

WISSENSCHAFTLICH-TECHNISCHE BERICHTE

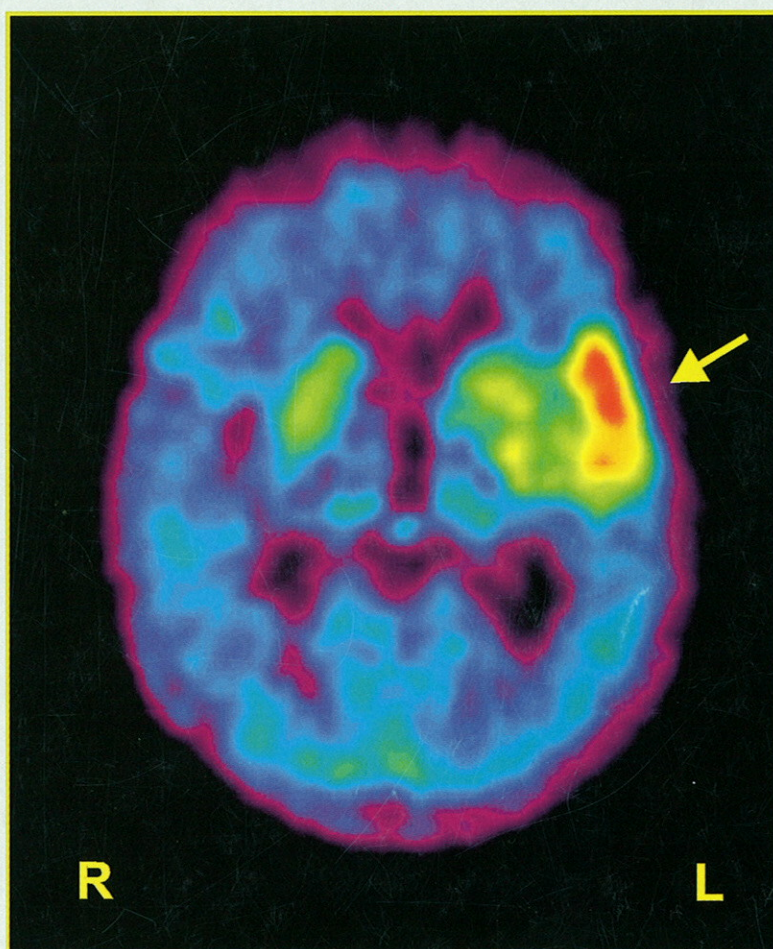
FZR-270

September 1999

ISSN 1437-322X



Institute of Bioinorganic and Radiopharmaceutical Chemistry



Report

January 1998 - June 1999

Cover Picture:

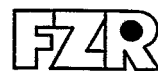
3-O-Methyl-6- ^{18}F fluoro-DOPA in a patient with recurrent glioblastoma. For further treatment planning an accurate delineation of the recurrent tumour is mandatory. An intense accumulation of the newly synthesized amino acid tracer depicts areas of viable tumour tissue in the left temporal lobe (arrow). Nonpathologic slightly increased uptake is found in the basal ganglia.

Forschungszentrum Rossendorf e. V.

Postfach 51 01 19; D-01314 Dresden
Bundesrepublik Deutschland
Telefon (03 51) 260 31 70
Telefax (03 51) 260 32 32
E-Mail johannsen@fz-rossendorf.de

FORSCHUNGSZENTRUM ROSSENDORF

WISSENSCHAFTLICH-TECHNISCHE BERICHTE



FZR-270

September 1999

**Institute of Bioinorganic and
Radiopharmaceutical Chemistry**

Report

January 1998 - June 1999

Editor:

Prof. Dr. B. Johannsen

Editorial staff: S. Seifert

CONTENTS

FOREWORD	VI
I. EDITORIAL	1
II. RESEARCH REPORTS	
TUMOUR AGENTS AND TUMOUR DIAGNOSIS	
1. Preparation of 3-O-Methyl-6-[¹⁸ F]Fluoro-L-DOPA F. Füchtner, J. Steinbach, R. Lücke, C. Smuda, B. Johannsen	13
2. Metabolism of 6-[¹⁸ F]Fluoro-3-O-Methyl-L-3,4-Dihydroxyphenylalanine in the Rat G. Vorwieger, R. Bergmann, R. Syhre, F. Füchtner, J. Steinbach, P. Brust, B. Johannsen	17
3. Metabolism of 6-[¹⁸ F]Fluoro-3-O-Methyl-L-3,4-Dihydroxyphenylalanine in Newborn Piglets G. Vorwieger, P. Brust, R. Bergmann, R. Bauer ¹ , B. Walter ¹ , F. Füchtner, J. Steinbach	21
4. First Results of 3-O-Methyl-6-[¹⁸ F]Fluoro-DOPA ([¹⁸ F]3-OMFD) in Patients with Glioblastoma Multiforme W. Burchert, B. Beuthien-Baumann, H. Alheit, J. Bredow, J. Steinbach, B. Johannsen, W.-G. Franke	24
5. Reaction of Neurotensin (8-13) and its Partially Reduced Congener with Unlabelled and ¹⁸ F-Labelled N-Succinimidyl 4-Fluorobenzoate (SFB) M. Scheunemann, P. Mäding, J. Steinbach, B. Johannsen, D. Tourwe	26
6. Experiments of the Synthesis of [¹⁸ F]Fluoromethyl Halides for Labelling Peptides P. Mäding, M. Scheunemann, J. Steinbach	29
7. Crystal and Solution Structures of the Rhenium(V) Gly-Gly-His Complex R. Jankowsky, W. Seichter, H. Spies, B. Johannsen	33
8. EXAFS Structure Analysis of a Rhenium Complex with Neurotensin Derivative ORP500 R. Jankowsky, B. Johannsen	38
9. Syntheses and Characterization of the Sulphamates of 17 ξ -Estradiols and 16 α -Fluoroestradiol J. Römer, J. Steinbach, H. Kasch	40
10. 17-Methyl-gona-1,3,5(10),13(17)-tetraene-3-ol J. Römer, H. Kasch, J. Steinbach, D. Scheller	47
11. ¹³ C NMR Spectroscopic Characterization of Some New Estrogen Sulphamates J. Römer, J. Steinbach, D. Scheller	49
12. Technetium and Rhenium-Labelled Steroids 7. Synthesis and Receptor Binding of Novel Progestine-Rhenium Complexes F. Wüst, M. B. Skaddan, K. E. Carlson, P. Leibnitz, J. A. Katzenellenbogen, H. Spies, B. Johannsen	51
13. Technetium and Rhenium-Labelled Steroids 8. "3+1" Mixed-Ligand Complexes According to the Integrated Design F. Wüst, H.-J. Pietzsch, P. Leibnitz, H. Spies	55

14. Nicotinamide-Substituted Complexes as Redox Markers 2. Synthesis of a ⁹⁹ Tc Dihydropyridine Mixed-Ligand Complex and Investigation of the Stability in Tissue Homogenates A. Rother, T. Kniess, M. Pütz, H. Jungclas, H. Spies	58
15. Evaluation of the In Vitro and In Vivo Properties of a Potential Tc-Labelled Inhibitor of the MDR Gene Product P-Glycoprotein R. Bergmann, P. Brust, H.-J. Pietzsch, M. Scheunemann, S. Seifert, B. Johannsen	62
16. Synthesis and Preliminary Evaluation of 9-[(3-[¹⁸ F]Fluoro-1-Hydroxy-2-Propoxy)-Methyl]guanine [¹⁸ F]FHPG in Rats B. Noll, St. Noll, P. Brust, M. Scheunemann, A. Jordanova, T. Knieß, M. Grote, J. Steinbach, M. Hausess, O. Koufaki, H. K.Schackert	68
17. The Diagnostic Value of [¹⁸ F]FDG Positron-Emission Imaging for Detection and Treatment Control of Malignant Germ Cell Tumours P. Tsatalpas, B. Beuthien-Baumann, T. Spiegel, J. Kropp, A. Manseck, C. Tiepolt, O. Hakenberg, W. Burchert, W.-G. Franke, M. P. Wirth	71
18. [¹⁸ F]FDG for the Staging of Patients with Differentiated Thyroid Cancer C. Tiepolt, B. Beuthien-Baumann, R. Hliscs, J. Bredow, A. Kühne, J. Kropp, W. Burchert, W.-G. Franke	75
BRAIN DOPAMINERGIC SYSTEMS	
19. The Pharmacokinetics of FDOPA in Newborn Piglets G. Vorwieger, R. Bergmann, B. Walter, R. Bauer, F. Füchtner, J. Steinbach, P. Brust	79
20. Characterization of Blood-Brain Transport of Large Neutral Amino Acids with 3-O-Methyl-[¹⁸ F]fluoro-DOPA H. Kuwabara, P. Brust, F. Füchtner, H. Stark, J. Steinbach	83
21. Regional Distribution of Cerebral Blood Volume in Newborn Piglets – Effect of Hypoxia/Hypercapnia R. Bergmann, R. Bauer, B. Walter, P. Brust	89
22. Effect of Hypoxia/Hypercapnia on Cerebral Blood Flow in Newborn Piglets R. Bauer, P. Brust, B. Walter, R. Bergmann	95
23. A New Tropane-Derived Rhenium Complex with High Affinity for the Dopamine Transporter A. Hoepfing, M. Reisgys, P. Brust, S. Seifert, H. Spies, R. Alberto, B. Johannsen	101
24. Investigations for an Improved Synthesis of TRODAT I. Heimbald, A. Hoepfing, S. Seifert	104
25. Potentially Dopamin Receptor-Binding Technetium and Rhenium Tracers: Synthesis and Characterization of Ligands Derived from Partial Structures of Epidepride M. Scheunemann, H.-J. Pietzsch, H. Spies, P. Brust, B. Johannsen	107
26. Implementation of the Catecholamine Analysis and Precolumn Technique in Amino Acid Determination with the Fluorescence Label Naphthalene-2,3-Dicarbaldehyde G. Vorwieger, R. Bergmann, P. Brust	110

27. Characterization of Impaired Brain Function in Persistent Vegetative State: Evaluation of Perfusion and Glucose Metabolism with Emission Tomography Techniques 115
B. Beuthien-Baumann, W. Handrick, T. Schmidt, W. Burchert, G. Schackert, W.-G. Franke

BRAIN SEROTONERGIC SYSTEMS

28. Synthesis of Enantiomerically Pure Thioester Precursors of [¹¹C]McN-5652 119
P. Gucker, J. Zessin, S. M. Ametamey, J. Steinbach
29. Improved Synthesis of [¹⁸F]Altanserin, a Radioligand for Imaging 5-HT_{2A} Receptors with PET 122
J. Zessin, K. Hamacher, F. Füchtner, H. Büttich, N. Dohn, J. Steinbach
30. Serotonin Receptor-Binding Technetium and Rhenium Complexes 124
21. Synthesis and Characterization of a Novel High-Affinity Tc-99m Ligand for the 5-HT_{2A} Receptor
H.-J. Pietzsch, M. Scheunemann, S. Seifert, P. Brust, H. Spies, B. Johannsen
31. Serotonin Receptor-Binding Technetium and Rhenium Complexes 127
22. Biological Evaluation of a Novel High-Affinity Tc-99m Ligand for the Serotonin-5-HT_{2A} Receptor
M. Kretzschmar, P. Brust, S. Elz, H. H. Pertz, H.-J. Pietzsch, M. Scheunemann, S. Seifert, J. Zessin, B. Johannsen
32. Serotonin Receptor-Binding Technetium and Rhenium Complexes 133
23. Design, Structure and in vitro Affinity of a 5-HT_{1A} Receptor Ligand Labelled with ^{99m}Tc - First Application of fac-[^{99m}Tc(OH₂)₃(CO)₃]⁺ in Bioorganometallic Chemistry
R. Alberto, R. Schibli, A. P. Schubiger, U. Abram, H.-J. Pietzsch, A. Drews, B. Johannsen

RADIOPHARMACEUTICAL CHEMISTRY

33. Automated Production of [¹¹C]Methyl Iodide 137
J. Zessin, P. Mäding, H. Krug, S. Gommlich, B. Jung, E. Lösel, N. Dohn, F. Füchtner, J. Steinbach
34. Synthesis of 5-Methoxy-[2-¹¹C]Indole by Reduction of 5-Methoxy-β,2-Dinitro-[β-¹¹C]Styrene 139
J. Zessin, J. Steinbach
35. Synthesis of 3-O-[¹¹C]Methyl-D-Glucose 141
P. Mäding, H. Kasper, J. Zessin, M. Gnauck, F. Füchtner, P. Brust, J. Steinbach
36. "3+1" Mixed-Ligand Oxorhenium(V) Complex with 1,2,3,4-Tetrahydroisoquinoline 143
A. Zablotska, I. Segal, E. Lukevics, H.-J. Pietzsch, T. Kniess, H. Spies
37. Tc-99m Labelled Fatty Acids on Basis of "n+1" Mixed-Ligand Complexes ? 145
H. Spies, H.-J. Pietzsch, J. Kropp, T. Fietz, C. Jung
38. ^{186/188}Re Labelling of Stents for the Prevention of Restenosis 148
B. Noll, H. Goerner, L. Dinckelborg, C. S. Hilger, E. Richter
39. Synthesis and Molecular Structure of Chloro(3-Thiapentane-1.5-Dithiolato)-Oxotechnetium(V) 151
B. Noll, P. Leibnitz, H. Spies

40. Synthesis and Molecular Structure of $[\text{Tc}(\text{CN}-\text{CH}_2-\text{COOCH}_3)_6]\text{TcO}_4$ B. Noll, P. Leibnitz, H. Spies	153
41. Crystal Structure of the Nitridorhenium(V) Complex $[\text{ReN}\{\text{Cme}_2\text{PPh Me}_2\}(\text{DMSMe}_2)_2]$ S. Seifert, P. Leibnitz ¹ , H. Spies	154
42. Reactions of Hydroxy Group Containing '3+1' Mixed-Ligand Oxorhenium(V) Complexes. Part 3. Synthesis and Physicochemical Investigation of O-Organosilicon Containing 3-Thia-, 3-Oxa- and 3-Methylazapentane-1,5-Dithiolato-Oxorhenium(V). A. Zablotska, I. Segal, A. Kemme, E. Lukevics, R. Berger, H. Spies	156
43. Artificial Guanidinium Hosts for Binding Pertechnetate H. Stephan, F. P. Schmidtchen, H. Spies, B. Johannsen	159
44. EXAFS Analysis of a Rhenium(I) Carbonyl Complex S. Seifert, J.-U. Künstler, H. Funke, A. Roßberg, C. Hennig, T. Reich, G. Bernhard, B. Johannsen	162
45. First XANES and EXAFS Measurements of Technetium Model Compounds at the Rossendorf Beamline ROBL T. Reich, H. Funke, C. Hennig, A. Roßberg, H.-J. Pietzsch, S. Seifert, J.-U. Künstler, G. Bernhard	165
46. Challenge Experiments with "3+1" Mixed-Ligand $^{99\text{m}}\text{Tc}$ Complexes and Glutathione: Influence of Structural Parameters on the Complex Stability A. Gupta, S. Seifert, R. Syhre, B. Johannsen	167
47. Identification of the Transchelation Product of "3+1" Mixed-Ligand Technetium and Rhenium Complexes with Glutathione A. Gupta, S. Seifert, R. Syhre, B. Johannsen	173
48. Stability of "3+1" Mixed-Ligand $^{99\text{m}}\text{Tc}$ Complexes in vitro: Inhibition of the GSH in the Blood Results in a Stabilization of the Complexes In Vitro A. Gupta, S. Seifert, R. Syhre, B. Johannsen	177
49. Reactivity of "3+1" $^{99\text{m}}\text{Tc}$ Complexes to Proteins S. Seifert, A. Gupta, R. Syhre	181
50. An Effective Pre-Labeling Method for Amino Acids with Activated $^{99\text{m}}\text{Tc}-\text{MAG}_3$ in Aqueous Solution T. Knieß, St. Noll, B. Noll, H. Spies	185
51. ^{186}Re -Labelling of an Endotheline Derivative B. Noll, L. Dinkelborg, H. Hilger	188
52. Capillary Electrophoresis of $^{99\text{m}}\text{Tc}$ Radiopharmaceuticals: Quality Control and pK Determination at the Tracer Level R. Jankowsky, B. Noll, H. Spies, B. Johannsen	190
53. Some Additions to the Determination of log P and pK _a Values by Using Reversed Phase HPLC R. Berger, H. Spies	194
54. Partition Coefficients for Steroidal Rhenium Coordination Compounds Determined by Using RP-HPLC R. Berger, F. Wüst, M. Reisgys, H. Spies	198

55. Miscellaneous Results of Determining Partition Coefficients and Ionization Constants for Rhenium and Technetium Coordination Compounds by Using HPLC R. Berger, F. Wüst, A. Zablotskaya, M. Reisgys, M. Friebe, H.-J. Pietzsch, M. Scheunemann, H. Spies, B. Johannsen	202
56. Influence of Transport Conditions of the [¹⁸ F]F ⁻ Water Target on the [¹⁸ F]FDG Synthesis St. Preusche, F. Füchtner, J. Steinbach	210
57. Improvements at the Rossendorf PET Cyclotron "CYCLONE 18/9" St. Preusche, H. Roß	213
58. Operation of the Rossendorf PET Cyclotron "CYCLONE 18/9" in 1998/1999 St. Preusche, J. Steinbach	215
59. Sources of Radiation Dose to Technologists by FDG-PET H. Linemann, E. Will, B. Beuthien-Baumann, A. Wittmüß, H. Schröder, H. Kutzner, A. Hauptmann	219
III. PUBLICATIONS, LECTURES, PATENTS AND AWARDS	223
IV. SCIENTIFIC COOPERATION	239
V. SEMINARS	245
VI. ACKNOWLEDGEMENTS	249
VII. PERSONNEL	251

FOREWORD

Basic and application-oriented research is carried out by the Institute of Bioinorganic and Radiopharmaceutical Chemistry as part of the research centre Forschungszentrum Rossendorf (FZR), a member of the research association Wissenschaftsgemeinschaft Gottfried Wilhelm Leibnitz.

Committed to research into essential problems of our time, the Institute focuses on investigations into radiotracers as molecular probes in order to contribute to a better understanding of chemical processes in the living organism on a nanomolar and picomolar level. The all-embracing theme is the search for radionuclide-labelled tracer molecules which bind to specific targets in the body.

When further developed into radiopharmaceuticals, the radiotracers permit medical research as well as diagnostic applications. Studies are performed in close cooperation with the Department of Nuclear Medicine of the Dresden University Hospital. For this purpose the Institute runs a centre for positron emission tomography (PET). A joint team of staff members from both the Institute and the Department of Nuclear Medicine work at this PET centre.

The reports presented here cover interdisciplinary research activities. The PET tracer group of the Institute studied the chemistry and radiopharmacy of ^{11}C and ^{18}F compounds. The bioinorganic group has dealt with the design, synthesis and characterization of radiometal-based radiotracers, primarily technetium and rhenium complexes. The biochemical group worked on the biological characterization of new radioactive compounds in cell and animal models and also on pharmacological and pathophysiological themes. Some first contributions from the joint medical group are also included in these reports.

The main research activities of the Institute were devoted to radiochemical and pharmacological studies of brain neurotransmitter-mediated processes and tumour targeting.

With respect to oncology, progress in tracer development is highlighted by the proposed concept of using 3-*O*-methyl-6- ^{18}F fluoro-L-DOPA for imaging brain tumours. Derived from biological studies of 6- ^{18}F fluoro-L-DOPA metabolites and the development of an improved synthesis of 3-*O*-methyl-6- ^{18}F fluoro-L-DOPA, the compound proved to be a substrate of an amino acid transporter and thus able to cross the blood-brain barrier with subsequent accumulation in brain tumours.

In 1998 a European Biomed project started on tumour-seeking receptor-binding peptides. The neurotensin molecule has meanwhile been modified and radiolabelled so as to maintain a high receptor-binding affinity. The structure is now being optimized in terms of optimal biodistribution by the groups collaborating on the project.

The main subject of CNS receptor ligand research at this moment is to design technetium-based molecules that are able to overcome the serious hurdle presented by the blood-brain barrier and to achieve high, subnanomolar binding affinities. During the period covered by these reports, studies of a large number of neutral mixed-ligand complexes confirmed the importance of the pKa value for transport of this class of compounds through the blood-brain barrier and showed how the pKa can be adjusted by appropriate substituents without impairing the receptor binding.

The requirement of subnanomolar affinity was met by the synthesis and autoradiographic evaluation of a novel $^{99\text{m}}\text{Tc}$ ligand for the serotonin 5-HT_{2A} receptor.

The metallotricarbonyl concept, which was quite recently introduced by the chelator chemistry group of the Paul Scherrer Institute (PSI), Switzerland, in the design of CNS receptor imaging agents based on technetium-99m, was successfully applied in cooperation with the PSI group. Ligands for the 5-HT_{2A} and 5-HT_{1A} receptors as well as the dopamine transporter were prepared and characterized.

The successes achieved so far have only been possible thanks to the dedication and commitment of the permanent and temporary staff, the Ph.D. students and collaborators inside and outside the research centre Forschungszentrum Rossendorf.

I would like to extend my thanks to all of them.

Rossendorf, September 1999



Prof. Dr. Bernd Johannsen

I. EDITORIAL

Radiotracers for Tumour Imaging with Positron Emission Tomography

P. Brust, J. Steinbach and B. Johannsen

Introduction

Positron emission tomography (PET) is a unique non-invasive diagnostic tool offering the possibility of *in vivo* quantitative measurements. Depending on the radiotracer used it produces dynamic images of various physiological functions at the molecular level which can be used to quantify vital processes, such as glucose metabolism, blood flow and perfusion, receptor-ligand interactions and oxygen utilization. So far PET studies have made substantial contributions to at least four clinical disciplines: cardiology, neurology, psychiatry and oncology.

A rapidly emerging clinical application of positron emission tomography (PET) is the detection and staging of cancer with the glucose analogue 2-¹⁸F-fluoro-2-deoxy-D-glucose (FDG). Early diagnosis in oncology is helpful for treatment by surgical intervention, which generally has the highest curative potential. Anatomic imaging modalities, such as CT and MRI, are clinically important high-resolution imaging techniques that are well suited for revealing structural abnormalities. However, the differentiation of neoplasms as being benign or malignant is still problematic. PET can reveal biochemical parameters of the neoplasms such as glucose, oxygen, or amino acid metabolism, or measure the receptor density status. These parameters may allow a completely new clinical perspective in the field of oncology.

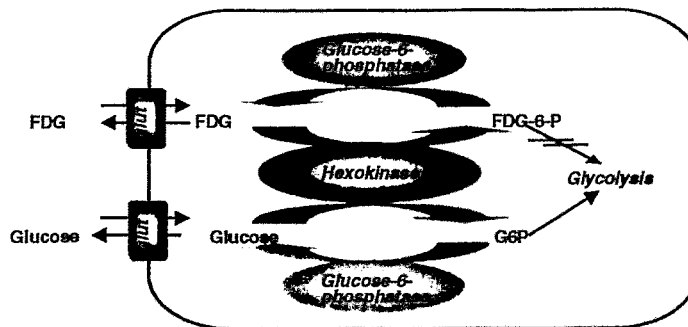


Fig. 1. Uptake and metabolism of glucose compared with FDG. After being transported into the cell glucose is metabolized via the glycolytic pathway to provide energy in form of ATP. The FDG is only phosphorylated and trapped because the activity of glucose-6-phosphatase is much lower than the activity of the hexokinase.

FDG for tumour imaging

PET using FDG as a metabolic marker has the potential to distinguish malignant processes from normal tissue by means of increased glucose metabolism (Fig. 1). Its higher spatial resolution compared with conventional scintigraphic methods leads to the widespread application of FDG-PET in oncology. Functional imaging with FDG-PET provides relevant diagnostic information complementary to morphologic imaging.

Knowledge of the normal physiological distribution of the radiotracer is required for the correct interpretation of FDG PET images. It has to be assured that benign pathological causes of FDG uptake are not confused with a malignant tumour. In a whole-body scan intense FDG activity can be seen in the brain, occasionally in the heart and due to the excretory route the urinary tract. Elsewhere, radiotracer activity is typically low. That allows sensitive demonstration of radiotracer accumulation in many tumor entities (Fig. 2). However, as a limitation one has to be aware that FDG uptake is nonspecific, which is related to the principle of FDG uptake and metabolism (Fig. 1). This offers the possibility of pitfalls that can be misinterpreted as cancer. Such pitfalls include variable physiological FDG uptake in various organs, in healing bones, sites of infection and aseptic inflammatory response [1].



Fig. 2. FDG-PET image of a patient with tumour bulk and singular metastases of Hodgkin's lymphoma in the mediastinum as well as metastases in the lower part of the right lung. FDG accumulation is seen in the brain, heart and bladder as well.

The clinical value of FDG-PET has been proved for a number of tumour entities and their metastases, e.g. bronchial, colorectal and pancreatic malignomas, nonsmall cell lung carcinomas, breast cancer, malignant lymphomas and others. Generally, FDG-PET can be very useful in clinically and radiologically "difficult-to-examine tumours," e.g., following tumour surgery. Qualitative assessment of the extent of the tumour spread provides prognostic information and allows for selection of an appropriate therapy. The identification of tumour spread to the axillary nodes or to more remote nodal groups, i.e., internal mammary or supraclavicular nodes, is probably the most practical information that qualitative FDG-PET can offer. For routine use in oncology a detailed assessment of the specific efficiency of PET has been indicated by a panel of recognized experts in the framework of an interdisciplinary consensus conference [2].

In the PET Center Rossendorf a total number of 484 tumour patients were studied between 1. Jan. 1998 and 30. Jun. 1999, among them 20 % with lymphoma and 20 % with squamous cell carcinoma as those with the highest incidence. Preliminary studies indicated that an early serial assessment of tumour metabolism by FDG-PET during an effective chemo- or radiotherapy may predict the subsequent response to such a therapy. (Fig. 3).

Another limitation of tumour imaging with FDG is the difficult visualization of gliomas because of the high uptake of this radiotracer in the normal brain. Also for imaging neuroendocrine tumours FDG-PET is only of limited value [3].

From this point of view it would be most useful to develop radiotracers utilizing tumour specific processes. Unfortunately the prerequisites for exploiting such processes are poor. The radiotracer accumulation caused by such targeted processes is usually low and the quality of the images may therefore be unsatisfactory.

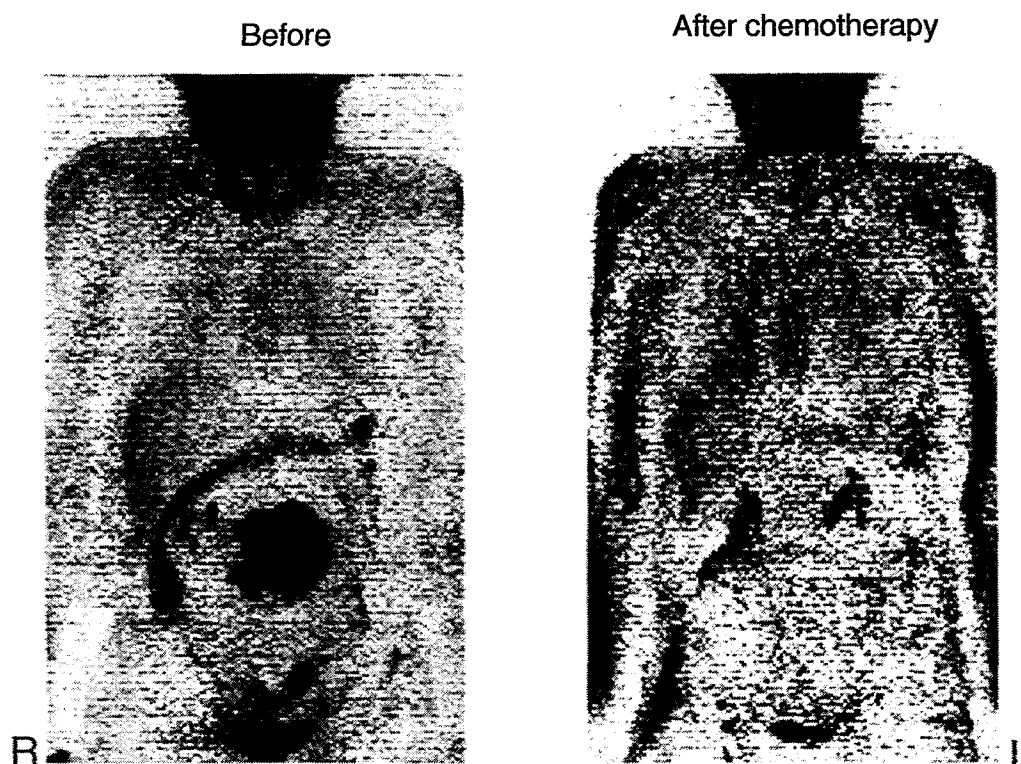


Fig. 3. FDG-PET image of a patient with abdominal metastasis of a seminoma (left). After completion of chemotherapy, with [^{18}F]FDG-PET no vital tumour is detected, although on CT residual tumour is still present.

To overcome this problem new radiodiagnostic tools for tumour imaging have to be considered. There are numerous new radiotracers whose particular distribution in the presence of cancer *in vivo* serves to distinguish medically relevant properties of the tumour cells with which they associate. These radiotracers include precursors of protein anabolism (e.g. amino acids), receptor ligands (e.g. peptides and steroids), substrates for enzymatic modification by the products of expression of specific genes (e.g. gancyclovir) and hypoxia markers (e.g. misonidazol).

Amino acids for brain tumours

New trends in PET applications for the study of brain tumours take the histological heterogeneity of these tumours into account and integrate PET data into their surgical management. The annual incidence of primary brain tumours is increasing. The prognosis for these tumours remains poor, with an expected survival of only a few years. The ability to diagnose, monitor, and treat CNS tumours has been improved by newly developed radiotracers for PET such as amino acid radiotracers.

The increased utilization of amino acids by tumours has been investigated for more than 40 years. Parameters such as membrane transport, metabolism and protein incorporation govern the fate of the amino acids in living tissue. The possibilities offered by PET of studying the amino acid metabolism

and protein synthesis have been evaluated within the framework of the European Community Medical and Public Health Research [4].

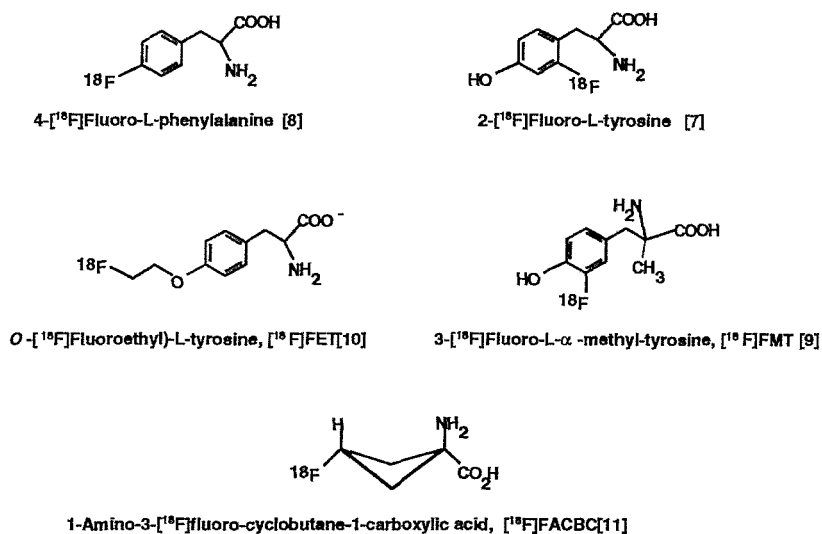


Fig. 4. ¹⁸F-labelled amino acids developed and evaluated as tumour-detecting PET tracers.

L-[¹¹C]Methionine has already proved to be useful in delineating brain tumours [5, 6]. However, this radiotracer has the disadvantage of a short half-life, which requires in-house radiosynthesis and repeated radiolabelling for each single PET study. An ¹⁸F-labelled amino acid tracer is therefore desirable for PET (Fig. 4). A number of such radiotracers have been developed and evaluated as tumour-detecting agents, e.g. 2-[¹⁸F]fluoro-L-tyrosine [7], 4-[¹⁸F]fluoro-L-phenylalanine [8], 3-[¹⁸F]fluoro-L-α-methyl-tyrosine (FMT) [9], O-[¹⁸F]fluoroethyl-L-tyrosine (FET) [10] and 1-amino-3-[¹⁸F]fluoro-cyclobutane-1-carboxylic acid (FACBC) [11].

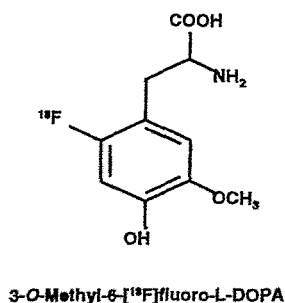


Fig. 5. The amino acid 3-O-methyl-6-[¹⁸F]fluoro-L-DOPA which may be used for tumour imaging with PET as proposed by the Rossendorf group [12].

Rather ineffective radiosynthesis still limits the use of these radiotracers. An efficient synthesis of 3-*O*-methyl-6- ^{18}F fluoro-L-DOPA has therefore been developed in Rossendorf (Fig. 5). Some first *in vivo* studies demonstrate the suitability of this radiotracer for tumour imaging [12].

Tumour receptor imaging

Tumour receptor imaging has great prospects for further PET investigations. The best-characterized systems for receptor-based imaging are estrogen-receptor imaging of breast cancer, somatostatin-receptor imaging of neuroendocrine tumours, and epidermal growth factor receptor imaging. The latter two systems are only available for SPECT. $^{99\text{m}}\text{Tc}$ -labelled antihuman epidermal growth factor receptor antibodies has been used in patients with tumours of epithelial origin [13-15]. The ^{131}I -labelled epidermal growth factor (EGF) has been used to localize squamous lung carcinoma with SPECT [16]. EGF is also a potential peptide radiopharmaceutical for the detection of brain tumours as many human gliomas overexpress the EGF receptor. For this purpose [^{111}In]DTPA-EGF was coupled to a delivery vector to enable brain tumour imaging [17]. Because of the higher spatial resolution PET imaging has an even greater potential. However, no suitable PET tracers are available so far.

Peptides

Bioactive peptides, such as peptide hormones, immunomodulators and growth promoters, have been found to modulate a wide variety of biological functions. Their effects are mediated by high-affinity receptors located on the membranes of the target cells. The widespread expression of high-density peptide receptors on the surface of tumour cells, which was recently demonstrated, makes these biomolecules attractive vectors for targeting those cells. Peptides may be used as tools for directing radionuclides for either diagnostic or therapeutic purposes specifically onto malignant cells. The development of the somatostatin analogue [^{111}In]octreoscan illustrates how advances in basic science are translated into health care [18, 19].

Despite successful labelling of peptides with ^{111}In , $^{99\text{m}}\text{Tc}$, ^{123}I and occasionally with ^{18}F [3, 18, 20-26] only a few of them have proved suitable for tumour receptor imaging. No PET tracer has as yet fulfilled the necessary criteria. Despite a high *in vitro* binding affinity, certain unfavourable features (a high nonspecific binding *in vivo*, rapid degradation, unacceptable accumulation in nontarget areas) prevented them from being useful.

One of the projects described in this annual report deals with the development of ^{18}F -labelled neurotensin analogues for tumour imaging. The work is embedded in a BIOMED2 shared-cost action with five other partners from European countries, which will hopefully ensure that the problems described can be solved.

Steroids

The use of PET with the estrogen analogue 16α - ^{18}F fluoro-estradiol (FES) to monitor the receptor function and response to hormonal therapy opens up intriguing new ways to monitor patients with breast cancer at a cellular level. Generally, ^{18}F -labelled estradiol derivatives are suitable for *in vivo* imaging of estrogen receptors, including functional receptor diagnosis. Their high specificity, established in animal experiments and in *in vitro* studies was reproduced in *in vivo* applications in humans. However, estrogen receptor scintigraphy is only of limited use for tumour screening or staging because only 50 – 70 % of mammary carcinomas are receptor positive [27].

On the other hand, targeting the progesterone receptors found in receptor-positive breast cancer provides a means of diagnosing the disease non-invasively. The advantages of visualizing the tumour through targeting these receptors include PET imaging to follow the progress of the tamoxifen therapy while the estrogen receptors are blocked [28].

Another therapeutic strategy is based on the assumption that the major source of estrogens in breast cancer cells is the conversion of estrone sulphate and dehydroepiandrosterone sulphate into estradiol and androstendiol by the enzymes estrone sulfatase and 17β -hydroxysteroid dehydrogenase [29, 30]. These estrogenic steroids delivered by the sulphated transport form act as mitogens to stimulate tumour growth [30, 31]. Inhibition of estrone sulfatase is therefore expected to inhibit also tumour growth. The concept has already proved its worth *in vitro* [29]. Highly potent estrone sulfatase in-

hibitors were recently developed in cooperation with the Jena Hans Knöll Institute. They offer the potential of tumour imaging after labelling with ^{18}F [33].

Hypoxia markers

Hypoxia occurs to a varying extent in a vast majority of rodent and human solid tumours. It results from an inadequate and disorganized tumour vasculature, and hence an impaired oxygen delivery. A probe for the non-invasive detection of tumour hypoxia could be very useful in the selection of patients for therapy. Tumour hypoxia is an important factor that limits the response to radiation in human cancers [34, 35]. In addition, hypoxic tumor cells are also resistant to some cytotoxic drugs [35, 36]. Nitroimidazoles and other compounds were designed to overcome the hypoxic cell problem by specifically sensitizing hypoxic cells to the effects of radiation. There has been considerable interest in imaging hypoxia with radiolabelled derivatives of these compounds. A fluorinated 2-nitroimidazole, N-(2-hydroxy-3,3,3-trifluoropropyl)-2-(2-nitro-1-imidazolyl) acetamide (SR 4554, CRC 94/17), was rationally designed for the measurement of tumour hypoxia by magnetic resonance spectroscopy (MRS) and imaging (MRI) [37]. Whole body ^{19}F -MRI in mice demonstrated that SR 4554 and related metabolites were mainly concentrated in tumour, liver and bladder. But rather high doses had to be administered, which may prevent the use of SR 4554 in humans on account of the possible toxicity. However, this compound also has a potential for use in positron emission tomography.

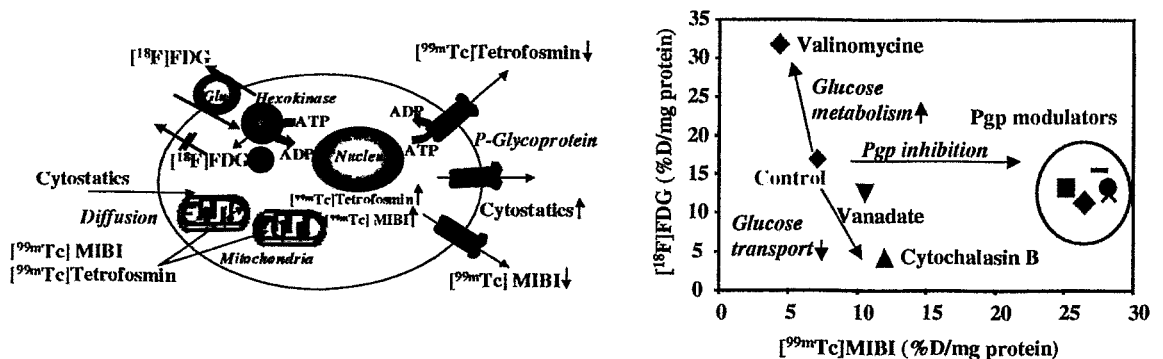


Fig. 6. Simultaneous investigation of P-glycoprotein (Pgp) expression and glucose metabolism in tumour cells.

Left: Schematic representation of the principles: Uptake of MIBI and tetrofosmin is caused by diffusion driven by the negatively charged membranes of mitochondria. Excess of cytostatics saturates the capacity of Pgp and results in decreased efflux and intracellular accumulation of the radiotracers MIBI and tetrofosmin. FDG is transported into the cell by a glucose transporter (glut) and is phosphorylated by hexokinase. The phosphorylated product is trapped within the cell. Effects of cytostatics on glucose metabolism are shown by increased or decreased accumulation of glucose phosphate.

Right: Effects of various drugs on the accumulation of MIBI and FDG by a Pgp expressing brain endothelial cell line. The typical effect of Pgp modulators, such as verapamil and colchicine is shown by the increased accumulation of MIBI. Other compounds (cytochalasin B, valinomycin) influence primarily glucose transport and metabolism.

Several imidazole derivatives have already been labelled with ^{18}F , such as ^{18}F fluoromisonidazole (FMISO), ^{18}F fluoroerythronitroimidazole (FETNIM) and ^{18}F fluoroethanidazole [38-40]. Despite encouraging preliminary results these compounds are expected to be of limited use in routine clinical practice [35].

Monitoring drug resistance

Cellular resistance to cytotoxic agents is the major cause of treatment failure in many human cancers. Overexpression of the P-glycoprotein (Pgp), present in the plasma membrane of various tumour cells and in several normal cell types, contributes to the multiple drug resistance (MDR) phenotype of many human cancers (Fig. 6). The expression of Pgp has to be studied as a prerequisite for the therapy. Available clinical radiopharmaceuticals to study the expression of Pgp include the lipophilic ^{99m}Tc cations MIBI and tetrofosmin [41-43].

Many clinical studies from various institutions and trials, including a variety of malignancies, indicate that both tumour uptake and clearance of [^{99m}Tc]MIBI are correlated with Pgp expression and may be used for the phenotypic assessment of MDR [44]. There is still a lack of PET tracers suitable for clinical monitoring of multiple drug resistance. Recently the Pgp function was measured *in vivo* with PET and [^{11}C]verapamil as radiolabelled Pgp substrate in rats having a Pgp-negative small-cell lung carcinoma and its Pgp-overexpressing subline [45]. These results show the feasibility of *in vivo* Pgp function measurement with PET under basal conditions and after modulation in solid tumours and in the brain. PET and radiolabelled Pgp substrates may therefore be useful as a clinical tools for selecting patients who might benefit from the addition of a Pgp modulator to MDR drugs.

As was recently shown in cell culture and animal experiments, the combined use of various radiotracers may be a tool for differentiating between individual tumours in terms of their sensitivity to therapeutic strategies (Fig. 6) [46].

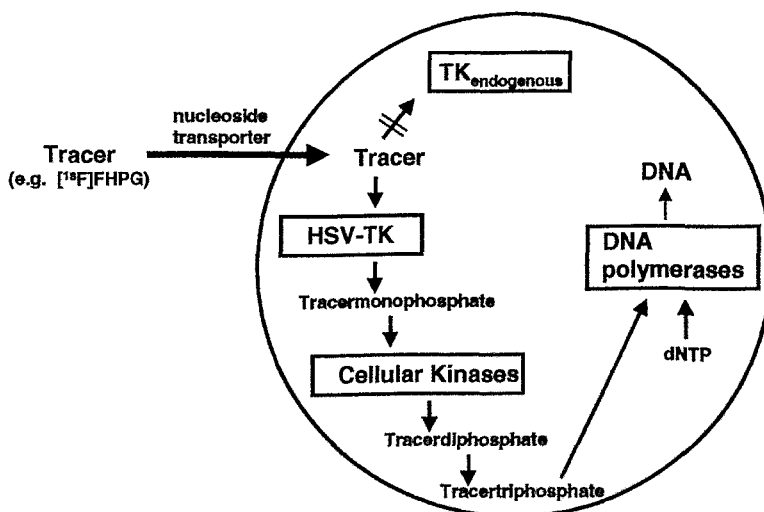


Fig. 7. Schematic representation of the principle of monitoring gene therapy with radiolabelled nucleoside analogues that are not substrates for human kinases but are converted by herpes simplex virus thymidine kinase (HSV-TK) and subsequently by cellular kinases to antimetabolites (inhibitors of DNA synthesis).

Tumour therapy

One of the most promising new treatments for cancer are gene therapy approaches. Phase I/II clinical trials for brain, breast, colon and other tumours are under way [47-49]. Cancer gene therapy includes gene delivery to tumour cells and the cellular expression of the specific transferred gene. Assessing the distribution and duration of gene expression is of prime importance for evaluating new gene ther-

apy approaches, and PET provides a tremendous potential for improvement over the currently used methods of monitoring gene transfer [35].

The herpes simplex virus thymidine kinase / ganciclovir system is one of the most widely investigated gene therapy approaches which has also been used for PET imaging (Fig. 7) [50, 51]. Several radiotracers have been developed for this purpose (Fig. 8) [52-59]. Generally, the *in vitro* and *in vivo* results obtained with these radiotracers demonstrated the validity of the concept. However it has been shown that the use of radiolabelled acyclovir and ganciclovir has limitations such as a poor sensitivity [51]. Other compounds lack selectivity. To overcome these problems, new radiotracers have to be developed. One of the most recent approaches is the synthesis and biological evaluation of [^{124}I]FIAU [60]. However, this radiotracer is only available on a limited number of sites, which complicates its routine use and encourages the search for other compounds.

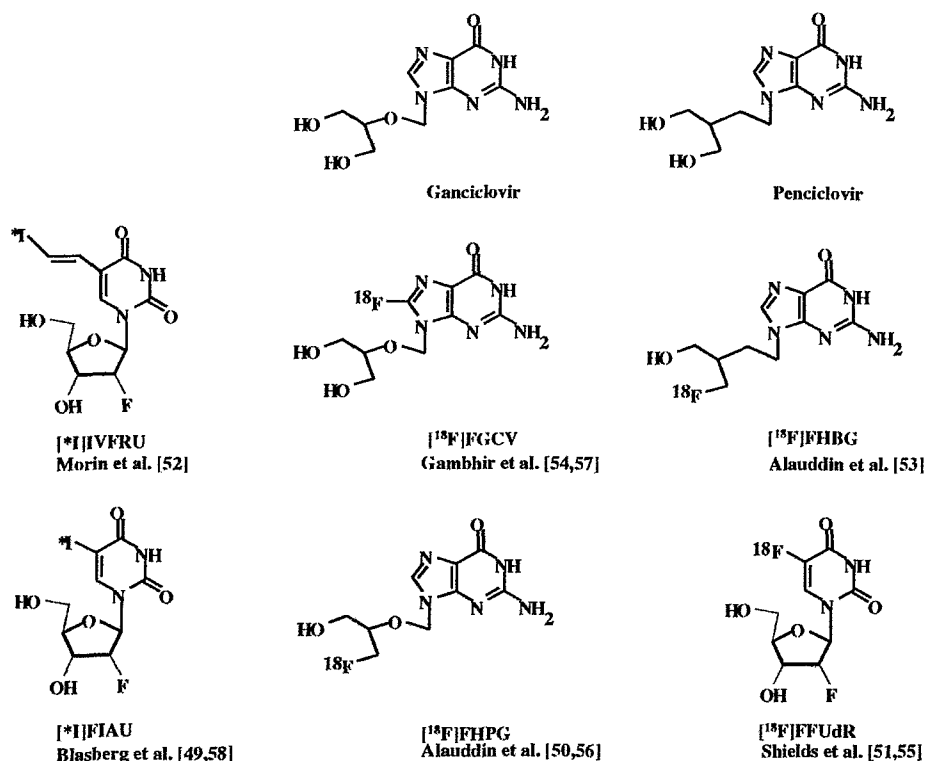


Fig. 8. Radiolabelled nucleoside analogues as potential imaging agents for monitoring gene therapy with herpes simplex virus thymidine kinase gene.

Another strategy for tumour therapy which was developed by the GSI Darmstadt with the support of the Rossendorf Research Center [61-65] is radiotherapy with heavy ions. Beams of heavy ions such as carbon make it possible to combine two advantageous properties: better targeting and higher biological efficiency. Particle beams have an inverse depth dose profile, with the maximum dose in the deep-seated tumour, a finite range, small lateral scattering, and a drastically increased biological efficiency in the tumour. These properties maximize the deletion effects on tumour cells [66]. In addition, particle beams can be directed with great precision within one or two millimetres, and can be monitored using positron emission tomography (PET).

In conclusion it can be said that PET has already been shown to contribute significantly to tumour research and clinical oncology. The development of new target-based imaging tools will provide even better possibilities for diagnosis and therapy in this field.

References

- [1] Shreve P. D., Anzai Y. and Wahl R. L. (1999) Pitfalls in oncologic diagnosis with FDG PET imaging: physiologic and benign variants. *Radiographics* **19**, 61-77.
- [2] Reske S. N., Bares R., Bull U., Guhlmann A., Moser E. and Wannemacher M. F. (1996) Clinical value of positron emission tomography (PET) in oncologic questions: results of an interdisciplinary consensus conference (in German). *Nuklearmedizin* **35**, 42-52.
- [3] Adams S., Baum R., Rink T., Schumm-Drager P. M., Usadel K. H. and Hör G. (1998) Limited value of fluorine-18 fluorodeoxyglucose positron emission tomography for the imaging of neuroendocrine tumours. *Eur. J. Nucl. Med.* **25**, 79-83.
- [4] Mazoyer B. M., Heiss W. D. and Comar D. (eds.) (1993) *PET Studies on Amino Acid Metabolism and Protein Synthesis*. Kluwer Academic Publishers, Dordrecht, p. 268.
- [5] Mineura K., Sasajima T., Kowada M., Ogawa T., Hatazawa J. and Uemura K. (1997) Early delineation of cerebral glioma using amino acid positron tracers. *Comput. Med. Imaging Graph.* **21**, 63-66.
- [6] Derlon J. M., Petit-Taboue M. C., Chapon F., Beaudouin V., Noel M. H., Creveuil C., Courtheoux P. and Houtteville J. P. (1997) The in vivo metabolic pattern of low-grade brain gliomas: a positron emission tomographic study using ^{18}F -fluorodeoxyglucose and ^{11}C -L-methylmethionine. *Neurosurgery* **40**, 276-287.
- [7] Coenen H. H., Kling P. and Stöcklin G. (1989) Cerebral metabolism of L-[2- ^{18}F]fluorotyrosine, a new PET tracer of protein synthesis. *J. Nucl. Med.* **30**, 1367-1372.
- [8] Kubota K., Ishiwata K., Kubota R., Yamada S., Takahashi J., Abe Y., Fukuda H. and Ido T. (1996) Feasibility of fluorine-18-fluorophenylalanine for tumor imaging compared with carbon-11-L-methionine. *J. Nucl. Med.* **37**, 320-325.
- [9] Inoue T., Tomiyoshi K., Higuichi T., Ahmed K., Sarwar M., Aoyagi K., Amano S., Alyafei S., Zhang H. and Endo K. (1998) Biodistribution studies on L-3-[fluorine-18]fluoro-alpha-methyl tyrosine: a potential tumor-detecting agent. *J. Nucl. Med.* **39**, 663-667.
- [10] Wester H. J., Herz M., Weber W., Heiss P., Senekowitsch-Schmidtke R., Schwaiger M. and Stöcklin G. (1999) Synthesis and radiopharmacology of O-(2-[^{18}F]fluoroethyl)-L-tyrosine for tumor imaging. *J. Nucl. Med.* **40**, 205-212.
- [11] Shoup T. M., Olson J., Hoffman J. M., Votaw J., Eshima D., Eshima L., Camp. V. M., Stabin M., Votaw D. and Goodman M. M. (1999) Synthesis and evaluation of [^{18}F]1-amino-3-fluorocyclobutane-1-carboxylic acid to image brain tumors. *J. Nucl. Med.* **40**, 331-338.
- [12] Füchtner F., Steinbach J., Vorwieger G., Bergmann R., Syhre R., Brust P., Beuthin-Baumann B., Burchert W., Zips D., Baumann M. and Johannsen B. (1999) 3-O-Methyl-6-[^{18}F]fluoro-L-DOPA - a promising substance for tumour imaging. *J. Labelled Compd. Radiopharm.* **42** (Suppl.1), S267-S269.
- [13] Iznaga-Escobar N., Torres L. A., Morales A., Ramos M., Alvarez I., Perez N., Fraxedas R., Rodriguez O., Rodriguez N., Perez R., Lage A., and Stabin M. G. (1998a) Technetium-99m-labeled anti-EGF-receptor antibody in patients with tumor of epithelial origin: I. Biodistribution and dosimetry for radioimmunotherapy. *J. Nucl. Med.* **39**, 15-23.
- [14] Iznaga-Escobar N., Torres Arocha L. A., Morales A., Ramos Suzarte M., Rodriguez Mesa N. and Perez Rodriguez R. (1998b) Technetium-99m-antiepidermal growth factor-receptor antibody in patients with tumors of epithelial origin: part II. Pharmacokinetics and clearances. *J. Nucl. Med.* **39**, 1918-1927.
- [15] Ramos-Suzarte M., Rodriguez N., Oliva J. P., Iznaga-Escobar N., Perera A., Morales A., Gonzalez N., Cordero M., Torres L., Pimentel G., Borrón M., Gonzalez J., Torres O., Rodriguez T. and Perez R. (1999) $^{99\text{m}}\text{Tc}$ -labeled antihuman epidermal growth factor receptor antibody in patients with tumors of epithelial origin: Part III. Clinical trials safety and diagnostic efficacy. *J. Nucl. Med.* **40**, 768-775.
- [16] Cuartero-Plaza A., Martínez-Miralles E., Rosell R., Vadell-Nadal C., Farre M. and Real F.X. (1996) Radiolocalization of squamous lung carcinoma with ^{131}I -labeled epidermal growth factor. *Clin. Cancer Res.* **2**, 13-20.

- [17] Kurihara A., Deguchi Y. and Partridge W. M. (1999) Epidermal growth factor radiopharmaceuticals: ^{111}In chelation, conjugation to a blood-brain barrier delivery vector via a biotin-polyethylene linker, pharmacokinetics, and in vivo imaging of experimental brain tumors. *Bioconjug. Chem.* **10**, 502-511.
- [18] O'Byrne K. J. and Carney D. N. (1996) Radiolabelled somatostatin analogue scintigraphy in oncology. *Anticancer Drugs* **7**(Suppl 1), 33-44.
- [19] Chianelli M., Mather S. J., Martin-Comin J. and Signore A. (1997) Radiopharmaceuticals for the study of inflammatory processes: a review. *Nucl. Med. Commun.* **18**, 437-455.
- [20] Kvoils L. K., Brown M. L., O'Connor M. K., Hung J. C., Hayostek R. J., Reubi J. C. and Lamberts S. W. (1993) Evaluation of a radiolabeled somatostatin analog (I-123 octreotide) in the detection and localization of carcinoid and islet cell tumors. *Radiology* **187**, 129-133.
- [21] Guhlke S., Wester H. J., Bruns C. and Stöcklin G. (1994) (2-[^{18}F]fluoropropionyl-(D)phe1)-octreotide, a potential radiopharmaceutical for quantitative somatostatin receptor imaging with PET: synthesis, radiolabeling, in vitro validation and biodistribution in mice. *Nucl. Med. Biol.* **21**, 819-825.
- [22] Bohdiewicz P. J., Scott G. C., Juni J. E., Fink-Bennett D., Wilner F., Nagle C. and Dworkin H. J. (1995) Indium-111 OncoScint CR/OV and F-18 FDG in colorectal and ovarian carcinoma recurrences. Early observations. *Clin. Nucl. Med.* **20**, 230-236.
- [23] Wester H. J., Brockmann J., Rösch F., Wutz W., Herzog H., Smith-Jones P., Stolz B., Bruns C. and Stöcklin G. (1997) PET-pharmacokinetics of ^{18}F -octreotide: a comparison with ^{67}Ga -DFO- and ^{86}Y -DTPA-octreotide. *Nucl. Med. Biol.* **24**, 275-286.
- [24] Santimaria M., Blok D., Feitsma R. I., Mazzi U. and Pauwels E. K. (1999) Experiments on a new phosphine-peptide chelator for labelling of peptides with Tc-99m. *Nucl. Med. Biol.* **26**, 251-258.
- [25] Decristoforo C. and Mather S. J. (1999) Preparation, $^{99\text{m}}\text{Tc}$ -labeling, and in vitro characterization of HYNIC and N3S modified RC-160 and [Tyr3]octreotide. *Bioconjug. Chem.* **10**, 431-438.
- [26] Gibson R. E., Fioravanti C., Francis B. and Burns H. D. (1999) Radioiodinated endothelin-1: a radiotracer for imaging endothelin receptor distribution and occupancy. *Nucl. Med. Biol.* **26**, 193-199.
- [27] Scheidhauer K., Scharl A. and Schicha H. (1998) Estrogen receptor scintigraphy. *Q. J. Nucl. Med.* **42**, 26-32.
- [28] Jonson S. D. and Welch M. J. (1998) PET imaging of breast cancer with fluorine-18 radiolabeled estrogens and progestins. *Q. J. Nucl. Med.* **42**, 8-17.
- [29] Li P. K., Chu G. H., Guo J. P., Peters A. and Selcer K. W. (1998) Development of potent non-estrogenic estrone sulfatase inhibitors. *Steroids* **63**, 425-432.
- [30] Reed M. J., Purohit A., Howarth N. M. and Potter B. V. L. (1994) Steroid sulphatase inhibitors: a new endocrine therapy. *Drugs Future* **19**, 673-680.
- [31] Kato S., Kitamoto T., Masuhiro Y. and Yanagisawa J. (1998) Molecular mechanism of a cross-talk between estrogen and growth-factor signaling pathways. *Oncology* **55**, 5-10.
- [32] Prall O. W., Rogan E. M. and Sutherland R. L. (1998) Estrogen regulation of cell cycle progression in breast cancer cells. *J. Steroid Biochem. Mol. Biol.* **65**, 169-174.
- [33] Kasch H., Schuhmann W., Römer J. and Steinbach J. (1998) Steroidsulfamate, Verfahren zu ihrer Herstellung und Anwendung derselben. Patentschrift vom 1.10. 1998 (Offenlegungstag) DE 19712488A1.
- [34] Moulder J. E. and Rockwell S. (1984) Hypoxic fractions of solid tumors: experimental techniques, methods of analysis, and a survey of existing data. *Int. J. Radiat. Oncol. Biol. Phys.* **10**, 695-712.
- [35] Hustinx R., Eck S. L. and Alavi A. (1999) Potential applications of PET imaging in developing novel cancer therapies. *J. Nucl. Med.* **40**, 995-1002.
- [36] Adams G. E. (1981) Hypoxia-mediated drugs for radiation and chemotherapy. *Cancer* **48**, 696-707.
- [37] Aboagye E. O., Kelson A. B., Tracy M. and Workman P. (1998) Preclinical development and current status of the fluorinated 2-nitroimidazole hypoxia probe N-(2-hydroxy-3,3,3-trifluoropropyl)-2-(2-nitro-1-imidazolyl) acetamide (SR 4554, CRC 94/17): a non-invasive diagnostic probe for the measurement of tumor hypoxia by magnetic resonance spectroscopy and imaging, and by positron emission tomography. *Anticancer Drug. Des.* **13**, 703-730.
- [38] Koh W. J., Rasey J. S., Evans M. L., Grierson J. R., Lewellen T. K., Graham M. M., Krohn K. A. and Griffin T. W. (1992) Imaging of hypoxia in human tumors with [F-18]fluoromisonidazole. *Int. J. Radiat. Oncol. Biol. Phys.* **22**, 199-212.

- [39] Yang D. J., Wallace S., Cherif A., Li C., Gretzer M. B., Kim E. E. and Podoloff D. A. (1995) Development of F-18-labeled fluoroerythronitroimidazole as a PET agent for imaging tumor hypoxia. *Radiology* **194**, 795-800.
- [40] Rasey J. S., Koh W. J., Evans M. L., Peterson L. M., Lewellen T. K., Graham M. M. and Krohn K. A. (1996) Quantifying regional hypoxia in human tumors with positron emission tomography of [¹⁸F]fluoromisonidazole: a pretherapy study of 37 patients. *Int. J. Radiat. Oncol. Biol. Phys.* **36**, 417-428.
- [41] Piwnica-Worms D., Rao V. V., Kronauge J. F. and Croop J. M. (1995) Characterisation of multi-drug resistance P-glycoprotein transport function with an organotechnetium cation. *Biochemistry* **34**, 12210-12220.
- [42] Hendrikse N. H., Franssen E. J. F., van der Graf W. T. A., Meijer C., Piers D. A., Vaalburg W. and de Vries E. G. (1998) ^{99m}Tc-sestamibi is a substrate for P-glycoprotein and the multidrug resistance-associated protein. *Brit. J. Cancer* **77**, 353-358.
- [43] Pauwels E. K. J., McCready V. R., Stoot J. H. M. B. and van Deurzen D. F. P. (1998) The mechanism of accumulation of tumour-localizing radiopharmaceuticals. *Eur. J. Nucl. Med.* **25**, 277-305.
- [44] Del Vecchio S., Ciarmiello A. and Salvatore M. (1999) Clinical imaging of multidrug resistance in cancer. *Q. J. Nucl. Med.* **43**, 125-131.
- [45] Hendrikse N. H., de Vries E. G., Eriks-Fluks L., van der Graaf W. T., Hospers G. A., Willemsen A. T., Vaalburg W. and Franssen E. J. (1999) A new in vivo method to study P-glycoprotein transport in tumors and the blood-brain barrier. *Cancer Res.* **59**, 2411-2416.
- [46] Bergmann R., Brust P., Pietzsch H.-J. and Johannsen B. (1998) Evaluation of the in vitro and in vivo properties of a potential Tc-labelled inhibitor of the MDR gene product P-glycoprotein (Abstract). *Eur. J. Nucl. Med.* **25**, 865.
- [47] Alavi J. B. and Eck S. L. (1998) Gene therapy for malignant gliomas. *Hematol. Oncol. Clin. North Am.* **12**, 617-629.
- [48] Boxhorn H. K. and Eck S. L. (1998) Gene therapy for breast cancer. *Hematol. Oncol. Clin. North Am.* **12**, 665-675.
- [49] Zwacka R. M. and Dunlop M. G. (1998) Gene therapy for colon cancer. *Hematol. Oncol. Clin. North Am.* **12**, 595-615.
- [50] Morin K. W., Knaus E. E. and Wiebe L. I. (1997) Non-invasive scintigraphic monitoring of gene expression in a HSV-1 thymidine kinase gene therapy model. *Nucl. Med. Commun.* **18**, 599-605.
- [51] Blasberg R. G. and Tjuvajev J. G. (1999) Herpes simplex virus thymidine kinase as a marker/reporter gene for PET imaging of gene therapy. *Q. J. Nucl. Med.* **43**, 163-169.
- [52] Alauddin M. M., Conti P. S., Mazza S. M., Hamzeh F. M. and Lever J. R. (1996) 9-[(3-[¹⁸F]-fluoro-1-hydroxy-2-propoxy)methyl]guanine ([¹⁸F]-FHPG): a potential imaging agent of viral infection and gene therapy using PET. *Nucl. Med. Biol.* **23**, 787-792.
- [53] Shields A. F., Grierson J. R., Kozawa S. M. and Zheng M. (1996) Development of labeled thymidine analogs for imaging tumor proliferation. *Nucl. Med. Biol.* **23**, 17-22.
- [54] Morin K. W., Atrazheva E. D., Knaus E. E. and Wiebe L. I. (1997) Synthesis and cellular uptake of 2'-substituted analogues of (E)-5-(2-[¹²⁵I]iodovinyl)-2'-deoxyuridine in tumor cells transduced with the herpes simplex type-1 thymidine kinase gene. Evaluation as probes for monitoring gene therapy. *J. Med. Chem.* **40**, 2184-2190.
- [55] Alauddin M. M. and Conti P. S. (1998) Synthesis and preliminary evaluation of 9-[(4-[¹⁸F]-fluoro-3-hydroxymethylbutyl]guanine ([¹⁸F]-FHBG): a new potential imaging agent for viral infection and gene therapy using PET. *Nucl. Med. Biol.* **25**, 175-180.
- [56] Gambhir S. S., Barrio J. R., Wu L., Iyer M., Namavari M., Satyamurthy N., Bauer E., Parrish C., MacLaren D. C., Borghesi A. R., Green L. A., Sharfstein S., Berk A. J., Cherry S. R., Phelps M. E. and Herschman H. R. (1998) Imaging of adenoviral-directed herpes simplex virus type 1 thymidine kinase reporter gene expression in mice with radiolabeled ganciclovir. *J. Nucl. Med.* **39**, 2003-2011.
- [57] Germann C., Shields A. F., Grierson J. R., Morr I. and Haberkorn U. (1998) 5-Fluoro-1-(2'-deoxy-2'-fluoro-beta-D-ribofuranosyl) uracil trapping in Morris hepatoma cells expressing the herpes simplex virus thymidine kinase gene. *J. Nucl. Med.* **39**, 1418-1423.
- [58] Alauddin M. M., Conti P. S., Mazza S. M., Hamzeh F. M. and Lever J. R. (1999) Evaluation of 9-[(3-[¹⁸F]-fluoro-1-hydroxy-2-propoxy)methyl]guanine ([¹⁸F]-FHPG) in vitro and in vivo as a probe for PET imaging of gene incorporation and expression in tumors. *Nucl. Med. Biol.* **26**, 371-376.

- [59] Gambhir S. S., Barrio J. R., Phelps M. E., Iyer M., Namavari M., Satyamurthy N., Wu L., Green L. A., Bauer E., MacLaren D. C., Nguyen K., Berk A. J., Cherry S. R. and Herschman H. R. (1999) Imaging adenoviral-directed reporter gene expression in living animals with positron emission tomography. *Proc. Natl. Acad. Sci. U S A.* **96**, 2333-2338.
- [60] Tjuvajev J. G., Avril N., Oku T., Sasajima T., Miyagawa T., Joshi R., Safer M., Beattie B., DiResta G., Daghighian F., Augensen F., Koutcher J., Zweit J., Humm J., Larson S. M., Finn R. and Blasberg R. (1998) Imaging herpes virus thymidine kinase gene transfer and expression by positron emission tomography. *Cancer Res.* **58**, 4333-4341.
- [61] Enghardt W. (1996) Positronen-Emissions-Tomographie bei der Schwerionentherapie. Ein Verfahren zur in-situ Kontrolle der Tumorbehandlung mit Strahlen schwerer Ionen. *Phys. Blätter* **52**, 874-875.
- [62] Pawelke J., Byars L., Enghardt W., Fromm W. D., Geissel H., Hasch B. G., Lauckner K., Manfraß P., Schardt D. and Sobiella M. (1996) The investigation of different cameras for in-beam PET imaging. *Phys. Med. Biol.* **41**, 279-296.
- [63] Pawelke J., Enghardt W., Haberer T., Hasch B. G., Hinz R., Krämer M., Lauckner K. and Sobiella M. (1997) In-Beam PET imaging for the control of heavy-ion tumour therapy. *IEEE Trans. Nucl. Sci.* **44**, 1492-1498.
- [64] Hinz R., Debus J., Enghardt W., Haberer T., Hasch B.G., Jäkel O., Lauckner K., Krämer M., Pawelke J. and Sobiella M (1998) Simultaneous control of the radiation therapy with heavy ions by positron emission tomography. *Proceedings of the 1998 IEEE Medical Imaging Conference*, Vol. III, pp. 2060-2063.
- [65] Enghardt W., Debus J., Haberer T., Hasch B.G., Hinz R., Jäkel O., Krämer M., Lauckner K. and Pawelke J. (1999) The application of PET to quality assurance of heavy-ion tumor therapy. *Strahlenther. Onkol.* **175** (Suppl. 2), 33-36.
- [66] Kraft G (1998) Radiotherapy with heavy ions: radiobiology, clinical indications and experience at GSI, Darmstadt. *Tumori* **84**, 200-204.

II. RESEARCH REPORTS

TUMOUR AGENTS AND TUMOUR DIAGNOSIS

1. Preparation of 3-O-Methyl-6-[¹⁸F]Fluoro-L-DOPA

F. Füchtner, J. Steinbach, R. Lücke, C. Smuda, B. Johannsen

Introduction

Since the middle of the 1990s we have been dealing with studies related to the dopaminergic system. 6-[¹⁸F]Fluoro-L-DOPA ([¹⁸F]FDOPA) was used as a radiotracer in our PET studies. In the analysis of the PET data 3-O-methyl-[¹⁸F]fluoro-L-DOPA ([¹⁸F]OMFD) has to be treated as one of the main metabolites [1]. For simplification of the compartment model we synthesized and studied [¹⁸F]OMFD. The substance is known to be rather stable in vivo [1].

By its chemical structure [¹⁸F]OMFD belongs to the group of amino acids and should have the potential of tumour affinity. Amino acids labelled with positron-emitting radionuclides play an important role as radiotracers in tumour imaging [2, 3, 4]. Some useful ¹⁸F-labelled amino acids for tumour imaging are known [4, 5, 6, 7]. Due to their potential for imaging tumour tissue, tumour growth and tumour staging, there exists a demand for a reliable and high-activity-level supply of ¹⁸F-labelled amino acids. The two procedures for [¹⁸F]OMFD synthesis described in the literature [8, 9] have the drawbacks of relatively low yields and complicated as well as time-consuming manufacturing processes. Here we describe an improved synthesis of [¹⁸F]OMFD which provides the substance in a high yield after a relatively short preparation time.

Experimental

An apparatus for routine production based on an electrophilic reaction was set up. The schematic layout of the [¹⁸F]OMFD preparation unit is shown in Fig. 1.

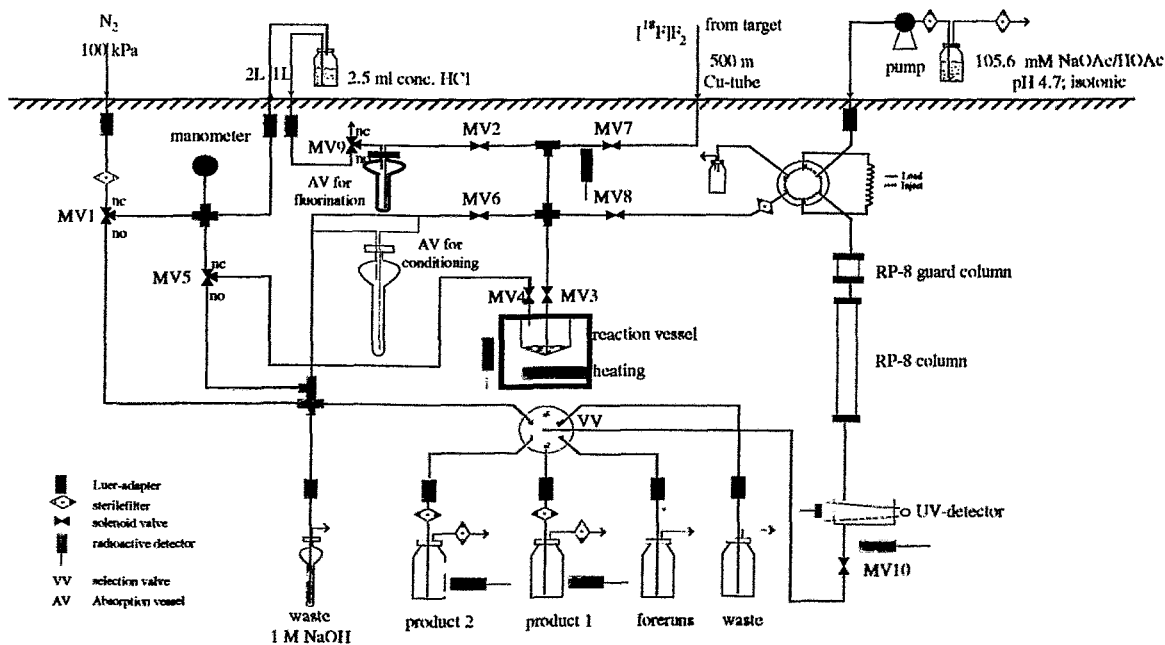
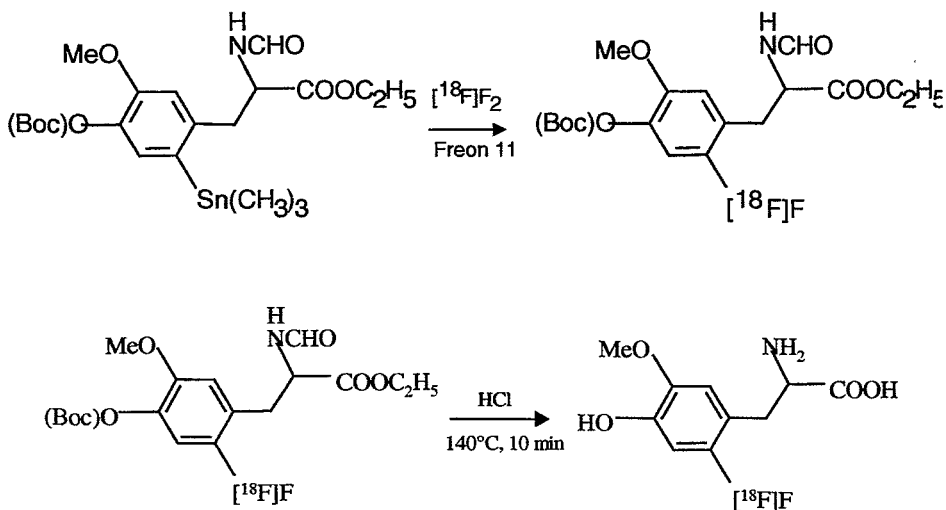


Fig. 1. Schematic presentation of the module for production of [¹⁸F]OMFD

Our synthesis starts with a new precursor, the N-formyl-3-O-methyl-4-O-boc-6-trimethylstannyl-L-DOPA-ethyl ester synthesized by BOZ Chem, Canada, according to our specifications. This

compound is derived from the [^{18}F]FDOPA precursor [10]. In contrast to the [^{18}F]FDOPA precursor, the methoxy group is already contained in this compound and is kept stable during the whole procedure. [^{18}F]F $_2$ is produced by the $^{20}\text{Ne}(d,\alpha)^{18}\text{F}$ reaction, using the 9 MeV deuterons from the Rossendorf cyclotron IBA 18/9 with Ne + F $_2$ (100 μmol) as the target gas. The target gas is discharged under its own pressure (1.2 MPa to start with) through the transporting copper tube (about 500 m). The [^{18}F]F $_2$ is transported to the synthesis unit using N $_2$ as a carrier gas with a pressure of 0.5 MPa. To increase the efficiency of absorption, the [^{18}F]F $_2$ is absorbed in a special Vigreux absorption column containing a precursor solution of 45 mg N-formyl-3-O-methyl-4-O-boc-6-trimethylstannyl-L-DOPA-ethyl ester in 15 ml trichlorofluoromethane (CFCl $_3$, Freon 11). This arrangement also makes it possible to measure the starting activity with a dose calibrator. Under these conditions the reaction between the precursor and the gaseous [^{18}F]F $_2$ takes about 10 minutes. The volume of the solvent is reduced to about 5 ml by evaporation during absorption.



After absorption of [^{18}F]F $_2$ 2.5 ml 12 M HCl are added and this mixture is transferred into the reaction vessel. The temperature is increased to 70 °C while the remaining solvent is evaporated by blowing in gaseous N $_2$. After evaporation the reaction vessel is closed and the temperature is increased to 140 °C for 10 minutes to reach the conditions for hydrolysis.

[^{18}F]OMFD is separated from the crude product by isocratic HPLC using isotonic acetate buffer as an eluent at pH 4.7 on an RP-8 column. The [^{18}F]OMFD-containing radioactive peak is eluted after about 19 minutes. After sterile filtration the product is ready for use as a radiopharmaceutical.

Conditions for preparative HPLC:

- column: LiChrosorb RP-8, 7 μm , 250 mm x 10 mm,
- guard column: LiChrospher RP-8, 5-20 μm , 30 mm x 9 mm,
- sample volume: 2.5 ml,
- injection loop: 10 ml,
- eluent: 105.6 mM of CH $_3$ COONa and CH $_3$ COOH, pH 4.7, isotonic, prepared with sterilized water (aqua ad iniectionabilia),
- flow rate: 3 ml/min,
- pressure: about 9 MPa,
- detection: UV, 1 mm path length, 280 nm, radioactivity.

According to the rules of good manufacturing practice (GMP), quality control of the final product is an essential part of quality assurance of radiopharmaceutical production. The quality of the product was characterized by HPLC, GC/MS and pharmaceutical data.

Results

The new precursor N-formyl-3-O-methyl-4-O-Boc-6-¹⁸F-fluoro-L-DOPA-ethyl ester facilitates stereoselective radiofluorination with [¹⁸F]F₂. As an advantage of this reaction only the desired isomer is generated, i.e. the 2- and 5-fluoroisomers do not occur.

The protective groups are completely cleaved by the partial hydrolysis while the methoxy group is solely affected to a small extent. The kinetics of hydrolysis is demonstrated in Fig. 2.

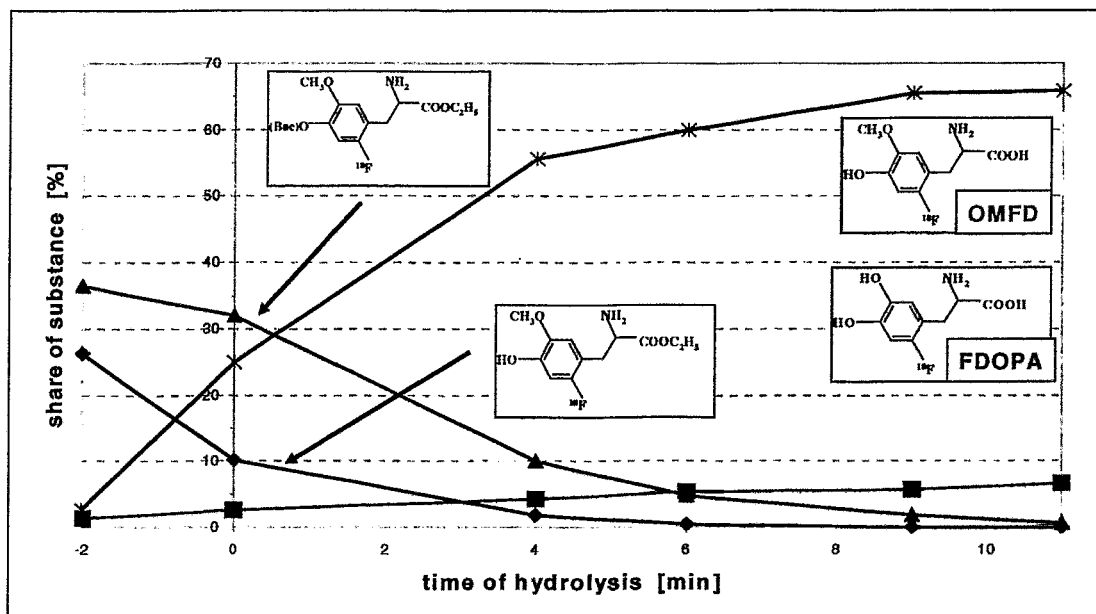


Fig. 2. Kinetics of the hydrolysis of N-formyl-3-O-methyl-4-O-Boc-6-¹⁸F-fluoro-L-DOPA-ethylester

The graph demonstrates that the maximum percentage of the desired product is achieved after 8 to 10 minutes. A longer reaction time causes cleavage of the methoxy group, which leads to an increased amount of [¹⁸F]FDOPA.

The total preparation time of [¹⁸F]OMFD after EOB, including radionuclide transport, takes about 50 minutes. The total [¹⁸F]OMFD yield is between 20 and 25 % (decay corrected, related to [¹⁸F]F₂) with a good reproducibility. The specific activity is 20 GBq/μmol. Depending on the starting activity, up to 1.5 GBq [¹⁸F]OMFD is available.

The product is characterized by the following quality parameters:

Parameter	Method	Limit	Average value
- Radiochemical purity:	HPLC	> 95 %	> 99 %
- Chemical purity:	HPLC	[OMFD] > 95 %	> 99 %
	GC/MS	[Freon 11] < 100 μg/ml	0.7-1.1 mg/ml
		[acetonitrile] < 100 μg/ml	< 3 μg/ml
		[acetone] < 100 μg/ml	< 25 μg/ml
- Pharmaceutical parameters:	pH	4 - 5	4.7
	Osmolality	280-320 mOsmol/kg	300 - 310 mOsmol/kg

Conclusion

As the improved synthesis procedure is simple and robust and the precursor is commercially available, it can be adapted to existing [^{18}F]FDOPA-modules. [^{18}F]OMFD can thus be easily obtained. The easy preparation of [^{18}F]OMFD and its biological behaviour make the compound seem promising for PET studies.

References

- [1] Wahl L., Chirakal R., Firna G., Garnett E.S. and Nahmias C. (1994) The distribution and kinetics of [^{18}F]6-fluoro-3-O-methyl-L-dopa. *J. Cereb. Blood Flow Metab.* **14**, 664-670.
- [2] Mazoyer B. M., Heis W. D. and Comar D. (1993) PET studies on amino acid metabolism and protein synthesis, Kluwer Academic Publisher.
- [3] Vaalburg W., Coenen H. H., Crouzel C., Elsinga P. H., Långström B., Lamaire C. and Meyer G.-J. (1992) Amino acids for the measurement of protein synthesis *in vivo* by PET. *Nucl. Med. Biol.* **19**, 227-237.
- [4] Wester H.-J., Herz M., Weber W., Heiss P., Senekowitsch-Schmidtke R., Schwaiger M. and Stöcklin G. (1999) Synthesis and radiopharmacology of O-(2-[^{18}F]fluoroethyl)-L-tyrosine. *J. Nucl. Med.* **40**, 205-212.
- [5] Inoue T., Tomiyoshi K. et al. (1998) Biodistribution studies on L-3-[fluorine-18]fluoro- α -methyl tyrosine: a potential tumor-detecting agent. *J. Nucl. Med.* **9**, 663-667.
- [6] Coenen H. H., Kling P. and Stöcklin G. (1989) Cerebral metabolism of 2-[^{18}F]fluorotyrosine: a new PET tracer of protein synthesis. *J. Nucl. Med.* **30**, 1367-1372.
- [7] Bodsch W., Coenen H. H., Stöcklin G., Takahashi K. and Hossmann K. A. (1988) Biochemical and autoradiographic study of cerebral protein synthesis with [^{18}F]- and [^{14}C]fluorophenylalanine. *J. Neurochem.* **50**, 979-983.
- [8] Adam M. J., Lu J. and Jivan S. (1994) Stereoselective synthesis of 3-O-methyl-6-[^{18}F]fluoro-dopa via fluorodestannylation. *J. Labelled Compd. Radiopharm.* **34**, 565-570.
- [9] Chirakal R., Firna G. and Garnett E. S. (1986) High yield synthesis of 6-[^{18}F]fluoro-L-dopa. *J. Nucl. Med.* **27**, 417-421.
- [10] Namavari M., Bishop A., Satyamurthy N., Bida G. and Barrio J. R. (1992) Regioselective radio-destannylation with [^{18}F]F $_2$ and [^{18}F]CH $_3$ COOF: a high yield synthesis of 6-[^{18}F]fluoro-L-dopa. *Appl. Radiat. Isot.* **43**, 989-996.

2. Metabolism of 6-[¹⁸F]Fluoro-3-O-Methyl-L-3,4-Dihydroxyphenylalanine in the Rat

G. Vorwieger, R. Bergmann, R. Syhre, F. Füchtner, J. Steinbach, P. Brust, B. Johannsen

Introduction

Tumour diagnostics by tomographical tools makes use of the usually higher metabolic activity of neoplastic tissue. Major metabolic processes include, first and foremost, protein biosynthesis and amino acid transport [1]. The xenobiotic L-amino acid OMFD (6-[¹⁸F]fluoro-3-O-methyl-L-3,4-dihydroxyphenylalanine) is known as an undesirable, virtually inert side product within FDOPA-PET (see chapter "Piglet pharmacokinetics of FDOPA" of this monograph). We synthesized the compound OMFD and investigated in the rat whether or not this metabolic stability can be absolutely relied upon. This is one aspect of assessment for the elucidation of conceivable tumour tracer properties of OMFD.

Methods

Male Wistar rats (8 weeks old, weighing 200 g on average) were anaesthetized and i.v. injected 125 MBq/kg OMFD equivalent to 12 µmol/kg. After tracer application the rats were left awake. Three animals at a time were anaesthetised 30, 60 and 120 min after tracer application. Blood and urine were drawn by heart and bladder aspiration. Then the animals were decapitated and tissue samples of brain, gut and pancreas were prepared.

Preanalytical processing of samples of the body fluids and tissues as well as HPLC separation with radiochromatography detection were performed as described in the chapter "Piglet metabolism of OMFD" in this monograph.

The percentages of total ¹⁸F for the metabolite substances were determined by integration of the radiochromatograms. The analytical recovery of the metabolite substances was arbitrarily assumed to be identical with the OMFD recovery.

The body distribution of the total ¹⁸F activity was determined by two approaches:

- withdrawal of an aliquot from the homogenate (before centrifugation) and determination of the 512 keV gamma activity in the well counter;
- normalizing for each sample the total peak areas of the radiochromatography detector with the detector counting efficacy.

The possible incorporation of OMFD-born activity into macromolecular structures was assessed on the basis of two pancreas samples. The pellets of those two samples were washed three times with a vast excess of precipitation reagent and thereafter measured in the well counter like homogenates. The total activities calculated in the two ways described above were moreover compared: the supernatants employed for HPLC separation were to contain only monomers and oligomers.

Results and Discussion

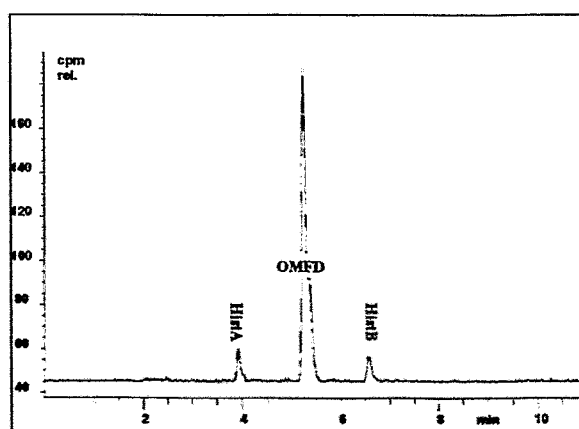


Fig. 1a. Representative radiochromatogram of tissue and plasma samples

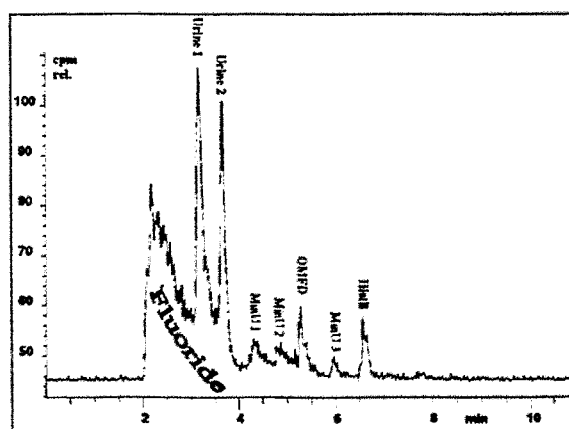


Fig. 1b. Representative radiochromatogram of urine samples

For the first time this work presents quantitative results of the OMFD tracer metabolism in living animals. With the exception of urine, all the investigated samples revealed mainly two products (HistA

and HistB; see traces in Figs. 1a and 1b). HistA and HistB are probably identical with the appropriate OMFD products in piglet plasma. The percentage relations between OMFD, HistA and HistB represent a tissue-specific metabolism pattern (Figs. 2a - 2d). Two additional trace substances which never shared more than 2 % of the total ^{18}F occurred predominantly in the gut. Neither they nor fluoride, which as an impurity or product instability accounted for about 5 mole percent of the OMFD preparation, were taken into account in Fig. 2.

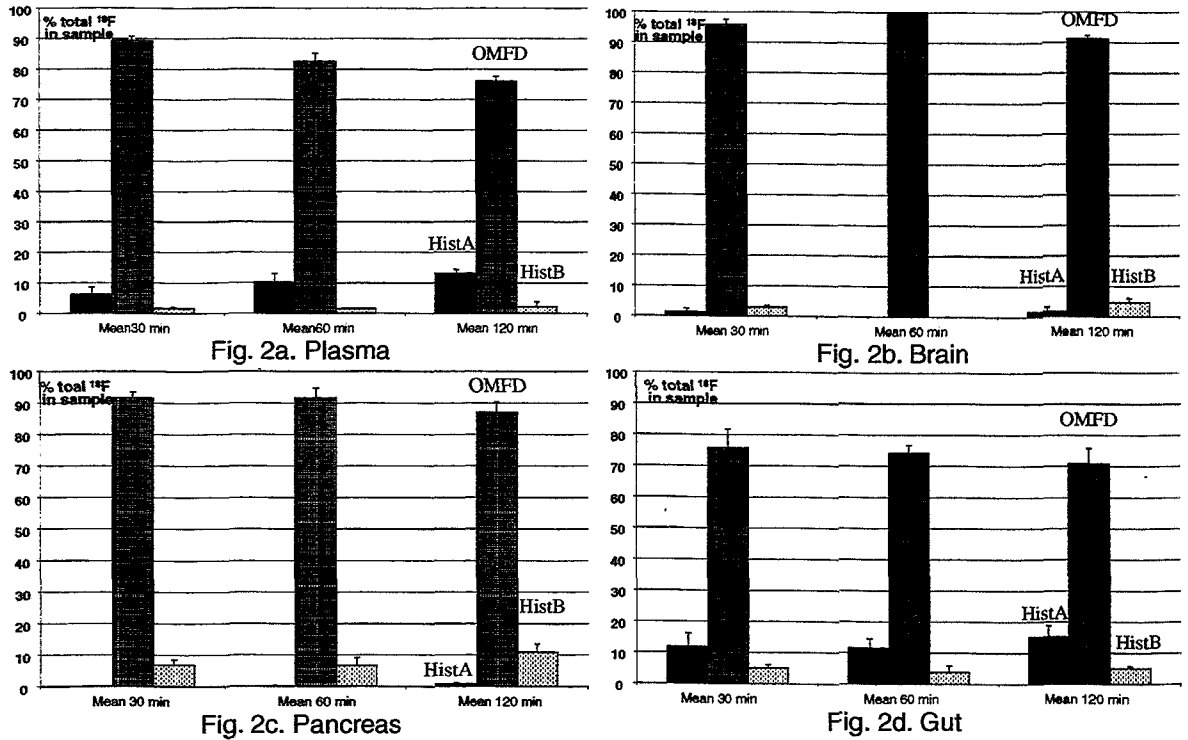


Fig. 2. Distribution of ^{18}F activity amongst OMFD and its main metabolites; mean ($n = 3$) + SD.

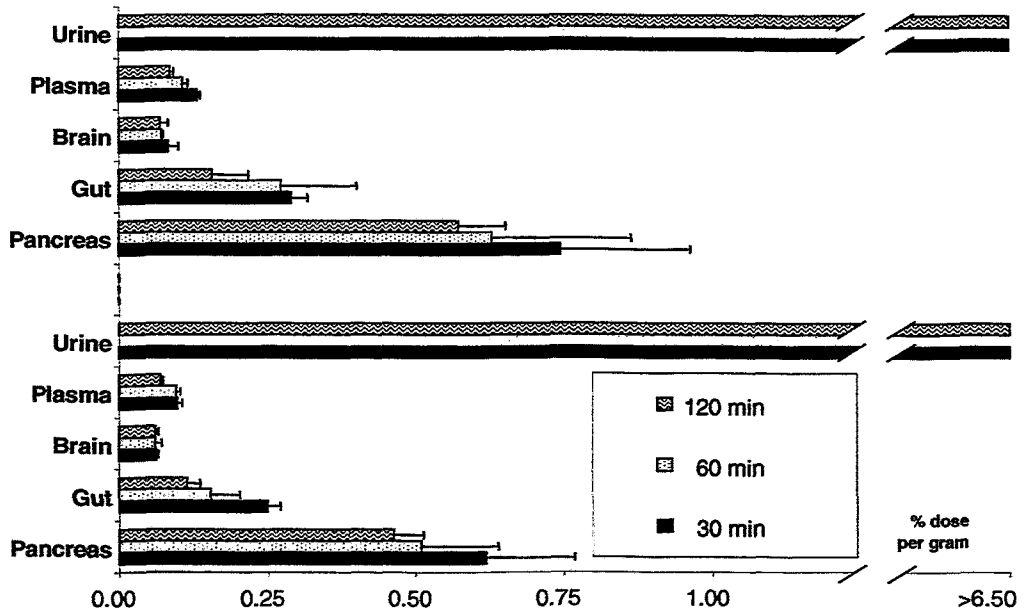


Fig. 3a. Time course of total ^{18}F activity (mean + SD; $n = 3$), zoomed for low activity details, determined from homogenate (upper columns) and total HPLC area (lower columns)

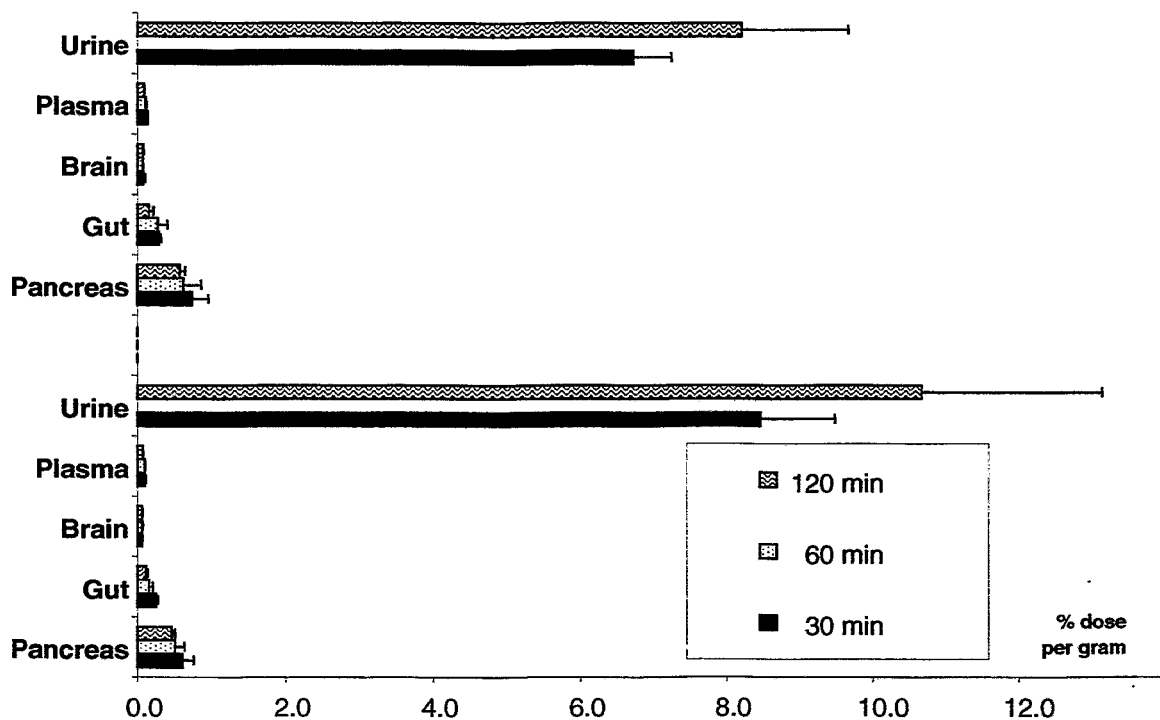


Fig. 3b. Time course of total ^{18}F activity (mean + SD; n = 3), determined from homogenate (upper columns) and total HPLC area (lower columns)

HistA and HistB are probably first-degree products of OMFD belonging to the category of Phase II of biotransformation [CHIRAKAL, Chemist's view of imaging centers]. For identification of these two substances we propose in the first place: HistA = OMFD glucuronide, HistB = 5-S-cysteinyl-OMFD. Phase I reactions of OMFD – decarboxylation, transamination, β -hydroxylation are conceivable – did not occur due to a lack of oblique terminal products or intermediates such as homovanillic acid, vanillylmandelic acid and 3-methoxytyramine.

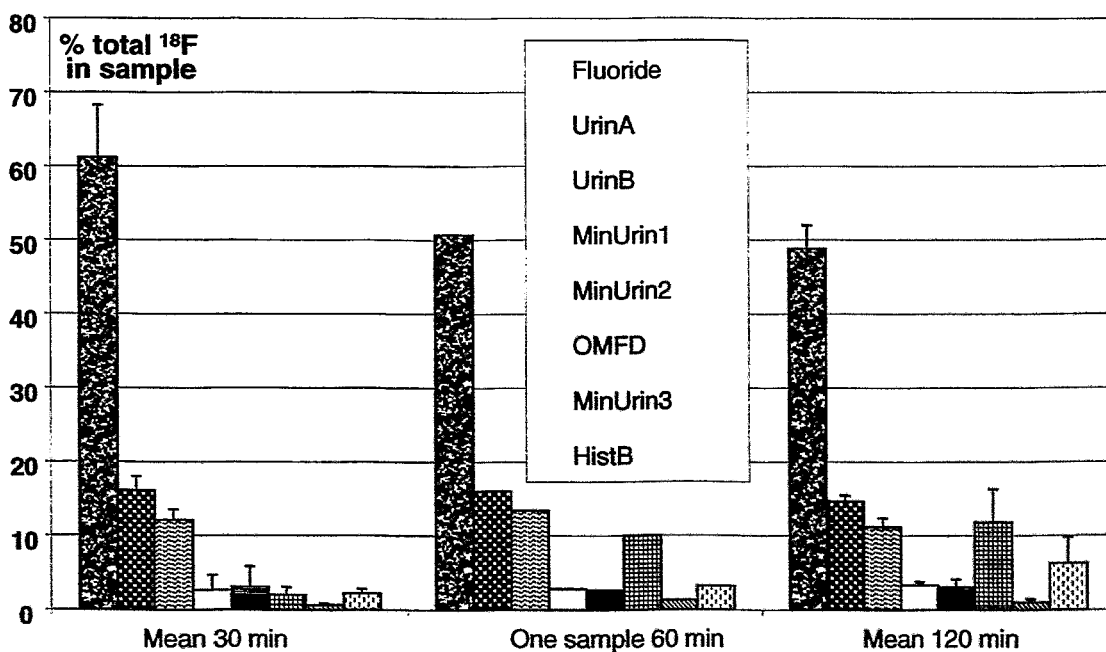


Fig. 4. Distribution of ^{18}F activity amongst all detected substances in urine; mean (n = 3) + SD (30 and 120 min p.i.); 60 min just one sample available.

We were able to confirm the long biological half life of OMD [2] for OMFD (see slow decrease of total activity in Fig. 3). The total activity plot (Fig. 3a) shows that among all the investigated tissues pancreas has the highest mass based activity content though still no enrichment compared with the whole body average (1 g body weight = 0,5 %). OMFD itself is responsible for the high pancreas values (see Fig. 2c). This finding supports the suitability of OMFD as a tumour tracer.

Kidney excretion obviously is the main excretion path. A typical urine chromatogram (Fig. 1b) indicates that the activity is basically made up of 2 hydrophilic species which do not occur in tissues (UrinA and UrinB, presumably different OMFD sulphates). Interestingly, the fractions of OMFD and HistB increase in time (Fig. 4). HistA is not found in urine. Three quantitatively insignificant substances (MinUrin1-3) each never exceed 5 per cent each of the total urine activity. The impurity fluoride obviously undergoes a rapid enrichment in urine. If we want to consider only the OMFD metabolism as such, the urine columns in Fig.3 are overestimated by about 100 %.

The following two arguments show that a possible involvement of OMFD in the protein biosynthesis (t-RNA bonding, peptide bonding) cannot include more than 4.5 % of the administered tracer.

- (1) 4.5 or 3.3 % of the initial sample activity could not be desorbed from the protein pellet even by washing it three times with vast surplus volumes of the precipitation solution.
- (2) The congruent behaviour of the total activities determined by the two methods in the investigated tissues is shown clearly by the data presented in Fig.3. The values in the supernatants applied to the HPLC, which are regularly about 20 % lower (the radioactivity recovery of the HPLC system itself is well documented at 100 %) have to be considered a systemic error of the conversion factor [well counter / radiochromatography detector], i.e. they are due to imprecise calculation of the effective dilution volume during the preanalytical procedure.

The plasma kinetics of the piglet experiments (see chapter "Piglet pharmacokinetics" in this monograph; 2 - 50 min p.i.) and of this rat study (30, 60 and 120 min p.i.) can be combined without hesitation, they fit together. This indicates that differences between animal species are negligible.

References

- [1] Wester H. J., Herz M., Weber W., Heiss P., Senekowitsch-Schmidtke R., Schwaiger M. and Stöcklin G. (1999) Synthesis and radiopharmacology of O-(2-[¹⁸F]fluoroethyl)-L-tyrosine for tumor imaging. *J. Nucl. Med.* **40**, 205-212.
- [2] Rose S., Jenner P. and Marsden C. D. (1988) The effect of carbidopa on plasma and muscle levels of L-Dopa, dopamine, and their metabolites following L-Dopa administration to rats. *Movement Disorders* **3**, 117-125.

3. Metabolism of 6-[¹⁸F]Fluoro-3-O-Methyl-L-3,4-Dihydroxyphenylalanine in Newborn Piglets

G. Vorwieger, P. Brust, R. Bergmann, R. Bauer¹, B. Walter¹, F. Füchtner, J. Steinbach

¹Institut für Pathophysiologie, Friedrich-Schiller-Universität, Jena

Introduction

Positron emission tomographic (PET) studies of the dopamine metabolism with the tracer 6-[¹⁸F]fluoro-L-3,4-dihydroxyphenylalanine (FDOPA) are impaired by in vivo generation of the metabolite 6-[¹⁸F]fluoro-3-O-methyl-L-3,4-dihydroxyphenylalanine (OMFD). This labelled molecule, formed mainly peripherally by the action of catechol-O-methyltransferase on FDOPA, crosses the blood-brain barrier and contributes substantially to brain radioactivity. Especially with Carbidopa premedication, this drawback is the more pronounced the longer the scanning procedure lasts. Corrections for this radioactivity in the brain have been proposed. They are based upon the assumption that regional variations of OMFD pharmacokinetics within the brain are negligible. Studies in humans with OMFD have shown that this assumption is valid [1]. In that study the distribution volume of OMFD was close to unity, and a single, reversible compartment was adequate for modelling the measured time course of OMFD.

Analysis of human plasma samples for labelled metabolites [1] showed that more than 95 % of the radioactivity was at all times associated with OMFD. In nonhuman primates a crude fractionation of the plasma metabolites revealed that only the negatively charged metabolites which should not cross the blood-brain barrier (which are, for example, extractable with an anion exchange column) were found in the plasma in significant quantities (<13 %) [2]. None of the studies mentioned provided chromatograms of the separations. There are no data available of the metabolism of OMFD in the brain or in peripheral organs.

Until now OMFD has thus been regarded as virtually not undergoing any further metabolism. It is therefore expected to be a good tracer for amino-acid transport processes in living subjects. We recently used OMFD to quantify the amino-acid transport at the BBB in piglets with PET [3]. The blood-brain transfer constant of OMFD (K_1) was estimated from the brain and plasma time activity curves. When there was a significant metabolism of OMFD, these data had to be corrected for the presence of labelled metabolites.

We intended to examine mutual metabolism of OMFD in the plasma and brain of newborn piglets. Verification of the expected metabolic stability would promote (a) investigation of the LNAA transporter, (b) judgement of its tissue distribution properties, and (c) differential identification of further "second-order"-FDOPA metabolites, all of this mainly with respect to the validation of the FDOPA PET model for the in vivo visualisation of catecholaminergic functionalities.

Materials and Methods

Animal experiments were performed as recently published [4]. After euthanasia by injection of saturated KCl solution, the brain of the animals was removed within 30 s, stored on ice and immediately dissected. Each brain tissue sample was submerged in 2.5 ml of the solvent CCl₄ which was pre-cooled to -20 °C.

Metabolite analysis was carried out by gradient HPLC in the following configuration: Hewlett-Packard 1050 quaternary gradient pump, autosampler (0.5 ml sample loop; injection volume 360 µl), UV detector ($\lambda = 280$ nm), all parts of the Hewlett-Packard 1050 system, and a flow scintillation analyser (150 TR, Canberra Packard) with a PET flow cell (100 µl volume; energy window: 15 - 2000 keV). The analytes were separated on a C 18 reverse-phase column (250 x 4 mm, LiChrosorb, 7 µm) fitted with a guard column (4 x 4 mm, LiChrospher 100 RP-18, 5 µm), at a temperature of 30 °C. A binary gradient was chosen at a flow rate of 1.5 ml/min (start: 0% B, 4 min : 25 % B, 10 min 80 % B, 10.1 min 100 % B, 11.2 min: 100 % B, 12.8 min 0 % B, 16 min : 0 % B; total method time: 16 min). Mobile phase A consisted of 70 mM KH₂PO₄, 1.5 mM sodium octyl sulphate, 0.1 mM EDTA, adjusted to pH 3.4 with H₃PO₄. Mobile phase B was prepared by adding two parts (vol/vol) MeCN to one part "A". After every 30 samples the system was re-equilibrated with water and MeCN. At the same time the guard columns were renewed and the flow direction reversed. The sequence of sample measurement was randomized.

Results and Discussion

The OMFD PET scans we accompanied by HPLC separations of brain extracts and plasma from three animals. No other substances were detected in the brain tissue extracts. This means that with our limit of detection the sum of possible metabolites is less than 2 % of the total activity.

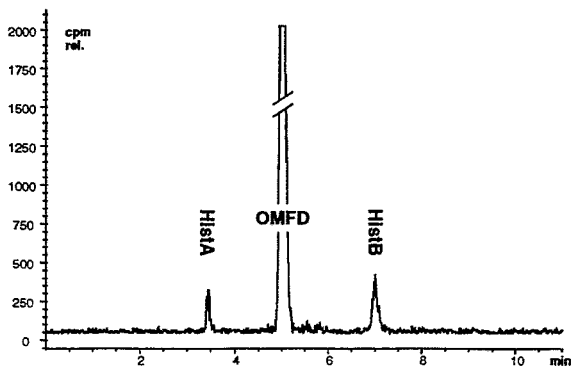


Fig. 1. Representative radiochromatogram of a plasma sample

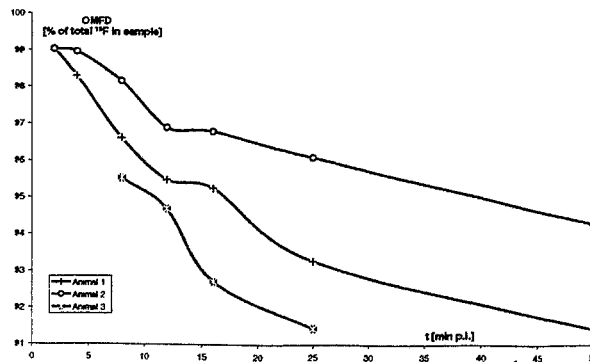


Fig. 2. Kinetics of the tracer OMFD ([^{18}F]6-fluoro-3-O-methyl-L-3,4-dihydroxyphenylalanine) in piglet plasma.

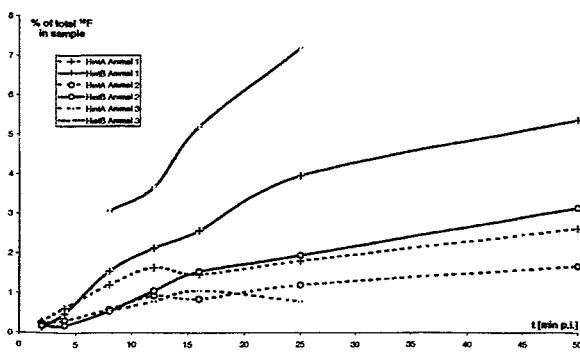


Fig. 3. Kinetics of the two metabolites HistA and HistB in piglet plasma

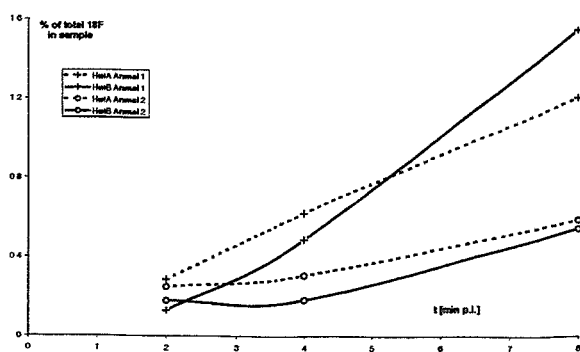


Fig. 4. Early p.i. kinetics of the two metabolites HistA and HistB.

As opposed to those groups who previously checked the plasma for OMFD metabolism, we found significant amounts of metabolites. Only two substances occurred in the traces. We named them HistA and HistB (see trace in Fig.1). All available data are presented in Figs. 2 - 4. The values are normalized to the total activity at each time point and decay corrected. The ordinate parameter [% of total ^{18}F] is thus plotted linearly against time p.i.. The resulting graphs correspond in good approximation to the monoexponential clearance (in the case of OMFD) and input function (HistA and HistB) even without curve fitting. A comparison of the initial kinetics of both metabolites suggests that HistA is formed at a higher rate (Fig. 4). In all the following samples however the HistB concentration exceeds that of HistA.

The identity of the two metabolites is discussed in a section "OMFD metabolism in the rat" of this monograph. Among other compounds, the glucuronide of OMFD (HistA) and 5-Cysteinyl-OMFD (HistB) are to be taken into consideration.

Our results imply that in modelling investigations with OMFD the desired precision determines the sampling frequency of the blood plasma. We suppose that in most cases a single analysis after PET scanning should be sufficient. From this value the input function for the brain tissue can be extrapolated into linearly extended graphs of the OMFD clearance (Fig. 2). This suggestion does not apply to other tissues with significant metabolite fractions.

The activity in the brain ROIs of the PET images can be exclusively attributed to OMFD itself. No OMFD metabolite compartment is necessary for brain tissue.

References

- [1] Wahl L., Chirakal R., Firnau G., Garnett E. S. and Nahmias C. (1994) The distribution and kinetics of [^{18}F]6-fluoro-3-O-methyl-L-dopa in the human brain. *J Cereb. Blood Flow Metab.* **14**, 664-670.
- [2] Doudet D. J., McLellan C. A., Carson R., Adams H. R., Miyake H., Aigner T. G., Finn R. T. and Cohen R. M. (1991) Distribution and kinetics of 3-O-methyl-6-[^{18}F]fluoro-L-dopa in the rhesus monkey brain. *J. Cereb. Blood Flow Metab.* **11**, 726-734.
- [3] Kuwabara H., Brust P., Steinbach J. and Johannsen B. (1999) Blood-brain transport of large neutral amino acids (LNAAAs) studied with [^{18}F]3-O-methyl-fluoro-L-DOPA. *J. Nucl. Med.* **40**, 145P.
- [4] Brust P., Bauer R., Vorwieger G, Walter B, Bergmann R., FÜchtner F., Steinbach J., Zwiener U. and Johannsen B. (1999) Upregulation of the aromatic amino acid decarboxylase under neonatal asphyxia. *Neurobiol. Dis.* **6**, 131-139.

4. First Results of 3-O-Methyl-6-[¹⁸F]Fluoro-DOPA ([¹⁸F]3-OMFD) in Patients with Glioblastoma Multiforme

W. Burchert, B. Beuthien-Baumann¹, H. Alheit², J. Bredow¹, J. Steinbach, B. Johannsen, W.-G. Franke¹

TU Dresden, ¹Klinik und Poliklinik für Nuklearmedizin und ²Klinik und Poliklinik für Strahlentherapie und Radioonkologie

Introduction

Patients with brain tumours such as glioblastoma multiforme generally face a grim prognosis. Even after intensive therapy such as tumour resection and postoperative radiotherapy, the incidence of tumour recurrence is high. For some patients one further therapeutic option in case of tumour recurrence is stereotactic radiotherapy. For this treatment modality the confirmation of the suspected recurrence and the exact definition of the tumour borders is mandatory. In some cases this cannot be achieved with only CT or MRI, so that the application of additional imaging modalities is desirable. Some promising results in brain tumour diagnostics with positron emission tomography (PET) and radiolabelled amino acids have been published [2-4]. The upregulation of amino acid transporters occurs as part of the malignant transformation of the tumour cells [5]. Since in normal brain tissue the amino acid uptake is low, a good tumour to non-tumour contrast can be expected. Incorporation of the PET data into treatment planning by image fusion could therefore be helpful for definition of the target volume for stereotactic radiotherapy.

Since most of the radiolabelled amino acids applied for PET show limitations concerning synthesis (low yield of tracer) or the short half life of the radioisotope (¹¹C, $t_{1/2}$: 20 min), further research is being carried out for an optimized amino acid.

One new amino acid without the above-mentioned limitations is 3-O-methyl-6-[¹⁸F]fluoro-DOPA ([¹⁸F]3-OMFD), a naturally occurring metabolite of dopamine [1]. Some first *in vitro* studies revealed promising results in terms of the tracer uptake in the cells of a human tumour cell line. Furthermore, a high tumour uptake and low tracer retention in the body was found for nude mice bearing human squamous cell carcinomas (unpublished data, Biochemistry Dep.).

These encouraging results of the *in vitro* and *in vivo* experiments seemed to justify the application of this substance to humans. Furthermore, [¹⁸F]3-OMFD is well known as a nontoxic metabolite occurring in [¹⁸F]DOPA-PET studies. The first investigations were performed in patients with glioblastoma multiforme in which the conventional diagnostic procedures were inconclusive and a stereotactic radiotherapy was considered because of a tumour recurrence was very likely.

Materials and Methods

Patients: 4 PET scans with [¹⁸F]3-OMFD were performed in 3 patients (2 female, 1 male; age 57 - 60 years). All patients suffered from histologically confirmed glioblastoma multiforme. In their medical history all of them underwent neurosurgery and postoperative radiotherapy. Two of the patients underwent a second operation because of tumour recurrence, one patient already had a second course of radiotherapy with a stereotactic approach. One patient was re-evaluated 3 months after stereotactic radiotherapy because of suspected progress of the disease.

Imaging procedure: PET imaging of the brain was performed, using a dedicated full-ring scanner (ECAT EXACT HR⁺, Siemens /CTI, Knoxville, Tenn., U.S.A.). Dynamic acquisition over 90 min. was started after intravenous injection of 330 MBq [¹⁸F]3-OMFD. Following the dynamic sequence of the brain, a distribution study of the body from the orbits to the pelvis was performed.

The data were reconstructed by measured attenuation correction. They were visually and semiquantitatively evaluated, using regions of interest.

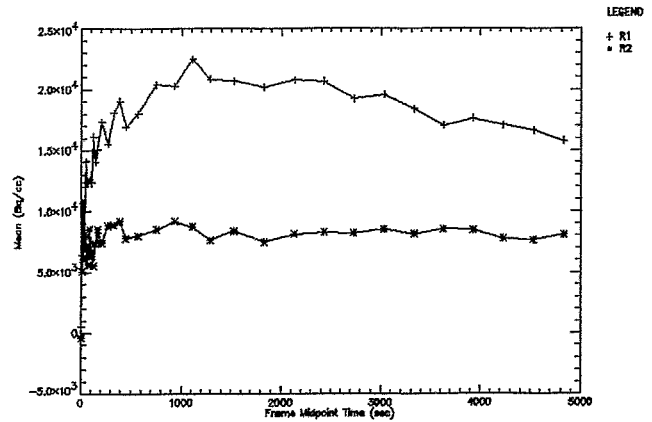
No adverse reactions were observed after tracer application.

Results and Discussion

In all three patients the recurrence of the brain tumour was visualized with a high degree of contrast by [¹⁸F]3-OMFD-PET (Fig. 1A). A comparison of the radiotracer uptake in the tumour and the contralateral normal brain tissue revealed a tumour to non tumour ratio of 2.2 ± 0.5 . The maximal tracer uptake was observed between 12 min and 25 min p.i.. The [¹⁸F]3-OMFD uptake is dependent on the amino acid transport (unpublished data, Biochemistry Dep.) and is not integrated into proteins. Since [¹⁸F]3-OMFD is not fixed within the cells, a loss of tracer over time can be observed. This decline of activity is more pronounced in tumour tissue than in normal brain tissue (Fig. 1B).



A



B

Fig. 1. Transaxial slice of a [^{18}F]3-OMFD-PET brain scan of a patient with recurrent glioblastoma multiforme. The tumour shows a high radiotracer uptake (R1) in the left temporal lobe. For quantitative analysis regions of interest are placed in the tumour region and in contra lateral reference brain tissue (A). Uptake kinetics of [^{18}F]3-OMFD in the tumour region (+) and reference brain tissue (*) (B).

In addition to the tracer uptake in the tumour tissue, all patients exhibited a low tracer accumulation in the basal ganglia. 3-O-methy-6-DOPA, as a metabolite of dopamine, seems to have some affinity to the basal ganglia. The physiology behind this phenomenon will have to be further investigated. In the whole body scan the tracer uptake in muscle and most of the internal organs was low. The tracer accumulation in the kidneys and urinary tract is due to physiological elimination (Fig. 2).

These first investigations with [^{18}F]3-OMFD showed encouraging results with respect to tumour visualization and localization in glioblastoma multiforme. The diagnostic accuracy and the application to various tumour entities will have to be further evaluated in controlled studies.

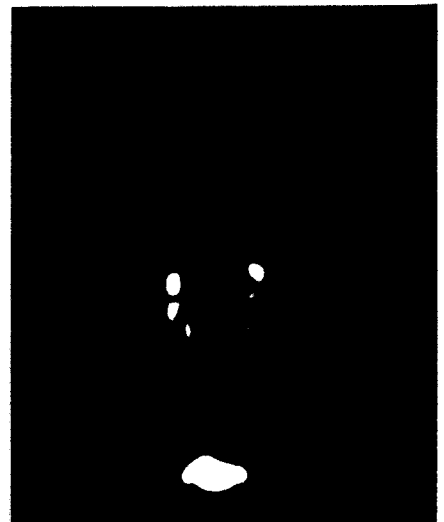


Fig. 2. Anterior-posterior projection of a [^{18}F]3-OMFD whole body scan

References

- [1] Firnau G., Sood S., Chirakal R., Nahmias C. and Garnett E. S. (1987) Cerebral metabolism of 6- ^{18}F fluoro-L-3,4-dihydroxyphenylalanine in the primate. *J. Neurochem.* **48**, 1077-1082.
- [2] Goldman S., Levivier M., Piroette B., Brucher J. M., Wikler D., Damhaut P., Dethy S., Brotchi J. and Hildebrand J. (1997) Regional methionine and glucose uptake in high-grade gliomas: a comparative study on PET-guided stereotactic biopsy [published erratum appears in *J. Nucl. Med.* 1997 Dec;38(12):2002]. *J. Nucl. Med.* **38**, 1459-1462.
- [3] Inoue T., Shibasaki T., Oriuchi N., Aoyagi K., Tomiyoshi K., Amano S., Mikuni M., Ida I., Aoki J. and Endo K. (1999) ^{18}F alpha-methyl tyrosine PET studies in patients with brain tumors. *J. Nucl. Med.* **40**, 399-405.
- [4] Wester H. J., Herz M., Weber W., Heiss P., Senekowitsch-Schmidtke R., Schwaiger M. and Stocklin G. (1999) Synthesis and radiopharmacology of O-(2- ^{18}F fluoroethyl)-L-tyrosine for tumor imaging. *J. Nucl. Med.* **40**, 205-212.
- [5] Wienhard K., Herholz K., Coenen H. H., Rudolf J., Kling P., Stocklin G. and Heiss W. D. (1991) Increased amino acid transport into brain tumors measured by PET of L- (2- ^{18}F)fluorotyrosine [see comments]. *J. Nucl. Med.* **32**, 1338-1346.

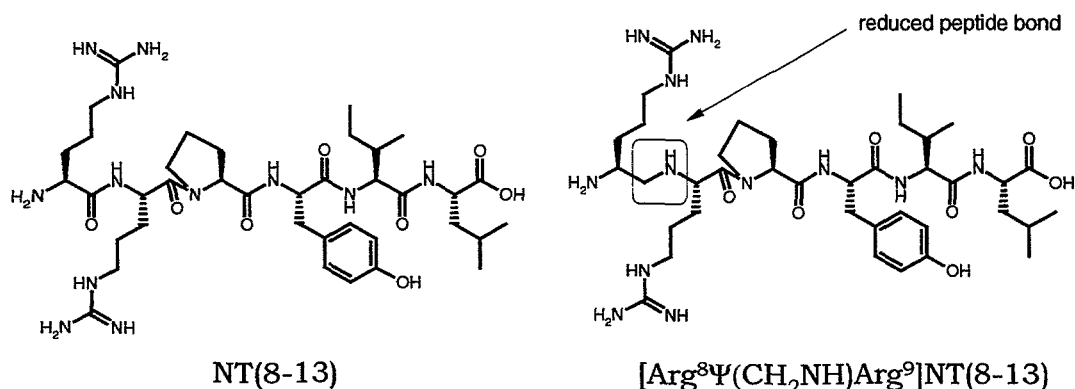
5. Reaction of Neurotensin (8-13) and its Partially Reduced Congener with Unlabelled and ^{18}F -Labelled N-Succinimidyl 4-Fluorobenzoate (SFB)

M. Scheunemann, P. Mäding, R. Bergmann, J. Steinbach, B. Johannsen, D. Tourwe¹
¹Vrije Universiteit Brussel, Belgium

Introduction

A promising approach for tracking tumours is the utilisation of radiolabelled peptides of specific affinity to receptors located on these tumours. Since neurotensin receptors were found in several tumour cell lines, such as small cell lung cancer [1], human colon [2] and pancreas cancer [3], the development of ^{18}F -radiolabelled derivatives of neurotensin, which bind to these receptors with high affinity, attracted our interest.

Investigation of the structure-affinity relationship of various neurotensin analogues showed that the hexapeptide NT (8-13) is the smallest biologically active fragment [4]. We therefore started our labelling experiments with this peptide fragment as well as smaller analogues containing either arginine or lysine as N-terminal amino acid (Arg-Tyr, Lys-Arg).



During the last decade only a few approaches to ^{18}F labelling of proteins and peptides using the [^{18}F]fluorobenzoyl group have been described. *Zalutsky and co-workers* reported on their experience in the preparation of N-succinimidyl-4- [^{18}F]fluorobenzoate ([^{18}F]SFB) and the subsequent labelling of the antibody F(ab')₂ [5]. In 1993 the same group used this procedure to label a small peptide (HCO-Nle-Leu-Phe-Nle-Tyr-Lys) in order to develop a potential agent for PET imaging of infection or inflammation [6]. In both papers the synthesis of the target molecule [^{18}F]SFB was described by a three-step procedure starting from 4-trimethylammonium benzaldehyde.

Among other prosthetic groups *Stöcklin et al.* investigated the labelling behaviour of the substituted benzoyl moiety for the introduction of [^{18}F] into proteins [7]. The authors used the triflate salt of ethyl 4-trimethylammonium benzoate as the starting material for the preparation of [^{18}F]SFB.

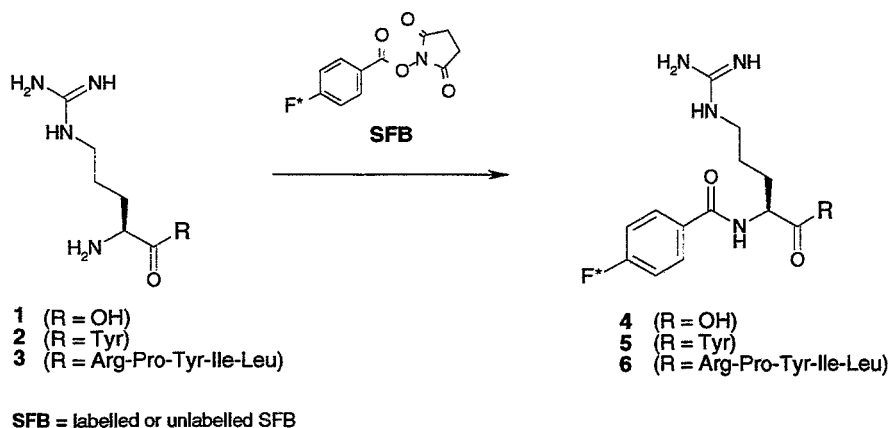
Preparation of *n.c.a.* N-succinimidyl-4- [^{18}F]fluorobenzoate

The synthesis of the authentic N-succinimidyl-4-fluorobenzoate has been published [7]. Radiosynthesis required a similar approach in which the ^{18}F was introduced at an early stage of the reaction sequence. Starting from trimethylammonium benzoate, which was converted into the ^{18}F -labelled ester, a saponification step yielded the salt of the acid. Finally, the carboxylic group was activated by means of *O*-(N-succinimidyl) N,N,N',N'-tetramethyluronium tetrafluoroborate in acetonitrile at 90°C. This method proved to be successful in achieving radiochemical yields of up to 50% calculated for the three-step procedure (decay corrected).

Peptide modification – Initial attempts at ^{18}F labelling of NT(8-13) and its smaller analogues

We began by examining the regioselectivity of nonlabelled SFB in its reaction with small peptides and (*S*)-arginine (**1**). The latter compound represents the N-terminal unit of the NT(8-13) sequence.

The other goal at the start of our studies was to compare the reaction conditions for labelling the amino acid derivatives given in the literature. Reaction of the activated fluorobenzoic acid derivative (unlabelled SFB) with two equivalents arginine (**1**) in a mixture of water and dioxane at 22°C, followed by extractive workup by means of butanol, exclusively afforded the desired acylated amino acid **4**.



Proton NMR clearly demonstrates the success of α -N-acylation, while no product was detected resulting from the attack of the guanidino function.

For our initial labelling experiments of NT(8-13) with [^{18}F]SFB we chose conditions similar to those described by *Wester et al.* [8]. Surprisingly, the attempt to convert NT(8-13) (**3**) and even Arg-Tyr (**2**) following this protocol (borate buffer, pH = 8.8 – 9.1, 22°C) gave rise to a mixture of radioactive products in each case. A similar complex product mixture was obtained by using unlabelled SFB. Apparently, the acylation of an amino group located at a tertiary carbon by means of SFB is more affected than the corresponding reaction at an amino group connected to a secondary carbon atom.

By contrast, the reaction of Lys-Arg both with labelled and unlabelled SFB yielded a predominant product together with smaller amounts of various unknown side products. In this case the kinetically preferred reaction presumably takes place at the ϵ -amino group of the lysyl moiety. The better chemoselectivity of the lysine-containing peptide is probably due to the lower steric hindrance and acidity of the protonated ϵ -amino group compared with the α -amino group in lysine. In fact, SFB has so far been described as a labelling agent solely for peptides containing lysine sequences.

To enlarge the field of application we investigated the reactivity of nonradioactive SFB in various solvent systems. We found that terminal Arg-peptides react with good chemoselectivity in an aprotic solvent such as DMF with triethylamine as a base or in buffered aqueous solutions with pH values lower than 8.5 at 22°C. Our labelling experiments then revealed that [^{18}F]SFB reacts with N-terminal Arg-peptides such as NT(8-13) or the metabolically stabilised pseudopeptide [Arg $^{\delta}\Psi(\text{CH}_2\text{NH})\text{Arg}^{\eta}$]NT(8-13) with reasonable to good chemoselectivity in aqueous buffered solutions, preferably at pH 8.3. To shorten the period of time necessary for the complete consumption of [^{18}F]SFB, we found it advisable to heat the mixture to 35 – 40 °C for 20 min.

The diluted reaction mixture was then subjected to chromatographic purification using semipreparative reversed-phase HPLC. The radioactivity corresponding to the desired product was collected and diluted with water. The solution was concentrated on an RP-18 cartridge. After washing with water, the purified ^{18}F -labelled peptide was eluted from the cartridge with a small amount of ethanol.

The radioactive product was identified by chromatographic comparison with a reference compound. The reactions carried out with nonradioactive SFB were shown to yield the corresponding 4-FB peptides. Their structural identity was confirmed by proton NMR and MS studies.

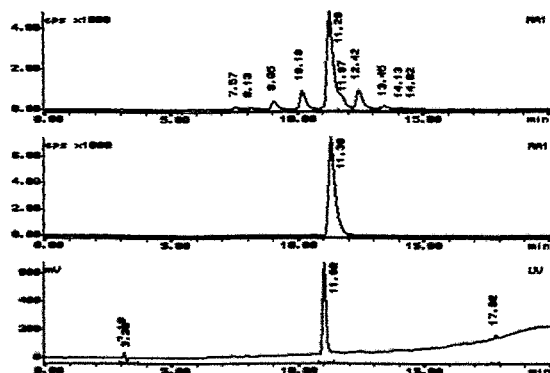


Fig. 1.
 a) HPLC of the reaction product of NT(8-13) and [^{18}F]SFB in phosphate buffer (pH 8.3, 40 min at 45°C).
 b) Purified product from the product mixture of a)
 c) Purified nonradioactive 4-FB-NT(8-13).

The forthcoming work will be focused on optimising the pH value for selective conversion within a smaller time range.

This work is supported by the European Union (BMH4-CT98-3198).

References and Notes

- [1] Davis T., Crowell S., McInturff B., Louis R. and Gillespie T. (1991) Neurotensin may function as a regulatory peptide in small cell lung cancer. *Peptides* **12**, 17–23.
- [2] Amar S., Kitabgi P. and Vincent, J.-P. (1986) Activation phosphatidyl inositol turnover by neurotensin receptors in the human colonic adenocarcinoma cell line HT29. *FEBS Letters* **201** (1), 31–36.
- [3] Ishizuka J., Townsend C. M. and Thompson J. C. (1993) Neurotensin regulates growth of human pancreatic cancer. *Annals of Surgery* **217**, 439–446.
- [4] Granier C., Van Rietschoten J., Kitabgi P., Poustis C. and Freychet P. (1982) Synthesis and characterisation of neurotensin analogues for structure/activity relationship studies. Acetyl-neurotensin (8-13) is the shortest analogue with full binding and pharmacological activities. *Eur. J. Biochem.* **124**, 117-125.
- [5] Vaidyanathan G. and Zalutsky M. R. (1992) Labeling proteins with fluorine-18 using *N*-succinimidyl 4-¹⁸F]fluorobenzoate. *Nucl. Med. Biol.* **19**, 275–281.
- [6] Vaidyanathan G., Affleck D. A., Welsh P. and Zalutsky M. R. (1993) Fluorine-18 labeled chemotactic peptide: A potential agent for the imaging of focal infection 10th International Symposium on Radiopharmaceutical Chemistry – Abstracts 365–367.
- [7] Wester H.-J., Hamacher K. and Stöcklin G. (1996) A comparative study of n.c.a. fluorine-18 labeling of proteins via acylation and photochemical conjugation *Nucl. Med. Biol.* **23**, 365–372.
- [8] Wester H. J., Krummeich Ch., Fixmann A., Förmer A., Müller-Gärtner H. W. and Stöcklin G. (1995) 11th International Symposium on Radiopharmaceutical Chemistry – Abstracts: 513-515.

6. Experiments of the Synthesis of [¹⁸F]Fluoromethyl Halides for Labelling Peptides

P. Mäding, M. Scheunemann, J. Steinbach

Introduction

Aiming at receptor-binding neuropeptides for tumour diagnosis with PET, we are interested in labelling peptides by means of [¹⁸F]fluoroalkylation, especially [¹⁸F]fluoromethylation. The [¹⁸F]fluoromethyl group ([¹⁸F]FCH₂) is the smallest prosthetic group for indirect labelling with ¹⁸F. It is to be expected that a fluoromethylated peptide has only little change in the size and polarity in comparison with the starting peptide. The receptor affinity of the fluoromethylated peptide should be similar to that of the starting peptide. Another advantage is the one-step procedure for synthesizing the fluoromethylation agent.

But the fluoromethylation of peptides also has its risks: the selectivity of the fluoromethylation agent for amino groups of the peptide may be lower compared with fluoroacylation agents such as N-succinimidyl 4-fluorobenzoate. The stability of the fluoromethyl-amino group is unknown.

Experimental

Materials

Fluoromethyl bromide (98 %) was purchased from ABCR GmbH & Co., Germany, sodium fluoroacetate (pract. ≥ 95 %) from Fluka, iodine (double-sublimated) and sodium iodide (pure) from Laborchemie Apolda, Germany.

Analysis

To determine the extent of conversion and the radiochemical purity and to identify the labelled product, an HPLC system (JASCO) was used, including a pump, a Rheodyne injector with a 20 µl loop, a LiChrospher WP300 RP-18 column (5 µm, 250 mm x 3 mm, Merck) and a UV detector coupled in series with a radioactivity detector FLO-ONE\Beta 150TR (Canberra Packard). The HPLC analyses were carried out at a flow rate of 0.5 ml/min with mixtures of MeCN and water containing 0.2 % TFA. The gradient of the eluents was: 0 min - 10 % MeCN/ 90 % water; 10 min - 60 % MeCN/ 40 % water; 14 min - 100 % MeCN/ 0 % water; 20 min - 100 % MeCN/ 0 % water.

Syntheses

Silver salt of fluoroacetic acid

A solution of silver nitrate (44 g = 259 mmol) in 40 ml water was added to a stirred solution of sodium fluoroacetate (25 g = 250 mmol) in 45 ml water, with a colourless salt precipitating. After stirring for 1 h the salt was filtered through a frit glass filter, washed with water and dried. Colourless crystals, yield: (40.7 g, 88.1 %).

Conversion of silver fluoroacetate with iodine

A mixture of the silver salt of fluoroacetic acid (10 g = 54 mmol) and iodine (34.2 g = 135 mmol) was slowly heated in a special distillation apparatus under a slight helium stream. The decarboxylation occurred at about 120 °C with iodine sublimating. When the reaction mixture was then heated up to 230 °C, iodine as well as a small amount of a strongly acidic, water-soluble liquid was distilled from it, probably fluoroacetic acid.

Fluoromethyl iodide

Fluoromethyl bromide (1.74 g = 15.4 mmol) was transferred from the storage vessel into a cooled 10 ml vial (-78 °C) with septum. A solution of sodium iodide (2.37 g = 15.8 mmol) in 2.9 ml acetone was added to the cooled substance while stirring. The reaction mixture was slowly heated to room temperature and sodium bromide was separated. After stirring for 3 h the reaction mixture was extracted with water (3 x 6 ml). The organic phase was dried with Na₂SO₄. In this way purified fluoromethyl iodide was obtained. Pale yellow liquid, yield: (1.3 g, 52.8 %).

Radiosyntheses

$[^{18}\text{F}]$ fluoromethyl bromide

A mixture of irradiated $[^{18}\text{O}]\text{H}_2\text{O}$ containing n.c.a. $[^{18}\text{F}]\text{HF}$ and K222/ K_2CO_3 solution (1.5 ml of 86 % MeCN with 15 mg (= 40 μmol) kryptofix and 2.77 mg (= 20 μmol) K_2CO_3) was dried by means of a vacuum and a nitrogen stream at 100 °C. The reaction mixture was carefully dried by repeated addition and evaporation of abs. MeCN (3 x 1 ml). After addition of 1 ml abs. MeCN and 100 μl dibromomethane the reaction mixture was heated at 100 °C. By means of an N_2 stream of 10 ml/min the $[^{18}\text{F}]$ fluoromethyl bromide was driven into a cooled trap with an appropriate solvent.

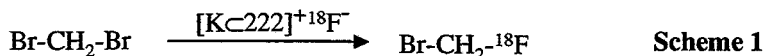
$[^{18}\text{F}]$ fluoromethyl iodide

A mixture of irradiated $[^{18}\text{O}]\text{H}_2\text{O}$ containing n.c.a. $[^{18}\text{F}]\text{HF}$ and K222/ K_2CO_3 solution was carefully dried as mentioned above. After addition of abs. MeCN and diiodomethane the $[^{18}\text{F}]$ fluoromethyl iodide formed at room temperature or an elevated temperature was driven (N_2 stream: 10 ml/min) into a cooled trap with a solvent. For detailed reaction conditions see Table 1.

Results and Discussion

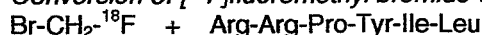
Synthesis of $[^{18}\text{F}]$ fluoromethyl bromide

Coenen et al. [1] prepared $[^{18}\text{F}]$ fluoromethyl bromide by nucleophilic substitution of $[^{18}\text{F}]$ fluoride for one bromide of dibromomethane according to Scheme 1:

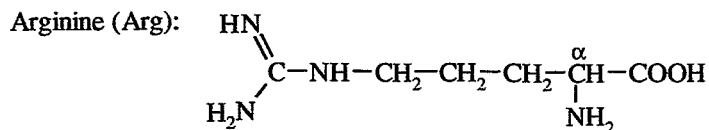


This reaction is very sensitive to moisture and other impurities. We tested this reaction in a closed as well as in an open system. In a closed system it is not possible to obtain $[^{18}\text{F}]$ fluoromethyl bromide in acceptable yields. We therefore optimized this conversion in an open system with a special apparatus. The volatile $[^{18}\text{F}]$ fluoromethyl bromide was driven by a nitrogen stream from the reaction mixture into a cooled trap. In this way the gaseous ^{18}F -labelled product was obtained in radiochemical yields of up to 53 %. The synthesis and purification of $[^{18}\text{F}]$ fluoromethyl bromide, especially the separation of the dibromomethane, have to be optimized to be used for labelling of peptides.

Conversion of $[^{18}\text{F}]$ fluoromethyl bromide with NT(8-13)



The arginine sequences of NT(8-13) contain two reactive guanidine functions in the pharmacophoric group.



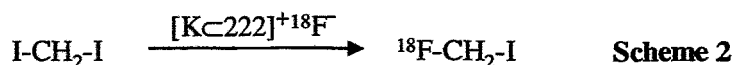
Because of the different pK_a values of the α -amino (9.04) and the guanidyl group (12.84) of the Arg(8), it should be possible to label only the α -amino group (the N-terminal region) by pH-controlled $[^{18}\text{F}]$ fluoro-methylation.

But initial attempts at converting $[^{18}\text{F}]$ fluoromethyl bromide with NT(8-13) in methanol using sodium acetate as a buffer failed at room temperature as well as at higher temperatures (75 °C and 120 °C). The reason may be the low reactivity of $[^{18}\text{F}]$ fluoromethyl bromide for amino groups. At 120 °C the $[^{18}\text{F}]$ fluoromethyl bromide gradually began to decompose.

For further $[^{18}\text{F}]$ fluoromethylation experiments we wanted to use $[^{18}\text{F}]$ fluoromethyl iodide, which has a better reactivity.

Synthesis of $[^{18}\text{F}]$ fluoromethyl iodide

The preparation of this labelling agent was described in [2] by nucleophilic substitution of the $[^{18}\text{F}]$ fluoride for one iodide of diiodomethane according to Scheme 2 in yields of 35-40 %:



Conversions of some model compounds having an amino, mercapto or carboxyl function with $[^{18}\text{F}]$ fluoromethyl iodide yielded the corresponding $[^{18}\text{F}]$ fluoromethylated products [3]. The first use of

[¹⁸F]fluoromethyl iodide to prepare a potential radiopharmakon was also carried out in [2]. In this way the so-called fluticasone propionate, a synthetic corticosteroid, was labelled with ¹⁸F by [¹⁸F]fluoromethylation of a carboxylic acid function.

We also tested the synthesis of [¹⁸F]fluoromethyl iodide according to [2] in a closed as well as in an open system, but the radiochemical yields were very low (about 2 %). The reason for that could be impurities in the reaction mixture which react with [¹⁸F]fluoromethyl iodide. In addition to unconverted [¹⁸F]fluoride a nonpolar ¹⁸F-labelled product in the reaction mixture was detected by HPLC. We tried to optimize the reaction conditions (see Table 1) such as reaction temperature (from room temperature up to 110 °C), reaction time, purity and amount of the solvent and the diiodomethane. So far these efforts have not been successful.

Table 1. Results of experiments for synthesizing [¹⁸F]fluoromethyl iodide under various reaction conditions

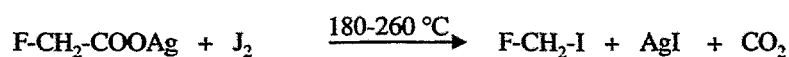
No.	Reaction vessel	Solvent	Methylene iodide	Reaction temperature	Total yield [%]	Radiochemical purity [%]
1	SA	1 ml MeCN	100 µl	RT, 70 °C, 110 °C	1.6	86.6
2	SA	1 ml MeCN	100 µl (dest.)	RT - 100 °C	2.0	87.9
3	SA	1 ml MeCN	100 µl (dest.)	RT, 45 °C, 65 °C, 80 °C	0.4	83.6
4	vial	1 ml MeCN	100 µl (dest.)	RT, 60 °C, 100 °C	2.5	45.9
5	vial	1 ml MeCN	100 µl (dest.)	RT, 60 °C, 100 °C	1.8	65.3
6	vial	1 ml dimethoxyethan (dest.)	100 µl (dest.)	RT	0	
				60 - 100 °C	2.5	44.1
7	SA	1 ml MeCN	70 µl (freeze-dried)	RT - 100 °C	2.6	89.1
8	SA without light	1 ml MeCN	100 µl	15 min RT		
				5 min 100 °C	2.3	93.2
9	SA	100 µl MeCN	10 µl	2.5 min RT ¹⁾		
				9 min RT	0.9	22.4
10	SA	without solvent	100 µl	2.5 min RT ¹⁾		
				5 min RT		
				10 min 100 °C	5.6	49.9
11	SA	without solvent	100 µl (dest.)	10 min 100 °C	4.2	60.3
			addition at 100 °C			

SA = special apparatus

¹⁾ without N₂ stream

Besides these attempts we also synthesized and tested the unlabelled fluoromethyl iodide.

Synthesis of fluoromethyl iodide



Scheme 3

There are several methods to prepare this compound.

One way to synthesize fluoromethyl iodide consists in the conversion of diiodomethane with mercury(I) fluoride (yield: 15 %; [4]) or mercury(II) fluoride (yield: 20 %; [5]).

Another method of preparing fluoromethyl iodide (yield: 55 %) is described in [6] by conversion of the silver salt of fluoroacetic acid with iodine under decarboxylation (Hundsdiecker reaction) according to Scheme 3. The silver salt of fluoroacetic acid can be precipitated by reaction of sodium fluoroacetate with silver nitrate in aqueous solution.

We tested this procedure. The decarboxylation of the prepared silver salt of fluoroacetic acid was observed while heating this salt with iodine, but the desired fluoromethyl iodide was not obtained. Only a small amount of a strongly acidic, water-soluble liquid was distilled from the reaction mixture, probably fluoroacetic acid.

We synthesized the fluoromethyl iodide using the Finkelstein exchange reaction of fluoromethyl bromide (b.p. 19 °C) with sodium iodide [7] according to Scheme 4.



The synthesis was improved as follows: The conversion was carried out in acetone as a solvent instead of MEK [7] at room temperature for 3 h. The reaction mixture was worked up by repeated extraction with water to separate the acetone and the inorganic salts from the final product. This convenient procedure avoids the fractionated distillation of fluoromethyl iodide from the solvent. Fluoromethyl iodide was obtained in yields of about 53 %.

Conversion of fluoromethyl iodide with Arg-Tyr as model peptide

Experiments of the conversion of fluoromethyl iodide with Arg-Tyr-HOAc were carried out in methanol by means of tetrabutylammonium hydroxide as a base. The possible formation of a fluoromethylated Arg-Tyr was observed using Arg-Tyr-HOAc, Bu₄NOH and FCH₂I in a molar ratio of about 1:3:3 at elevated temperatures (100 °C).

Further investigations are under way.

References

- [1] Coenen H. H., Colosimo M., Schüller M. and Stöcklin G. (1986) Präparation of n.c.a. [¹⁸F]CH₂BrF via aminopolyether supported nucleophilic substitution. *J. Labelled Compd. Radiopharm.* **23**, 587-595.
- [2] Zheng L. and Berridge M. S. (1997) Labelling of [¹⁸F]fluticasone propionate with [¹⁸F]fluoriodomethane. *XIth International Symposium on Radiopharmaceutical Chemistry*, Uppsala, Abstract p. 43-45.
- [3] Zheng L. and Berridge M. S. (1997) Synthesis of fluorine-18 labeled fluoromethyl iodide, a synthetic precursor for fluoromethylation of radiopharmaceuticals. *J. Nucl. Med.* **38**, 177P.
- [4] Van Arkel A. E. and Janetzky E. (1937) Fluor-jod-methan. *Recl. Trav. Chim. Pays-Bas* **56**, 167-168.
- [5] Burton D. J. and Greenlimb P. E. (1975) Fluoro olefins. VII. Preparation of terminal vinyl fluorides *J. Org. Chem.* **40**, 2796-2801.
- [6] Haszeldine R. N. (1952) The reactions of metallic salts of acids with halogens. Part III. Some reactions of salts of fluorohalogenoacetates and of perfluoro-acids. *J. Chem. Soc.* **1952**, 4259-68.
- [7] Hine J., Ehrenson S. J. and Brader W. H. (1956) The effect of halogen atoms on the reactivity of other halogen atoms in the same molecule. VI. The S_N2 reactivity of methylene and polymethylene halides. *J. Am. Chem. Soc.* **78**, 2282-84.

7. Crystal and Solution Structures of the Rhenium(V) Gly-Gly-His Complex

R. Jankowsky, W. Seichter¹, H. Spies, B. Johannsen

¹Institut für Organische Chemie, TU Bergakademie Freiberg

Introduction

In modern radiopharmaceutical research, ^{99m}Tc radiotracers basing on biologically active peptides are of growing interest for imaging of infections, inflammations, thrombi and tumors [1 - 4]. The successful design of peptide radiotracers decisively depends on the specific and stable metal binding to the peptide. That can be accomplished by the use of peptidic chelators, which can be easily attached to the peptide by solid phase synthesis [5 - 9]. Thus, the finding of specific metal binding peptide sequences remains to be a key task in basic radiopharmaceutical research. Previously, the rhenium(V) and technetium(V) binding properties of cysteinyl-containing model peptides were elucidated and successfully applied to the design of larger, biologically active systems [10 - 13]. Considering other peptidic donor groups, the histidine residue bearing an imidazole moiety can be expected to serve as a further anchor group for metal complexation [14, 15]. In the present study, we report on the rhenium(V) binding of the tripeptide Gly-Gly-His, which represents a model of the N-terminus of the human serum albumin (HSA) and is known to complexate other metals specifically [16]. The work deals with the crystal structure as well as the solution structures as studied by X-ray diffraction (XRD), capillary electrophoresis (CE) and X-ray absorption spectroscopy (EXAFS), respectively.

Experimental

The Re(V)-Gly-Gly-His complex was synthesized by common ligand exchange reactions starting from the Re gluconate precursor. Crystals were obtained from aqueous solution. The crystal structure was elucidated by XRD at the TU Bergakademie Freiberg, the solution structures were studied by a combined CE-EXAFS method as described previously [13]. EXAFS measurements were performed at HASYLAB, Hamburg, Germany at beamline X1.1 using transmission techniques and analyzed as described [13].

Results and Discussion

Crystal structure. The crystal structure is marked by the formation of a dimeric system. It consists of two rhenium nuclei which are coordinated by tetradentately acting peptide molecules at each nucleus. Bridging of the molecular moieties is realized by the peptide carboxyl groups (Fig. 1).

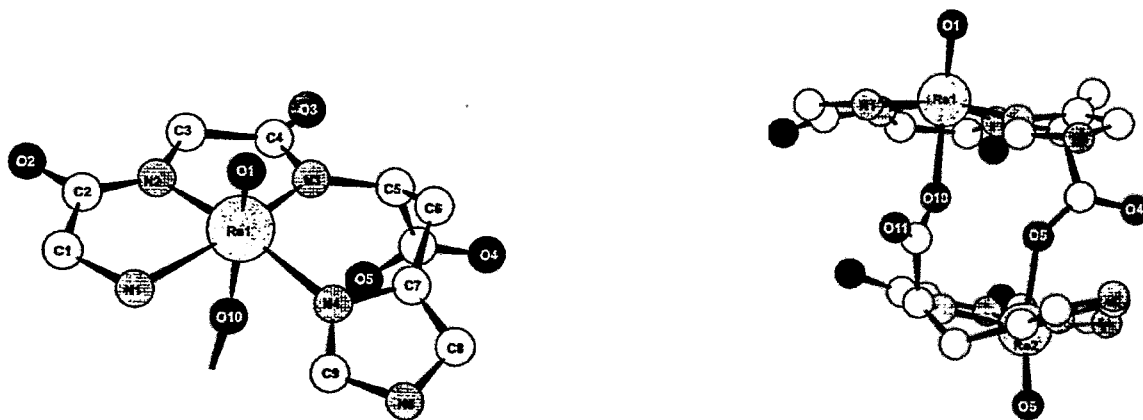


Fig. 1. Crystal structure of the Re Gly-Gly-His complex. Left sketch, monomeric nucleus moiety; right sketch, dimeric complex

At each nucleus, the metal complexation is accomplished by a formal N_4 coordination mode of the amine, amide and imidazole nitrogens. The *trans* coordination of carboxyl groups at each nucleus

leads to octahedral, neutral metal cores. Considering the bond lengths, deprotonation of the coordinating amide nitrogens takes place during metal complexation, while the coordinating amine and imidazole nitrogens remain protonated. Bond lengths are in good agreement with structural data from known rhenium complexes with similar donor atoms [11, 14, 15].

Solution structure. For the elucidation of the solution structure of the complex, an electrophoretic mobility curve was recorded using the capillary electrophoresis technique. It is shown with the corresponding pH-dependent UV spectra in Fig. 2.

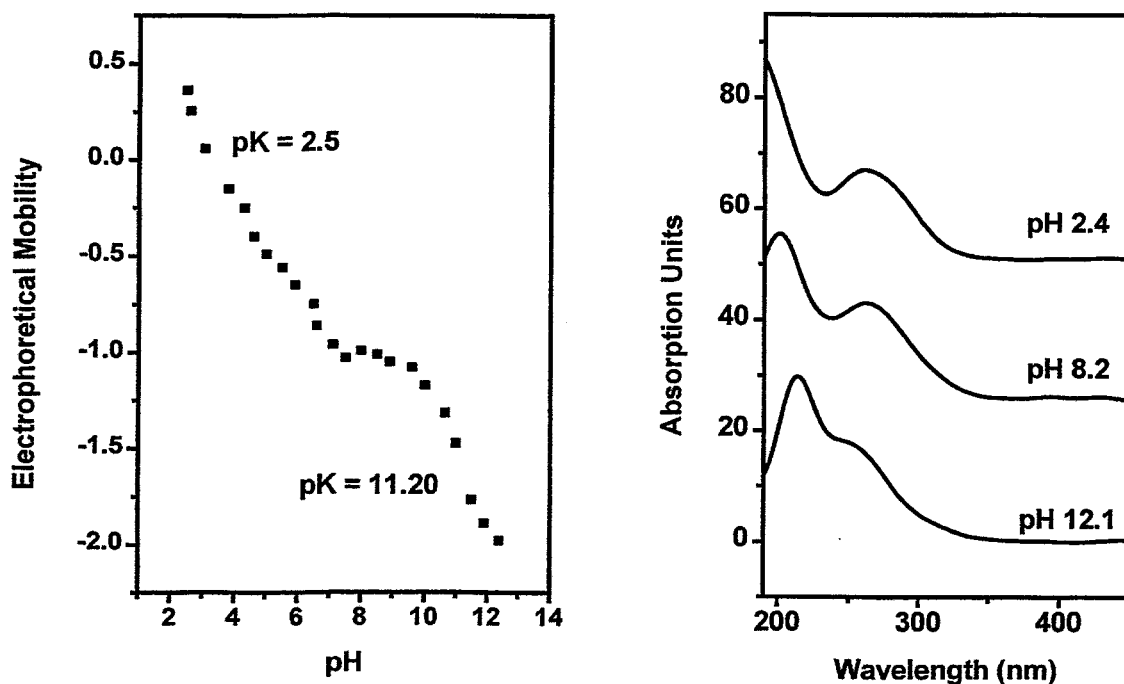


Fig. 2. Electrophoretic mobility curve of the Re Gly-Gly-His complex with corresponding UV spectra

Two steps were detected, where at each step the complex charge changes significantly. Furthermore, the UV spectra show different absorption patterns over the pH range which gives rise to the assumption that the metal surrounding is different at the three pH-values. The complex charge changes from cationic to anionic under acidic and alkaline conditions, respectively.

For the assignment of the electrophoretic mobilities to certain complex structures, EXAFS measurements were carried out at solid state, at pH 2.5 and at pH 12.4 (Fig. 3). At neutral pH, complex precipitation prevented an EXAFS analysis in solution.

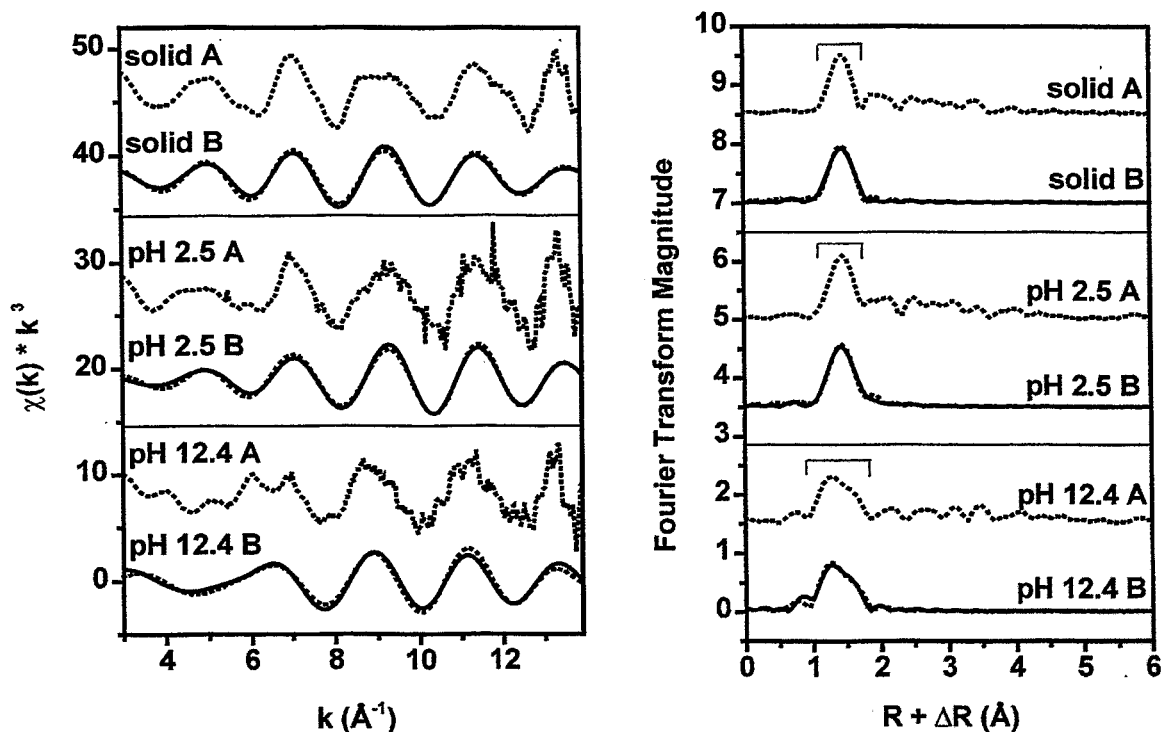
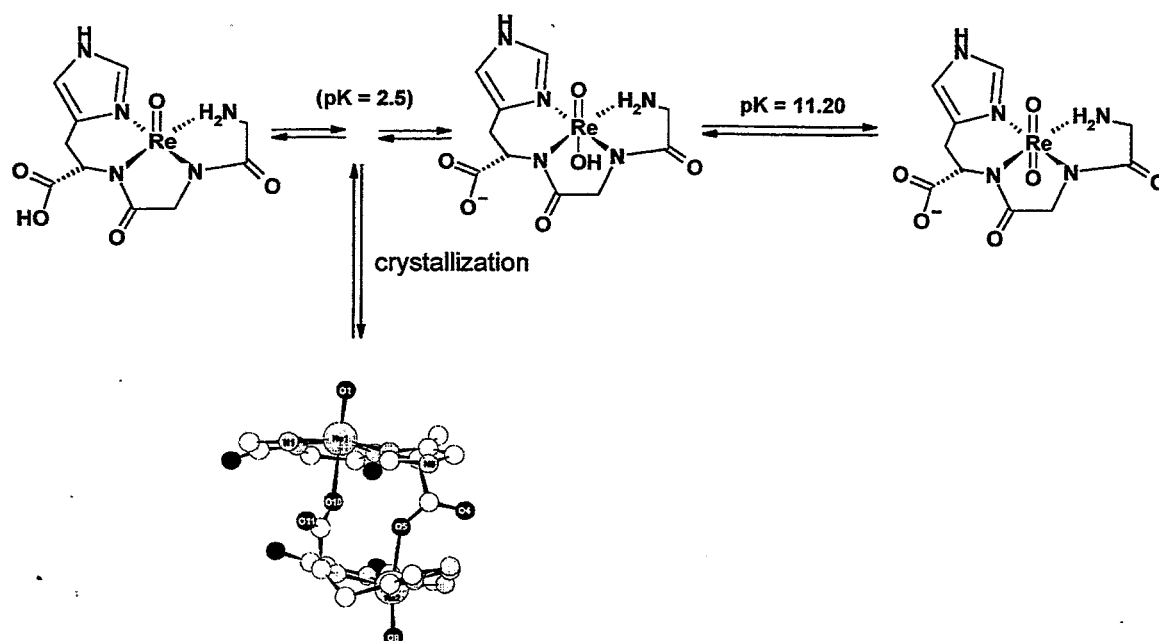


Fig. 3. EXAFS patterns and Fourier transforms of the Re Gly-Gly-His complex. A, experimental data and Fourier transforms with filtering windows; B, Fourier filtered data according to the filtering windows (dotted lines) and EXAFS fit data (solid lines)

EXAFS analysis of the solid complex confirmed the dimeric structure as analyzed by XRD. At higher distances to the central atom, significant multiple scattering effects were detected which are obviously caused by both the coordinating peptide backbone and the imidazole ring system. Within these back-scattering contributions, no resolution was possible by EXAFS fits. However, such a pattern may be considered as a fingerprint for coordinating peptide backbones and imidazole rings. The EXAFS measurement at pH 2.5 showed some slight changes, which is in agreement with the complex charge under acidic conditions. As a result of the EXAFS analysis, a formal N_4 coordination of the oxo metal core without involvement of a trans coordinated carboxyl oxygen atom could be concluded. Thus, at acidic pH a monomeric complex with a free protonated carboxyl group is existent. The plateau at pH 8 in the electrophoretical mobility curve could not be analyzed. However, due to the anionic complex charge, a complex structure similar to the crystal structure can be excluded. More probably, a hydroxyl group in *trans* position of the metal core is present under these conditions. At alkaline pH, two shortly bound oxygen atoms were detected at the metal core, which belong to a rhenium dioxo core. The ligand coordination mode does not change at this pH, thus the second step in the electrophoretical mobility curve can be assigned to the formation of a rhenium dioxo core under basic conditions. With respect to the CE and EXAFS data, the following scheme of the complex solution structure can be concluded.

Scheme 1.



References

- [1] Reubi J. C. (1997) Regulatory peptide receptors as molecular targets for cancer diagnosis and therapy. *Q. J. Nucl. Med.* **41**, 63-70.
- [2] Fischman A. J., Babich J. W. and Strauss H. W. (1993) A ticket to ride: peptide radiopharmaceuticals. *J. Nucl. Med.* **34**, 2253-2263.
- [3] Thakur M. L. (1995) Radiolabelled peptides: now and the future. *Nucl. Med. Comm.* **16**, 724-732.
- [4] Liu S., Edwards D. S. and Barrett J. A. (1997) ^{99m}Tc labeling of highly potent small peptides. *Bioconj. Chem.* **8**, 621-636
- [5] Knight L. C., Radcliffe R., Maurer S., Rodwell J. D. and Alvarez V. (1994) Thrombus imaging with technetium-99m synthetic peptides based upon the binding domain of a monoclonal antibody to activated platelets. *J. Nucl. Med.* **35**, 282-288.
- [6] Pearson D. A., Lister-James J., McBride M. C., Wilson D. M., Martel L. J., Civitello E. R. and Dean R. T. (1996) Thrombus imaging using technetium-99m-labeled high-potency GPIIb/IIIa receptor antagonists. Chemistry and initial biological studies. *J. Med. Chem.* **39**, 1372-1382.
- [7] Liu S., Edwards D. S., Looby R. J., Poirier M. J., Rajopadhye M., Bourque J. P. T. R. and Carroll S. (1996) Labeling cyclic glycoprotein IIb/IIIa receptor antagonists with ^{99m}Tc by the preformed chelate approach: effects of chelators on properties of ^{99m}Tc -chelator peptide conjugates. *Bioconjug. Chem.* **7**, 196-202.
- [8] Bogdanov A., Petherick P., Marecos E. and Weissleder R. (1997) *In vivo* localization of diglycyl-cysteine-bearing synthetic peptides by nuclear imaging of oxotechnetate transchelation. *Nucl. Med. Biol.* **24**, 739-742.
- [9] George A. J. T., Jamar F., Tai M. S., Heelan B. T., Adams G. P., McCartney J. E., Houston L. L., Weiner L. M., Oppermann H., Peters A. M. and Huston J. S. (1995) Radiometal labelling of recombinant proteins by a genetically engineered minimal chelation site: technetium-99m coordination by single-chain Fv antibody fusion proteins through a C-terminal cysteinyl peptide. *Proc. Natl. Acad. Sci. USA* **92**, 358-8362.
- [10] Johannsen B., Jankowsky R., Noll B., Spies H., Reich T., Nitsche H., Dinkelborg L. M., Hilger C. S. and Semmler W. (1997) Technetium coordination ability of cysteine-containing peptides: X-ray absorption spectroscopy of a ^{99}Tc labelled endothelin derivative. *Appl. Rad. Isot.* **48**, 1045-1050.

- [11] Jankowsky R., Kirsch S., Reich T., Spies H. and Johannsen B. (1998) Solution structures of rhenium(V) oxo peptide complexes of glycyglycylcysteine and cysteinylglycine as studied by capillary electrophoresis and X-ray absorption spectroscopy. *J. Inorg. Biochem.* **70**, 99-106.
- [12] Kirsch S., Jankowsky R., Spies H. and Johannsen B. (1997) Rhenium(V) oxo complexes with glycyglycylcysteine and glycyglycylcysteinylglycine: complexation behaviour in aqueous solution. *Annual Report 1997*, Institute of Bioinorganic and Radiopharmaceutical Chemistry, FZR-200, pp. 79-81.
- [13] Jankowsky R., Kirsch S., Noll B., Spies H. and Johannsen B. (1997) Technetium coordination features of cysteine-containing peptides: two ways to obtain direct labelled peptides. An EXAFS study of an endothelin and an LHRH derivative. *Annual Report 1997*, Institute of Bioinorganic and Radiopharmaceutical Chemistry, FZR-200, pp. 72-76.
- [14] Kremer C., Kremer E., Dominguez S., China E., Mederos A. and Castineiras A. (1996) Synthesis, characterization and potentiometric studies of trans-dioxorhenium(V) complexes. X-ray crystal structure of $\text{ReO}_2(\text{tn})_2\text{l}^*\text{H}_2\text{O}$. *Polyhedron* **15**, 4341-4347.
- [15] Kremer C., Gancheff J., Kremer E., Mombru A. W, Gonzalez O., Mariezcurrena R., Suescun L., Cubas M. L. and Ventura O. N. (1997) Structural and conformational analysis of Tc^{V} and Re^{V} di-oxo complexes. X-ray crystal structure of $\text{TcO}_2(\text{tn})_2\text{l}^*\text{H}_2\text{O}$. *Polyhedron* **16**, 3311-3316.
- [16] Metal Ions in Biological Systems, Vol. 1, Ed. H. Sigel, Cel Dekker, New York, 1975

8. EXAFS Structure Analysis of a Rhenium Complex with Neurotensin Derivative ORP500

R. Jankowsky, B. Johannsen

ORP500, a peptide derived from the peptide hormone neurotensin, consists of ten amino acids and has the sequence (dimethyl)-Gly-Ser-Cys-Gly-Lys-Lys-Pro-Tyr-Ile-Leu (Fig. 1). The N-terminal end of the peptide chain neurotensin(8-13) is attached to the tripeptide (dimethyl)-Gly-Ser-Cys, an analogue to the peptide Gly-Gly-Cys, which possesses strong coordination abilities to Re(V).

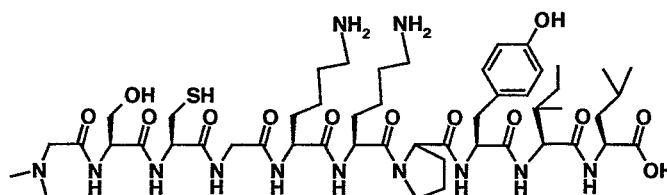


Fig. 1. Sequence of the neurotensin derivative ORP500

Extended X-ray absorption fine structure (EXAFS) spectroscopy was applied to investigate the complex coordination spheres. The sample was freeze-dried. Fluorescence detection was used because of the small sample amount. The EXAFS data and their Fourier transformation are shown in Fig. 2.

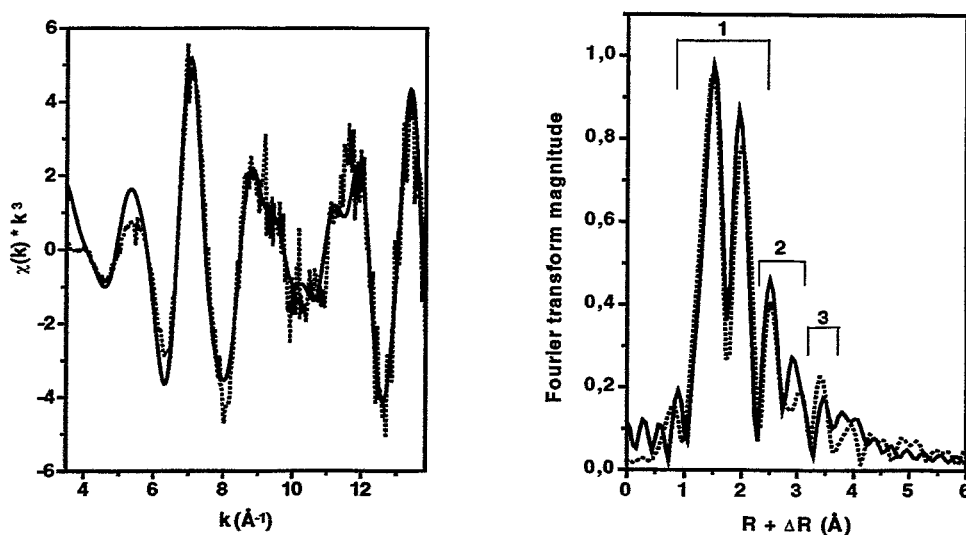


Fig. 2. Left: Experimental EXAFS data (dotted) vs. fit data (solid) of the rhenium(V) oxo ORP500 complex.

Right: Fourier transformation corresponding to the experimental EXAFS data (dotted) vs. fit data (solid) and three filtering regions.

Several coordination shells, partly clearly resolved, are visible in the Fourier transformation of the experimental EXAFS data. For the first filtered coordination sphere (Fig. 2), one oxygen atom at a distance to rhenium of 1.70 Å, three nitrogen atoms at a distance of 2.06 Å and a sulphur atom at a distance of 2.33 Å were found. The absorption edge position of the rhenium(V) oxo ORP500 complex was determined to be 10 529 eV. These characteristic features indicate an oxidation state of + 5 for rhenium.

Table 1. EXAFS fit results for the rhenium (V)oxo ORP500 complex

Backscattering atom	CN	R (Å)	σ^2 (Å ²)	ΔE_0 (eV)
O ¹	1.1(2)	1.70(1)	0.001(1)	-16.1(5)
N ¹	3.1(7)	2.06(1)	0.007(2)	-16.1(5)
S ¹	0.7(4)	2.33(1)	0.002(1)	-16.1(5)
C ²	6 ^e	3.00(2)	0.007(3)	-18.9(8)
C (MS) ^{a,2}	6 ^e	3.11(2)	0.002(2)	-18.9(8)
C (MS) ^{b,2}	6 ^e	3.15(2)	0.005(3)	-18.9(8)
O (MS) ^{c,3}	2 ^e	4.03(2)	0.005(3)	-15.2(4)
O (MS) ^{d,3}	2 ^e	4.09(2)	0.006(2)	-15.2(4)

CN: Number of coordinating atoms, R: distance to rhenium central atom,

σ^2 : Debye-Waller factor, ΔE_0 : Energy shift, Energy shifts were linked during several fits,

¹ First filtered coordination sphere,

² Second filtered coordination sphere,

³ Third filtered coordination sphere,

^a Multiple scattering along the Re-N-C path,

^b Multiple scattering along the Re-N-C-N path,

^c Multiple scattering along the Re-C-O path,

^d Multiple scattering along the Re-C-O-C path,

^e CNs were constraint during fits.

The detected distance of 2.06 Å for the nitrogen atoms is likely a mean value for two amide nitrogen atoms and one amine nitrogen atom corresponding to the rhenium(V) oxo Gly-Gly-Cys complex. This assumption is supported by an increased Debye-Waller factor for this coordination shell.

The sulphur atom at 2.33 Å resulted from the involvement of cysteinyl-SH in coordination of rhenium. Therefore, formal SN₃ coordination is obtained with very similar binding parameters to the rhenium (V) oxo Gly-Gly-Cys complex.

The second filtered coordination sphere in the Fourier transformation of experimental EXAFS data shows six carbon atoms with a mean distance to rhenium of 3.00 Å. This sphere was fitted with multiple scattering functions along the Re-N-C and Re-N-C-N paths. Values were obtained show the involvement of the peptide backbone chain in the metal chelate ring.

For the third filtered coordination sphere, multiple scattering along the Re-C-O and Re-C-O-C paths was found. This shows the involvement of amide nitrogen atoms of the peptide in coordination of rhenium.

From EXAFS fit results, the structure of the rhenium(V) oxo ORP500 complex as shown in Fig. 3 can be concluded. This complex shows a coordination sphere analogous to the rhenium(V) oxo Gly-Gly-Cys complex respectively the rhenium(V) oxo (dimethyl)-Gly-Ser-Cys complex.



Fig. 3. Structure of the rhenium(V) oxo ORP500 complex

9. Syntheses and Characterization of the Sulphamates of 17 ξ -Estradiols and 16 α -Fluoroestradiol

J. Römer, J. Steinbach, H. Kasch¹
¹Hans Knöll Institut, Jena

Introduction

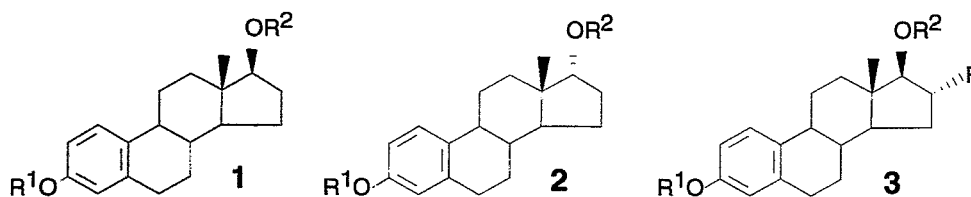
In the 1970s papers about sulphamates of 3-hydroxy-estra-1,3,5(10)-trienes were published for the first time [1 - 4]. They related to sulphamates of artificial steroids with a contraceptive effect.

Attention has now been focused again on estrogen sulphamates by some remarkable new insights. First, estrogen sulphamates were found to act as sulphatase inhibitors in the body [5]. Second, taken orally they were found to pass freely through the liver and thus to offer a much greater oral bioavailability than the mother steroids [6].

These new insights are remarkable in two ways. The first discovery promises a new approach to combating cancer [5] as sulphatase activity occurs particularly in placenta and mammary tumours. The second discovery opens up new ways of hormone therapy [6] and of oral contraception [7].

The first discovery could also be of significance in PET tracer chemistry. If, for example, 16 α -[¹⁸F]fluoroestradiol can be routinely converted into sulphamates, a new tracer should become available for the sulphatase receptor. This tracer could supply some first imaging agents for sulphatase activity in placenta and mammary tumours.

Three sulphamates are conceivable for 16 α -fluoroestradiol. These three sulphamates, their properties and conditions of formation have to be known for successful sulphamoylation of 16 α -[¹⁸F]fluoroestradiol. It was therefore necessary to work out production processes. Estradiol (**1a**) and 17 α -estradiol (**2a**) were available as commercial standard steroids. These unsubstituted diols and 16 α -fluoroestradiol (**3a**) as well as the relevant sulphamates are compiled in Scheme 1.

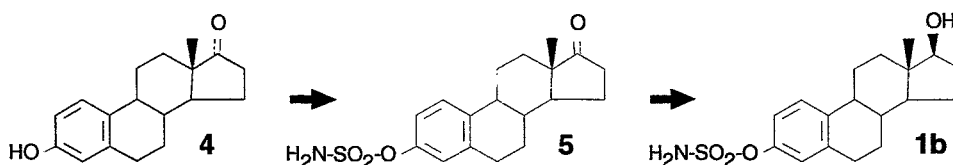


Scheme 1

	R ¹	R ²
a	H	H
b	H ₂ N-SO ₂	H
c	H	SO ₂ -NH ₂
d	H ₂ N-SO ₂	SO ₂ -NH ₂

Results and Discussion

Using sulphamoyl chloride (SCI), the first preparatory sulphamoylation experiments were carried out with estrone (**4**) according to a method specified by Howarth et al. [8]. Estrone-3-sulphamate (**5**) was obtained according to Scheme 2. We found confirmed [2] that the formation of the 3-amido-sulphonyloxy-estra-1,3,5(10)-triene structure is accompanied by a hypsochromic shift of the absorption maximum of the 3-hydroxy-estrogens by about 10 nm. The absorption maximum of **5** was found at 270 nm. In all the following syntheses the hypsochromic shift was useful for identifying the 3-amido-sulphonyloxy-estra-1,3,5(10)-triene structure.



Scheme 2

Howarth et al. [8] sulphamatized **4** in DMF and used NaH as a deprotonation agent. In our case this procedure required a great excess of reagents and was too time-consuming. Because of its high boiling point DMF was not a suitable solvent for an automatic synthesis apparatus, which was to be used later. We therefore replaced it by MeCN and tested Spillane's solid-liquid phase transfer process [9]. We were able to show that a few 3-amido-sulphonyloxy-estra-1,3,5(10)-trienes which are not accessible through [8] can be favourably synthesized in this way. The process was used for all sulphamates mentioned in Scheme 1.

Table 1. Physical data found for all steroids from Scheme 1

Steroid	Melting point [°C]	R _f value ^{a)}	RT (spec.) ^{b)}	UV _{max} [nm]
1a	177 - 179	0.27	1.000	284
1b	170 - 172	0.16	0.791	270
1c	158 - 161	0.29	0.729	282
1d	184 - 186	0.21	0.674	270
2a	223 - 226	0.30	0.922	284
2b	183 - 186	0.14	0.767	270
2c	^{c)}	0.28	0.721	282
2d	171 - 176	0.21	0.667	270
3a	199 - 202	0.32	0.775	284
3b	183 - 189	0.17	0.698	270
3c	141 - 143	0.27	0.698	282
3d	160 - 166	0.21	0.651	270

a) Silica gel plates as carriers and toluene / ethyl acetate (3:1) as solvent

b) RT (spec.) = RT (steroid) / RT (**1a**)

c) Became rearranged during heating and showed the melting point of the rearranged product (see [10])

The sulphamoylation of estradiols always yielded product mixtures which had to be separated by an efficient process. HPLC proved to be the method of choice. We used a preparative RP₁₈ column. Elution was by pure MeCN at a flow rate $v = 7$ ml/min. The retention times found in this system for **1a**, **2a** and **3a** and for the sulphamates obtained from them are compiled in Table 1. The longest retention time (12.9 min) was found for estradiol (**1a**). It was equated to 1. All other retention times in Table 1 were related to 12.9 min.

In addition to HPLC, thin-layer chromatography (TLC) on silica gel plates was used to check the purity of the synthesized sulphamates. The solvent was toluene/ethyl acetate (3 : 1). The R_f values found are also included in Table 1. In addition, Table 1 comprises the melting points of all compounds from Scheme 1 and their UV maxima.

Sulphamoylation of estradiol (1a)

After addition of the stoichiometric amount of SOCl₂ and double the stoichiometric amount of anhydrous Na₂CO₃, vigorous stirring of a solution of estradiol (**1a**) in anhydrous MeCN yielded three reaction products as well as unreacted **1a** after a short reaction time at room temperature. One of them was produced in a distinctly bigger yield than the other two. It proved to be estradiol-17β-sulphamate (**1c**). Schwarz *et al.* [11] were also surprised by this because their earlier experiments with 17α-ethinyl estradiol [3] had always shown that sulphamoylation was strictly confined to the phenolic OH group.

With the stoichiometric amount of SCl the yield of sulphamates was small. It grew along with the amount of SCl. The amount of estradiol-3,17 β -disulphamate (**1d**) increased in particular. The yield of estradiol-3-sulphamate (**1b**) always remained the lowest.

To obtain **1c** in amounts of about 50 mg, reaction batches of 100 mg of estradiol (**1a**) and the treble stoichiometric amount of SCl were needed. With the tenfold amount of reagent the formation of **1d** finally predominated. Sulphamoylation of estradiol (**1a**) did not offer favourable conditions for the preparation of **1b**.

In an alternative process for the preparation of **1b** according to Schwarz and Elger [7] estrone sulphamate (**5**), which was easy to prepare from estrone (**4**), was reduced in THF/MeOH with NaBH₄. The reaction sequence is shown in Scheme 2.

The retention times of the estradiol sulphamates increased in the order **1d** < **1c** < **1b**. But the sequence of the R_f values indicated by TLC differed from the retention times: **1b** < **1d** < **1c**.

Sulphamoylation of 17 α -estradiol (2a)

When the same sulphamoylation conditions were used for 17 α -estradiol (**2a**) as for **1a**, three reaction products were again obtained in addition to unreacted **2a**. The elution sequence was the same as above, i.e. **2d** < **2c** < **2b**, and the main product was 17 α -estradiol-17 α -sulphamate (**2c**). Excessive SCl caused the quantitative reaction of **2a** with the formation of **2c** and **2d** after only 1 hour's stirring. Different reaction conditions (CH₂Cl₂ instead of MeCN as reaction medium, higher temperature, long reaction time) also yielded a non-polar by-product at R_f = 15.8 min [10]. This by-product was not formed when the sulphamoylation occurred in MeCN at room temperature.

While the sulphamates **1b**, **1c**, **1d** as well as 17 α -estradiol-3-sulphamate (**2b**) and 17 α -estradiol-3,17 α -disulphamate (**2d**) were stable compounds, 17 α -estradiol-17 α -sulphamate (**2c**) proved to be very delicate. Studies showed that **2c** formed the above-mentioned non-polar by-product [10] on mere exposure to air. By boiling in MeCN **2c** was completely transformed into the non-polar product [10]. TLC again showed a sequence of the R_f values which differed from the retention times. With **2b** < **2d** < **2c**, the sequence was the same as above. TLC showed further that the above-mentioned by-product was also formed on the TLC plate.

Sulphamate of 16 α -fluoroestradiol (3a)

The required 16 α -fluoroestradiol (**3a**) was prepared according to a specification by Lim et al. [12] and purified by preparative HPLC.

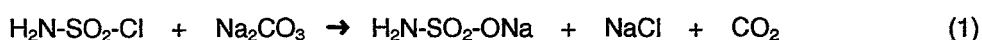
At first glance sulphamoylation of **3a** only seemed to yield two products. It turned out, however, that 16 α -fluoroestradiol-3-sulphamate (**3b**) and 16 α -fluoroestradiol-17 β -sulphamate (**3c**) had the same retention time (9.0 min). The latter dominated to an extent that the absorption maximum of **3b** (λ = 270 nm) was not even noticed in the mixture, i.e. predominantly 16 α -fluoroestradiol-3,17 β -disulphamate (**3d**) and 16 α -fluoroestradiol-17 β -sulphamate (**3c**) were found. No formation of non-polar products was observed. It was therefore not necessary to restrict the production conditions to room temperature and MeCN as in the case of 17 α -estradiol (**2a**).

Some experiments conducted for optimization are compiled in Table 2. While the amount of substrate remained the same, the amounts of reagent and of anhydrous Na₂CO₃ were varied. The solvent was dichloromethane. Each batch was stirred in a bath of 50 °C. Samples were taken after 2 and 4 hours and analysed by HPLC. Table 2 shows the peak distribution after the second sampling. It has to be taken into account that the peak of **3c** contained a small amount of **3b**.

Table 2: Optimum reaction conditions for the synthesis of 16 α -fluoroestradiol-17 β -sulphamate (**3c**) and 16 α -fluoroestradiol-3,17 β -disulphamate (**3d**)

Experiment	Reaction conditions			Product distribution		
	Substrate 3a [mg] / [mmol]	SCl [mg] / [mmol]	Na ₂ CO ₃ [mg] / [mmol]	3d [%]	3c [%]	Rest of 3a [%]
1	15 / 0.052	62 / 0.54	100 / 0.94	80	9	0
2	14 / 0.048	66 / 0.57	19 / 0.18	12	40	45
3	17 / 0.059	62 / 0.54	0 / 0	3	30	65
4	17 / 0.059	13 / 0.11	106 / 1.00	8	39	51

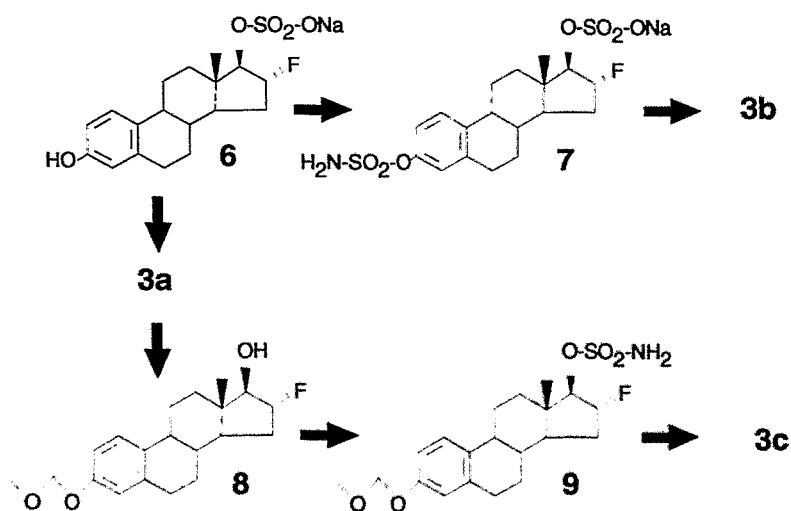
In experiments 1, 2 and 3 about the same amount of substrate **3a** and excessive reagent ($m(\text{SCl}) : m(\mathbf{3a}) \approx 10 : 1$) was used. When there was also sufficient alkali as in experiment 1 ($m(\text{soda}) : m(\text{SCl}) \approx 2 : 1$), 16α -fluoroestradiol (**3a**) was completely converted and a high yield of disulphamate **3d** obtained. When there was not enough alkali (experiment 2), only part of **3a** was sulphamated, chiefly to 16α -fluoroestradiol- 17β -sulphamate (**3c**). A partial conversion occurred even without alkali (experiment 3). Disulphamate was practically not formed in this process. When only double the molar amount of reagent was used for sulphamoylation (experiment 4), **3a** was only partially sulphamated in spite of the presence of excessive alkali, and a similar result as that of experiment 2 was obtained. The conditions of experiment 1 were suitable for preparation of disulphamate **3d**, while sulphamatization in the absence of alkali was useful for preparation of **3c**, although with qualifications. First, **3c** was never obtained pure but always contained small amounts of **3b**. Second, it was advisable to recover the unconverted **3a**. Third, the yield of **3c** was not increased by addition of further SCl.. The conditions of experiments 2 and 4 are unsuitable for sulphamoylation. This is due to the fact that SCl and Na_2CO_3 can also react with each other (see Eq. (1)) so that after a certain reaction time the deficient reactant is used up. The results of experiments 2 and 4 were therefore between the results of experiments 1 and 3.



Two alternative processes were devised for preparing the pure monosulphamates **3b** and **3c**, starting from 16α -fluoroestradiol- 17β -sodium sulphate (**6**) or from 3-O-methoxymethyl- 16α -fluoroestradiol (**8**) (see Scheme 3). The starting material **6** was obtained from 16α -fluoroestradiol- 17β -hydrogensulphate, an intermediate compound in the synthesis of **3a** [13], by treatment with a cation exchanger in the Na^+ form.

Sulphamoylation of 16α -fluoroestradiol- 17β -sodium sulphate (**6**) yielded 3-O-amidosulphonyl- 16α -fluoroestradiol- 17β -sodium sulphate (**7**). The reaction was sluggish. The following hydrolysis was carried out according to an elegant procedure [12] by refluxing a solution of **7** in anhydrous MeOH in the presence of an H^+ -charged cation exchanger. All available sulphamate **7** was converted into **3b**. Unreacted **6** yielded **3a**.

3-O-Methoxymethyl- 16α -fluoroestradiol (**8**) was synthesized from **3a**. The sulphamoylation of **8** occurred in a quantitative process, yielding 3-O-methoxymethyl- 16α -fluoroestradiol- 17β -sulphamate (**9**). The subsequent hydrolysis yielded pure **3c**, as was confirmed by TLC and MS.



Scheme 3

Experimental

Chemicals

Aldrich, Fluka and Sigma were the suppliers of commercial reagents and solvents. SCI was prepared according to [14] from chlorosulphonyl isocyanate, 16 α -fluoroestradiol (**3a**) according to a modified specification [13] from estra-1,3,5(10)-triene-3,16 β ,17 β -triol.

Equipment

The melting points were determined using a "GalenTMIII" microheating stage (Reichert Division of the Vienna Leica AG) with a digital temperature measuring system. ¹³C NMR spectra were recorded with a DRX 500 spectrometer (Bruker). A Merck-Hitachi HPLC system was used for the chromatographic analyses. It comprised an L-6200A gradient pump, a Rheodyne injector with a 500 μ l loop, an RP column SP 250/21 Nucleosil 100-7C₁₈ (Macherey & Nagel) and an L-4500 DAD diode array detector. The eluent was pure MeCN, the flow rate was 7 ml / min. UV absorption was measured at $\lambda = 275$ nm.

General sulphamylation specification

The chosen substrate (**1a** or **2a** or **3a**) was dissolved in a suitable solvent (MeCN or CH₂Cl₂), adding freshly heated and recooled Na₂CO₃ (anhydrous, the tenfold molar amount related to the substrate) to the solution. SCI (at least the double and not more than the 8fold molar amount related to the substrate) was added while stirring vigorously. Stirring was then continued for a few hours at room temperature or a higher temperature. The end of the reaction was determined by HPLC control. Processing: The batch was stirred into diluted HCl, followed by double extraction with ether, washing of the combined organic phases, evaporation of the ether, take-up of the residue in a suitable amount of MeCN. HPLC: The injection volume depended on the efficiency of separation. Per 0.1 mmol of substrate about 1 ml of MeCN was added to the extracted substance mixture. The injection volume was chosen in the range from 0.2 to 0.5 ml. Obtaining the product: The peaks of interest were separately collected in beakers. MeCN was boiled down to 10 ml on the heating plate. The MeCN solution of **2c** was an exception. This solution was carefully boiled down in the rotary evaporator at not more than 45° C, then covered with a layer of argon and the sealed flask kept in the refrigerator. The solutions of the other peaks were left to stand open overnight and the solid crystalline product was weighed the following morning.

Syntheses

- Estradiol-3-sulphamate (**1b**), estradiol-17 β -sulphamate (**1c**) and estradiol-3,17 β -disulphamate (**1d**)

(a) **1a** (85 mg, 0.3 mmol) was dissolved in MeCN (anhydrous; 15 ml) in a round-bottomed flask. Addition of Na₂CO₃ (anhydrous; 265 mg, 2.5 mmol). After setting a high stirring speed, SCI (116 mg, 1 mmol) was added. Stirring time at room temperature: 2 hours, reaction control by HPLC. Processed as usual and taken up in 2 ml of MeCN. Preparative HPLC with 8 times 0.25 ml injection solution, separate collection of the peaks of **1d**, **1c** and **1b**, product obtained as usual. White crystals. Weighed products: **1d** (11 mg = 25.6 μ mol), **1c** (38 mg = 108 μ mol), **1b** (6 mg = 17 μ mol).

(b) 500 mg of Na₂CO₃ (4.7 mmol) and 350 mg of SCI (3 mmol) were added to a similar-sized batch of **1a** in MeCN, which was otherwise treated as above described. HPLC indicated no **1a** and very little **1b**. Weighed products: **1d** (68 mg = 158 μ mol), **1c** (25 mg = 71 μ mol).
- Estradiol-3-sulphamate (**1b**) from estrone (**4**)

4 (135 mg, 0.5 mmol) was dissolved in MeCN (anhydrous, 15 ml) in a round-bottomed flask and Na₂CO₃ (anhydrous; 510 mg, 5 mmol) and SCI (310 mg, 2.7 mmol) were added to it. The solution was stirred vigorously for 6 hours at room temperature. Processed as usual, preparative HPLC, product obtained as usual. Weight of estrone sulphamate (**5**): 92 mg = 0.26 mmol; yield: 52 %. The white product **5** was dissolved in a mixture of THF (2.5 ml) and EtOH (2.5 ml). NaBH₄ (20 mg, 0.5 mmol) was added to this batch in an ice bath and stirred for 2 hours. HPLC control, processed as usual, HPLC purification with 5 times 0.25 ml, product obtained as usual. Weight of **1b**: 52 mg (0.15 mmol). Yield related to estrone (**4**): 30 %.

3) 17 α -estradiol-3-sulphamate (2b), 17 α -estradiol-17 α -sulphamate (2c) and 17 α -estradiol-3,17 α -disulphamate (2c)

(a) **2a** (90 mg, 0.33 mmol) was dissolved in MeCN (anhydrous; 15 ml) in a round-bottomed flask. Addition of Na₂CO₃ (anhydrous; 370 mg, 3.5 mmol). After setting a high stirring speed, SCl (230 mg, 2 mmol) was added. Stirring time at room temperature: 1 hour, reaction control by HPLC. Processed as usual and residue taken up with 2.5 ml of MeCN. Preparative HPLC with 10 times 0.25 ml injection solution, separate collection of the peaks of **2d**, **2c** and **2b**. Product distribution: **2d** (14 %), **2c** (42 %), **2b** (10 %), remainder of **2a** (34 %). Processed as usual and products **2d** and **2b** obtained as usual. Weighed products: **2d** (17 mg = 39.5 μ mol), **2b** (9 mg = 25.6 μ mol). The MeCN solution of **2c** was boiled down to 2 ml at 45 °C in the rotary evaporator. The remaining MeCN was dispelled with argon. A tan coloured product was obtained. Quick weighing showed the product to be 48 mg (136.7 μ mol).

(b) A batch of 83 mg (0.305 mmol) of **2a**, 10 ml of MeCN, 507 mg (4.8 mmol) of Na₂CO₃ and 290 mg (2.5 mmol) of SCl was vigorously stirred at room temperature for 2 hours. HPLC indicated only the 2 peaks of **2d** and **2c**. Product distribution: **2d** (70 %), **2c** (30 %). Processed and products obtained as above described. Weighed products: **2d** (81 mg = 188 μ mol) and **2c** (20 mg = 57 μ mol).

4) 16 α -fluoroestradiol-3,17 β -disulphamate (3d)

3a (110 mg, 0.38 mmol) was dissolved in CH₂Cl₂ (40 ml) in a 100 ml round-bottomed flask, and anhydrous Na₂CO₃ (600 mg, 5.65 mmol) was added to it. SCl (480 mg, 4.15 mmol) was added while stirring vigorously, and stirring was continued for 4 hours in a bath of 50 °C. Reaction control by HPLC. The solvent was dispelled in the rotary evaporator. Processed as usual, residue taken up in 5 ml of MeCN, then preparative HPLC with 10 times 0.5 ml injection solution. Only the peak of **3d** was collected. Product obtained as usual. Weight of **3d**: 108 mg (251 μ mol) of a white crystalline product. Yield: 66 %.

5) 16 α -fluoroestradiol-17 β -sulphamate (3c)

3a (87 mg, 0.3 mmol) was dissolved in THF (anhydrous; 5 ml) in a 15 ml round-bottomed flask. NaH (60 % suspension, 30 mg, 0.75 mmol; freed from mineral oil by means of hexane, then suspended in 3 ml THF) was added to it. Methoxymethyl chloride (0.04 ml, 0.5 mmol) was added to 0.5 ml THF and this reagent solution stirred into the batch. HPLC showed good conversion after 2 hours' stirring. Processed as usual by ether extraction. The residue was 3-O-methoxymethyl-16 α -fluoroestradiol (**8**) as a yellow oil.

To the oil were added CH₂Cl₂ (anhydrous, 5 ml), anhydrous Na₂CO₃ (150 mg, 1.42 mmol) and SCl (110 mg, 0.95 mmol). The batch was vigorously stirred for 2.5 hours in a bath of 50 °C. HPLC showed almost complete conversion to 3-O-methoxymethyl-16 α -fluoroestradiol-17 β -sulphamate (**9**). The batch was filtered, filter and soda were washed with CH₂Cl₂. The filtrate was boiled down in the rotary evaporator.

Four times 1 ml of 0.1 M hydrochloric MeCN solution was added to the residue of sulphamoylation with its content of **9** and the mixture evaporated to dryness in the rotary evaporator [16]. The solid residue was processed as usual, the residue taken up in MeCN (2.5 ml). Preparative HPLC with 10 times 0.25 ml injection solution, peak collection and preparation of the product as usual yielded 55 mg of white crystalline **3c** equivalent to 150 μ mol. The yield was 50 % related to **3a**.

6) 16 α -fluoroestradiol-3-sulphamate (3b)

A batch of 16 α -fluoroestradiol-17 β -sodium sulphate (**6**) (93 mg, 0.237 mmol), MeCN (30 ml), anhydrous Na₂CO₃ (510 mg, 4.8 mmol) and SCl (510 mg, 4.4 mmol) was vigorously stirred at room temperature for 1 hour. The MeCN was dispelled in the rotary evaporator, 10 ml of fresh MeCN was added and again dispelled. This was repeated five times, each time adding 10 ml MeCN. Each time a white, caked residue remained on the inside of the flask. The cation exchanger (CAT; H⁺ form, washed neutral, 12 mmol capacity) was treated with 4 portions of MeOH (anhydrous, 10 ml each) and then put into the above flask with 3 portions of MeOH (10 ml each). The batch was re-fluxed for 2 hours in a bath of 95 – 100 °C. The methanolic solution was then a very pale yellow and clear. It reacted acid and contained **3b** and **3a** in the ratio 1 : 2. The methanolic solution was filtered off. The filter with the CAT was washed several times with a little MeOH. The combined filtrates were boiled down in the rotary evaporator. After the usual process 3 ml of MeCN were added

to the residue of the concentrated ether extract. HPLC with 6 times 0.5 ml injection solution. Only **3b** was collected. Product obtained as usual. Weight: 21 mg of a white product. This is equivalent to 60 μmol of **3b**. The yield was 25.2 %, related to **6**.

References

- [1] Schwarz S., Weber G. and Kühner F. (1970) Sulphamate des 17α -Ethinylestradiols. *Z. Chem.* **10** 299-300.
- [2] Schwarz S. and Weber G. (1974) Steroidsulphamate. *Z. Chem.* **14** 15-16.
- [3] Schwarz S. and Weber G. (1975) Phasentransfer-katalysierte Veresterung von Estrogenen mit Sulfonylchloriden. *Z. Chem.* **15**, 270-272.
- [4] Schwarz S., Weber G. and Schreiber M. (1975) Sulfonyloxyderivate von Estrogenen. *Pharmazie* **30**, 17-21.
- [5] Reed M. J., Purohit A., Howarth N. M. and Potter B. V. L. (1994) Steroid sulphatase inhibitors: A new endocrine therapy. *Drugs Future* **19**, 673-679.
- [6] Elger W., Schwarz S., Hedden A., Reddersen G. and Schneider B. (1995) Sulphamates of various estrogens with increased systemic and reduced hepatic estrogenicity at oral application. *J. Steroid Biochem. Molec. Biol.* **55**, 395-403.
- [7] Schwarz S. and Elger W. (1996) Estrogen sulphamates, a novel approach to oral contraception and hormone replacement therapy. *Drugs Future* **21**, 49-61.
- [8] Howarth N. M., Purohit A., Reed M. J. and Potter B. V. L. (1994) Estrone sulphamates: potent inhibitors of estrone sulfatase with therapeutical potential. *J. Med. Chem.* **37**, 219-221.
- [9] Spillane W. J., Taheny A. P. and Kearns M. M. (1982) Versatile synthesis of sulphamate esters by phase-transfer methods. *J. Chem. Soc., Perkin I*, 677-679.
- [10] Römer J., Kasch H., Steinbach J. and Scheller D. (1999) 17-Methyl-gona-1,3,5(10),13(17)-tetraene-3-ol. *This report*, pp. 47-48.
- [11] Schwarz S., Thieme I., Richter M., Undeutsch B., Henkel H. and Elger W. (1996) Synthesis of estrogen sulphamates: compounds with a novel endocrinological profile. *Steroids* **61**, 710-717.
- [12] Lim J. L., Lei Zheng, Berridge M. S. and Tewson T. J. (1996) The use of methoxymethyl- $16\beta,17\beta$ -epiestriol-O-cyclic sulfone as the precursor in the synthesis of F-18 16α -fluorestradiol. *Nucl. Med. Biol.* **23**, 911-915.
- [13] Römer J., Steinbach J. and Kasch H. (1996) Studies on the synthesis of 16α - ^{18}F fluorestradiol. *Appl. Radiat. Isot.* **47**, 395-399.
- [14] Appel R. and Berger G. (1958) Über das Hydrazodisulphamid. *Chem. Ber.* **91**, 1339-41.

10. 17-Methyl-gona-1,3,5(10),13(17)-tetraene-3-ol

J.Römer, H.Kasch¹, J.Steinbach, D.Scheller²
¹Hans Knöll Institut, Jena; ² TU Dresden

Introduction

In the preparation of sulphamates of 17 α -estradiol [1] a non-polar product was observed, which occurred in particular when the reaction batches had been heated. This non-polar product was formed from 17 α -estradiol-17 α -sulphamate (**1**) and was a stable compound. Its structure was chiefly determined by ¹H NMR and ¹³C NMR. It proved to be 17-methyl-gona-1,3,5(10),13(17)-tetraene-3-ol (**2**).

Experimental

The ¹³C NMR spectrum was recorded with a DRX 500 spectrometer (Bruker). A ¹H NMR spectrum was also prepared, and the two-dimensional methods COSY, HSQC, HMBC and NOESY were used to clear up its structure.

Synthesis:

MeCN (5 ml) was added to 17 α -estradiol-17 α -sulphamate (**1**) (HPLC purified, 13 mg, 39 μ mol). The clear solution was slowly boiled down to 1 ml on the heating plate and then restored to 5 ml by adding MeCN. HPLC indicated the complete conversion of **1** and the formation of a non-polar product with a retention time of 15.6 min. Evaporation of MeCN at room temperature yielded a fine white product. Weight: 8.5 mg. This is equivalent to 33.5 μ mol of **2**. The yield was 86 % related to **1**.

Results and Discussion

17-Methyl-gona-1,3,5(10),13(17)-tetraene-3-ol (**2**) was first prepared by Arunachalam et al. [2] by refluxing 17 α -iodoestra-1,3,5(10)-triene-3-ol (**3**) for 24 hours (!) in 2-propanol in the presence of NaI. The melting point indicated by the authors was 95 °C. But we found a quick and complete conversion of **1** \rightarrow **2** and 132 - 135° C for the chromatographically pure product. That is to say, compared with the substituent 17 α -I, the 17 α -O-SO₂-NH₂ group is a much better leaving group.

The ¹H NMR spectrum also contradicted structure **I** as there were no additional olefinic protons. But it contained a methyl group at 1.65 ppm as a singlet. Its location, the fact that there was no cleavage and the HMBC suggested a methyl group at a double bond. Structure **II** was in agreement with this result. The assumption of structure **II** and the chemical shifts found in the ¹³C NMR spectrum indicated the assignments shown in Table 1.

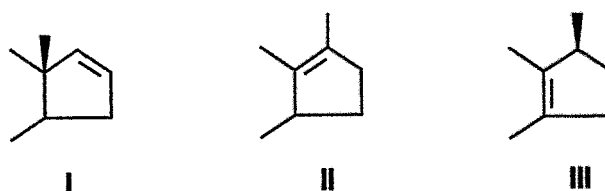


Table 1. Assignments suggested for the chemical shifts of the non-polar product

C atom	δ [ppm]	C atom	δ [ppm]	C atom	δ [ppm]
1	127.9	7	28.4	13	129.1
2	113.5	8	49.8	14	53.1
3	154.8	9	42.9	15	28.3
4	115.8	10	132.7	16	37.8
5	139.2	11	32.2	17	136.7
6	30.9	12	26.4	17-CH ₃	14.0

As expected, a comparison of the chemical shifts of the six Ring A carbon atoms of Table 1 with the values of the 3-hydroxy-estra-1,3,5(10)-trienes shows good agreement. The values also agreed for C(6) and C(7). On the basis of this certain relationship it was possible to clearly define the assignment of the protons to the carbon chains 7 - 8 - 14 - 15 - 16 and 9 - 11 - 12, using the two-dimensional

spectrums. The definite assignment of the protons also pointed to a $\Delta^{13(17)}$ structure II. The assignments of the protons of compound 2 are compiled in Table 2.

Table 2. Assignment of the chemical shifts of the H atoms in the ^1H NMR spectrum of compound 2

H atom	δ [ppm]	H atom	δ [ppm]	H atom	δ [ppm]
1-H	7.18	8 β -H	1.00	14 α -H	2.30
2-H	6.65	9 α -H	2.39	15 α -H	1.39
4-H	6.56	11 α -H	2.46	15 β -H	2.13
6 α -H	}2.77 a)	11 β -H	1.14	16 α -H	}2.26 b)
6 β -H				16 β -H	
7 α -H	1.39	12 α -H	1.98	17-CH ₃	1.65
7 β -H	1.94	12 β -H	2.67		

a) Location of centroid; it holds that $\delta(6\beta) > \delta(6\alpha)$

b) Location of centroid

References

- [1] Römer J., Steinbach J. and Kasch H. (1999) Syntheses and characterization of the sulphamates of 17 ξ -estradiols and 16 α -fluoroestradiol. *This report*, pp. 40-46.
- [2] Arunachalam T., Longcope Ch. and Caspi E. (1979) Iodoestrogens, syntheses, and interaction with uterine receptors. *J. Biol. Chem.* **254**, 5900-05.

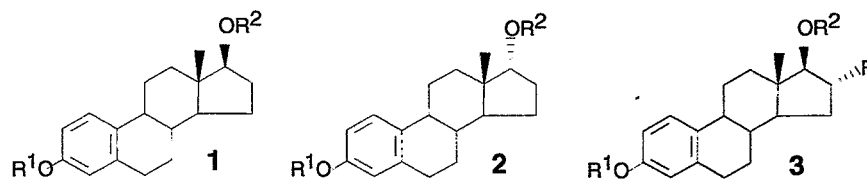
11. ^{13}C NMR Spectroscopic Characterization of Some New Estrogen Sulphamates

J. Römer, J. Steinbach, D. Scheller¹

¹ TU Dresden

Introduction

All sulphamates **b**, **c**, **d** shown in Scheme 1 were described in the above paper [1]. They were clearly characterized by ^{13}C NMR spectroscopy.



	R ¹	R ²
a	H	H
b	H ₂ N-SO ₂	H
c	H	SO ₂ -NH ₂
d	H ₂ N-SO ₂	SO ₂ -NH ₂

Experimental

The ^{13}C NMR spectra were recorded using a DRX 500 spectrometer (Bruker).

Results and Discussion

The chemical shifts found for estradiol (**1a**) and its three sulphamates, 17 α -estradiol (**2a**) and its three sulphamates and 16 α -fluoroestradiol (**3a**) and its three sulphamates are compiled in Table 1.

A 3-O-sulphamate group influences in particular the chemical shifts of the Ring A carbon atoms. We found a distinct high-field shift for the signal of C(3) and distinct low-field shifts for the signals of C(2) and C(4). The signals of the atoms C(1) and C(5) were hardly influenced at all. But the unshielding effect on C(10), which led to the signals of C(5) and C(10) lying side by side, was remarkable. This is a characteristic feature of the presence of a 3-amidosulphonyloxy-estra-1,3,5(10)-triene.

A 17 ξ -O-sulphamate group mainly influenced only the chemical shift of C(17), but unlike the 3-O-sulphamate group it did this by causing a low-field shift of the signal. The above-mentioned influences were all present in the 3,17 ξ -disulphamates.

A comparison of the spectra of estradiol (**1a**) and 16 α -fluoroestradiol (**3a**) showed that fluorine as a substituent influences in particular the Ring D carbon atoms. The coupling constants strongly confirmed the 16 α orientation. It was to be expected that the signals of the Ring D carbon atoms are split into doublets in the spectra of the fluorosteroids **3a** - **3d**. The coupling constant $^1J(\text{C},\text{F})$ was found to be - 178.5 Hz, which agrees with the value for fluorocyclopentane quoted in the literature (- 173.5 Hz) [2]. The coupling constants $^2J(\text{C},\text{F})$ were 21.7 Hz for C(17) and 23.1 Hz for C(15). The coupling constants $^3J(\text{C},\text{F})$ for C(14) turned out to be 4.9 Hz and for C(13) 6.1 Hz. Because of the greater dihedral angle the larger value of C(13) can only be explained by 16 α -F in the Karplus equation. 16 β -F would have caused a larger value for C(14).

Table 1. ^{13}C chemical shifts of estradiol (**1a**) and its sulphamates, of 17α -estradiol (**2a**) and its sulphamates and of 16α -fluoroestradiol (**3a**) and its sulphamates

C atom	1a	1b	1c	1d	2a	2b	2c	2d	3a	3b	3c	3d
1	126.0	126.9	127.2	127.0	127.1	127.6	127.1	127.1	126.0	126.4	126.0	126.3
2	112	119.5	113.8	119.6	113.5	120.1	113.5	119.7	112.6	118.9	112.6	118.9
3	154.0	148.7	156.0	148.9	155.1	149.4	155.2	149.0	154.3	148.0	154.3	148.1
4	115.0	122.4	116.1	122.6	116.0	123.1	116.0	122.6	115.1	121.9	115.0	121.8
5	137.8	139.6	138.7	139.2	138.8	139.7	138.7	139.0	137.7	138.7	137.4	138.2
6	29.4	29.9	30.6	29.9	30.6	30.7	30.5	30.0	29.4	29.2	29.1	29.0
7	27.1	27.4	28.4	27.4	29.0	28.9	28.8	28.3	27.1	26.8	26.9	26.6
8	38.7	39.0	40.2	38.8	40.0	40.0	39.9	39.4	38.1	37.6	37.8	37.4
9	43.7	44.6	45.2	44.5	44.5	45.0	44.2	44.3	43.7	43.8	43.3	43.5
10	131.5	139.0	132.3	138.9	132.7	140.3	132.3	139.3	131.2	138.4	130.6	138.1
11	26.1	26.7	27.4	26.5	27.1	27.3	26.9	26.5	25.7	25.5	25.4	25.2
12	36.5	37.1	37.7	36.8	32.7	32.9	32.5	32.2	36.4	36.2	35.9	35.9
13	43.0	43.6	44.4	43.7	46.3	46.5	46.3	45.9	43.8	43.7	43.9	43.9
14	49.8	50.5	50.5	49.8	49.0	48.9	49.4	49.3	47.7	47.7	47.2	47.2
15	22.8	23.4	24.0	23.5	25.1	25.3	24.9	24.6	31.5	31.5	31.3	31.4
16	29.7	30.1	28.9	28.2	32.3	32.6	31.0	30.7	101.1	101.0	97.9	97.8
17	81.3	81.7	90.2	89.9	80.5	80.6	91.2	90.3	87.0	86.9	94.0	93.8
18	10.8	11.3	12.2	11.9	17.8	17.9	17.3	16.8	12.0	12.0	12.4	12.4

Reference

- [1] Römer J., Steinbach J. and Kasch H. (1999) Syntheses and characterization of the sulphamates of 17β -estradiols and 16α -fluoroestradiol. *This report*, pp. 40-46.

12. Technetium and Rhenium-Labelled Steroids

7. Synthesis and Receptor Binding of Novel Progesterone-Rhenium Complexes

F. Wüst, M. B. Skaddan¹, K. E. Carlson¹, P. Leibnitz², J. A. Katzenellenbogen¹, H. Spies, B. Johannsen

¹Department of Chemistry, University of Illinois, Urbana, IL, USA

²Bundesanstalt für Materialforschung, Berlin

Introduction

In an effort to develop radiopharmaceuticals useful for diagnostic imaging of steroid receptor-positive breast tumours, several progesterone receptor ligands containing a bulky N₂S₂ (e.g. BAT, MAMA) rhenium and technetium chelate have been explored. The complexes obtained represent stereoisomers which were not completely separable. The remarkably high receptor affinity of some of these conjugates is compromised by a high nonspecific binding due to high lipophilicity [1].

To extend our current research aimed at technetium tracers capable of binding to steroid hormone receptors, we explored the usefulness of small-sized neutral mixed-ligand complexes, thioether-carbonyl complexes and organometallic complexes. In our preliminary investigations, rhenium was used as a model for the radioactive technetium. Starting from 21-hydroxyprogesterone (deoxycorticosterone), we prepared various progesterone-rhenium chelates containing the rhenium metal at the oxidation states +5, +3 and +1.

Experimental

Starting from commercially available deoxycorticosterone, the 21-hydroxy group was converted into a thiol group, N-formyl amine group and dithioether unit required for the formation of rhenium complexes according to the "n+1" mixed-ligand design and dithioether-carbonyl design. The attachment of a cyclopentadienyltricarbonylrhenium(I) moiety was accomplished by an ester formation involving the 21-hydroxy group.

Results and Discussion

21-Mercaptoprogestosterone **1** was subjected to standard conditions [2] for the formation of the "3+1" mixed-ligand complexes **2** and **3** by means of two different oxorhenium(V) precursors **4** and **5** (Fig. 1).

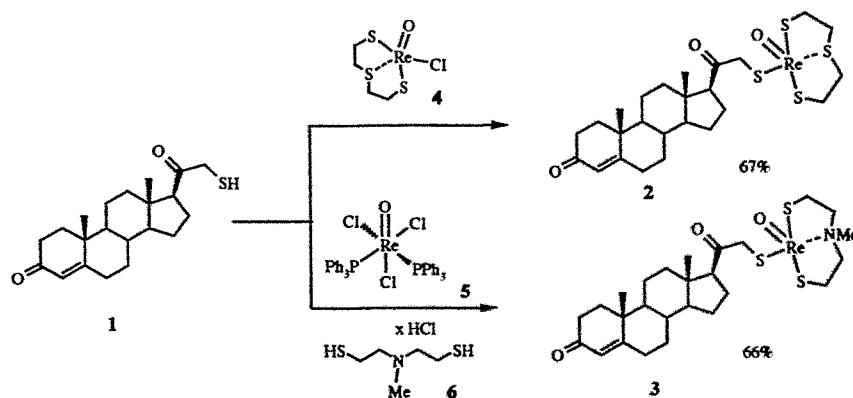


Fig. 1. Synthesis of "3+1" mixed-ligand complexes

The reaction of the chlorine containing oxorhenium(V) precursor **4** with thiol **1** in refluxing acetonitrile gave the "SSS" mixed-ligand complex **2** in a good yield (67 %) as brown crystals. The alternative "SNMeS" complex **3** was obtained by the reaction of the oxorhenium(V) precursor **5** with the monodentate thiol ligand **1** and tridentate "SNMeS" ligand **6** in refluxing 1 N methanolic NaOAc.

Suitable crystals of **2** for X-ray single crystal analysis were obtained by slow crystallization of **2** from acetone/n-hexane solution at room temperature. The X-ray structure of complex **2** is shown in Fig. 2.

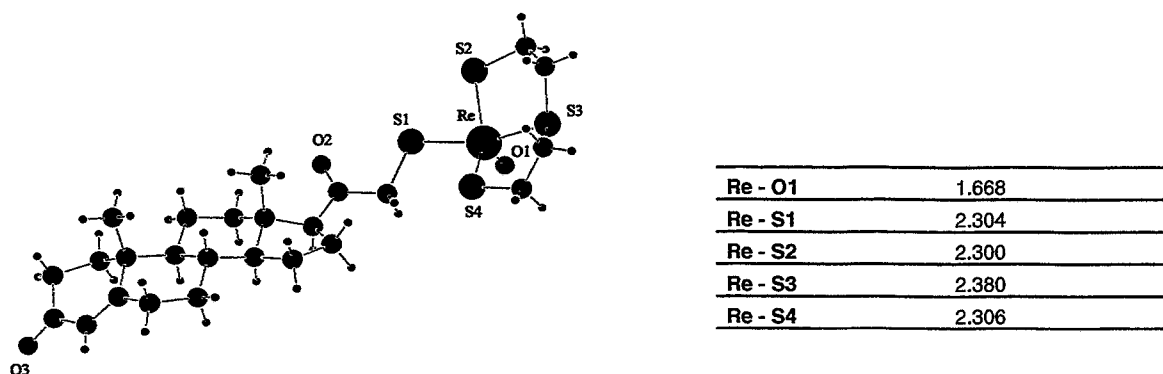


Fig. 2. X-ray structure and selected bond lengths [\AA] of complex **2**

The four sulphur donor atoms are arranged in a square-pyramidal geometry around the oxorhenium(V) core as is typical of "SSS"-coordinated "3+1" mixed-ligand complexes. The square-pyramidal chelate moiety exhibits an *anti*-like orientation with respect to the β -orientated methyl groups at positions 10 and 13 of the progesterone molecule.

Alternatively, a "4+1" mixed-ligand design [2] is based on rhenium and technetium in the oxidation state +3. The tetradentate ligand $\text{N}(\text{CH}_2\text{CH}_2\text{-SH})_3$ fills four of the five coordination sites of the metal(III) core, the remaining position being occupied by a monodentate isocyanide ligand. The "4+1" complex **9** was conveniently prepared in one step by reaction of the phosphane-containing tripodal rhenium(III) precursor **8** with an isocyanide generated in situ. Starting from formamide **7**, we used POCl_3 /diisopropylamine as a dehydrating agent to prepare the corresponding isocyanide. The isocyanide immediately undergoes a substitution of the phosphane ligand in **8**. This procedure avoids the isolation of the free isocyanide, and gives complex **9** in a modest yield (53 %) as an olive-green solid (Fig. 3).

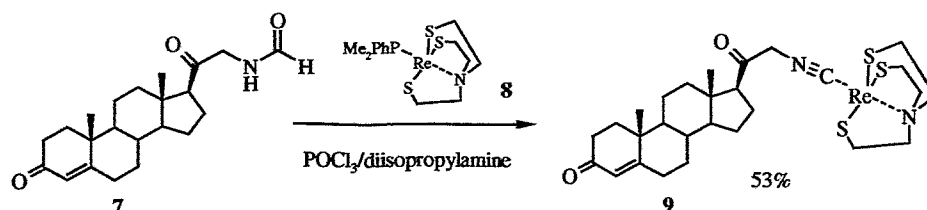


Fig. 3. Synthesis of "4+1" mixed-ligand complex **9**

A bromotricarbonylrhenium(I) moiety was attached to the dithioether **10** as inaugurated by *Alberto et al.* [3]. The two soft donor sulphur atoms of the dithioether unit replace two of the three bromine atoms of precursor **11**, to give the neutral rhenium(I) complex **12** in a good yield (79 %) (Fig. 4).

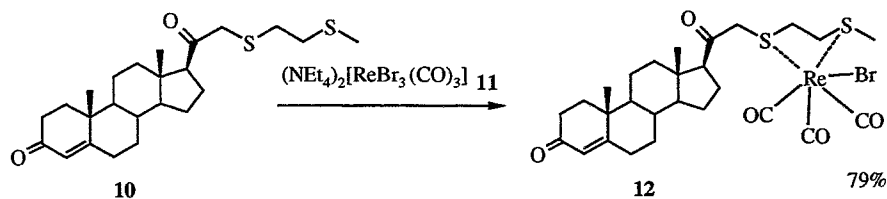


Fig. 4. Synthesis of complex **12**

^1H NMR analysis of complex **12** reveals the formation of a 1:1 diastereomeric mixture. The attachment of the tricarbonyl bromo rhenium(I) core through the thioether sulphur leads to a rhenium(I) chelate where the rhenium is a stereogenic centre (Fig. 5). Furthermore, the coordination of the thioether sulphur also results in the formation of chiral sulphur donor atoms.

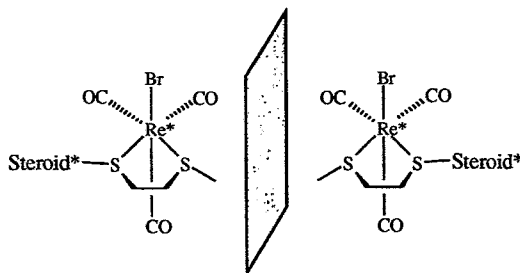


Fig. 5. Diastereomeric rhenium complexes

An organometallic cyclopentadienyltricarbonylrhenium(I) complex **15** was synthesized in an excellent yield (96 %) by coupling 21-hydroxyprogesterone **13** with cyclopentadienyl tricarbonyl rhenium(I) carboxylic acid **14** by means of 1-ethyl-3-(3-dimethylaminopropyl)carbodiimide (EDC) as the dehydrating agent and DMAP as the catalytic base (Fig. 6). Rhenium(I) precursor **14** was easily obtained by a central metal exchange reaction starting from ferrocene dimethylester [4].

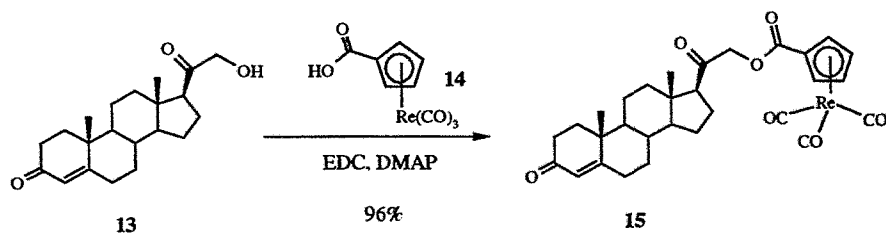


Fig. 6. Synthesis of cyclopentadienyltricarbonylrhenium(I) complex **15**

The complexes were used in a competitive receptor-binding assay (rat uterine cytosol, 0 °C) to determine their binding to the progesterone receptor (PgR) (Table 1).

Table 1. Relative binding affinities (RBAs) of 21-substituted progesterone rhenium complexes for the progesterone receptor ($RBA_{RU\ 5020} = 100$).

Compound	RBA (0 °C)
2	4.7
3	9.0
9	1.5
12	0.02
15	2.2

The best affinity of 9 % ($RU\ 5020 = 100\ %$) was obtained with "3+1" mixed-ligand complex **3** containing a NMe group as the central donor atom in the tridentate ligand part. This value reflects a relative binding affinity of 75 % compared with the parent molecule progesterone.

We described the preparation of several new PgR binding ligands labelled with rhenium by four different means - three inorganic complexes and one organometallic complex - and we have shown that some of these have substantial binding affinity for the progesterone receptor. Further investigations concerning the in vivo stability of all complexes are planned using the corresponding technetium-99m complexes.

References

- [1] O'Neil J. P., Carlson K. E., Anderson C. J., Welch M. J. and Katzenellenbogen J. A. (1994) Progestin radiopharmaceuticals labeled with technetium and rhenium: Synthesis, binding affinity, and in vivo distribution of a new progestin N_2S_2 -metal conjugate. *Bioconjugate Chem.* **5**, 182-193.
- [2] Spies H., Fietz T., Glaser M., Pietzsch H.-J. and Johannsen B. (1995) The "n+1" concept in the synthesis strategy of novel technetium and rhenium tracers. In: *Technetium and Rhenium in Chemistry and Nuclear Medicine 4* (M. Nicolini, G. Bandoli, U. Mazzi Eds.) SGEEditoriali, Padova, pp. 243-246.
- [3] Alberto R., Schibli R., Egli A., Schubiger P. A., Herrmann W. A., Artus G. M., Abram U. and Kaden T. A. (1995) Metal carbonyl syntheses XXII. Low pressure carbonylation of $[MOCl_4]^-$ and $[MO_4]^-$ technetium(I) and rhenium(I) complexes $[NEt_4]_2 [MCl_3 (CO)_3]$. *J. Organomet. Chem.* **493**, 119-127.
- [4] Spradau T. W. and Katzenellenbogen J. A. (1998) Preparation of cyclopentadienyltricarbonyl-rhenium complexes using a double ligand-transfer reaction. *Organometallics* **17**, 2009-2017.

13. Technetium and Rhenium-Labelled Steroids

8. "3+1" Mixed-Ligand Complexes According to the Integrated Design

F. Wüst, H.-J. Pietzsch, P. Leibnitz¹, H. Spies

¹Bundesanstalt für Materialforschung, Berlin

Introduction

The synthesis of metal-containing complexes capable of mimicking the steric structure of steroids represents an alternative integrated design for the synthesis of steroid receptor-binding ligands. Here the characteristics of the metal-containing complex are associated with the steric and functional contours of the receptor ligand.

Studies of the potent nonsteroidal estrogen diethylstilbestrol (DES) showed that the ER can accommodate a second phenol ring that mimics the 17 β -hydroxy-substituted D-ring. DES has been shown to possess a trans-stilbene structure and the distance between both oxygen atoms, which plays an important role in receptor binding, is 12.13 Å. This distance is close to that of 3,17 β -estradiol (10.9 - 11.0 Å) [1, 2].

The further expansion of metal-containing steroid mimics on oxorhenium(V) and oxotechnetium(V) complexes according to the "3+1" mixed-ligand concept and knowledge of the structural requirements for binding to the ER [1, 2] resulted in the design of an oxometal(V) complex (Fig. 1.) as a DES mimic.

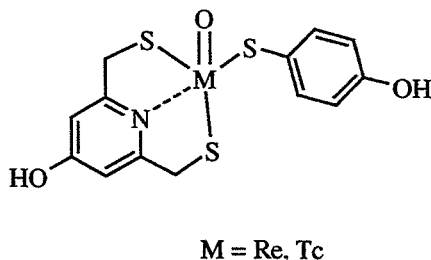


Fig. 1. "3+1" mixed-ligand complex as a DES mimic

Results and Discussion

In our preliminary investigations we simplified the structure of the target molecule by removing the hydroxy group of the pyridine ring. Thus, commercially available 2,6-dimethanopyridine **1** could be used. Its conversion into the corresponding tridentate "SNS" ligand **2** is shown in Fig. 2.

Chlorination of the alcohol **1** by means of thionyl chloride in chloroform generated the corresponding chloro derivative. Treatment of the dichloro compound with thiourea in refluxing EtOH yielded the isothiuronium salt, which was then saponified with NaOH to release thiol **2** in a total yield of 50%.

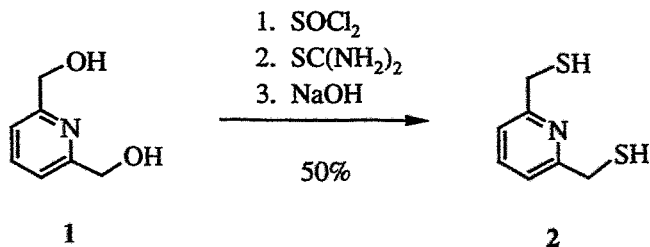


Fig. 2. Synthesis of the tridentate "SNS"-ligand **2**

The formation of the "3+1" mixed-ligand complexes **6** - **8** was achieved by the common reaction of the oxorhenium(V) precursor **6** with the monodentate thiols **3** - **5** and the tridentate "SNS" ligand **2** (Fig. 3.). The complexes **7** - **9** were obtained in moderate yields of 48 % - 57 %.

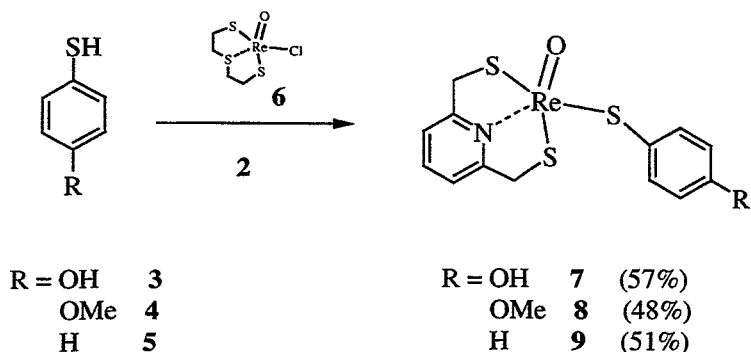


Fig. 3. Complex formation of the steroid mimics **7** - **9**

For compound **8** crystals suitable for an X-ray single crystal analysis were obtained. The X-ray structure of complex **8** is given in Fig. 4.

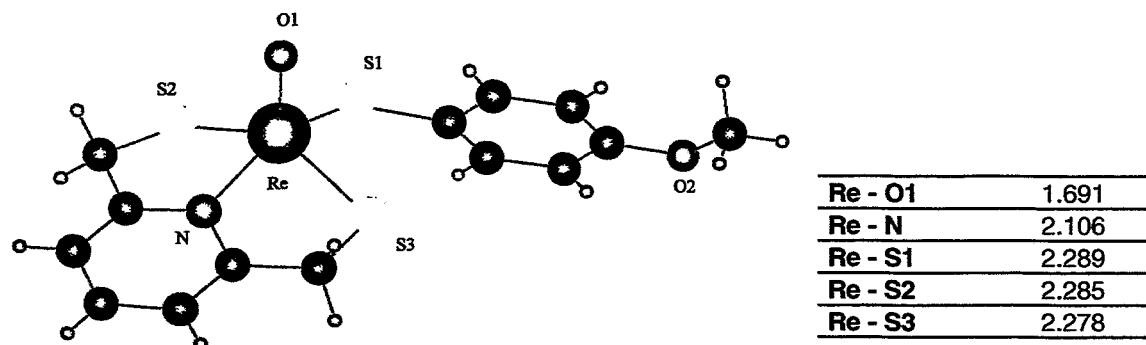


Fig. 4. X-ray structure of complex **8** and selected bond lengths (Å)

Complex **8** exhibits the usual square-pyramidal arrangement of the four donor atoms (SNS-S) around the $[\text{Re}=\text{O}]^{\text{O}+}$ core. The tridentate ligand part used represents a novel set of donor atoms capable of forming "3+1" mixed-ligand complexes, being two benzylic sulphur atoms and a pyridine nitrogen. The pyridine nitrogen is less basic than the central tertiary amine nitrogen of the "SNMeS" ligand, which is otherwise employed.

In an even more simplified structure according to the Integrated Design complex **10** is used. Simple reaction of 4-hydroxy thiophenol **3** with the chlorine-containing oxorhenium(V) precursor **6** afforded complex **10** in a 33 % yield (Fig. 5.).

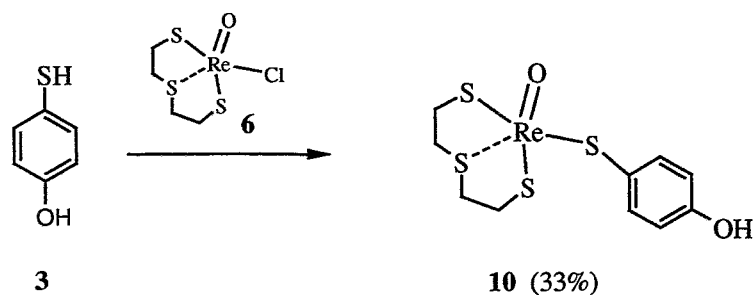


Fig. 5. Synthesis of complex 10

All complexes display the characteristic Re=O stretching band in the IR-spectra, being 961 cm^{-1} for **10**, 965 cm^{-1} for **7**, 965 cm^{-1} for **8** and 968 cm^{-1} for **9**.

References

- [1] von Angerer E. (1995) In: Molecular Biology Intelligence Unit. The estrogen receptor as target for the rational drug design. R. G. Landes, Company Ed. Springer-Verlag, Heidelberg.
- [2] Anstead G. M., Carlson K. E. and Katzenellenbogen J. A. (1997) The estradiol pharmacophore: Ligand structure-estrogen receptor binding affinity relationship and a model for the receptor binding site. *Steroids* **62**, 268-303.

14. Nicotinamide-Substituted Complexes as Redox Markers

2. Synthesis of a ^{99}Tc Dihydropyridine Mixed-Ligand Complex and Investigation of the Stability in Tissue Homogenates

A. Rother¹, T. Knieß, M. Pütz¹, H. Jungclas¹, H. Spies

¹Universität Marburg, Fachbereich Kernchemie

Introduction

Diagnostic nuclear medicine provides valuable information on a variety of disease states. In recent years there has been an increasing interest in tracers able to visualise biochemical reactions in vivo. For imaging the various redox processes occurring in the organism the development of redox-active radiotracers is needed. The search for Tc tracers in this field is in its infancy. First technetium complexes with 2-nitroimidazoles that are enzymatically reducible in the organism and accumulate in hypoxic tissue and in tumour cells were studied in vivo some years ago [1, 2]. Recently ^{64}Cu -labeled complexes based on bis(thiosemicarbazone) and bis(salicylaldimine) ligands were prepared and tested for cell uptake under normoxic and hypoxic conditions [3]. Looking for technetium chelates bearing a pyridinium salt/dihydropyridine moiety by analogy to the NAD^+/NADH redox system we developed a mixed-ligand rhenium pyridinium complex [4]. Re serves as a surrogate for $^{99\text{m}}\text{Tc}$ and describes the reduction with sodium dithionite to the dihydropyridine compound. In the present paper we report the synthesis of a ^{99}Tc pyridinium salt complex according to the "3+1" principle and its characterisation by ^1H NMR-, ^{13}C NMR spectroscopy and X-ray structure analysis. After conversion to the corresponding 1,4-dihydropyridine compound the stability of the ^{99}Tc dihydropyridine complex in buffer, tissue homogenates, blood plasma and cerebrospinal fluid and its dependence on temperature was investigated.

Experimental

General

HPLC-investigations were carried out with an analytical RP18 column (Lichrospher 100 RP-18, 5 μm , MERCK) and a semi-preparative RP column (Ultrasorb 5 ODS, 20 μm , PHENOMENEX) using a 3:1 mixture of iso-propanol/phosphate buffer (10 mmol, pH = 7.0) as eluent with a flow rate of 0.2 ml/min or 0.8 ml/min respectively. The products were determined by UV absorbance at 254 nm and by β -detection with a scintillation detector (Ramona 90, RAYTEST). The NMR spectra were recorded on an FT-Spectrometer ARX 500 (BRUKER) in DMSO-d_6 . The UV/VIS spectroscopic measurements were carried out with a diode array spectrometer with 1024 diodes (J & M ANALYTISCHE MESSTECHNIK). The x-ray structure analysis was performed on a Image Plate Detector System (STOE) with MoK_α x-rays (71.07 pm) and calculated with the programs Stoe Expose, Stoe Cell and Stoe Integrate.

Preparation of [^{99}Tc](1-Methyl-3-pyridinyl-ethylcarbamoyl-thiolato)(3-thiapentan-1,5-dithiolato)oxotechnetium(V)-iodide **2**.

54 ml of an aqueous $\text{NH}_4^{99}\text{TcO}_4$ solution ($c = 4.64 \text{ mmol/l}$, 250 μmol) was added to 5.45 g (25 mmol) sodium d-gluconate dissolved in 10 ml water. Reduction to ^{99}Tc gluconate was carried out by addition of 15 ml 0.02 M solution of stannous chloride (20 mmol) in 0.1M HCl. After complete reduction 486 mg (1.5 mmol) 3(2-mercaptoethyl carbamoyl)-1-methylpyridinium iodide **1** dissolved in 5 ml water was added followed by 25 ml acetonitrile after 25 minutes and 39 mg (250 μmol) 3-thia-1,5-pentanedithiol dissolved in 5 ml acetonitrile. The reaction mixture was evaporated to 5 ml and the product was purified by preparative HPLC. Yield: 96 mg (163 μmol , 65 %), M.p. 190 – 194 °C.

^1H NMR (DMSO-d_6) δ [ppm]: 2.26 (2H, td), 3.03 (2H, td), 3.67 (2H, q), 3.86 (2H, t), 4.08 (2H, dd), 4.30 (2H, dd), 4.39 (3H, s), 8.22 (1H, t), 8.88 (1H, d), 9.09 (1H, d), 9.30 (1H, t), 9.39 (1H, s);

^{13}C NMR (DMSO-d_6) δ [ppm]: 34.94 (CH_2), 42.64 (CH_2), 43.04 ($2\times\text{CH}_2$), 45.74 ($2\times\text{CH}_2$), 48.22 (CH_3), 127.33 (C_{ar}), 133.29 (C_{ar}), 142.63 (C_{ar}), 145.45 (C_{ar}), 147.07 (C_{ar}), 161.19 (CO).

Preparation of [^{99}Tc](1-Methyl-3-(1,4)dihydropyridinyl-ethylcarbamoyl-thiolato)(3-thiapentan-1,5-dithiolato)oxotechnetium(V) **3**

8.0 ml diethyl ether was added to 0.6 g (3.45 mmol) sodium dithionite and 0.48 g (3.45 mmol) sodium carbonate dissolved in 2.0 ml water. To this biphasic system 10 mg (17 μmol) **2** dissolved in 0.5 ml water was added and the mixture was refluxed for 20 minutes with vigorous stirring. After cooling the organic layer was separated and at -18°C concentrated in vacuum to 1.0 ml. This ethereal solution of

the product **3** is stable for one day at $-18\text{ }^{\circ}\text{C}$ and was used for the UV/VIS spectrometric investigations without purification.

*UV/VIS spectrometric investigations of kinetic and stability of the **3** in buffer and tissue homogenate*

For investigation of the kinetics of **3** in different media 0.1 M phosphate buffers at pH 6.7 - 7.6 were used. The homogenates of kidney, liver and brain were diluted with phosphate buffer pH = 7.4. Blood plasma and cerebrospinal fluid were used without dilution. The measurements were performed at $20\text{ }^{\circ}\text{C}$ and at $37\text{ }^{\circ}\text{C}$ with 1.0 cm standard cuvettes in a temperature-controlled cuvette holder. For the kinetic measurements 100 μl of the ethereal solution of **3** was added to 2.0 ml buffer in the cuvette and the diethyl ether was removed by passing a stream of argon. The samples were measured at regular intervals of 10 seconds over a period of 15 minutes. The decrease in the absorption at 365 nm served as the criterion for the decay of the dihydropyridine complex.

Results and Discussion

The synthesis of the (1-methyl-3-pyridinyl ethylcarbamoyl thiolato)-(3-thiapentan-1,5-dithiolato)oxotechnetium(V) iodide **2** was carried out according to the "3+1" principle by reaction of ^{99}Tc gluconate with the monodentate ligand 3(2-mercaptoethyl carbamoyl)-1-methyl pyridinium iodide **1** [4] and the tridentate 3-thia-1,5-pentanedithiol (Fig. 1). The corresponding 4:1 complex of monodentate ligand and technetium is observed as intermediate [4]. After addition of the tridentate the resulting complex **2** was purified by HPLC.

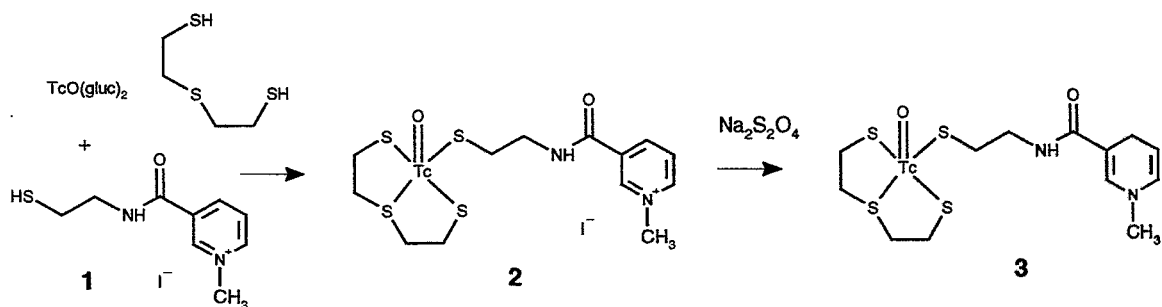


Fig. 1. Reaction pathway for the synthesis of the ^{99}Tc complexes **2** and **3**.

The molecular structure of complex **2** was established by crystallographic means. The X-ray structure reveals that the monodentate and the tridentate ligand form a square pyramid with distorted basal surface and the oxygen in an axial position (Fig. 2). The Tc-O bond distance was found to be 1.68 \AA , the average Tc-S bond distance is 2.32 \AA whilst the thioether metal bond has a distance of 2.37 \AA because of the coordinative character of this bond.

The reduction of **2** to the complex **3** with sodium dithionite in pure 0.1 M potassium carbonate was not a successful way to isolate the dihydropyridine because the basic conditions lead to rapid decomposition of the complex. So we looked for an alternative procedure that was realised by using a biphasic system diethyl ether/water according to a literature procedure [6]. After vigorous stirring the lipophilic dihydropyridine complex **3** accumulated in the organic phase and could be separated. UV/VIS investigations showed that the dihydropyridine in ethereal solution is stable for 24 hours whereas in alkaline solution it rapidly decomposes.

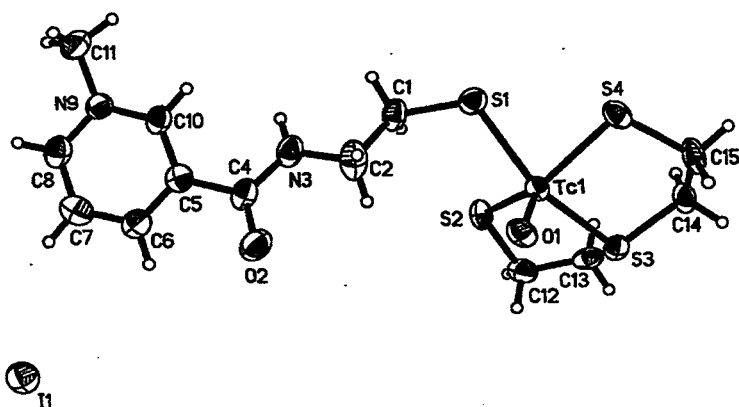


Fig. 2. Molecular structure of **2**. Selected bond length [Å] and angles [°]: Tc-O1 1.680(6), Tc-S1 2.320(3), Tc-S2 2.288(3), Tc-S3 2.372(3), Tc-S4 2.294(3), O1-Tc-S1 105.3(3), O1-Tc-S2 114.6(3), O1-Tc-S3 101.8(3), O1-Tc-S4 114.8(3)

For the kinetic investigations of the stability the UV spectrum of the dihydropyridine complex **3** was recorded in phosphate buffer at various pH's. The samples were measured at regular intervals of 10 seconds over a period of 15 minutes. Dihydropyridines are characterized by a strong UV absorption at 360 nm [7] that decrease with oxidation to the pyridinium salt. Figure 3a shows a typical UV/VIS spectrum of **3** at pH = 6.97 and 20 °C. The declining absorption at 360 nm was used as a basis for the decay of the dihydropyridine complex. The increasing band at 270 nm is characteristic of the pyridinium salt that had a maximum absorption at 265 nm. The appearance of an isobestic point at 315 nm may serve as proof of a pure two-compound system. The drop in the absorption at 360 nm over time described an exponential function and in this way the half life of the re-oxidation was established as a criterion for the stability. In Figure 3b the decay of the dihydropyridine complex **3** depending as a function of time is shown and it is obvious that 600 seconds after start of the measurement mostly all of the dihydropyridine had decomposed.

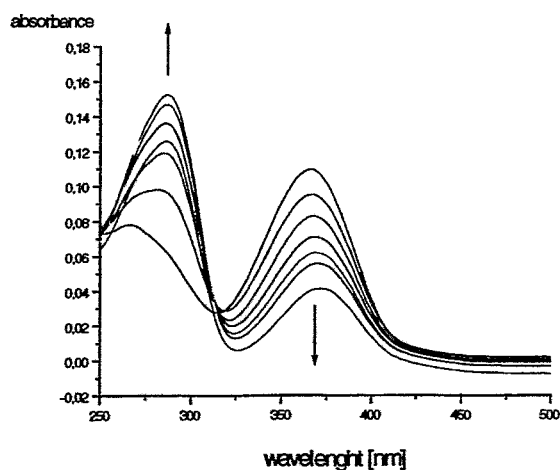


Fig. 3a. UV/VIS spectrum of complex **3** at pH = 6.97 over 10 minutes, the arrows show the course of measurement.

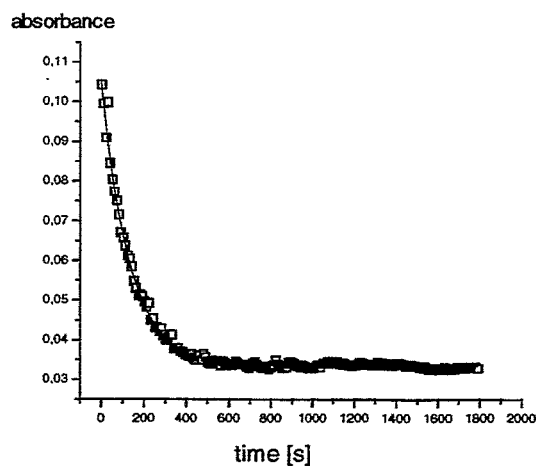


Fig. 3b. Exponential decrease in the absorption of **3** at 360 nm at pH = 6.97 over the time.

To investigate the stability of **3** as a function of pH and temperature 0.1 M phosphate buffers were used with the physiological relevant values between pH = 6.7 - 7.6 at 20 °C and at 37 °C. The tissue homogenates of kidney, liver and brain were diluted with 0.1 M phosphate buffer (pH = 7.4) and tested at 37 °C. Because of the turbidity of the biological materials caused by suspended particles that could not be removed by centrifugation, the probes had a high background UV absorption. The absorbance

at 360 nm was near 2.0 and the decreasing extinction values can only show tendencies. Table 1 gives an overview of the half-lives of the complex **3** in various media and selected temperatures.

Table 1. Half-life times of complex **3** in various media and selected temperatures

pH	Temperature [°C]	Media	Half-life time [s]
6.72	37	phosphate buffer	178
6.79	20	phosphate buffer	53
6.94	37	phosphate buffer	134
6.97	20	phosphate buffer	117
7.15	37	phosphate buffer	107
7.17	20	phosphate buffer	160
7.34	37	phosphate buffer	80
7.60	37	phosphate buffer	41
7.60	20	phosphate buffer	394
7.40	37	kidney homogenate	102
7.40	37	liver homogenate	45
7.40	37	brain homogenate	144
7.40	37	blood plasma	133

Considering the half-life times it is remarkable that the stability decreases with increasing pH, whereas at room temperature the relationship is inverted. In liver homogenate a significantly faster decomposition than in other tissue homogenates was observed and in blood plasma the dihydropyridine is more stable which is in accordance to previous work by Bodor et al. [8]. In cerebrospinal fluid the complex is notably more stable than in all other media. No exponential course of decomposition was observed here, the concentration of **3** declines linearly.

As a result of the studies of the stability of the dihydropyridine complex **3** in buffer and tissue homogenate it must be concluded that the dihydropyridine ^{99m}Tc-mixed-ligand complex **3** with half-lives between 40 and 400 seconds is not stable enough for further biological experiments and preparation of the corresponding ^{99m}Tc derivative is not useful. Future work will focus on improvements to the stability of the dihydropyridine by introduction of electron withdrawing substituents such as benzyl or isopropyl at the pyridinium nitrogen. Bromine substitution in the 5-position of the pyridinium ring and the utilisation of the chinolinium salt/dihydrochinoline system also has a stabilising effect [5]. Another option might be to employ a tetradentate ligand system where a higher stability of the chelate against the reducing media sodium dithionite/alkali is expected.

References

- [1] Ballinger J. R., Wan Min Kee J. and Rauth A. M. (1996) In vitro and in vivo evaluation of a technetium-99m labeled 2-nitroimidazole (BMS 181321) as a marker of tumor hypoxia. *J.Nucl.Chem.* **37**, 1023-1030.
- [2] Nunn A., Lindner K. and Strauss H. W. (1995) Nitroimidazoles and imaging hypoxia. *Eur. J. Nucl. Med.* **22**, 265-280.
- [3] Dearling J. L. J., Mullen G. E. D., Lewis J. S., Rae M. T., Zweit J. and Blower P. J. (1998) Hypoxia-targeting radiopharmaceuticals: selective uptake of copper-64 complexes by hypoxic cells in vitro. *Eur. J. Nucl. Med.* **25**, 854.
- [4] Knies T., Spies H., Brandau W. and Johannsen B. (1998) Nicotinamide-substituted complexes as redox markers. 1. Synthesis and UV investigation of rhenium and technetium mixed-ligand systems. *J. Labelled Comp. Radiopharm.* **41**, 605-614.
- [5] Pop E. (1997) Optimization of the properties of brain specific chemical delivery systems by structural modifications. *Current Med. Chem.* **4**, 279-294.
- [6] Wong Y. S., Marazano C., Gnecco D. and Das C. (1994) 1,4-Dihydropyridines from dithionite reduction of pyridinium salts without electron-withdrawing groups as substituents. *Tetrah. Lett.* **35**, 707-710.
- [7] Lehninger A. L., Nelson D. L. and Cox M. M. (1994) Prinzipien der Biochemie, *Spectrum Akadem. Verlag, Heidelberg*, p. 458.
- [8] Bodor N. and Abdelalim A. M. (1984) Improved delivery through biological membranes XIX: Novel redox carriers for brain-specific chemical delivery systems. *J. Pharm. Sci.* **74**, 241-245.

15. Evaluation of the In Vitro and In Vivo Properties of a Potential Tc-Labelled Inhibitor of the MDR Gene Product P-Glycoprotein

R. Bergmann, P. Brust, H.-J. Pietzsch, M. Scheunemann, S. Seifert, B. Johannsen

Introduction

Resistance of malignant tumours to chemotherapy is a major cause of treatment failure [1 – 3]. One of the important mechanisms is overexpression of the human multidrug resistance gene (MDR1) [4]. On the other hand, MDR gene transfer and expression in bone marrow cells followed by autologous bone marrow transplantation in patients with advanced cancer is seen as a strategy to minimize the risks of high-dose chemotherapy [5]. Monitoring the functional expression of the gene products or the successful gene transfer may be a prerequisite for the therapy, i.e. it is required to study the functional expression of the gene products. Its overexpression has been demonstrated to contribute to the multidrug resistance (MDR) phenotype of many human cancers. The gene product P-glycoprotein (Pgp) is present in the plasma membrane not only of tumour cells but also of several normal tissues, including the brain endothelial cells forming the blood-brain barrier (BBB) and the intestinal epithelium [6]. It acts as an energy-dependent efflux pump which allows the transport of a wide range of structurally and functionally unrelated cytotoxic drugs out of tumour cells, including doxorubicine, vincristine, vinblastine and many others (for review see [7]). These substances tend to be lipophilic, cationic compounds [8]. Additionally, a number of drugs called MDR modulators have been identified that are non-toxic in themselves (calcium channel blockers, anti-arrhythmics, antidepressants and many others) but can reverse Pgp-mediated MDR. These drugs, such as verapamil, quinidine and cyclosporin-A, make MDR tumour cells sensitive to coadministered cytotoxic agents. However many of them are of limited clinical use due to side effects in the relevant doses [9]. On the other hand they may be of potential use for the development of radiopharmaceuticals for PET and SPECT imaging. Thus, [^{11}C]daunorubicin and [^{11}C]verapamil both have potential for in vivo probing of Pgp with PET [10, 11]. The only available clinical radiopharmaceuticals for studying the expression of Pgp with SPECT are the lipophilic $^{99\text{m}}\text{Tc}$ cations hexakis(2-methoxy-isobutyl-isonitrile)technetium(I), [$^{99\text{m}}\text{Tc}$]sestamibi, [12, 13] and trans-dioxo-bis(diphosphine)-technetium(V), [$^{99\text{m}}\text{Tc}$]tetrofosmin, (for review see [14]. Some $^{99\text{m}}\text{Tc}$ (III)-complexes of the Q-series are currently under investigation [15].

It was recently suggested that a set of structural elements was required for an interaction of drugs with Pgp. The recognition elements were formed by 2 or 3 electron donor groups with a fixed spatial separation [16]. The investigation of neutral and monoprotonated forms of a large number of compounds revealed that, in parallel with the commonly recognized critical sites (such as polycyclic ring systems and N-substituted moiety), the molecular profile of hydrophobicity is a specific structural determinant for the anti-MDR activity of these drugs [17]. Based on these findings we examined various '3+1' mixed-ligand technetium(V) and rhenium(V) complexes containing electron donor groups such as protonable nitrogen and aromatic moieties as prerequisites for MDR modulation [18 – 20]. We demonstrate that one of these novel complexes shows a strong inhibition of Pgp-mediated transport function in vitro (immortalized rat brain endothelial cells) and in vivo (organ distribution in rats). These experiments were performed in comparison with classical MDR modulators. A multitracers approach was used to investigate simultaneously the effects of Pgp modulators on the function of Pgp and basic physiological and metabolic parameters such as the glucose metabolism. Toxic effects resulting in disturbances of the cell metabolism may thus also be observed in these in vitro and in vivo studies.

Experimental

Preparation of the complexes and tracers used

Synthesis of the ligands, the preparation of the oxorhenium(V) and the Tc-99 complexes (Fig. 1), the complex purification, and the quality control technique were based on the previously described general methods after minor modification [18]. The preparation of the n.c.a. $^{99\text{m}}\text{Tc}$ complex 3-thiapentane-1,5-dithiolato){[N-(3-phenylpropyl)-N-2(3-quinazoline-2,4-dionyl)ethyl]aminoethylthiolato}oxotechnetium(V) using a ligand-exchange reaction followed by HPLC purification was described in detail [22].

[^3H]vinblastine (670 GBq/mmol) and [^3H]vincristine (370 GBq/mmol) were obtained from Amersham Buchler, Braunschweig, Germany. [^3H]colchicine (2.73 TBq/mmol) was purchased from NEN/DuPont, Germany. 2-[^{18}F]fluoro-2-deoxy-D-glucose was kindly provided by the Rossendorf PET Center [21]. [$^{99\text{m}}\text{Tc}$]sestamibi (Cardiolite, Du Pont Pharma GmbH, Germany) and [$^{99\text{m}}\text{Tc}$]tetrofosmin (Myoview, Amersham, Germany) were prepared from commercially available kits according to manufacturer's instructions and added to the control solution (see below) at a final concentration of 1 MBq/ml (<10 nM in all experiments).

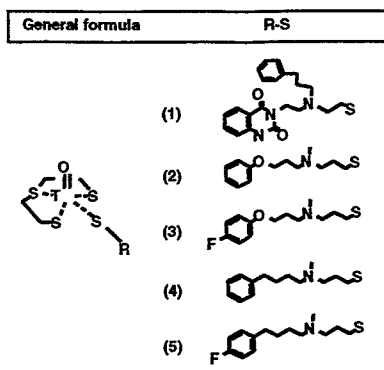


Fig. 1. "3+1" mixed-ligand ^{99m}Tc complexes

Tracer uptake studies

Immortalized rat brain microvessel endothelial cells (RBE4) (23,24) were plated on tissue culture plates 24-well flat bottom Cell⁺® (Sarstedt, Inc., Newton, USA). Cells were grown in culture medium consisting of α -minimal essential medium (α -MEM)/Ham's F10 (GIBCO, Eggenstein; Germany) (1:1 vol/vol), supplemented by 2 mM glutamin, 10 % heat-inactivated fetal calf serum (Sigma, Deisenhofen, Germany) 1 ng/ml of basic fibroblast growth factor (bFGF) (Boehringer Mannheim) and 300 $\mu\text{g}/\text{ml}$ of geneticin (G418) (Sigma, Deisenhofen, Germany) in humidified 5 % $\text{CO}_2/95$ % air at 37 °C. In the 24-well cell culture plates the cells reached confluence after 3 - 4 days. The experiments were conducted at confluence with cell densities between 10^5 - 10^6 cells per well (equivalent to about 100 - 150 μg protein) of passage 30 - 40.

The solution used for the transport experiments was a modified culture medium consisting of α -minimal essential medium (α -MEM)/Ham's F10 (GIBCO, Eggenstein; Germany) (1:1 vol/vol), supplemented by 2 mM glutamin, and 1 % (v/v) albumin. The wash solution for clearing the extra-cellular space was phosphate-buffered solution containing Mg^{++} (0.5 mM) and Ca^{++} (0.9 mM). The uptake studies were performed using various tracers with up to four different isotopic labels, (^3H , ^{18}F , ^{99m}Tc , ^{99}Tc). The experiments were initiated by washing each of the 24-wells in the plate with α -MEM and by loading them with α -MEM containing the Pgp inhibitor under review (10 μM). After a preincubation period of 60 min the solutions were aspirated from the wells and replaced by 0.5 ml per well of the radioactive incubation medium to initiate transport. In addition to the radiotracers the media contained various drugs or $^{99}\text{Tc}(\text{V})$ complexes in concentrations ranging from 1 nM to 10 mM. At the end of the incubation period (after 60 min) the well plates were transferred onto ice (4 °C). Aliquots of the incubation medium from each well were used to calculate the free tracer concentration in the supernatant. The remaining medium was then aspirated and the cells were carefully rinsed four times with 1 ml of ice-cold washing solution. The remaining cells were solubilized by shaking them with 500 μl of modified 0.1 N NaOH with 1% sodium dodecyl sulphate. Aliquots were obtained for γ - and β -counting and for protein determination by the method of Lowry. All samples (aliquots of the stock incubation medium, of the supernatant after incubation and of the solubilised cells) were transferred to 4 ml vials containing Ultima Gold counting solution (Canberra-Packard, Dreieich, Germany). These vials were assayed for gamma activity in a multichannel well-type sodium iodine gamma counter (COBRA II, Packard Instrument Company, Meriden, USA) using two energy windows (110 - 180 keV and 450 - 1500 keV). After a minimum of 10 half-lives of the short-lived isotopes used (^{18}F , ^{99m}Tc), the count vials were assayed in a multichannel well-type beta counter (TRICARB, Packard Instrument Company, Meriden, USA) using two energy windows to determine the ^3H (0-20 keV) as well as ^{99}Tc contents (20-2000 keV) in the samples.

Animal experiments

Animal experiments were carried out according to the relevant national regulations. 0.5 MBq of ^{99m}Tc complex was injected into the tail veins of 5-6 weeks old Wistar rats. At 30 min p.i. the rats were sacrificed by heart puncture under ether anaesthesia. Selected organs were isolated for weighing and counting.

Calculations

All data were corrected for background, spill over, and decay. The amount of accumulated tracer in the cells was presented as a percentage of the total radioactivity per mg cell protein. The data (means \pm S.D.) were obtained in quadruplicate from preparations of the same cell culture in at least two independent experiments. Statistical analysis was performed using the two-tailed t-test with equal variances. Values of $p < 0.05$ (*), $p < 0.01$ (**), $p < 0.005$ (***) were considered significant.

Results and Discussion

In this study we describe the *in vitro* and *in vivo* properties of the complex 3-thiapentane-1,5-dithiolato)[[N-(3-phenylpropyl)-N-2(3-quinazoline-2,4-dionyl)ethyl]aminoethylthiolato]oxotechnetium(V) ($^{99/99m}\text{Tc1}$) and structurally related compounds as potential inhibitors of Pgp. As shown in Fig. 1 all these complexes contain a tridentate S,S,S donor ligand and a monodentate thiolato ligand of variable structure. Fig. 2 shows the effect of these compounds and of various known Pgp modulators on the accumulation of [^{99m}Tc]sestamibi in RBE4 cells, an immortalised cell line of brain endothelial cells.

Among the complex compounds only those with a higher frequency of the electron donor groups in the molecule ($^{99}\text{Tc1-3}$) show a considerable inhibition of Pgp as revealed by an increased accumulation of [^{99m}Tc]sestamibi (see Fig. 2). Complex $^{99/99m}\text{Tc1}$ was further characterized using also [^3H]vinblastine, [^3H]vincristine, [^3H]colchicine, [^{99m}Tc]tetrofosmine and the n.c.a. $^{99m}\text{Tc1}$ itself as substrates for the Pgp. As shown in Table 2 $^{99}\text{Tc1}$ significantly increases the accumulation of all these radiotracers with the exception of its ^{99m}Tc congener which was competitively decreased.

Table 1. Effects of Pgp modulators and various coordination compounds on the accumulation of ^{99m}Tc sestamibi in RBE4 cells (% of control).

Substance	Mean	S.D.	p	Substance	Mean	S.D.	P
Control	100.0	31.4		($^{99}\text{Tc1}$)	312.6	25.1	**
Vinblastin	321.2	20.1	***	($^{99}\text{Tc2}$)	277,8	5,8	***
Verapamil	312.6	11.3	***	($^{99}\text{Tc3}$)	231,0	10,8	**
Cytochalasine B	233.6	12.0	**	($^{99}\text{Tc4}$)	101,8	3,1	n.s.
Reserpine	365.0	15.5	**	($^{99}\text{Tc5}$)	95,7	4,7	n.s.

Table 2. Effects of Pgp modulators (10 μM) and complex (1) (10 μM) on the accumulation of various Pgp substrates in RBE4 cells.

%D/mg protein	^{99m}Tc -sestamibi	^{99m}Tc -tetrofosmin	$^{99m}\text{Tc1}$	^3H -colchicine	^3H -vinblastine	^3H -vincristine
Control	31.9 \pm 3.3	8.1 \pm 1.5	50.4 \pm 3.7	30.7 \pm 0.7	53.2 \pm 5.5	45.4 \pm 5.6
Verapamil	54.4 \pm 4.6	17.5 \pm 0.2**	60.3 \pm 2.3**	47.0 \pm 3.7*	80.7 \pm 6.0*	72.4 \pm 8.8**
Reserpine	62.4 \pm 5.7***	21.0 \pm 2.1**	66.3 \pm 2.2**	49.0 \pm 4.4***	93.9 \pm 9.5**	76.6 \pm 11.8*
$^{99}\text{Tc1}$	45.1 \pm 6.4*	22.3 \pm 1.8***	33.1 \pm .5***	36.8 \pm 1.3 **	79.4 \pm 10.6*	81.0 \pm 2.5***

To study possible side effects of **1** on the cell metabolism a multitracer approach was used. The cells were simultaneously incubated with [^{99m}Tc]sestamibi or $^{99m}\text{Tc1}$ and [^{18}F]FDG. Two-dimensional scatter plots of both ^{99m}Tc tracer accumulations vs. [^{18}F]FDG accumulation show typical changes of known Pgp inhibitors including $^{99/99m}\text{Tc1}$ (Fig. 2). They show that the side effects of compounds may be separated from the direct effects on Pgp. Valinomycin increases only the accumulation of $^{99m}\text{Tc1}$ but decreases the accumulation of [^{99m}Tc]sestamibi. However, it strongly increases the accumulation of [^{18}F]FDG. The effects of $^{99}\text{Tc1}$ on the *in vivo* distribution of [^{99m}Tc]sestamibi and [^{18}F]FDG in rats are also comparable with the effects of verapamil, an established Pgp inhibitor and Ca-channel blocker. (Fig. 3). After pretreatment with both verapamil and $^{99}\text{Tc1}$, an increase in the [^{99m}Tc]sestamibi accumulation was found in the heart, adrenal bodies and kidneys, i.e. in organs in which Pgp is expressed.

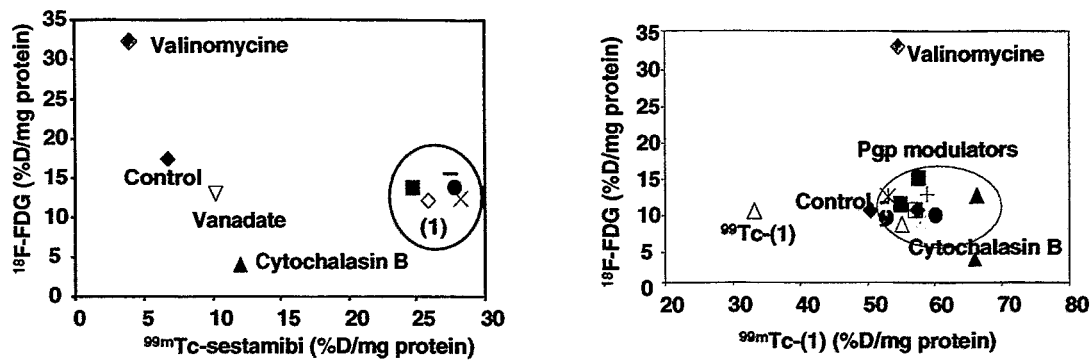


Fig. 2. Effects of various Pgp modulators on the accumulation of accumulation of [^{99m}Tc]sestamibi (left) or $^{99m}\text{Tc}1$ (right) and [^{18}F]FDG in RBE4 cells

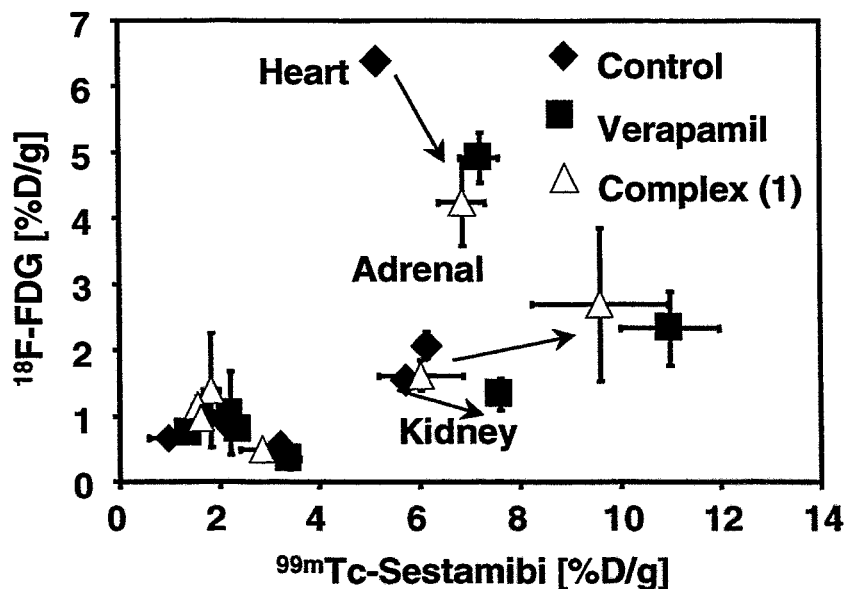


Fig. 3. Effects of verapamil (5 mg/kg body weight) and complex $^{99m}\text{Tc}1$ (5 mg/kg body weight) on the accumulation of [^{99m}Tc]sestamibi and [^{18}F]FDG in rats

Up to now the clinical radiopharmaceuticals available for studying the expression of the Pgp have been the lipophilic ^{99m}Tc cations (^{99m}Tc]sestamibi, [^{99m}Tc]tetrofosmin) as well as [^{99m}Tc]Q57, [^{99m}Tc]Q58, and [^{99m}Tc]Q63 [13 – 15]. All these complexes are transported by Pgp.

In this study, we have shown that the structurally different complex (3-thiapentane-1,5-dithiolato)[N-(3-phenylpropyl)-N-2(3-quinazoline-2,4-dionyl)ethyl]aminoethylthiolato]oxotechnetium(V) ($^{99m}\text{Tc}1$) also serves as a substrate and inhibitor of Pgp.

The RBE4 cells used for the in vitro studies express Pgp, which is functionally active [25, 26]. The cellular accumulation of Pgp substrates after inhibition of Pgp is commonly used as a measure of the capacity of Pgp [27]. It has been suggested that Pgp affects both the influx and efflux [28]. In addition, the amount of this accumulation may not only depend on Pgp but also on the type of the intracellular target of the drug (e.g. mitochondrial inner membrane, tubulin or DNA) and the tightness of binding.

In the present study, we used drugs with various targets to exclude the possibility of unspecific effects. Two of them [^{99m}Tc]sestamibi and [^{99m}Tc]tetrofosmin are nonmetabolized metallopharmaceuticals with a nontitratable delocalized monocationic charge which have been shown to be transported by P-glycoprotein [12]. They lack the usual structural features which were previously thought important for

recognition by P-glycoprotein, such as basic nitrogen atoms, titratable protons, or aromatic residues. As classical substrates of Pgp, [^3H]vinblastine, [^3H]vincristine, and [^3H]colchicine were used in the experiments simultaneously with $^{99\text{m}}\text{Tc}$. Under normal conditions the direct and linear correlation of the uptake of the three tracers at different levels of PGP inhibition may be interpreted as a sign of the strong influence of the PGP on the drug accumulation process in the cells.

Complex $^{99}\text{Tc1}$ was selected in our study from a number of other coordination compounds on account of its ability to increase the accumulation of [$^{99\text{m}}\text{Tc}$]sestamibi, which was expected to have an effect on Pgp. In addition, this compound significantly increased the accumulation of all the other Pgp radiotracers studied, which is strong evidence of a direct interaction with Pgp. The various radiotracers are expected to bind to different binding sites. There is evidence from photoaffinity labelling and from binding studies with [^3H]vinblastine [29] that Pgp has at least two allosterically coupled drug acceptor sites.

One of the drawbacks in studying the function of Pgp is the lack of specificity of the classical Pgp inhibitors. The drugs commonly used to inhibit Pgp may thus also influence the metabolism of the cells. Since ATP is needed as a co-substrate for the transporter disturbances of the energy metabolism may indirectly influence its function. Using a multi-tracer approach (co-administration of [$^{99\text{m}}\text{Tc}$]sestamibi and [^{18}F]FDG), we demonstrate in this paper that the inhibition of Pgp by our novel complex $^{99}\text{Tc1}$ does not influence basic metabolic parameters of the cells which is important for the suitability as radiopharmaceutical. Valinomycin, which is also known to interact with the Pgp, was used as a positive control (30). It dramatically increases the accumulation of [^{18}F]FDG and [^3H]vinblastine (data not shown) without changing the accumulation of [$^{99\text{m}}\text{Tc}$]sestamibi. It also increases the accumulation of $^{99\text{m}}\text{Tc1}$, suggesting various intracellular targets for this complex and for [$^{99\text{m}}\text{Tc}$]sestamibi. [^3H]valinomycin serves as an ionophor for K^+ ions at the mitochondria and depolarizes the mitochondrial membrane potential causing a decreased cellular accumulation of [$^{99\text{m}}\text{Tc}$]sestamibi [31]. In our study it also inhibits Pgp, as revealed by the increased accumulation of [^3H]vinblastine, resulting in unchanged [$^{99\text{m}}\text{Tc}$]sestamibi accumulation as the net effect.

In summary, $^{99/99\text{m}}\text{Tc1}$ was shown to have biochemical and pharmacological properties of a Pgp substrate and inhibitor of the Pgp-mediated efflux of sestamibi, vinblastine and colchicine. It may therefore be considered as a candidate reversal agent and could serve as a template for the development of nonradioactive Re(V) analogues as Pgp inhibitors. The in vivo distribution of the $^{99\text{m}}\text{Tc1}$ is similar to [$^{99\text{m}}\text{Tc}$]sestamibi. However, further experiments are needed to show the potential of $^{99\text{m}}\text{Tc1}$ as a radiopharmaceutical for monitoring the function of Pgp in vivo.

References

- [1] Gottesman M. M. and Pastan I. (1988) The multidrug transporter, a double-edged sword. *J. Biol. Chem.* **263**, 12163-12166.
- [2] Stein U., Shoemaker R. H. and Schlag P. M. (1996) MDR1 gene expression: evaluation of its use as a molecular marker for prognosis and chemotherapy of bone and soft tissue sarcomas. *Eur. J. Cancer* **32A**, 86-92.
- [3] Woodhouse J.R. and Ferry D.R. (1995) The genetic basis of resistance to cancer chemotherapy. *Ann. Med.* **27**, 157-167.
- [4] Gottesman M.M. and Pastan I. (1993) Biochemistry of multidrug resistance mediated by the multidrug transporter. *Ann. Rev. Biochem.* **62**, 385-427.
- [5] Hesdorffer C., Ayello J., Ward M., Kaubisch A., Vahdat L., Balmaceda C. et al. (1998) Phase I trial of retroviral-mediated transfer of the human MDR1 gene as marrow chemoprotection in patients undergoing high-dose chemotherapy and autologous stem-cell transplantation. *J. Clin. Oncol.* **16**, 165-172.
- [6] Schinkel A. H. (1998) Pharmacological insights from P-glycoprotein knockout mice. *Int. J. Clin. Pharmacol. Ther.* **36**, 9-13.
- [7] Preiss R. (1998) P-glycoprotein and related transporters. *Int. J. Clin. Pharmacol. Ther.* **36**, 3-8.
- [8] Ford J., Hait W.N. (1990) Pharmacology of drugs that alter multidrug resistance in cancer. *Pharmacol. Rev.* **42**, 156-199.
- [9] Scheulen M. E. (1998) Clinical relevance of P-glycoprotein with respect to the application of resistance modifiers. *Int. J. Clin. Pharmacol. Ther.* **36**: 41-45.
- [10] Eriks-Fluks E., Elsinga P. H., Hendrikse N. H., Franssen E. J. and Vaalburg W. (1998) Enzymatic synthesis of [4-methoxy- ^{11}C]daunorubicin for functional imaging of P-glycoprotein with PET. *Appl. Radiat. Isot.* **49**, 811-813.
- [11] Elsinga P. H., Franssen E. J., Hendrikse N. H., Fluks L., Weemaes A. M., van der Graaf W. T. et al. (1996) Carbon-11-labeled daunorubicin and verapamil for probing P-glycoprotein in tumors

- with PET. *J. Nucl. Med.* **37**, 1571-1575.
- [12] Piwnica-Worms D., Rao V. V., Kronauge J. F. and Croop J. M. (1995) Characterisation of multi-drug resistance P-glycoprotein transport function with an organotechnetium cation. *Biochemistry* **34**, 12210-12220.
- [13] Hendrikse N. H., Franssen E. J. F., van der Graf W. T. A., Meijer C., Piers D. A., Vaalburg W. et al. (1998) ^{99m}Tc -sestamibi is a substrate for P-glycoprotein and the multidrug resistance-associated protein. *Brit. J. Cancer* **77**, 353-358.
- [14] Pauwels E. K. J., McCready V. R., Stoot J. H. M. B. and van Deurzen D. F. P. (1998) The mechanism of accumulation of tumour-localizing radiopharmaceuticals. *Eur. J. Nucl. Med.* **25**, 277-305.
- [15] Crankshaw C. L., Marmion M., Luker G. D., Rao V., Dahlheimer J., Burleigh B. D. et al. (1998) Novel Technetium (III)-Q complexes for functional imaging of multidrug resistance (MDR1) P-glycoprotein. *J. Nucl. Med.* **39**, 77-86.
- [16] Seelig A. (1998) How does P-glycoprotein recognize its substrates? *Int. J. Clin. Pharmacol. Ther.* **36**, 50-54.
- [17] Pajeva I. and Wiese M. (1998) Molecular modeling of phenothiazines and related drugs as multi-drug resistance modifiers: a comparative molecular field analysis study. *J. Med. Chem.* **41**, 1815-1826.
- [18] Johannsen B., Scheunemann M., Spies H., Brust P., Wober J., Syhre R., et al. (1996) Technetium (V) and rhenium(V) complexes for 5-HT_{2A} serotonin receptor binding: structure-affinity considerations. *Nucl. Med. Biol.* **23**, 429-438.
- [19] Johannsen B., Berger R., Brust P., Pietzsch H.J., Scheunemann M., Seifert S. et al. (1997) Structural modification on receptor-binding technetium-99m complexes in order to improve brain uptake. *Eur. J. Nucl. Med.* **24**, 316-319.
- [20] Spies H., Pietzsch H.-J. and Johannsen B. (1999) The "n+1" mixed ligand approach in the design of specific technetium radiopharmaceuticals: Potentials and problems. In: *Technetium, Rhenium and Other Metals in Chemistry and Nuclear Medicine* 5(M. Nicolini, U. Mazzi Eds.), SGEEditoriali, Padova, pp. 101-108.
- [21] Seifert S., Pietzsch H.-J., Scheunemann M., Spies H., Syhre R. and Johannsen B. (1998) No carrier added preparations of ,3+1' mixed-ligand ^{99m}Tc complexes. *Appl. Radiat. Isot.* **49**, 5-11.
- [22] Füchtner F., Steinbach J., Mäding P. and Johannsen B. (1996) Basic hydrolysis of 2-[^{18}F]fluoro-1,3,4,6-tetra-O-acetyl-D-glucose in the preparation of 2-[^{18}F]fluoro-2-deoxy-D-glucose. *Appl. Radiat. Isot.* **47**, 61-66.
- [23] Roux F., Durieu-Trautmann O., Chaverot N., Claire M., Maily P., Bourre J. M. et al. (1994) Regulation of gamma glutamyl transpeptidase and alkaline phosphatase activities in immortalised rat brain microvessel endothelial cells. *J. Cell Physiol.* **159**, 101-113.
- [24] Regina A., Koman A., Piciotti M., El Hafny B., Center M. S., Bergmann R. et al. (1998) Mrp1 multidrug resistance-associated protein and P-glycoprotein expression in rat brain microvessel endothelial cells. *J. Neurochem.* **71**, 705-715.
- [25] Bergmann R., Roux F., Drewes L. R. and Brust P. (1995) PCR analysis of blood-brain barrier specific transporters in RBE4 cells. *Annual Report 1995*, Institute of Bioinorganic and Radiopharmaceutical Chemistry, FZR-122, pp. 161-164.
- [26] Begley D. J., Lechardeur D., Chen Z. D., Rollinson C., Bardoul M., Roux F. et al. (1996) Functional expression of P-glycoprotein in an immortalised cell line of rat brain endothelial cells, RBE4. *J. Neurochem.* **67**, 988-995.
- [27] Bae K. T. and Piwnica-Worms D. (1997) Pharmacokinetic modeling of multidrug resistance P-glycoprotein transport of gamma-emitting substrates. *Q. J. Nucl. Med.* **41**, 101-110.
- [28] Gottesman M. M., Currier S., Bruggemann E., Lelong I., Stein W. and Pastan I. (1994) The multidrug transporter: Mechanistic considerations. *Cell Biol. Membr. Transp. Proc.* **41**, 17.
- [29] Malkhandi J., Ferry D. R., Boer R., Gekeler V., Ise W. and Kerr, D. J. (1994) Dexniguldipine-HCl is a potent allosteric inhibitor of [^3H]vinblastine binding to P-glycoprotein of CCRF ADR 5000 cells. *Eur. J. Pharmacol.* **288**, 105-114.
- [30] Sharom F. J., Diodato G., Yu X. H. and Ashbourne, K. J. D. (1995) Interaction of the P-glycoprotein multidrug transporter with peptides and ionophores. *J. Biol. Chem.* **270**, 10334-10341.
- [31] Chiu M. L., Kronauge J. F. and Piwnica-Worms D. (1990) Effect of mitochondrial and plasma membrane potentials on accumulation of hexakis(2-methoxyisobutylisonitrile)technetium(I) in cultured mouse fibroblasts. *J. Nucl. Med.* **31**, 1646-1653.

16. Synthesis and Preliminary Evaluation of 9-[(3-¹⁸F]-Fluoro-1-Hydroxy-2-Propoxy)-Methyl]guanine [¹⁸F]FHPG in Rats

B. Noll, St. Noll, P. Brust, M. Scheunemann, A. Jordanova, T. Knieß, M. Grote, J. Steinbach, M. Hauses¹, O. Koufaki¹, H. K. Schackert¹

¹Technische Universität Dresden, Universitätsklinikum, Chirurgische Forschung

Gene therapy with the transfer of Herpes simplex virus type 1 thymidine kinase (HSV1-tk) has shown promise in animal models. The efficiency of this method is currently being evaluated in the treatment of human brain tumours and a variety of other human cancers. Many nucleoside analogues are known to localize selectively HSV1-tk transfected cells and show a very high specificity for the viral enzyme, especially acyclic nucleosides such as ganciclovir [1, 2, 3]. Apart from that ganciclovir undergoes only minimal metabolism in vivo by the host-tk. The use of reporter genes encoding proteins to metabolise the [¹⁸F]-PET (Positron Emission Tomography) tracer into trapped products provides a novel approach to monitoring the expression of reporter genes in living animals [4, 5]. This study was designed to investigate the biological behaviour of the [¹⁸F]-labelled ganciclovir ([¹⁸F]FHPG) in rats with regard to its application as PET tracer for monitoring the gene transfer in tumours. The preparation of the non-radiolabelled FHPG and the PET precursor, the labelling procedure with fluor-18, the biodistribution in rats and the determination of metabolites are described.

*Synthesis of the PET precursor **4** and the non radiolabelled reference compound **6***

The synthesis was modified according to a procedure described in [1, 7] and follows the route shown in Fig. 1. The sodium salt of 9-[(1,3-dihydroxy-2-propoxy)methyl]guanine **1** was neutralized with 0.1 N hydrochloric acid and recrystallized from water to form the free nucleobase 9-[(1,3-dihydroxy-2-propoxy)methyl]guanine **2** which reacts with p-anisylchlorodiphenyl-methane to produce N²-(p-anisylidiphenylmethyl)-9-[[1-(p-anisylidiphenylmethoxy)-3-hydroxy-2-propoxy]methyl]guanine **3** in a 35 % yield. Tosylation of **3** yields N²-(p-anisylidiphenylmethyl)-9-[[1-(p-anisylidiphenylmethoxy)-3-(p-toluolsulfonyloxy)-2-propoxy]methyl]guanine **4** (75 %), which was fluorinated with potassium fluoride and kryptofix 2.2.2. in acetonitrile to yield N²-(p-anisylidiphenylmethyl)-9-[[1-(p-anisylidiphenylmethyl)-3-fluoro-2-propoxy]methyl]-guanine **5**. To split off the protection groups, **5** was refluxed with acetic acid producing the desired product 9-[(1-hydroxy-3-fluoro-2-propoxy)methyl]guanine **6** in a yield of 85 %. **6** was 95 % pure and analysed by elemental analysis, including determination of the fluorine content and ¹H NMR. Compound **4** was used as a precursor for the following ¹⁸F-labelling procedure.

¹⁸F-labelling procedure

[¹⁸F]Fluoride was produced by irradiating ¹⁸O – enriched water (98 %, 1,35 ml) with protons (25 µA, 18 MeV, 120 min) using the facilities of IBA "Cyclon 18/9" cyclotron at the FZR.

The precursor **4** was radiolabelled by [¹⁸F]-fluorination of the tosylate-protected 3-hydroxymethyl-group with potassium [¹⁸F]fluoride (1.85 GBq) in the presence of kryptofix 2.2.2. After hydrolysis of the methoxytrityl groups the final product 9-[(3-¹⁸F]-fluoro-1-hydroxy-2-propoxy)methyl]guanine was purified by HPLC on a RP18 column and identified by co-injection of the unlabelled reference of **6**. The radiochemical purity amounts to >99 % with a specific activity of 14.8 MBq/µmol.

Biodistribution studies

Biodistribution studies were carried out in six week old male Wistar rats (Tierzucht Schoenwalde) according to the national regulations for animal research. The animals were anaesthetized by i.p. injection of 1300 mg/kg urethane. The body temperature was monitored and kept at 37 °C. 1.5 - 3.0 MBq of [¹⁸F]ganciclovir (in 0.5 ml saline) were injected into the tail vein. The animals (4-6 per time point) were sacrificed by heart puncture 5, 60, and 120 min post injection (p.i.). Samples of the blood, plasma and urine were taken for investigation of the labelled metabolites by TLC and of the binding to erythrocytes. Organs of interest were removed, blotted dry and weighed. The activity was measured in a Packard COBRA II gamma counter. Reference samples of the injected solution and aliquots of the blood and urine were measured as well. After correction for physical decay, the percentage of the injected dose per organ (% I.D.) and per gram organ (% I.D./g) was calculated for each organ.

For erythrocyte binding a blood sample was centrifuged for 2 min at 14,000 rpm (JOUAN A 14). The plasma was separated from the blood and counted. 700 µl saline solution was added, followed by renewed centrifugation. The supernatant was taken and measured. The procedure was repeated five times and the activity bound to erythrocytes was measured and related to the total activity of the blood sample.

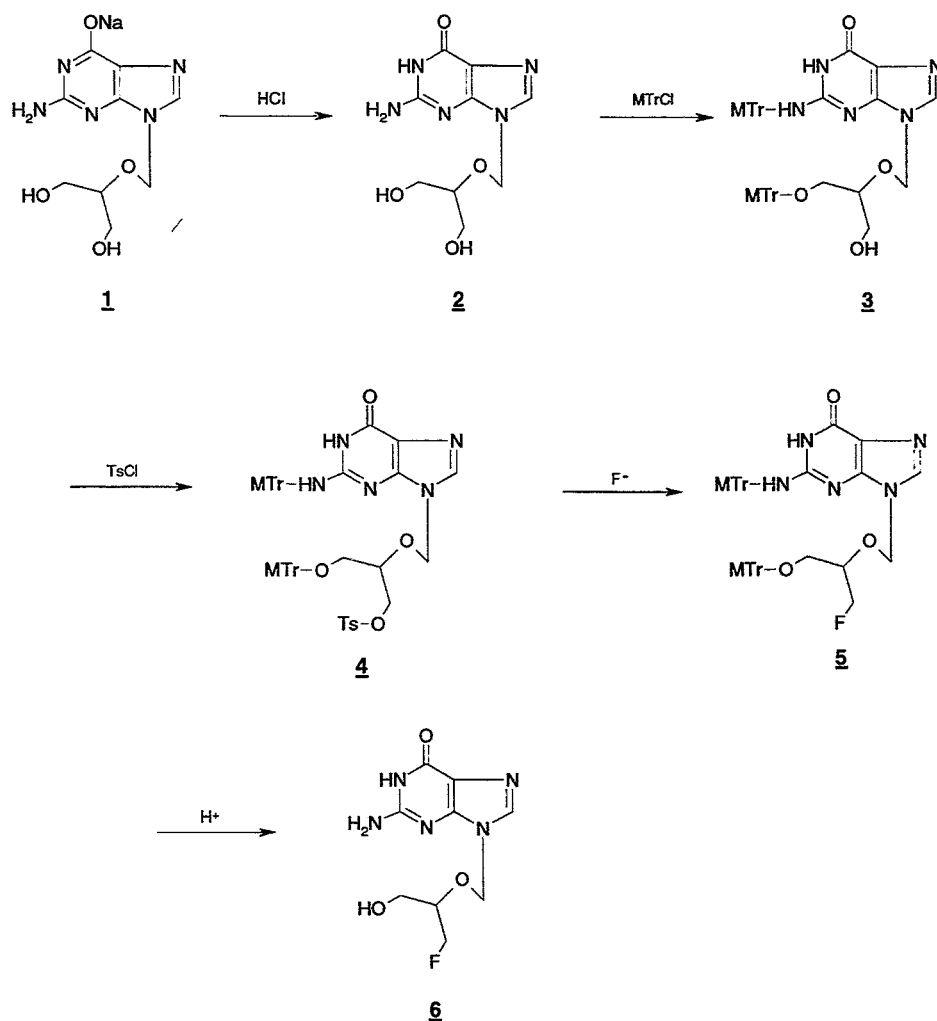


Fig. 1. Reaction route of the preparation of the PET precursor and the inactive reference compound

Analysis of metabolites

For determination of metabolites, urine and plasma samples are checked by thin-layer chromatography on RP-18 (Merck) aluminium sheets and methanol / water (9:1) as the eluent. The chromatograms were evaluated by measuring the radioactivity (the urine and the short-time plasma samples) on a linear analyser (Berthold) and the chromatograms with the lowest activity level (long-time plasma samples) on a FUDJI BAS 2000 device. The R_f value of 9-[(3-¹⁸F]-fluoro-1-hydroxy-2-propoxy)-methyl]guanine is 0.7. With sufficient differences in R_f it was possible to separate both ganciclovir and fluoroganciclovir on this TLC system.

Results and Discussion

The nonradioactive reference compound fluoroganciclovir was obtained in a high purity. The product was characterised by ¹H NMR, elemental analysis and mass spectrometry. The identity of the ¹⁸F-labelled ganciclovir with the nonradioactive reference compound was determined by HPLC. The radiochemical purity of the ¹⁸F-labelled ganciclovir exceeded 99 % and the yield of the radiopharmaceutical preparation amounted to 12 % (time corrected).

The distribution of [¹⁸F]GCV in the various tissues of male Wistar rats is summarized in Table 1.

Table 1. Biodistribution data of [¹⁸F]ganciclovir in male Wistar rats at 5, 60, and 120 min post injection (p.i.).

%Dose/g	5 min	60 min	120 min
Blood	0.650±0.049	0.056±0.008	0.020±0.004
Brain-total	0.044±0.016	0.009±0.002	0.005±0.001
Pancreas	0.923±0.092	0.066±0.002	0.042±0.013
Spleen	1.378±0.105	0.130±0.023	0.051±0.017
Adrenals	0.879±0.031	0.102±0.009	0.074±0.035
Kidney	3.685±0.467	0.287±0.048	0.115±0.015
Fat	0.203±0.026	0.034±0.022	0.020±0.017
Muscle	0.258±0.018	0.148±0.033	0.051±0.008
Heart	0.524±0.019	0.062±0.005	0.018±0.002
Lung	0.909±0.092	0.085±0.003	0.036±0.009
Thymus	0.655±0.034	0.060±0.010	0.022±0.003
Liver	1.581±0.134	0.117±0.017	0.044±0.006
Femur	0.471±0.039	0.089±0.015	0.043±0.008

[¹⁸F]GCV shows a relatively fast blood clearance. The erythrocyte binding of the tracer was negligible (5 min: 6.73 ± 0.92 %, 60 min: 6.83 ± 1.93 %, 120 min: 8.44 ± 3.73 %). An initial high uptake of the tracer was found in the spleen, kidney and liver, which decreased rapidly in time. The lowest uptake was found in the brain, indicating a negligible penetration across the blood-brain barrier. The absence of metabolites both in the plasma and in the urine is in accordance with the results obtained with ganciclovir in a clinical study concerning its antiviral activity [6].

The rapid blood and organ clearance and the in vivo stability of [¹⁸F]GCV is expected to be advantageous for in vivo monitoring of the gene transfer in tumours. After transfer of the Herpes simplex virus thymidine kinase gene into tumours metabolization and trapping of [¹⁸F]GCV should occur. Thus, a reasonable target-to-background ratio may be expected within the physical half-life of the tracer.

References

- [1] Alauddin M. M., Conti P. S., Mazza S. M., Hamzeh F. M. and Lever J. R. (1996) 9-[(3-[¹⁸F]-fluoro-1-hydroxy-2-propoxy)methyl]guanine ([¹⁸F]-FHPG): a potential imaging agent of viral infection and gene therapy using PET. *Nucl. Med. Biol.* **23**, 787-792.
- [2] Gambhir S. S., Barrio J. R., Phelps M. E., Iyer M., Namavari M., Satyamurthy N., Wu L., Green L. A., Bauer E., Maclaren D. C., Nguyen K., Berk A. J., Cherry S. R. and Herschman H.R. (1999) Imaging adenoviral-directed reporter gene expression in living animals with positron emission tomography. *Proc. Natl. Acad. Sci.* **96**, 2333-2338.
- [3] Gambhir S. S., Barrio J. R., Wu L., Iyer M., Namavari M., Satyamurthy N., Bauer E., Parrish C., Maclaren D. C., Borghei A. R., Green L. A., Sharfstein S., Berk A. J., Cherry S. R., Phelps M. E. and Herschman H. R. (1998) Imaging of adenoviral-directed herpes simplex virus type 1 thymidine kinase reporter gene expression in mice with radiolabelled ganciclovir. *J. Nucl. Med.* **39**, 2003-2011.
- [4] Moolten F. L., Vonderhaar B. K. and Mroz P. J. (1996) Transduction of the herpes thymidine kinase gene into pre-malignant murine mammary epithelial cells renders subsequent breast cancers responsive to ganciclovir therapy. *Hum. Gene Ther.* **7**, 1197-1204.
- [5] Tjuvajev J. G., Avril N., Oku T., Sasajima T., Miyagawa T., Joshi R., Safer M., Beattie B., Diresta G., Daghighian F., Augensen F., Koutcher J., Zweit J., Humm J., Larson S. M., Finn R. and Blasberg R. (1998) Imaging herpes virus thymidine kinase gene transfer and expression by positron emission tomography *Cancer Research* **58**, 4333-4341.
- [6] Alauddin M. M., Shahinian A., Kundu R. K., Gordon E. M. and Conti P. S. (1999) Evaluation of 9-[(3-[¹⁸F]-fluoro-1-hydroxy-2-propoxy)methyl]guanine [¹⁸F]FHPG in vivo as a probe for PET imaging of gene incorporation and expression in tumours. *Nucl. Med. Biol.* **26**, 371-376.
- [7] Martin J. C., McGee D., Jeffrey G., Hobbs D. W., Smee D. F., Mathews T. R. and Verheyden J. P. H. (1986) Synthesis and anti-herpes-virus activity of acyclic 2'-deoxyguanosine analogues related to 9-[1,3-dihydroxy-2-propoxy)methyl]guanine. *J. Med. Chem.* **29**, 1384-1389.

17. The Diagnostic Value of [¹⁸F]FDG Positron-Emission Imaging for Detection and Treatment Control of Malignant Germ Cell Tumours

P. Tsatalpas¹, B. Beuthien-Baumann², T. Spiegel¹, J. Kropp², A. Manseck¹, C. Tiepolt², O. Hakenberg¹, W. Burchert, W.-G. Franke², M. P. Wirth¹
TU Dresden, ¹Klinik und Poliklinik für Urologie und ²Klinik und Poliklinik für Nuklearmedizin

Introduction

The role of positron emission tomography (PET) with 2-[¹⁸F]fluoro-2-deoxy-D-glucose ([¹⁸F]FDG) is currently under evaluation in genitourinary tumours [1, 2, 7-10, 13]. Recent studies showed that in many tumour types the uptake of [¹⁸F]FDG is increased compared with normal tissue [4, 11]. Effective chemotherapy was found to reduce the [¹⁸F]FDG uptake prior to volumetric changes in morphological imaging techniques such as computed tomography (CT) [5, 6, 12]. In this study the potential of [¹⁸F]FDG-PET for the detection and therapy control of testicular germ cell tumours was investigated.

Materials and Methods

Patients: Twenty-three consecutive patients with histopathologically confirmed testicular germ cell tumours were included in the study from June 1997 to July 1998. The histological diagnosis was seminoma in ten patients (43 %), a combined tumour in nine (39 %), embryonic carcinoma in three (13 %), and one patient (4 %) had a combined testicular tumour. Tumour staging was assessed according to the international workshop on staging and treatment of testicular cancer in Lugano [16]. Eleven pts. were classified as stage I (48 %), six pts. as stage II (26 %), and six pts. as stage III (26 %). 16 patients received chemotherapy, six patients underwent retroperitoneal lymphadenectomy. One patient received a bone-marrow support in addition to high-dose chemotherapy and one patient underwent mediastinal lymph-node dissection with resection of pulmonary residual tumour masses after chemotherapy. Four of seven patients with a Stage I seminoma received an adjuvant radiation therapy (26 Gy), two an adjuvant monochemotherapy with two series of carboplatin. A total of 32 PET scans were carried out. The scans were performed either after initial diagnosis (n = 21) and/or within 3 to 45 days after chemotherapy was completed (stage II-III patients only, n = 11).

PET imaging: PET studies were carried out after the patients had fasted for 6-12 hours. Plasma glucose levels at the time of the [¹⁸F]FDG injection were within physiological limits. Patients with diabetes mellitus were excluded. [¹⁸F]FDG was produced in-house by a modified method as described by [3]. 330 MBq [¹⁸F]FDG per patient were intravenously injected. Fifteen of the twenty-one initial scans and all scans after chemotherapy were carried out using an ECAT EXACT HR⁺ PET scanner (Siemens/CTI, Knoxville, Tenn., USA). The reconstructed image resolution was about 6-7 mm FWHM. Attenuation correction was performed by a 10 min transmission scan in selected bed positions (BP). 60 min after injection the emission scan was acquired for 10 min per BP. Six of the twenty-one initial [¹⁸F]FDG scans (185 MBq per patient) were performed using a dual head coincidence gamma camera (SoluS EPIC MCD, ADAC Laboratories, Milpitas, Calif., USA). Iteratively reconstructed images had a resolution of about 15 mm. The visual analysis was graded as positive, indeterminate or negative for malignancy. In studies performed with the dedicated PET scanner quantitative image analysis of tumour uptake was performed by calculating the standardized uptake values (SUVs) in selected areas [14].

CT imaging: Thirty-four CT scans (23 initial and 11 after chemotherapy) were acquired with a third- or fourth-generation CT scanner corresponding to all PET studies (10 mm slice thickness; oral and intravenous contrast medium). CT scans for initial staging were interpreted as suspicious of metastatic lymphatic spread, when the lymph node was larger than 1.5 cm and of organ metastases when characteristic radiological signs such as contrast enhancement after intravenous contrast medium application were seen.

Tumour markers: Tumour marker levels of AFP and b-HCG were available in all patients entered into the study. AFP > 9 ng/ml and b-HCG > 5 U/l were considered pathological.

Validation and statistics: Validation was carried out either by histology (n = 7) or by clinical follow-up for 6 to 11 months (n = 16). The absence of disease after therapy was assumed if the patients were without progression in CT and tumour markers were negative for at least 6 months without further therapy. Tissue for histology was obtained by retroperitoneal lymphadenectomy (n = 6) and thoracotomy (n = 1). Sensitivity, specificity, positive and negative predictive values and accuracy were deter-

mined for PET and CT. Differences between PET and CT for parameters of diagnostic value were evaluated by the chi-square test. The accepted limit to indicate statistical significance was $p < 0.05$.

Results and Discussion

Pathological accumulation of [^{18}F]FDG was detected in 9 of 21 (43 %) of the initial PET studies. All lesions with pathological findings represented metastatic lesions confirmed either by histology or clinical follow-up (Fig. 1). Twelve of 21 primary PET studies (57 %) were graded as negative in accordance with clinical and CT findings.

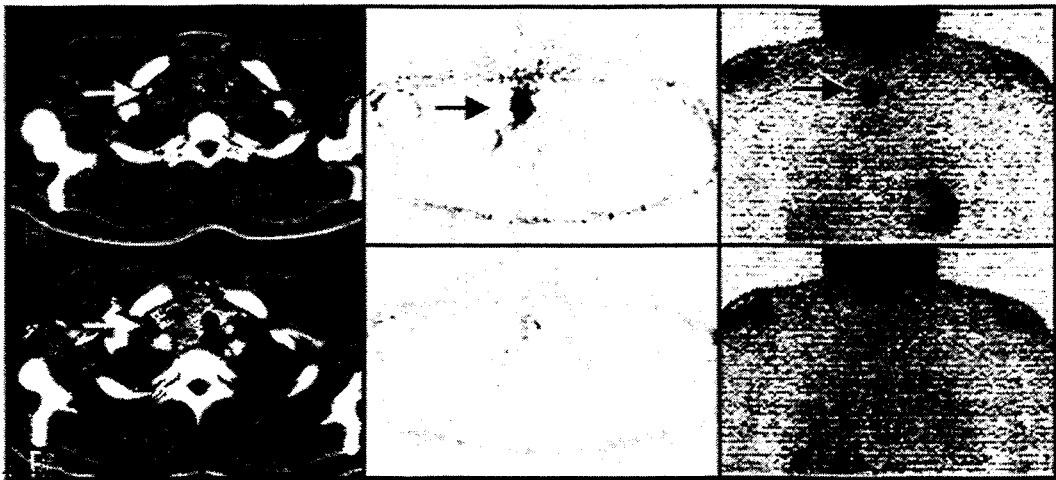


Fig. 1. A 54 year-old patient with left sided seminoma. CT transversal slices (left), corresponding PET slices (middle) and PET projection images (right) are shown (upper row prior to therapy, bottom row after chemotherapy). Before chemotherapy the mediastinal lymph node metastasis showed intensive accumulation of labelled glucose, while the CT was inconclusive with respect to the dignity of the mass (arrow). After two cycles of chemotherapy no viable tumour tissue was detected with PET.

Pretherapeutic PET (Table 1) was more sensitive (0.90 vs. 0.60) and had a higher negative predictive value (0.92 vs. 0.73) than CT. However, these differences did not reach statistical significance. Specificity and positive predictive value were comparable to the CT results.

Table 1. Overall diagnostic value of PET versus CT

	Sensitivity	Specificity	PPV	NPV
<i>Before therapy</i>				
<i>(n = 21)</i>				
PET	0.90	1.00	1.00	0.92
CT	0.60	1.00	1.00	0.73
<i>After therapy</i>				
<i>(n = 11)</i>				
PET	1.00	0.60	0.20	1.00
CT	1.00	0.60	0.20	1.00

PET = positron emission tomography; CT = X-ray computed tomography; PPV = positive predictive value; NPV = negative predictive value

After chemotherapy 5 of 11 patients (45 %) showed a pathological accumulation of [^{18}F]FDG. In one of the patients the [^{18}F]FDG accumulation represented persistent disease. In the 4 other cases, new lesions were found in the posttherapeutic PET (lung and neck), whereas the initial lesions had com-

pletely disappeared. These new [¹⁸F]FDG accumulations were due to inflammatory reactions proved by histology after thoracotomy (1 of 4 cases), antibiotic treatment and clinical follow-up (3 of 4 cases).

Six of the eleven (55 %) PET scans after chemotherapy showed no accumulation of [¹⁸F]FDG, although in four of these six patients residual tumour masses were identified by CT. After retroperitoneal lymphadenectomy in three cases, these masses were shown by histology to be scar tissue and an ectopic seminal vesicle without vital tumour cells. One patient with a residual retroperitoneal tumour mass is still without progression after 8 months. The other two patients with negative PET scans after chemotherapy also showed a complete remission with respect to control CT and serologic tumour markers. They are still in remission after a follow-up period of 8 to 11 months.

After chemotherapy no significant differences were found between PET and CT results in the overall tumour detection rate. Considering infradiaphragmatic lesions only (Table 2), PET was shown to be superior to CT in specificity (1.0 vs. 0.60; $p < 0.05$) and positive predictive value (1.0 vs. 0.20; n.s.). Regarding supradiaphragmatic lesions (Table 3) CT was found to be more specific (1.0 vs. 0.60; $p < 0.05$) and to have a higher positive predictive value (1.0 vs. 0.20; n.s.) than PET.

Our preliminary results demonstrate [¹⁸F]FDG positron imaging to be a useful diagnostic tool for initial staging and treatment control in patients with germ cell tumours. The possible advantages compared

Table 2. Diagnostic value of PET versus CT in infradiaphragmatic tumour lesions

	Sensitivity	Specificity	PPV	NPV
<i>Before therapy</i> (n = 21)				
PET	0.85	1.00	1.00	0.93
CT	0.71	1.00	1.00	0.87
<i>After therapy</i> (n = 11)				
PET	1.00	1.00	1.00	1.00
CT	1.00	0.60	0.20	1.00

PET = positron-emission tomography; CT = X-ray computed tomography; PPV = positive predictive value; NPV = negative predictive value

Table 3. Diagnostic value of PET versus CT in supradiaphragmatic tumour lesions

	Sensitivity	Specificity	PPV	NPV
<i>Before therapy</i> (n = 21)				
PET	0.80	1.00	1.00	0.94
CT	0.60	1.00	1.00	0.89
<i>After therapy</i> (n = 11)				
PET	1.00	0.60	0.20	1.00
CT	1.00	1.00	1.00	1.00

PET = positron-emission tomography; CT = X-ray computed tomography; PPV = positive predictive value; NPV = negative predictive value

with CT are not yet clearly defined due to the limited number of investigated patients. A limitation of this method seem to be supradiaphragmatic inflammatory processes after chemotherapy resulting in false positive PET findings. However, in infradiaphragmatic lesions PET proved to be superior to CT. The combined use of both imaging methods should therefore be preferred at the moment in order to achieve maximal diagnostic accuracy. Further investigations are needed to improve the imaging scheme for PET to avoid false positive results caused by inflammatory changes post chemotherapy.

References

- [1] Bachor R., Kocher F., Gropengiesser F., Reske S. N. and Hautmann R. E. (1995) Positron emission tomography. Introduction of a new procedure in diagnosis of urologic tumors and initial clinical results. *Urologe A*. **34**, 138-142.
- [2] Cremerius U., Effert P. J., Adam G., Sabri O., Zimmy M., Wagenknecht G., Jakse G. and Buell U. (1998) FDG PET for detection and therapy control of metastatic germ cell tumor. *J. Nucl. Med.* **39**, 815-822.
- [3] Fuechtner F., Steinbach J., Maeding P. and Johannsen B. (1996) Basic hydrolysis of 2-[¹⁸F]fluoro-1,3,4,6-tetra-O-acetyl-D-glucose in the preparation of 2-[¹⁸F]fluoro-2-deoxy-D-glucose. *Appl. Radiat. Isot.* **47**, 61-66.
- [4] Goldberg M. A., Lee M. J., Fischman A. J., Mueller P. R., Alpert N. M. and Thrall J. H. (1993) Fluorodeoxyglucose PET of abdominal and pelvic neoplasms: potential role in oncologic imaging. *Radiographics*. **13**, 1047-1062.
- [5] Haberkorn U., Strauss L. G., Dimitrakopoulou A., Seiffert E., Oberdorfer F., Ziegler S., Reisser C., Doll J., Helus F. and van Kaick G. (1993) Fluorodeoxyglucose imaging of advanced head and neck cancer after chemotherapy. *J. Nucl. Med.* **34**, 12-17.
- [6] Hoekstra O. S., Ossenkoppelle G. J., Golding R., van Lingen A., Visser G. W., Teule G. J. and Huijgens P. C. (1993) Early treatment response in malignant lymphoma, as determined by planar fluorine-18-fluorodeoxyglucose scintigraphy. *J. Nucl. Med.* **34**, 1706-1710.
- [7] Kosuda S., Kison P. V., Greenough R., Grossman H. B. and Wahl R. L. (1997) Preliminary assessment of fluorine-18 fluorodeoxyglucose positron emission tomography in patients with bladder cancer. *Eur. J. Nucl. Med.* **24**, 615-620.
- [8] Muller-Mattheis V., Reinhardt M., Gerharz C. D., Furst G., Vosberg H., Muller-Gartner H. W. and Ackermann R. (1998) [Positron emission tomography with [¹⁸F]-2-fluoro-2-deoxy-D-glucose (¹⁸FDG-PET) in diagnosis of retroperitoneal lymph node metastases of testicular tumors]. *Urologe A*. **37**, 609-620.
- [9] Nuutinen J. M., Leskinen S., Elomaa I., Minn H., Varpula M., Solin O., Soderstrom K. O., Joensuu H. and Salminen E. (1997) Detection of residual tumours in postchemotherapy testicular cancer by FDG-PET. *Eur. J. Cancer*. **33**, 1234-1241.
- [10] Stephens A. W., Gonin R., Hutchins G. D. and Einhorn L. H. (1996) Positron emission tomography evaluation of residual radiographic abnormalities in postchemotherapy germ cell tumor patients. *J. Clin. Oncol.* **14**, 1637-1641.
- [11] Strauss L. G. and Conti P. S. (1991) The applications of PET in clinical oncology. *J. Nucl. Med.* **32**, 623-648; discussion 649-650.
- [12] Wahl R. L., Zasadny K., Helvie M., Hutchins G. D., Weber B. and Cody R. (1993) Metabolic monitoring of breast cancer chemohormonotherapy using positron emission tomography: initial evaluation. *J. Clin. Oncol.* **11**, 2101-2111.
- [13] Wilson C. B., Young H. E., Ott R. J., Flower M. A., Cronin B. F., Pratt B. E., McCready V. R. and Horwich A. (1995) Imaging metastatic testicular germ cell tumours with ¹⁸FDG positron emission tomography: prospects for detection and management. *Eur. J. Nucl. Med.* **22**, 508-513.
- [14] Woodward H., Gigler R., Freed B. and Russ G. (1975) Expression of tissue isotope distribution. *J. Nucl. Med.* **16**, 958-959.

18. [¹⁸F]FDG for the Staging of Patients with Differentiated Thyroid Cancer

C. Tiepolt¹, B. Beuthien-Baumann¹, R. Hliscs¹, J. Bredow¹, A. Kühne¹, J. Kropp¹, W. Burchert, W.-G. Franke¹

¹TU Dresden, Klinik und Poliklinik für Nuklearmedizin

Introduction

In patients with differentiated thyroid cancer, positron emission tomography (PET) using [¹⁸F]-fluorodeoxyglucose (FDG) has been demonstrated to provide additional diagnostic information compared with ¹³¹I whole body scanning. It was found to be particularly useful in cases of suspected local recurrence, regional lymph node metastases or distant metastatic spread [1, 2]. The availability of PET for routine clinical use is limited by the great expense of a full-ring tomograph. The coincidence gamma camera was therefore proposed as a cost-effective alternative for FDG imaging. In spite of the technical limitations of gamma camera coincidence imaging, some first results indicate the usefulness in clinical settings [3, 4]. The aim of this study was to investigate the diagnostic accuracy of coincidence imaging and PET with regard to the staging of patients with differentiated thyroid cancer.

Materials and Methods

Patients: Twenty-three patients with differentiated thyroid cancer with positive ¹³¹I whole body scans (n = 20) and/or elevated thyroglobulin levels (n = 20) were included in this study. All patients had undergone thyroidectomy and at least four radioiodine treatments for metastases. At the time of initial the diagnosis, 17 patients had lymph node or distant metastases verified by chest X-ray, computerized tomography, or by histology.

Study design: All patients were investigated with both dedicated PET and coincidence camera on the same day. Prior to the injection the patients fasted for at least 4 hours. The reference scan with a dedicated ring tomograph was performed 60 minutes after the intravenous injection of 300-370 MBq of [¹⁸F]FDG. Then coincidence imaging with the dual head gamma camera was carried out 210-240 minutes after tracer application. Due to a radioiodine whole-body scan being performed at roughly the same time, 11 patients were off levothyroxine when the FDG scan was performed.

PET imaging: We used an ECAT Exact HR+ (Siemens/CTI) with BGO detectors and an axial field of view of 15.2 cm. Six bed positions overlapping by 1 cm were acquired in 2D mode for 10 minutes each.

Coincidence gamma camera imaging: A Solus EPIC MCD (ADAC Laboratories) with a 5/8 inch NaI crystal and an axial field of view of 38 cm was used. Two to three bed positions covering head, neck and chest and overlapping by 35 % were acquired in three-dimensional (3D) mode with 32 angles of 40 s each.

¹³¹I whole body scanning: An ¹³¹I whole body scan was performed 72 hours after oral administration of a therapeutic dose of ¹³¹I-NaI (3,700 MBq) for treatment of metastases using a dual head gamma camera equipped with high-energy collimators (Genesis, ADAC Laboratories).

Data analysis: Images obtained with both modalities were read by two experienced investigators (CT, BB-B) who were blinded to the FDG-PET results when evaluating the coincidence gamma camera scans. The size of each lesion was derived from the PET images, applying a 50 % intensity isocontour as the outline of the tumour.

Results and Discussion

By the combined use of [¹⁸F]FDG and ¹³¹I-NaI 123 lesions were detected (100 %). 55/123 (45 %) lesions were visualized with ¹³¹I whole body scan, 66/123 (54 %) with coincidence imaging, and 101/123 (82 %) with dedicated PET.

A lesion-by-lesion comparison between the images obtained with dedicated PET and the coincidence camera showed concurrence in 65 % of cases. The analysis of various anatomical areas showed 61 % agreement in the head and neck and 73 % in the chest. Of 23 bone metastases detected by ¹³¹I whole body scan, 14 lesions were revealed by dedicated PET, but only 6 by coincidence imaging.

The analysis according to size showed that the coincidence camera detected 98 % of the lesions larger than 1.5 cm and 56 % of the lesions between 1 and 1.5 cm that were seen with the PET scanner. Lesions smaller than 1 cm (n = 16) could only be imaged with the dedicated PET scanner.

Compared with ^{131}I , [^{18}F]FDG showed additional lymph node metastases in 6 patients when imaged with the coincidence camera, and in 8 patients when imaged with the PET scanner (Fig. 1).

The therapeutic strategy was changed as a result of the additional diagnostic information provided by the [^{18}F]FDG scan in 2/23 patients. In these cases both the dedicated PET scanner and the coincidence camera showed radioiodine negative lymph node metastases which were subsequently removed by surgery.

Two patients who had known metastases demonstrated by the ^{131}I whole-body scan were misstaged as M0 by both imaging modalities employing [^{18}F]FDG.

The same N stage as with the PET scanner was obtained with the coincidence camera in 21/23 patients (Fig. 2). The same M stage was assigned to 21/23 patients, resulting in an overall agreement of coincidence camera and PET scanner in 19/23 patients. Those metastases that were missed by coincidence imaging but were relevant to TNM staging were small (< 1.5 cm) mediastinal lymph nodes in two cases (in one of which the PET scan was the only diagnostic procedure showing evidence of disease activity), small (< 1.5 cm) metastases in the lung in one patient, and a lesion in the thoracic spine in another patient. The misstaging of 4 patients by coincidence imaging did not, however, alter therapeutic management of these patients.

Coincidence imaging using a modified gamma camera offers a cost-effective alternative to a dedicated PET scanner for imaging oncological patients with [^{18}F]FDG. This new technology has, however, not been fully evaluated in clinical settings.

This study showed a relative sensitivity of 65 % for coincidence imaging compared with dedicated PET. This is slightly more than the results published by Shreve *et al.* who found a relative sensitivity of 55 % in 31 patients. For lesions located in the chest an identical relative sensitivity of 73 % was reported. The overall lower sensitivity may have been caused by the low detection rate for abdominal lesions (23 %) in this heterogeneous patient population [5].

Without attenuation correction it proved difficult to assign lesions located at the border between lung and mediastinum to one or the other anatomical structure. Due to the lower usable spatial resolution, this effect was more pronounced with the coincidence gamma camera imaging than with the dedicated PET system. A study of Shreve *et al.* reported similar results [5]. Furthermore, the generally poorer image quality of the coincidence camera makes the distinction of pathological from physiological FDG uptake more difficult [5]. As attenuation correction improves geometric distortion as well as edge definition of lesions, it will lead to a better visualization and localization. An increased sensitivity can therefore be expected [6].

Taking into account the severe technical limitations of coincidence imaging outlined above, it seems encouraging that 19/23 patients in our selective cohort were staged correctly according to the TNM system with dedicated PET as a reference. The incorrect staging of four patients was due to chest lesions smaller than 1.5 cm.



Fig. 1. A 67-year-old man with metastatic differentiated thyroid cancer. Coronal images from the coincidence camera (left) and PET (right) showed an increased uptake in mediastinal lymph node metastases. Whereas the contrast in the PET image was equal in all lesions, in the coincidence image it was lower in the smaller lesions. One lesion (in the left jugular region) was not recognizable in the coincidence image without knowledge of the PET results.

Patient management changed as a result of the FDG scan in two cases with raised serum thyroglobulin and lymph node metastases, which showed no uptake of radioiodine. These lesions were detected with both PET and the coincidence gamma camera.

Although the accurate detection of lesions with coincidence imaging is limited to a size larger than 1.5 cm, the staging was affected in 17 % of the patients in this population. Due to technical limitations, FDG scanning with a coincidence gamma camera is at present not suitable for clinical imaging of patients with thyroid cancer. For future applications it is expected that the application of attenuation correction will improve the clinical accuracy of the coincidence gamma camera.

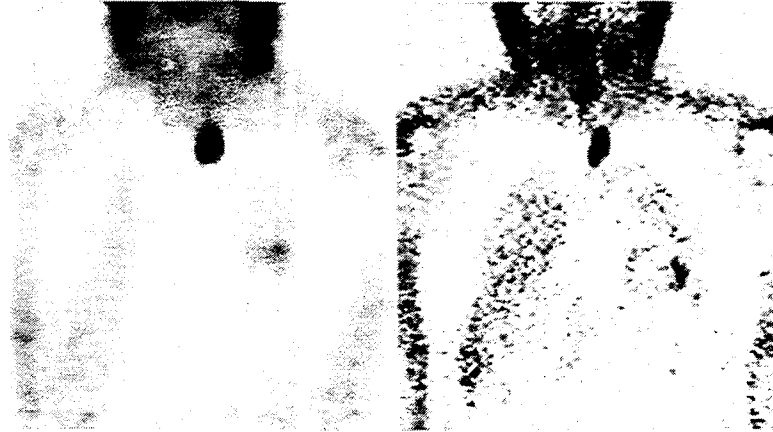


Fig. 2. A 60-year-old man was investigated with ^{18}F -FDG because of raised thyroglobulin and a (false) negative ^{131}I whole body scan. The ^{18}F -FDG images obtained with the coincidence camera (left) and the PET scanner (right) clearly showed an increased uptake in the paratracheal region. Surgery and histology confirmed this finding.

References

- [1] Dietlein M., Scheidhauer K., Voth E., Theissen P. and Schicha H. (1997) Fluorine-18 fluorodeoxyglucose positron emission tomography and iodine-131 whole-body scintigraphy in the follow-up of differentiated thyroid cancer. *Eur. J. Nucl. Med.* **24**, 1342-1348.
- [2] Feine U., Lietzenmayer R., Hanke J. P., Held J., Wöhrle H. and Müller-Schauenburg W. (1996) Fluorine-18-FDG and iodine-131-iodide uptake in thyroid cancer. *J Nucl Med.* **37**, 1468-1472.
- [3] Delbeke D., Patton J. A., Martin W. H. and Sandler M. P. (1999) FDG PET and dual-head gamma camera positron coincidence detection imaging of suspected malignancies and brain disorders. *J. Nucl. Med.* **40**, 110-117.
- [4] Weber W., Young C., Abdel-Dayem H. M., Skafianakis G., Weir G., Shreve P., Swamy C., Gates M., Rijk P., Parker A., Valk P., Leung A., Caputo G., Sollito R., Hines H. and Wagner H. (1998) Assessment of pulmonary lesions with 18-FDG positron imaging using a gamma camera operated in coincidence. *J. Nucl. Med.* **39**, 108P.
- [5] Shreve P. D., Steventon R. S., Deters E. C., Kison P. V., Gross M. D. and Wahl R. L. (1998) Oncologic diagnosis with 2-[fluorine-18]fluoro-2-deoxy-D-glucose imaging: dual-head coincidence gamma camera versus positron emission tomographic scanner. *Radiology* **207**, 431-437.
- [6] Bengel F. M., Ziegler S. I., Avril N., Weber W., Laubenbacher C. and Schwaiger M. (1997) Whole-body positron emission tomography in clinical oncology: comparison between attenuation-corrected and uncorrected images [see comments]. *Eur. J. Nucl. Med.* **24**, 1091-1098.

BRAIN DOPAMINERGIC SYSTEMS

19. The Pharmacokinetics of FDOPA in Newborn Piglets

G. Vorwieger, R. Bergmann, B. Walter¹, R. Bauer¹, F. Füchtner, J. Steinbach, P. Brust
¹Institut für Pathophysiologie, Friedrich-Schiller Universität, Jena

Introduction

Positron emission tomography (PET) after i.v. application of FDOPA provides, among other things, information about the enzyme kinetics in dopamine metabolism (for review see [4]). Its application to newborn piglets represents a new animal model which requires chemical quantification of radiotracer metabolism in the brain target tissue as well as in plasma. The results of this quantification are shown here on a temporary level and discussed with regard to commonly accepted FDOPA PET modelling.

Methods

Newborn piglets were injected with 50 MBq/kg equivalent to 10 $\mu\text{mol/kg}$ FDOPA [2].

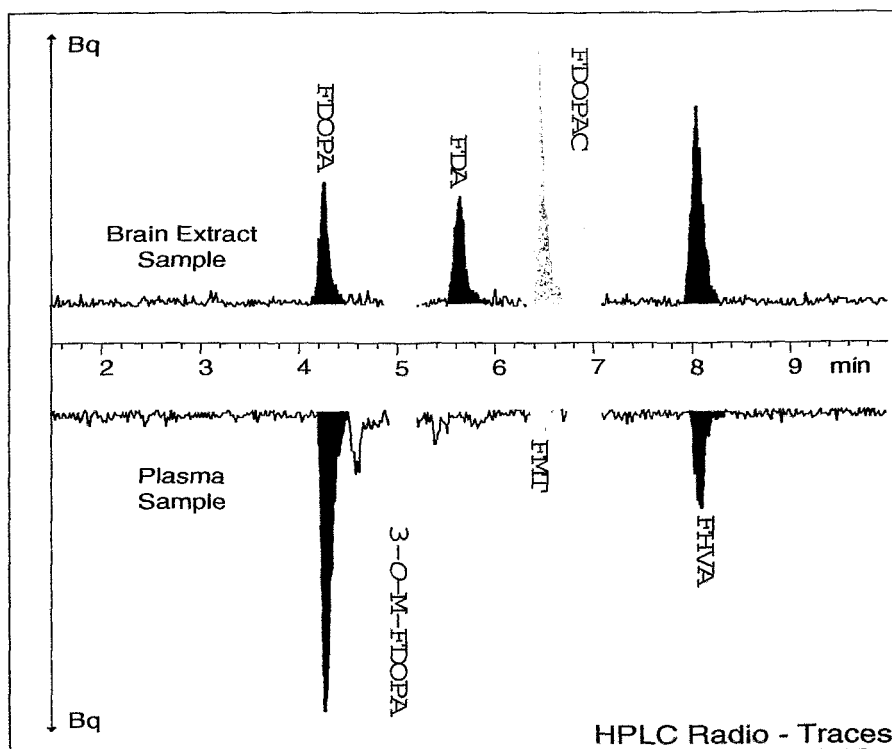


Fig. 1. Representative HPLC radiotracers of brain extract and plasma.
Colours and abbreviations as in Fig. 3.

Five brain regions (cerebellum, frontal cortex, mesencephalon, nucleus caudatus and putamen) were chosen for tissue metabolite analysis after euthanasia at different times p.i.. Preanalytical preparation and HPLC of that tissue and of blood plasma were accomplished by an application [7] specially developed for the purpose, aimed at fast sample throughput (short half life of ^{18}F), recovery of all the potential FDOPA metabolites and low detection limit. Further sample throughput enhancement was achieved by simultaneous use of two analytical columns coupled by a switching valve. Fig. 1 shows representative chromatograms of brain extract and plasma with the individual peaks coloured as in the pathway scheme (Fig. 3).

Results

The plasma total activity soon after injection passed a brief maximum and then approximated a steady state at a 1/1 plasma/brain ratio (Fig. 2). In the brain the ^{18}F activity never covered more than six substances. Their relative kinetics, together with the plasma kinetics of the identical substances, are arranged according to the generally accepted pathway and biodistribution succession (Fig. 3).

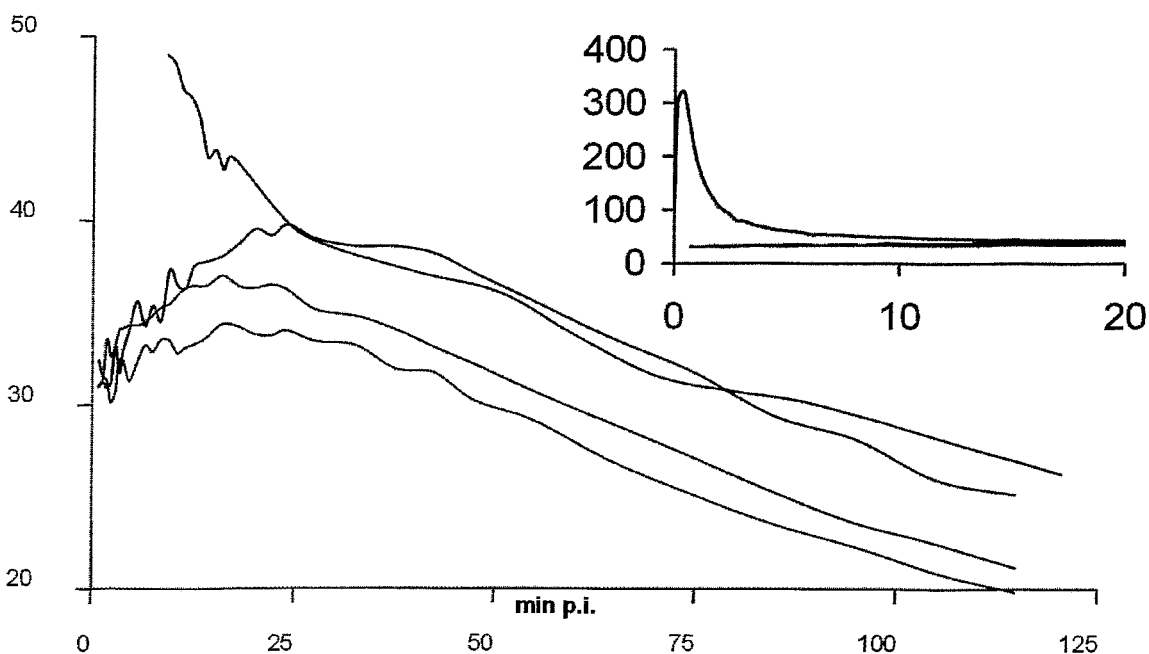


Fig. 2: Normalised total ^{18}F activity of the plasma and brain versus time (ordinate: $1000 \times (\% \text{dose/g})$). Graph colours as in Fig. 3.

Among the five extracted brain regions we suggest to classify three types of metabolism (table + Fig. 3). Since we worked without peripheral AADC inhibition, we obtained a complex plasma metabolite pattern: the plasma activity was mainly formed by four substances (FDOPA, 3-O-M, FDOPAC, FHVA). FMT and FDA belonged to the minor plasma metabolites the sum of which never exceeded 15 % of total ^{18}F .

Table 1. Brain metabolism classification

Type	Region	FDOPA turnover	FDA storage
I	cerebellum / cortex	slow	negligible
II	mesencephalon	fast	negligible
III	Nucleus caudatus / putamen	intermediate	significant

Discussion

During the first few minutes p.i. the FDOPA brain metabolism showed considerable dynamics with quantitative changes higher than during all the remaining PET acquisition time (total 120 min). In the piglets this contradicts prolonged data acquisition procedures yielding the diagnostically discriminating variables (such as k_4). The rapidly accumulating major metabolite FHVA as well as FMT and FDOPAC are by definition regarded as non BBB diffusible. We emphasise that FMT accounted for as much as 35 % of total brain activity (peak at 4 min p.i.). Expressed as total activity this implies that the most concentrated ^{18}F species occurring in piglet brain are FHVA, FDOPAC and FMT.

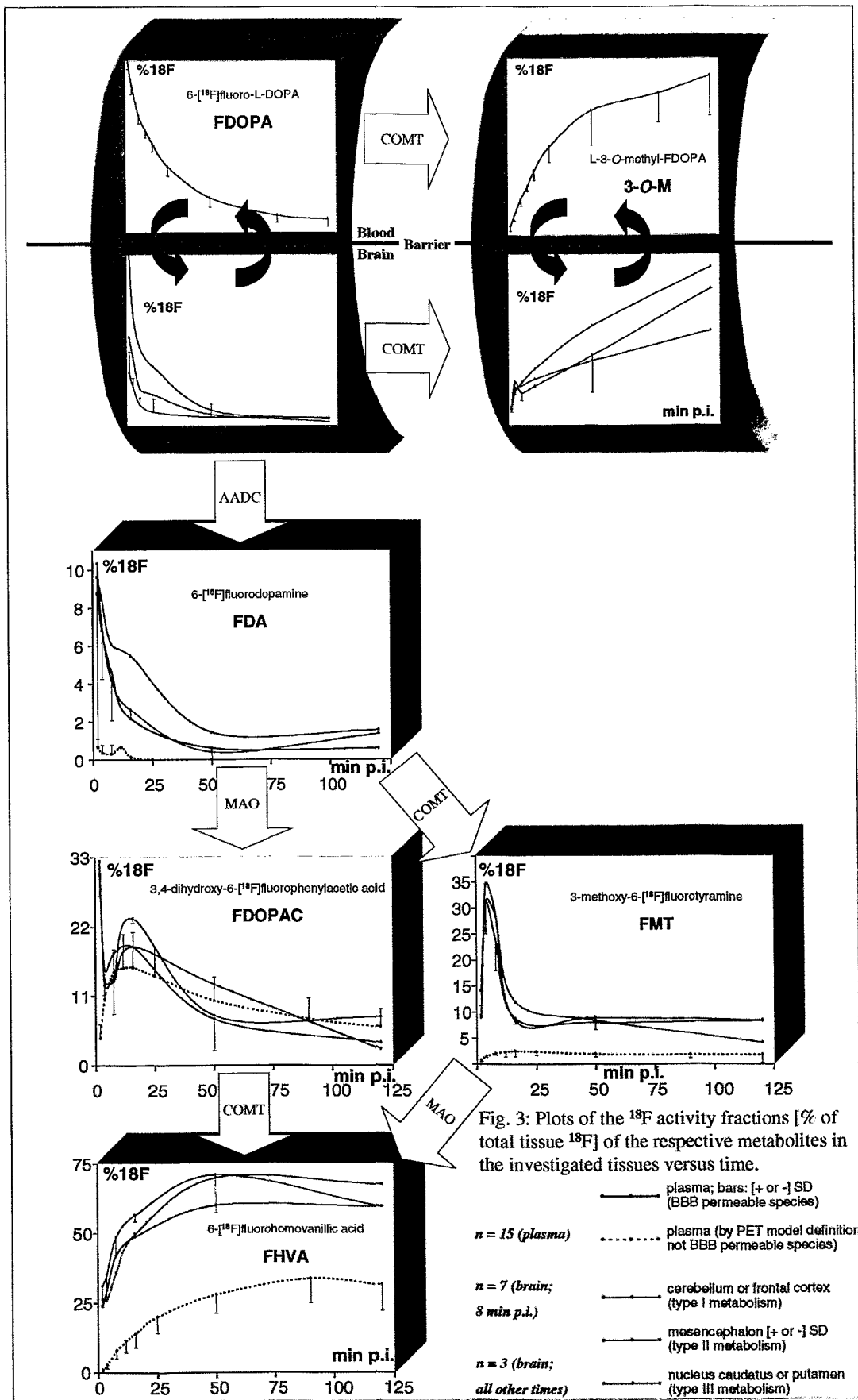


Fig. 3. Plots of the ¹⁸F activity fractions [% of total tissue ¹⁸F] of the metabolites in the investigated tissues versus time.

In recent PET modelling FMT has been generally neglected on the assumption that it represents less than 5 % of total activity. In endogenous metabolism methoxytyramine may be indicative for dopamine release into interstices [1].

The rapid pathway passage does not meet substantial postulates of slope-intercept plots (that is: FDA and its acidic metabolites are trapped in the brain target regions; brain clearance processes of FDOPAC and FHVA do not significantly alter tissue activity because of their low percentage up to 50 min p.i. For review see [4]). The metabolite pattern changes during the first few minutes p.i. are possibly part of a qualitatively distinct episode that describes xenobioticum detoxification (violation of tracer principle by the injected FDOPA amounts; [8]) rather than endogenous turnover rates.

As against the results in adult animals, the same magnitude of metabolism was found in reference regions (cerebellum, cortex) and target regions (nc. caud., putamen). However, this might have been expected from experiments on the ontogenesis of CNS AADC activity [3] and tissue extract analysis revealing high endogenous HVA contents[5]. The contribution of an immature BBB has to be considered as well. Nevertheless, we found small but partially significant differences in normalised ¹⁸F contents of FDOPA, FHVA, the sum of amines and the sum of AADC products between the three metabolic types with plausible signs (t = 8 min p.i.; n = 7; data not shown). These differences may reflect the only specific volume of transmitter metabolism and thus the appropriate ontogenetic maturation level of the dopaminergic system (dopamine storage [6], precursor and terminal product accumulation of the transmitter).

Conclusion

Without peripheral AADC inhibition in neonatal piglets, there emerge two features which interfere with the use of FDOPA PET for striatal AADC investigation: (1) The properties of the much higher concentrated FDA products conceal the desired target process. (2) The widespread distribution of AADC in the brain does not leave a well suitable PET reference region. Feature (1) is treated by implementation of compartment models which take FDA metabolites into account (k_a , describes the loss of tissue activity by FDOPAC and FHVA diffusion). Feature (2) is treated by the choice of the **plasma slope-intercept plot** instead of the **tissue slope-intercept plot** together with properly performed plasma metabolite analyses.

References

- [1] Brown E. E., Damsma G., Cumming P. and Fibiger H. C. (1991): Interstitial 3-methoxytyramine reflects striatal dopamine release: An in vivo microdialysis study. *J. Neurochem.* **57**, 701-707.
- [2] Brust P., Bauer R., Walter B., Bergmann R., Füchtner F., Vorwieger G., Steinbach J., Johannsen B. and Zwiener U. (1998): Simultaneous measurement of [¹⁸F]FDOPA metabolism and cerebral blood flow in newborn piglets. *Int. J. Devl. Neurosci.* **16**, 353-364.
- [3] Commissiong J. W. (1985): Monoamine metabolites: their relationship and lack of relationship to monoaminergic neuronal activity. *Biochem. Pharmacol.* **34**, 1127-1131.
- [4] Cumming P. and Gjedde A. (1998): Compartmental analysis of DOPA decarboxylation in living brain from dynamic positron emission tomograms. *Synapse* **29**, 37-61.
- [5] Shaywitz I. A., Anderson G. M. and Cohen D. J. (1985): Cerebrospinal fluid (CSF) and brain monoamine metabolites in the developing rat pup. *Dev. Brain Res.* **17**, 225-232.
- [6] Tennyson V. M., Barrett R. E., Cohen G., Cote L., Heikkila R. and Mytilineou C. (1972): The developing neostriatum of the rabbit: correlation of fluorescence histochemistry, electron microscopy, endogenous dopamine release, and [³H]dopamine uptake. *Brain Res.* **46**, 251-285.
- [7] Vorwieger G., Brust P., Bergmann R., Bauer R., Walter B., Füchtner F., Steinbach J. and Johannsen B. (1998): HPLC analysis of the metabolism of 6-[¹⁸F]fluoro-L-DOPA in the brain of neonatal pigs. In: *Quantitative functional brain imaging with positron emission tomography*, (Carson R.E., Daube-Witherspoon M.E. and Herscovitch P., eds.) Academic Press, New York, pp. 285-292.
- [8] Hartvig P., Agren H., Reibring L., Tedroff J., Bjurling P., Kihlberg T. and Langström B (1991): Brain kinetics of L-[β-¹¹C]DOPA in humans studied by positron emission tomography. *J. Neural Transm.* **86**, 25-41.

Abbreviations not declared above

BBB	blood brain barrier;	AADC	aromatic amino acid decarboxylase
CNS	central nervous system;	COMT	catechol-O-methyl transferase
MAO	monoamine oxidase		

20. Characterization of Blood-Brain Transport of Large Neutral Amino Acids with 3-O-Methyl- ^{18}F Fluoro-DOPA

H. Kuwabara¹, P. Brust, F. Füchtner, H. Stark², J. Steinbach

¹Department of Neurosurgery, West Virginia University Morgantown, USA

²Leibniz-Institut für Neurobiologie Magdeburg

Introduction

In preceding papers, we have demonstrated that it requires, not the unidirectional blood-brain clearance constant (K_1^*), but two Michaelis-Menten constants to describe blood-brain transport of glucose [1]. The two constants, relative maximal transport of OMG (T_{\max}^*) and the half-saturation constant of glucose (K_t), can be obtained when K_1^* is measured with PET at a range of plasma glucose levels. In the study, the two constants were estimated in a group of subjects, assuming common values among individuals. It is necessary, however, to estimate the two constants in a single individual and in a single region in order to examine changes in the constants in neurological conditions in which pathological changes in the constants are expected.

Blood-brain transport of large neutral amino acids (LNAAs) is also shown to obey the Michaelis-Menten equation [2, 3]. Recently, Miyagawa *et al.* [4] demonstrated an up-regulation of LNAA transport in brain tumors.

In this study, we introduced a new method for estimating the Michaelis-Menten constants of blood-brain LNAA transport in a single subject with one PET study with ^{18}F fluoro-O-methyl-L-DOPA (OMFD), a specific tracer of the transport.

Theory

In the following, we present a theoretical basis for measuring parameters of blood-brain transport of LNAAs in one OMFD-PET study. In the proposed experiments, concentrations of LNAAs are increased gradually when OMFD is in a near steady-state following an intravenous injection (e.g., 40 minutes after injection). In such experiments, rate constants which describe the kinetics of individual LNAAs and OMFD are time-variant. In addition, the fact that a number of LNAAs compete for the same facilitated transport makes equations complicated. For this reason, only critical equations will be presented in this paper. Details can be found elsewhere [5]. According to the Michaelis-Menten equation, K_1 of i -th LNAA (denoted by suffix i) is given by:

$$K_{1i}(t) = \frac{T_{\max_i}}{K_{t_i} (1 + \sum_{j=1}^n C_{a_j}(t) / K_{t_j})} \quad \dots \quad (1)$$

where K_{1i} , K_{t_i} , and $C_{a_i}(t)$ are the maximal transport, half-saturation constant, and concentration in plasma of the i -th LNAA. The equation for k_{2i} , the brain-blood clearance rate constant of the i -th LNAA, can be obtained by replacing $C_{a_i}(t)$ by $M_{e_i}(t)$, the content of i -th LNAA in the brain in the equation. (Strictly speaking, the concentration and the content should be discriminated. However, we treat them equally in this paper for the sake of simplicity). Similarly, K_1^* of OMFD is given by:

$$K_1^*(t) = \frac{T_{\max}^*}{K_t^* (1 + \sum_{j=1}^n C_{a_j}(t) / K_{t_j})} \quad \dots \quad (2)$$

where T_{\max}^* and K_t^* are the maximal transport and half-saturation constant of OMFD. The $K_1 - k_2$ ratios are common among LNAAs and the OMFD tracer. Thus, the ratio, denoted by $V_e(t)$ is given by:

$$V_e(t) = \frac{1 + \sum_{j=1}^n M_{e_j}(t) / K_{t_j}}{1 + \sum_{j=1}^n C_{a_j}(t) / K_{t_j}} \quad \dots \quad (3)$$

It is likely that the utilization of the i -th LNAA remains constant (c_i) despite the gradual increase in plasma concentrations of LNAAs during the experiment. The utilization is given by:

$$c_i = K_{1_i}(t) \cdot C_{a_i}(t) - k_{2_i}(t) \cdot M_{e_i}(t) \quad \dots \quad (4)$$

as the difference between the amount of the LNAA which enters the brain (the first term) and the amount of the LNAA which returns to the circulation (the second term). The equation is divided by $K_{1_i}(t) \cdot K_{1_i}$ to obtain:

$$C_{a_i}(t) / K_{1_i} - M_{e_i}(t) / K_{1_i} / V_e(t) = c_i / [K_{1_i} \cdot K_{1_i}] \quad (5)$$

In the right-hand side of the equation, $K_{1_i}(t) \cdot K_{1_i}$ is replaced by $T_{\max_i} / (1 + \sum_{j=1}^n C_{a_j}(t) / K_{1_j})$, according to Equation (1), to obtain:

$$C_{a_i}(t) / K_{1_i} - M_{e_i}(t) / K_{1_i} / V_e(t) = [c_i / T_{\max_i}] \cdot (1 + \sum_{j=1}^n C_{a_j}(t) / K_{1_j}) \quad (6)$$

The equation for each LNAA is added across LNAAs to obtain:

$$\sum_{i=1}^n C_{a_i}(t) / K_{1_i} - \sum_{i=1}^n M_{e_i}(t) / K_{1_i} / V_e(t) = \sum_{i=1}^n [c_i / T_{\max_i}] \cdot (1 + \sum_{j=1}^n C_{a_j}(t) / K_{1_j}) \quad \dots(7)$$

The left-hand side of the equation can be modified as follows:

$$1 + \sum_{i=1}^n C_{a_i}(t) / K_{1_i} - (1 + \sum_{i=1}^n M_{e_i}(t) / K_{1_i}) / V_e(t) - 1 + 1 / V_e(t) \quad (8)$$

The first two terms cancel each other, according to Equation (3). Thus Equation (7) can be rearranged to:

$$1 / V_e(t) = 1 + \sum_{i=1}^n [c_i / T_{\max_i}] \cdot (1 + \sum_{j=1}^n C_{a_j}(t) / K_{1_j}) \quad (9)$$

Further more, Equation (9) can be modified as follows using Equation (2):

$$1 / V_e(t) = 1 + \sum_{i=1}^n [c_i / T_{\max_i}] \cdot [T_{\max_i}^* / K_{1_i}^*] / K_{1_i}^* \quad (10)$$

Since $V_e(t)$ is common among LNAAs and OMFD, Equation (10) is multiplied by $K_{1_i}^*(t)$ to obtain:

$$k_2^*(t) = K_{1_i}^*(t) + \sum_{i=1}^n [c_i / T_{\max_i}] \cdot [T_{\max_i}^* / K_{1_i}^*] \quad (11)$$

Separately, the kinetics of OMFD is described by the following differential equation:

$$dM_e^*(t) / dt = K_{1_i}^*(t) \cdot C_a^*(t) - k_2^*(t) \cdot M_e^*(t) \quad (12)$$

In this equation, $k_2^*(t)$ is replaced by Equation (11) and $K_{1_i}^*(t)$ by Equation (2) to obtain:

$$dM_e^*(t) / dt = [T_{\max_i}^* / K_{1_i}^*] \left\{ \frac{C_a^*(t) - M_e^*(t)}{1 + \sum_{i=1}^n C_{a_i}(t) / K_{1_i}} - [\sum_{i=1}^n c_i / T_{\max_i}] \cdot M_e^*(t) \right\} \quad (13)$$

There are two constants to estimate by least squares optimization, namely $T_{\max_i}^* / K_{1_i}^*$ and $\sum_{i=1}^n c_i / T_{\max_i}$. Practical application of the equation will be discussed in Methods.

Methods

We studied 5 pigs (~6 weeks old, body weight~20 kg) in this project under isoflurane anesthesia. Each pig was studied with OMG twice at least 4 hours before the OMFD study. We confirmed that the pigs were normoglycemic at least one hour before the OMFD study, although plasma glucose concentration was modified in the OMG experiments. At time 0, a bolus of ~300 Bq (two thirds of the total dose) was given intravenously over one minute and PET data acquisition was started. Starting at 20 minutes, the remaining one third dose of OMFD was continuously infused throughout the study. Starting at 40 minutes, either physiological saline (n = 3) or amino acid solution (n = 2) were infused at a constant rate throughout the study. A total of 38 frames were recorded with the Siemens ECAT EXACT HR+ PET. There were 6 thirty-second frames, 7 one-minute frames, 5 two-minute frames, and 20 five-minute frames. Arterial blood was sampled from the femoral artery using an HPLC fraction collection system at a constant speed for the first 20 minutes. Blood samples were collected into a tube every 20 seconds for the first 6 minutes then every minute thereafter. Blood samples were taken manually every 5 minutes after 20 minutes. Samples were immediately placed on ice. The radioactivity in plasma was determined with the Wallac 1480 Wizard 3" automatic gamma counter which was cross-calibrated with the PET. Concentrations of LNAAs were determined on arterial plasma taken at 10 minute intervals after 35 minutes.

All data were processed as described in detail in a separate paper. The radioactivity was corrected for physical decay to time 0. The radioactivity in arterial plasma was expressed in nCi/ml as a function of time. Regional radioactivity data sets were also obtained as functions of time and expressed in nCi/g. The regions included left and right frontal, temporal, parietal, and occipital lobes, and cerebellum. We obtained K_1 and k_2 of OMFD in the 12 brain regions for each animal using data obtained during the first 40 minutes. In the amino acid infusion experiments, we assumed that regional estimates of K_1 represented K_1 for plasma LNAAs concentrations at 35 minutes (i.e., pre-infusion) of the regions. Regional K_1 estimates were used later as described below.

We found that measured radioactivity was subject to error due to relatively low counts toward the end of study. In order to minimize the uncertainty, $M_e^*(t)$ was fitted by a sum of two exponentials as follows:

$$M_e^*(t) = A^*(t) - v_0 \cdot C_a^*(t) = \sum_{i=1}^2 e^{-a_i t + b_i} \quad (14)$$

where v_0 is the effective vascular volume to subtract intravascular radioactivity ($v_0 = 0.035$ ml/g). The derivative of $M_e^*(t)$, $dM_e^*(t)/dt$, was obtained by differentiating Equation (14) as follows:

$$dM_e^*(t)/dt = -\sum_{i=1}^2 a_i \cdot e^{-a_i t + b_i} \quad (15)$$

Since the values of K_1 for individual LNAAs are not known for young pigs, we used values reported for the rat brain [2,6] after averaging, assuming that the pig values were proportional to the rat values [7]. Thus:

$$\sum_{i=1}^6 C_{a_i}(t) / K_{t_i} [pig] = \beta \cdot \sum_{i=1}^6 C_{a_i}(t) / K_{t_i} [rat] \quad (16)$$

where β is a factor to account for the proportionality. Six LNAAs were considered in this study. The K_{t_i} values used were 0.42 for valine, 0.115 for methionine, 0.193 for isoleucine, 0.0895 for leucine, 0.112 for tyrosine, and 0.0655 for phenylalanine (units are $\mu\text{mol/ml}$). The sum was also fitted by a sum of two exponentials as follows:

$$\sum_{i=1}^6 C_{a_i} / K_{t_i} [rat] = p - \sum_{j=1}^2 e^{-q_j t + r_j} \quad (17)$$

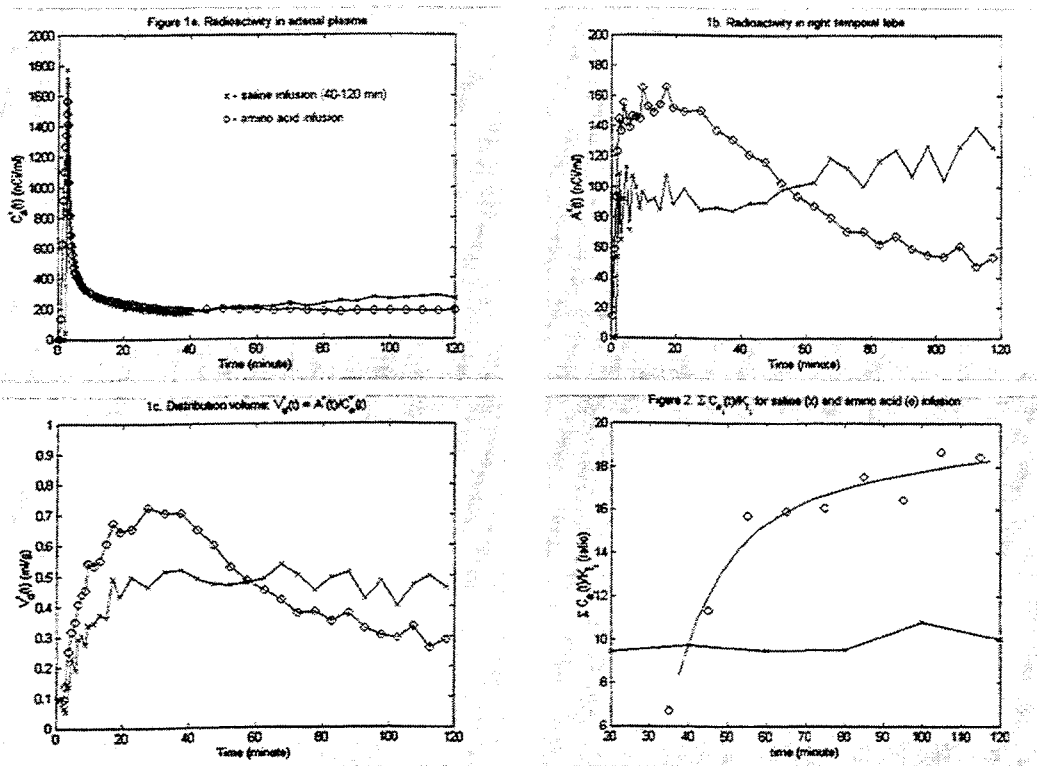
Equation (13) can be re-written as:

$$dM_e^*(t)/dt = \alpha \cdot \frac{C_a^*(t) - M_e^*(t)}{1 + \beta \cdot \sum C_{a_i}(t) / K_{t_i}} - \gamma \cdot M_e^*(t) \quad (18)$$

where α is T_{\max} / K_1^* , and γ is $[T_{\max}^* / K_1^*] \cdot \sum_{i=1}^6 c_i / T_{\max}$. In a preliminary study, we found that the residual square sum changed little when β was changed in step wise from 0.1 to 7.2. Thus, we chose regional values of β which minimized the difference between calculated values of K_1^* , given by $\alpha / (1 + \beta \cdot \sum_{i=1}^6 C_{a_i}(35))$, and the estimates of the regions. We assumed that concentrations of LNAAs in plasma remained constant before amino acid solution infusion started at 40 minutes.

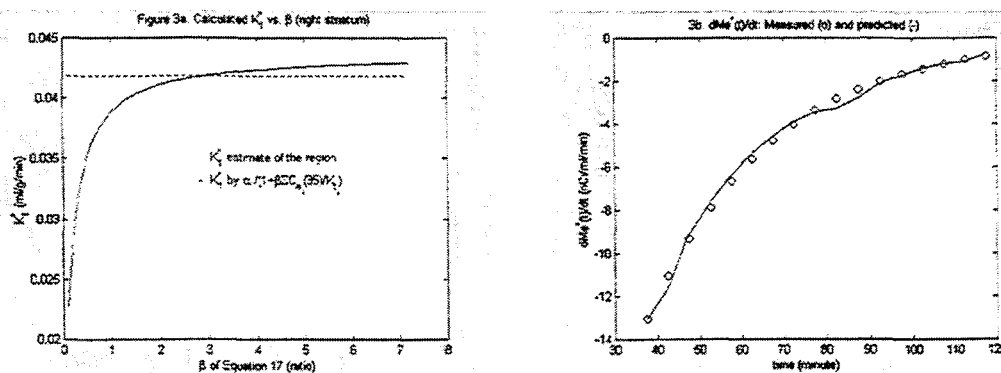
Results and Discussion

The radioactivity in arterial plasma is shown in Fig. 1a for one experiment with saline infusion (marked with x) and one experiment with amino acid infusion (o). The present infusion method kept $C_a(t)$ relatively constant throughout the experiment in all studies. The radioactivity in the right temporal lobe is shown in Fig. 1b for the two experiments. In the experiment with saline infusion, $A(T)$ increased constantly over time because $C_a(t)$ also increased slightly over time in this experiment. However, the distribution volume ($A(T)$ over $C_a(t)$) remained constant as shown in Fig. 1c.



When $A(T)$ changes relatively little over time as is the case with this experiment, the distribution volume must be close to the $K_1 - k_2$ ratio (Equation (12)). In the experiment with amino acid infusion, $A(T)$ decreased slowly over time despite $C_a(t)$ remaining constant after 40 minutes. The distribution volume decreased from 0.7 at 40 minutes to 0.3 at 120 minutes.

The sum of the concentration-half saturation constant ratios, given by Equation (16), remained constant in saline infusion experiments. One example is shown in Fig. 2 with x. The sum of the ratios increased rapidly from 6 at pre-infusion (35 minutes) to 18 at 120 minutes in this amino acid infusion experiment (shown by o in the figure). In another amino acid infusion experiment, the sum increased somewhat less from 6.5 at 35 minutes to 14.4 at 120 minutes. The curve in the figure indicated the best fit by Equation (18).



As described in the Method, β was fixed to estimate α and γ of Equation (18). The value of β was changed step wise from 0.1 to 7.2 (step size: 0.1) and α and γ were estimated for each β . K_1^* was calculated by Equation (2) as $\alpha / (1 + \beta \cdot \sum_{i=1}^6 C_{a_i}(35) / K_i)$. In Fig. 3a, calculated K_1^* was plotted against β . The calculated K_1^* should represent K_1^* before amino acid infusion and should be equal to the estimate of K_1^* using the data obtained during the first 40 minutes (shown by the dotted line in the figure). It was noted, however, that the choice of β may suffer uncertainty because the paths of the two K_1^* crossed where calculated K_1^* approached an asymptote, as evidenced in the figure. For this reason, we chose the mean β across regions. The values were 3.5 for one experiment (shown in the figure) and 2.2 in the other experiment. In Fig. 3b (right panel), measured $dM_e^t(t)/dt$ (strictly speaking, calculated $dM_e^t(t)/dt$ using Equation (15)) were shown by circles and predicted $dM_e^t(t)/dt$ (calculated by Equation (18)) by the curve. In all regions, the two were close to each other. The best estimates of T_{max}/K_1^* ($=\alpha$) averaged 0.87 ± 0.15 (g/ml) in one amino acid infusion experiment and 0.26 ± 0.06 in the other. The values were quite different between the two animals. The value from the second animal was close to the value for the human striatum (0.22 g/ml) we obtained in a previous experiment [7]. In the human study, T_{max}/K_1^* was obtained as the best estimate across 6 subjects using [18 F]fluoro-L-DOPA. The estimates of $\sum_{i=1}^6 c_i / T_{max_i}$ ($=\gamma / \alpha$) averaged 0.034 ± 0.010 (ratio) in one animal and 0.057 ± 0.010 in the other. These values indicated that only about 0.6~0.9 % of LNAAs were used in the pig brain relative to the maximal transport. If values of individual K_i change in parallel in a pathological condition, estimates of β should change accordingly. However, it is not certain whether such changes in β can be detected by this method at this point.

Summary

1. We introduced the theory for regional measurements of the Michaelis-Menten constants of blood-brain transport of LNAAs.
2. We demonstrated that the theory described actual data.
3. The estimates of T_{max}/K_1^* for the pig brain was close to the value we obtained for the human striatum using [18 F]fluoro-L-DOPA.
4. The current study indicated that only about 0.6~0.9% of LNAAs were used in the pig brain relative to the maximal transport.

References

- [1] Kuwabara H., Brust P., Bergmann R., Mäding P. and Steinbach J. (1999) Blood-Brain transport of glucose studied with [^{11}C]3-O-methylglucose and [^{18}F]fluoro-deoxyglucose. See part 2 of this report.
- [2] Pardridge W. M. and Oldendorf W. H. (1975) Kinetic analysis of blood-brain barrier transport of amino acids. *Biochim. Biophys. Acta* **401**, 128-136.
- [3] Knudsen G. M., Hasselbalch S., Toft P. B., Christensen E., Paulson E. and Lou H. (1995) Blood-brain barrier transport of amino acids in healthy controls and in patients with phenylketoneuria. *J. Inher. Metab. Dis.* **18**, 653-664.
- [4] Miyagawa T., Oku R., Uehara H., Desai R., Beattie B., Tjuvajev J. and Blasberg R. (1998) "Facilitated" amino acid transport is upregulated in brain tumors. *J. Cereb. Blood Flow Metab.* **18**, 500-509.
- [5] Kuwabara H. and Brust P. (1999) Blood-Brain transport of glucose studied with [^{11}C]O-methylglucose and [^{18}F]fluoro-deoxyglucose. Manuscript in preparation.
- [6] Smith Q., Momma S., Aoyagi M. and Rapoport S. I. (1987) Kinetics of neutral amino acid transport across the blood-brain barrier. *J. Neurochem.* **49**, 1651-1658.
- [7] Kuwabara H., Nishizawa S., Cumming P., Shiraishi M., Diksic M. and Gjedde A. (1999) Effects of dietary protein on kinetics of [^{18}F]fluoro-L-DOPA. *J. Cereb. Blood Flow Metab.*, submitted.

21. Regional Distribution of Cerebral Blood Volume in Newborn Piglets – Effect of Hypoxia/Hypercapnia

R. Bergmann, R. Bauer¹, B. Walter¹, P. Brust

¹Institut für Pathophysiologie, Friedrich-Schiller-Universität Jena

Introduction

Cerebral blood volume (CBV) is an important factor in cerebral hemodynamics as well as a key parameter in brain tracer studies. The newborn piglet has been shown to be a good model for the study of brain blood flow and metabolism and this model has now been well standardized (for review see [1]). However, apparently up until now an estimation of regional CBV has not been performed. In order to establish in vivo tracer studies for further investigations of normal and disturbed brain functions in newborn piglets, knowledge of regional distribution of CBV is necessary.

The aim of this study was to determine the regional distribution of CBV that occur under normal conditions and under conditions of vasodilatation induced by hypoxia/hypercapnia.

Material and Methods

The animal experiments were performed according to the German Law on the Protection of Animals. The study was approved by the committee of the Saxon state government for animal research (75-9185.81-4.6/95).

Fourteen newborn piglets (aged 5 to 7 days old, body weight 2373 ± 381 g) of both sexes were utilized in this study. All animals were anesthetized with 0.25 - 0.5 % isoflurane in 70 % nitrous oxide and 30 % oxygen. Body temperature, heart rate, mean arterial blood pressure (MAP), arterial and brain venous pH, $p\text{CO}_2$, and $p\text{O}_2$, oxygen saturation and hemoglobin values were monitored. A central venous catheter was introduced through the left external jugular vein and was used for tracer injection and for volume substitution (Ringer/lactate solution: 5 ml/h). A polyurethane catheter (PU 3.5 Ch, Sherwood, England) was advanced through the right femoral artery into the abdominal aorta 1 cm above the aortic bifurcation for blood sampling and for arterial blood pressure monitoring. Seven animals were held under unchanged conditions and served as sham operated control (normoxic group). Another seven animals underwent a change in their inspired gas composition (FiO_2 was lowered from 0.35 to 0.11 in exchange for nitrogen and about 10 % CO_2 was added) and served as the hypoxia/hypercapnia group. At the 15th minute of hypoxia/hypercapnia the animals were injected with 30 - 40 MBq $^{99m}\text{TcO}_4^-$ intravenously. Five minutes later the animals were killed by decapitation immediately following intracardial injection of about 1ml saturated KCl solution, which stopped myocardial function. The brain was removed within 90 seconds and further dissected for CBV measurements. In blood samples obtained immediately before death and in brain tissue samples radioactivity of ^{99m}Tc was measured in a well counter (COBRA II, Packard Instrument Company, Meriden, CT, and U.S.A.). Cerebral blood volume (CBV) was calculated using the following formula: $\text{CBV} = (\text{tissue radioactivity} \square \text{blood weight}) / (\text{blood radioactivity} \square \text{tissue weight})$ and expressed as percentage of sample weight.

Data are reported as means \pm SD. Comparisons between both animal groups were performed using the t-test for independent samples and Bonferroni correction for multiple use. Differences were considered significant when $P < 0.05$.

Results

Table 1 summarizes the values for MAP, heart rate, arterial blood gases, and catecholamines during baseline conditions and after fifteen minutes of hypoxia/hypercapnia. The baseline values are within the physiological range and consistent with other data obtained from anesthetized and artificially ventilated newborn piglets [2]. The supposed degree of moderate hypoxia/hypercapnia, i.e. a reduction of arterial $p\text{O}_2$ of about twenty five per cent of baseline value in addition to nearly doubling arterial $p\text{CO}_2$, led to a significant increase of MAP and heart rate together with a several fold increase of epinephrine and norepinephrine ($p < 0.05$). Moreover, arterial oxygen content and also brain AVDO₂ were reduced to about one third ($p < 0.05$). However, under this condition of hypoxia/hypercapnia brain oxidative metabolism has obviously not been compromised. Regional CBV was significantly higher in the lower brain stem and cerebellum compared with the values from thalamus and white matter ($p < 0.05$).

Table 1. Physiological values and blood catecholamines of newborn piglets obtained during baseline conditions and in the 15th minute of hypoxia/hypercapnia.

	Control group n = 7		Hypoxia/hypercapnia group n = 7			
	baseline		baseline		hypoxia/hypercapnia	
Heart rate (min ⁻¹)	217	± 25	201	± 23	261	± 19 *
MABP (mmHg)	68	± 3	68	± 9	79	± 4 *
Arterial pH	7.42	± 0.04	7.46	± 0.02	7.23	± 0.05 *
Arterial pCO ₂ (mm Hg)	39	± 3	36	± 1	68	± 5 *
Arterial pO ₂ (mm Hg)	120	± 12	128	± 8	32	± 5 *
Arterial O ₂ content (μmol/ml)	4.1	± 0.7	4.2	± 0.9	1.4	± 0.3 *
AVDO ₂ (mmol/l)	2.5	± 0.4	2.5	± 0.4	0.7	± 0.2 *
Epinephrine (pg/ml)	175	± 40	217	± 169	1239	± 979 *
Norepinephrine (pg/ml)	504	± 315	481	± 442	7807	± 5245 *
Dopamine (pg/ml)	204	± 38	145	± 68	262	± 94 *

(Values are means ± SD. AVDO₂ indicates difference of arterial and brain venous blood content of oxygen. * P < 0.05, comparison between baseline stage and the stage of hypoxia/hypercapnia.)

Hypoxia/hypercapnia induced a considerable change in CBV. There were considerable differences among different regions in the brain. The increase in percentage of the CBV was higher in structures with lowest baseline values; i.e. the thalamus (66 % increase) and white matter (62 % increase). However, absolute values remained significantly higher within the lower brain stem, cerebellum and cerebral cortex (p < 0.05).

Discussion

The newborn piglet has been shown to be an appropriate model for the study of cerebral blood flow and metabolism [1]. However, to the best of one's knowledge measurement of regional CBV has not been done before in newborn piglets. A considerable number of studies which presented parameters of cerebral oxidative metabolism under different experimental conditions, including various sedation states have been performed in newborn piglets [3 - 9]. Usually the CBV is measured by determining the brain distribution space for nondiffusible red cell and / or plasma markers. Typical tracers include ⁵¹Cr-, ⁵⁵Fe-, ^{99m}Tc-, or C¹⁵O labelled red cells, or ^{99m}Tc- or radioiodine-labeled albumin. Recently, as a new principle paramagnetic contrast media like Gd-complexes are used to determine quantitatively the intravascular volume by using contrast MRI techniques [10, 11]. The obtained magnetic resonance imaging of cerebral blood volume (CBV) estimates correlated well with values obtained by ¹⁵O labelled carbon monoxide (C¹⁵O) PET. However, PET CBV values were approximately 2.5 times larger than absolute MRI CBV values, supporting a hypothesized sensitivity of MRI to small vessels [12]. In addition to their expenses, these attractive approaches appear to be of limited value for use in smaller mammals because of the limited possibility to determine exactly the input (arterial) function in MRI and in difficulty to differentiate intracranial blood volume compartments and the extracranial compartment with appropriate exactness due to a reduced spatial resolution (> 5-8 mm) in PET [12], accordingly. In regard to the chosen method of intraparenchymal CBV we used a method based on labeling plasma and red cells together, which allows calculation of blood volume without any correction. Therefore, this method avoids hematocrit sources of error because all methods based on separate red blood cell or

plasma labelling alone require a correction for the difference between large-vessel and cerebral hematocrit [13].

Table 2. Cerebral blood volume (CBV) of different brain regions obtained during baseline conditions and in the 15th minute of hypoxia/hypercapnia in newborn piglets.

Index		Regional CBV (ml \square 100g ⁻¹)	
		control group n = 6	H/H group n = 7
1	lower brainstem	2.23 \pm 0.22	3.29 \pm 0.34*
2	cerebellum	2.60 \pm 0.60	3.55 \pm 0.39*
3	thalamus	1.55 \pm 0.40 ^{§1,2}	2.58 \pm 0.42* ^{§1,2}
4	cerebral cortex	2.01 \pm 0.31	3.07 \pm 0.31*
5	white matter	1.50 \pm 0.37 ^{§1,2}	2.43 \pm 0.36* ^{§1,2,4}

(Values are means \pm SD. * [§] P < 0.05, * indicates the comparison between baseline stage and the stage of hypoxia/hypercapnia; [§] indicates the comparison between different brain regions, given by the index column.)

Since we obtained brain tissue samples just after induction of cardiac arrest by intravenous potassium chloride and subsequent brain removal, parenchymal blood volume was measured. We used ^{99m}Tc-pertechnetate as a blood marker because evidence exist that both red blood cell membranes and serum proteins could bind ^{99m}Tc-pertechnetate with a similar degree of affinity and kinetic stability [14]. Moreover, ^{99m}Tc-pertechnetate distribution between red blood cells and plasma is suggested to be finished within a few seconds [13]. Unbiased CBV estimation is based on the prerequisite that tracer amount and distribution (e.g. in this study ^{99m}Tc-pertechnetate bound on erythrocytes and serum proteins) has not been affected either by the procedure of the killing, brain removal and brain sample processing. No separate study was carried out to determine if a secondary mismatch occurred, but it has been assumed that through the method, sequence, and timing such mismatch can be largely excluded. In detail, the procedure to gain brain tissue samples was initiated by intracardial injection of a small volume of saturated KCl solution, which led immediately (within 2 - 3 seconds after onset of KCl injection) to a simultaneous arrest of both ventricles. Simultaneously, decapitation was performed after tipping the forwards by about 75° so that effluence of blood from the head was largely prevented. Therefore, a dilution of the head blood by the injected KCl solution can be virtually excluded because dissection of all cervical vessels occurred immediately after intracardial KCl injection. Moreover, head repositioning by incline forwards after removal greatly prevents blood congestion as well as blood effluence. Indeed, using the procedure of decapitation should aid reduction of transmural pressure within cerebral circulation making arterial branches reduce in diameter. The effects on capillary beds and venous branches should have been rather small if not abolished because the head repositioning in order to prevent blood effluence resulted in a positive hydrostatic pressure similar to in vivo conditions of intracerebral venous pressure. Therefore, the normal filling of the venous branches and of parts of the capillary bed should not have been changed due to the procedure of brain removal. Furthermore, considering that the change in capacity of arterial branches due to the reduced transmural pressure would have been counteracted by a dilation of the resistive vessels due to terminal anoxia and acidic waste accumulation, a corruption of CBV estimation by procedure used here would seem to be minimal.

We chose to determine intraparenchymal blood volume as that part of total cerebral blood volume, which deals mainly with microcirculation [13, 15]. Therefore, the approach used here provides unbiased data of intraparenchymal CBV, which are of particular concern for instance in studies using tracer kinetics methods in newborn piglets [16].

We found under normoxic/normocapnic conditions considerable regional differences of CBV with the highest values in the brain stem and the lowest values in the forebrain white matter (p < 0.05). CBV of the cerebral cortex was found to be similar to data measured in adult rat forebrain after in vivo micro-

wave fixation [17]. Other studies, however, reported considerably lower parenchymal CBV values (about half) in adult rats [13, 15, 18]. In these studies CBV measurements were done after decapitation. Estimation of CBV in young rats after killing by saturated potassium chloride and brain dissection yielded CBV values, which were slightly higher than in adult rats [19]. As extensively discussed measurement of CBV in brain tissue samples after brain removal is markedly influenced by the methods, which were used. Todd and co-worker pointed out when the CBV is measured in small samples of brain tissue obtained after animals are killed either by drug overdose or decapitation, the resultant values would be lower than those obtained from in vivo methods or those obtained when the brain was fixed in situ before removal because of tracer loss from the tissue during processing [17]. Keyeux *et al.* argued that a higher CBV value after in situ fixation by focussed microwave irradiation could be due to the absence of bleeding during decapitation and dissection and also to the brain sample contamination by extraparenchymal components, since microwave fixation makes peeling off the meninges impossible [20]. We used brain tissue samples, which were carefully stripped of their meningeal coverings so that penetrating arterial branches, capillaries and intraparenchymal veins are included into CBV estimation. Extracerebral contamination appears almost excluded. Therefore in newborn piglets the parenchymal CBV seems to be somewhat higher than in adult animals.

Two different mechanisms appear to be responsible for cerebral vasodilatation under hypoxia/hypercapnia. Hypoxia *per se* induces pial artery dilation by neuronal derived nitric oxide (NO) in newborn piglets via formation of cGMP and the subsequent release of opioids [21]. Hypercapnia-induced cerebral vasodilatation is prostanoid-associated [22] and NO independent [23] in the newborn pig. Studies in cerebral microvascular smooth muscle cells derived from newborn pigs suggest that arteriolar dilation in response to hypercapnia requires the presence of an intact endothelium and is accompanied by an indomethacine-sensitive increase in cortical adenosine 3', 5'-cyclic monophosphate (cAMP) [24]. We assume that under hypoxia/hypercapnia used here a maximum dilation of cerebral resistive vessels occurred in newborn piglets.

As a consequence of this vasodilation, hypoxia/hypercapnia induced a moderate increase in CBV in all brain regions studied (36 to 66 %) ($p < 0.05$). The moderate increase in intracerebral CBV may reflect predominantly the enlargement of the resistive vessel branches. However, minor increase of cerebral venous pressure as might result from upstream basilar dilation cannot be excluded, because cerebral venous pressure has not been measured in this study. A capillary recruitment obviously does not exist in the adult brain during the high flow situation of hypercapnia [25], and the brain circulation appears to be different from peripheral vascular beds by having a continuous capillary perfusion. According to our data derived from newborn piglets it seems also to be true for the immature brain, considering that only a moderate CBV increase resulted under hypoxia/hypercapnia in comparison to a tremendous CBF elevation (see following report).

One study was reported where cerebral erythrocyte volume (CEV) was monitored together with other parameters of cerebral oxygen delivery and uptake in newborn piglets during normal conditions and various stages of blood gas manipulation [26]. CEV was measured by erythrocytes labeled with ^{99m}Tc -pertechnetate and scintillation detection over the head. Surprisingly, no significant changes in CEV were detected throughout this study. This was obviously caused by methodological problems in regard to the used CEV measurement procedure since extracranially counted radioactivity as a measure of cerebral erythrocyte volume is contaminated by radioactivity emitted by labeled red blood cells from vessel beds outside the brain, mainly from venous plexus at the base of the skull and from adjacent extracranial tissue, e.g. nasal mucosa. The authors stated that despite all their efforts to reduce extracranial contamination, e.g. shielding within the oral cavity and animal body surface by lead, about 30 % of the detected radioactivity was assumed to be resulted from Compton scatter from the subdural venous plexus at the base of the skull and from adjacent extracranial tissue. However the assumption that extracerebral erythrocyte volume varied parallel to CEV throughout the various experimental states remains rather unlikely. Changes in blood gas composition which induce a marked redistribution of circulating blood which is accompanied by gradual increase in sympathetic tone should lead to opposite responses of cerebral and adjacent extracerebral blood volume, e.g. vasodilatation of brain vessels (see above) and vasoconstriction of respective extracerebral vessels especially within the adjacent nasal mucosa, particularly the nasal venous sinusoids since nasal mucosa blood flow and tone of the capacitance vessels are strictly controlled by sympathetic tone [18, 27].

In summary, newborn piglets under normoxic and normocapnic conditions exhibit a comparatively enlarged intraparenchymal CBV. Moderate hypoxia and hypercapnia induced a increase in CBV caused by vasodilatation of cerebral vessels.

References

- [1] Raju T. N. (1992) Some animal models for the study of perinatal asphyxia. *Biol. Neonate* **62**, 202-214.
- [2] Lerman J., Oyston J. P., Gallagher T. M., Miyasaka K. A. G., Volgyesi G. A. and Burrows F. A. (1990) The minimum alveolar concentration (MAC) and hemodynamic effects of Halothane, Isoflurane, and Sevoflurane in newborn swine. *Anesthesiology* **73**, 717-721.
- [3] Armstead W. M. and Kurth C. D. (1994) Different cerebral hemodynamic responses following fluid percussion brain injury in the newborn and juvenile pig. *J. Neurotrauma* **11**, 487-497.
- [4] Bauer R., Zwiener U., Buchenau W., Hoyer D., Witte H., Lampe V., Burgold K. and Zieger M. (1989) Restricted cardiovascular and cerebral performance of intra-uterine growth retarded newborn piglets during severe hypoxia. *Biomed. Biochim. Acta* **48**, 697-705.
- [5] Busija D. W. and Leffler C. W. (1987) Hypothermia reduces cerebral metabolic rate and cerebral blood flow in newborn pigs. *Am. J. Physiol.* **253**, H869-H873.
- [6] Busija D. W., Leffler C. W. and Pourcyrous M. (1988) Hyperthermia increases cerebral metabolic rate and blood flow in neonatal pigs. *Am. J. Physiol.* **255**, H343-H346.
- [7] Laptook A. R., Corbett R. J., Ruley J. and Olivares E. (1992) Blood flow and metabolism during and after repeated partial brain ischemia in neonatal piglets. *Stroke* **23**, 380-387.
- [8] Laptook A. R., Stonestreet B. S. and Oh W. (1983) Brain blood flow and O₂ delivery during hemorrhagic hypotension in the piglet. *Pediatr. Res.* **17**, 77-80.
- [9] Leffler C. W. and Busija D. W. (1987) Prostanoids and pial arteriolar diameter in hypotensive newborn pigs. *Am. J. Physiol.* **252**, H687-H691.
- [10] Rosen B. R., Belliveau J. W., Buchbinder B. R., McKinstry R. C., Porkka L. M., Kennedy D. N., Neuder M. S., Fisel C. R., Aronen H. J., Kwong K. K. *et al.* (1991) Contrast agents and cerebral hemodynamics. *Magn. Reson. Med.* **19**, 285-292.
- [11] Rosen, B.R., Belliveau, J.W., Vevea, J.M. and Brady, T.J. (1990) Perfusion imaging with NMR contrast agents, *Magn Reson Med*, **14**, 249-265.
- [12] Ostergaard L., Smith D. F., Vestergaard Poulsen P., Hansen S. B., Gee A. D., Gjedde A. and Gyldensted C. (1998) Absolute cerebral blood flow and blood volume measured by magnetic resonance imaging bolus tracking: comparison with positron emission tomography values. *J. Cereb. Blood Flow Metab.* **18**, 425-432.
- [13] Keyeux A., Ochrymowicz Bemelmans D., Van Eyll C. and Charlier A. (1993) Total cerebral blood volume calculated from a model of [^{99m}Tc]pertechnetate distribution in the head. *J. Appl. Physiol.* **74**, 2886-2895.
- [14] Hays M. J. and Green F. A. (1973) In vitro studies of ^{99m}Tc-pertechnetate binding by human serum and tissues. *J. Nucl. Med.* **14**, 149-158.
- [15] Cremer J. E. and Seville M. P. (1983) Regional brain blood flow, blood volume, and haematocrit values in the adult rat. *J. Cereb. Blood Flow Metab.* **3**, 254-256.
- [16] Brust P., Bauer R., Walter B., Bergmann R., Füchtner F., Vorwieger G., Steinbach J., Johannsen B. and Zwiener U. (1998) Simultaneous measurement of [¹⁸F]FDOPA metabolism and cerebral blood flow in newborn piglets. *Int. J. Dev. Neurosci.* **16**, 353-364.
- [17] Todd M. M., Weeks J. B. and Warner D. S. (1993) Microwave fixation for the determination of cerebral blood volume in rats. *J. Cereb. Blood Flow Metab.* **13**, 328-336.
- [18] Rinder J. and Lundberg J. M. (1996) Nasal vasoconstriction and decongestant effects of nitric oxide synthase inhibition in the pig. *Acta Physiol. Scand.* **157**, 233-244.
- [19] Hansen T. W. R. and Bratlid D. (1989) Cerebral blood volumes in young rats with and without in situ saline flushing of cerebral vasculature. *Biol. Neonate* **56**, 15-21.
- [20] Keyeux A., Ochrymowicz Bemelmans D. and Charlier A. A. (1995) Induced response to hypercapnia in the two-compartment total cerebral blood volume: influence on brain vascular reserve and flow efficiency. *J. Cereb. Blood Flow Metab.* **15**, 1121-1131.
- [21] Wilderman M. J. and Armstead W. M. (1997) Role of PACAP in the relationship between cAMP and opioids in hypoxia-induced pial artery vasodilation. *Am. J. Physiol.* **41**, H1350-H1358.
- [22] Wagerle L. C. and Mishra O. P. (1988) Mechanism of CO₂ response in cerebral arteries of the newborn pig: role of phospholipase, cyclooxygenase, and lipoxxygenase pathways. *Circ. Res.* **62**, 1019-1026.
- [23] Zuckerman S. L., Armstead W. M., Hsu P., Shibata M. and Leffler C. W. (1996) Age dependence of cerebrovascular response mechanisms in domestic pigs. *Am. J. Physiol.* **271**, H535-H540.

- [24] Parfenova H. and Leffler C. W. (1996) Effects of hypercapnia on prostanoid and cAMP production by cerebral microvascular cell cultures. *Am. J. Physiol.* **270**, C1503-C1510.
- [25] Göbel U., Klein B., Schröck H. and Kuschinsky W. (1989) Lack of capillary recruitment in the brains of awake rats during hypercapnia. *J. Cereb. Blood Flow Metab.* **9**, 491-499.
- [26] Brun N. C., Moen A., Borch K., Saugstad O. D. and Greisen G. (1997) Near-infrared monitoring of cerebral tissue oxygen saturation and blood volume in newborn piglets. *Am. J. Physiol.* **273**, H682-H686.
- [27] Bamford O. S. and Eccles R. (1983) The role of sympathetic efferent activity in the regulation of brain temperature. *Pflügers Arch.* **396**, 138-143.

22. Effect of Hypoxia/Hypercapnia on Cerebral Blood Flow in Newborn Piglets

R. Bauer¹, P. Brust, B. Walter¹, R. Bergmann

¹Institut für Pathophysiologie, Friedrich-Schiller-Universität Jena

Introduction

Cerebral blood flow (CBF) is an important factor in cerebral hemodynamics as well as a key parameter in brain tracer studies. A linear relationship is suggested between CBF and cerebral blood volume (CBV) according to the fundamental equation derived by Meier and Zierler [1]. This equation states that the mean transit time (MTT) of a tracer equals the ratio between the volume of distribution of the tracer in the organ and the blood flow rate through the organ. Therefore it has to be assumed that the relation between CBV and CBF is a continuously changing function which is predestined by momentary metabolic requirements and that one parameter alone cannot be used as a reliable index for the other [2].

The newborn piglet has been shown to be a good model for the study of CBF and metabolism and this model has now been well standardized (for review see [3]).

The aim of this study was to determine the regional distribution of CBV, CBF, and MTT that occur under normal conditions and under conditions of vasodilatation induced by hypoxia/hypercapnia. We tested the hypothesis that the marked increase of regional cerebral blood flow is predominantly caused by reduced MTT rather than increased regional CBV during hypoxia/hypercapnia.

Material and Methods

The animal experiments were performed according to the German Law on the Protection of Animals. The study was approved by the committee of the Saxon state government for animal research (75-9185.81-4.6/95).

Fourteen newborn piglets (aged 5 to 7 days old, body weight 2373 ± 381 g) of both sexes were utilized in this study. All animals were anesthetized with 0.25 - 0.5 % isoflurane in 70 % nitrous oxide and 30% oxygen. Body temperature, heart rate, mean arterial blood pressure (MAP), arterial and brain venous pH, $p\text{CO}_2$, and $p\text{O}_2$, oxygen saturation and hemoglobin values were monitored. A central venous catheter was introduced through the left external jugular vein and was used for tracer injection and for volume substitution (Ringer/lactate solution: 5 ml/h). The left ventricle was cannulated retrogradely via the right common carotid artery with a polyurethane catheter (PU 3.5 Ch, Sherwood, England) for colored microsphere (CMS) injection and placement was verified by pressure tracings and at autopsy. A polyurethane catheter (PU 3.5 Ch, Sherwood, England) was advanced through the right femoral artery into the abdominal aorta 1 cm above the aortic bifurcation for blood sampling, for withdrawing the reference sample of CMS method and for arterial blood pressure monitoring.

Seven animals were held under unchanged conditions and served as sham operated control (normoxic group). Another seven animals underwent a change in their inspired gas composition (FiO_2 was lowered from 0.35 to 0.11 in exchange for nitrogen and about 10 % CO_2 was added) and served as the hypoxia/hypercapnia group. Physiological measurements were performed at the 15th minute of hypoxia/hypercapnia. Five minutes later the animals were killed by decapitation immediately following intracardial injection of about 1ml saturated KCl solution, which stopped myocardial function.

Regional CBF was measured by means of the reference sample color-labeled microsphere technique. Absolute flow to tissues measured by colored microspheres were calculated by the formula: $\text{flow}_{\text{tissue}} = \text{number of microspheres}_{\text{tissue}} \cdot \eta$ ($\text{flow}_{\text{reference}} / \text{number of microspheres}_{\text{reference}}$). Flows are expressed in milliliters per minute per 100g of tissue by normalizing for tissue weight. Cerebrovascular resistance (CVR) was calculated as the quotient of mean arterial blood pressure divided by forebrain blood flow. Assuming the oxygen capacity of hemoglobin to be 1.39 ml O_2 /g hemoglobin in piglets [4], blood O_2 -content was calculated as equal to g hemoglobin/ml \cdot 1.39 ml O_2 /g hemoglobin \cdot % O_2 -saturation and expressed in $\mu\text{Mol}/\text{min} \cdot 100$ g. Dissolved oxygen was added by calculation, using the measured $p\text{O}_2$ and the temperature-corrected solubility coefficient of oxygen. Because the sagittal sinus drains the cerebral cortex, cerebral white matter, and some deep gray structures (basal ganglia, hippocampus), blood flow measured to the cerebrum included these structures. CMRO_2 was obtained by multiplying

blood flow to the cerebrum by the cerebral arteriovenous O₂ content difference (avDO₂). Cerebral O₂ delivery (cDO₂) was calculated as the product of cerebral blood flow times the arterial O₂ content. Data are reported as means ± SD. Comparisons between both animal groups were performed using the t-test for independent samples and Bonferroni correction for multiple use. Differences were considered significant when P < 0.05.

Results

The values for MAP, heart rate, arterial blood gases, and catecholamines during baseline conditions and after fifteen minutes of hypoxia/hypercapnia are shown Table 1 of the previous report. Under this condition of hypoxia/hypercapnia brain oxidative metabolism has obviously not been compromised. Because of an unadapted cerebral blood flow increase to the forebrain (p < 0.05) due to a considerable reduction of CVR (p < 0.05) an elevated brain oxygen delivery occurred (p < 0.05) whereas CMRO₂ remained unchanged (Table 1).

Table 1. Forebrain cerebral blood flow and parameters of brain oxidative metabolism of newborn piglets obtained during baseline conditions and in the 15th minute of hypoxia/hypercapnia.

	Control group	Hypoxia/hypercapnia group	
	n = 7 Baseline	Baseline	n = 7 Hypoxia/hypercapnia
Forebrain CBF (ml • 100g ⁻¹ • min ⁻¹)	64 ± 11	70 ± 13	274 ± 74*
Forebrain CVR (mmHg • 100g • min • ml ⁻¹)	1.08 ± 0.15	0.99 ± 0.19	0.30 ± 0.08*
Cerebral O ₂ -delivery (μmol • 100g ⁻¹ • min ⁻¹)	274 ± 90	303 ± 70	364 ± 60*
CMRO ₂ (μmol • 100g ⁻¹ • min ⁻¹)	164 ± 54	182 ± 39	183 ± 45
Oxygen extraction ratio	0.58 ± 0.03	0.61 ± 0.09	0.52 ± 0.17

(Values are means ± SD. CMRO₂ indicates cerebral metabolic rate off oxygen.

* P < 0.05, comparison between baseline stage and the stage of hypoxia/hypercapnia.)

The levels of regional CBF and MTT were considerably different during baseline conditions (Table 2). The highest perfusion rate was found in the lower brain stem and cerebellum, whereas white matter exhibited the lowest values, which was about 38 % less than those of brain stem and cerebellum (p < 0.05). Under baseline conditions MTT was significantly prolonged within the cerebral cortex compared with the thalamic MTT (p < 0.05). Hypoxia/hypercapnia induced a considerable change in brain perfusion with a vast increase of CBF and marked shortening of MTT. However there were considerable differences among different regions in the brain. The strongest increase of perfusion rate was found in the lower brain stem with an improvement of 6.7 fold, which resulted in a significantly higher rCBF in comparison to those of the cerebral cortex and white matter (Table 2, p < 0.05). MTT shortening was pronounced in all regions - between 22 % of baseline value in the lower brainstem and 49% in white matter (p < 0.05).

Table 2. Cerebral blood flow (CBF), cerebral blood volume (CBV) and mean transit time (MTT) of different brain regions obtained during baseline conditions and in the 15th minute of hypoxia/hypercapnia in newborn piglets.

Index	Regional CBF (ml • 100g ⁻¹ • min ⁻¹)		Regional MTT (s)	
	Control group n = 6	H/H group n = 7	Control group n = 6	H/H group n = 7
1 lower brain-stem	69 ± 11	460 ± 131*	2.09 ± 0.50	0.46 ± 0.14*
2 cerebellum	70 ± 10	369 ± 104*	2.22 ± 0.31	0.61 ± 0.17*
3 thalamus	62 ± 9	393 ± 107*	1.53 ± 0.38	0.42 ± 0.14*
4 cerebral cortex	56 ± 4	258 ± 72*	2.34 ± 0.42 ^{§§}	0.79 ± 0.27* ^{§§}
5 white matter	43 ± 7 ^{§ 1,2,3}	150 ± 42* ^{§ 1,2,3}	2.06 ± 0.52	1.05 ± 0.35* ^{§ 1,2,3}

(Values are means ± SD. * § P < 0.05, * indicates the comparison between baseline stage and the stage of hypoxia/hypercapnia; § indicates the comparison between different brain regions, given by the index column.)

Discussion

The newborn piglet has been shown to be an appropriate model for the study of cerebral blood flow and metabolism [3]. Therefore, a considerable number of studies which presented parameters of cerebral oxidative metabolism under different experimental conditions, including various sedation states have been performed in newborn piglets [5 - 8]. Mild sedation by volatile anesthetics and analgesia by nitrous oxide (used here) has no detectable influence on cardiovascular response in newborn piglets [9]. Furthermore, pancuronium administered in newborn piglets for neuromuscular blocking while ventilation is controlled does not alter systemic hemodynamic status [10]. Cerebral blood flow and cerebral O₂ uptake values presented in this study were similar to values obtained from newborn piglets which were treated with other drugs for general anesthesia which were indicated to not alter brain oxidative metabolism and therefore the accompanying cerebral blood flow [11]. However studies in awake and unrestrained newborn piglets showed considerably higher regional perfusion rates in the brain and also higher cerebral oxygen uptake [12]. The reason for that could be the reduced sensory input and abolished motor function due to immobilization and artificial ventilation. There is, however, no evidence that cerebrovascular response to hypoxia and hypercapnia under general anesthesia used here is basically different to that in unbiased conditions [13]. Therefore the study design is appropriate estimating regional CBF, and MTT under baseline normoxic and normocapnic state and during conditions of cerebrovascular dilation induced by combined moderate hypoxia and hypercapnia which is able to effect a compensatory blood flow increase in order to maintain an adequate brain oxygen uptake under compromised conditions. Indeed, systemic hypoxia/hypercapnia induces a circulatory redistribution even in immature mammals which favors the blood flow towards the heart, brain and adrenals in expense of the other organs and tissues. This is mainly affected by an increase in sympathoadrenal activity. However, in contrast to older animals cardiovascular response in newborns is mainly caused by circulating catecholamines because of delayed central sympathetic maturity. Indeed, Lee and Downing have shown that hypoxia-induced cardiovascular responses were observed in intact and ganglionic blockade piglets, but no changes occurred in adrenalectomized piglets [14]. Direct stimulation of adrenal medulla and extramedullary chromaffin cells by reduced arterial pO₂ is mainly responsible for increased catecholamine release in newborn rats early after birth [15]. Neurogenic activation via increased efferent sympathetic tone appears to be rather unlikely since peripheral chemoreceptors remain insensitive shortly after birth. Resetting takes several days even in precocial animals like newborn lambs [16]. Therefore, sympathetic activity is mainly reflected by changes in circulating catecholamines and may serve as a relevant indicator for an adequate response of cardiovascular regulation due to systemic hypoxia/hypercapnia in newborns.

We used the colored microsphere method for regional cerebral blood flow measurement, which was evaluated in this lab for use on newborn piglets [25]. This method enables a multiple quantitative estimation of the nutritive circulation during a short period of time (e.g. 2 to 3 minutes after intracardial microsphere injection). In contrast to CBF determination by diffusible tracers the use of particles as indicators of nutritive flow has been shown to be appropriate even during high perfusion states [17].

Moderate hypoxemia combined with hypercapnia, which simulates blood gas changes typical for respiratory distress in newborns, leads to an exceeding CBF increase so that cerebral oxygen delivery surpasses baseline value but cerebral O₂ uptake remains not altered (Table 2). The reason for this high increase in non-adapted cerebral blood flow should be a dilation of cerebral resistive vessels, which appeared to be not more completely controlled by metabolic demands since cerebral oxygen metabolism remained obviously unchanged, but cerebral O₂-delivery was inadequately increased ($p < 0.05$). This assumption is supported by findings in parallel studies on newborn piglets. We studied effects of hypoxic hypoxia alone and of combined hypoxia/hypercapnia on CBF and the cerebral oxidative metabolism. We found that hypoxia alone induced a balanced CBF increase of about 160 %, whereas cerebral O₂-delivery and CMRO₂ remained constant. In contrast, combined hypoxia/hypercapnia led to a further CBF increase with a concomitant increase of cerebral O₂-delivery, but CMRO₂ remained unchanged [18].

Two different mechanisms appear to be responsible for cerebral vasodilatation under these conditions. Hypoxia *per se* induces pial artery dilation by neuronal derived nitric oxide (NO) in newborn piglets via formation of cGMP and the subsequent release of opioids [19]. Hypercapnia-induced cerebral vasodilation is prostanoid-associated [20] and NO independent [21] in the newborn pig. Studies in cerebral microvascular smooth muscle cells derived from newborn pigs suggest that arteriolar dilation in response to hypercapnia requires the presence of an intact endothelium and is accompanied by an indomethacin-sensitive increase in cortical adenosine 3', 5'-cyclic monophosphate (cAMP) [22]. We assume that under hypoxia/ hypercapnia used here a maximum dilation of cerebral resistive vessels occurred in newborn piglets.

A capillary recruitment obviously does not exist in the adult brain during the high flow situation of hypercapnia [23], and the brain circulation appears to be different from peripheral vascular beds by having a continuous capillary perfusion. According to our data derived from newborn piglets it seems also to be true for the immature brain, considering that only a moderate CBV (see previous report) increase resulted under hypoxia/hypercapnia in comparison to the tremendous CBF elevation. According to the law of continuity of flow, in the case of continuous capillary perfusion, blood flow regulation is under unique control of vasomotion. Because the cerebral arteries, as well as pial arteries and arterioles represent the main part of cerebral resistive vessels [24], cerebral perfusion is mainly regulated outside the parenchyma itself. Therefore, under conditions of marked vasodilation like combined hypoxia/hypercapnia with concomitantly marked CVR decrease, an increased pressure gradient throughout the microcirculating branch has to be assumed because pressure decrease along the resistive vessels was considerably reduced. As a consequence, perfusion velocity through intraparenchymal vessels, mainly shaped by the capillary network, must be increased, as shown in this study by a considerable shortening of MTT. In regard to the disproportionate shortening of MTT in comparison to the changes in intraparenchymal CBV increase there is no prediction about the behavior of extraparenchymal CBV which represents about 75 per cent of total CBV [17] and includes main branches of resistive vessels which are predominantly enlarged due to hypoxia/hypercapnia. Nevertheless, MTT shortening appears to be a direct consequence of cerebral vasodilation. Further influences, like increased cerebral perfusion pressure may be additional factors influencing perfusion velocity within cerebral microcirculation. However, the observed small but significantly increased arterial blood pressure of $117 \pm 13\%$ obviously did not seriously affect the marked CBF increase to $393 \pm 79\%$ and MTT shortening to $32 \pm 11\%$ due to hypoxia/hypercapnia. Indeed, there was no correlation between arterial blood pressure and forebrain CBF during normoxic conditions ($R^2 = 0.092$) as well as at hypoxia/hypercapnia ($R^2 = 0.056$), as expected, since arterial blood pressure was in all cases above the autoregulatory threshold considerably lower in newborns than in older animals [25,26] but only insubstantially increased.

More relevant for microcirculatory exchange function should be that parenchymal MTT was considerably reduced which reflects a marked increase in blood flow velocity within the microcirculation. Therefore, the contact time for substance exchange within the capillaries could be critically reduced and

should surpass a possible increment in exchange area. This could be assumed to be due to a slightly increased filling of the capillary network.

In summary, newborn piglets under normoxic and normocapnic conditions exhibit a comparatively enlarged intraparenchymal CBV. Moderate hypoxia and hypercapnia induced a marked increase in cerebral blood flow, which appears to be caused by an increased perfusion velocity, expressed by a strongly reduced mean transit time. Concomitant CBV increase remains moderate.

References

- [1] Meier P. and Zierler K. L. (1954) On the theory of the indicator -dilution method for measurement of blood flow and volume. *J. Appl. Physiol.* **6**, 731-744.
- [2] Raichle M. E. (1979) Quantitative in vivo autoradiography with positron emission tomography. *Brain Res. Rev.* **1**, 47-68.
- [3] Raju T. N. (1992) Some animal models for the study of perinatal asphyxia. *Biol. Neonate* **62**, 202-214.
- [4] Busija D. W., Leffler C. W. and Pourcyrous M. (1988) Hyperthermia increases cerebral metabolic rate and blood flow in neonatal pigs. *Am. J. Physiol.* **255**, H343-H346.
- [5] Armstead W. M. and Kurth C. D. (1994) Different cerebral hemodynamic responses following fluid percussion brain injury in the newborn and juvenile pig. *J. Neurotrauma* **11**, 487-497.
- [6] Busija D. W., Leffler C. W. and Pourcyrous M. (1988) Hyperthermia increases cerebral metabolic rate and blood flow in neonatal pigs. *Am. J. Physiol.* **255**, H343-H346.
- [7] Laptook A. R., Corbett R. J., Ruley J. and Olivares E. (1992) Blood flow and metabolism during and after repeated partial brain ischemia in neonatal piglets. *Stroke* **23**, 380-387.
- [8] Leffler C. W. and Busija D. W. (1987) Prostanoids and pial arteriolar diameter in hypotensive newborn pigs. *Am. J. Physiol.* **252**, H687-H691.
- [9] Gootman P. M., Buckley N. M., Gootman N., Crane L. A. and Buckley B. J. (1978) Integrated cardiovascular responses to combined somatic afferent stimulation in newborn piglets. *Biol. Neonate* **34**, 187-198.
- [10] Easa D., Uyehara C. F., Stevens E. L., Finn K. C., Balaraman V. and Sim H. (1993) Pancuronium does not alter the hemodynamic status of piglets after normoxia or hypoxia. *Pediatr. Res.* **33**, 365-372.
- [11] Anday E. K., Lien R., Goplerud J. M., Kurth C. D. and Shaw L. M. (1993) Pharmacokinetics and effect of cocaine on cerebral blood flow in the newborn. *Dev. Pharmacol. Ther.* **20**, 35-44.
- [12] Leffler C. W., Busija D. W. and Beasley D. G. (1987) Effect of therapeutic dose of indomethacin on the cerebral circulation of newborn pigs. *Pediatr. Res.* **21**, 188-192.
- [13] Leffler C. W. (1997) Prostanoids: Intrinsic modulators of cerebral circulation. *News Physiol. Sci.* **12**, 72-77.
- [14] Lee J. C., Werner J. C. and Downing E. (1980) Adrenal contribution to cardiac responses elicited by acute hypoxia in piglets. *Am. J. Physiol.* **239**, H751-H755.
- [15] Mojet M. H., Mills E. and Duchon M. R. (1997) Hypoxia-induced catecholamine secretion in isolated newborn rat adrenal chromaffin cells is mimicked by inhibition of mitochondrial respiration. *J. Physiol.* **504**, 175-89.
- [16] Hanson M. A. (1988) The importance of baro- and chemoreflexes in the control of the fetal cardiovascular system. *J. Dev. Physiol.* **10**, 491-511.
- [17] Keyeux A., Ochrymowicz Bemelmans D. and Charlier A. A. (1995) Induced response to hypercapnia in the two-compartment total cerebral blood volume: influence on brain vascular reserve and flow efficiency. *J. Cereb. Blood Flow Metab.* **15**, 1121-1131.
- [18] Bauer R., Walter B., Kluge H., Würker E. and Zwiener U. (1995) Different amount of CBF increase during hypoxia and hypoxia/hypercapnia, but unchanged CMRO₂ in newborn piglet. *Pflügers Archiv Suppl* **429**, R136.
- [19] Wilderman M. J. and Armstead W. M. (1997) Role of PACAP in the relationship between cAMP and opioids in hypoxia-induced pial artery vasodilation. *Am. J. Physiol.* **41**, H1350-H1358.
- [20] Wagerle L. C. and Mishra O. P. (1988) Mechanism of CO₂ response in cerebral arteries of the newborn pig: role of phospholipase, cyclooxygenase, and lipoxigenase pathways. *Circ. Res.* **62**, 1019-1026.
- [21] Zuckerman S. L., Armstead W. M., Hsu P., Shibata M. and Leffler C. W. (1996) Age dependence of cerebrovascular response mechanisms in domestic pigs. *Am. J. Physiol.* **271**, H535-H540.
- [22] Parfenova H. and Leffler C. W. (1996) Effects of hypercapnia on prostanoid and cAMP production by cerebral microvascular cell cultures. *Am. J. Physiol.* **270**, C1503-C1510.

- [23] Göbel U., Klein B., Schröck H. and Kuschinsky W. (1989) Lack of capillary recruitment in the brains of awake rats during hypercapnia [see comments]. *J. Cereb. Blood Flow Metab.* **9**, 491-499.
- [24] Bauer R., Hoyer D., Walter B., Gaser E., Kluge H. and Zwiener U. (1997) Changed systemic and cerebral hemodynamics and oxygen supply due to gradual hemorrhagic hypotension induced by an external PID-controller in newborn swine. *Exp. Toxic. Pathol.* **49**, 469-476.
- [25] Hernandez M. J., Brennan R. W. and Bowman G. S. (1980) Autoregulation of cerebral blood flow in the newborn dog. *Brain Res.* **184**, 199-202.

23. A New Tropane-Derived Rhenium Complex with High Affinity for the Dopamine Transporter

A. Hoeping, M. Reisgys, P. Brust, S. Seifert, H. Spies, R. Alberto¹, B. Johannsen
¹Paul Scherrer Institut, Villigen, Switzerland

Introduction

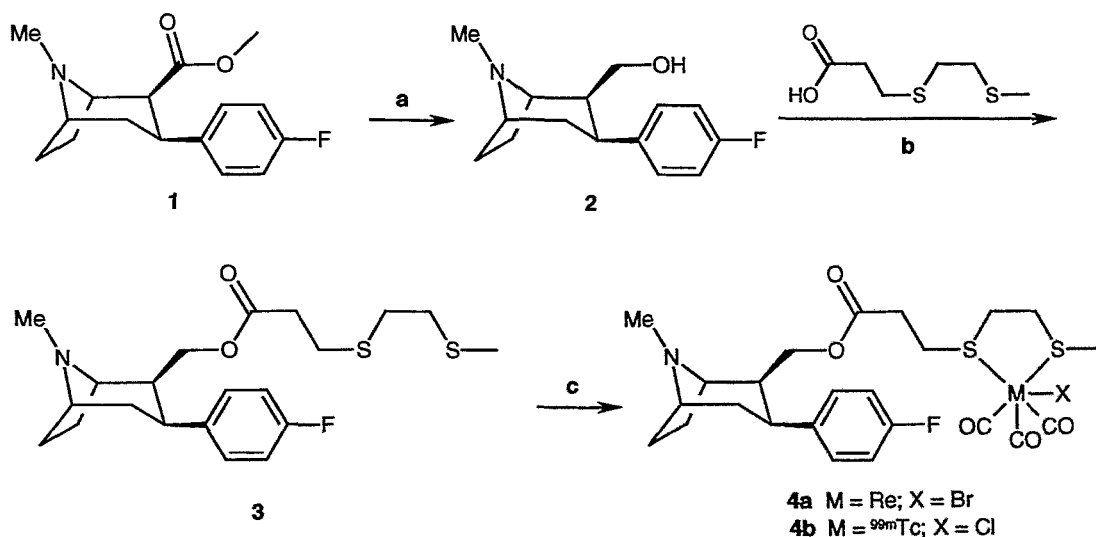
Parkinson's disease is characterized by a significant loss of dopaminergic neurons in the basal ganglia. A decreased specific striatal uptake may therefore indicate early pathological states and allow a diagnosis, preferably by a radiotracer [1]. Considerable efforts have been made to incorporate a ^{99m}Tc-containing unit into a CNS receptor-targeted agent [2 – 7].

Here we describe the synthesis of the new DAT-binding ligand 4,7-dithiaoctanoic acid (3β-(4-fluorophenyl)tropan-2β-yl)-methyl ester and its coordination reaction with the tricarbonylmethyl centre of Re and ^{99m}Tc-forming complexes of the common formula [MXⁿS₂(CO)₃] ("S₂" = RS(CH₂)₂SR). We also report *in vitro* competition binding studies of **3** and the rhenium complex **4** with DAT, the serotonin transporter (5-HTT) and the norepinephrine transporter (NET).

Experimental

Starting from CFT, the new chelating ligand **3** was prepared by introduction of a dithioether unit into the 2β-position. The synthesis route is shown in Scheme 1. The desired product **3** was obtained in a quantitative yield.

Scheme 1. Synthesis of ligand **3** and the complexes **4a,b**.



Reagents: **a** DIBAL, toluene, 0 °C, 85 – 95 %; **b** EDCI, DMPA, CH₂Cl₂, 25 °C, quant.;
c (NEt₄)₂[MX₃(CO)₃] (M = Re, X = Br; M = ^{99m}Tc, X = Cl), MeOH, 25 °C.

The synthesis of the rhenium complex **4a** was performed by reaction of **3** with (NEt₄)₂ [ReBr₃ (CO)₃] in methanol [16]. After work-up **4a** was obtained in a 83 % yield.

Elemental analysis, mass spectra and IR spectra clearly indicate the proposed structure of **4a**. The tricarbonyl rhenium core is characterized by the strong vibration bands at 2032, 1940 and 1904 cm⁻¹. An additional C=O band at 1728 cm⁻¹ belongs to the ester group. The mass spectrum (FAB⁺) shows the molecular peak at *m/z* 762. The synthesis of the corresponding ^{99m}Tc complex **4b** was carried out by reaction of **3** with the analogue ^{99m}Tc precursor according to [17]. Purification and characterization of the complex was completed by HPLC (R_f = 6.2 min). The complex was obtained in a 60 – 65 % yield of 97 % radiochemical purity.

Results and Discussion

The binding affinities of the compounds **3** and **4a** for DAT, NET and 5-HTT, determined by competitive binding assays using [³H]CFT, [³H]nisoxetine and [³H]paroxetine as radioligands [21, 22], revealed a high affinity for cloned human DAT and a moderate affinity for NET and 5-HTT. Most remarkably, the dithioether-containing CFT3 has an affinity higher by one order of magnitude than CFT, and this high affinity is not diminished by complexation. Reserving poor statistics, the rhenium complex **4a** binds even more strongly to the high affinity site than the chelator **3** (Table 1).

Our IC₅₀ values obtained on cloned human DAT expressed in CHO cells are about four times lower than those found by Pristupa *et al.* [25], using COS-7 cells. Because of inconsistencies in the literature in describing one or two binding sites, we also calculated the affinities assuming only a single binding site and found a higher affinity for **4a** (IC₅₀ = 1.5 nM ± 0.4 nM) than for **3** (IC₅₀ = 3.2 nM ± 0.3 nM). It is known that CFT also binds to 5-HTT and NET. Our data (Table 1) shows that the introduction of rhenium into the chelating tropane derivative **3** decreases the affinity towards 5-HTT but, interestingly, increases the affinity towards NET.

Table 1. Binding data (IC₅₀ values) of β-CFT, **3** and **4** to the monoamine transporters. Data are means ± S.E.M. (n = 3 - 4).

	DAT high affine (nM)	DAT low affine (nM)	NET (nM)	5-HTT (nM)
β-CFT	2.62 ± 1.06	139 ± 72	834 ± 45 [17]	759 ± 47 [17]
3	0.227 ± 0.202	5.69 ± 1.20	16.3 ± 0.6	28.5 ± 4.6
4	0.146 ± 0.042	20.3 ± 16.1	7.3 ± 1.1	71.8 ± 1.4

Considering the high affinities of **3** and the complex **4a**, it is assumed that the chelating group of **3** or the chelate in **4a** are active parts in the ligand-transporter interaction. The increased lipophilicity of **3** and **4a** compared with **1** may enhance the interaction of the ligand molecule with the transporter, which is characterized by hydrophobic interaction and an assumed hydrogen bond. This argument is consistent with the previously reported results by Kozikowski regarding a 2-vinyl substituted cocaine analogue [26] and by Carroll regarding 2-heterocyclic substituted derivatives [27]. Both reports also suggest that hydrophobic interaction may contribute to the binding to the DAT.

Conclusions

The results show that the M(I) carbonyl/dithioether ligand system is a valuable tool for the design and synthesis of receptor-affine technetium and rhenium complexes. In the present case the introduction of a dithioether chelator into the tropane moiety causes an increase in affinity in the subnanomolar range which is further enhanced by complexation.

References

- [1] Tedroff J., Aquilonius S. M., Hartvig P. G. and Langstrom B. (1996) Functional positron emission tomographic studies of striatal dopaminergic activity - changes induced by drugs and nigrostriatal degeneration in Parkinson's Disease. In: Battistin L., Scarlato G., Caraceni T., Ruggieri S., Eds., Lippincott-Raven Publ. Vol. 69, pp. 443-448.
- [2] Johannsen B., Scheunemann M., Spies H., Brust P., Wober J., Syhre R. and Pietzsch H.-J. (1996) Technetium(V) and rhenium(V) complexes for 5-HT_{2A} serotonin receptor binding: Structure-affinity considerations. *Nucl. Med. Biol.* **23**, 429-438.
- [3] Samnick S., Brandau W., Sciuk J., Steinsträßer A. and Schober O. (1995) Synthesis, characterization and biodistribution of neutral and lipid-soluble ^{99m}Tc-bisaminoethanethiol spiperone. *Nucl. Med. Biol.* **22**, 573-583.
- [4] Madras B. K., Jones A. G., Mahmood A., Zimmerman R. E., Garada B., Holman B. L., Davison A., Blundell P. and Meltzer P. C. (1996) Technetium: a high-affinity ^{99m}Technetium probe to label the dopamine transporter in brain by SPECT imaging. *Synapse* **22**, 239-246.

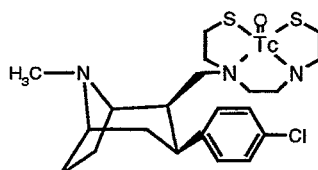
- [5] Kung M. P., Stevenson D. A., Plössl K., Meegalla S. K., Beckwith A., Essman W. D., Mu M., Lucki I. and Kung H. F. (1996) [Tc-99m]TRODAT-1: A novel technetium-99m complex as a dopamine transporter imaging agent. *Eur. J. Nucl. Med.* **24**, 372-380.
- [6] Meegalla S. K., Plössl K., Kung M. P., Chumpradit S., Stevenson D. A., Kushner S. A., McElgin W. T., Mozley P. D. and Kung H. F. (1997) Synthesis and characterization of technetium-99m-labeled tropanes as dopamine transporter-imaging agents. *J. Med. Chem.* **40**, 9-17.
- [7] Europ. Pat. Appl. 972012322.
- [8] Reigys M., Wüst F., Alberto R., Schibli R., Schubiger P. A., Pietzsch H.-J., Spies H. and Johannsen B. (1997) Synthesis of rhenium(I) and technetium(I) carbonyl/dithioether ligand complexes bearing 3,17 β - estradiol. *Bioorg. Med. Chem. Lett.* **7**, 2243-2246.
- [9] Meltzer P. C., Blundell P., Jones A. G., Mahmood A., Garada B., Zimmerman R. E., Davison A., Holman B. L. and Madras B. K. (1997) A technetium-99m SPECT imaging agent which targets the dopamine transporter in primate brain. *J. Med. Chem.* **40**, 1835-1844.
- [10] Hoepfing A., Breikreuz D., Berger R., Brust P., Jungclas H., Kretzschmar M., Seifert S., Spies H., Syhre R. and Johannsen B. Improved synthesis and biological evaluation of ^{99m}Tc-Technepine and comparison with a modified Technepine containing a hexyl linker (Hexyltechnepine). Publication in preparation.
- [11] Lewin A. H., Gao Y., Abraham P., Boja J. W., Kuhar M. J. and Carroll F. I. (1992) 2 β -substituted analogs of cocaine. Synthesis and inhibition of binding to the cocaine receptor. *J. Med. Chem.* **35**, 135-140.
- [12] Kozikowski A. P., Saiah M. K. E., Johnson K. M. and Bergmann J. S. (1995) Chemistry and biology of the 2 β -alkyl-3 β -phenyl analogs of cocaine: subnanomolar affinity ligands that suggest a new pharmacophore model at the C-2 position. *J. Med. Chem.* **38**, 3086-3093.
- [13] Carroll F. I., Kotian P., Gray J. L., Abraham P., Kuzemko M. A., Lewin A. H., Boja J. W. and Kuhar M. J. (1993) 3 β -(4'-chlorophenyl)tropan-2 β -carboxamides and cocaine amide analogs: new high affinity and selective compounds for the dopamine transporter. *Med. Chem. Res.* **7**, 468-472.
- [14] Xu L. F. and Trudell M. L. (1996) Stereoselective synthesis of 2 β -carbomethoxy-3 β - phenyltropane derivatives. Enhanced stereoselectivity observed for the conjugate addition reaction of phenylmagnesium bromide derivatives with anhydro dichloromethane. *J. Heterocycl. Chem.* **33**, 2037-2039.
- [15] Madras B. K., Spealman R. D., Fahey M. A., Neumeyer J. L., Saha J. K. and Milius R. A. (1989) Cocaine receptors labeled by [³H]2 β -carbomethoxy-3 β -(4-fluorophenyl)tropane. *Mol. Pharmacol.* **36**, 518-524.
- [16] Gracz L. M. and Madras B. K. [³H]WIN 35,428 ([³H]CFT) binds to multiple charge-states of the solubilized dopamine transporter in primate striatum. *J. Pharmacol. Exp. Ther.* **273**, 1224-1234.
- [17] Pristupa Z. B., Wilson J. M., Hoffman B. J., Kish S. J. and Niznik H. B. (1994) Pharmacological heterogeneity of the cloned and native human dopamine transporter: disassociation of [³H]WIN 35,428 and [³H]GBR 12,935 binding. *Mol. Pharmacol.* **45**, 125-135.
- [18] Meegalla S., Plössl K., Kung M.-P., Stevenson D. A., Liable-Sands L. M., Rheingold A. L. and Kung H. F. (1995) First example of a ^{99m}Tc complex as a dopamine transporter imaging agent. *J. Am. Chem. Soc.* **117**, 11037-11038.
- [19] Zoghbi S. S., Tamagnan R. M., Baldwin R. M., Gao Y., Neumeyer J. L., Baldessarini R., Charney D. S., Seibyl J. S. and Innis R. B. (1997) Synthesis of a dopamine transporter binding cyclopentadiene phenyltropane conjugate complexed with rhenium and Tc-99m. *J. Nucl. Med. (Abstracts)*, P 368.
- [20] Kozikowski A. P., Roberti M., Xiang L., Bergmann J. S., Callahan P. M., Cunningham K. A. and Johnson K. M. (1992) Structure-activity relationship studies of cocaine: replacement of the C-2 ester group by vinyl argues against hydrogen-bonding and provides an esterase-resistant, high-affinity cocaine. *J. Med. Chem.* **35**, 4764-4766.
- [21] Kotian P., Mascarella S. W., Abraham P., Lewin A. H., Boja J. W., Kuhar M. J. and Carroll F. I. (1996) Synthesis, ligand binding, and quantitative structure-activity relationship study of 3 β -(4'-substituted phenyl)-2 β -heterocyclic tropanes: evidence for an electrostatic interaction at the 2 β -position. *J. Med. Chem.* **39**, 2753-2763.

24. Investigations for an Improved Synthesis of TRODAT

I. Heimbold, A. Hoeping, S. Seifert

Introduction

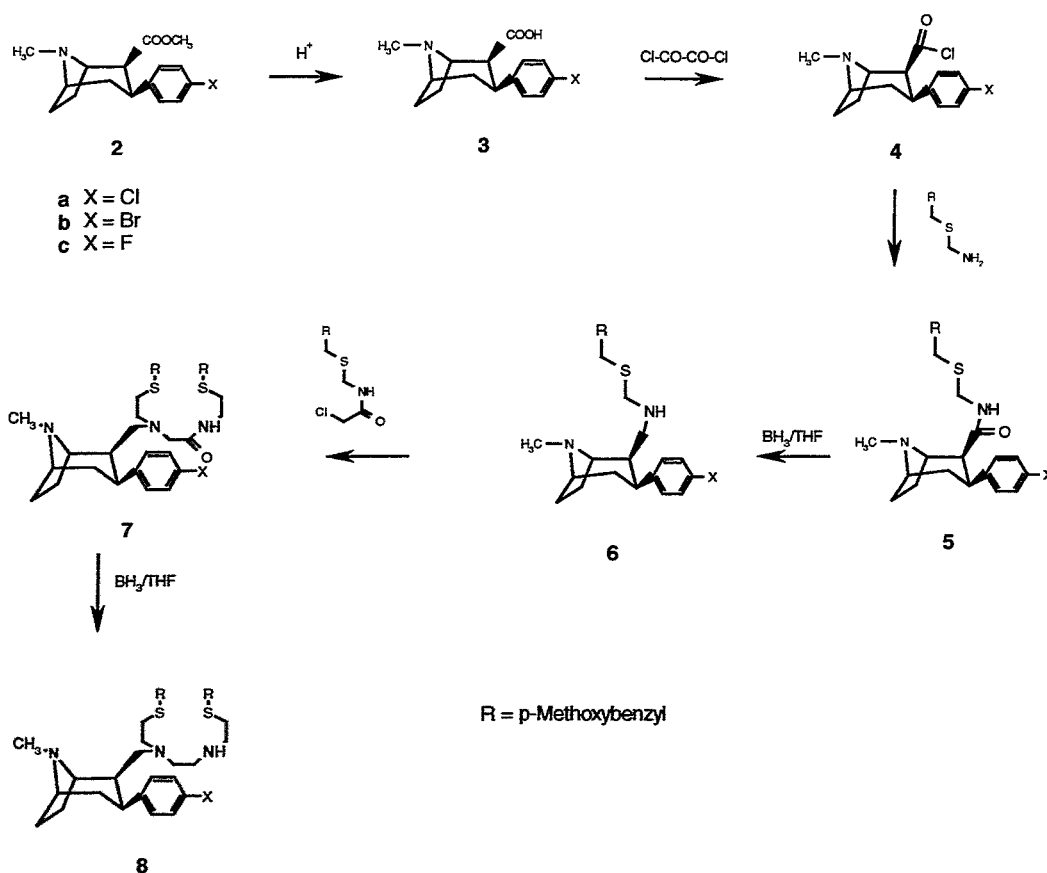
Recent publications by Kung and coworkers described [^{99m}Tc]TRODAT-1 **1** to be a useful imaging agent in the evaluation of the status of CNS dopamine transporters in humans [1 - 4].



[^{99m}Tc]TRODAT-1 **1**

The authors describe a sequential synthesis of TRODAT starting from 2 β -carbomethoxy-3 β -phenyltropanes [1] as shown (Scheme 1).

Scheme 1.



Deprotection of the thiol functions occurs with $\text{Hg}(\text{OAc})_2$ followed by radiolabelling with sodium [^{99m}Tc]pertechnetate.

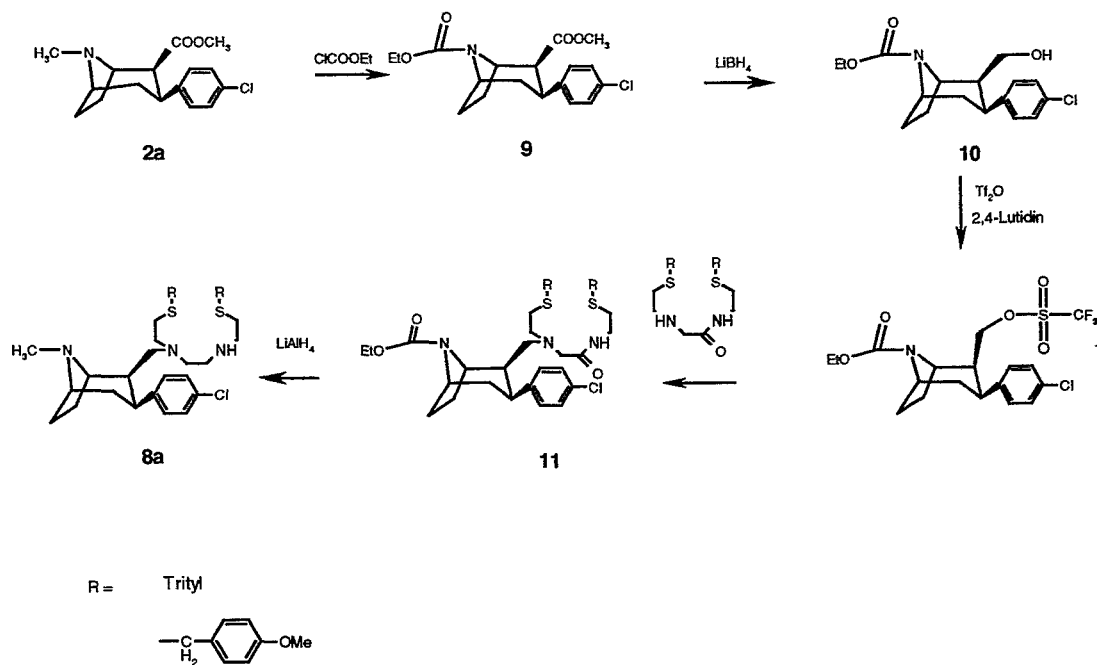
The interest of our group in further investigations of TRODAT made it attractive to look for an improved synthetic route to obtain this compound.

Results and Discussion

In our opinion some modifications of the original synthesis would be favorable. Therefore we developed the following new synthetic strategy (Scheme 2).

Varying the synthesis by Kung and co-workers we investigated the combination of the complete MAMA ligand with the tropane molecule and we tried to find protecting groups for the thiol functions of the MAMA ligand which give the possibility to carry out the deprotection reaction simultaneously with the ^{99m}Tc labelling reaction. Good experiences in this case were made in our group with trityl groups.

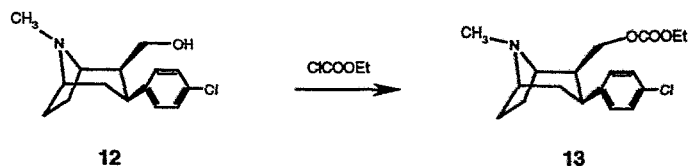
Scheme 2.



The 2 β -carbomethoxy-3 β -(4-chlorophenyl)tropane **2a** was prepared following previously described methods [5]. Protection of the tropane amine function of **2a** occurs by refluxing it in ethylchloroformate (98 % yield). In the next step the methylester **9** was reduced to the alcohol **10** in 96 % yield, using LiBH_4 in diethylether at room temperature.

It is not possible to prepare 2 β -(hydroxymethyl)-3 β -(4-chlorophenyl)tropane [5] and protect the tropane amine function in the next step because of the reaction of ethylchloroformate with the hydroxy group (Scheme 3).

Scheme 3.



Treating **10** with trifluoromethansulfonic anhydride in methylenechloride at $-10\text{ }^\circ\text{C}$ yields the corresponding triflate, which reacted - without separation - with the MAMA ligand and was stirred at room temperature for one day. Purification occurs by flash chromatography on silica gel with first ether/methylenechloride/methanol (10 : 5 : 0.1) and second ether/ethylacetate/methanol/ NH_4OH (10 : 8.5 : 1 : 0.5). Yields between 50 % and 70 % of **11** were reached.

Reduction of trityl-protected **11** to **8a** with LiAlH_4 was not possible because of instability of the trityl groups against the reducing agent. Therefore we had to look for another useful protecting group.

$^{99\text{m}}\text{Tc}$ labelling investigations with p-methoxybenzyl-protected **8a** (yielded by Kung synthesis) in a strong acidic medium showed that it is possible to carry out deprotection simultaneously with the labelling reaction (yield about 50 %). Now we study the coupling reaction of the p-methoxybenzyl-protected MAMA ligand with the triflate of **10** and the following reduction. First encouraging results were reached but yields must be improved.

References

- [1] Meegalla S. K., Plössl K., Kung M.-P., Chumpradit S., Stevenson D. A., Kushner S. A., McElgin W. T., Mozley P. D. and Kung H. F. (1997) Synthesis and characterization of technetium-99m-labeled tropanes as dopamin transporter-imaging agents. *J. Med. Chem.* **40**, 9-17.
- [2] Kung M.-P., Stevenson D. A., Plössl K., Meegalla S. K., Beckwith A., Essman W. D., Mu M., Lucki I. and Kung H. F. (1997) [$^{99\text{m}}\text{Tc}$]TRODAT-1: a novel technetium-99m complex as a dopamine transporter imaging agent. *Eur. J. Nucl. Med.* **24**, 372-380.
- [3] Kung H. F., Kim H.-J., Kung M.-P., Meegalla S. K., Plössl K. and Lee H.-K. (1996) Imaging of dopamine transporters in humans with technetium-99m TRODAT-1. *Eur. J. Nucl. Med.* **23**, 1527-1530.
- [4] Dresel S., Kung M.-P., Huang X.-F., Plössl K., Hou C., Meegalla S. K., Patselas G., Mu M., Saffer J. R. and Kung H. F. (1999) Simultaneous SPECT studies of pre- and postsynaptic dopamine binding sites in baboons. *J. Nucl. Med.* **40**, 600-666 and literature cited therein.
- [5] Kozikowski A. P., Saiah M. K. E., Johnson K. M. and Bergmann J. S. (1995) Chemistry and biology of the 2 β -alkyl-3 β -phenyl analogues of cocaine: subnanomolar affinity ligands that suggest a new pharmacophore model at the C-2 position. *J. Med. Chem.* **38**, 3086-3093.

25. Potentially Dopamine Receptor-Binding Technetium and Rhenium Tracers: Synthesis and Characterisation of Ligands Derived from Partial Structures of Epidepride

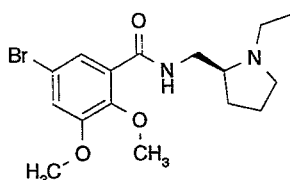
M. Scheunemann, H.-J. Pietzsch, H. Spies, P. Brust, B. Johannsen

Introduction

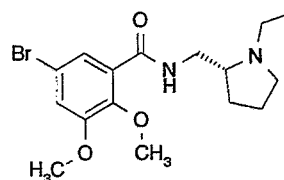
During the last four decades numerous substituted benzamides have been developed as potential antipsychotic agents due to their ability to block dopamine D-2 receptors [1].

Amongst this class of compounds the 2-methoxy or 2,3-dimethoxybenzoic acid amides are highly potent and selective D-2 receptor antagonists. Especially amides having a 2-pyrrolidinylmethyl side chain, such as *raclopride*, *sulpiride* or *epidepride*, attracted attention because of their good penetration through the blood-brain barrier and an exceptionally good receptor-binding profile [2].

As part of a project concerned with the synthesis of Tc complexes for *in vivo* imaging of neuroreceptors by SPECT, we decided to apply the structure of *epidepride* and its bromo-analogue *FLB 457* as the lead for our investigations.

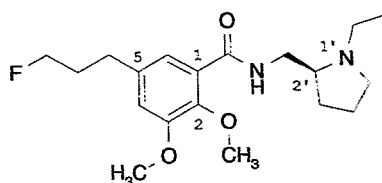


FLB 457
Ki: 0.018 nmol

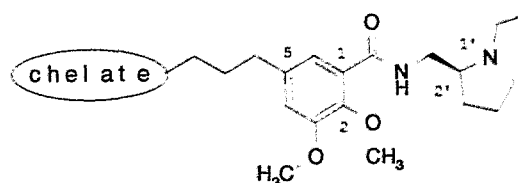


NCQ 114
Ki: 14.5 nmol

Previous studies by *Hall and co-workers* showed that steric bulk at the side chain of the pyrrolidine nitrogen may affect the receptor-binding potency [3]. Furthermore, the stereochemistry at the 2'-position is crucial for its neuroactivity, as only the *S*-enantiomer exhibits the desired picomolar affinity to the D-2 receptor. In an attempt to attenuate the detrimental effect of the fluoro alkyl substituent on the pyrrolidine amino group, *Mukherjee* reported on a new class of fluorinated neuroleptics as candidates for use as radiotracers for PET [4].



FPMB (ref. [4])

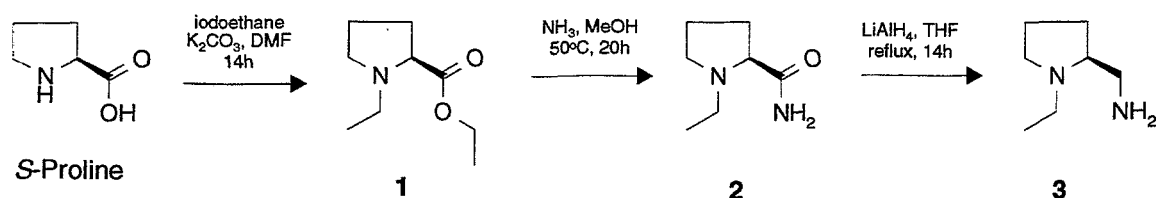


In these derivatives, which show a high affinity to the D-2 receptor, the fluorine atom is incorporated as a 3-fluoropropyl group on the benzene ring.

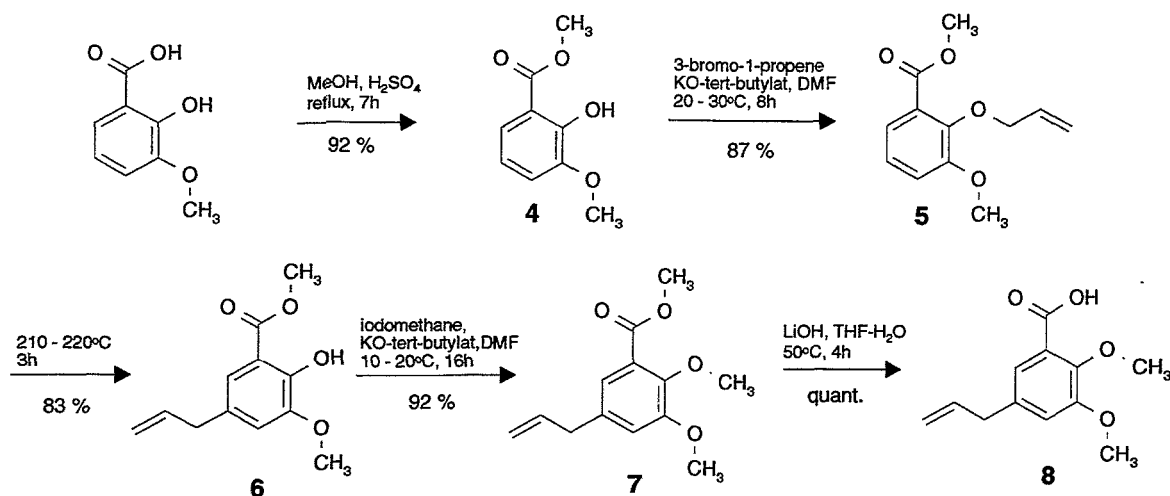
These disclosures prompted us to choose the 5-position at the benzene ring rather than the 1'-position of the pyrrolidine ring for linkage of a suitable Tc-chelating unit.

Chemistry

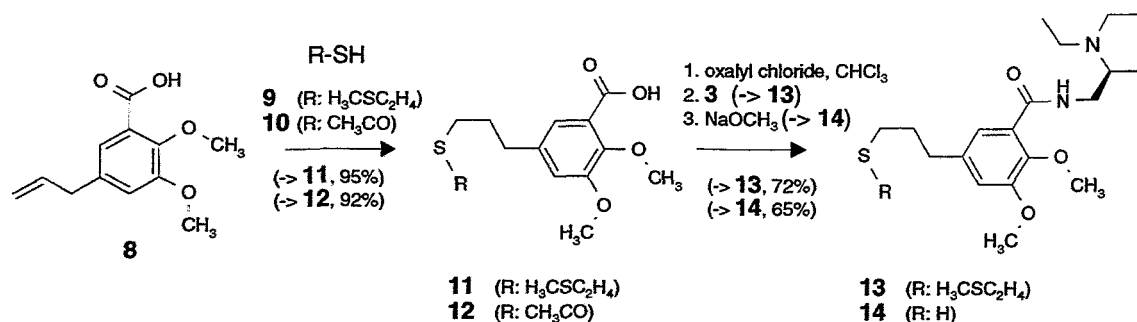
(*S*)-2-Aminomethyl)-*N*-ethylpyrrolidine was prepared following a procedure described in the literature [5]. Natural (*S*)-proline was both esterified and simultaneously *N*-ethylated by treatment of the amino acid with iodo ethane in dry DMF. Then the ester (**1**) was transformed into the amide (**2**) in the presence of methanolic ammonia in a closed vial at 50°C for 20 hours. Finally the reduction of the amide to the desired amino compound (**3**) was accomplished by reaction with lithium aluminium hydride in THF.



For the preparation of an appropriately derivatized benzoic acid we started from commercially available 2-hydroxy-3-methoxy benzoic acid. After its esterification with methanol in the presence of sulphuric acid, the resulting ester (**4**) was alkylated by means of 3-bromo-1-propene in DMF at room temperature to yield the allyl ether (**5**). Claisen rearrangement was effected by heating the allyl ether at 210 – 220°C for 3 hours [6].



For the methylation of the phenolic hydroxy group with iodomethane we used reaction conditions similar to the allylation step. Finally the ester (**7**) was saponified to yield the substituted benzoic acid (**8**) in a 61% overall yield.



2,3-Dimethoxy-5-allylbenzoic acid (**8**) represents a valuable starting material for a number of reactions leading to appropriate chelators for technetium in various oxidation stages.

For our purpose we selected on the main two transformations. A chelating unit containing two sulphur donors was at first attached to the olefinic group of **8** by radical addition of 2-methyl-thioethyl thiol (**9**). The intermediate benzoic acid (**11**) was then coupled to the pyrrolidine derivative (**3**) by its carboxylic acid chloride, which was obtained by treatment with oxalyl chloride in chloroform.

In a similar manner heating of **8** with a surplus of thiol acetic acid (**10**) yielded the *S*-acetyl-protected derivative **12**. Again the carboxylic group in **12** was activated by the oxalyl chloride under mild conditions (< 20°C). Without isolating the acid chloride intermediate, the *S*-acetyl derivative of **14** was obtained in a 73% yield after reaction with **3** at 20°C for 10 h. Deprotection proceeded efficiently (90% yield) and cleanly in MeOH in the presence of sodium methanolate at 0 – 18°C for 2 h.

The ¹H and ¹³C NMR spectra of **7**, **8** and **11** – **14** clearly confirm the success of the addition step, the

coupling to amine **3** and removal of the protecting group from the precursor of **14**. With **13** and **14** in hand, we have already started to prepare neutral Tc complexes both on a c.a. and n.c.a. level.

References

- [1] Florvall L. and Ögren S.-O. (1982) Potential neuroleptic agents. 2,6 -Dialkoxybenzamide derivatives with potent dopamine receptor blocking activities. *J. Med. Chem.* **25**, 1280–1286 and references given therein.
- [2] Högberg T., de Paulis T., Johansson L., Kumar Y., Hall H. and Ögren S. (1990) Potential antipsychotic agents. 7. Synthesis and antidopaminergic properties of the atypical highly potent (*S*)-5-bromo-2,3-dimethoxy-*N*-[(1-ethyl-2-pyrrolidinyl)methyl]benzamide and related compounds. A comparative study. *J. Med. Chem.* **33**, 2305–2309.
- [3] Hall H., Högberg T., Halldin C., Bengtsson S. and Wedel I. (1991) Synthesis and binding properties of the fluorinated substituted benzamide [³H]NCQ 115, a new selective dopamine D₂ receptor ligand. *Eur. J. Pharmacol.* **201**, 1–10.
- [4] Mukherjee J. (1991) Fluorinated benzamide neuroleptics 2. Synthesis and radiosynthesis of (*S*)-*N*-[(1-ethyl-2-pyrrolidinyl)methyl]-5-(3-[¹⁸F]fluoropropyl)-3-substituted-2-methoxybenzamides. *Appl. Radiat. Isot.* **42**, 713–721.
- [5] Högberg T., Råmsby S. and Ström P. (1989) Efficient stereoconservative synthesis of 1-substituted (*S*)- and (*R*)-2-aminomethylpyrrolidines. *Acta. Chem. Scand.* **43**, 660–664.
- [6] Claisen L. (1919) Über eine Synthese des Eugenols. *Liebigs Ann.* **418**, 113–120.

26. Implementation of the Catecholamine Analysis and Precolumn Technique in Amino Acid Determination with the Fluorescence Label Naphthalene-2,3-dicarbaldehyde

G. Vorwieger, R. Bergmann, P. Brust

Various projects currently under investigation necessitate measurement of extracellular indicator molecule concentrations, many of them being primary amines (Table 1). In the past decades, neurochemical research generally included brain microdialysis as a suitable tool for such tasks. Surgical know-how and standard amino acid analysis were established in our group as early as in 1994 [5].

Table 1. Implication of primary amine solutes in recent research subjects

Subject	Indicator solutes	Function of indicator solute
role of dopamine metabolism in the pathogenesis of asphyxia-induced brain injury	glutamate, taurine, glycine, γ -aminobutyric acid (GABA)	modulator of aminergic transmission, excitatory and inhibitory amino acids (excitotoxic index)
role of dopamine metabolism in the pathogenesis of asphyxia-induced brain injury	dopamine (DA), 3-methoxytyramine, norepinephrine, DOPA	neurotransmitter, marker for DA release and catalyst of radical genesis
[^{18}F]fluoro-DOPA Positron Emission Tomography	fluoro-DA, fluoro-DOPA, etc.	inactive carrier of radiotracer: kinetics and metabolism
fluorinated peptide-receptor tracers	neurotensin fragments	visualization of receptor densities, undesirable cleavage products
serotonergic system and depression	serotonine	neurotransmitter
brain trauma	citrulline	marker for nitric oxide synthesis

Since 1995 trace analysis of primary amines by derivatization with naphthalene-2,3-dicarbaldehyde (NDA) and HPLC separation/fluorescence detection of the resulting cyanobenzisoindole (CBI) derivatives has been consistently applied. Components of the application ensuring a desirable high sensitivity and reproducibility have already been developed and described [4].

In this work the inclusion of catechol analytes as additional modules in the application and the extended HPLC-configuration "reconcentration of the CBI-derivatives on a precolumn" will be verified. The reconcentration, along with the benefits mentioned in the discussion, is a prerequisite for experimental manipulations such as dilution with catechol protection solution and removal of excessive reagents by precipitation.

Methods

A compromise was to be found between the high reactivity of the catechol group in alkaline solutions and the alkaline pH optimum of the derivatization reaction. In orientating trials with DOPA and DA we found undesirable side reactions leading to spontaneous browning (oxidation, condensation producing melanines) which were visible to the naked eye. A catechol protection solution CPS (yet to be published) was therefore introduced. As an alternative to the automatized reactions described in [4], all derivatizations mentioned in this report were performed by the following manual procedure:

mix 1 vol. acidified sample/standard with 0.25 vol. CPS + cyanide and 0.5 vol. methanolic NDA, allow for reaction (1 min), add the stopping reagent (0.5 vol., tryptamine excessive to NDA; containing CPS), allow another 5 min for reaction, centrifuge at 12,000 x g for 5 min. A tightly sealable glass microvial that withstands centrifugation was chosen to prevent adsorption and NDA recrystallisation due to methanol evaporation.

All other conditions were the same as described in the experimental section in [4].

For the precolumn/reconcentration experiment the following modifications were introduced: precolumn Waters SENTRY guard 3.9 mm diameter x 20mm length, Symmetry C18 5 μ , mobile phase unchanged, load of 200 μ l sample at a flow 0.3 ml/min. Backflush onto the analytical column (4.6 x 150 mm high-speed column packed with Symmetry C18 3.5 μ , Waters) with a steep MeCN gradient beginning with a high elution power, pH adjusted to 6.4, flow 1.5 ml/min. Switching valve: 6 port (Valco cheminert) with microbore port diameter, pneumatic actuator with high-speed switching assembly. The temperature of both columns was maintained at 30 $^{\circ}$ C within a Jetstream 2 (Eppendorf BIOTRONIK) column oven.

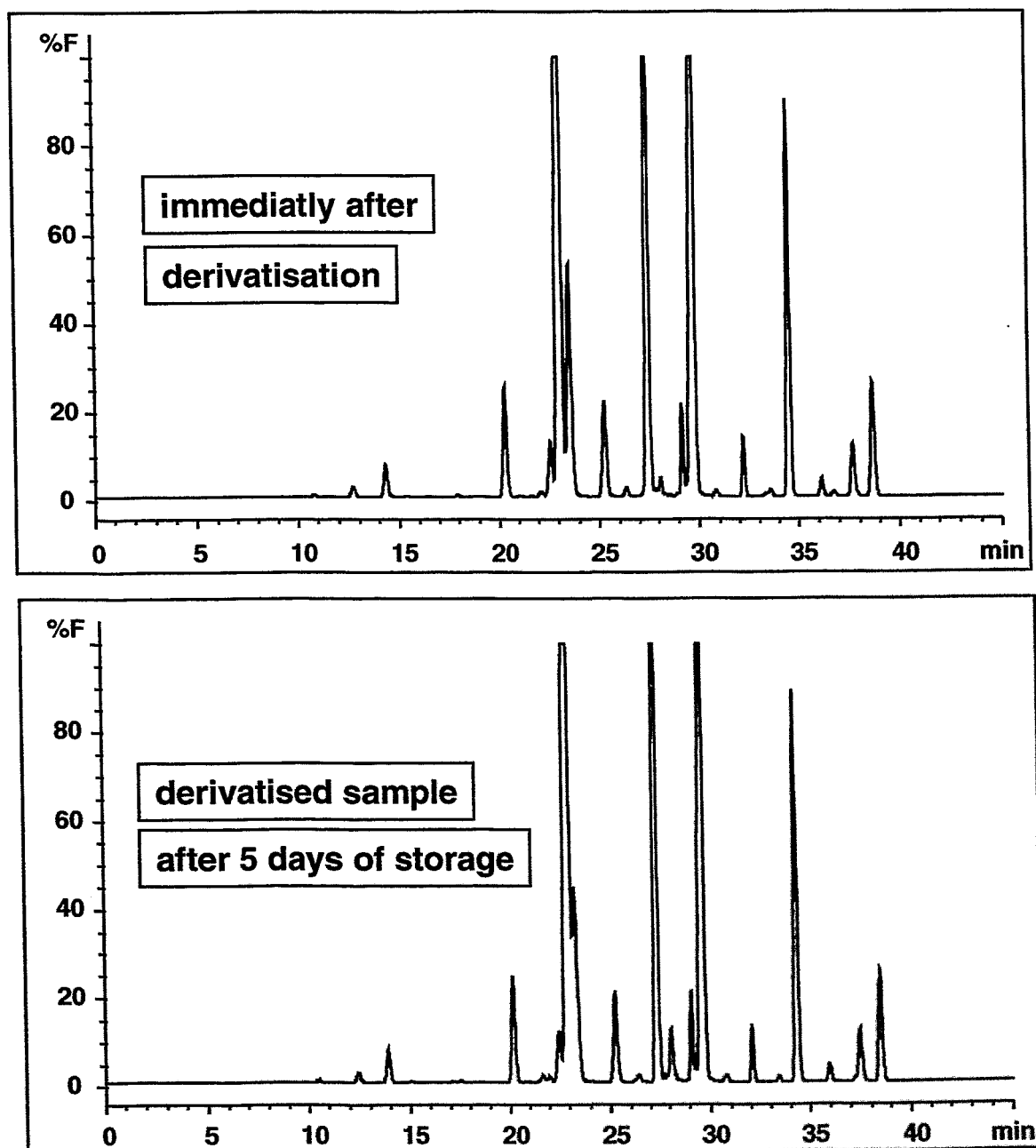


Fig. 1. Fluorescence traces of one and the same sample (deproteinised human plasma) immediately after derivatisation (top) and after 5 days of storage at room temperature in the dark (bottom)

Results and Discussion

CBI derivatives of (deproteinized) human plasma amines were rendered stable for 5 days of storage at room temperature in the dark. Even within such a complex sample matrix there is no significant change in peak areas (Fig. 1).

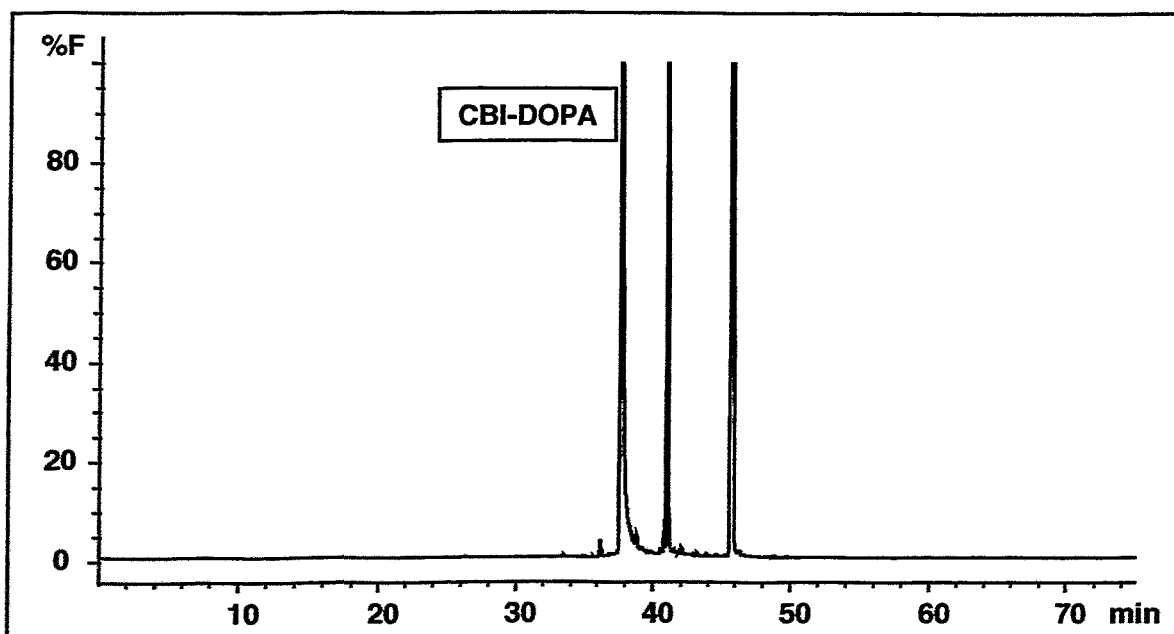
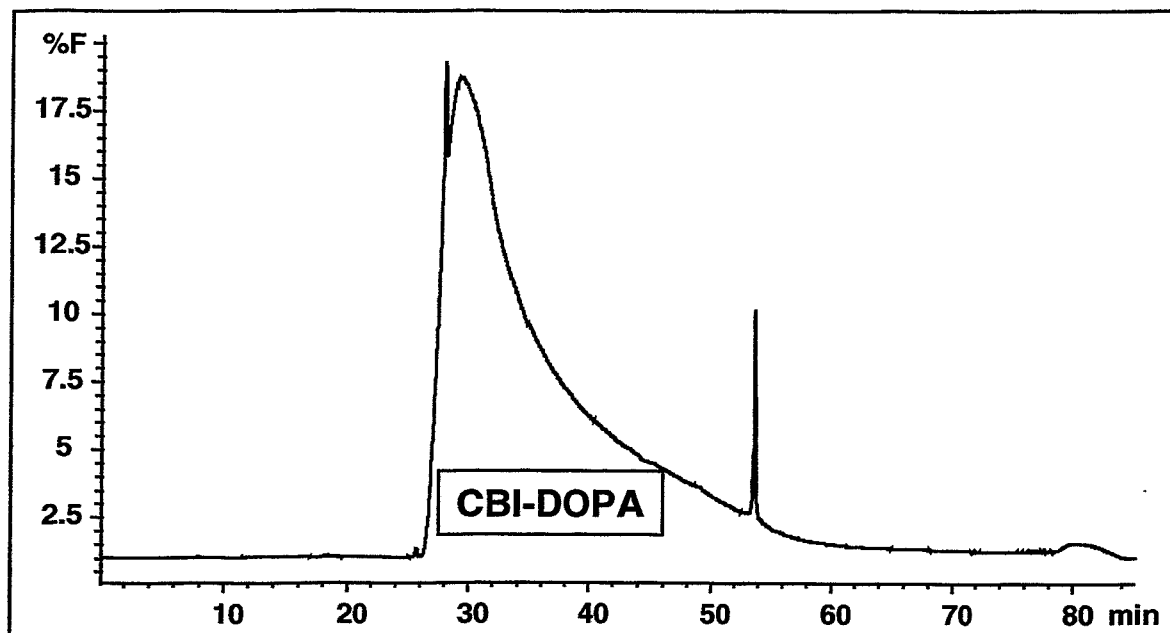


Fig. 2. Fluorescence traces demonstrating the results of DOPA derivatisation by the conventional procedure (top) and by addition of CPS (bottom).

This stability allows measurement of large sample sequences, i.e. at least one autosampler tray (34 samples, their measurement takes about a day) also without autosampler cooling devices. The stability of CBI-dopamine and CBI-DOPA was verified in separate experiments with standard compounds (data not shown).

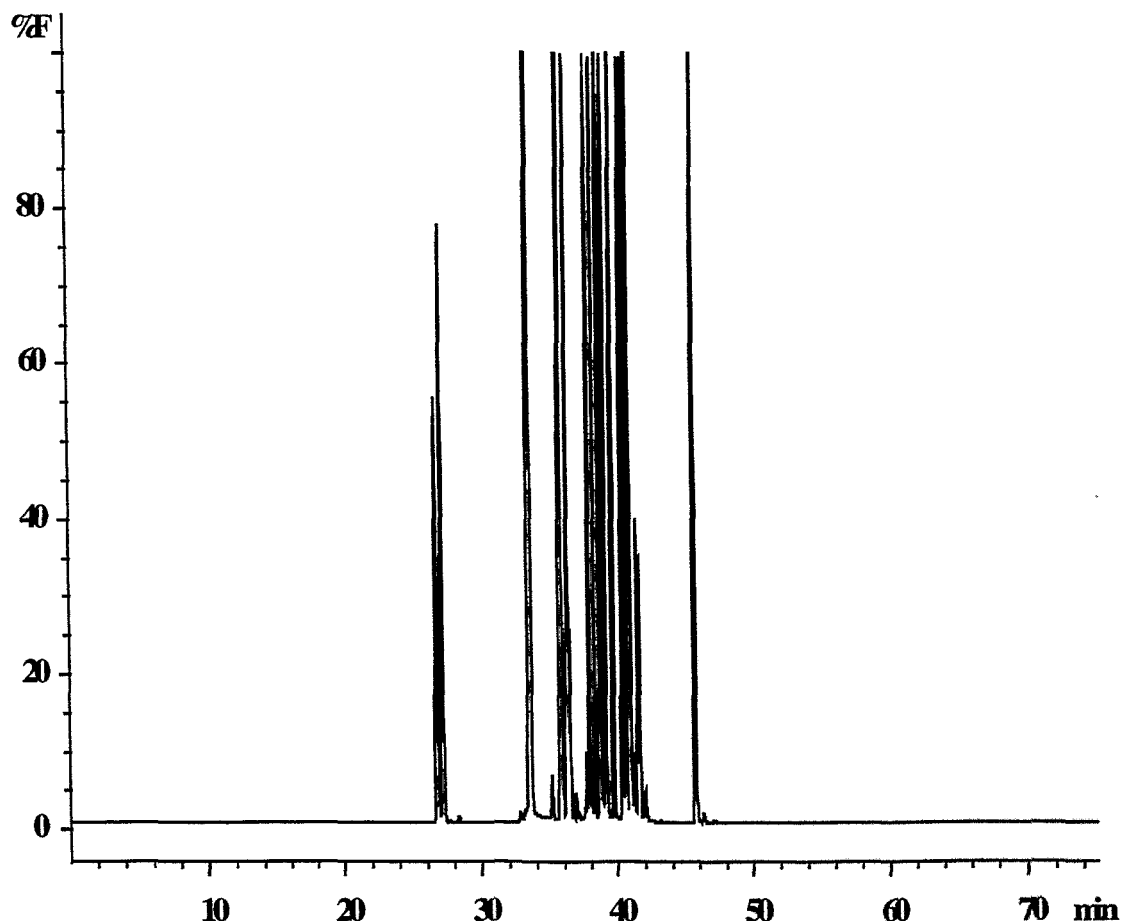


Fig. 3. Fluorescence trace of CBI derivatives of proteinogenic amino acids and DA on line reconcentrated from a large sample volume and backflushed with a steep gradient.

The trace in Fig. 2 (top) is the result of DOPA analysis without CPS. The multitude of polycondensation products gives rise to a broad signal agglomerate which moreover exhibits a strong memory phenomenon on the column (the latter is not shown). With CPS there remains just common peak tailing as compared to neutral amino-acid CBIs (Fig. 2 bottom). We assume that this remaining problem, which of course impairs the detection limit, can be abolished by a lower pH of the mobile phase.

The catecholamines are commonly determined by HPLC with electrochemical detection ECD. With ECD the only selectivity criterion is the oxidation potential, which of course is not group specific. A noisy background and restrictions in gradient use are ECD characteristics. To our knowledge there have been just 3 papers until now reporting on the contemporary fluorescence analysis of amino acids and catecholamines by derivatisations with NDA or the related ortho-phthalaldehyde OPA [1, 2, 3]. Two of them [2, 3] are restricted to online (to CE) derivatizations.

Here we demonstrate the integration of catecholamines into an amino-acid protocol. It is no longer necessary to split the samples volumes, which are anyway minute, into an amino acid and a catecholamine analysis. The fluorescence detection of the derivatives is moreover more sensitive than electrochemical detection.

Fig. 3 is the result of a precolumn/reconcentration experiment with a commercially available amino acid standard solution stocked up with DA. Though we used just a rather short precolumn, all solutes but aspartic acid (15 %) and glutamic acid (60 %) were quantitatively recovered. These acidic species can probably be included in the range of quantitative recovery by lowering the pH of the loading mobile phase, adding to it basic ion pairing reagents, and elongating the precolumn.

The in vivo experimental procedures can thus be performed quite independently of any analytical demands, keeping the benefits of low limit of detection [4].

The capability of quantitative reconcentration abolishes handling difficulties because n * microlitre sample volumes can be taken up immediately in convenient volumes of stabilization solution.

The analytical column receives the sample via backflush in an optimized manner (within its own mobile phase, guaranteed free of particles, the only dilution being the dispersion of the valve void volume). Thus, as in the demonstrated case, the employment of high-speed columns becomes possible. Difficult separating processes, e.g. CBI-arg and CBI-citrulline, can be carried out by all available specific tools of HPLC, regardless of any matrix problems.

References

- [1] Kawasaki T., Higuchi T., Imai K. and Wong O. S. (1989) Determination of dopamine, norepinephrine, and related trace amines by prechromatographic derivatisation with naphthalene-2,3-dicarboxaldehyde. *Anal. Biochem.* **180**, 279-285.
- [2] Robert F., Bert L., Denoroy L. and Renaud B. (1995) Capillary zone electrophoresis with laser-induced fluorescence detection for the determination of nanomolar concentrations of noradrenaline and dopamine: application to brain microdialysate analysis. *Anal. Chem.* **67**, 1838 – 1844.
- [3] Gilman S. D. and Ewing A. G. (1995) Analysis of single cells by capillary electrophoresis with on-column derivatisation and laser-induced fluorescence detection. *Anal. Chem.* **67**, 58 – 64.
- [4] Vorwieger G., Bergmann R., Brust P. and Johannsen B. (1996) Studies on a HPLC method to assay the concentrations of amines in brain microdialysates based on naphthalene-2,3-dicarbaldehyde derivatisation and fluorescence detection. *Annual Report 1996*, Institute of Bioinorganic and Radiopharmaceutical Chemistry, FZR-165, pp. 139-143.
- [5] Bergmann R. and Brust P. (1994) Use of brain microdialysis for studying changes of amino acid concentrations in the brain interstitial space. *Annual Report 1994*, Institute of Bioinorganic and Radiopharmaceutical Chemistry, FZR-73, pp. 151-157.

27. Characterization of the Impaired Brain Function in Persistent Vegetative State: Evaluation of Perfusion and Glucose Metabolism with Emission Tomography Techniques

B. Beuthien-Baumann¹, W. Handrick², T. Schmidt³, W. Burchert, G. Schackert², W.-G. Franke¹

¹TU Dresden, ¹Klinik und Poliklinik für Nuklearmedizin, ²Klinik und Poliklinik für Neurochirurgie, ³Rehabilitationsklinik Pulsnitz

Introduction

The persistent vegetative state is characterized by a comatose state with a preserved sleep-wake cycle, but without detectable awareness [1]. Most often this syndrome is due to a severe brain injury. For many patients this state is irreversible, but some of them show improvement after intensive rehabilitation efforts [2]. To further characterize the extent of functional brain damage we evaluated brain perfusion and cerebral glucose metabolism in this patient group.

Materials and Methods

Patients: 16 patients (3 female, 13 male, age 18-67 years, median age 47.5 years) with persistent vegetative state and dilated ventricular system were investigated. The persistent vegetative state developed after a head trauma or cerebral haemorrhage. The time interval between the initial brain injury and the scanning procedure was 2.5 to 11 months. Blood glucose levels at the time of investigation were within physiological limits, none of the patients was diabetic.

Imaging procedures: Brain perfusion was assessed with Single Photon Emission Computed Tomography (SPECT) using a 3-headed gamma camera (Multi SPECT III, Siemens). Ten minutes after injection of 750 MBq Tc-99m-ECD (Neurolite, DuPont) a static tomographic acquisition was performed.

The cerebral glucose metabolism was measured with dynamic Positron Emission Tomography (PET) using a dedicated full-ring PET scanner (ECAT EXACT HR⁺, Siemens /CTI, Knoxville, Tenn., USA). A dynamic data acquisition over 60 min was performed after intravenous injection of 300 MBq [¹⁸F]FDG (in-house production [3]). Several pseudo-arterial blood samples were taken at the same time to determine the input function of the tracer. The actual blood glucose level for quantitative analysis of the cerebral glucose metabolism was measured 20 min and 40 min after the start of the scan. Quantitative parametric images of the regional metabolic rate of glucose were derived using the Gjedde-Patlak approach [4 - 6].

After reconstruction of both data sets, image fusion of PET and SPECT data was performed (MPITOOL, [7, 8]). Differences in glucose metabolism and perfusion were qualitatively evaluated by visual analysis. Furthermore, quantitative data were derived from anatomically defined 'regions of interest' (ROI) according to the vascular territories of the main brain arteries.

For a direct comparison of perfusion and MRGlc, the values derived by ROI analysis were normalized to the total counts (SPECT) and MRGlc (PET) of grey matter.

Statistical data evaluation using the paired and unpaired t-test was performed with commercial software (StatView, SAS Institute Inc.). A p-value of < 0,05 was used as level of significance.

Results and Discussion

Visual analysis of the data revealed that all patients showed substantial defects of regional perfusion and metabolism. The cerebral glucose metabolism was impaired even in brain areas not primarily affected by the trauma. In the lesion area the defect of the glucose metabolism was more extensive than the perfusion defect (Fig. 1). Quantitative analysis of the absolute cerebral metabolic rate of glucose (MRGlc) revealed significantly lower values in the cortical and subcortical areas than the normal controls (Fig. 2). This difference was not significant in the areas of the brain stem and the vermis of the cerebellum. These findings are in accordance with the literature, in which reduced values of the cerebral glucose metabolism are described in patients with a persistent vegetative state [9 - 11].

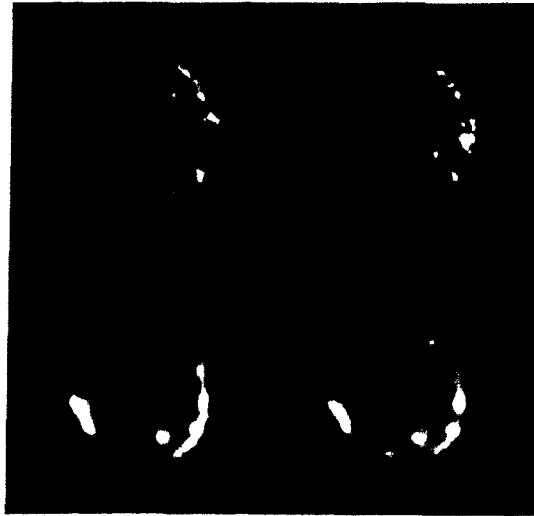


Fig. 1. A 46-year-old patient 3 months after brain trauma. Upper row [¹⁸F]FDG-PET, lower row ^{99m}Tc-ECD-SPECT. Regional hyperperfusion (arrow) with relatively low glucose metabolism.

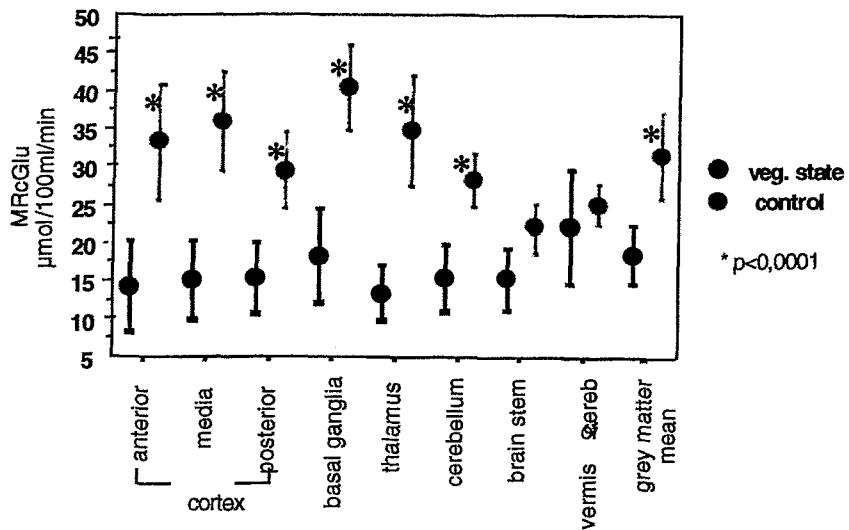


Fig. 2. Comparison of MRGlu in various brain regions in vegetative state and controls.

Concerning the relative glucose metabolism and perfusion, the glucose metabolism of cortical regions was more severely impaired than the perfusion (Table 1). In lesions and even more clearly in their border zones, perfusion was better preserved than the glucose metabolism (Fig. 3). No significant differences between normalized MRGlc and normalized perfusion were found in subcortical areas, brain stem and vermis of the cerebellum.

Under physiological conditions there is a close correlation between brain perfusion and cerebral glucose metabolism [12]. A dissociation of these two parameters in cortical areas was found in this study. The higher perfusion indices in cortical areas seem to represent changes in the sense of 'luxury perfusion'. Therefore, the evaluation of the viability of brain tissue seems to be more predictive with [¹⁸F]FDG-PET than with ^{99m}Tc-ECD-SPECT.

Nevertheless, to assess the prognostic value of both imaging modalities with respect to the clinical outcome a longer follow-up of the patients is needed.

Table 1. Comparison of normalized PET and normalized SPECT in various brain regions

Region	n-PET	n-SPECT	p =
	Mean ± SD	Mean ± SD	
Anterior *	0,83 ± 0,28	0,91 ± 0,31	< 0,05
Media *	0,88 ± 0,23	0,95 ± 0,24	< 0,05
Posterior *	0,85 ± 0,21	1,10 ± 0,23	< 0,05
Basal ganglia	1,10 ± 0,34	1,00 ± 0,21	n. s.
Thalamus	0,81 ± 0,23	0,75 ± 0,17	n. s.
Cerebellum	0,86 ± 0,20	1,08 ± 0,12	< 0,05
Brain stem	0,80 ± 0,11	0,68 ± 0,13	< 0,05
Vermis of cerebell.	1,15 ± 0,35	1,12 ± 0,16	n. s.

n.s. = not significant

* territories of the main brain arteries

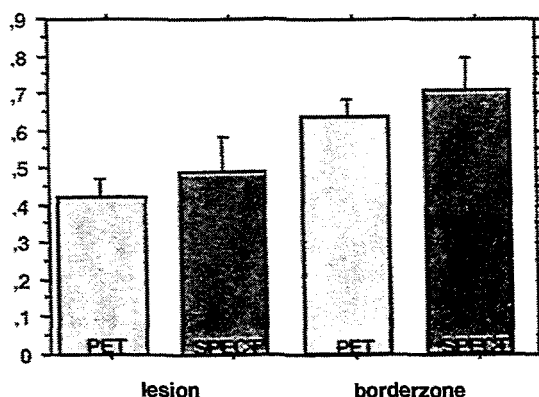


Fig. 3. Comparison of normalized PET and normalized SPECT in brain lesions and their border zones

References

- [1] Fuechtner F., Steinbach J., Maeding P. and Johannsen B. (1996) Basic hydrolysis of 2-¹⁸F]fluoro-1,3,4,6-tetra-O-acetyl-D-glucose in the preparation of 2-¹⁸F]fluoro-2-deoxy-D-glucose. *Appl. Radiat. Isot.* **47**, 61-66.
- [2] Gjedde A. (1982) Calculation of cerebral glucose phosphorylation from brain uptake of glucose analogs in vivo: a re-examination. *Brain Res.* **257**, 237-274.
- [3] Levy D. E., Sidtis J. J., Rottenberg D. A., Jarden J. O., Strother S. C., Dhawan V., Ginos J. Z., Tramo M. J., Evans A. C. and Plum F. (1987) Differences in cerebral blood flow and glucose utilization in vegetative versus locked-in patients. *Ann. Neurol.* **22**, 673-682.
- [4] Patlak C. S. and Blasberg R. G. (1985) Graphical evaluation of blood-to-brain transfer constants from multiple- time uptake data. Generalizations. *J. Cereb. Blood Flow Metab.* **5**, 584-590.
- [5] Patlak C. S., Blasberg R. G. and Fenstermacher J. D. (1983) Graphical evaluation of blood-to-brain transfer constants from multiple- time uptake data. *J. Cereb. Blood Flow Metab.* **3**, 1-7.

- [6] Pietrzyk U., Herholz K., Fink G., Jacobs A., Mielke R., Slansky I., Wurker M. and Heiss W. D. (1994) An interactive technique for three-dimensional image registration: validation for PET, SPECT, MRI and CT brain studies. *J. Nucl. Med.* **35**, 2011-2018.
- [7] Pietrzyk U., Herholz K. and Heiss W. D. (1990) Three-dimensional alignment of functional and morphological tomograms. *J. Comput. Assist. Tomogr.* **14**, 51-59.
- [8] Pilon M. and Sullivan S. J. (1996) Motor profile of patients in minimally responsive and persistent vegetative states. *Brain Inj.* **10**, 421-437.
- [9] Rudolf J., Ghaemi M., Ghaemi M., Sobesky J., Haupt W., Szeliés B., Grond M. and Heiss W.-D. (1999) Alterations of cerebral glucose metabolism and benzodiazepine receptor binding in acute and persistent vegetative state. *J Cereb Blood Flow Metabol.* **19**, S839.
- [10] Rudolf J., Ghaemi M., Haupt W. F., Szeliés B. and Heiss W. D. (1999) Cerebral glucose metabolism in acute and persistent vegetative state. *J Neurosurg Anesthesiol.* **11**, 17-24.
- [11] The multi-society task force on PVS. (1994) Medical aspects of the persistent vegetative state (First of two parts). *n Engl J Med.* **330**, 1499-1508.
- [12] Wienhard K., Wagner R. and Heiss W.-D. (1989) PET - Grundlagen und Anwendungen der Positronen-Emissions-Tomographie. Springer-Verlag Berlin, Heidelberg, New York.

BRAIN SEROTONERGIC SYSTEMS

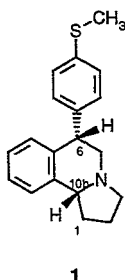
28. Synthesis of Enantiomerically Pure Thioester Precursors of [^{11}C]McN-5652

P. Gucker¹, J. Zessin, S. M. Ametamey¹, J. Steinbach

¹Center of Radiopharmaceutical Science, Paul-Scherrer-Institut Villigen (Switzerland)

Introduction

The radioligand [^{11}C]McN-5652 (trans-1,2,3,5,6,10b-hexahydro-6-[4-(^{11}C)methylthio]-phenyl]pyrrolo-[2,1-*a*]-isoquinoline, [^{11}C]-**1**) is a potent tracer for imaging serotonin uptake sites with positron emission tomography (PET) [1, 2]. In vivo investigations in baboons and humans have shown that satisfactory target-to-non-target ratios (hypothalamus to cerebellum ratio) of 1.5 – 1.8 are only obtained using the biologically active (+)-enantiomer [3, 4].



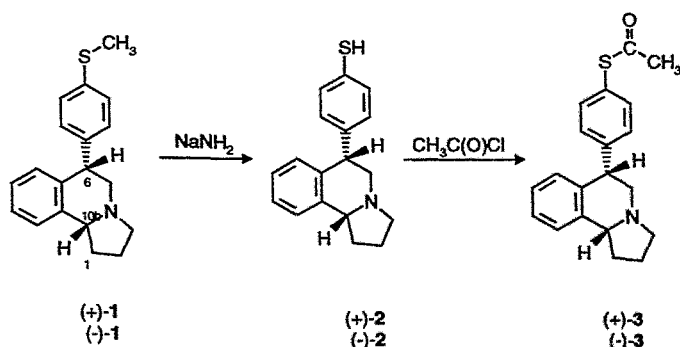
[^{11}C](+)-McN-5652 is prepared by methylation of the normethyl compound **2** with [^{11}C]methyl iodide [5]. The normethyl precursor **2** can be prepared by demethylation of **1** by treatment with sodium thiomethoxide [5]. The stability of the thiol **2** was increased by conversion into a thioester as thiol acetate **3** or butyrate [6]. The demethylation using sodium thiomethoxide is accompanied by a conformational change which reduces the portion of the desired trans diastereomer to about 40%. This isomerization reaction is avoided by demethylation using sodium amide in liquid ammonia [7].

(+)-McN-5652, the starting compound for the precursor synthesis, is not commercially available. The known preparation method of (+)-**1** is based on resolution of racemic **1** by recrystallization of the (+)-tartrate [8], but this procedure gives no satisfactory results [9].

This problem can be prevented by a stereoconservative synthesis utilizing the 6-(4-bromophenyl) analogues of **1** as key intermediates [9]. However, this procedure requires time-consuming preparation of the bromophenyl compound.

In this paper we describe a route for preparation of the enantiomerically pure thioester precursors (+)-**3** and (-)-**3** starting from racemic McN-5652. The preparation is based on the resolution of racemic **1** by crystallization with (+)- and (-)-di-*p*-toluoyltartaric acid. The S-demethylation was performed by treatment of (+)-**1** or (-)-**1** with sodium amide (see Scheme 1).

Scheme 1. Synthesis of the thioester precursor for [^{11}C]McN-5652



Experimental

Reagents and solvents were obtained from commercial suppliers and were used without purification. Racemic McN-5652 was prepared starting from 2-phenylpyrrolidine and 4-methylthiomandelic acid according to literature procedures [8, 10].

^1H NMR spectra were recorded with a Varian INOVA 400 NMR spectrometer. The chemical shifts are expressed in ppm relative to tetramethylsilane. CDCl_3 or benzene- d_6 were used as solvent and internal standard. The enantiomeric purity was determined by NMR spectra of the (+)-Mosher's acid salts ((+)- α -methoxy- α -(trifluoromethyl)phenylacetic acid, (+)-MTPA) of **1** as described by Villani *et al.* [11].

Optical rotations (589 nm) were obtained by using a JASCO Digital Polarimeter DIP-370.

HPLC analyses were performed with the following chromatographic systems:

Chemical purities were determined with a Purospher RP 18 column (125 mm x 3 mm, 5 μm) eluted isocratically with acetonitrile/water (50/50) containing 0.1 M ammonium formate at a flow rate of 0.5 ml/min. The enantiomeric purity was determined with a Chirobiotic T column (250 mm x 4.6 mm, 5 μm) eluted isocratically with methanol/acetic acid/triethylamine (100/0.1/0.05) at a flow rate of 1 ml/min.

Resolution of racemic trans-1,2,3,5,6,10b-hexahydro-6-[4-(methylthio)-phenyl]pyrrolo-[2,1-a]-isoquinoline

Racemic McN-5652 as a free amine was dissolved in acetonitrile, filtered and added to a solution of (+)-dip-toluoyltartaric acid in acetonitrile. The combined solutions were left to stand at ambient temperature for 24 h. The precipitate was separated, dried, dissolved in hot ethanol, and left to stand at room temperature for 3 days to give off-white crystals.

A sample was converted into the (-)-tartrate, which showed an optical rotation of $[\alpha]_D^{21} -51.90$ (MeOH, c 0.236). ^1H NMR of the (+)-MTPA salt showed an enantiomeric excess (ee) of (-)-**1** > 98 %

The mother liquors of previous crystallizations were evaporated. The residue was partitioned between aqueous NaOH and dichloromethane. The resulting oil was dissolved in acetonitrile, combined with a solution of (-)-dip-toluoyltartaric acid in acetonitrile, and left to crystallize at ambient temperature for 1 day to produce off-white crystals, which were enriched with (+)-**1** (determined by HPLC of the (+)-MTPA salt, ee > 98 %). A sample was converted into the (+)-tartrate: $[\alpha]_D^{21} +50.50$ (MeOH, c 0.221).

*Trans-1,2,3,5,6,10b-hexahydro-6-[4-(acetylthio)-phenyl]pyrrolo-[2,1-a]-isoquinoline ((+)-**3**, (-)-**3**)*

The thioesters (-)-**3** or (+)-**3** respectively were prepared by demethylation of (-)-**1** or (+)-**1** with sodium amide in liquid ammonia and subsequent reaction of the resulting thiol with acetyl chloride as reported in [7].

*Radiosynthesis of (+)- and (-)-trans-1,2,3,5,6,10b-hexahydro-6-[4-([^{11}C]methylthio)-phenyl]pyrrolo-[2,1-a]-isoquinoline ([^{11}C](+)-**1**, [^{11}C](−)-**1**)*

[^{11}C](+) or [^{11}C](−)-McN-5652 were prepared by hydrolysis of the thioester precursor (+)-**3** or (-)-**3** followed by methylation of the resulting thiol with [^{11}C]methyl iodide according to the literature procedure [9].

Results and Discussion

The parent McN-5652 ((±)-**1**) was prepared starting from 2-phenylpyrrolidine and 4-methylthiomandelic acid in a five-step synthesis as reported in [8,10]. Initially, we tried to resolve the racemic product by repeated crystallization of the (+)-tartrate from ethanol or acetonitrile similar to [8]. These operations produced no enrichment of any enantiomer, which confirms the results of Huang *et al.* [9]

In an alternative method, we tested the recrystallization of racemic **1** with (+)-di-p-toluoyltartaric acid. Unexpectedly, the initial crystallization from acetonitrile yielded (-)-**1** in an enantiomeric purity of about 90 %.

Optically pure (-)-**1** (ee > 98 %) was obtained after an additional recrystallization from ethanol. The mother liquors of the initial crystallizations were enriched with the (+)-enantiomer (ee > 90 %). Another crystallization of the recovered amine with (-)-di-p-toluoyltartaric acid from acetonitrile produced optically pure (+)-**1** (ee > 98 %).

The enantiomeric purity was determined by ^1H NMR spectra of the McN-5652 enantiomers with (+)-MTPA. In addition to ^1H NMR, analysis of the enantiomeric composition was performed by chiral

HPLC. A separation of (+)-1 and (-)-1 was achieved using the glycopeptide teicoplanine as chiral stationary phase.

The separated enantiomers of 1 were converted into the related thiols 2 by treatment with sodium amide in liquid ammonia as described in a former report [7]. The thioesters (+)-3 or (-)-3 respectively were obtained by reaction of the intermediate thiol enantiomers with acetylchloride.

A sample of (+)-3 was converted into McN-5652 by hydrolysis with potassium hydroxide and subsequent methylation with methyl iodide. The product was identified as optically pure (+)-McN-5652 by chiral HPLC analysis. In case of (-)-3, an analogous result was obtained. These results established that no racemization occurred during S-demethylation of enantiomerically pure 1 by treatment with sodium amide.

The thioester precursors (+)-3 or (-)-3 respectively were used for ¹¹C-labelling of (+)-McN-5652 or (-)-McN-5652 in a similar procedure as reported [9]. [¹¹C](+)-1 or [¹¹C](-)-1 were obtained in an overall radiochemical yield of 22 % (corrected for decay, related to [¹¹C]CO₂). The radiochemical purity was >98 %. The products were identified by chiral HPLC as enantiomerically pure [¹¹C](+)-1 or [¹¹C](-)-1, which confirms that no racemization occurred during the thioester synthesis and the labelling step.

Conclusion

Enantiomerically pure thioester precursor of [¹¹C](+)-McN5652 and [¹¹C](-)-McN5652 can be prepared, starting from racemic McN5652. The key step is the resolution of (±)-1 by recrystallization with (+)- and (-)-di-p-toluoyltartaric acid, yielding (+)-1 and (-)-1 in an enantiomeric purity > 98 %.

References

- [1] Suehiro M., Scheffel U., Dannals R. F., Ravert H. T., Ricaurte G. A. and Wagner H. N. (1993) A PET radiotracer for studying serotonin uptake sites: Carbon-11-McN5652Z. *J. Nucl. Med.* **34**, 120-127.
- [2] Suehiro M., Scheffel U., Ravert H. T., Dannals R. F. and Wagner H. N. (1993) [¹¹C](+)McN5652 as a radiotracer for imaging serotonin uptake sites with PET. *Life Sci.* **53**, 883-892.
- [3] Szabo Z., Scheffel U., Suehiro M., Dannals R. F., Kim S. E., Ravert H. T., Ricaurte G. A. and Wagner H. N. (1995) Positron emission tomography of 5-HT transporter sites in the baboon brain with [¹¹C]McN5652. *J. Cereb. Blood Flow Metab.* **15**, 798-805.
- [4] Szabo Z., Kao P. F., Scheffel U., Suehiro M., Mathwes W. B., Ravert H. T., Musachio J. L., Marneco S., Kim S. E., Ricaurte G. A., Wong D. F., Wagner H. N. and Dannals R. F. (1995) Positron emission tomography imaging of serotonin transporters in the human brain using [¹¹C](+)McN5652. *Synapse* **20**, 20-37.
- [5] Suehiro M., Ravert H. T., Dannals R. F., Scheffel U. and Wagner H. N. (1992) Synthesis of a radiotracer for studying serotonin uptake sites with positron emission tomography: [¹¹C]McN-5652-Z. *J. Labelled Compd. Radiopharm.* **31**, 841-848.
- [6] Suehiro M., Musachio J. L., Dannals R. F., Mathwes W. B., Ravert H. T., Scheffel U. and Wagner H. N. (1995), *Nucl. Med. Biol.* **22**, 543-545.
- [7] Zessin J., Steinbach J. and Johannsen B. (1997), Improved synthesis of the thioester precursor of [¹¹C](+)-McN-5652-Z. *J. Labelled Compd. Radiopharm.* **40**, 815-816.
- [8] Maryanoff E. B., McComsey D. F., Gardocki J. F., Shank R. P., Costanzo M. J., Nortey S. O., Schneider C. R. and Setler P. E. (1987) Pyrroloisoquinoline antidepressants. 2. In-depth exploration of structure-activity relationships. *J. Med. Chem.* **30**, 1433-1454.
- [9] Huang Y., Mahmood K., Simpson N. R., Mason N. S. and Mathis C. A. (1997) Stereoconservative synthesis of the enantiomerically pure precursors of [¹¹C](+)-McN 5652 and [¹¹C](-)-McN 5652. *J. Labelled Compd. Radiopharm.* **41**, 9-17.
- [10] Sorgi K. L., Maryanoff C. A., McComsey D. F., Graden D. W. and Maryanoff E. B. (1990) Asymmetric induction in an enammonium-iminium rearrangement. Mechanistic insight via NMR, deuterium labeling, and reaction rate studies. Application to the stereoselective synthesis of pyrroloisoquinoline antidepressants. *J. Am. Chem. Soc.* **112**, 3567-3579.
- [11] Villani F. J., Costanzo M. J., Inners R. R. Mütter M. S. and McClure D. E. (1986) Determination of enantiomeric purity of tertiary amines by ¹H NMR of α-methoxy-α-trifluoromethylphenylacetic acid complexes. *J. Org. Chem.* **51**, 3715-3718.

29. Improved Synthesis of [¹⁸F]Altanserin, a Radioligand for Imaging 5-HT_{2A} Receptors with PET

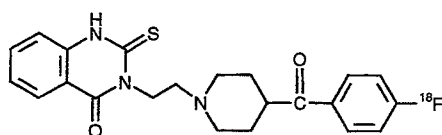
J. Zessin, K. Hamacher¹, F. Füchtner, H. Büttich², N. Dohn, J. Steinbach

¹Forschungszentrum Jülich GmbH, Institut für Nuklearchemie; ²Zentralabteilung Neue Beschleuniger

Introduction

Serotonin (5-HT) receptors are involved in the regulation of several brain processes as well as in various neurological or psychiatric diseases. PET investigations of the receptor conditions, using suitable radiotracers, therefore improve understanding of the causes of such diseases. A special PET tracer for investigation of the 5-HT₂ receptors is [¹⁸F]altanserin because of its high affinity (K_i 0.13 nM) and high selectivity for the 5-HT₂ receptor [1]. The structure of altanserin (Scheme 1) is related to ketanserin and characterized by the fluorobenzoyl moiety.

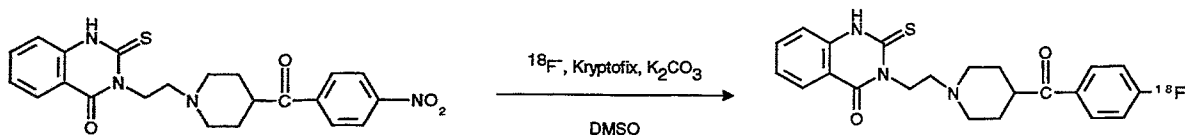
Scheme 1. Structure of [¹⁸F]altanserin



[¹⁸F]Altanserin is prepared by nucleophilic substitution of the nitro group of nitroaltanserin with [¹⁸F]fluoride (Scheme 2) [1]. The radiochemical yield depends on the reaction conditions and on the amount of precursor used. [¹⁸F]Altanserin was obtained in a yield of 2 - 20 % (using 5 - 15 mg nitroaltanserin) with conventional heating (30 min, 135 °C) [1]. The radiochemical yield was increased to 50 % by fluorination in a microwave oven [1].

The purification of [¹⁸F]altanserin was performed by solid phase extraction followed by preparative HPLC. The HPLC eluent was removed by solid phase extraction using an RP18 cartridge.

Scheme 2. Synthesis of [¹⁸F]altanserin



Due to the lack of a suitable microwave oven for radiochemical conversion, we were forced to use the preparation of [¹⁸F]altanserin by conventional heating. Our investigations led to an improved synthesis method, which is described in the present report.

Experimental

Most of the reagents and solvents were obtained from commercial suppliers, altanserin was a gift from Janssen Pharmaceutica.

HPLC analyses of the chemical and radiochemical purity were performed with a LiChrospher 60 select B column (250 mm x 4 mm) isocratically eluted with acetate buffer (pH 4.4)/THF/methanol (550/324/126) at a flow rate of 0.8 ml/min.

Purification by semipreparative HPLC was carried out by using a LiChrospher 60 select B column (250 mm x 10 mm). The column was isocratically eluted with phosphate buffer (pH 5.6)/THF/methanol (550/324/126) at a flow rate of 5 ml/min.

Purification of nitroaltanserin

Nitroaltanserin (300 mg) was suspended in THF (8 ml). The resulting suspension was refluxed for 30 min and filtered hot. The filter cake was washed with hot THF (4 ml). The collected filtrates were evaporated to yield a beige solid.

Yield: 195 mg (65 %)

Melting point: 201 – 206 °C

Radiosynthesis of [¹⁸F]altanserin in a microwave oven

A solution of Kryptofix 2.2.2 (15 mg) and K₂CO₃ (3 mg) dissolved in a mixture of water (0.2 ml) and acetonitrile (1 ml) was added to water (0.1 ml) containing [¹⁸F]fluoride. The water was evaporated by heating the resulting solution at 120 °C in a nitrogen stream while repeatedly adding several portions of acetonitrile (0.5 ml). The dry residue was dissolved in dry DMSO (1 ml) containing nitroaltanserin (nonpurified, 3 - 5 mg). The sealed reaction vessel was placed in the microwave oven and heated several times.

Samples of the reaction mixture were analysed by HPLC to determine the course of the reaction.

Radiosynthesis of [¹⁸F]altanserin by conventional heating

The aqueous solution of [¹⁸F]fluoride was evaporated in the presence of Kryptofix 2.2.2 and potassium carbonate as described above. The nitroaltanserin solution (3-5 mg of purified nitroaltanserin in 1 ml DMSO) was added to the resulting residue. The reaction mixture was heated at 140 °C for 25 min and diluted with HPLC eluent. It was purified by semipreparative HPLC as described above. The eluent containing [¹⁸F]altanserin was collected and diluted with water (eluent/water ratio 1:2). The solution was passed through a C18 cartridge (Chromafix from Macherey & Nagel, 200 mg, prewashed with 5 ml ethanol and 10 ml water). The cartridge was washed with water (10 ml). The product was eluted with absolute ethanol (1 ml). For use of [¹⁸F]altanserin in biochemical studies, saline (9 ml) was added and the resulting solution was filtered through a 0.22 µm sterile filter. Chemical and radiochemical purity was determined by the described methods.

Results and Discussion

Initially we carried out the synthesis of [¹⁸F]altanserin by using a modified home microwave oven. The heating cavity of the oven was reduced to a size suitable for a 2 ml reaction vessel. The reaction mixture (1 ml) was irradiated with a microwave power of 30 W. Under these conditions nitroaltanserin was completely decomposed within 20 s during the fluorination step without formation of [¹⁸F]altanserin. Further experiments using the microwave-assisted synthesis of [¹⁸F]altanserin were not carried out because regulation of the power of the microwave oven proved to be very expensive.

Radiofluorination of nitroaltanserin by conventional heating proceeded without complete decomposition of the precursor. After fluorination, the resulting reaction mixture contained about 15 % [¹⁸F]altanserin (decay-corrected, determined by HPLC).

Nitroaltanserin is very slightly soluble in most common solvents, which makes purification very difficult. In the original procedure this precursor was therefore used as a crude product [1]. We found that nitroaltanserin can be purified by extraction of crude nitroaltanserin with hot THF. Using purified nitroaltanserin, the yield of the fluorination step increased to 25 – 35 %. Under these conditions the amount of nitroaltanserin can be reduced to 3 – 4 mg. By contrast, Lemaire *et al.* [1] obtained radiochemical yields of 20 % with 9 mg crude nitroaltanserin.

Furthermore, the synthesis time was reduced by simplifying purification of [¹⁸F]altanserin, which was performed by semipreparative HPLC. The retention time of [¹⁸F]altanserin was reduced from 55 min to 17 min by using a smaller HPLC column.

The improved synthesis of [¹⁸F]altanserin was completed after 85 min. The overall radiochemical yield ranged from 12 to 27 % (decay-corrected, related to [¹⁸F]fluoride).

References

- [1] Lemaire C., Cantineau R., Guillaume M., Plenevaux A. and Christiaens L. (1991) Fluorine-18-altanserin: A radioligand for the study of serotonin receptors with PET: Radiolabeling and *in vivo* biological behavior in rats. *J. Nucl. Med.* **32**, 2266 – 2272.

30. Serotonin Receptor-Binding Technetium and Rhenium Complexes

21. Synthesis and Characterization of a Novel High-Affinity Tc-99m Ligand for the 5-HT_{2A} Receptor

H.-J. Pietzsch, M. Scheunemann, S. Seifert, P. Brust, H. Spies, B. Johannsen

Introduction

In contrast to the successful development of [^{99m}Tc]TRODAT as a ligand for the dopamine transporter [1] the search for Tc-99m complexes with affinity for post-synaptic CNS receptors have not yet reached the same stage of development. The differences in the topology and structural features of the receptors as opposed to the dopamine transporter [2] as well as the at least 10fold lower concentrations in the brain may be recognized as the principal factors for these difficulties [3].

As one of the consequences for the design of serotonin-5-HT_{2A} receptor binding Tc-99m complexes we have dealt with for some years [4 - 6], an affinity of < 1nM is believed to be a prerequisite for further progress. Aiming at such a high affinity, we have pursued our design concept starting from the selective, high affinity 5-HT_{2A} receptor antagonist ketanserin as lead structure for 5-HT_{2A} receptor binding ligands.

Here we report on the synthesis of a new high-affinity Tc-99m ligand that meets the requirement of subnanomolar affinity. The complex has been evaluated by several *in vitro* receptor binding assays (radioligand binding and functional experiments) [7].

Results and Discussion

Previous studies have shown that already quite simple technetium hybrid molecules of type I (Figure 1) may exhibit nanomolar affinity for the 5-HT_{2A} receptor [4, 5]. These ketanserin-derived complexes combine an aromatic moiety and a protonable nitrogen in an appropriate spacer distance with a neutral technetium chelate representing a mixed ligand "3+1" unit.

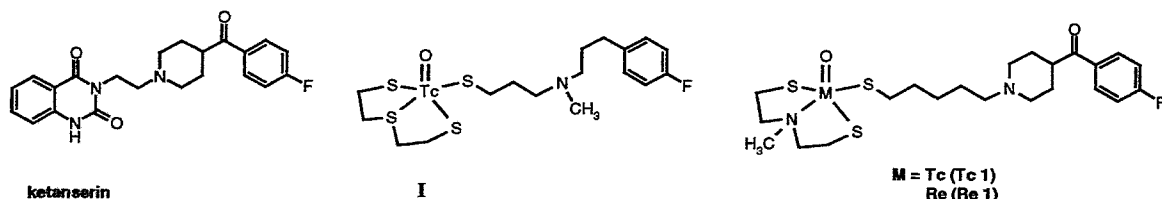


Fig. 1. Serotonin-5-HT_{2A} receptor binding Tc complex I derived from ketanserin as lead structure and a novel Tc-99m ligand Tc 1 with subnanomolar affinity for the serotonin-5-HT_{2A} receptor.

The new technetium complex Tc 1 has resulted from modification of spacer length and tridentate ligand of the chelate unit. The 4-(4-fluoro)benzoyl piperidine portion derived from ketanserin, which contributes much to an effective binding of 5-HT_{2A} receptor antagonists, has been conserved.

The rhenium complex Re 1 has been synthesized as a surrogate for the Tc-99m complex for use in receptor binding assays and for complete structural characterization. Elemental analysis as well as NMR data clearly indicated the purity and composition of the compound. Co-injections of [^{99m}Tc]Tc 1 and Re 1 into HPLC under various elution conditions showing similar retention times confirm the structural identity of both substances.

Synthesis of the monodentate thiol ligand 6

The synthesis of monodentate thiol ligand 6 was performed by a new method using a ring opening reaction of 2-thianone 3 as the key step (Scheme 1).

Prior to this ring opening reaction 4-(4-fluoro)benzoyl piperidine 1 was protected by 1,2-ethanediol, using a three-step procedure to give the ketal 2. The aminolysis of 2-thianone 3 with 2 was carried out in chloroform at ambient temperature for 3 h. The convenience of the purification of the resulting am-

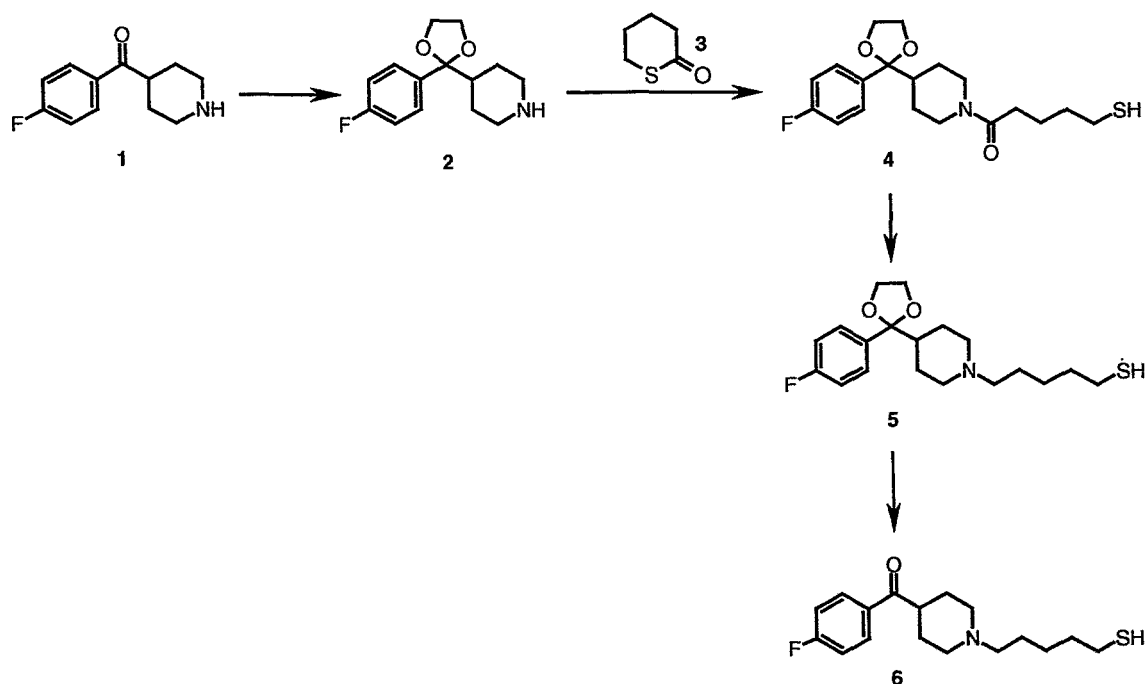
¹ for part 20 see FZR-Annual Report 1997, pp. 18-20.

² submitted for publication in Nucl. Med. Biol. 1999

ide **4** is mainly due to its nonbasic properties. Thus, simple washing of the reaction mixture with diluted acid removes any basic starting material.

Reduction of the amide group is accomplished with lithium aluminium hydride. The ^{13}C NMR spectrum of the product obtained indicates no contamination by unreacted amide. Finally, the ketal intermediate **5** was deprotected by treatment with 4 N HCl for 1 hour at 45 °C to give the monodentate thiol **6**. The isolated compound was homogeneous on TLC and showed satisfying elemental analysis in the form of its oxalate salt.

Scheme 1. Synthesis of the monodentate thiol ligand **6** via ring opening reaction of 2-thianone **3** as the key step



{[3-N-methyl-azapentane-1,5-dithiolato][5-(4-{4-fluorobenzoyl}piperidin-1-yl)pentyl-1-thiolato]}-oxorhenium(V) (**Re 1**)

Thiol **6** (104 mg, 0.26 mmol) and 3-(N-methyl)-azapentane-1,5-dithiol oxalate (58 mg, 0.24 mmol) were dissolved in MeOH (8 ml) at 50 °C. After addition of a methanolic solution of sodium acetate (1 M, 4 ml) and $\text{ReOCl}_3(\text{PPh}_3)_2$ (208 mg, 0.25 mmol) the suspension was stirred and heated under reflux for 2 h.

After cooling to room temperature, the reaction mixture was evaporated. The residue was partitioned between CHCl_3 (15 ml) and 5 % aqueous solution of NaHCO_3 (10 ml). The organic phase was dried (MgSO_4), evaporated and purified by liquid chromatography on silica gel with $\text{CHCl}_3/\text{MeOH}$ (18:1) as solvent to give the product as a green coloured fraction. The solvent of the separated fraction was removed and the residue was triturated with MeOH to afford the complex as dark green crystals: yield, 53.9 mg (34 %); m.p. 135 – 137 °C.

^1H NMR (400 MHz, CDCl_3): δ = 1.49 – 1.57 [m, 4H, $\text{N-CH}_2(\text{CH}_2)_2\text{-CH}_2$], 1.80 – 1.90 [m, 6H, $\text{CH}_2\text{-CH}_2\text{-S}$, Pip-3-H, Pip-5H] 2.0 – 2.14 [m, 2H, Pip-2- H_{ax} , Pip-6- H_{ax}], 2.36 [m, 2H, $\text{N-CH}_2(\text{CH}_2)_3$], 2.62 [m, 2H, $(\text{CH}_2)_2\text{-CH}_2\text{-S}$], 3.00 [m, 2H, Pip-2- H_{eq} , Pip-6- H_{eq}], 3.35 [s, 3H, NCH_3], 3.10 – 3.20, 3.50 – 3.58 and 3.72 [2m and br, 9H, Pip-4-H, $\text{N}(\text{CH}_2\text{-CH}_2\text{-S})_2$], 7.13 and 7.96 [AA'BB'-part of AA'BB'X-system, 4H, H_{arom}].

^{13}C NMR (100 MHz, CDCl_3): δ = 26.77, 27.20, 28.77, 32.74, 41.52, 43.88, 44.81, 52.59, 53.29, 58.96, 68.70, 115.69 (d, J = 22.2 Hz, 2C, C3), 130.83 (d, J = 9.2 Hz, 2C, C2), 132.48 (d, J = 2.8 Hz, 1C, C1), 165.54 (d, J = 253.9 Hz, 1C, C4), 201.10 (C=O).

Elemental analysis: Found: C, 39.97; H, 4.72; N, 4.13; S, 14.66.

$\text{C}_{22}\text{H}_{44}\text{FN}_2\text{O}_2\text{ReS}_3$ requires: C, 40.04; H, 5.19; N, 4.25; S, 14.66 %.

Preparation of the technetium-99 complex [⁹⁹Tc]Tc 1

⁹⁹Tc(V) gluconate was prepared by gradual addition of stannous chloride to an aqueous solution of ⁹⁹TcO₄⁻ (2 μmol/ca. 5 MBq) in an excess of sodium gluconate.

1 ml of the ⁹⁹Tc gluconate solution was diluted with 1 ml of ethanol. A solution of 2 μmol of 3-(N-methyl)azapentane-1,5-dithiol (HS-NMe-SH) and 2 μmol of the monodentate thiol **6** in 0.2 ml ethanol was added. The colour of the mixture turned to reddish-brown. After stirring for 30 min and adding 2 ml of water, the Tc compound was isolated by extraction of the reaction mixture with 2 ml of chloroform. The organic phase was washed twice with 1 ml of water and dried over Na₂SO₄.

The yields are in the range from 75 to 80 percent (related to technetium gluconate).

The radiochemical purity (98 %) of the technetium complex was determined by HPLC: Perkin Elmer 250 binary pump gradient elution, Hamilton PRP 1 reversed phase column (250 x 4 mm, 10 μm), mobile phases: acetonitrile and ammonium acetate buffer (0.05 M, adjusted to pH 4.0 with acetic acid), initial elution: for 2 min with 50 % acetonitrile and 50 % buffer, within 20 min the eluting solution was 100 % acetonitrile, flow rate: 2 ml/min.

For receptor binding studies a stock solution of the complex was prepared by evaporating the organic solvent under nitrogen and redissolving the residue in 1 ml of DMSO.

No carrier added preparation of the Tc-99m complex [^{99m}Tc]Tc 1

0.5 mg of an aqueous/ethanolic solution (200 μl) of the monothiol ligand **6** and 0.05 mg of the tridentate ligand dissolved in ethanol (10 μl) are added to a mixture of 1.0 ml pertechnetate eluate (100 – 500 MBq) and 0.5 ml propylene glycol. After increasing the pH of the solution with 150 μl 0.1 N NaOH the reduction of pertechnetate was performed by addition of 20 μl stannous chloride solution (1.0 – 2.0 mg SnCl₂ • 2 H₂O dissolved in 5.0 ml 0.1 N HCl) and heating for 20 min in a water bath at 50 °C.

Radiochemical purity: 90 – 95 % determined by HPLC (Hypersil ODS (250 x 4 mm), flow rate 1.0 ml/min, isocratic gradient mixture of 80 % methanol and 20 % 0.01 M phosphate buffer of pH 7.4).

For the separation of ligand excess the reaction mixture is loaded onto a semi-preparative PRP-1 column. The complex is eluted with a R_t value of 11.5 min and well separated from the ligands (R_t = 6.5 min and 13.9 min) using a linear gradient system of acetonitrile/0.1 % trifluoroacetic acid (A) and 0.1 % trifluoroacetic acid (B); [t(min)/A(%): [5/30], [10/80], [5/80], flow rate 3.0 ml/min, UV detection at 254 nm and γ-detection.

After neutralization of the complex fraction and adding of 200 μl propylene glycol the acetonitrile is evaporated under vacuum. The radiochemical purity of the final solution is > 95%. For the autoradiographic studies the solution is diluted with saline.

References

- [1] Meegalla S., Ploessl K., Kung M.-P., Stevenson D. A., Liable-Sands L. M., Rheingold A. L. and Kung H. F. J. (1995) First example of a ^{99m}Tc complex as a dopamine transporter imaging agent. *Am. Chem. Soc.* **117**, 11037-11038.
- [2] Newman A. H. (1998) Novel dopamine transporter ligands: the state of the art. *Med. Chem. Es.* **8** (1/2), 1-11.
- [3] Volkow N. D., Fowler J. S., Gatley S. J., Logan J., Wang G.-J., Ding Y. S. and Dewey S. (1996) PET evaluation of the dopamine system of the human brain. *J. Nucl. Med.* **37**, 1242-1256.
- [4] Johannsen B., Scheunemann M., Spies H., Brust P., Wober J., Syhre R. and Pietzsch H.-J. (1996) Technetium(V) and rhenium(V) complexes for 5-HT_{2A} serotonin receptor binding: structure-affinity considerations. *Nucl. Med. Biol.* **23**, 429-438.
- [5] Johannsen B., Berger R., Brust P., Pietzsch H.-J., Scheunemann M., Seifert S., Spies H. and Syhre R. (1997) Structural modification of receptor binding technetium-99m complexes in order to improve brain uptake. *Eur. J. Nucl. Med.* **24**, 316-319.
- [6] Johannsen B. and Spies H. (1997) Advances in technetium chemistry towards tc-99m receptor imaging agents. *Trans. Met. Chem.* **22**, 318-320.
- [7] Kretschmar M., Brust P., Elz S., Pertz H. H., Pietzsch H.-J., Scheunemann M., Seifert S., Zessin J. and Johannsen B. (1999) Serotonin receptor-binding technetium and rhenium complexes **23**. Biological evaluation of a novel high-affinity Tc-99m ligand for the serotonin-5-HT_{2A} receptor. *This report*, pp. 126-131.

31. Serotonin Receptor-Binding Technetium and Rhenium Complexes

22. Biological Evaluation of a Novel High-Affinity Tc-99m Ligand for the Serotonin-5-HT_{2A} Receptor

M. Kretzschmar, P. Brust, S. Elz¹, H. H. Pertz¹, H.-J. Pietzsch, M. Scheunemann, S. Seifert, J. Zessin, B. Johannsen

¹Freie Universität Berlin, Institut für Pharmazie

Introduction

Alterations in serotonergic neurotransmission have been implicated in various neuropsychiatric disorders, e.g. anxiety, depression and Alzheimer's disease. Changes in the density of the 5-HT_{2A} receptor were demonstrated *in vitro* on postmortem human brain [6, 15]. Modern imaging technology, such as positron emission tomography (PET) or single-photon computed tomography (SPECT), allows the visualization and quantification of these receptor-binding sites in living patients. [¹⁸F]Setoperone and [¹⁸F]altanserin were developed as PET tracer and are currently used for *in vivo* human application [2, 3, 4, 12].

In contrast to this achievement and in spite of the efforts many groups, the search for ^{99m}Tc complexes with an affinity to post-synaptic CNS receptors for the application of SPECT have not yet reached the same stage of development [10].

Aiming at a high-affinity serotonin-5-HT_{2A} receptor-binding ^{99m}Tc complex, we pursued our design concept, starting from the selective, high-affinity 5-HT_{2A} receptor antagonist ketanserin [21] as lead structure for 5-HT_{2A} receptor-binding ligands.

The synthesis of a new high-affinity ^{99m}Tc ligand (**Tc 1**) that meets the requirement of subnanomolar affinity was described in an accompanying report [17]. This study evaluates the complex and its rhenium congener (**Re 1**) by several *in vitro* receptor-binding assays (radioligand binding and functional experiments) and by *in vitro* autoradiography.

Experimental

Receptor-binding assays :

A. Brain homogenates

Binding assays using the [⁹⁹Tc]**Tc 1** and **Re 1** compounds for the 5-HT_{2A} receptor, the 5-HT_{1A} receptor and D₂ receptor were performed as previously described [18]. The procedures for the binding assays for the 5-HT and DA transporters were published recently [8, 9].

B. Functional receptor assays on isolated organs

The 5-HT_{2A} receptor assay on the rat tail artery using the **Re 1** compound was performed as published [16, 17]. Assays for histamine H₁ and muscarinic M₃ receptors of the guinea-pig whole ileal segments, adrenergic α_{1D} receptors of the rat thoracic aorta, histamine H₂ and adrenergic β₁ receptors of the spontaneously beating guinea-pig right atrium, 5-HT_{1B} receptors of the guinea-pig iliac artery were carried out on the model of Pertz and Elz [16]. Histamine H₃ receptors were measured on the field-stimulated guinea-pig ileal longitudinal muscle with adhering myenteric plexus [19] and 5-HT₃ receptors on quiescent guinea-pig ileal longitudinal muscle with adhering myenteric plexus and 5-HT₄ receptors of rat oesophageal muscular mucous membrane [7].

In vitro autoradiography

Male Wistar rats (210-230 g) and male piglets (1.8-2.9 kg) were used in the studies. After euthanasia the brains were removed and quickly frozen by immersion in isopentane/dry ice solution at -50 °C. 20 μm horizontal and sagittal sections were sliced on a cryostat microtome, thaw-mounted onto pre-treated slides and kept at -20 °C until use. Prior to the experiment, the slides were dried at room temperature and pre-incubated for 30 min in buffer containing 50 mM Tris-HCl (pH 7.4) and 120 mM NaCl. As described above the slides were then incubated for 1.5 h in buffer containing [^{99m}Tc]**Tc 1** compound (0.008 MBq/ml = 216 nCi/ml). After incubation, the slides were washed twice 10 min in ice-cold Tris buffer, rinsed in cold distilled water, and dried by cold air. Nonspecific binding was determined in the presence of 1 μM mianserin.

In order to determine the pharmacological specificity and selectivity of [^{99m}Tc]**Tc 1** receptor binding, 1 μM of various drugs was added to the incubation buffer, such as the 5-HT_{2A} receptor antagonist ketanserin, the 5-HT_{1A} receptor agonist 8-OH-DPAT, the dopamine receptor antagonist haloperidol and the α₁β₁ adrenergic receptor agonist (±) norepinephrine.

As a reference for the 5-HT_{2A} receptor distribution in the brain, additional slides containing the high-affinity 5-HT_{2A} receptor ligands [³H]ketanserin (1 nM) or [¹⁸F]altanserin (10 nM) were incubated in the same buffer. The nonspecific binding of these ligands was also determined in the presence of 1 μM of mianserin.

For autoradiography the method of radioluminography was used. The ^{99m}Tc and ¹⁸F-labelled sections were apposed to standard imaging plates for approximately 18 h whereas ³H-labelled sections were apposed to tritium-sensitive plates for 11 days. The imaging plates were scanned in the bio-imaging analyser BAS 2000 (FUJI photo film Co, Tokyo). The evaluation was carried out with the TINA 2.09 g program (RAYTEST, STRAUBENHARDT). After exposure the brain sections were stained with cresyl violet to match anatomical with functional information.

Results and Discussion

Receptor-binding assays

The **Tc 1** and **Re 1** were used in various receptor-binding assays to determine the affinity and selectivity of these ligands for the 5-HT_{2A} receptor. As shown in Table 1, both compounds have a similarly high affinity for this serotonin receptor subtype. They also display a high selectivity for the 5-HT_{1A} receptor, the 5-HT transporter (5-HTT) and the dopamine transporter (DAT). The selectivity for the dopamine D₂ receptor is much lower. However, for extrastriatal regions **Tc 1** meets some of the criteria of a good imaging agent. This lack of selectivity is not a general problem for brain imaging. It has been shown with ¹¹C-3-N-methylspiperone (NMSP), a ligand with high affinity to 5-HT_{2A} and D₂ receptors, that these two receptor types can be simultaneously measured with PET [22].

Table 1. Inhibition constants ($K_i \pm SD$) of [^{99m}Tc]**Tc 1** and **Re 1** for serotonin and dopamine receptors (5-HT_{1A}, 5-HT_{2A}, D₂) and transporters (5-HTT, DAT).

Complex	K_i (nM)				
	5-HT _{1A}	5-HT _{2A}	5-HTT	D ₂	DAT
[^{99m} Tc] Tc 1	142 ± 35	0.44 ± 0.10	1783 ± 671	12.9 ± 1.2	>15,000
Re 1	44.8 ± 2.6	0.25 ± 0.11	1150 ± 354	16.8 ± 0.9	n.det.

The subnanomolar 5-HT_{2A} receptor binding of **Re 1** was confirmed by functional *in vitro* antagonism of contractile effects evoked by 5-HT in rat arterial tissue. The vascular contraction of the rat tail artery elicited by 5-HT and related tryptamines is mediated by 5-HT_{2A} receptors [5]. This effect was antagonized by **Re 1** (10 - 1000 nM). The **Re 1**/receptor dissociation constant was similar to the K_i value obtained from inhibition of the radioligand binding in rat cortex under various experimental conditions (0.83 nM versus 0.25 nM). The selectivity of **Re 1** for some other 5-HT receptor subtypes was >1200 [17]. In a series of selectivity experiments vis-à-vis histamine, acetylcholine, and adrenergic receptors, **Re 1** showed a moderate competitive antagonist affinity for H₁ receptors of guinea-pig ileum and α_{1D} receptors of rat aorta. This behaviour is shared by ketanserin, which blocked the H₁ and α_{1D} receptors to a similar extent [16] and thus displayed similar selectivity ratios for these receptors (10 and 36) as **Re 1** [17].

In vitro autoradiography

The regional *in vitro* distribution and accumulation of [^{99m}Tc]**Tc 1** was measured in sections of rat and piglet brains. Autoradiograms of brain slices are shown in Fig. 1. Obviously, the ^{99m}Tc radioactivity accumulates predominantly in the frontal cortex, anterior olfactory nucleus and caudate putamen, areas known to have a high density of 5-HT_{2A} receptors [11, 12, 13, 14].

An almost identical regional labelling pattern of the brain sections was found with [³H]ketanserin (Fig. 2), [¹⁸F]altanserin [1] (Fig. 3) and [^{99m}Tc]**Tc 1**, with the exception of the tracer accumulation in the thalamus. Larger amounts of ^{99m}Tc radioactivity were measured in this region. 55 % of the total binding in the thalamus of the rat was displaced by mianserin (Fig. 4). The displacement of [³H]ketanserin was only 35 %. In the piglet too a higher binding of [^{99m}Tc]**Tc 1** was found compared with [³H]ketanserin (Fig. 4). It is possible that the ^{99m}Tc complex occupies binding sites in the thalamus other than 5-HT_{2A} receptors. As was shown using the functional receptor assays, the **Re** congener has a rather high affinity also for the α_{1D} and histamine H₁ receptors [17] which are found at relatively high densities in the thalamus [12, 20]. For example in our studies the α₁β₁ adrenergic agonist (±) norepinephrine dis-

placed 15 % of the total [^{99m}Tc]Tc 1 binding in the thalamus (Fig. 5). A slightly higher accumulation of [^{99m}Tc]Tc 1 was also found in the white matter (corpus callosum, internal and external capsula) and in the medullary substance of the cerebellum. The accumulation in these lipid-rich areas may be caused by the considerable lipophilicity of the compound.

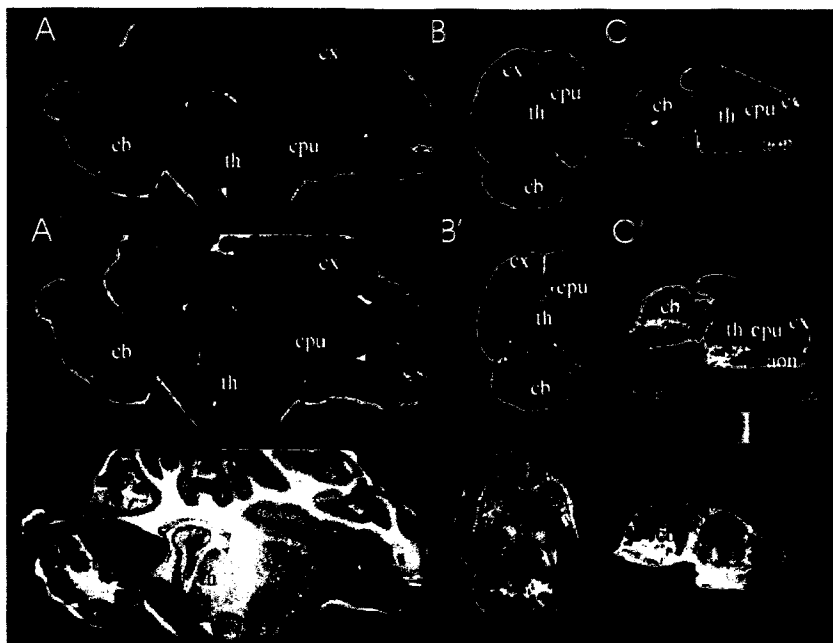


Fig.1. In vitro autoradiograms (above) and histological image (below) of sagittal (A, C) and horizontal (B) brain sections of piglets (A) and rats (B, C) showing the distribution of [^{99m}Tc]Tc 1. A - C: control sections without displacer, A' - C': consecutive sections after displacement by mianserin. Cx = frontal cortex, cpu = caudate putamen, th = thalamus, cb = cerebellum, aon = anterior olfactory nucleus.



Fig. 2. In vitro autoradiograms (above) and histological image (below) of sagittal (A, C) and horizontal (B) brain sections of piglets (A) and rats (B, C) showing the distribution of [^3H]ketanserin.

A - C: control sections without displacer, A' - C': consecutive sections after displacement by mianserin. Cx = frontal cortex, cpu = caudate putamen, th = thalamus, cb = cerebellum, aon = anterior olfactory nucleus.

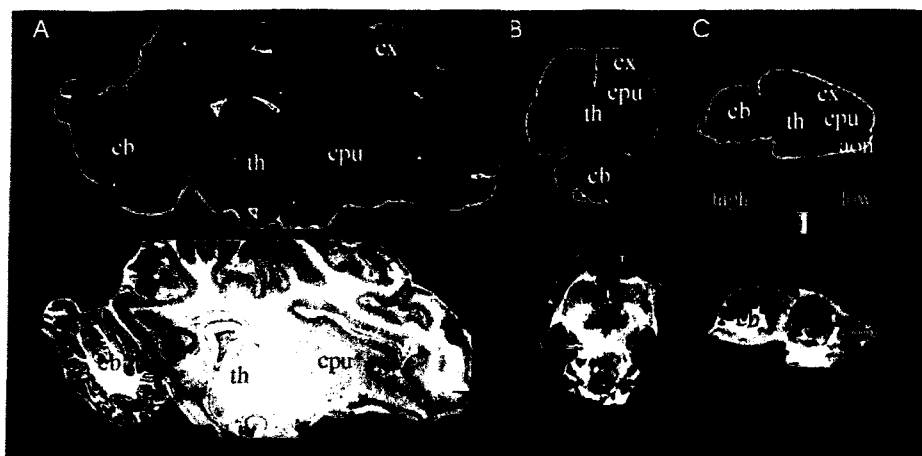


Fig. 3. In vitro autoradiograms (above) and histological image (below) of sagittal (A, C) and horizontal (B) brain sections of piglets (A) and rats (B, C) showing the distribution of [^{18}F]altanserin. Cx = frontal cortex, cpu = caudate putamen, th = thalamus, cb = cerebellum, aon = anterior olfactory nucleus.

The binding of [$^{99\text{m}}\text{Tc}$]Tc 1 in the various brain regions can be inhibited by the 5-HT $_{2A}$ antagonists mianserin (rat: between 55 and 32 %; piglet: between 47 and 10 %) and ketanserin (rat: between 41 and 6 %; piglet: between 37 and 0 %) (Fig. 5).

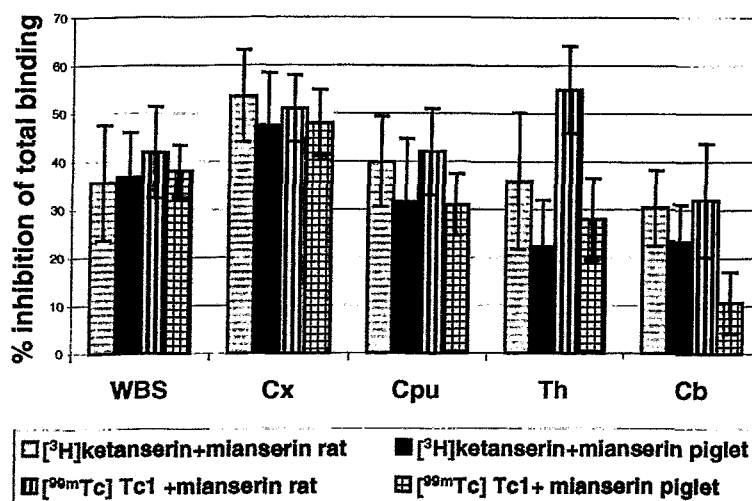


Fig. 4. Comparison of the inhibition of [^3H]ketanserin binding (specific 5-HT $_{2A}$ receptor binding) and [$^{99\text{m}}\text{Tc}$]Tc 1 binding by mianserin in various regions of the brain of rats (n = 5) and piglets (n = 3). WBS = whole brain section, Cx = frontal cortex, Cpu = caudate putamen, Th = thalamus, Cb = cerebellum

The dopamine receptor antagonist haloperidol also significantly inhibited the binding of [$^{99\text{m}}\text{Tc}$]Tc 1 in various brain areas (Fig. 5). This result is in agreement with the studies by Leysen *et al.* [13] who found that the [^3H]ketanserin binding was displaced by haloperidol ($K_i = 22$ nM) in the rat prefrontal cortex. With the 5-HT $_{1A}$ agonist 8-OH-DPAT no inhibition of binding was observed in most regions of the brain (Fig. 5). These results agree with the noticeable binding affinity to the dopamine D $_2$ receptor ($K_i = 13$ nM) as well as with the relatively low 5-HT $_{1A}$ receptor-binding affinity ($K_i = 142$ nM) found in the receptor-binding studies. (Table 1) [17].

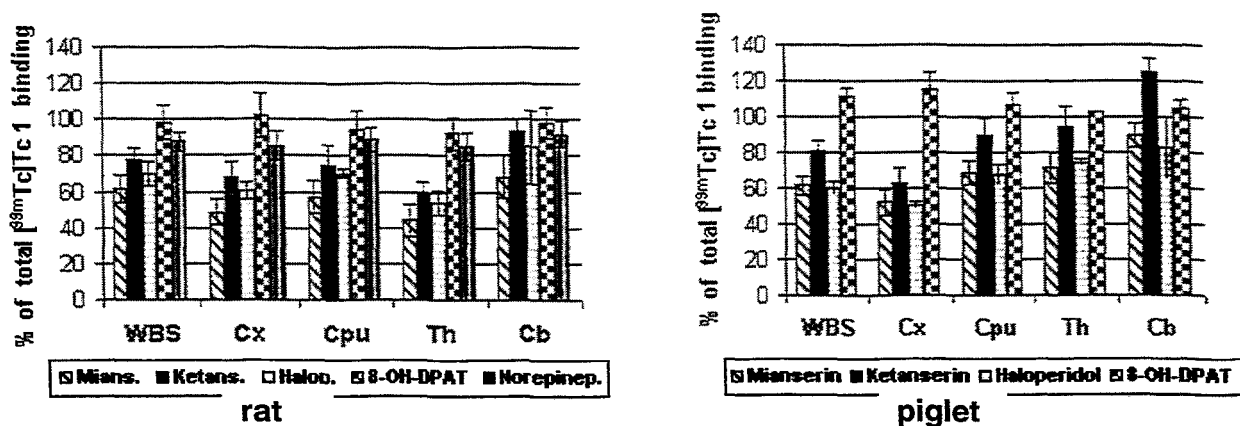


Fig. 5. Effect of the equimolar administration of several drugs on in vitro [^{99m}Tc]Tc 1 binding in various rat (left) and piglet (right) brain regions (percentage of total complex binding)

In conclusion, it was shown that among the ^{99m}Tc compounds studied so far the new [^{99m}Tc]Tc 1 ligand exhibits the highest affinity to the serotonin-5-HT_{2A} receptor in the subnanomolar range with obvious visualization of the in vitro binding in areas of the brain known to have a high density of serotonin-5-HT_{2A} receptors.

References

- [1] Biver F., Lotstra F., Monclus M., Dethy S., Damhaut P., Wikler D., Luxen A. and Goldman S. (1997) *In vivo* binding of [^{18}F]altanserin to rat brain 5-HT₂ Receptors: A film and electronic autoradiographic study. *Nucl. Med. Biol.* **24**, 357-360.
- [2] Blin J., Baron J. C., Dubois B., Crouzel C., Fiorelli M., Attar-Levy D., Pillon B., Fournier D., Vidailhet M. and Agid Y. (1993) Loss of brain 5-HT₂ receptors in Alzheimer's disease. In vivo assessment with positron emission tomography and [^{18}F] setoperone. *Brain* **116** (Pt 3) 497-510.
- [3] Blin J., Pappata S., Kiyosawa M., Crouzel C. and Baron J.C. (1988) [^{18}F]setoperone: a new - high affinity ligand for positron emission tomography study of the serotonin-2 receptors in baboon brain in vivo. *Eur. J. Pharmacol.* **147**, 73-82.
- [4] Blin J., Sette G., Fiorelli M., Bletry O., Elghozi J.L., Crouzel C. and Baron J.C. (1990) A method for the in vivo investigation of the serotonergic 5-HT₂ receptors in the human cerebral cortex using positron emission tomography and ^{18}F -labeled setoperone. *J. Neurochem.* **54**, 1744-1754.
- [5] Bradley P.B., Humphrey P.P.A. and Williams R.H. (1985) Tryptamine-induced vasoconstrictor responses in rat caudal arteries are mediated predominantly via 5-hydroxytryptamine receptors. *Br. J. Pharmacol.* **84**, 915-925.
- [6] Cross A.J., Slater P., Perry E.K. and Perry R.H. (1988) An autoradiographic analysis of serotonin receptors in human temporal cortex: Changes in Alzheimer-type dementia. *Neurochem. Int.* **13**, 89-96.
- [7] Elz S. and Keller A. (1995) Preparation and *in vitro* pharmacology of 5-HT₄ receptor ligands. Partial agonism and antagonism of metoclopramide analogous benzoic esters. *Arch. Pharm. Pharm. Med. Chem.* **328**, 585-594.
- [8] Hoepfing A., Brust P., Berger R., Spies H., Machill S., Scheller D. and Johannsen B. (1998) Novel rhenium complexes derived from α -tropanole as potential ligands for the dopamine transporter. *Bioorg. Med. Chem.* **6**, 1663-1672.
- [9] Hoepfing A., Reisgys M., Brust P., Seifert S., Spies H., Alberto R. and Johannsen B. (1998) TROTEC-1: A new high-affinity ligand for labeling of the dopamine transporter. *J. Med. Chem.* **41**, 4429-4432.
- [10] Holm R. K. and Katzenellenbogen J. A. (1997) Technetium-99m labeled receptor-specific small-molecule radiopharmaceuticals: recent developments and encouraging results. *Nucl. Med. Biol.* **24**, 485-498.
- [11] Hrdina P.D. and Vu T.B. (1993) Chronic fluoxetine treatment upregulates 5-HT uptake sites and 5-HT₂ receptors in rat brain: an autoradiographic study. *Synapse* **14**, 324-331.
- [12] Lemaire C., Cantineau R., Guillaume M., Plenevaux A. and Christiaens L. (1991) Fluorine-18-

- altanserin: a radioligand for the study of serotonin receptors with PET: radiolabeling and in vivo biologic behavior in rats. *J. Nucl. Med.* **32**, 2266-2272.
- [13] Leysen J.E., Niemegeers C.J.E., van Nueten J.M. and Laduron P.M. (1982) [³H]ketanserin (R41468), a selective ³H-ligand for serotonin₂ receptor binding sites. Binding properties, brain distribution, and functional role. *Mol. Pharm.* **21**, 301-314.
- [14] Pazos A., Cortes R. and Palacios J. M.(1985) Quantitative autoradiographic mapping of serotonin receptors in the rat brain. II. Serotonin-2 receptors. *Brain Res.* **346**, 231-249.
- [15] Perry E. K., Perry R. H., Candy J. M., Fairbairn A. F., Blessed G., Dick D. J. and Tomlinson B. E. (1984) Cortical serotonin-2 receptor binding abnormalities in patients with Alzheimer's disease: Comparisons with Parkinson's disease. *Neurosci. Lett.* **51**, 353-357.
- [16] Pertz H. H. and Elz S. (1995) In-vitro pharmacology of sarpogrelate and the enantiomers of its major metabolite: 5-HT_{2A} receptor specificity, stereoselectivity and modulation of ritanserin-induced depression of 5-HT contractions in rat tail artery. *J. Pharm. Pharmacol.* **47**, 310-316.
- [17] Pietzsch H.-J., Scheunemann M., Kretzschmar M., Seifert S., Elz S., Brust P., Spies H., Syhre R. and Johannsen B. (1999) Synthesis and autoradiographical evaluation of a novel high-affinity Tc-99m ligand for the serotonin-5-HT_{2A} receptor. *Nucl. Med. Biol.* in press.
- [18] Pietzsch H.-J., Scheunemann M., Brust P., Wober J., Spies H. and Johannsen B. (1997) *Annual Report 1996*, Institute of Bioinorganic and Radiopharmaceutical Chemistry, FZR-165, pp 9-12.
- [19] Schlicker E., Kathmann M., Reidemeister S., Stark H. and Schunack W. (1994) Novel histamine H₃ receptor antagonists: affinities in an H₃ receptor binding assay and potencies in two functional H₃ receptor models. *Br. J. Pharmacol.* **112**, 1043-1048. Erratum: (1994) *Br. J. Pharmacol.* **113**, 657.
- [20] Soria-Jasso L. E., Bahena-Trujillo R. and Arias-Montano J. A. (1997) Histamine H1 receptors and inositol phosphate formation in rat thalamus. *Neurosci. Lett.* **225**, 117-120.
- [21] Van Nueten J. M., Janssen P. A. J., van Beek J., Xhonneux R., Verbeuren T. J. and Vanhoutte P. M. (1981) Vascular effects of ketanserin (R 41 468), a novel antagonist of 5-HT₂ serotonergic receptors. *J. Pharmacol. Exp. Ther.* **218**, 217-230.
- [22] Wong D. F., Wagner H. N. Jr, Dannals R. F., Links J. M., Frost J. J., Ravert H. T., Wilson A. A., Rosenbaum A. E., Gjedde A., Douglass K. H., Petronis J. D., Folstein M. F., Toung J. K. T., Burns H. D. and Kuhar M. J. (1984) Effects of age on dopamine and serotonin receptors measured by positron tomography in the living human brain. *Science* **226**, 1393-1396.

32. Serotonin Receptor-Binding Technetium and Rhenium Complexes

23. Design, Structure and In Vitro Affinity of a 5-HT_{1A} Receptor Ligand Labelled with ^{99m}Tc -First Application of fac-[^{99m}Tc(OH₂)₃(CO)₃]⁺ in Bioorganometallic Chemistry**

R. Alberto¹, R. Schibli¹, A. P. Schubiger¹, U. Abram², H.-J. Pietzsch, A. Drews, B. Johannsen
¹Center for Radiopharmacy, Paul Scherrer Institute, CH-5232 Villigen, Switzerland
²Institut für Radiochemie

Introduction

Organometallic complexes exhibit unique features, which make them very attractive mainly in catalysis but, more recently, their application in life science has become a field of growing interest as well [1]. Beside investigations on the metabolic behaviour of pure organometallic compounds, bioorganometallic chemistry, as introduced by Jaouen and coworkers [2] stands for the combination of an organometallic moiety and a bioactive molecule which targets different type of receptors. For the latter purposes, the metal complex should be "innocent" but provide major advantages in metabolic stability and interference with binding properties of the biomolecule.

We present herein the first example where the organometallic tricarbonyl moiety "fac-[^{99m}Tc(CO)₃]⁺" was successfully applied for the straight forward labelling of a biomolecule designed for binding to the serotonergic receptor 5-HT_{1A} in the central nervous system [3].

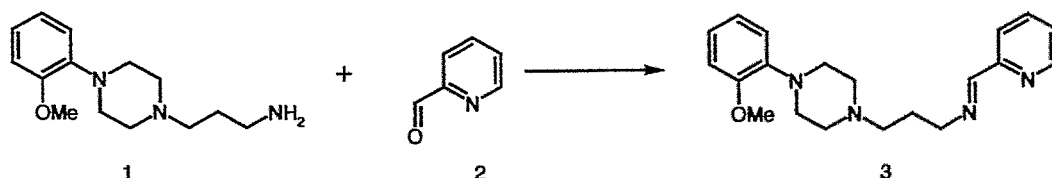
Results and Discussion

Bioorganometallic chemistry comprises the combination of an organometallic transition metal complex and a targeting biomolecule. If ever such a combination should be applied in nuclear medicine, the synthesis has to be convenient, fast and requires one or two steps only. A useful precursor is represented by the organometallic aquo-complex [^{99m}Tc(OH₂)₃(CO)₃]⁺ **1** for which we recently presented a convenient one step kit procedure directly from saline in high yield [4].

Potential ^{99m}Tc complexes attached to CNS receptor ligands have to be neutral in charge and lipophilic to cross the blood-brain barrier. Thus, we have focused our interest on neutral bidentate amine ligands (N'N'). The occupation of two coordination sites by such a set of donors entails the coordination of charge neutralizing Cl⁻ at the third position. Whereas aliphatic diamines were found to be weak (or slow) chelators, all combination of nitrogen donors containing an aromatic amine group were extremely efficient. In particular Schiff Base ligands can be prepared just by reacting an aliphatic amine, which is a frequent functionality in biomolecules, with a corresponding aromatic aldehyde of choice.

To exemplify this, we have derivatized a receptor ligand from the class of arylpiperazines, which belongs to the most thoroughly studied molecules for the 5-HT_{1A} subclass of serotonergic receptors [5]. In particular, 4-(3-aminopropyl)-1-(2-methoxyphenyl)piperazine **1** was reacted with 2-pyridine carbaldehyde **2** to yield compound **3**, a Schiff Base type ligand attached to the bioactive moiety (Scheme 1). Labelling was achieved by incubating the precursor **1** with the corresponding amount of **3**. After 10 min at 90 °C the radiolabelled biomolecule **4** was formed in almost quantitative yield.

Scheme 1. Preparation of the derivatized aryl piperazine **3** from 4-(3-aminopropyl)-1-(2-methoxyphenyl)piperazine **1** and 2-pyridine carbaldehyde **2**

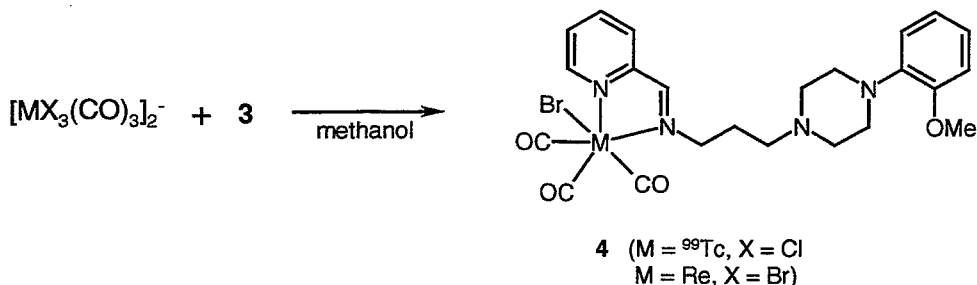


To get unambiguous evidence for the composition of the compounds, we have synthesized the corresponding complex with long-lived ⁹⁹Tc. Formation of the complex **4** was carried out by the reaction of

* for part 22 see this report, pp. 126-131.
** J. Am. Chem. Soc., in press

$[\text{}^{99}\text{TcCl}_3(\text{CO})_3]_2^-$ in methanol [6] with 1 eq. of ligand **3** at r. t. (Scheme 2). Crystals could be grown directly from the solvent and the structure was elucidated by X-ray analysis. HPLC comparison of the cold, macroscopic complex and the material prepared on the n. c. a. level finally established their identity.

Scheme 2. Synthesis of complexes **4** by the reaction of $[\text{MX}_3(\text{CO})_3]_2^-$ in methanol with 1 eq. of ligand **3**



The molecular structure of **4** is given in Fig. 1. The technetium acts as a chirality center. Consequently, two enantiomeric forms of the labelled compound exist with $^{99\text{m}}\text{Tc}$. Since the complex is far away from the effective binding site of the optically inactive receptor ligand, it can be anticipated that interference and decrease of affinity should not be initiated by this chiral center.

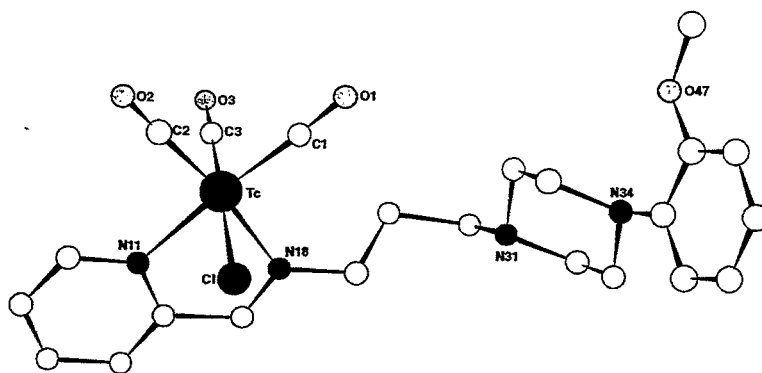


Fig. 1. Molecular structure of the 5-HT_{1A} receptor binding ^{99}Tc complex **4**

In vitro receptor binding assays

To assess the retention of biological activity and selectivity, the *in vitro* binding affinities of **4** with cold rhenium instead of Tc were tested. The affinity (IC_{50} values) to the 5-HT_{1A} receptor was 5 ± 2 nM (competitor [^3H]8-OH-DPAT).

The selectivity (competitor in brackets) was investigated with the following other receptors: 5-HT_{2A} ([^3H]ketanserin), dopamin-D₂ ([^3H]spiperone) 5-HT-transporter ([^3H]paroxetine) and D-transporter ([^3H]WIN35,428). In all cases the affinity was found to be > 1 mM. The rhenium labelled compounds revealed, thus, a very good selectivity for the 5-HT_{1A} receptor. Due to the chemical relationship between Re and Tc, the values for the latter one are not significantly different [7]. The good selectivity justifies further investigations on the *in vivo* behaviour and in particular the brain uptake of CNS receptor ligands labelled with the "fac- $[\text{}^{99\text{m}}\text{Tc}(\text{CO})_3]$ " moiety.

Conclusion

In conclusion, it was shown for the first time, that organometallic complexes such as $[^{99m}\text{Tc}(\text{OH}_2)_3(\text{CO})_3]^+$ can be applied in purely aqueous systems for the labelling of derivatized bioactive molecules under retention of their receptor affinity. Thus, the concept of bioorganometallic chemistry could be established on a routinely applicable base. Unique advantages in comparison to other concepts emerge from the partially organometallic coordination sphere of the label. In particular, very low biomolecule concentration, high kinetic stabilities and flexibility in the choice of ligands make this type of precursor very attractive for routine use.

References

- [1] Severin K., Bergs R. and Beck W. (1998) Bioorganometallic chemistry - transition metal complexes with alpha-amino acids and peptides. *Angew. Chem. Int. Ed. Engl.* **37**, 1634-1654.
Chen H., Ogo S. and Fish R. (1996) *J. Bioorganometallic Chemistry*. 8. The molecular recognition of aromatic and aliphatic amino acids and substituted aromatic and aliphatic carboxylic acid guests with supramolecular (5-pentamethylcyclopentadienyl)rhodium-nucleobase, nucleoside, and nucleotide cyclic trimer hosts via non-covalent – and hydrophobic interactions in water: steric, electronic, and conformational parameters. *Am. Chem. Soc.* **118**, 4993-5001.
- [2] Top S., El Hafa H., Vessières A., Quivy J., Vaissermann J., Hughes D. W., McGlinchey M. J., Mornon J.-P., Thoreau E. and Jaouen G. J. (1995) Rhenium carbonyl complexes of beta-estradiol derivatives with high affinity for the estradiol receptor: an approach to selective organometallic radiopharmaceuticals. *Am. Chem. Soc.* **117**, 8372-8380.
- [3] Glennon R. A. (1992) *Drug Dev. Res.* **26**, 251-257.
- [4] Alberto R., Schibli R., Egli A., Schubiger P. A., Abram U. and Kaden Th. A. (1998) A novel organometallic aqua complex of technetium for the labeling of biomolecules: Synthesis of $[\text{Tc-}^{99m}(\text{OH}_2)_3(\text{CO})_3]^+$ from $[(\text{TcO}_4)\text{Tc-}^{99m}]$ in aqueous solution and its reaction with a bifunctional ligand *J. Am. Chem. Soc.* **120**, 7987-7988.
- [5] Kulkarni S. K. and Aley K. O. (1988) *Drugs Today* **24**, 175-183. Glennon R. A., Westkaemper R. B. and Bartyzer P. Serotonin receptor subtypes; Peroutka S. J., Ed.; Wiley-Liss: New York 1991; pp 19-64. Cliffe I. A. and Fletcher A. (1993) *Drugs Future* **18**, 631-642. Wilson A. A., Inaba T., Fischer N., Dixon L. M., Nobrega J., DaSilva J. N. and Houle S. (1998) Derivatives of WAY 100635 as potential imaging agents for 5-HT1A receptors: syntheses, radiosyntheses, and *in vitro* and *in vivo* evaluation. *Nucl. Med. Biol.* **25**, 769-776.
- [6] Alberto R., Schibli R., Egli A., Schubiger P. A., Herrmann W. A., Artus G. M., Abram U. and Kaden Th. A. (1995) Metal carbonyl syntheses; low pressure carbonylation of $[\text{MOCl}_4]^-$ and $[\text{MO}_4]^-$, M = Tc, Re, $[\text{NEt}_4]_2[\text{MCl}_3(\text{CO})_3]$. *J. Organomet. Chem.* **493**, 119-127.
- [7] Deutsch E., Libson K., Vanderheyden J.-L., Ketring A. R. and Maxon H. R. (1986) The chemistry of rhenium and technetium as related to the use of isotopes of these elements in therapeutic and diagnostic nuclear medicine. *Nucl. Med. Biol.* **13**, 465-477.

RADIOPHARMACEUTICAL CHEMISTRY

33. Automated Production of [^{11}C]Methyl iodide

J. Zessin, P. Mäding, H. Krug¹, S. Gommlich¹, B. Jung, E. Lösel, N. Dohn, F. Füchtner, J. Steinbach
¹Zentralabteilung Forschungs- und Informationstechnik

Introduction

[^{11}C]Methyl iodide is one of the most important precursors for syntheses of ^{11}C -labelled tracers used in investigations with positron emission tomography (PET). Studying regions with a low density of the target such as brain receptors requires radiotracers of a high specific radioactivity. A prerequisite for the production of [^{11}C]methyl iodide of a high specific radioactivity is a large quantity of starting radioactivity. Under these conditions the preparation has to take place in hot cells with a remote-controlled system or an automated synthesis apparatus.

A synthesis apparatus for automated preparation of [^{11}C]methyl iodide was developed in our PET centre. The preparation is based on the reduction of [^{11}C]CO₂ to [^{11}C]methanol by using lithium aluminium hydride, followed by conversion of the released methanol into [^{11}C]methyl iodide by treatment with hydroiodic acid [1].

The results obtained in the automated synthesis of [^{11}C]methyl iodide are presented in the following paper.

Experimental

General

The automated apparatus for preparation of [^{11}C]methyl iodide consists of a synthetic unit, a control unit based on SIEMATIC S5 blocks and a control PC. The apparatus was controlled by using the InTouch software from Wonderware. A schematic picture of the synthetic unit is shown in Fig.1.

[^{11}C]CO₂ was produced by the $^{14}\text{N}(p,\alpha)^{11}\text{C}$ reaction on an IBA Cyclone 18/9 cyclotron. For most experiments the nitrogen target (nitrogen 99.999 % with 0.2 % oxygen) was irradiated with a beam current of 5 μA for 4 min giving, on average, 3.9 GBq of [^{11}C]carbon dioxide (EOB). Production of 37 GBq [^{11}C]CO₂ required an irradiation of 25 μA for 12 min.

Hydroiodic acid, 2-thionaphthol, dimethyl formamide (DMF) and tetrabutyl ammonium hydroxide (methanolic solution) were purchased from commercial suppliers and used without purification. THF was dried by distillation over lithium aluminium hydride in a nitrogen atmosphere as reported by Harada and Hayashi [2]. The lithium aluminium hydride solution was prepared by dissolving solid LiAlH₄ in dry THF. The saturated solution was diluted with dry THF in a ratio of 1:19. These preparative steps were carried out in a glove box under nitrogen.

[^{11}C]Methyl iodide

[^{11}C]Carbon dioxide was trapped in a Carbosphere (Alltech) loop at ambient temperature and released at 110 °C. [^{11}C]CO₂ was transferred by a nitrogen stream into the LiAlH₄ solution (1.3 ml). The THF was evaporated by heating the reaction vessel under reduced pressure. After cooling the reaction vessel, hydroiodic acid (1.7 ml) was added. The reaction mixture was heated to 165 °C and the [^{11}C]methyl iodide was distilled over NaOH on charcoal and Sicapent (Merck) into a cooled vial.

2-[^{11}C]Methylthionaphthol

[^{11}C]Methyl iodide was trapped in a solution of 2-thionaphthol (5 mg, 31 μmol) and tetrabutyl ammonium hydroxide (40 μmol , as 1 M methanolic solution) in dimethyl formamide (0.4 ml) while cooling with dry ice/methanol. Then the reaction mixture was warmed to room temperature.

A small sample of the reaction mixture was analysed with HPLC (Purospher 125mm x 3 mm, 5 μm ; water/acetonitrile (50:50) with 0.1 M ammonium formate as eluent, flow rate of 0.8 ml/min) to determine the specific radioactivity.

Results and Discussion

In the first experiments the reaction parameters and process times for adsorption of [^{11}C]CO₂ on the Carbosphere loop, desorption, evaporation of THF and release of [^{11}C]methyl iodide by treatment with hydroiodic acid were optimized. The synthesis of [^{11}C]methyl iodide using the optimized parameter set was completed after 7.7 ± 0.1 min (without transfer of [^{11}C]CO₂ from the cyclotron to the automatic synthesis system).

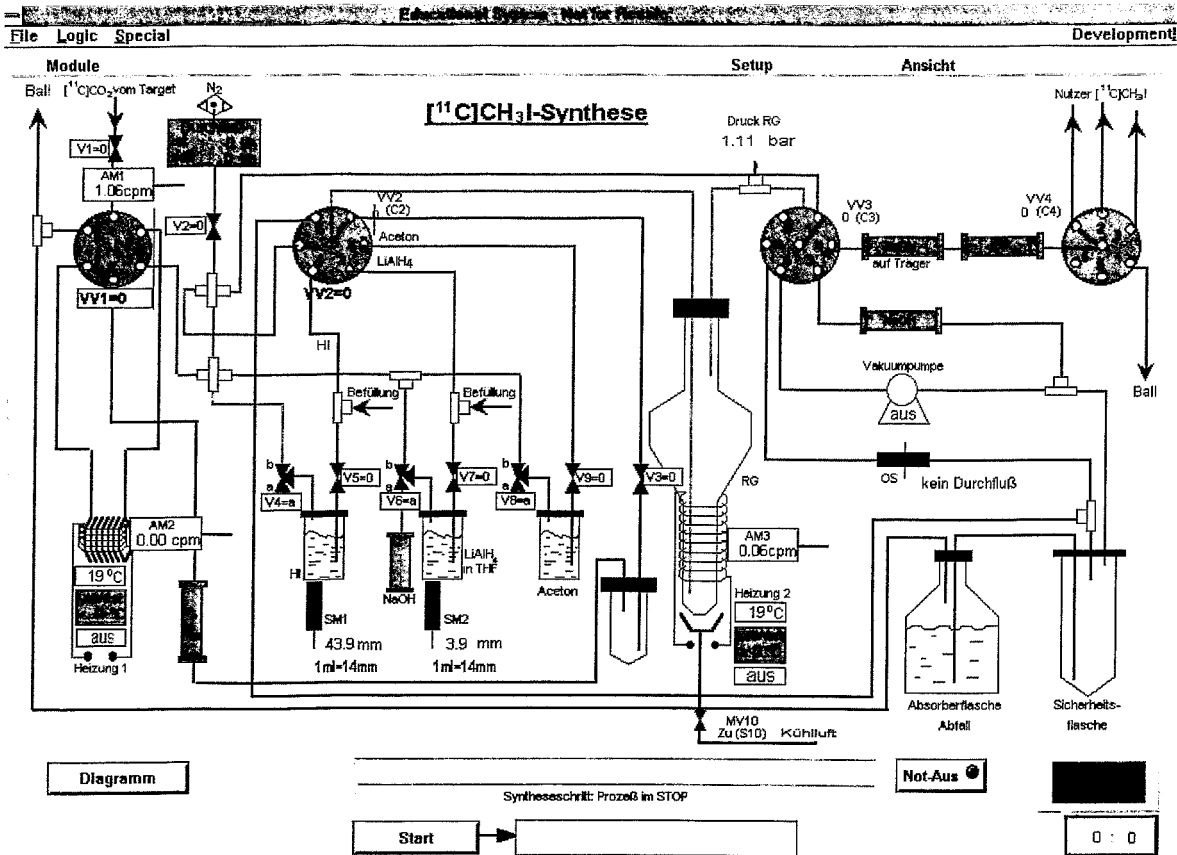


Fig. 1. Scheme of the synthetic unit for automated production of $[^{11}\text{C}]\text{methyl iodide}$

Starting from 3,900 MBq $[^{11}\text{C}]\text{CO}_2$, 1,450 – 1,750 MBq $[^{11}\text{C}]\text{methyl iodide}$ were produced. The reproducible radiochemical yield of $[^{11}\text{C}]\text{CH}_3\text{I}$ in relation to $[^{11}\text{C}]\text{CO}_2$ was $66 \pm 5 \%$ (decay-corrected). An exact determination of the loss of radioactivity was not possible. A loss of radioactivity was observed during evaporation of THF (1 – 5 % of the starting radioactivity). After the release of $[^{11}\text{C}]\text{methyl iodide}$, the hydroiodic acid solution in the reaction vessel contained about 1 % of the starting radioactivity. The detection of the residual radioactivity in the Carbosphere loop and in the gaseous waste was not possible.

The radiochemical purity of $[^{11}\text{C}]\text{methyl iodide}$ produced using the automatic synthesis apparatus was about 98 %. The $[^{11}\text{C}]\text{methyl iodide}$ was converted into 2- $[^{11}\text{C}]\text{methylthionaphthol}$ as this compound has a stronger UV absorbance than methyl iodide, which is useful for determination of the specific radioactivity. At the end of the synthesis, the mean specific radioactivity was 125 mCi/ μmol .

In single experiments the preparation started with 37 GBq $[^{11}\text{C}]\text{CO}_2$ (EOB) yielding 16 GBq $[^{11}\text{C}]\text{methyl iodide}$. The specific radioactivity of $[^{11}\text{C}]\text{methyl iodide}$ was 1.7 Ci/ μmol .

In summary, it can be said that the new synthesis apparatus is suitable for automated preparation of $[^{11}\text{C}]\text{methyl iodide}$ in good radiochemical yields and specific radioactivities in short synthesis times.

References

- [1] Crouzel C., Långström B., Pike V. W. and Coenen H. H. (1987) Recommendations for a practical production of $[^{11}\text{C}]\text{methyl iodide}$. *Appl. Rad. Isot.* **38**, 601-603
- [2] Harada N. and Hayashi N. (1993) Measurement of the carbon source which is responsible for dilution in carbon-11 labelling reactions. *Appl. Rad. Isot.* **44**, 629-630

34. Synthesis of 5-Methoxy-[2-¹¹C]Indole by Reduction of 5-Methoxy-β,2-Dinitro-[β-¹¹C]Styrene

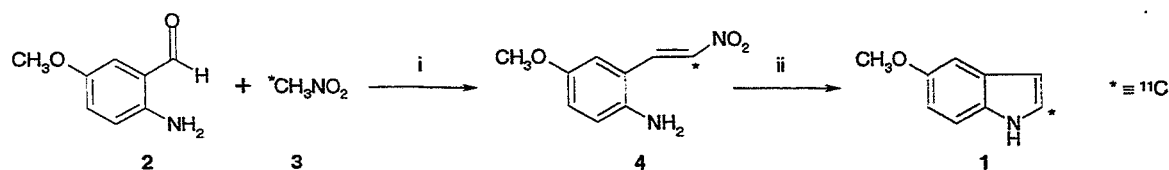
J. Zessin, J. Steinbach

Introduction

The indole ring is the basic structure of many biologically active compounds. Many of these substances labelled with a positron emitter such as ¹¹C or ¹⁸F may be potential radiotracers for the positron emission tomography (PET). In particular the application of ¹¹C-labelled tracers requires efficient preparation methods on account of the short half life (*t*_{1/2} = 20.38 min). The reduction of β,2-dinitro-[β-¹¹C]styrene with titanium(III) chloride was recognized as a first practicable method of synthesizing ¹¹C-ring labelled indole [1].

In this paper the synthesis of a 5-substituted indole derivative utilizing this method is described. 5-Methoxy-[2-¹¹C]indole **1** was prepared by reduction of 5-methoxy-β,2-dinitro-[β-¹¹C]styrene **4** with titanium(III) chloride. The intermediate **4** was obtained from condensation of 5-methoxy-2-nitrobenzaldehyde **2** with nitro-[¹¹C]methane **3** (Scheme 1).

Scheme 1. Synthesis of 5-methoxy-[2-¹¹C]indole **1**. Reaction conditions: i, ammonium acetate, glacial acetic acid, 140 °C; ii, titanium(III) chloride, glacial acetic acid, room temperature



Experimental

General

Glacial acetic acid, ammonium acetate, titanium(III) chloride and 5-hydroxy-2-nitro-benzaldehyde were purchased from commercial suppliers and were used without purification. Nitro-[¹¹C]methane was prepared *via* [¹¹C]methyl iodide according to the method of Schoeps et al. as described in [2].

¹H NMR spectra were recorded on a Varian INOVA 400 NMR spectrometer.

HPLC analyses were performed on a JASCO system with a PUROSPHER RP 18 column (125 mm x 3 mm, 5 μm) isocratically eluted with acetonitrile/water (40:60) containing 0.1M ammonium formate at a flow rate of 0.5 ml/min. Semipreparative HPLC was performed with a NULEOSIL 120 RP 18 column (250 mm x 10 mm, 7 μm) isocratically eluted with acetonitrile/water (50:50) at a flow rate of 4 ml/min.

5-Methoxy-2-nitrobenzaldehyde (2)

5-Hydroxy-2-nitrobenzaldehyde (5.0 g, 30 mmol) was dissolved in a potassium hydroxide solution (2.73 g in 30 ml water). Dimethyl sulphate (4.1 g, 32.5 mmol) was added to this solution. Then the reaction mixture was heated at 100 °C for 30 min. The methoxy compound was extracted with dichloromethane. The organic layers were washed with sodium hydroxide solution and water, dried with sodium sulphate and evaporated to yield a lightbrown solid.

Yield: 2.3 g (42 %)

Melting point: 77 – 79 °C

NMR data: δ_H (400 MHz, solvent CDCl₃, standard: SiMe₄): 3.90 [3H, s, OCH₃], 7.10 [1H, m, C₃H], 7.21 [1H, m, C₆H], 8.10 [1H, m, C₄H], 10.42 [1H, s, CHO]

5-Methoxy-β,2-dinitro-[β-¹¹C]styrene (4)

5-Methoxy-2-nitrobenzaldehyde (10 mg, 55 μmol) and ammonium acetate (25 mg, 325 μmol) were dissolved in glacial acetic acid (250 μl). Nitro-[¹¹C]methane was trapped in this solution. The sealed reaction vessel was heated at 145 °C for 10 min. The reaction mixture was diluted with 1 ml HPLC eluent and purified by semipreparative HPLC. The eluent containing **3** was diluted with water (10 ml)

and passed through a C18 cartridge. After washing with water, compound **3** was eluted with glacial acetic acid (1 ml).

5-Methoxy-[2-¹¹C]indole (1)

Titanium(III) chloride (6 mg, 40 μ mol) was placed in a sealed reaction vial, which had been purged with nitrogen. The eluate from solid phase extraction containing **3** was added to this vial. After 6 min at room temperature a sample of the reaction mixture was dissolved in the HPLC eluent, filtered and analysed by HPLC.

Results and Discussion

The procedure of preparing 5-methoxy[2-¹¹C]indole **1** is illustrated in Scheme 1. The two-step synthesis involves the condensation of 5-methoxy-2-nitrobenzaldehyde **2** with nitro-[¹¹C]methane **3** to yield 5-methoxy- β ,2-dinitro-[β -¹¹C]styrene **4**. After purification the intermediate **4** was converted into **1** by reduction with titanium(III) chloride.

The preparation of 5-methoxy- β ,2-dinitro-[β -¹¹C]styrene **4** being investigated here is a modification of a procedure earlier published for synthesis of β ,2-dinitro-[β -¹¹C]styrene [1]. The condensation reaction was carried out in glacial acetic acid catalysed by ammonium acetate (10 min, 140 °C). Under these conditions 27 % of **3** (determined by HPLC, decay-corrected) were converted into **1**. In comparison with the preparation of unsubstituted β ,2-dinitro-[β -¹¹C]styrene [1], the 5-methoxy group causes a less incorporation of nitro-[¹¹C]methane.

The reduction of β ,2-dinitro-[β -¹¹C]styrene with titanium(III) chloride in the presence of the catalyst ammonium acetate proceeded without formation of indole. The dinitrostyrene was completely decomposed [1]. Ammonium acetate was therefore removed by solid phase extraction, using a C18 cartridge. Reduction of purified compound **4** with titanium(III) chloride in glacial acetic acid (6 min, room temperature) yielded a product mixture which contained the desired 5-methoxy-[2-¹¹C]indole in a percentage of 7 % (determined by HPLC, decay-corrected). The parent **4** was almost completely converted.

The yield of **1** increased when the purification of **4** was performed by semipreparative HPLC. The radiochemical yield of **4** after HPLC purification and removal of the HPLC eluent by solid phase extraction was 14 % (decay-corrected, related to compound **3**). In addition to ammonium acetate, unreacted 5-methoxy-2-nitrobenzaldehyde was removed in the course of this purification procedure. The reduction reaction can therefore be carried out with a smaller amount of the reduction agent titanium(III) chloride. The resulting product mixture contained the 5-methoxy-[2-¹¹C]indole **1** in a percentage of 26 % (determined by HPLC, decay-corrected), which is equivalent to a decay-corrected radiochemical yield of 4 % (in relation to **3**). The synthesis of **1** starting from **3** was completed after 40 min.

In conclusion it shall be pointed out that the reduction of β ,2-dinitro-[β -¹¹C]styrenes with titanium(III) chloride can be provide a practicable route to ¹¹C-ring labelled indole derivatives with substituents at the benzene ring. This was demonstrated by the preparation of 5-methoxy-[2-¹¹C]indole **1**.

References

- [1] Zessin J. and Steinbach J. (1998) ¹¹C-Labeling of Heterocyclic Aromatic Compounds in Ring Positions: Synthesis of [2-¹¹C]Indole. *J. Labelled Compd. Radiopharm.* **41**, 669-676.
- [2] Schoeps K.-O., Stone-Elander S. and Halldin C. (1989) On-line synthesis of [¹¹C]nitroalkanes. *Appl. Radiat. Isot.* **40**, 261 – 262.

35. Synthesis of 3-O-[¹¹C]Methyl-D-Glucose

P. Mäding, H. Kasper, J. Zessin, M. Gnauck, F. Füchtner, P. Brust, J. Steinbach

Introduction

Unlike the established radiopharmaceutical 2-[¹⁸F]fluoro-2-deoxy-D-glucose ([¹⁸F]FDG), 3-O-[¹¹C]methyl-D-glucose ([¹¹C]MG; **4**) is not metabolized in the living body [1, 2]. Both tracers share, however, the same transport in the tissue via the glucose transporter [3]. Therefore, the ¹¹C-labelled radiotracer **4** is especially suitable for investigating glucose transport and its alteration under pathological conditions. For PET animal experiments in this field, we had to work out a more convenient procedure to prepare [¹¹C]MG based on the known synthesis process [4].

Experimental

Materials

Diacetone-D-glucose (**1**; purum, ≥ 98 %) was purchased from Fluka, and potassium hydride (35 % in paraffin oil) from Merck. As reference substances were used: 3-O-methyl-D-glucose 97 % (Aldrich) and D(+)-glucose waterfree for biochemical use (Merck).

Analysis

To determine the extent of the reaction conversion, the radiochemical and chemical purity and the specific radioactivity of [¹¹C]MG, an HPLC system (Hewlett Packard) was used, including a gradient pump (series 1050), an autosampler (series 1050), a CarboPac PA 1 column (4 x 250 mm, Dionex), an electrochemical detector (ECD) coupled in series with a radioactivity detector (A 100, Canberra Packard). The mobile phase consisted of 0.1 M NaOH at a flow rate of 1 ml/min. This method is based on an anion-exchange separation mechanism and allows isocratic separation of carbohydrates (further details are given in [5]).

The osmolality was determined by an Osmomat 030-D from Gonotec, Berlin, Germany. The measurements of the pH values were performed by the microprocessor pH-Meter pH 3000 from WTW, Weilheim, Germany.

Synthesis of the precursor solution of the potassium salt of diacetone-D-glucose (2)

A suspension of 35 % potassium hydride in paraffin oil (1g; 8.7 mmol) was washed with pentane and then with freshly distilled THF to remove the paraffin oil by decantation of the solvent. A solution of **1** (150 mg; 0.58 mmol) in 5 ml THF was added to a stirred suspension of the purified KH in 10 ml THF. This mixture was stirred at room temperature for 1.5 h and then refluxed for 30 min. After cooling to room temperature the suspension was filtered through a frit glass filter. The clear yellow precursor solution of **2** was stored at 4 °C for use within 4 weeks.

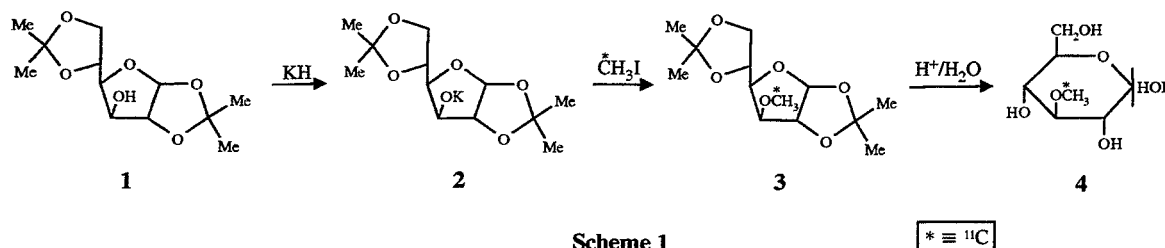
Radiosynthesis

[¹¹C]CO₂ was produced on the cyclotron Cyclone 18/9 (IBA) by the ¹⁴N(p,α)¹¹C nuclear reaction. [¹¹C]Methyl iodide was prepared by the classic one-pot method [6] involving the reduction of [¹¹C]CO₂ with LiAlH₄, hydrolysis of the intermediate organometallic complex and subsequent iodization of the [¹¹C]methanol formed with HI.

[¹¹C]MeI was trapped in a cooled 2 ml vessel (-78 °C) containing the precursor solution of **2** (250 µl). For methylation the well-sealed vessel was heated at 120 °C for 3 min. Then the THF was evaporated by means of a stream of nitrogen gas. 0.5 M HCl (0.6 ml) was added to the residue. The mixture was heated at 120 °C for 2 min. After cooling to room temperature the solution was neutralized by addition of 0.5 M NaOH (0.6 ml) and a solution of physiological phosphate buffer (pH 7.2; 0.7 ml). The resulting solution was transferred to a 10 ml syringe. The reaction vessel was washed with water (2.8 ml) and this solution was also drawn up into the 10 ml syringe. The radioactive solution was put through a sterile filter into a sealed sterile flask containing an aqueous solution of 5.85 % NaCl (0.37 ml).

Results and Discussion

[¹¹C]MG (4) was synthesized according to Scheme 1 by methylation of the potassium salt of diacetone-D-glucose (2) with [¹¹C]methyl iodide followed by acidic hydrolysis of the ketal groups of the [¹¹C]methyl-diacetone-D-glucose (3) formed.



The preparation of 4 in this way is described in [4]. But we have modified this procedure for our purposes:

- changing the solvent for preparing the precursor 2 and for the methylation reaction, i.e. substitution of THF for diethyl ether;
- preparation of the precursor 2 from compound 1 using KH instead of K;
- reduction of the methylation time from 6 min to 3 min, reduction of the hydrolysis time from 6 min to 2 min;
- using 0.5 M aqueous HCl instead of 0.5 M aqueous methanolic HCl for hydrolysis;
- simple working-up of the reaction mixture without HPLC purification.

We performed 34 production runs for animal experiments which yielded 686 ± 212 MBq [¹¹C]MG. The [¹¹C]MG was obtained in radiochemical yields of 56.1 ± 11.2 % (decay-corrected) with specific radioactivities of 12 - 42 mCi/μmol (450 - 1550 MBq/μmol) within 16 min, starting from [¹¹C]MeI.

Quality parameters of [¹¹C]MG:

- | | |
|-----------------------------------|--------------------------|
| • radiochemical purity | > 96 % |
| • content of D-glucose | 0.47 ± 0.22 mg/ml |
| • content of 3-O-methyl-D-glucose | 0.0244 ± 0.017 mg/ml |
| • pH | 7.1 ± 2.2 |
| • osmolality | 335 ± 30 mOsmol/kg |

Acknowledgements

The excellent analytical assistance by Mr. C. Smuda and Mrs. R. Hüller is gratefully acknowledged.

References

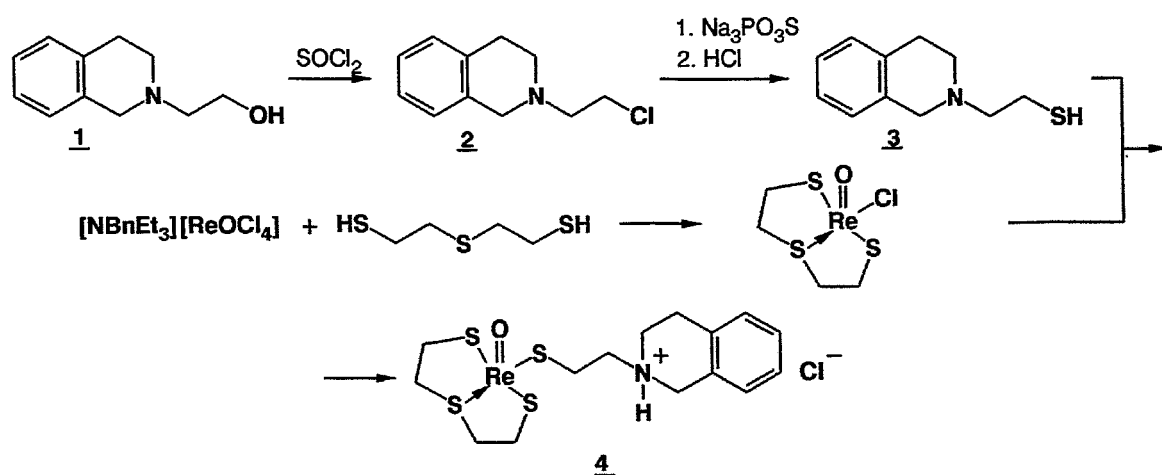
- [1] Seider M. J. and Kim H. D. (1979) Cow red blood cells. I. Effect of purines, pyrimidines, and nucleosides in bovine red cell glycolysis. *Am. J. Physiol.* **236**, C255-61
- [2] Pesquero J., Albi J. L., Gallardo M. A., Planas J. and Sanchez J. (1992) Glucose metabolism by trout (*Salmo trutta*) red blood cells. *J. Comp. Physiol. [B]* **162**, 448-54
- [3] Johnson J. H., Newgard C. B., Milburn J. L., Lodish H. F. and Thorens B. (1990) The high Km glucose transporter of islets of Langerhans is functionally similar to the low affinity transporter of liver and has an identical primary sequence. *J. Biol. Chem.* **265**, 6548-51
- [4] Kloster G., Müller-Platz C. and Laufer P. (1981) 3-[¹¹C]Methyl-D-glucose, a potential agent for regional cerebral glucose utilization studies: synthesis, chromatography and tissue distribution in mice. *J. Labelled Compd. Radiopharm.* **18**, 855-863
- [5] Füchtner F., Neubert K. and Steinbach J. (1994) Determination of the chemical and radiochemical purity and specific radioactivity of [¹⁸F]FDG by HPLC. *Annual Report 1993*, Institute of Bioinorganic and Radiopharmaceutical Chemistry, FZR-32, 17-23
- [6] Crouzel C., Långström B., Pike V. W. and Coenen H. H. (1987) Recommendations for a practical production of [¹¹C]methyl iodide. *Appl. Radiat. Isot.* **38**, 601-603

36. '3+1' Mixed-Ligand Oxorhenium(V) Complex with 1,2,3,4-Tetrahydroisoquinoline

A. Zablotka¹, I. Segal¹, E. Lukevics¹, H.-J. Pietzsch, T. Kniess, H. Spies
¹Latvian Institute of Organic Synthesis, Riga

It has been reported that some tetrahydro(iso)quinoline-containing ligands display affinity to serotonin (5HT_{1A}) and dopamine receptors [1, 2]. In addition, we found earlier that some tetrahydro-, tetrahydroiso- and tetrahydrosilaisoquinoline derivatives exhibited the sedative action [3-5]. One may therefore expect that the tetrahydro(iso)quinoline moiety may serve as an anchor group in the design of receptor-affine rhenium and technetium complexes. As an access to such compounds we synthesized the first prototype of '3+1' mixed-ligand oxorhenium(V) complexes with 1,2,3,4-tetrahydroisoquinoline-containing monodentate (Scheme 1).

Scheme 1. Reaction pathway for synthesis of tetrahydroisoquinoline containing oxorhenium(V) complex **4**



N-(2-hydroxyethyl)-1,2,3,4-tetrahydroisoquinoline obtained by condensation of 1,2,3,4-tetrahydroisoquinoline with 2-iodoethanol in the presence of triethylamine was further converted into N-(2-mercaptoethyl)-1,2,3,4-tetrahydroisoquinoline suitable for complexation. Thus, the reaction of aminoalcohol **1** with thionyl chloride produced the aminoalkyl chloride **2** in a 59% isolated yield. The subsequent treatment of **2** with sodium thiophosphate dodecahydrate in dimethylformamide [6] followed by acid hydrolysis resulted in mercaptane **3** in a 30 % yield (after isolation).

N-(2-mercaptomethyl)-1,2,3,4-tetrahydroisoquinoline **3** was further used for complexation with (3-thiapentane-1,5-dithiolato)oxorhenium(V) chloride to obtain the desired mixed-ligand complex **4**. The newly prepared complex was characterized by elemental analysis, ¹H and ¹³C NMR and IR spectroscopy. Fig. 1 shows the infrared spectrum with the Re=O band at 967 cm⁻¹.

The molecular structure, brain receptor-binding *in vitro*, psychotropic activity and acute toxicity *in vivo* of compound **4** are under investigation and the results will be published in the subsequent paper.

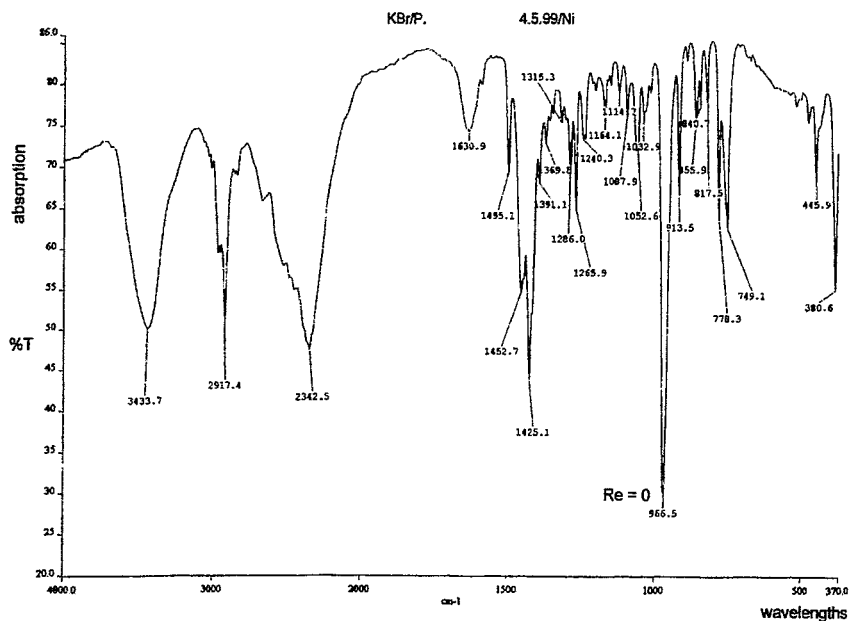


Fig. 1 IR spectrum of compound 4

References

- [1] Heier R. F., Dolak L. A., Duncan J. N., Hyslop D. K., Lipton M. F., Martin I. J., Mauragis M. A., Piercey M. F., Nichols N. F., Schreur P. J. K. D., Smith M. W. and Moon M. W. (1997) Synthesis and biological activity of (R)-5,6-dihydro-N,N-dimethyl-4H-imidazo[4,5,1-ij]quinoline-5-amine and its metabolites. *J. Med. Chem.* **40**, 639-646.
- [2] Mokrosz M. J., Bojarski A. J., Duszynska B., Tatarczynska E., Klodzinska A., Deren-Wesolek A., Charakchieva-Minol S. and Chojnacka-Wojcik E. (1999) 1,2,3,4-Tetrahydroisoquinoline derivatives: a new class of 5-HT_{1A} receptor ligands. *Bioorg. Med. Chem.* **7**, 287-295.
- [3] Lukevics E., Segal I., Zablotskaya A. and Germane S. (1996) Organosilicon derivatives of aminoalcohols in the series of tetrahydroquinoline, tetrahydroisoquinoline and tetrahydroisaisoquinoline. *Chem. Heterocycl. Comp.* **32**, 682-688.
- [4] Lukevics E., Germane S., Segal I. and Zablotskaya A. (1997) Derivatives of amino acids in the tetrahydroquinoline, tetrahydroisoquinoline and tetrahydroisaisoquinoline series. *Chem. Heterocycl. Comp.* **32**, 234-238.
- [5] Lukevics E., Segal I., Zablotskaya A. and Germane S. (1997) Synthesis and neurotropic activity of novel quinoline derivatives. *Molecules* **2**, 180-185.
- [6] Bieniarz C. and Cornwell M. J. (1993) A facile high-yielding method for the conversion of halides to mercaptanes. *Tetrahedron Lett.* **34**, 939-942.

37. Tc-99m Labelled Fatty Acids on Basis of "n+1" Mixed-Ligand Complexes ?

H. Spies, H.-J. Pietzsch, J. Kropp¹, T. Fietz, C. Jung²

¹TU Dresden, Universitätsklinikum Carl Gustav Carus, Klinik und Poliklinik für Nuklearmedizin

²Universität Marburg, Fachbereich Kernchemie

Introduction

Although some efforts have been made to develop Tc-99m-labeled fatty acid analogues, poor recognition of those compounds as substrates for beta-oxidation has prevented their application [1-3]. Reasons for failure may come from the nature of the chelate, that is has been chosen to attach at the omega position of a fatty acid and in the nature of this fatty acid itself. The majority of previously known chelates used for binding technetium to a fatty acid moiety are almost without exception square-pyramidal oxotechnetium(V) complexes of tetradentate complexing agents, in which the properties, and thus the *in vivo* behavior, is strongly influenced by the coupling to the polar Tc=O unit (Fig. 1).

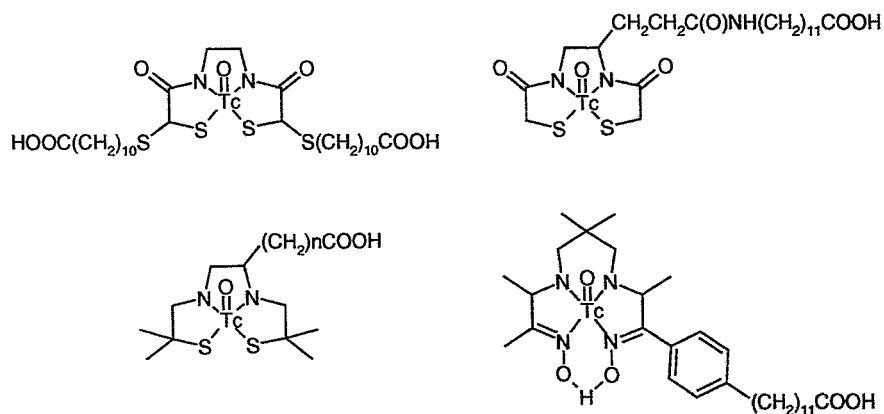


Fig. 1. Tc complexes intended as fatty acid analogues showing no uptake in myocardium [1 - 3].

Intended working strategy

It is to be expected, but remains to be proven, that ligands that allow extensive shielding of the metal, may particularly suitable to be combined with fatty acids. We want to apply the "n+1" mixed-ligand approach [4, 5] (Fig. 2), with emphasis on the "4+1"-version [6], to the synthesis of new types of Tc-99m-labelled fatty acid analogs in the hope to make them acceptable as substrates for energy production in living cells.

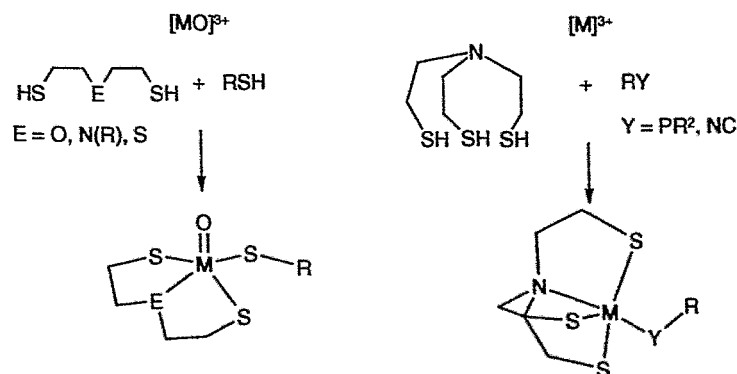


Fig. 2. "3+1" and "4+1" complexes as two versions of the "n+1" concept [4 - 6].

Concerning the nature of the fatty acid sequence, "modified" fatty acids as used to be labeled with ^{18}F and ^{123}I will preferably be used. Fig. 3 shows schematically the intended working program that aims at "thia" acids bearing a lipophilic mixed-ligand chelate unit at the omega-position.

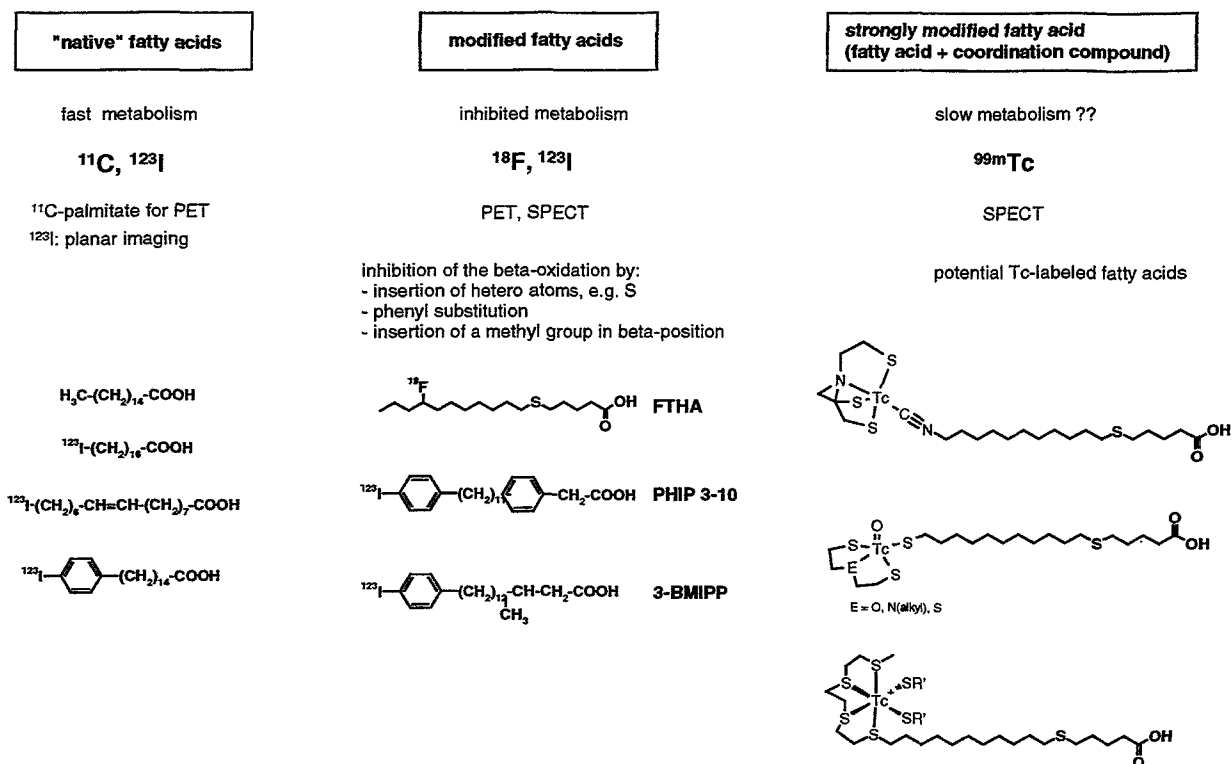


Fig. 3. Intended development of Tc-99m-labelled fatty acid analogs; from [^{123}I]iodine "native" fatty acids to [$^{99\text{m}}\text{Tc}$]Tc coupled "modified" fatty acids

Preliminary results

To become familiar with synthesis and handling of this class of high-lipophilic acids, **1** was synthesized as a representative of omega-mercapto substituted fatty acids and used for the preparation of "3+1" mixed ligand complexes **2** according to Fig. 4 [7]. Both species were obtained in moderate yields and were characterized by elemental analysis, ^1H NMR and IR spectroscopy. Lipophilicity/pH profiles (determination of P_{HPLC} at different pH values as described in [8]) show the form expected for highly lipophilic carboxylic acids.

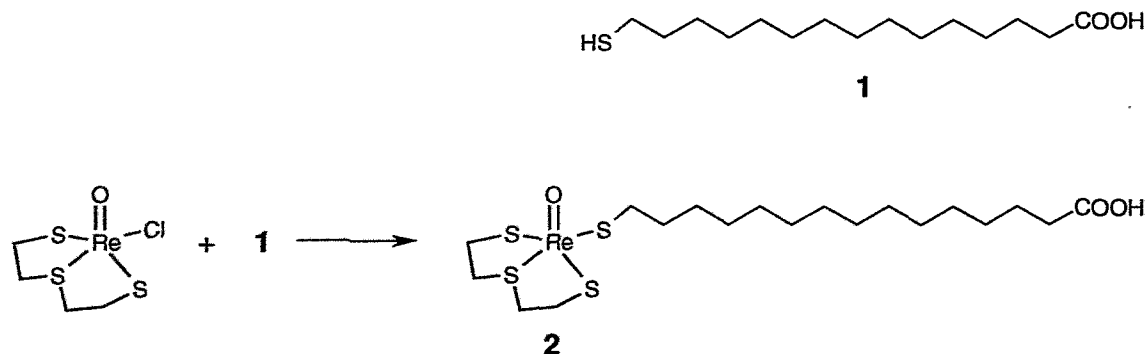


Fig. 4. Reaction scheme for the synthesis of long-chain fatty acid "3+1" Re complexes [7].

References

- [1] Mach R. H. and Kung H. F. (1991) Synthesis and biodistribution of a new class of Tc-99m-labeled fatty acid analogs for myocardial imaging. *Nucl. Med. Biol.* **18**, 215-226.
- [2] Alagui H., Vidal M., Riche F., du Moulinet d'Hardemare A., Mathieu J. P. and Pasqualini R. (1995) Synthesis and evaluation of ^{99m}Tc labelled fatty acids. In: *Technetium and Rhenium in Chemistry and Nuclear Medicine 4* (M. Nicolini, G. Bandoli, U. Mazzi Eds.) SGEEditoriali, Padova, pp. 325-328.
- [3] Jones jr. G. S., Elmaleh D. R., Strauss H. W. and Fishman A. J. (1994) Synthesis and biodistribution of a new ^{99m}technetium fatty acid. *Nucl. Med. Biol.* **21**, 117-124.
- [4] Spies H., Fietz T., Glaser M., Pietzsch H.-J. and Johannsen B. (1995) The n+1 concept in the synthesis strategy of novel technetium and rhenium tracers. In: *Technetium and Rhenium in Chemistry and Nuclear Medicine 4* (M. Nicolini, G. Bandoli, U. Mazzi Eds.) SGEEditoriali, Padova, pp. 243-246.
- [5] Spies H. and Johannsen B. (1995) Functionalization of technetium complexes to make them active *in vivo*. *Analyst* **120**, 775-777.
- [6] Spies H., Glaser M., Pietzsch H.-J., Hahn F. E., Kintzel O. and Lügger T. (1994) Trigonal-bipyramidale Technetium- und Rhenium-Komplexe mit vierzähligen tripodalen NS₃-Liganden. *Angew.Chem.* **106**, 1416-1418.
- [7] Jung C. Diplomarbeit 1999, Universität Marburg, Fachbereich Kernchemie.
- [8] Berger R., Fietz T., Glaser M., Spies H. and Johannsen B. (1995) Determination of partition coefficients for coordination compounds by using HPLC. *Annual Report 1995*, Institute of Bioinorganic and Radiopharmaceutical Chemistry, FZR-122, pp. 69-72.

38. ^{186/188}Re Labelling of Stents for the Prevention of Restenosis

B. Noll, H. Goerner, L. Dinckelborg¹, C. S. Hilger¹, E. Richter²

¹Research Laboratories of Schering AG, Berlin

²Forschungszentrum Rossendorf, Institut für Ionenstrahlphysik und Materialforschung

Intracoronary implantations of stents allow an improved revascularization of obstructive coronary artery disease compared to the conventional balloon angioplasty. Despite this progress restenosis is still significant. The use of ionizing radiation is a promising approach to prevent restenosis after stent implantation.

There are several approaches for delivering radioactive gamma or beta rays to decrease the proliferation response by coronary irradiation. One way is the use of liquid filled balloons containing solutions with beta- and gamma-emitting radionuclides [1]. Another approach, catheter-based vascular brachytherapy, uses wires or wire coils of radioactive metals, which are centred within the vessel lumen. The very high activity level of sources for vascular brachytherapy needed because of the short exposure time being available during the treatment leads to a significant radiation exposure for both the patient and the laboratory staff [2].

An attractive concept for irradiation of the vessel wall is the use of stents implanted with low activities of a β -emitting radioisotope to inhibit the proliferative process in arteries [3]. For this purpose, pre-loading of the stents with a radioisotope can be carried out, e.g. by implanting ³²P. This, however, has to be done by means of accelerator facilities remote from the site of stent application. To overcome this and other limitations, we searched for a convenient method to label stents with the rhenium isotopes ¹⁸⁶Re and ¹⁸⁸Re directly at the site of application. The labelling procedure should allow individual preparations with easily adjusted radiation doses as well as the preparation in a similar easy way as ^{99m}Tc radiopharmaceuticals are prepared in a hospital.

Results and Discussion

Several methods for the labelling of stents were developed in cooperation with the Research Laboratories of Schering AG. Because of intellectual property reasons they are not disclosed in detail in this report.

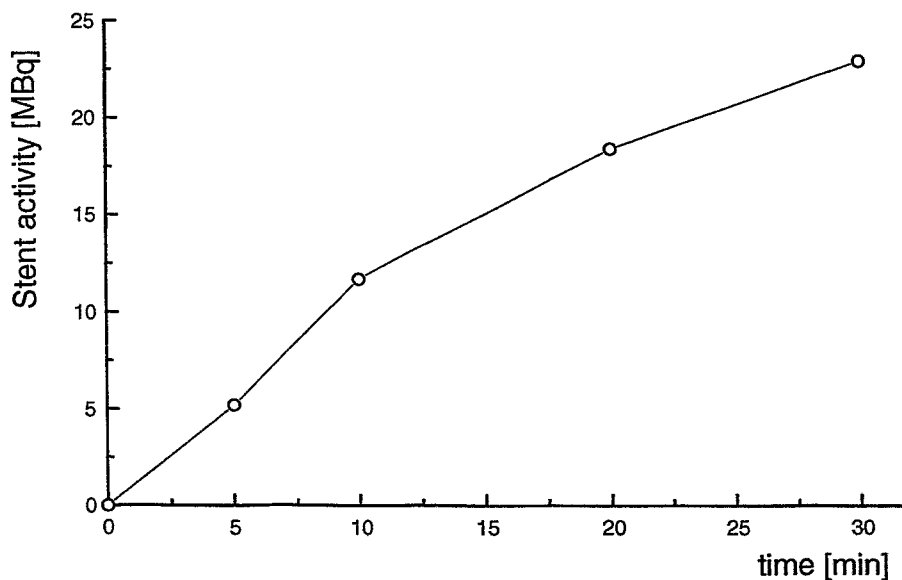


Fig. 1. Dependence of the ^{186}Re uptake on the labelling time

Using this technology, the ^{186}Re deposition on the stent surface increases with the time (Fig.1). Within a labelling time of ten minutes no significant modification of the metallic grain was observed by electron microscopy (500 fold scale-up).

Furthermore, the amount of bound ^{186}Re in dependence on the activity in the labelling solution was investigated. Up to 2 MBq/mg stent in the labelling solution a linear increase of ^{186}Re uptake was observed (Fig.2).

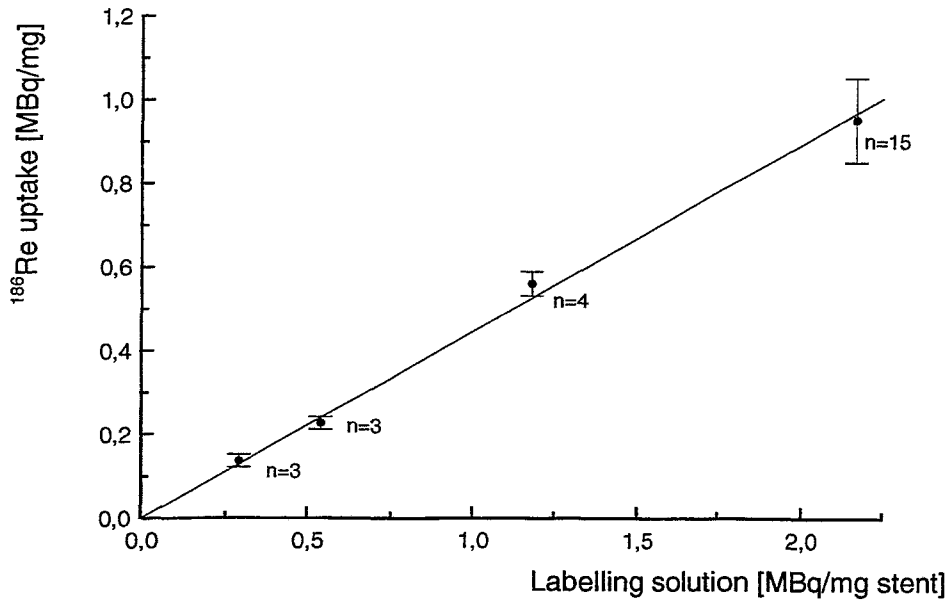


Fig. 2. ¹⁸⁶Re uptake on stents in dependence on the activity of the labelling solution, n = number of labelled stents.

Because of the strong linearity between the amount of activity in the labelling solution and the ¹⁸⁶Re uptake on the stent we consider this as the preferred control variable in the labelling process. Thus, a reproducible method for labelling of stents was developed. There is, however, still an increase of the tenacity of the deposited radioactivity to achieve. In preliminary studies, the stability was investigated by incubation of the labelled stents in isotonic saline solution and in human blood at 37 °C. Under these conditions, ¹⁸⁶Re was released from the stent surface. After 24 h incubation about 50 - 60 % of the start activity remains deposited. In further experiments the stability of the deposited ¹⁸⁶Re on the stent will be improved by e. g. coating the stent with an organic polymer.

References

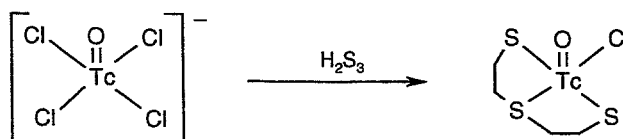
- [1] Waksman R., Robinson K. A., Crocker I. R., Gravanis M. B., Palmer S. J., Wang C., Cipolla G. D. and King S. B. 3rd (1995) Intracoronary radiation before stent implantation inhibits neointima formation in stented porcine coronary arteries. *Circulation* **92**, 1383-1386.
- [2] Meerkink D., Tardif J. C., Crocker I. R., Arsenault A., Joyal M., Lucier G., King S. B. 3rd, Williams D. O., Serruys P. W. and Bonan R. (1999) Effects of intracoronary beta-radiation therapy after coronary angioplasty: an intravascular ultrasound study. *Circulation* **99**, 1660-1665.
- [3] Fischell T. A. and Hehrlein C. (1998) The radioisotope stent for the prevention of restenosis. *Herz* **23**, 373-379.

39. Synthesis and Molecular Structure of Chloro(3-Thiapentane-1,5-Dithiolato)-Oxotechnetium(V)

B. Noll, P. Leibnitz¹, H. Spies

¹Bundesanstalt für Materialforschung und -prüfung Berlin

Tetrachlorooxotechnetate(V) $[\text{TcOCl}_4]^{2-}$ and the tridentate ligand HS-CH₂CH₂-S-CH₂CH₂-SH (H_2S_3) react in acetonitrile to produce the (chloro)oxotechnetium(V) complex $[\text{TcO}(\text{S}_3)\text{Cl}]$ according to the following reaction scheme:



The new Tc complex is an analogue to the neutral Re(V) complex that was described earlier [1]. The chlorine at the Tc core can be replaced by monodentate thiols in a subsequent step forming "3+1" complexes. A new precursor for the synthesis of derived mixed-ligand Tc complexes has thus become available.

Synthesis:

132 mg $(\text{C}_6\text{H}_5)_4\text{As}[\text{TcOCl}_4]$ (0.2 mmol) are dissolved in 10 ml acetonitrile. 0.2 mmol 3-thiapentane-1.5-dithiol dissolved in 2 ml acetonitrile are slowly added to the reaction mixture while stirring and cooling to -20 °C under argon. The colour changes from yellowish green to dark green. After stirring for 30 min the completeness of the reaction is controlled by TLC (silicagel / acetone), the R_f is 0.6. After reducing the volume of the solution by slow evaporation in an argon stream, yellowish green prismatic crystals are recrystallized from acetonitrile. The yield is about 70 %.

The complex was identified by elemental analysis, infrared spectroscopy, and X-ray crystal structure determination.

Elemental analysis: (found C, 16.01; H, 2.72; S, 31.21, $\text{TcOC}_4\text{H}_8\text{S}_3\text{Cl}$ requires
C, 15.92; H, 2.67; S, 31.88 %)

IR absorption: $\lambda_{\text{max}}/\text{cm}^{-1}$ 956 (TcO)

Melting point: >340 °C (decomp.)

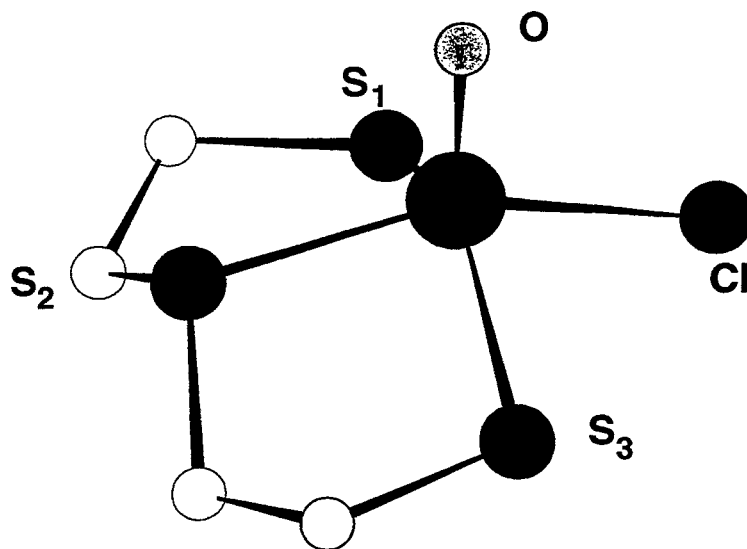


Fig. 1. CELLGRAPH drawing of the TcOCIS_3

The structure was confirmed by X-ray crystallography. The X-ray data were collected at room temperature (296 K) with an ENRAF-NONIUS CAD 4 diffractometer, graphite monochromatized Mo K_α radiation ($\lambda = 0.71073 \text{ \AA}$)

Crystal structure analysis shows the square-pyramidal arrangement, where the tridentate H_2S_3 ligand and the chloro atom form the square. The bond lengths of $\text{Tc}=\text{O}(1)$, $\text{Tc}-\text{O}(2)$ and $\text{Tc}-\text{S}$ in $[\text{TcOCIS}_3]$ are found in the region expected. This complex can be used as a precursor for preparation of a variety of Tc complexes by analogy with the corresponding rhenium precursor.

References

- [1] Fietz T., Spies H., Pietzsch H.-J. and Leibnitz P. (1995) Synthesis and molecular structure of chloro(3-thiapentane-1,5-dithiolato)oxotechnetium(V). *Inorg.Chim.Acta* 231, 233-236.

40. Synthesis and Molecular Structure of $[\text{Tc}(\text{CN-CH}_2\text{-COOCH}_3)_6]\text{TcO}_4$

B. Noll, P. Leibnitz¹, H. Spies

¹Bundesanstalt für Materialforschung und -prüfung Berlin

Organometallic homoleptic isocyanide compounds of technetium are described both at c.a. and n.c.a. level [1, 2]. They were prepared either from the $[\text{Tc}(\text{diphosphine})_2\text{Cl}_2]^+$ precursor in organic solution or directly by reduction of pertechnetate in the presence of isocyanides under while heating the reaction mixture.

We observed an uncommon formation of a Tc(I) hexakisisonitrile complex $[\text{Tc}(\text{CN-CH}_2\text{-COOCH}_3)_6]\text{TcO}_4$ when Tc(V) gluconate in aqueous solution was heated in the presence of the isonitrile ligand. The complex was extracted into methylene chloride, purified by column chromatography on silica gel and crystallized from methanol. The resulting compound contained the pertechnetate anion as a counter ion. A possible explanation is that Tc(V) disproportionates to the oxidation states +1 and +7 when Tc(V) gluconate is attacked by the isonitrile.

The structure was confirmed by X-ray crystallography. The X-ray data were collected at room temperature (296 K) with an ENRAF-NONIUS CAD 4 diffractometer, graphite monochromatized Mo K_α radiation ($\lambda = 0.71073 \text{ \AA}$). Crystal structure analysis shows the symmetric coordination of the six carbon atoms of the isonitrile ligand at the technetium central atom. The bond length of Tc-C is found in the region expected (2.033 Å) [3]. The geometry around the Tc central atom is octahedral. The pertechnetate counter ion is fixed within the molecular packing of the Tc complex.

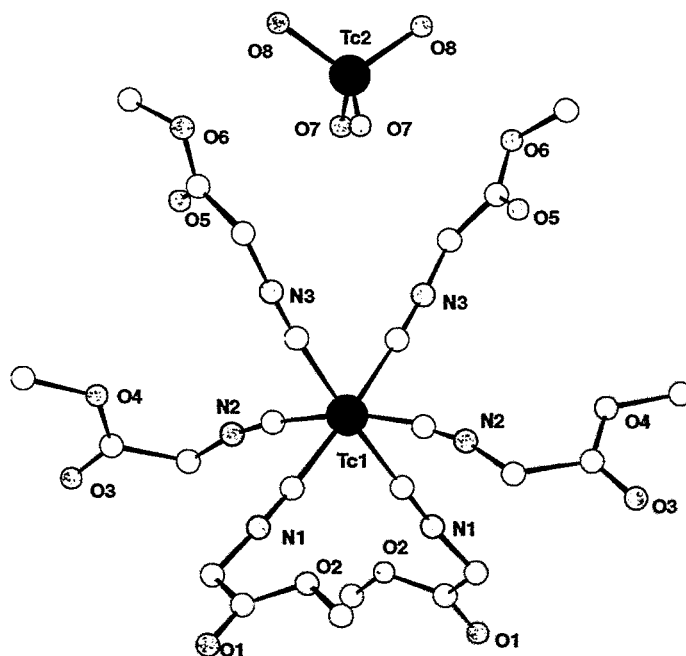


Fig. 1. CELLGRAPH drawing of the $[\text{Tc}(\text{CN-CH}_2\text{-COOCH}_3)_6]\text{TcO}_4$

References

- [1] Jones A. G., Davison A., Abrams M. J., Brodack J. W., Costello C. E., Kassis A. I., Uren R. F., Simon M., Stemp L. and Holman B. L. (1982) A new class of water soluble low valent technetium unipositive cations: Hexakisisonitrile technetium(I) salts. *J. Labelled. Compd. Radiopharm.* **19**, 1594-1595.
- [2] Jones A. G., Abrams M. J., Davison A., Brodack J. W., Toothaker A. K., Adelstein S. J. and Kassis A. I. (1984) Biological studies of a new class of technetium complexes: the hexakis(alkylisonitrile)technetium(I) cations. *Nucl. Med. Biol.* **11**, 225-234.
- [3] Rochon F. D., Melanson R. and Kong P. C. (1996) Synthesis and crystal structure of mixed-ligand Tc(I) complexes with dimethylphenylphosphine and t-butylisonitrile. (1996) *Inorg. Chim. Acta* **245**, 251-256.

41. Crystal Structure of the Nitridorhenium(V) Complex [ReN{CMe₂PPh Me₂}(DMSMe₂)₂]

S. Seifert, P. Leibnitz¹, H. Spies

¹Bundesanstalt für Materialforschung und -prüfung Berlin

The preparation and partial characterization of nitridorhenium(V) complexes with DMSA and DMSdimethylester as ligands were described some years ago [1]. By elemental analysis and NMR studies it was found that a phosphine molecule remains in the complex after the ligand exchange reaction of ReNCl₂(Me₂PhP)₃ with the DMS ligands and that a solvent acetone reacts with the ReN core. However, the formulation [ReN(C(CH₃)₂)(PMe₂Ph)(DMSMe₂)₂] was still rather speculative and had to be clarified by mass spectrometry and X-ray analysis.

Mass spectrometric analyses show that in addition to the DMS ligands and the phosphine molecule a component with the mass of 42 (CH₃-C-CH₃) is part of the molecule ion (m/z = 795, 797). A reaction product with condensed acetone was not found [2, 3].

When methylethylketone is used as solvent instead of acetone, the formation of a similar complex of the mass m/z = 810, 812 is observed. The resulting complex [ReN{C(CH₃)(C₂H₅)PMe₂Ph}(DMSMe₂)₂] is formed by addition of CH₃-C-C₂H₅ to the ReN core. Moreover, an additional complex [ReN{C(CH₃)(C₂H₅)CH₂C(O)C₂H₅PMe₂Ph}(DMSMe₂)₂] of the mass m/z = 881, 883 is found by FAB-MS. As described for other ReN complexes [2, 3] this complex is formed by acid condensation of two solvent molecules and addition of the reaction product to the ReN core.

The X-ray analysis of the complex [ReN{C(CH₃)₂PMe₂Ph}(DMSMe₂)₂] leads to a surprising result. The phosphine molecule is bound to the central C atom of the added solvent molecule and not, as expected, directly to the Re atom (Fig. 1).

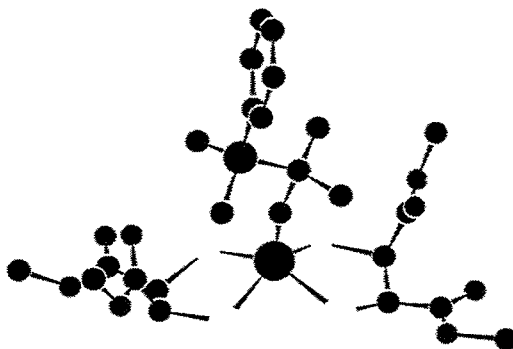
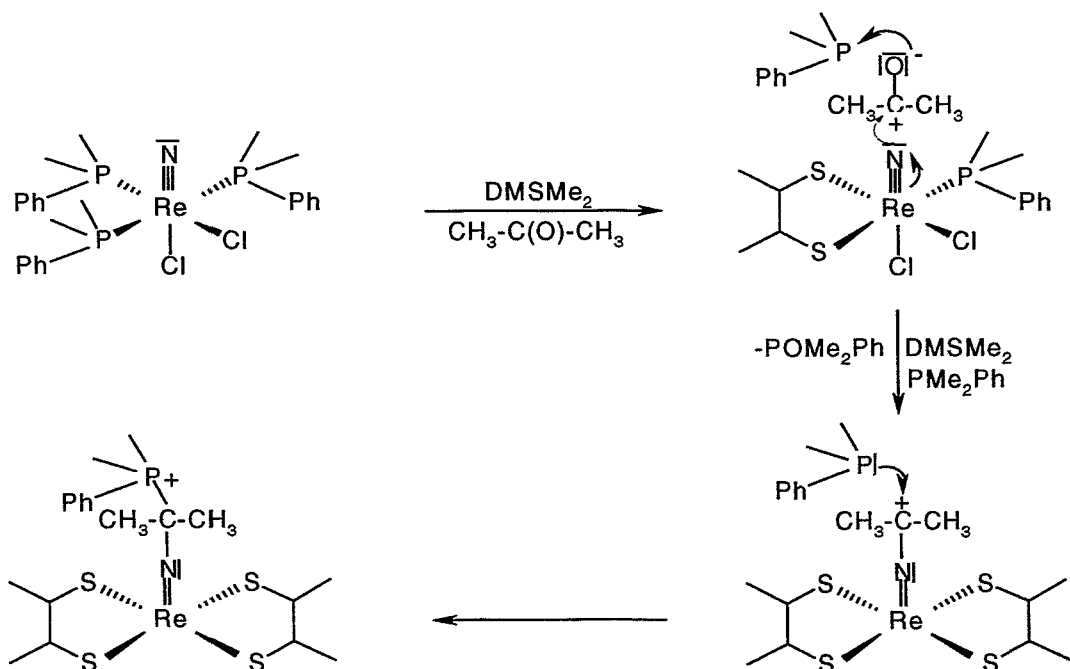
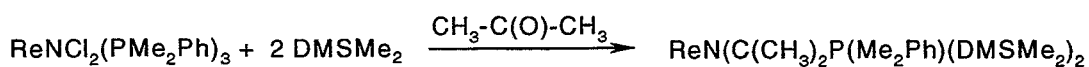


Fig. 1. X-ray crystal structure of the complex [ReN{C(CH₃)₂PMe₂Ph}(DMSMe₂)₂]

The resulting chain Re=N-C-P has never been described before and shows an angle N1-C13-P1 of 99.5°. The Re-N bond length of 1.697 Å is in the range of a double bound nitrogen atom. The Re-S distances are of the order generally found for these complexes.

The exceptional configuration found by X-ray analysis can possibly be explained by the reductive attack of a free phosphine molecule on a solvent molecule and following formation of a carbonium ion and phosphine oxide. The resulting electrophilic agent is added onto the nitrido atom and the unusual Re-N-C-P configuration is formed by the nucleophilic attack of a second phosphine (Scheme 1).

Scheme 1.



References

- [1] Seifert S., Schneider F., Pietzsch H.-J. and Spies H. (1994) Preparation and characterization of nitridorhenium(V) DMSA complexes. *Annual Report 1993*, Institute of Bioinorganic and Radio-pharmaceutical Chemistry, FZR-32, pp. 95-99.
- [2] Bishop M. W., Chatt J., Dilworth J. R., Dahlstrom P., Hyde J. and Zubieta J. (1981) Reactions of coordinated nitride to generate novel rhenium and molybdenum imido complexes: the crystal and molecular structures of $[\text{Mo}(\text{NCPh}_3)(\text{S}_2\text{CNMe}_2)_3]\text{BF}_4$ and $[\text{Mo}(\text{NSO}_2\text{Ph})(\text{S}_2\text{CNMe}_2)_3]\text{PF}_6$. *J. Organomet. Chem.* **213**, 109-124.
- [3] Ritter S. and Abram U. (1994) Die Bildung von Nitrenkomplexen durch Kondensation von Aceton an koordinierten Nitridoliganden. Darstellung und Strukturen von *fac*- $[\text{Re}\{\text{NC}(\text{CH}_3)_2\text{CH}_2\text{C}(\text{O})\text{CH}_3\}_3\text{X}_3(\text{Me}_2\text{PhP})_2]$ -Komplexen (X = Cl, Br). *Z. anorg. allg. Chem.* **620**, 1786-1792.

42. Reactions of Hydroxy-Group-Containing '3+1' Mixed-Ligand Oxorhenium(V) Complexes.

Part 3*. Synthesis and Physico-Chemical Investigation of O-Organosilicon-Containing 3-Thia-, 3-Oxa- and 3-Methylazapentane-1,5-Dithiolato-Oxorhenium(V)

A. Zablotska¹, I. Segal¹, A. Kemme, E. Lukevics¹, R. Berger, H. Spies
¹Latvian Institute of Organic Synthesis, Riga

To investigate the influence of substituents on the physico-chemical and biological properties a series of neutral oxorhenium(V) complexes **1-10** was synthesized in which the oxorhenium(V) core ReO^{3+} is coordinated with a tridentate 3-thia-, 3-oxa- and 3-methylazapentane-1,5-dithiolato as well as with a hydroxy- or triorganylsiloxy-containing monodentate thiolate. In the synthesis of novel O-silylated oxorhenium complexes **6-10** silylation experiments were performed, starting from '3+1' mixed-ligand rhenium complexes **1-5** in which the monodentate ligand part contains a hydroxy group. A ligand containing the hydroxy group was first fixed at the complex core first and then the silyl group was introduced by silyl halogenides in the presence of triethylamine (Scheme 1).

The structure of the synthesized compounds was proved by the elemental analysis, ^1H and ^{29}Si NMR spectroscopy. The molecular structures of complexes **5**, **8** and **10** was established by X-ray analysis. No additional coordination of the silicon atom in organosilicon oxorhenium complexes was observed. But the ^{29}Si resonance for (2-trimethylsiloxyethanethiolato)[3-(N-methyl)azapentane-1,5-dithiolato]oxorhenium(V) **10** is shifted strongly down-field, suggesting the deshielding anisotropic effect of rhenium on the silicon atom in solution.

X-ray analysis revealed the presence of two crystallographic independent molecules per unit cell for (2-hydroxyethanethiolato)[3-(N-methyl)azapentane-1,5-dithiolato]oxorhenium(V) **5** (Fig. 1). A disorder of C atoms in α -position to the N atom of the tridentate ligand with its occupation factors ratio of approximately 2:3 was observed in one of them.

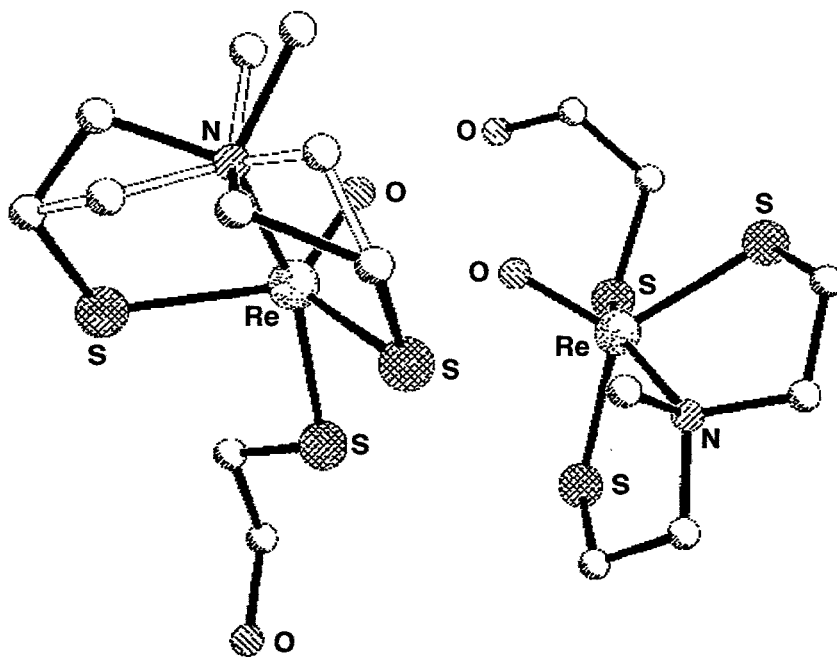
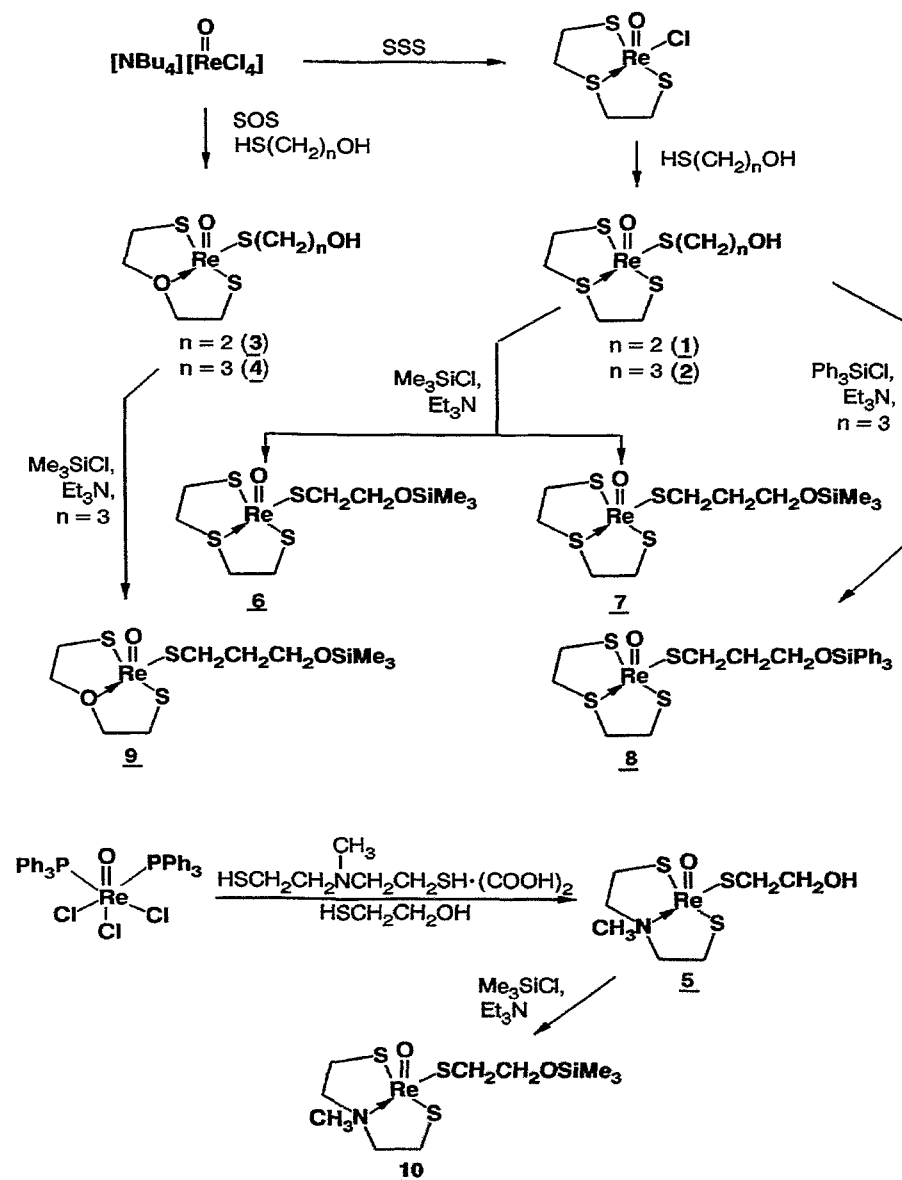


Fig. 1. Molecular structures of two conformers of (2-hydroxyethanethiolato)[3-azapentane(N-methyl)-1,5-dithiolato]oxorhenium(V) **5**

Scheme 1



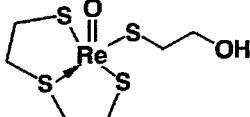
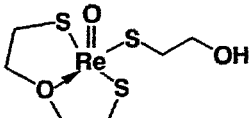
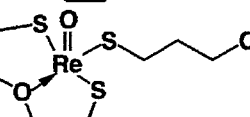
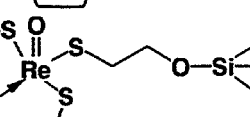
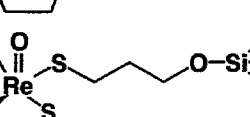

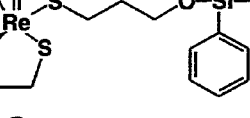
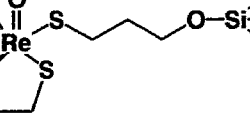
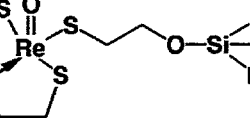
To evaluate the difference between the silylated and parent compounds, their lipophilicity was determined by a HPLC procedure (Table 1). The data obtained adequately describes (a) the effect of the organosilicon-substituent introduction, (b) the sequence concerning 3-thia-, 3-oxa- and 3-(N-methyl)aza ligands, and (c) the side chain length. For unsilylated complexes 1 and 3-5 log P values are under 1. For the silylated ones these values vary from 2.4 to 5.4 and depend on the increase in the steric bulk about the silicon atom. The maximal value, 5.4, was found for (3-triphenylsiloxypropanethiolato)(3-thiapentane-1,5-dithiolato)oxorhenium(V) **8**. Log P for (3-trimethylsiloxypropanethiolato)(3-thiapentane-1,5-dithiolato)oxorhenium(V) **9** is about two times smaller (Table 1).

For both silylated and unsilylated complexes the tendency of log P to increase from aza to oxa and further to thia is consistent with the electronic effect caused by S, O and N atoms of the tridentate ligands.

The influence of the carbon chain length of monodentate ligands for the complexes 3-4 and 6-7 is also reasonable.

The synthesized compounds are tested *in vivo* for psychotropic activity caused obviously by the introduction of the silyl group.

Table 1. Lipophilicity data

Denotation	Structure	P _{HPLC}	log P _{HPLC}
<u>1</u>		2.66 ± 0.06	0.4249
<u>3</u>		2.06 ± 0.12	0.3139
<u>4</u>		2.73 ± 0.04	0.4362
<u>6</u>		577 ± 14	2.7612
<u>7</u>		982 ± 48	2.9921
<u>8</u>		237360 ± 23000	5.3754
<u>9</u>		760	2.8808
<u>10</u>		275 ± 8	2.4393
<u>5</u>		1.66 ± 0.02	0.2201

* Part 2 has been published in *Annual Report 1997*, FZR-200, pp. 116-117.

References

- [1] Fietz T., Spies H., Zablotskaya A. and Scheller D. (1997) Reactions of hydroxy-group containing "3+1" mixed-ligand rhenium(V) compounds. Part 1: Silylation of "3+1" mixed-ligand complexes. *Annual Report 1997*, Institute of Bioinorganic and Radiopharmaceutical Chemistry, FZR-200, pp. 113-116.
- [2] Spies H., Fietz T., Zablotskaya A., Belyakov S. and Lukevics E. (1999) Organosilicon containing rhenium(V) complexes with mixed ligands. *Chem. Heterocycl. Comp.* **35**, 116-125.

43. Artificial Guanidinium Hosts for Binding Pertechnetate

H. Stephan, F. P. Schmidtchen¹, H. Spies, B. Johannsen

¹Institut für Organische Chemie und Biochemie, Technische Universität München

Introduction

Noncovalent binding of pertechnetate may be of considerable interest as a new approach to labelling organic compounds with technetium without any reduction step, and for removal of pertechnetate as an environmental contaminant. Special requirements have to be met in the first envisaged area of application, particularly as specific imaging agents, including

- high kinetic stability of the host-pertechnetate complex in the presence of competitive anions such as chloride and bicarbonate
- adjustment of the shape, charge, redox properties and lipophilicity of the complex
- host-guest complex may be conjugated to targeting molecules in order to govern the biodistribution.

This objective should be realizable on the basis of modular assembled supramolecular receptors that can provide multi-point fixation of pertechnetate as shown in Fig. 1.

Thus, the receptor should have a framework that is complementary to the charge and topology of tetrahedral pertechnetate. The receptor may be ditopic, with the coordination centre 1 designed for charge compensation and both coordination groups operating by ion-dipole binding. In the latter nexus hydrogen bonds are the most prominent and prototypical representatives of dipolar elements. The spacer moiety makes it possible to adjust the stability and lipophilicity, and most important, to introduce biomolecules without disturbing the coordination centre.

Recently we developed ditopic guanidinium receptors as selective extractants for tetrahedral oxoanions [1]. In this paper we report the binding behaviour of guanidinium compounds towards pertechnetate.

Liquid-liquid partition of ⁹⁹TcO₄⁻ in a CHCl₃/aqueous buffer system was chosen to characterize the binding properties of various host compounds.

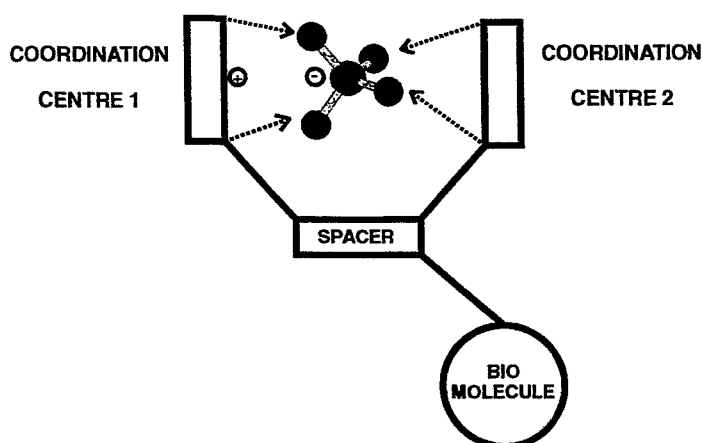
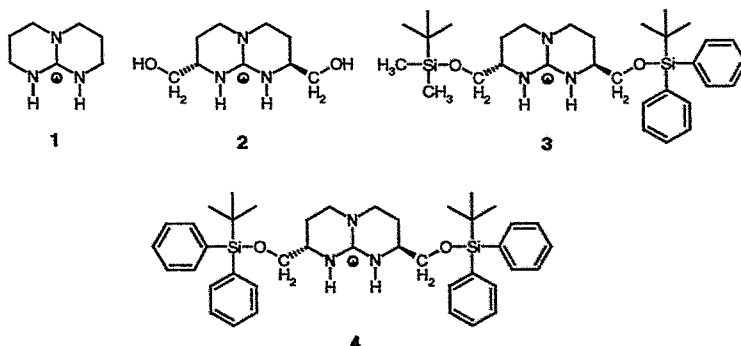


Fig. 1. Conception for the complexation of pertechnetate

Experimental

All chemicals were reagent grade and used as obtained. Compound 1 was received from Fluka, the bicyclic guanidinium hosts 2 - 4 were synthesized as described earlier [2] and used as chlorides.

The extraction studies were performed at 25 ± 1°C in 2 ml microcentrifuge tubes by mechanical shaking. The phase ratio V_(org):V_(w) was 1:1 (0.5 ml each); the shaking period was 30 min. The extraction equilibrium was achieved during this period. All samples were centrifuged after extraction. The



pertechnetate concentration in both phases was determined radiometrically using the β -radiation measurements of $^{99}\text{TcO}_4^-$ (Amersham) in a liquid scintillation counter (Tricarb 2500, Canberra-Packard). The aqueous solution was adjusted using 0.05 M 4-(2-hydroxyethyl)piperazine-1-ethanesulphonic acid (HEPES)/NaOH buffer.

Results and Discussion

Fig. 2 shows the results of pertechnetate extraction with the guanidinium hosts 1 – 4. It can be seen that the most lipophilic compounds 3 and 4 are capable of transferring pertechnetate with high efficiency from water into trichloromethane. The distribution ratios D_{TcO_4} are of the same order of magnitude as obtained for extractants that are mainly used for pertechnetate such as tetraphenylarsonium [3 - 5], tetraphylphosphonium [6] and trioctylmethylammonium chloride (Aliquat 336) [7, 8]. The extractability is lowered with decreasing lipophilicity of the guanidinium hosts (cf. 1 and 2), but even the highly hydrophilic derivative 1 extracts pertechnetate with unprecedented efficiency. This finding points to the reinforcement of binding caused by using two hydrogen bonds in addition to electrostatic attraction. As expected, the guanidinium hosts investigated form clean 1:1 complexes with pertechnetate in the organic phase [9]. In the presence of the competitive anions chloride and bicarbonate the pertechnetate extraction decreases. But even at a huge excess of these anions pertechnetate is still extracted with high efficiency. Thus, more than 60% of pertechnetate is transferred into trichloromethane with guanidinium host 4 ($C_{4(\text{org})} = 1 \cdot 10^{-3}$ M in CHCl_3) at a concentration ratio = 1 : 1000 for $\text{TcO}_4 : \text{Cl}^- (\text{HCO}_3^-)$.

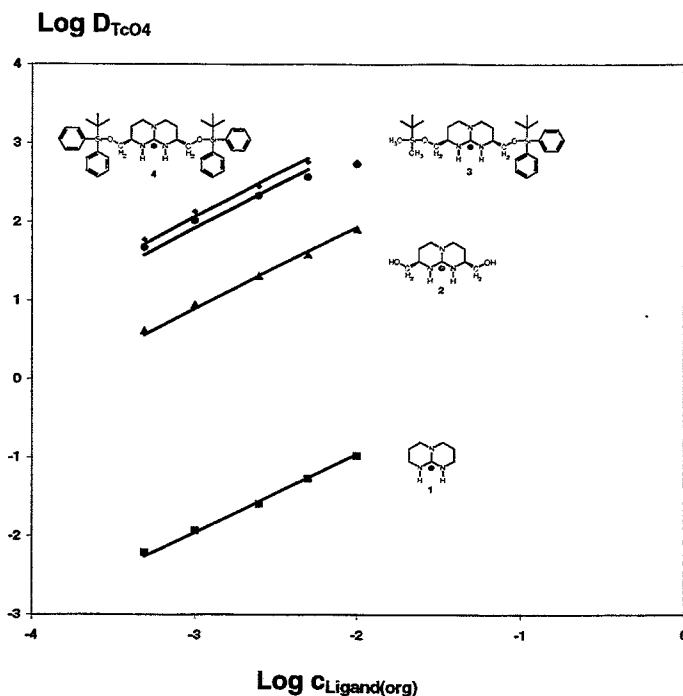


Fig. 2. Extraction of pertechnetate with bicyclic guanidinium compounds 1 – 4

[KTcO_4] = $1 \cdot 10^{-4}$ M; pH = 7.4 (HEPES/NaOH buffer); [ligand] = $5 \cdot 10^{-4}$.. $1 \cdot 10^{-2}$ M in CHCl_3 ; points represent the experimental data; lines correspond to 1:1 complex formation.

Summary

Guanidinium hosts may serve to complex pertechnetate. Lipophilic derivatives transfer this tetrahedral anion from water to trichloromethane with high efficiency. A remarkable selectivity of pertechnetate over chloride and bicarbonate was obtained. Structural modifications of host molecules in terms of complex stability and lipophilicity are under way.

We conclude that supramolecular receptors having at least one guanidinium unit are very promising for direct complexation of pertechnetate.

References

- [1] Stephan H., Gloe K., Schiessl P. and Schmidtchen F. P. (1995) Lipophilic ditopic guanidinium receptors: selective extractants for tetrahedral oxoanions. *Supramol. Chem.* **5**, 273-280.
- [2] Kurzmeier H. and Schmidtchen F. P. (1990) Abiotic anion receptor functions. A facile and dependable access to chiral guanidinium anchor groups. *J. Org. Chem.* **55**, 3749-3755.
- [3] Omori T., Muraoka Y. and Suganuma H. (1994) Solvent extraction mechanism of pertechnetate with tetraphenylarsonium chloride. *J. Radioanal. Nucl. Chem.* **178**, 237-243.

- [4] Omori T., Asahina K. and Suganuma H. (1995) Mechanism of solvent extraction of pertechnetate with tetraphenylarsonium chloride. *J. Radioanal. Nucl. Chem.* **191**, 99-104.
- [5] Kopunec R., Abudeab F. N. and Maikova I. (1996) Extraction characteristics of pertechnetate with tetraphenylarsonium chloride in the presence of chloride, nitrate and perchlorate anions. *J. Radioanal. Nucl. Chem.* **208**, 207-228.
- [6] Kopunec R., Abudeab F. N. and Skraskova S. (1998) Extraction of pertechnetate with tetraphenylphosphonium in the presence of various acids, salts and hydroxides. *J. Radioanal. Nucl. Chem.* **230**, 51-60.
- [7] Rohal K. M., van Seggen D. M., Clark J. F., McClure M. K., Chambliss C. K., Strauss St. H. and Schroeder C. (1996) Solvent extraction of pertechnetate and perrhenate ions from nitrate-rich acidic and alkaline aqueous solution. *Solvent. Extr. Ion. Exch.* **14**, 401-416.
- [8] Bonnesen P. V., Moyer B. A., Presley D. J., Armstrong V. S., Haverlock T. J., Counce R. M. and Sachleben R. A. (1996) Alkaline-side extraction of technetium from tank waste using crown ethers and other extractants. Oak Rich National Laboratory (ORNL)-Report 13241.
- [9] The slope of the $\text{Log } D_{\text{TcO}_4^-} \text{ vs } \text{Log } C_{\text{Ligand}}$ diagram is 1 indicating 1:1 complex formation in the organic phase.

44. EXAFS Analysis of a Rhenium(I) Carbonyl Complex

S. Seifert, J.-U. K nstler, H. Funke¹, A. Ro bberg¹, C. Hennig¹, T. Reich¹, G. Bernhard¹, B. Johannsen¹
¹Institut f r Radiochemie

Introduction

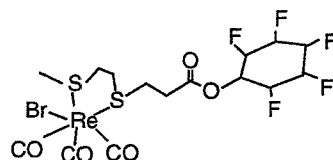
After joint EXAFS experiments at the Hamburger Synchrotronstrahlungslabor (Hasylab) and the Stanford Synchrotron Radiation Laboratory (SSRL), EXAFS measurements of various rhenium complexes were performed, using for the first time the sophisticated Rossendorf Beamline (ROBL) facility at the European Synchrotron Radiation Facility (ESRF) in Grenoble. Being a collaboration between the Institute of Radiochemistry and the Institute of Bioinorganic and Radiopharmaceutical Chemistry, this analysis serves as a stepping stone towards preparing future EXAFS experiments with ⁹⁹Tc carbonyl complexes.

Rhenium and technetium carbonyl complexes of the general formula [M(CO)₃XL] (M = Re, Tc; X = Br⁻, Cl⁻; L = bidentate thioether or Schiff base ligand) are at present under investigation for the development of neutral receptor-affine complexes which are able to cross the blood-brain barrier and to bind to receptors of the central nervous system. Some of the rhenium carbonyl thioether complexes are fully characterized by X-ray analysis and other chemical methods, the data of which may be used for comparison with the EXAFS results.

Experimental

The EXAFS spectra of the Re L_{III} and Br K-edges of the same sample were measured in transmission mode, using the Si(111) double-crystal monochromator in fixed-exit mode.

The sample consists of 20 mg of the following rhenium complex: This complex was mixed with Teflon powder as matrix material and pressed into a pellet. The EXAFS spectra were evaluated, using the program package EXAFSPAK [1], and phases and amplitudes were calculated with the scattering code FEFF6.



Results

To obtain a satisfactory fit result for the Re spectra, the individual scattering paths Re-C, Re-S, and Re-Br and the multiple scattering path along the carbonyl group, i.e. Re-C-O, have to be included (see Fig. 1 and Tab. 1).

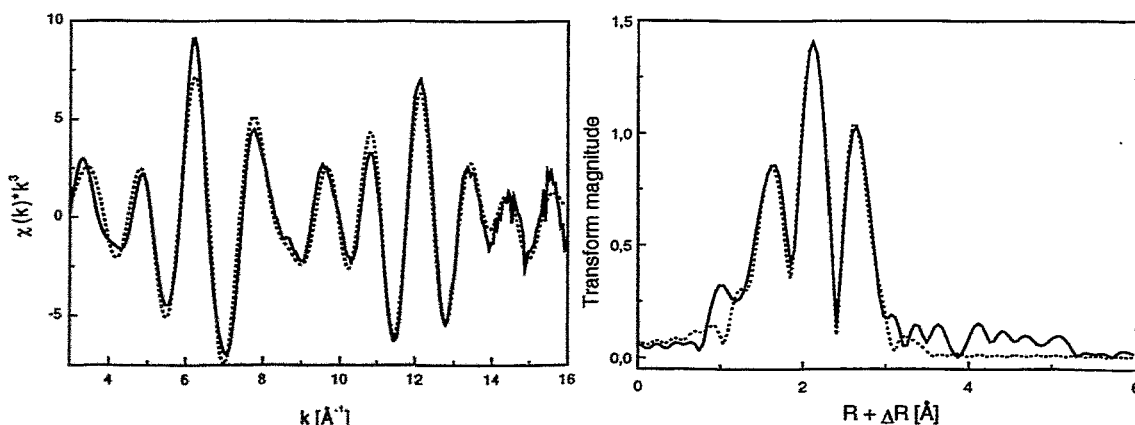


Fig. 1. Re L_{III} edge EXAFS spectrum and Fourier transform of the rhenium(I) carbonyl complex (solid line: experimental data, dotted line: fit).

Table 1. Comparison of bond distances obtained by EXAFS measurement and X-ray analyses data of similar complexes ($\Delta R_{\text{EXAFS}} < 0.02 \text{ \AA}$)

Path	EXAFS			XRD ¹⁾	XRD ²⁾
	N	σ^2 ³⁾	R[\AA]	R[\AA]	R[\AA]
Re-C1	2.7	1.8	1.92	1.92	1.98
Re-C2				1.90	1.94
Re-C3				1.90	1.92
Re-Br	0.9	3.3	2.62	2.64	2.61
Re-S1	2.4	3.6	2.49	2.47	2.54
Re-S2				2.46	2.53
Re-C-O (3 legs)	2.7 ⁴⁾	3.0	3.07	3.07	no data
Re-C-O (4 legs)	2.7	3.0	3.06	3.06	

¹⁾ $\text{Re}(\text{CO})_3\text{Br}(\text{CH}_3\text{-S-C}_2\text{H}_4\text{-S-CH}_3\text{-CCH})$, [2]

²⁾ $\text{Re}(\text{CO})_3\text{Br}(\text{Cl-C}_2\text{H}_4\text{-S-C}_2\text{H}_4\text{-S-C}_2\text{H}_4\text{-Cl})$, [3]

³⁾ Debye Waller factors in 10^{-3} \AA^2

⁴⁾ The degeneracy of 2 was taken into account

The EXAFS scan of the same compound with Br as the central atom produces a more complicated spectrum dominated by the heaviest possible back-scatterer, rhenium. Apart from the main scattering path Br-Re, the nearly linear multiple scattering paths Br-Re-C and Br-Re-C-O make the main contributions to the radial distribution function (Fig. 2). The evaluated bond length is 2.6 \AA .

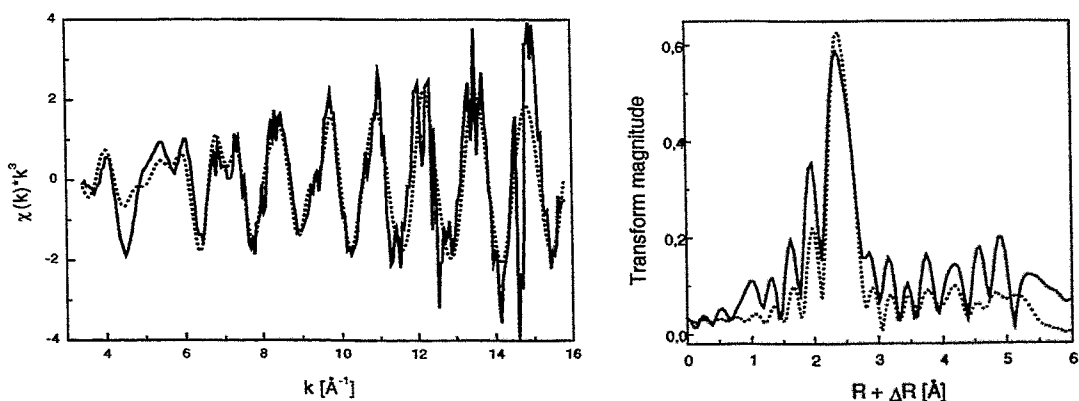


Fig. 2. Br K-edge EXAFS spectrum and Fourier transform of the rhenium(I) carbonyl complex (solid line: experimental data, dotted line: fit).

Measurements of the inner coordination spheres of rhenium carbonyl complexes with different dithioether ligands, using X-ray crystal-structure methods, show Re-Br distances between 2.61 and 2.64 Å [2, 3]. The EXAFS-results presented are consistent with these data.

References

- [1] George G. N. and Pickering I. J. (1995) EXAFSPAK. *Stanford Synchrotron Radiation Laboratory*, Stanford, CA, USA.
Zabinsky S. I., Rehr J. J., Ankudinov A., Albers R. C. and Eller M. J. (1995) Multiple-scattering calculations of X-ray-absorption spectra. *Phys. Rev.* **B52**, 2995-3009.
- [2] Reisgys M. (1998) Rhenium- und Technetiumkomplexe mit Thioetherliganden. *Thesis*, TU Dresden.
- [3] Alberto R., Schibli R., Angst D., Schubiger P. A., Abram U., Abram S. and Kaden Th. A. (1997) Application of technetium and rhenium carbonyl chemistry to nuclear medicine. Preparation of $[\text{NEt}_4][\text{TcCl}_3(\text{CO})_3]$ from $[\text{NBu}_4][\text{TcO}_4]$ and structure of $[\text{NEt}_4][\text{Tc}_2(\mu\text{-Cl})_3(\text{CO})_6]$; structures of the model complexes $[\text{NEt}_4][\text{Re}_2(\mu\text{-OEt})_2(\mu\text{-OAc})(\text{CO})_6]$ and $[\text{ReBr}\{\{-\text{CH}_2\text{S}(\text{CH}_2)_2\text{Cl}\}_2\}(\text{CO})_3]$ *Transition Met. Chem.* **22**, 597-601.

45. First XANES and EXAFS Measurements of Technetium Model Compounds at the Rossendorf Beamline ROBL

T. Reich¹, H. Funke¹, C. Hennig¹, A. Roßberg¹, H.-J. Pietzsch, S. Seifert, J.-U. Künstler, G. Bernhard¹
¹Institut für Radiochemie

Technetium K-edge EXAFS measurements on model compounds demonstrate the superb quality of the radiochemistry endstation of ROBL for X-ray absorption spectroscopy.

Experimental

The structure of novel Tc complexes has been studied successfully in the framework of a collaboration between the Institute of Radiochemistry and the Institute of Bioinorganic and Radiopharmaceutical Chemistry over the last few years [1, 2].

In order to evaluate the possibilities of the new Rossendorf Beamline (ROBL) for Tc EXAFS studies, we prepared four samples for a first experiment with ⁹⁹Tc at ROBL. The samples were 127 mM NaTcO₄(aq), 1.3 mM NaTcO₄(aq), KTcO₄(s), and TcO₂·nH₂O(s). Except for the 1.3 mM Tc solution, the amount of Tc in the samples yielded an edge jump of ~1 across the Tc K absorption edge at 21 keV. These samples were measured in transmission mode using the Si(111) double-crystal monochromator in fixed-exit mode with an additional feedback system to minimize beam intensity fluctuations. The Tc K-edge EXAFS spectrum of the dilute solution was recorded using a four pixel Ge fluorescence detector. The energy scale of the XANES scans was calibrated with a Mo metal foil (Mo K-edge at 20004.3 eV). For the EXAFS analysis, the first inflection point of the pre-edge absorption peak for the NaTcO₄(aq) sample was defined as 21044 eV [3].

Results and Discussion

Fig. 1 displays the raw Tc K-edge k³-weighted EXAFS spectrum of NaTcO₄(aq). The spectrum of the 127 mM Tc solution was recorded in a single sweep up to k = 21 Å⁻¹. During this sweep the counting time per data point was gradually increased from 2 to 20 sec. To our knowledge, this is the first Tc EXAFS spectrum of a liquid sample where it was possible to observe the fine structure of the X-ray absorption spectrum over an energy range of 1700 eV. In addition, this spectrum is an impressive demonstration of the superb quality and stability of all beamline components. It follows from the best theoretical fit to the data (Fig. 1) that Tc is surrounded by 4 oxygen atoms (N = 4.1±0.1) at a distance of 1.72±0.01 Å (σ² = 0.0013±0.0004 Å²). The EXAFS spectrum of the 100 times more dilute NaTcO₄(aq) sample is also shown in Fig. 1 and represents an average of four sweeps measured in fluorescence mode. The intensity of the Tc Kα fluorescence line was 1.2 x 10⁵ counts/sec. The total count rate processed by the fluorescence detector was 6.4 x 10⁵ counts/sec. Under these conditions, it was possible to analyze the Tc K-edge k³-weighted EXAFS spectrum of the 1.3 mmol Tc solution up to k = 15 Å⁻¹. The structural parameters obtained are the same as for the TcO₄⁻ ion in the concentrated solution, i.e., N = 3.9±0.2, R = 1.72±0.01 Å, and σ² = 0.0016±0.0003 Å². Our structural parameters agree with a previous Tc K-edge EXAFS measurement of a 0.2 M NH₄TcO₄(aq) sample [3].

Fig. 2 displays the Tc K-edge XANES spectra of KTcO₄(s), and TcO₂·nH₂O(s). The energy of the main absorption edge defined by the first-derivative method increases from 21061.6 eV to 21065.8 eV as the Tc valence increases from IV to VII. This energy shift of 4.2 eV is in qualitative agreement with previous measurements [3]. The shape of the Tc K-edge XANES spectra reflects the symmetry of the oxygen atoms surrounding Tc. The most distinct feature of the TcO₄⁻ ion, which has T_d symmetry, is the pre-edge peak at 21050.8 eV. The XANES features can be used as a probe to determine the Tc speciation as it has been shown, for example, in cement waste forms [3].

In summary, the Tc K-edge X-ray absorption measurements on Tc model compounds showed that high-quality data can be obtained for liquids and solids at the new Rossendorf Beamline. We conclude that ROBL provides excellent experimental conditions to study the structure of solid and liquid Tc complexes with a large variety of organic and inorganic ligands covering a Tc concentration range of at least two orders of magnitude.

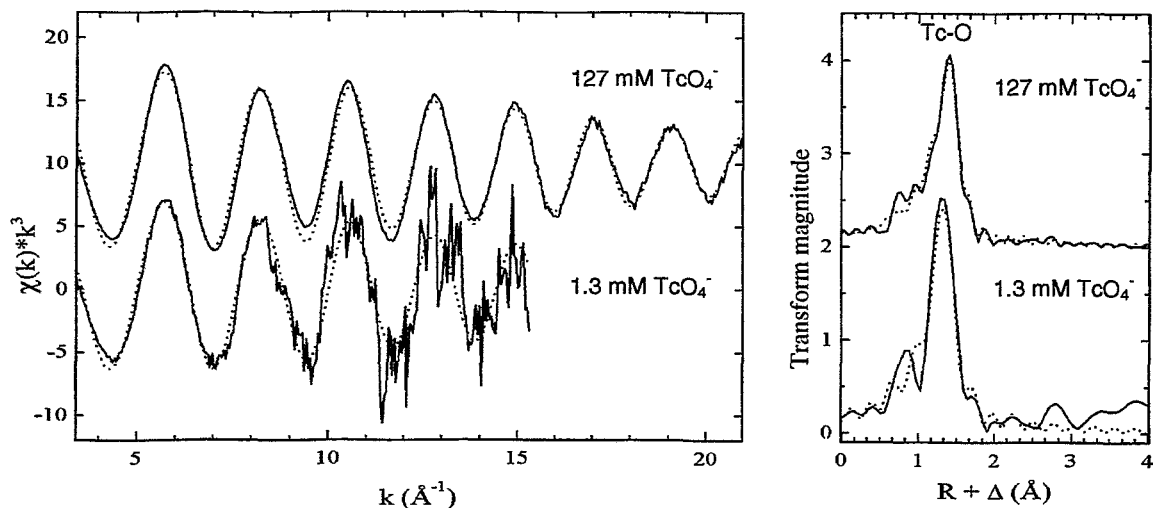


Fig. 1. Raw k^3 -weighted Tc K-edge EXAFS spectra (left) and corresponding Fourier transforms (right) of experimental data (solid line) and theoretical fits (dots) for 127 mM (top) and 1.3 mM (bottom) $\text{NaTcO}_4(\text{aq})$.

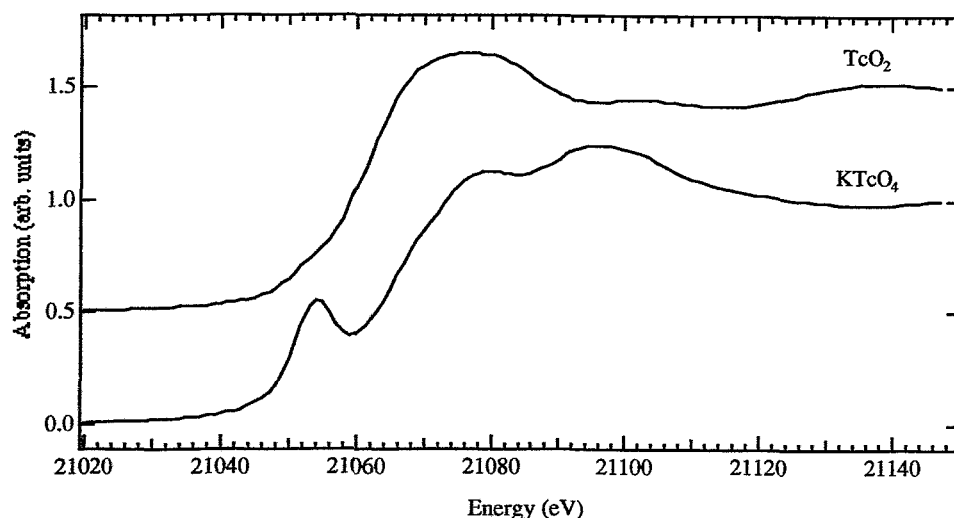


Fig. 2. Raw Tc K-edge XANES spectra of $\text{TcO}_2 \cdot n\text{H}_2\text{O}(\text{s})$ (top) and $\text{KTcO}_4(\text{s})$ (bottom).

References

- [1] Johannsen B., Jankowsky R., Noll B., Spies H., Reich T., Nitsche H., Dinkelborg L. M. and Hilger C. S. (1997) Technetium coordination ability of cysteine-containing peptides: X-ray absorption spectroscopy of a Tc-99 labelled endothelin derivative. *Appl. Radiat. Isot.* **48**, 1045-1050.
- [2] Jankowsky R., Kirsch S., Reich T., Spies H. and Johannsen B. (1998) Solution structures of rhenium (V) oxo peptide complexes of glycylglycylcysteine and cysteinylglycine as studied by capillary electrophoresis and X-ray absorption spectroscopy. *J. Inorg. Biochem.* **702**, 99-106.
- [3] Allen P. G., Siemering G. S., Shuh D. K., Bucher J. J., Edelstein N. M., Langton C. A., Clark S. B., Reich T. and Denecke M. A. (1997) Technetium speciation in cement waste forms determined by X-ray absorption fine structure spectroscopy. *Radiochim. Acta* **76**, 77-86 and references therein.

46. Challenge Experiments with "3+1" Mixed-Ligand ^{99m}Tc Complexes and Glutathione: Influence of Structural Parameters on the Complex Stability

A. Gupta, S. Seifert, R. Syhre, B. Johansen

Introduction

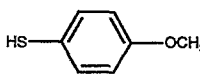
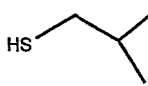
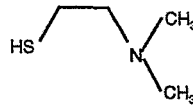
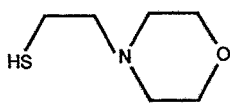
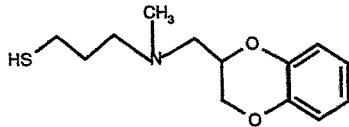
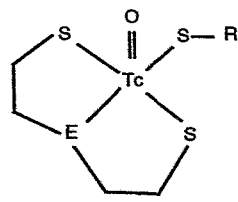
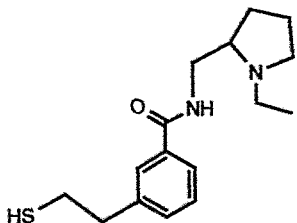
"3+1" mixed-ligand ^{99m}Tc complexes, containing a tridentate ligand and a monodentate ligand, are of particular interest in the development of new technetium-99m radiopharmaceuticals. An important point is the stability of these complexes in the various biologically relevant fluids. The "3+1" mixed-ligand ^{99m}Tc complexes proved to be stable in saline, phosphate buffer of pH = 7.4 and in plasma.

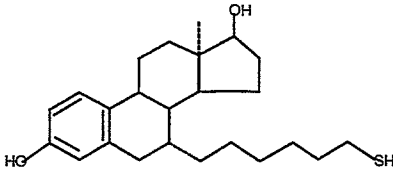
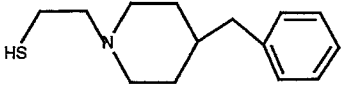
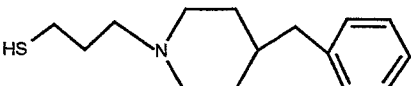
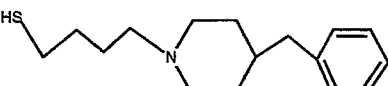
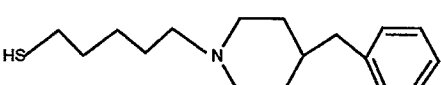
In blood, however, the complexes are converted. The assumption of a ligand exchange in terms of replacement of the monodentate ligand by GSH is quite reasonable as recently shown by us and others [1, 2, 3].

In fact, there is a high concentration of glutathione (GSH) in the erythrocytes (approx. 2 mM) compared with plasma (approx. 10 μM), and in other cases GSH was even considered a converting agent [4, 5].

Challenge experiments are a useful tool for estimating the stability of complex compounds to transchelation processes [6]. Systematic studies with GSH as a challenger were therefore carried out with a number of "3+1" mixed-ligand ^{99m}Tc complexes of the general formula $[\text{}^{99m}\text{TcO}(\text{SES})(\text{RS})]$ (E = S, NMe). To investigate the influence of the structure of the tridentate as well as the monodentate ligands on the stability the following complexes were used.

Table 1. General formula and numbering scheme of the "3+1" mixed-ligand ^{99m}Tc complexes

General formula	R-SH	E = S	E = NMe
		1a	1b
		2a	2b
		3a	3b
		4a	4b
$[\text{}^{99m}\text{TcO}(\text{SES})(\text{RS})]$ E = S, NMe		5a	5b
		6a	6b

		—	7b
		—	8b (C2)
		—	9b (C3)
		—	10b (C4)
		—	11b (C5)

Experimental

Preparation of complexes

The ^{99m}Tc complexes were prepared by direct reduction of pertechnetate with stannous chloride in an optimized mixture of various amounts of the ligands and propylene glycol according to Seifert *et al.* [7, 8].

Approx. 150 – 200 MBq of the ^{99m}Tc pertechnetate eluate were added to 1 ml propylene glycol and filled up to 2 ml with a solution of 0.9 % sodium chloride. After mixing approx. 40 μg of the tridentate ligand (diluted in acetone or methanol), 0.5 mg of the monodentate ligand (diluted in 100 μl H_2O), 100 μl 0.1 N NaOH and 20 μl stannous chloride solution (1.0 – 2.0 mg SnCl_2 dissolved in 5 ml 0.1 N HCl) were added and the reaction mixture was heated at 50 $^\circ\text{C}$ for 20 minutes.

The complexes were purified by HPLC with a semipreparative PRP-1 column (Hamilton, 305 x 7 mm, 10 μm , flow rate 2.0 ml/min) using a linear gradient system ($t[\text{min}]/\%B$): (5/30),(10/80), (10/80) of H_2O 0.1 % trifluoroacetic acid (A) and acetonitrile 0.1 % trifluoroacetic acid (B). The effluent from the column was monitored by γ -detection and UV detection. After adding 200 μl propylene glycol and removing acetonitrile by vacuum evaporation, the separated neutralized complex fraction was stable for more than 8 h.

Challenge experiments

For the challenge experiments about 1 MBq of the HPLC-purified ^{99m}Tc complexes was diluted in 0.1 M phosphate buffer (pH = 7.4 20 % propylene glycol) containing 1 mM or 10 μM solution of GSH to a final volume of 200 μl . The reaction mixture was incubated at 37 $^\circ\text{C}$ in a thermoshaker. After various lengths of time the reaction products were analysed by HPLC.

HPLC analyses

HPLC analyses were carried out with a PRP-3 column (Hamilton, 150 x 4 mm, 10 μm , flow rate 1.0 ml/min) using a linear gradient system ($t[\text{min}]/\%B$): (5/0),(5/70), (10/70) of 10 mM phosphate buffer of pH = 7.4 (A) and acetonitrile (B). The effluent from the column was monitored by γ -detection.

Results and Discussion

Influence of the nature of tridentate ligands

Remarkable differences are observed between the complexes containing the tridentate ligand with E = S and the complexes containing the tridentate ligand with E = NMe. In all investigated cases the SNMeS complexes are much more stable to transchelation with glutathione than SSS complexes. Most of the so-called SSS complexes are so fast converted with GSH concentrations of 1 mM that the time course of conversion could not be followed and only the transchelation product is found after 1 - 2 minutes. To compare the influence of the monodentate ligands we later studied these complexes with GSH concentrations of only 10 μ M.

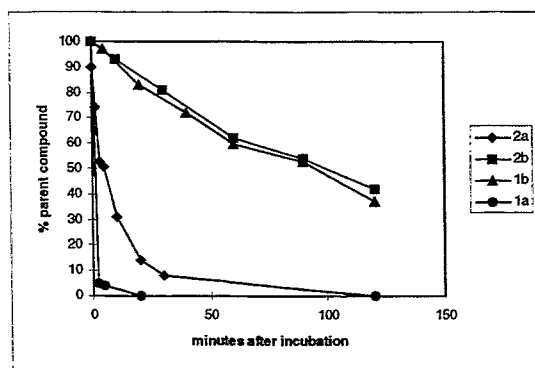


Fig. 1. Time course of the conversion of the "3+1" mixed-ligand ^{99m}Tc complexes **1a/1b** and **2a/2b** in the glutathione challenge

2. Influence of the nature of monodentate ligands

Variation of the monodentate ligand does not remarkably alter the different kinetics of complexes with the E = S tridentate ligand versus E = NMe. When we compared the complexes with constant tridentate ligand and varying monodentate ligands for both types (E = S and E = NMe), we observed exactly the same tendency. The complexes with the monodentate ligand **2** and with the monodentate ligand **1** have almost the same relatively high stability. The most stable of all investigated complexes was that with the monodentate ligand **7**. All the other complexes are converted faster into the transchelation product. All these complexes have a nitrogen atom in the side chain of the monodentate ligand. This nitrogen atom is therefore assumed to have a destabilizing effect. This effect was investigated by varying the spacer between the nitrogen atom and the coordinated sulphur atom as well as the ability of this nitrogen to be protonated.

For the complexes with the E = NMe tridentate ligand the challenge experiment was performed with an initial GSH concentration of 1 mM. After 120 min the GSH concentration in the reaction mixture was still $0.85 \text{ mM} \pm 0.04$ and so that the GSH concentration was considered to be almost constant. The time course of the converting reaction therefore fits the equation for a pseudo first order reaction and the parameter k thus obtained is a direct measure of the stability of the complex to conversion with GSH.

For the complexes with the E = S tridentate ligand the challenge experiment was performed with an initial GSH concentration of 10 μ M. In this case the time course of the converting reaction becomes a plateau. The reason for this behaviour seems to be the parallel autoxidation of the GSH so that the GSH content during the challenge experiment cannot be considered to be constant for low GSH concentrations. Unfortunately, we were not in a position to measure the glutathione in this challenge experiment because the detection limit of the test system used was 25 μ M. For these complexes the following equation was used to fit the time courses (parameter not shown):

$$y = y_0 + A_1 * e^{-(x-x_0)/k}$$

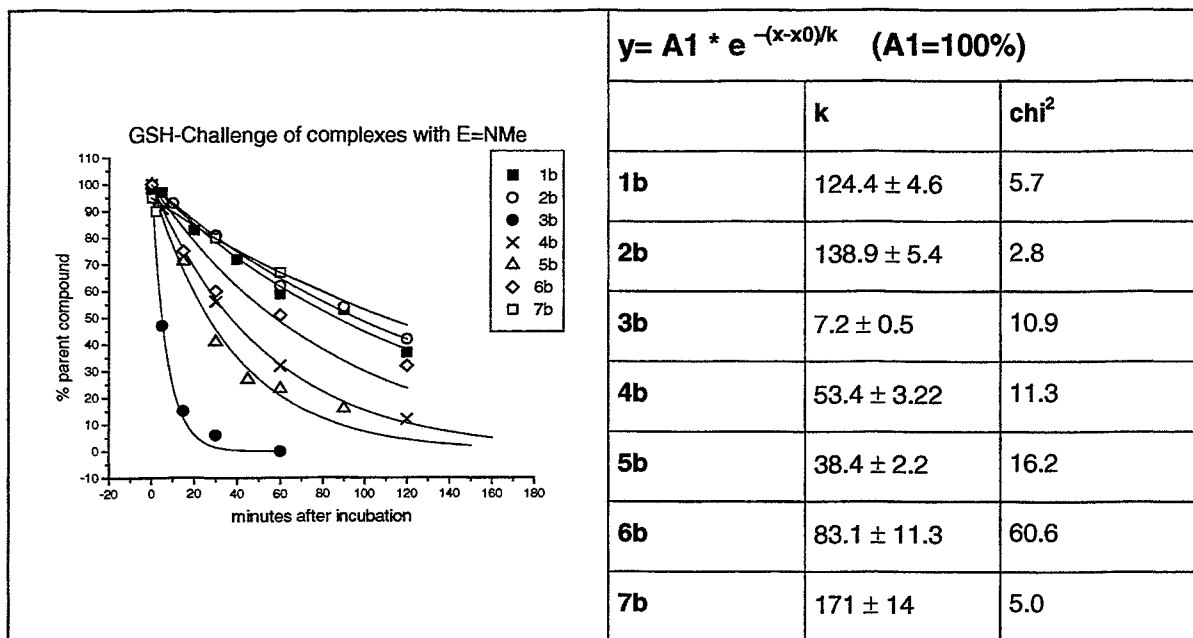


Fig. 2. Time course of the conversion of the "3+1" mixed-ligand ^{99m}Tc complexes with E = NMe in the glutathione challenge with 1 mM GSH

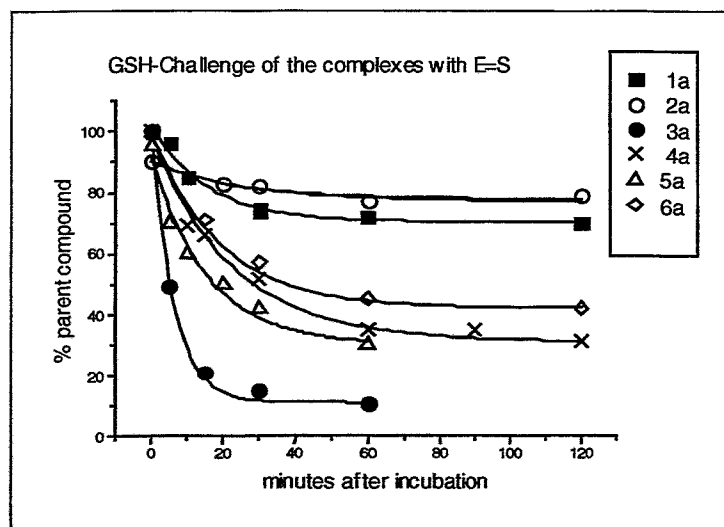


Fig. 3. Time course of the conversion of the "3+1" mixed-ligand ^{99m}Tc complexes with E = S in the glutathione challenge with 10 μM GSH

3. Influence of the nitrogen atom of the monodentate ligand

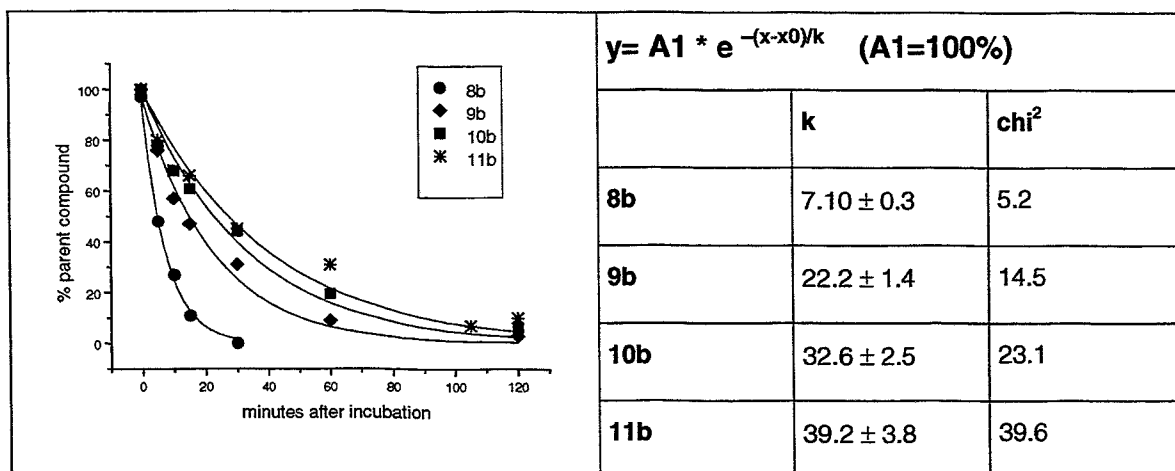


Fig. 4. Time course of the conversion of the "3+1" mixed-ligand ^{99m}Tc complexes with E = NMe in the glutathione challenge with 1 mM GSH

Interestingly, the compounds with the monodentate ligands **8b** and **3b** are converted the fastest. These compounds both have an ethylene spacer between the nitrogen atom and the coordinated sulphur atom. In Fig. 4 it is shown that the stability to GSH conversion increases with increasing spacer length between the technetium core and the nitrogen atom. But even with five spacer carbon atoms the stability of the complexes containing nitrogen in the monodentate ligand does not reach the stability of the complexes containing the monodentate ligands **1** and **2**. An exception in this range is compound **4b** where the nitrogen atom is an element of a morpholine ring system. This compound also has the ethylene spacer but it shows the same stability as the compounds **10b**, **11b** and **5b**. This is not surprising when the destabilizing effect of the nitrogen is explained by an electron-withdrawing(-I) effect of the protonated nitrogen that weakens the metal-sulphur bond of the complex. Because all compounds except compound **4b** have a pKa between 8.5 and 9.55 [9], the nitrogen of those compounds should be protonated under our working conditions of pH = 7.4. Compound **4b** has a pKa of about 7.1, which means that the oxygen of the morpholine ring weakens the base strength of the nitrogen atom and increases in this way the stability of the metal-sulphur bond compared to complexes **8b** and **3b**.

The stability tendencies found can be summed up as follows:

Complexes with the E = NMe tridentate ligand are much more stable than those with the E=S tridentate ligand.

A nitrogen atom in the monodentate ligand has a destabilizing effect, which can be explained by an -I-effect of the nitrogen on the complex core.

Compounds with an ethylene spacer between the nitrogen atom and the coordinated sulphur atom are the fastest converted compounds.

References

- [1] Syhre R., Seifert S., Spies H., Gupta A. and Johannsen B. (1998) Stability versus reactivity of "3+1" mixed-ligand technetium-99m complexes in vitro and in vivo. *Eur. J. Nucl. Med.* **25**, 793-796.
- [2] Pelecanou M., Pirmettis I. C., Nock B. A., Papadopoulos M., Chiotellis E., Stassinopoulou C. I. (1998) Interaction of [ReO(SNS)(S)] and [99mTc(SNS)(S)] mixed ligand complexes with glutathione: isolation and characterization of the product. *Inorg. Chim. Acta* **281**, 148-152.
- [3] Nock B. A., Maina T., Yannoukakos D., Ioannis C., Papadopoulos M. and Chiotellis E. (1999) Glutathione-mediated metabolism of technetium-99m SNS/S mixed ligand complexes: a proposed mechanism of brain retention. *J. Med. Chem.* **42**, 1066-1075.
- [4] Neirinckx R. D., Burke J. F., Harrison R. C., Forster A. M., Andersen A. R. and Lassen N. (1988) The retention mechanism of technetium-99m HMPAO: intracellular reaction with glutathione. *J. Cereb. Blood Flow Metab.* **8**, 4-12.
- [5] Xue L. Y., Noujaim A. A., Sykes T. R., Woo T. K. and Wang X. B. (1997) Role of transchelation in the uptake of ^{99m}Tc-MAB in liver and kidney. *Q. J. Nucl. Med.* **41**, 10-18.
- [6] Nock B., Tsoukalas C., Maina T., Pirmettis I., Papadopoulos M., Spies H., Johannsen B. and Chiotellis E. (1997) Comparative stability versus cysteine of mixed ligand ^{99m}Tc complexes containing monothiols of different nucleophilicity. *Eur. J. Nucl. Med.* **24**, 179.
- [7] Seifert S., Pietzsch H.-J., Scheunemann M., Spies H., Syhre R. and Johannsen B. (1998) No carrier added preparations of "3+1" mixed-ligand ^{99m}Tc complexes. *Appl. Radiat. Isot.* **49**, 5-11.
- [8] Seifert S., Pietzsch H.-J., Scheunemann M., Spies H. and Johannsen B. (1997) Serotonin receptor-binding technetium and rhenium complexes. 17. Different routes of n.c.a. preparation of "3+1" ^{99m}Tc complexes. *Annual Report 1997*, Institute of Bioinorganic and Radiopharmaceutical Chemistry, FZR-200, pp. 10-13.
- [9] Berger R., Friebe M., Pietzsch H.-J., Scheunemann M., Noll B., Fietz T., Spies H. and Johannsen B. (1996) Lipophilicity and ionization properties of some amine bearing technetium and rhenium "3+1" mixed-ligand complexes with same ligand structure. *Annual Report 1996*, Institute of Bioinorganic and Radiopharmaceutical Chemistry, FZR-165, pp. 43-47.

47. Identification of the Transchelation Product of "3+1" Mixed-Ligand Technetium and Rhenium Complexes with Glutathione

A. Gupta, S. Seifert, R. Syhre, B. Johannsen

Introduction

The "3+1" mixed -ligand ^{99m}Tc complexes, developed for radiopharmaceutical application and proved to be stable in saline, phosphate buffer of pH 7.4 and in plasma, are shown to be subject to conversion with GSH into a more hydrophilic metabolite [3]. GSH, the most abundant sulphhydryl compound in tissues, is present in almost all animal cells investigated in relatively high concentrations (0.5 mM to 12 mM). It is quite reasonable to assume that the "3+1" mixed-ligand ^{99m}Tc complexes react with GSH in vivo and in vitro forming the complex shown in Fig. 1 [3]. For some complexes this reaction has been proven [6, 7].

To further support this explanation "3+1" mixed-ligand rhenium complexes as well as the ^{99m}Tc complexes with varied tridentate ligands and GSH for a monodentate ligand were synthesized and compared with the product resulting from GSH challenge experiments.

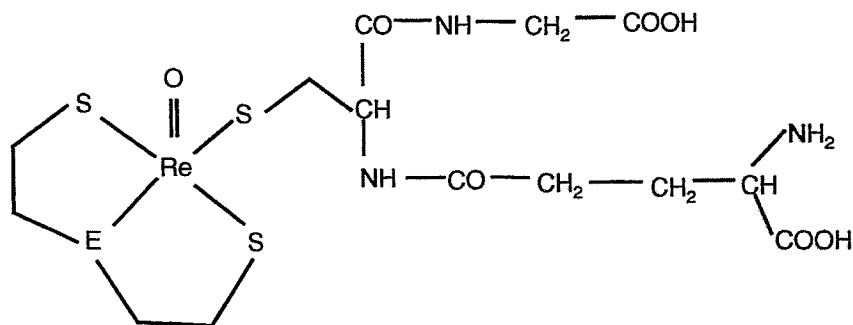


Fig. 1. General formula of the supposed transchelation product of the "3+1" mixed-ligand technetium or rhenium complexes (E = S or E = NMe) with glutathione

Experimental

Preparation of [ReO(SSS)(glutathione)]

An equimolar amount of glutathione (50.9 mg, 0.166 mmol) diluted with acetonitril/water (50/50) and 0.166 mmol triethylamine (21 μl) were added to a stirred and refluxed solution of chloro(3-thiapentane-1,5-dithiolato)oxorhenium(V) (65 mg, 0.166 mmol) in acetonitrile (10 ml)[4]. After a period of 60 minutes the reaction mixture was evaporated to dryness. The residue was again dissolved in a mixture of acetonitrile/water (50/50) and the soluble part separated from the insoluble residue. Then the solution was again evaporated to dryness and the residue washed with methanol. The residue was again dissolved in a mixture of acetonitrile / water and a solid reddish brown powder was formed by addition of diethyl ether.

Preparation of [ReO(SNMeS)(glutathione)]

The complex was prepared by ligand exchange, starting from the gluconate precursor (0.125 mmol) [5] by adding a fourfold molar excess of glutathione (150 mg, 0.5 mmol) dissolved in water. After the solution had turned from blue to red the tridentate ligand dissolved in water was added in a molar ratio of 1:1 (30.1 mg). After a period of 120 minutes the reaction mixture was evaporated to dryness. The residue was dissolved in water and purified by liquid chromatography over silica gel with a mixture of methanol/water (80/20). The green fraction was collected and again evaporated to dryness. To completely remove the glutathione excess the residue was again dissolved in water and purified by HPLC (semipreparative PRP-1 column, Hamilton, 305 x 7 mm, 10 μm , flow rate 2.0 ml/min using a linear gradient system (t[min]/%B): (5/20),(10/80), (10/80) of H₂O 0.1 % trifluoroacetic acid (A) and acetonitrile 0.1 % trifluoroacetic acid (B)). After purification the complex was precipitated as a green solid by slow evaporation of the mixture of methanol/diethylether.

Preparation of [ReO(SSS)(glutathione)] by GSH challenge of [ReO(SSS)(S-CH₂CH₂-N(CH₃)₂)]
100 mg of glutathione were added to 13 mg of (0.026 mmol) [ReO(SSS)(S-CH₂CH₂-N(CH₃)₂)] dissolved in water. After complete ligand exchange the glutathione excess was removed by HPLC as described above. After evaporation of the solvent the residue was dissolved in a mixture of acetonitrile/water and a solid reddish brown powder was formed by addition of diethyl ether.

Preparation of the n.c.a. complex [TcO(SSS)(Glutathione)]

The ^{99m}Tc complexes were prepared by direct reduction of pertechnetate with stannous chloride in an optimized mixture of amounts of the ligands and propylene glycol according to Seifert *et al.* [1, 2]. Approx. 150 - 200 MBq of the ^{99m}Tc pertechnetate eluate were added to 1 ml propylene glycol and filled up to 2 ml with a solution of 0.9 % sodium chloride. After mixing approx. 40 µg of the tridentate ligand diluted in acetone, 0.5 mg of glutathione (diluted in 100 µl H₂O), 100 µl 0.1N NaOH and 20 µl stannous chloride solution (1.0 - 2.0 mg SnCl₂ dissolved in 5 ml 0.1 N HCl) were added and the reaction mixture was heated at 50 °C for 20 minutes.

The complex were purified by HPLC as described above.

HPLC analysis of the Tc and Re complexes

HPLC analyses were carried out with a PRP-3 column (Hamilton, 150 x 4 mm, 10 µm, flow rate 1.0 ml/min) using a linear gradient system (t[*min*]/%B): (5/0), (5/70), (10/70) of 10 mM phosphate buffer of pH = 7.4 (A) and acetonitrile (B). The effluent from the column was monitored by γ-detection.

Infrared spectroscopy of the Re complexes

The complexes were compressed into KBr pellets and measured on a CARL ZEISS JENA infrared spectrometer against air.

Capillary electrophoresis and UV spectroscopy of the Re complexes

Capillary electrophoresis was performed using a HEWLETT PACKARD device equipped with a diode array UV detection system. The analysis was performed with a non-coated silica capillary (24.5 cm, ID 50 µm) in borate buffer (50 mM, pH 9.3).

¹H NMR

The complexes were recorded in DMSO-d₆ on an INOVA 400 spectrometer.

Fast atom bombardment mass spectrometry

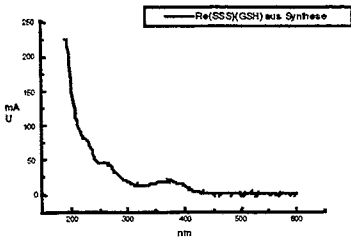
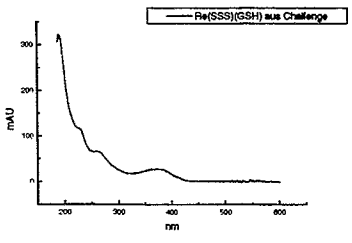
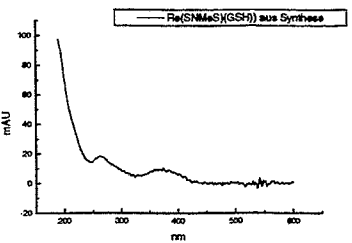
FAB⁺ mass spectra of the Re complexes were recorded with a MAT 95 spectrometer (Finnigan) by mixing 1 µl sample solution with 5 µl glycerol and bombarding it with caesium atoms of low energy of about 150 eV at room temperature.

Results and Discussion

The data in Table 1 show that the supposed challenge products with glutathione are available by a standard synthesis procedure for "3+1" mixed-ligand rhenium complexes. As shown for the SSS complex, the complex corresponds to the complex resulting from the glutathione challenge of other "3+1" rhenium complexes in terms of congruent UV, IR and NMR spectra.

The "3+1" ^{99m}Tc complex with GSH was also obtained by the standard n.c.a. synthesis procedure and was shown to have the same retention time in the HPLC analysis as the above-characterized rhenium complex as well as the product resulting from challenge experiments and the metabolite resulting from *in vitro* incubation of "3+1" ^{99m}Tc mixed-ligand complexes with whole blood. Furthermore, the ligand-exchange reaction leading to the GSH complex proved to be reversible. It was shown that after complete turnover of the parent compound into the challenge product it was possible to reconstitute the parent compound by an excess of the original monodentate ligand.

Table 1. Chemical data of the "3+1" mixed-ligand rhenium complexes containing glutathione as monodentate ligand

Re(SSS)(GSH) synthesis	Re(SSS)(GSH) challenge	Re(SNMeS)(GSH) synthesis
HPLC: $R_f = 4.67\text{min}$	$R_f = 4.61\text{min}$	$R_f = 4.58\text{min}$
HPCE: $R_f = 11.9\text{min}$	$R_f = 12.3\text{min}$	$R_f = 12.3\text{min}$
UV-spectra: 		
MS: 659(48), 660(5), 661(100)M+1, 662(10),663(11)	-----	679(46),680(13),681(100) M+Na, 682(27),683(15)
Elemental analysis: found: C,23.9 H,3.8 N,5.8 S,16.9 C ₁₄ H ₂₄ O ₇ ReS ₄ N ₃ ·2H ₂ O requires: C,24.1 H,3.9 N,6.0 S18.4	found: C,23.9 H,3.5 N,4.5 S,13.7 C ₁₄ H ₂₄ O ₇ ReS ₄ N ₃ ·x2TFA requires: C,24.3 H,2.95 N,4.7 S,14.4	found: C,26.4 H,4.5 N,7.6 S,13.2 C ₁₅ H ₂₇ O ₇ ReS ₃ N ₃ ·x2H ₂ O requires: C,26.0 H,4.36 N,8.0 S,13.8
red powder	red powder	green powder
IR: $\nu_{\text{max}}/\text{cm}^{-1}$ (KBr): 958.2(Re=O), 1522.4 (CO-NH), 1646.9 (CO-NH), 1724.4(COOH), 3290.6(NH), 3388 (OH)	$\nu_{\text{max}}/\text{cm}^{-1}$ (KBr): 961.6(Re=O), 1529.8 (CO-NH), 1648.6 (CO-NH), 1724.4(COOH), 3284.8NH), 3390 (OH)	$\nu_{\text{max}}/\text{cm}^{-1}$ (KBr): 952.4(Re=O), 1526.9 (CO-NH), 1650 (CO-NH), 1729.2(COOH), 3247.4(NH), 3391.7 (OH)
¹ H NMR in DMSO-D ₆ [δ]: signals of tridentate: 2.25(2H), 3.02(2H),4.05(2H), 4.29(2H) signals of monodentate: 1.80/1.89 (2H), 2.31(2H) 3.68(4H), 4.54(1H) 8.34(1H), 8.59(1H)	signals of tridentate: 2.23(2H), 3.02(2H),4.04(2H), 4.29(2H) signals of monodentate: 1.95(2H), 2.32(2H), 3.73(4H), 4.59(1H) 8.34(2H),	signals of tridentate: 2.59(2H), 3.53(2H),3.18(xH), 3.24(CH ₃) signals of monodentate: 1.82,1.90 (2H), 2.29(2H), 3.67(4H), 4.51(1H), 8.31(1H), 8.46(1H)

For solubility or synthetic reasons the complexes contain either 2 mole water or trifluoroacetic acid as shown by ¹H, ¹³C and ¹⁹F NMR.

The trifluoroacetic acid results from HPLC purification.

The results show that the reaction of the "3+1" mixed-ligand rhenium complexes with GSH as well as direct synthesis lead to a "3+1" mixed-ligand rhenium complex with GSH as a monodentate ligand. The formation of a metabolite of the same structure can therefore be assumed for "3+1" mixed-ligand ^{99m}Tc complexes in vivo as well as in challenge experiments with GSH.

References

- [1] Seifert S., Pietzsch H.-J., Scheunemann M., Spies H., Syhre R. and Johannsen B. (1998) No carrier added preparations of "3+1" mixed-ligand ^{99m}Tc complexes. *Appl. Radiat. Isot.* **49**, 5-11.
- [2] Seifert S. Pietzsch H.-J., Scheunemann M., Spies H. and Johannsen B. (1997) Serotonin receptor-binding technetium and rhenium complexes. 17. Different routes of n.c.a. preparation of "3+1" ^{99m}Tc complexes. *Annual Report 1997*, Institute of Bioinorganic and Radiopharmaceutical Chemistry, FZR-200, pp. 10-13.
- [3] Syhre R., Seifert S., Spies H., Gupta A. and Johannsen B. (1998) Stability versus reactivity of "3+1" mixed-ligand technetium-99m complexes in vitro and in vivo. *Eur. J. Nucl. Med.* **25**, 793-796.
- [4] Fietz Th.(1996) Oxorhenium(V)-Komplexe mit „3+1“ Gemischtligandkoordination. Dissertation
- [5] Noll B., Kniess T., Friebe M., Spies H. and Johannsen B. (1996) Rhenium(V) gluconate - a suitable precursor for the preparation of rhenium(V) complexes. *Isotopes Environ. Health Stud.* **32**, 21-29.
- [6] Pelecanou M., Pirmettis I. C., Nock B. A., Papadopoulos M., Chiotellis E. and Stassinopoulou C. I. (1998) Interaction of $[\text{ReO}(\text{SNS})(\text{S})]$ and $[\text{}^{99m}\text{Tc}(\text{SNS})(\text{S})]$ mixed ligand complexes with glutathione: isolation and characterization of the product. *Inorg. Chim. Acta* **281**, 148-152.
- [7] Nock B. A., Maina T., Yannoukakos D., Ioannis C., Papadopoulos M. and Chiotellis E. (1999) Glutathione-mediated metabolism of technetium-99m SNS/S mixed ligand complexes: a proposed mechanism of brain retention. *J. Med. Chem.* **42**, 1066-1075.

48. Stability of "3+1" Mixed-Ligand ^{99m}Tc Complexes In Vitro: Inhibition of the GSH in the Blood Results in a Stabilization of the Complexes In Vitro

A. Gupta, S. Seifert, R. Syhre, B. Johannsen

Introduction

When the "3+1" mixed-ligand ^{99m}Tc complexes are incubated in blood, they are converted into hydrophilic products. If the tridentate ligand is SNMeS, only one product occurs, but with SSS as the tridentate ligand two products are found. Glutathione (GSH) is responsible for this conversion [1]. In challenge experiments of the "3+1" mixed-ligand ^{99m}Tc complexes against GSH, a relationship between the complex stability and the structure of the tridentate or monodentate ligand is elucidated. The supposed challenge products were synthesized with Re and chemically characterized (see previous reports).

Here we report on the incubation studies performed to elucidate the influence of the structure of the monodentate ligand on the in vitro stability of the complexes. Further we give a detailed description of the inhibition experiments performed to support the GSH hypothesis.

Table 1. General formula and numbering scheme of the "3+1" mixed-ligand ^{99m}Tc complexes

General formula	R-SH	E = S	E = NMe
		1a	1b
		2a	2b
 E = S, NMe		3a	3b
		4a	4b
		5a	5b
		6a	6b

Experimental

Preparation of complexes

The ^{99m}Tc complexes were prepared by direct reduction of pertechnetate with stannous chloride in an optimized mixture of ligand amounts and propylene glycol according to Seifert *et al.* [2, 3].

Approx. 150 – 200 MBq of [^{99m}Tc]pertechnetate were added to 1 ml propylene glycol and filled up to 2 ml with a solution of 0.9 % sodium chloride. After mixing approx. 40 μg of the tridentate ligand (diluted with acetone or methanol), 0.5 mg of the monodentate ligand (diluted with 100 μl H_2O), 100 μl 0.1 N NaOH and 20 μl stannous chloride solution (1.0 – 2.0 mg SnCl_2 dissolved in 5 ml 0.1 N HCl) were added and the reaction mixture was heated at 50 $^\circ\text{C}$ for 20 minutes.

The complexes were purified by HPLC with a semi-preparative PRP-1 column (Hamilton, 305 x 7 mm, 10 μm , flow rate 2.0 ml/min), using a linear gradient system (t[min]/%B): (5/30), (10/80), (10/80) of H_2O 0.1 % trifluoroacetic acid (A) and acetonitrile 0.1 % trifluoroacetic acid (B). The effluent from the column was monitored by γ -detection and UV detection. After adding 200 μl propylene glycol and removing acetonitrile by vacuum evaporation, the separated neutralized complex fraction was stable for more than 8h.

GSH inhibition

For GSH-depletion experiments the whole blood was incubated with 2 % diethylmaleate (DEM) for 1 h before the complex was added [4, 5]. After that time it was shown that the GSH content of the blood had decreased under the detection limit.

GSH determination

The GSH determination in whole blood was performed according to the procedure of Coutelle *et al.* [6, 7, 8]. 50 μl of blood were haemolysed by addition of 100 μl of water and deproteinized by further addition of 50 μl metaphosphoric acid. After centrifugation for 5 min (10000g) the supernatant solution (125 μl) was diluted with 375 μl of buffer (phosphate buffer 0.05 M, EDTA 0.005 M pH = 7.4). This solution was analysed for GSH and GSSG, using the DTNB-GSSG reductase recycling procedure first reported by Owens and Belcher [9] and later modified by Tietze [10] and Griffith [11].

In vitro studies

About 5 - 7 MBq of the ^{99m}Tc complexes in 0.1 M phosphate buffer pH = 7.4 / 20 % propylene glycol were incubated in 500 μl of whole blood or plasma at 37 $^\circ\text{C}$. After the incubation time the blood is centrifuged and the supernatant plasma was analysed by HPLC.

HPLC analyses

HPLC analyses were carried out with a PRP-3 column (Hamilton, 150 x 4 mm, 10 μm , flow rate 1.0 ml/min) using a linear gradient system (t[min]/%B): (5/0), (5/70), (10/70) of 10mM phosphate buffer of pH = 7.4 (A) and acetonitrile (B). The effluent from the column was monitored by γ -detection.

Results and Discussion

In vitro stability of the complexes in blood

For all complexes with the E = S tridentate ligand, no parent compound was detectable in the plasma part of whole blood after 1 - 2 minutes. It was therefore not possible to observe differences between the used monodentate ligands for this class of complexes. On the other hand these complexes as well as their metabolites show a tendency to label protein components of the plasma so that more than one metabolite peak occurs in the chromatogram. Generally about 40 – 50 % of the activity in the blood sample are found in the plasma fraction.

By contrast incubation in the blood of complexes with the E = NMe tridentate ligand results in only one conversion product with the same retention time as the challenge product. The conversion is also much slower than that of complexes with the E = S tridentate ligand, so that it was possible to observe the time course for these complexes.

Concerning the influence of the monodentate ligand on the stability of the complexes in vitro incubation in whole blood shows a similar tendency as the GSH challenge assays (see previous reports). That means that complexes with nitrogen in the side chain of the monodentate ligand are less stable than those with an aromatic or aliphatic monodentate ligand (**1b**, **2b**). In the challenge experiments as also in vitro the complex with dimethylcystamine as a monodentate ligand is the compound that is converted the fastest. There are minor differences in the time courses of the complexes **6b**, **4b** and **5b** com-

pared with the challenge experiments. As reasons for these differences in the whole blood, interaction with proteins and the various modes of transport of the complexes and their conversion products through the membrane of the erythrocytes may be assumed.

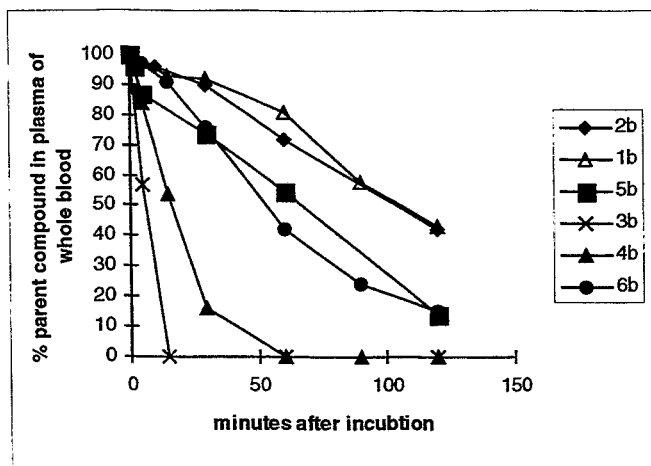


Fig. 1. Portion of parent complex of Tc species in plasma at various incubation time

Depletion of GSH in whole the blood

For the complexes **5a** and **4b** it could be shown that the depletion of GSH with DEM in the whole blood leads to a stabilization of the complex against conversion in the blood (Fig. 2). For control a blood sample was preincubated at room temperature without diethylmaleate (DEM) for the same period of time as the sample with DEM. After preincubation the ^{99m}Tc "3+1" complex was added. It was shown that after standing for about 4 h at 25 °C the GSH concentration in the blood was still 1.0 mM, whereas after 4 h incubation with DEM no GSH was detectable. In another control experiment it was also shown that there is no reaction between our complexes and DEM (Fig. 2B). In Fig. 2D it is shown that in the whole rat blood preincubated for 4 h at 25 °C without DEM the complex **4b** is converted into one more hydrophilic metabolite while no conversion occurs in the blood sample preincubated for the same period of time with DEM (Fig. 2C).

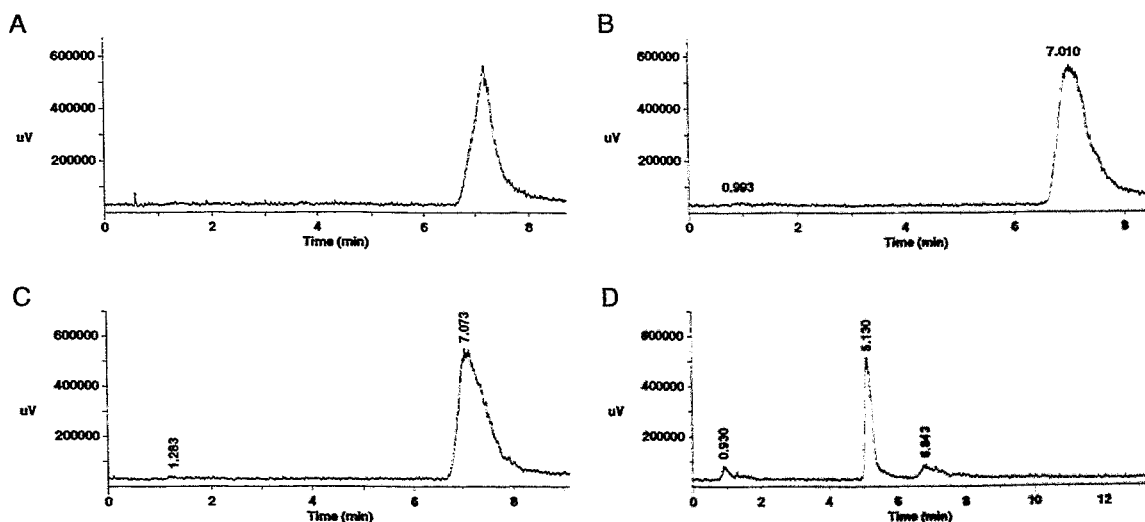


Fig 2. HPLC patterns of compound **4b**. A. parent compound, B. after 60minutes incubation in rat plasma containing 2 % DEM, C. plasma part of whole blood after 30 minutes incubation in the whole blood containing 2 % DEM, D. plasma part of whole blood after 30 minutes incubation in the whole blood.

These results support the assumption that GSH is the converting agent in whole blood and is responsible for the instability of the "3+1" mixed-ligand complexes in vitro. The principle of the in vitro conversion seems to be similar to that of the GSH challenge experiments.

References

- [1] Syhre R., Seifert S., Spies H., Gupta A. and Johannsen B. (1998) Stability versus reactivity of "3+1" mixed-ligand technetium-99m complexes in vitro and in vivo. *Eur. J. Nucl. Med.* **25**, 793-796.
- [2] Seifert S., Pietzsch H.-J., Scheunemann M., Spies H., Syhre R. and Johannsen B. (1998) No carrier added preparations of "3+1" mixed-ligand ^{99m}Tc complexes. *Appl. Radiat. Isot.* **49**, 5-11.
- [3] Seifert S., Pietzsch H.-J., Scheunemann M., Spies H. and Johannsen B. (1997) Serotonin receptor-binding technetium and rhenium complexes. 17. Different routes of nca preparation of "3+1" ^{99m}Tc complexes. *Annual Report 1997*, Institute of Bioinorganic and Radiopharmaceutical Chemistry, FZR-200, pp. 10-13.
- [4] Neirinckx R. D., Burke J. F., Harrison R. C., Forster A. M., Andersen A. R. and Lassen N. (1988) The retention mechanism of technetium-99m HMPAO: intracellular reaction with glutathione. *J. Cereb. Blood Flow Metab.* **8**, 4-12.
- [5] Ecobichon D. J. (1984) Glutathione depletion and resynthesis in laboratory animals. *Drug. Chem. Toxicol.* **7**, 345-355.
- [6] Anderson M. E. (1985) Determination of glutathione and glutathione disulphide. *Methods Enzymol.* **113**, 548-555.
- [7] Coutelle C. (1992) Optimisation du dosage spectrophotométrique du glutathion sanguin total et oxydé: comparaison avec une méthode fluorimétrique. *Ann. Biol. Clin.* **50**, 71-76.
- [8] Ellman G. L. (1959) Tissue sulfhydryl groups. *Arch. Biochem. Biophys.* **82**, 70-77.
- [9] Owens C. W. I. and Belcher R. V. (1965) A colorimetric micromethod for determination of glutathione. *J. Biochem.* **94**, 705.
- [10] Tietze F. (1969) Enzymic method for quantitative determination of nanogramme amounts of total and oxidized glutathione: application to mammalian blood and other tissues. *Anal. Biochem.* **27**, 502.
- [11] Griffith O. W. (1980) Determination of glutathione and glutathione disulfide using glutathione reductase and vinyl-2-pyridine. *Anal. Biochem.* **106**, 207.

49. Reactivity of "3+1" ^{99m}Tc Complexes to Proteins

S. Seifert, A. Gupta, R. Syhre

Introduction

Mixed-ligand 3+1 complexes containing a tridentate dithiol and a monothiol exhibit reactivity towards thiols. Ligand exchange with glutathione (GSH) is considered to be the main reason for the observed instability of the complexes in blood [1, 2]. *In vitro* and *in vivo* studies of 3+1 ^{99m}Tc complexes have shown that structural differences of the tridentate ligand as well as the monothiolato ligand influence the stability of these complexes in the blood and in the plasma. It was found that complexes with an S(NR)S configuration (R = Me, Et, Pr) of the tridentate ligand are much more stable than complexes with an SSS moiety [3]. Moreover, the stability of the complexes decreases when the monodentate ligand contains an amino nitrogen in its side chain. Another important parameter for the stability of these complexes with nitrogen in the side chain of the monothiolato ligand is the number of C atoms between the SH group and the nitrogen atom [4]. On the basis of systematic stability studies performed with a number of 3+1 complexes possibilities of labelling SH-containing components of the blood with ^{99m}Tc were investigated.

Experimental

Preparation of complexes. The ^{99m}Tc complexes were prepared by direct reduction of pertechnetate with stannous chloride in an optimized mixture of ligand amounts and propylene glycol (PG) and purified by HPLC [5, 6].

HPLC analyses. HPLC analyses were carried out with a PRP-3 column (Hamilton, 150 x 4 mm, 10 μm , flow rate 1.0 ml/min) using a linear gradient system [t(min)/%B]: (5/0), (10/70), (5/70) of 10 mM phosphate buffer (PBS) of pH 7.4 (A) and acetonitrile (B). For plasma and blood analyses a Supelguard column (20 x 4.6 mm, 10 μm , flow rate 1.0 ml/min) was used with a linear gradient of 95 % A to 40 % A in 15 min [A: isopropanol/0.1 % TFA (10/90), B: isopropanol/0.1 % TFA (90/10)].

***In vitro* studies.** HPLC-purified ^{99m}Tc complexes were dissolved in 0.1 M PBS of pH 7.4 containing 15 % PG. *In vitro* incubation at 37° C was carried out in a thermoshaker for various lengths of time. 500 μl samples of 0.1 M PBS, pH 7.4 containing the ^{99m}Tc complex and 2 – 3 mg rat or human albumin or globulin were used. For incubation in rat or human plasma, 50 - 100 μl of the ^{99m}Tc complex solution (5 - 10 MBq) were added to a suspension of pre-washed erythrocytes as well as to heparinized whole blood. The reactions were stopped in an ice bath and the reaction products analysed by HPLC.

Results and Discussion

For all tested complexes a correlation was visible between the stability to GSH and the *in vitro* stability in plasma and blood. All complexes shown in Fig. 1 are unstable in the whole blood of rats and humans.

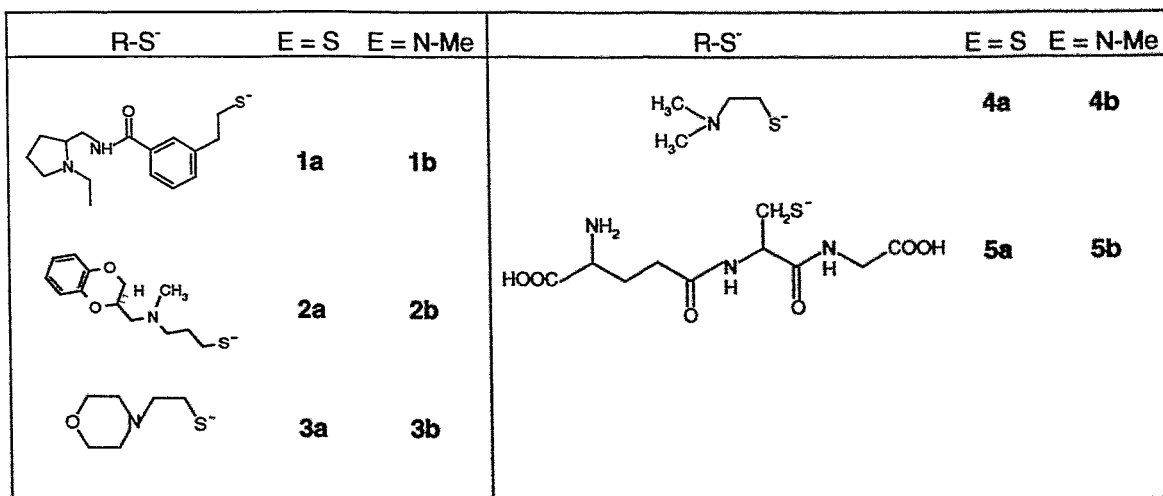


Fig. 1. 3+1 mixed-ligand [$^{99m}\text{TcO}(\text{SES}/\text{RS})$] complexes 1 – 5 used for stability and reactivity studies

In accordance with their high glutathione content, these solutions undergo, at various rates, a ligand-exchange reaction with GSH to yield the $[^{99m}\text{TcO}(\text{SES}/\text{GS})]$ complex. While most of the investigated complexes are stable in plasma, the complexes **4a** and **5a** are converted.

The following HPLC analyses were performed with a Supelguard column, which is recommended for the separation of proteins. The retention times of the ^{99m}Tc complexes **1** – **5** are shorter than those of the reaction products with plasma and blood proteins, which are eluted at the same times as the main components of the plasma (albumin and globulin) and blood (R_t values between 8 and 13 minutes).

Incubation with plasma, albumin and globulin:

The more stable complexes **1** – **3**, **4b** and **5b** do not undergo further reaction with plasma components (Fig. 2). However, complexes **4a** and **5a** react with albumin and one of the globulin fractions of the plasma (Fig. 3). It is remarkable that other plasma proteins eluted at 10 and 11 minutes are not labelled.

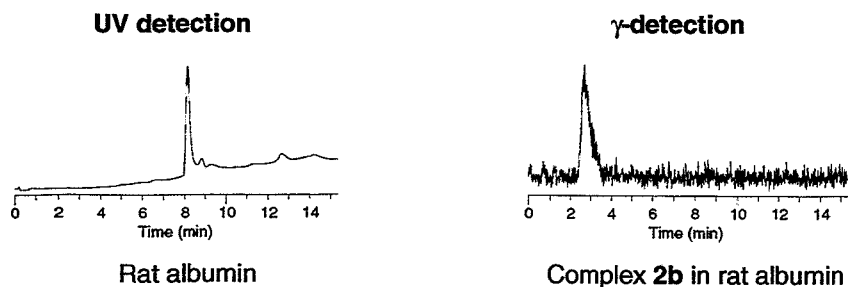


Fig. 2. HPLC patterns of the incubation of complex **2b** with a 3 % rat albumin solution

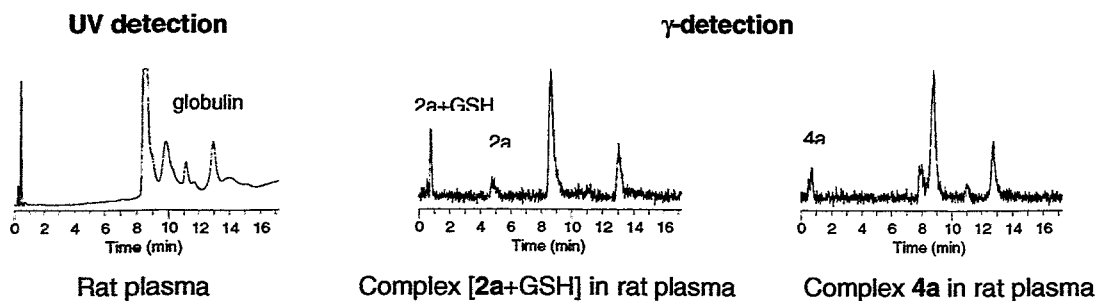


Fig. 3. HPLC analyses of incubation samples of the complexes **4a** and **5a** with rat plasma. Complex **5a** was prepared in a challenge experiment of **2a** with GSH; incubation time 30 minutes.

The reaction is reversible. Adding an excess of another monothiol R-SH to the plasma solution results in the formation of the 3+1 complex with this monothiol (Fig. 4). The final product is eluted in the same retention time of 5.5 min as the complementary rhenium complex $[\text{ReO}(\text{SSS}/\text{RS})]$.



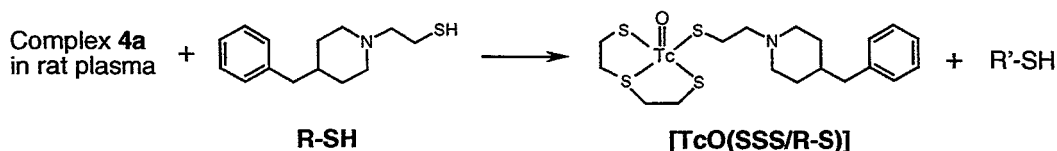
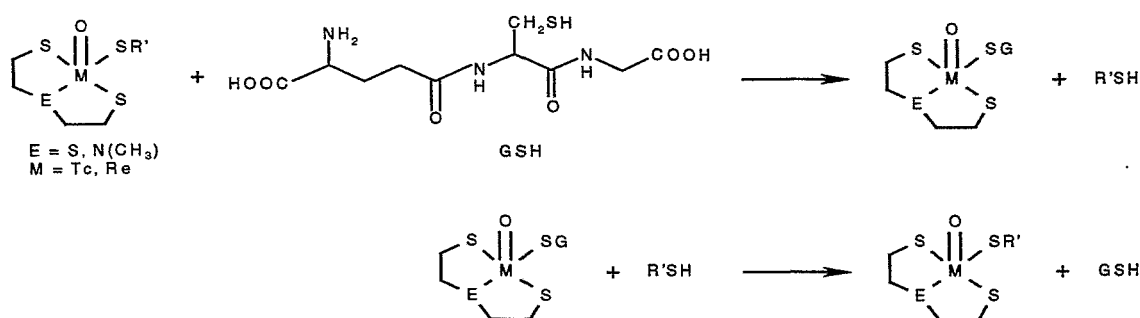


Fig. 4. Reaction of labelled albumin and globulin fractions with the monothiol R-SH yielding the 3+1 complex [$^{99m}\text{TcO}(\text{SSS/RS})$]

The same reversibility was found for the ligand-exchange reaction with GSH (Scheme 1). The original 3+1 complex reacts with an excess of GSH to yield the 3+1 $\text{TcO}(\text{SES/GS})$ complex. The reaction product can be re-converted by adding a higher excess of the original mercaptide ligand [7]. An equilibrium reaction obviously exists, depending on the concentration of monodentate ligand in the reaction solution.

Scheme 1.



The example shows that SH-containing peptides are also able to substitute the mercaptide ligand in the 3+1 complex.

Albumin from bovine serum was also successfully labelled in this way. The labelling with complex **4a** failed when rat plasma was inhibited by adding diethylmaleate (DEM) to the incubation solution.

It is concluded that the unstable 3+1 complexes **4a** and **5a** can also form 3+1 complexes with proteins such as albumin or globulin. The proteins containing at least one free SH-group react as monodentate thiol ligands, substituting the dimethylcysteamine or glutathione ligand in the original complexes.

Incubation with rat blood

The incubation of complex **2b** with the whole blood of rats results in the labelling of an unknown component of the blood which is eluted in HPLC after 10.4 minutes (Fig. 5). After centrifugation most of the radioactivity remains in the erythrocytes as an unchanged complex **2b** [8].

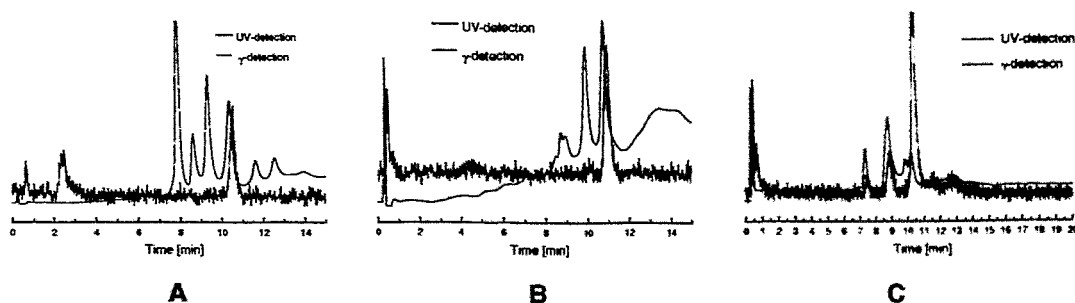


Fig. 5. Reactions of the complexes **2a** and **2b** with rat blood and pre-washed erythrocytes.
A: **2b** in rat blood (supernatant), **B:** **2a** in a suspension of erythrocytes,
C: **2a** in rat blood (supernatant); 30 min incubation time

The presence of the free complex **2b** in the incubation solution, which is eluted after 2.5 minutes, confirms the higher stability of that type of complex. Only traces of the metabolization product [$^{99m}\text{TcO}(\text{SNMeS}/\text{GS})$] (**5b**) are found ($R_t = 0.7$ min). It seems that primarily the [$^{99m}\text{TcO}(\text{SNMeS}/\text{GS})$] complex is formed, which immediately undergoes a ligand-exchange reaction with one of the components of the blood ($R_t = 10.4$ min) in a secondary step. The albumin and globulin fractions as well as a third component ($R_t = 9.4$ min) are not labelled. Complex **2a**, however, reacts with albumin and globulin after metabolization by GSH.

When complex **2a** is incubated with a suspension of pre-washed red blood cells, the same component is labelled as in the whole blood. No free complex **2a** is found in this solution. It is obviously completely converted into complex **5a**, which reacts with the unknown component. As observed for complex **2b** in the whole blood, the component with $R_t = 9.4$ min is not labelled.

In both cases the incubation solutions are red. Perhaps a protein released by haemolysis is labelled and serves as the monodentate ligand in the 3+1 complex formed.

Conclusions

- Some of our 3+1 ^{99m}Tc complexes can react with the plasma and blood proteins which replace the monodentate ligand in the complexes.
- The reversibility of the reaction confirms that only the monothiol ligand is exchanged.
- All investigated 3+1 complexes are metabolized in the whole blood *in vitro* and *in vivo* into GSH-containing complexes which are able to label a protein component of the blood.
- While the [$^{99m}\text{TcO}(\text{SNMeS}/\text{GS})$] complex is stable in rat and human plasma, the more unstable [$^{99m}\text{TcO}(\text{SSS}/\text{GS})$] complex **5a** as well as the [$^{99m}\text{TcO}(\text{SSS}/\text{DMCA})$] complex **4a** react with albumin and globulin.
- The usefulness of this new labelling procedure for proteins and peptides should be examined.

References

- [1] Syhre R., Berger R., Brust P., Pietzsch H.-J., Seifert S., Scheunemann M., Spies H. and Johannsen B. (1997) Structural modification of the tridentate ligand of n.c.a. "3+1"oxotech-netium(V) mixed-ligand technetium-99m complexes and their effects on the distribution and retention behaviour in rats. *Annual Report 1997*, Institute of Bioinorganic and Radiopharmaceutical Chemistry, FZR-200, pp. 58-60.
- [2] Pelecanou M., Pirmettis I. C., Nock B. A., Papadopoulos M., Chiotellis E. and Stassinopoulou C. I. (1998) Interaction of [$\text{ReO}(\text{SNS})(\text{S})$] and [$^{99m}\text{TcO}(\text{SNS})(\text{S})$] mixed ligand complexes with glutathione: isolation and characterization of the product. *Inorg. Chim. Acta* **281**, 148-152.
- [3] Syhre R., Seifert S., Spies H., Gupta A. and Johannsen B. (1998) Stability versus reactivity of "3+1" mixed-ligand technetium-99m complexes *in vitro* and *in vivo*. *Eur. J. Nucl. Med.* **25**, 793-796.
- [4] Gupta A., Seifert S., Syhre R. and Johannsen B. (1999) Challenge experiments with "3+1" mixed-ligand ^{99m}Tc complexes and glutathione: influence of structural parameters on the complex stability. *This report*, pp. 165-170.
- [5] Seifert S., Pietzsch H.-J., Scheunemann M., Spies H., Syhre R. and Johannsen B. (1998) No carrier added preparations of "3+1" mixed-ligand ^{99m}Tc complexes. *Appl. Radiat. Isot.* **49**, 5-11.
- [6] Seifert S., Pietzsch H.-J., Scheunemann M., Spies H. and Johannsen B. (1997) Serotonin receptor-binding technetium and rhenium complexes. 17. Different routes of n.c.a. preparation of "3+1" ^{99m}Tc complexes. *Annual Report 1997*, Institute of Bioinorganic and Radiopharmaceutical Chemistry, FZR-200, pp. 10-13.
- [7] Gupta A., Seifert S., Syhre R. and Johannsen B. (1999) Identification of the transchelation product of "3+1" mixed-ligand technetium and rhenium complexes with glutathione. *This report*, pp. 171-174.
- [8] unpublished data.

50. An Effective Pre-Labeling Method for Amino Acids with Activated $^{99m}\text{Tc-MAG}_3$ in Aqueous Solution

T. Knieß, St. Noll, B. Noll, H. Spies

Introduction

Mercaptoacetyltriglycine (MAG_3) as an excellent ^{99m}Tc chelator has suitable properties for being used as a bifunctional chelating agent (BFCA) since its carboxylic group is not necessary for complexation and is therefore available for coupling with biomolecules. Some time ago we described a new pre-labelling method for coupling Re- and Tc- MAG_3 complexes to amines and nucleobases using O-(benzotriazol-1-yl)-N,N,N',N'-tetramethyl-uronium-tetrafluoroborate (TBTU) [1]. However, as this procedure is limited to aprotic solvents we looked for a pre-labelling procedure with $^{99m}\text{Tc-MAG}_3$ in aqueous media that can be applied to water-soluble compounds such as amino acids, peptides and oligonucleotides. Only a few papers are known on this topic where the $^{99m}\text{Tc-MAG}_3$ complex was coupled to biomolecules when the method suffered from low yields [2, 3, 4]. Here we describe a pre-labelling method that makes use of a $^{99m}\text{Tc-MAG}_3$ -activated ester for coupling to amino acids, esters and also a fatty acid in aqueous solution in good yields.

Experimental

General

HPLC investigations were carried out with a VYDAC C18 column, using a gradient of 0.01 M phosphate buffer pH = 6.0 / acetonitrile at a flow rate of 1.0 ml/min. The ^{99m}Tc compounds were determined by γ -detection, impurities such as unreacted 2,3,5,6-tetrafluorophenol were detected by UV absorbance at 230 nm. The purification of the intermediates was performed with cartridges for solid phase extraction RP 18 (LiChrolut, MERCK).

Labelling of $^{99m}\text{Tc-MAG}_3$ and coupling to amino acids and amino esters (general procedure)

103 MBq $^{99m}\text{TcO}_4^-$ generator eluate diluted with 2.0 ml water was added to a commercial MAG_3 kit. After 30 minutes the solution was acidified with 100 μl 1.0 M HCl and the mixture was eluted on an activated RP 18 cartridge. The pure $^{99m}\text{Tc-MAG}_3$ fraction was re-eluted with 800 μl acetonitrile. 20 mg 2,3,5,6-tetrafluorophenol dissolved in 50 ml acetonitrile and 50 mg N'-(3-dimethyl-aminopropyl)-N-ethylcarbodiimide hydrochloride (EDC) dissolved in 100 μl 90 % acetonitrile were added to this solution. After 30 minutes the mixture was diluted with 5.0 ml water and the active ester was separated by elution through an RP 18 cartridge. After washing with diethyl ether the product was removed from the cartridge with acetonitrile. The organic layer was removed in a stream of nitrogen and the residue was dissolved in 1.0 ml water. 4.0 mg of amino acid (amino ester) in 500 μl phosphate buffer pH = 9.2 was added to this solution and after 30 minutes the product was purified by HPLC. The total reaction time was 2 hours and the product had an activity of 51 MBq (overall yield: 49 %).

Results and Discussion

The pre-labelling with $^{99m}\text{Tc-MAG}_3$ in aqueous solution was carried out in the order described in Figure 1. As a first step the activated ester of $^{99m}\text{Tc-MAG}_3$ was synthesized by reaction of the complex with 2,3,5,6-tetrafluorophenol in 90 % acetonitrile. Because both tetrafluorophenol and the coupling reagent EDC were used in great excess over the Tc complex, the product had to be separated by solid-phase extraction and the unreacted tetrafluorophenylester removed by washing with diethyl ether. In a second step the active ester was reacted with the amino acid in alkaline solution where the active ester bond was cleaved and the coupling to the amino group occurred.

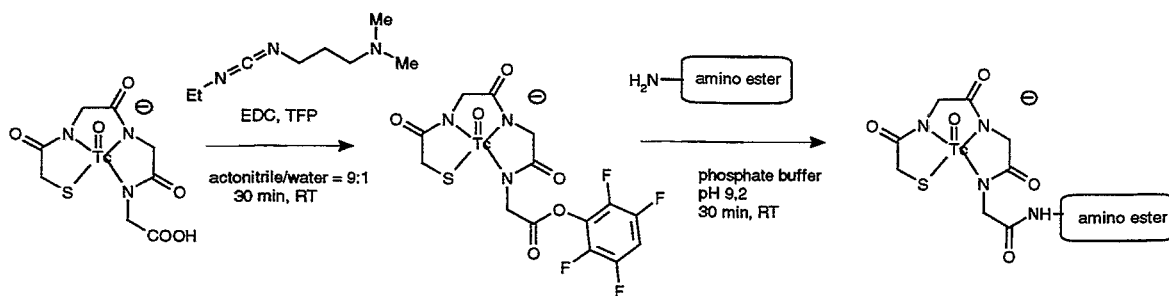


Fig.1. Course of the coupling reaction of $^{99m}\text{Tc-MAG}_3$ with amino acids and esters

The reaction steps and the purity of all intermediates were checked by HPLC. Figure 2 shows the radiochromatograms of the coupling to diglycine ethyl ester, starting from pure $^{99m}\text{Tc-MAG}_3$ (Fig.2a), the conversion into $^{99m}\text{Tc-MAG}_3$ -tetrafluorophenyl ester (Fig.2b) and the final product $^{99m}\text{Tc-MAG}_3$ diglycine ethyl ester (Fig.2c). It is remarkable that no by-products are observed and the reactions are fully completed. The chromatogram of the $^{99m}\text{Tc-MAG}_3$ diglycine ethyl ester detected by UV adsorbance is represented in Fig.2d, and some impurity by tetrafluorophenol with a retention time of 15.85 min is visible.

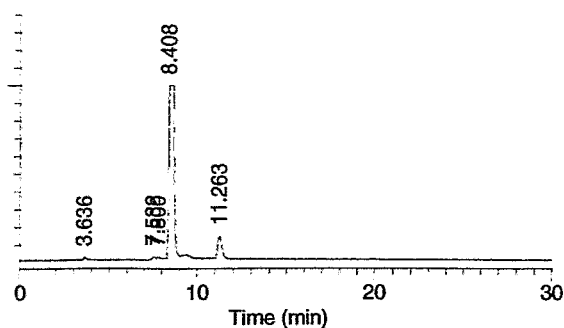


Fig. 2a. $^{99m}\text{Tc-MAG}_3$

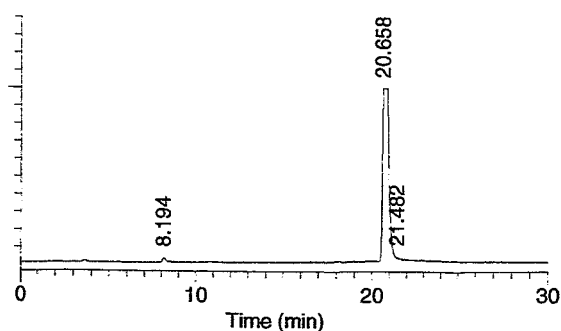


Fig. 2b. $^{99m}\text{Tc-MAG}_3$ tetrafluorophenyl ester

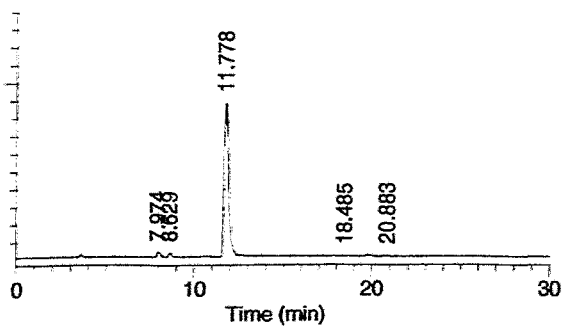


Fig. 2c. $^{99m}\text{Tc-MAG}_3$ diglycine ethyl ester (radiochromatogram)

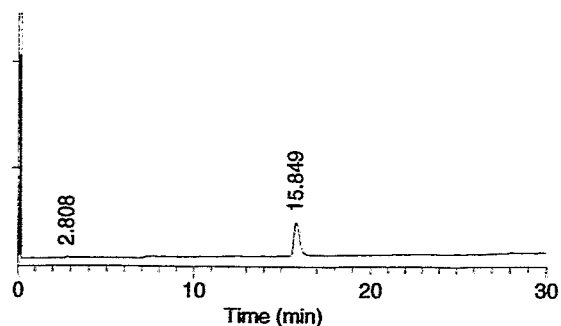


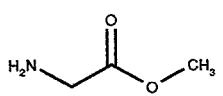
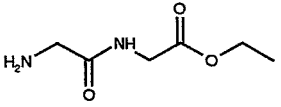
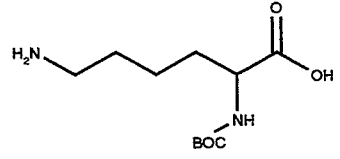
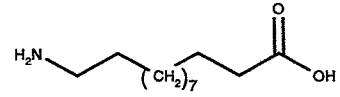
Fig. 2d. $^{99m}\text{Tc-MAG}_3$ diglycine ethyl ester (UV-chromatogram)

Fig. 2. HPLC analyses of the coupling of $^{99m}\text{Tc-MAG}_3$ to diglycine ethyl ester, (VYDAC C18, gradient 0.01 M phosphate buffer pH = 6.0 / acetonitrile, 1.0 ml/min)

Table 1 provides information on HPLC retention times and yields of products obtained by coupling some amino compounds to $^{99m}\text{Tc-MAG}_3$. The total yields were calculated by measuring the activity of the solution containing the product compared with the starting activity. The amino ester and the free amino acid N_α -BOC-lysine reacted with similar results, the reaction with the free fatty acid showed some impurities and a lower yield. Attempts of coupling nucleoside derivatives such as cytidine or cytidine monophosphate failed.

It can be summarized that the pre-labelling procedure is an advantageous method of coupling hydrophilic compounds such as amino acids or amino ester to $^{99m}\text{Tc-MAG}_3$ in aqueous solution. In the future this reaction is intended to be expanded to peptides and oligonucleotides.

Table 1. $^{99m}\text{Tc-MAG}_3$ coupled amino compounds, retention times and yields

Amino compound	Retention time	Total yield	
	glycine methyl ester	11.24 min	53 %
	diglycine ethyl ester	11.78 min	49 %
	N_α -BOC-lysine	11.32 min	51 %
	12-amino-laurinic acid	18.44 min	45 %

References

- [1] Kniess T., Noll St., Noll B. Spies H. and Johannsen B. (1998) Effective coupling of Re/Tc-MAG_3 complexes with amines and nucleobases in aprotic solvents. *J. Radioanal. Nucl. Chem.*, in press
- [2] Visser G. W. M., Gerretsen M., Herscheid J. D. M., Snow G. B. and van Dongen G. (1993) Labeling of monoclonal antibodies with Re-186 using the MAG_3 chelate for radioimmunotherapy of cancer, *J. Nucl. Med.* **34**, 1953-1963.
- [3] Verbeke K., Hjelstuen O., Debrock E., Cleynhens B. De Roo M. and Verbruggen A. (1995) Comparative evaluation of $^{99m}\text{Tc-HYNIC-HSA}$ and $^{99m}\text{Tc-MAG}_3\text{-HSA}$ as possible blood pool agents. *Nucl. Med. Commun.* **16**, 942-957.
- [4] Yoo T. M., Hye K., Chang C. W., Webber K. O., Le N., Kim I. S., Eckelman W. C., Pastan I., Carrasquillo J. A. and Paik C. H. (1997) Tc-^{99m} labeling and biodistribution of anti-TAC disulfide stabilized Fv fragment. *J. Nucl. Med.* **38**, 294-300.

51. ^{186}Re -Labelling of an Endothelin Derivative

B. Noll, L. Dinkelborg¹, H. Hilger¹
¹Schering AG

The radioactive isotopes of rhenium, ^{186}Re and ^{188}Re , are of interest in nuclear medicine for therapeutic use because of their nuclear properties. The labelling of peptides with Re-188 is described by several authors. Guhlke et al. explored a somatostatin analogue for its potential as a locally/regionally administered radiotherapeutic agent targeting somatostatin-receptor- positive tumours [1]. Savavy et al. describe the labelling of small molecule peptides (7-amino acid analogue of bombesin) with antagonistic activities as potential radiotherapeutic agents [2]. Tc-labelled endothelin derivatives were characterized for imaging experimentally induced atherosclerosis in vivo [3].

The aim of our work was to investigate the labelling of endothelin derivatives with rhenium-186/188 in analogy to technetium labelling. The compounds were labelled by means of $^{186}\text{Re(V)}$ gluconate [4]. To optimize the conditions experiments were carried out, including variation of the amounts of the reactants and the reaction time. In analogy to the ^{99}Tc labelling the ligand exchange reaction between the $^{186}\text{Re(V)}$ gluconate and the peptide Asp-Gly-Gly-Cys-Gly-CysPhe-(D-Trp)-Leu-Asp-Ile-Ile-Trp results in a product that contains two species, which are separable by HPLC [5].

Preparation and analysis

1.0 mg peptide is dissolved in 200 μl phosphate buffer solution pH 7.0 (SÖRENSEN) and stepwise added to the $^{186}\text{Re(V)}$ gluconate solution. After 45 min the reaction mixture is analysed by HPLC (Eurosphere RP 18, 250/4 mm, eluent A: 95 % 0.013 M phosphate buffer pH 7.4 / 5 % CH_3CN , eluent B: 25 % 0.013 M phosphate buffer pH 7.4 / 75 % CH_3CN , gradient elution: 5 min 80 % A, 5 min from 80 % A to 75 % A, 20 min 75 % A to 72 % A flow: 1 ml / min, 5 min 100 % B, flow 1.5 ml / min). For the semipreparative separation a sample volume of 200 μl was injected and the peak fractions were separated and frozen in a refrigerator to prevent the occurrence of perrhenate by radiolysis. The preparations took place under a nitrogen atmosphere, and a nitrogen stream was bubbled to all solutions. The HPLC analysis of the isolated isomers (complexes I and II) after 24 h storage at -20°C is shown in Fig. 1.

The reaction mixture was separated into ^{186}Re gluconate (R_t 2.0 min, about 10 %), $^{186}\text{ReO}_4^-$ (R_t 2.5 min, <5 %), ^{186}Re endothelin complex I (R_t 22.0 min, about 15 %), ^{186}Re endothelin complex II (R_t 25.0 min, about 25 %). The residual activity remained on the column under this separation conditions and was eluted with acetonitrile.

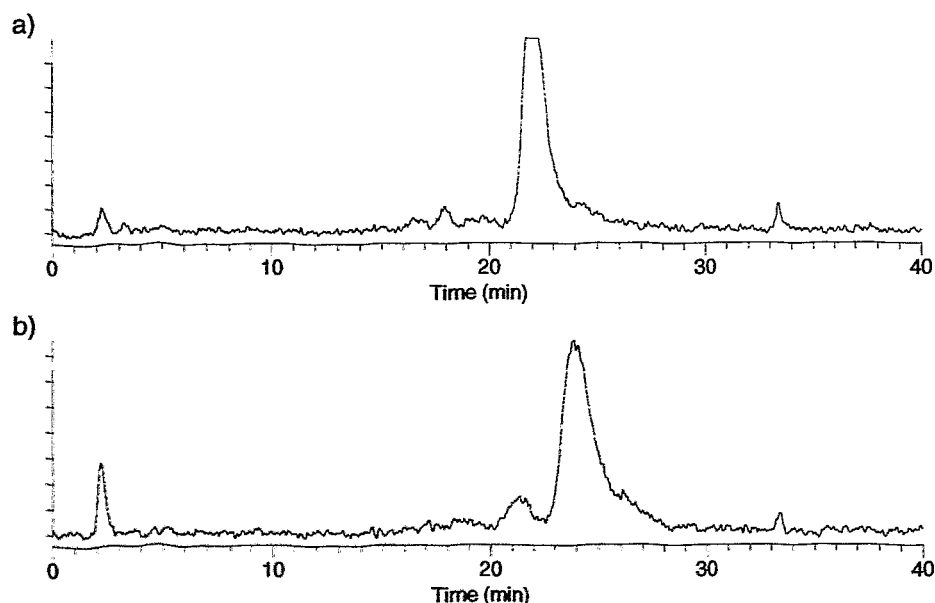


Fig. 1. The HPLC analysis of the separated fractions after 24 h storage at -20°C using a β -radioactivity detector. a) complex I, b) complex II

The stability of the ^{186}Re labelled endothelin to radiolytic effects is a prerequisite for the success of a possible therapeutical approach. The radiolysis was investigated without separating the ^{186}Re labelled endothelin into its isomers. The labelling preparation was separated from hydrophilic components on a solid-phase LiCrolut column (Merck, RP-18 endcapped / 200 mg). The high β -energy of the rhenium isotope initiated the radiolytic formation of perrhenate to up to 20 % within 5 h at room temperature. We found that storage in refrigerator at -20 or the addition of ascorbic acid to the preparations or the isolated fractions stabilize the ^{186}Re labelled endothelin complexes so that no radiolysis occurs. The ^{186}Re endothelin complexes were stable for over 24 h and useful for in vivo animal studies.

References

- [1] Guhlke S., Zamora P. O., Sartor J., Knapp F. F., Bender H., Rhodes B. A. and Biersack H. J. (1997) Ascorbic acid stabilization of Re-188- and I-131- radiolabeled peptides for radiotherapy. *Radiochim. Acta* **79**, 93-97.
- [2] Safavy A., Khazaeli M. B., Qin H. Y. and Buchsbaum D. J. (1997) Synthesis of bombesin analogues for radiolabeling with rhenium-188. *Cancer* **80**, 2354-2359.
- [3] Dinkelborg L. M., Duda S. H., Hanke H., Tepe G., Hilger C. S. and Semmler W. (1998) Molecular imaging of atherosclerosis using a technetium-99m-labeled endothelin derivative. *J. Nucl. Med.* **39**, 1819-22.
- [4] Noll B., Kniess T. and Spies H. (1996) Synthesis of ^{186}Re -Gluconate by stannous Chloride reduction of $^{186}\text{ReO}_4^-$. *Annual Report 1996*, Institute of Bioinorganic and Radiopharmaceutical Chemistry, FZR-165, pp. 106-107.
- [5] Johannsen B., Jankowsky R., Noll B., Spies H., Reich T., Nitsche H., Dinkelborg L. M. and Hilger C. S. (1997) Technetium coordination ability of cysteine-containing peptides: X-ray absorption spectroscopy of a Tc-99 labelled endothelin derivative. *Appl. Radiat. Isot.* **48**, 1045-1050.

52. Capillary Electrophoresis of ^{99m}Tc Radiopharmaceuticals: Quality Control and pK Determination at the Tracer Level

R. Jankowsky, B. Noll, H. Spies, B. Johannsen

Introduction

In radiopharmaceutical practice, quality control of radiotracers is of importance. Although the majority of analytical controls are done by thin-layer chromatography (TLC) and HPLC; the capillary electrophoresis (CE) as a micro-analytical technique becomes more and more relevant. Here we describe the construction of a γ -ray sensitive detector for CE and its usage for the quality control of the ^{99m}Tc radiopharmaceuticals ^{99m}Tc -MAG₃, ^{99m}Tc -DTPA, ^{99m}Tc -DMSA, ^{99m}Tc -HMPAO, ^{99m}Tc -EHIDA, ^{99m}Tc -MDP, ^{99m}Tc -EC, ^{99m}Tc -Q12, ^{99m}Tc -ECD and ^{99m}Tc -Tetrofosmin.

As a further application of CE, it can be used for the determination of pK values as important molecular parameters which decisively influence the biological behaviour of pharmaceuticals [1 - 3]. In the present work, we report on the pK determination of ^{99m}Tc -MAG₃ and ^{99m}Tc -EC using the radio-CE.

Experimental

For measurements, a $^{3\text{D}}$ CE device (Hewlett-Packard, Waldbronn, Germany) was used. It was equipped with a γ -ray sensitive flow detector consisting of a cylindric scintillation crystal. The schematic construction is given in Fig. 1.

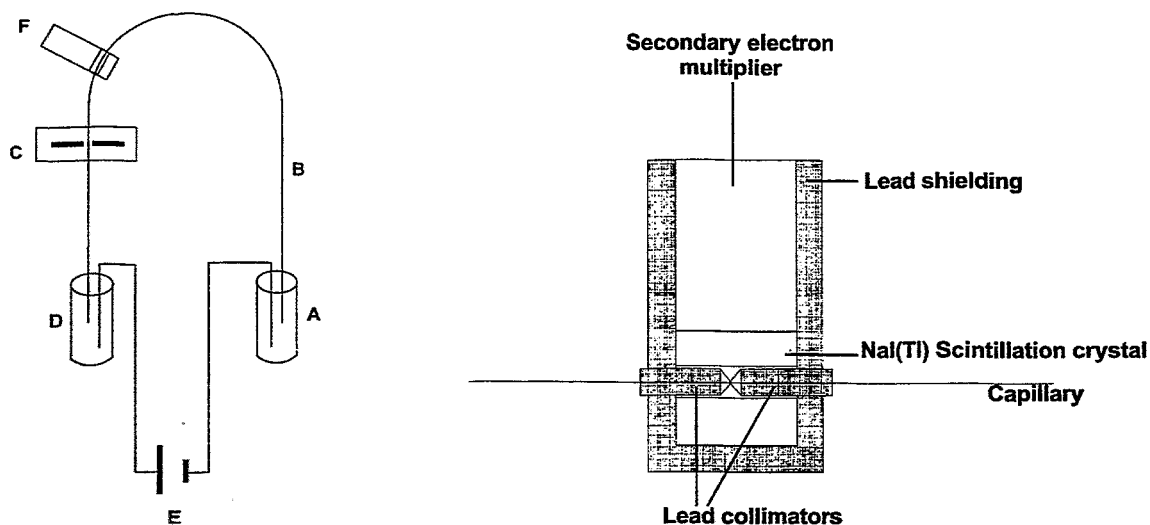


Fig. 1. Schematic construction of the CE radiodetector. Left sketch, arrangement of the detector at the CE device; A, capillary inlet; B, capillary; C, diode array detector; D, capillary outlet; E, high voltage supply; F, radioactivity detector. Right sketch, schematic construction of the detector.

^{99m}Tc radiopharmaceuticals were prepared according to instructions with $\text{Na}^{99m}\text{TcO}_4$ generator eluate or were purchased readily from the University Hospital of the Dresden University of Technology, respectively. For analytical CE runs, both conventional and pressure-modified capillary zone electrophoresis were used [4]. pK determinations of ^{99m}Tc -MAG₃ and ^{99m}Tc -EC were accomplished by measuring the relative electrophoretic mobility depending on the running buffer pH [5 - 8]. The mobilities were referred to the electrophoretic mobility of simultaneously measured internal standards [4].

Results and Discussion

Radioactivity detector. The constructed radioactivity detector showed linear response over a broad activity range and a low offset. The detection cell volume was determined to be 2.2 nl which ensures a high spatial resolution. However, due to the small detection cell volume, the detector possesses a rather low sensitivity. The lowest possible radioactivity amount is expected to be roughly 3 MBq ^{99m}Tc per 100 μl , depending on the amount of components in the sample.

Quality control. ^{99m}Tc -Tetrofosmin, ^{99m}Tc -Q12 and ^{99m}Tc -MIBI showed cationic migration behaviour (Fig. 2). This is in accordance to the proposed complex charges [9].

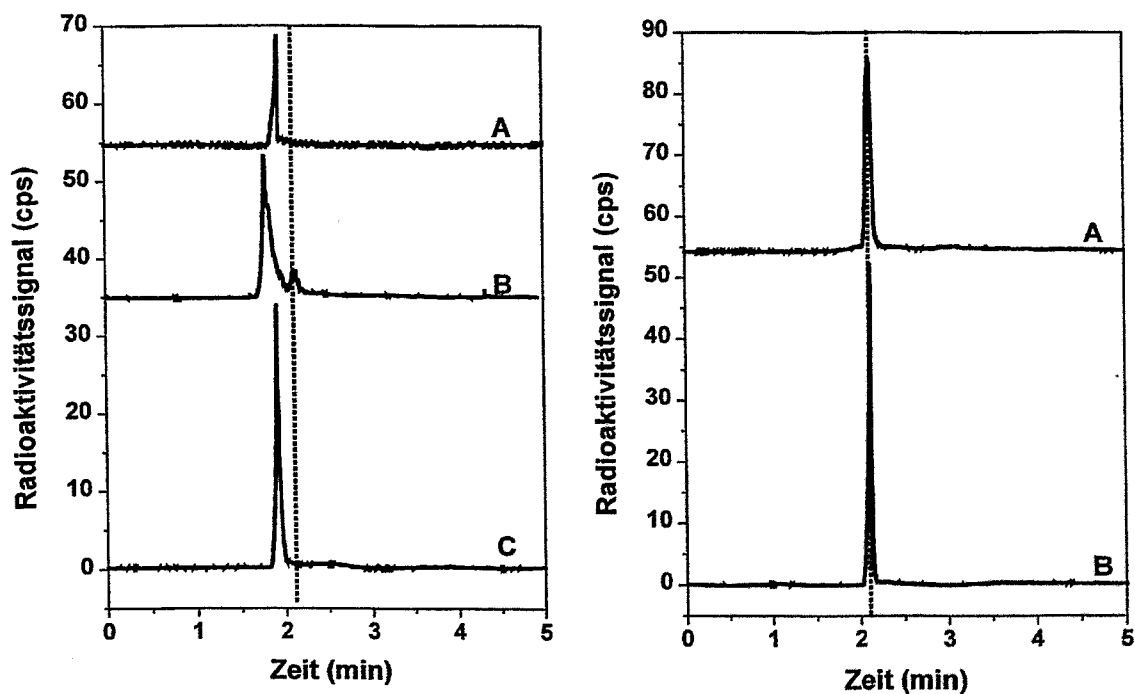


Fig. 2. Capillary zone electrophoresis of cationic and neutral ^{99m}Tc radiopharmaceuticals. The dotted lines represent the extrapolated detection time of a neutral marker. Left sketch, cationic complexes; A, ^{99m}Tc -Tetrofosmin; B, ^{99m}Tc -Q12; C, ^{99m}Tc -MIBI. Right sketch, neutral complexes; A, ^{99m}Tc -HMPAO; B, ^{99m}Tc -ECD.

For ^{99m}Tc -Q12, a complex mixture could be detected while ^{99m}Tc -Tetrofosmin and ^{99m}Tc -MIBI delivered single peaks. The migration times are different for the three cationic complexes showing the possibility to analyze them simultaneously. In case of neutral complexes, no separation can be achieved by capillary zone electrophoresis (Fig. 2). They do not exhibit any electrophoretic migration and are thus detected with the neutral marker. However, this result is in agreement with the proposed neutral complex structures [9]. For anionic complexes, it has to be distinguished between complexes of high and low electrophoretic mobility. The first are detectable by conventional capillary zone electrophoresis, while the latter are only analyzable by the pressure-modified capillary zone electrophoresis. ^{99m}Tc -EC, ^{99m}Tc -DTPA and ^{99m}Tc -EHIDA can be considered as low-mobile complexes. The ^{99m}Tc -EC and ^{99m}Tc -DTPA complexes exhibited single peaks in their electropherograms showing that uniform complex species are formed (Fig. 3).

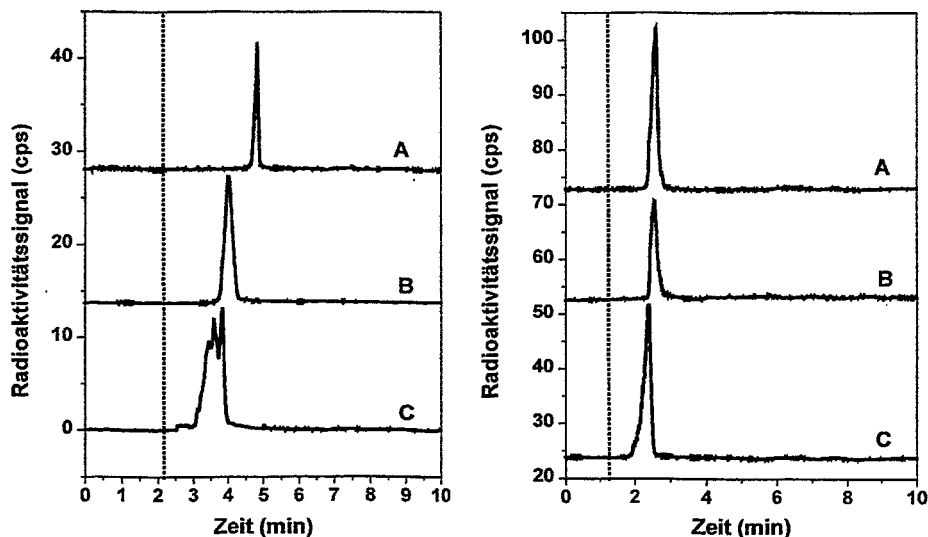


Fig. 3. Capillary zone electrophoresis of anionic ^{99m}Tc radiopharmaceuticals. The dotted lines represent the extrapolated detection time of a neutral marker. Left sketch, conventional capillary zone electrophoresis mode; A, ^{99m}Tc -EC; B, ^{99m}Tc -DTPA; C, ^{99m}Tc -EHIDA. Right sketch, pressure-modified capillary zone electrophoresis mode; A, ^{99m}Tc -MAG₃; B, ^{99m}Tc -DMSA; C, ^{99m}Tc -MDP.

In contrast, the ^{99m}Tc -EHIDA complex delivered a rather complicated peak pattern giving rise to the assumption that a variety of complex species are formed. For ^{99m}Tc -MAG₃, ^{99m}Tc -DMSA and ^{99m}Tc -MDP, the pressure-modified capillary zone electrophoresis was applied due to their high electrophoretic mobilities (Fig. 3). Remarkably, ^{99m}Tc -MAG₃ and ^{99m}Tc -DMSA showed nearly identical migration times which is obviously caused by the similar charge-size ratio of the complexes. ^{99m}Tc -MDP exhibits a broad peak, thus it can be assumed that several complex species with similar properties are formed.

pK determination. ^{99m}Tc -MAG₃ and ^{99m}Tc -EC bear free protonable carboxyl groups [9], whose pK values can be measured. For the determination of pK values, the complex structure-based thermodynamical equilibria constants of ligand deprotonations were employed to derive equations describing the relation between electrophoretic mobility and buffer pH [4]. The measured electrophoretic mobility curves of ^{99m}Tc -MAG₃ and ^{99m}Tc -EC are given in Fig. 3.

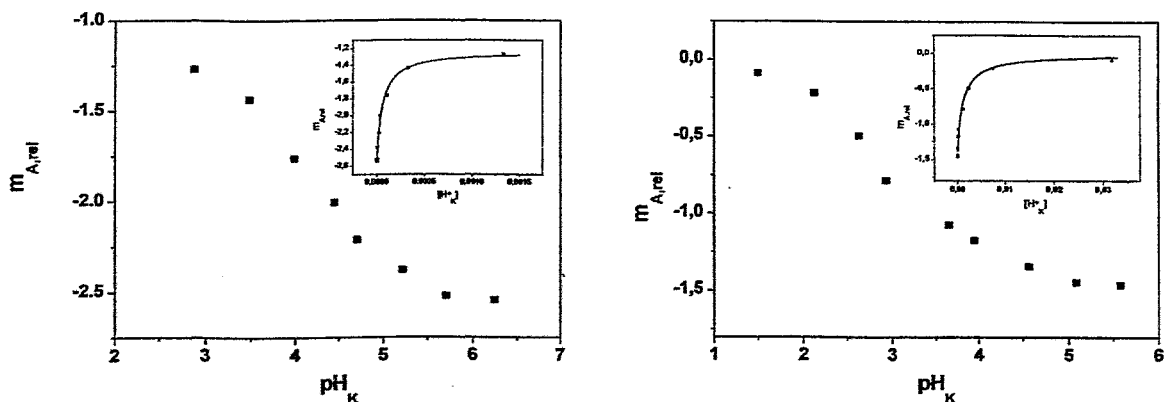


Fig. 4. Electrophoretic mobility curves of ^{99m}Tc -MAG₃ (left sketch) and ^{99m}Tc -EC (right sketch). The curve fitting using structure-based thermodynamical equations are shown as insets, respectively.

For both curves, sigmoidal decay properties could be obtained. The experimentally determined pK values are 4.22 and 2.90 for the $^{99m}\text{Tc-MAG}_3$ and $^{99m}\text{Tc-EC}$ complex, respectively. In case of $^{99m}\text{Tc-MAG}_3$, the value is higher than for carboxyl groups in comparable free peptides [10]. $^{99m}\text{Tc-EC}$ bears two free carboxyl groups, which are obviously chemically identical. That can be assumed, since only one step was obtained in the electrophoretic mobility curve. However, for $^{99m}\text{Tc-EC}$ the determined pK value is significantly increased comparing to the free cysteine [10], which could be due to the chemical modification of the ligand as well as to the metal complexation.

In summary, the CE equipped with a radioactivity detector proved to be a useful tool in both the analysis and the determination of pK values of ^{99m}Tc radiopharmaceuticals. Although few ^{99m}Tc radiopharmaceuticals show similar migration features under the described conditions, variation of the running conditions should improve the separation efficiency. Considering the pK determination, the radio-CE can be expected to become an essential tool in radiopharmaceutical research. Advantages are the small required sample amounts, possible automatization and very low running costs.

References

- [1] Gluck S. J., Steele K. P. and Benkő M. H. (1996) Determination of acidity constants of monoprotic and diprotic acids by capillary electrophoresis. *J. Chromatogr. A* **745**, 117-125.
- [2] Benet L. Z. and Goyan J. E. (1967) Potentiometric determination of dissociation constants. *J. Pharm. Sci.* **56**, 665-680.
- [3] Roda A., Minutello A. and Fini A. (1990) Bile acid structure-activity-relationship: evaluation of bile acid lipophilicity using 1-octanol/water partition coefficient and reverse phase HPLC. *J. Lipid. Res.* **31**, 1433-1443.
- [4] Jankowsky R., Friebe M., Noll B. and Johannsen B. (1999) Determination of dissociation constants of ^{99m}Tc radiopharmaceuticals by capillary electrophoresis. *J. Chromatogr. A* **833**, 83-96.
- [5] Beckers J. M., Everaerts F. M. and Ackermans M. T. (1991) Determination of absolute mobilities, pK values and separation numbers by capillary zone electrophoresis: effective mobility as a parameter for screening. *J. Chromatogr.* **537**, 407-428.
- [6] Cai J., Smith J. T. and Rassi Z. E. (1992) Determination of the ionization constants of weak electrolytes by capillary zone electrophoresis. *J. High Resolut. Chromatogr.* **15**, 30-32.
- [7] Ishihama Y., Oda Y. and Asakawa N. (1994) Microscale determination of dissociation constants of multivalent pharmaceuticals by capillary electrophoresis. *J. Pharm. Sci.* **83**, 1500-1507.
- [8] Castagnola M., Rossetti M., Cassiano L., Misiti F, Pennachietti L., Giardina B. and Messina I. (1996) Determination of peptide dissociation constants and stokes radius at different protonation stages by capillary electrophoresis. *Electrophoresis* **17**, 1925-1930.
- [9] Volkert W. A. and Jurisson S. (1996) Technetium-99m chelates as radiopharmaceuticals. In: *Topics Curr. Chem.* **176**, Ed. K. Yoshihara and T. Omori, pp. 123-148.
- [10] CRC Handbook of Chemistry and Physics, 73rd Edition, Ed. D. R. Lide, CRC Press, Boca Raton, 1992

53. Some Additions to the Determination of log P and pK_a Values by Using Reversed Phase HPLC

R. Berger, H. Spies

Introduction

As reported earlier, the lipophilicity (log P) and/or the ionization constants (pK_a) of certain organic bases can be determined by using reversed phase HPLC [1, 2].

A specific HPLC column (PRP-1) and elution system (acetonitrile/buffer) having a well-defined volume ratio are basic requirements for reliability in achieving correspondence between the retention times of the tested compounds and their octanol/water partition coefficients (P or log P). The more structure-related the tested substances are, the better the lipophilicity values obtained by HPLC correspond to P. The lipophilicity values of heterogenous compounds can only be compared with each other by referring to the chromatographic system used. Here we study the effects of deviations of the volume ratio in the elution system on the lipophilicity as well as on the ionization parameters of some organic bases and acids.

Results and Discussion

Amines:

In Table 1 we compare the lipophilicity values of amines obtained by reversed phase HPLC, using various organic modifier (acetonitrile) to buffer ratios, with log P values taken from the literature and from the internet. (The amines are arranged according to increasing pK_a values (cp. Table 2)).

Table 1. Experimental lipophilicity values and log P data from the literature and the internet for some amines

Amine	log P			Volume Ratio: Acetonitrile / Buffer				Δ ⁴ log P ²) - log P ^{HPLC}
	¹)	²)	³)	(3:1)		(2:1)		
				P _{HPLC}	log P _{HPLC}	P _{HPLC}	log P _{HPLC}	
o-Toluidine	1.30 *)	1.32	1.62	18.3	1.26	18	1.26	+ 0.06
Aniline	0.94 *)	0.90	1.08	7.6	0.88	7.7	0.89	+ 0.01
p-Toluidine	1.40 *)	1.39	1.62	13	1.11	13.5	1.13	+ 0.26
N-Ethylaniline	2.26	2.16	2.11	161	2.21	146	2.16	- 0.02
N,N-Dimethylaniline	2.46 *)	2.31	2.17	410	2.61	436	2.64	- 0.31
Pyridine	0.64 *)	0.65	0.80	1.7	0.23	1.4	0.15	+ 0.46
α-Picoline	-	1.11	1.35	2.5	0.40	2.2	0.34	+ 0.74
N,N-Diethylaniline	-	3.31	3.15	1800	3.26	2093	3.32	+ 0.02
2,4-Lutidine	-	-	1.90	4.2	0.62	3.6	0.56	~ + 1.31
Collidine	1.72	1.88	2.45	5.8	0.76	5.8	0.76	+ 1.12
Brucine	0.98 [3]	0.98	-	11	1.04	12	1.08	- 0.08
Benzylamine	1.09	1.09	1.07	2.2	0.34	2.6	0.43	+ 0.71

*) mean value ; taken from ¹) literature [4] if not notified otherwise;

²) WWW (<http://esc.syrres.com/~esc1/kowexpdb.htm>);

³) calculated by WWW (<http://esc.syrres.com/~esc1/kowint.htm>); ⁴) mean values

The lipophilicity constants (P) obtained from retention times are denoted by the index HPLC (P_{HPLC}). A modification of the volume ratio of acetonitrile to buffer from 3:1 to 2:1 does not essentially change the P_{HPLC} values.

These P_{HPLC} data differ to some extent from the log P values reported in the literature or internet. In the case of congeners of pyridine the log P_{HPLC} values are much smaller than the log P values from the literature [3, 4]. It is possibly on account of a nitrogen atom in the aromatic ring of the referring examples that the interaction with the stationary phase [poly(styrene-divinylbenzene)] is diminished and the appropriate retention times are thus reduced.

When the ionization constants of single ionizable compounds are determined, the influence of organic cosolvents (e.g. acetonitrile) on the pH value has to be taken into consideration. As cosolvents with

dielectric constants smaller than that of water weaken both acidic and basic groups, the pK_a of an acidic group is raised and that of a basic group lowered [5].

For a number of organic bases the pK_a values from the literature and those determined by HPLC using two acetonitrile to buffer ratios are compared in Table 2. The pK_a values were measured by potentiometric titration in pure aqueous solution or extrapolated into this medium. The addition of the organic modifier to the buffer diminishes the pK_a value. Thus, the third column contains the lowest pK_a values.

Table 2. pK_a values of some amines taken from the literature [6] and determined by HPLC using two volume ratios of acetonitrile to buffer

Amine	pK_a	pK_{HPLC} (2:1)	pK_{HPLC} (3:1)
o-Toluidine	4.44	3.49	2.67
Aniline	4.63	3.65	3.43
p-Toluidine	5.08	4.25	3.78
N-Ethylaniline	5.12	4.20	3.81
N,N-Dimethylaniline	5.15	4.01	3.81
Pyridine	5.25	4.15	3.83
α -Picoline	5.97	4.90	4.45
N,N-Diethylaniline	6.61	5.37	5.26
2,4-Lutidine	6.99	5.55	5.13
Collidine	7.43	6.17	5.87
Brucine	8.28	6.76	6.96
Benzylamine	9.33	7.90	7.98

Based on these data, calibration curves were defined for correction of the measured values of further organic bases (Figs. 1 and 2).

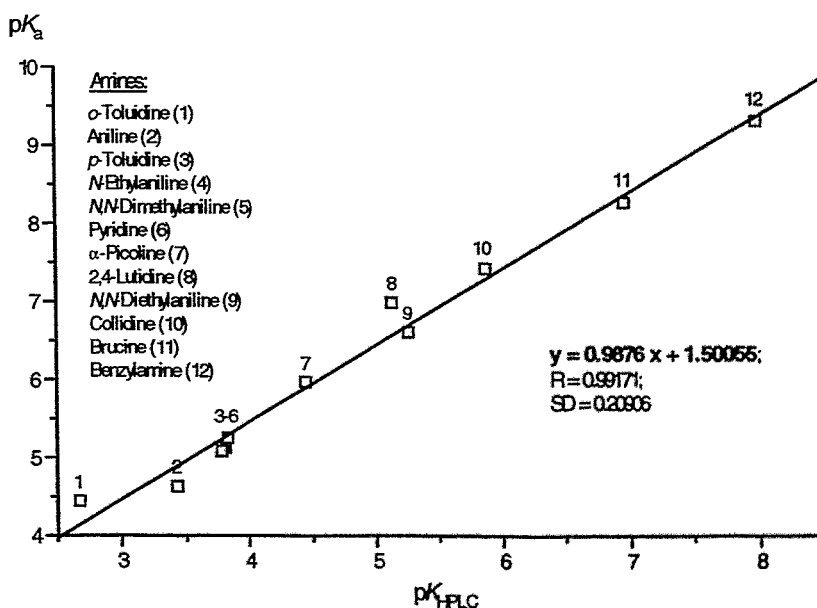


Fig. 1. Calibration curve for corrections of the pK_{HPLC} values of organic bases (acetonitrile/buffer = 3:1 (v/v))

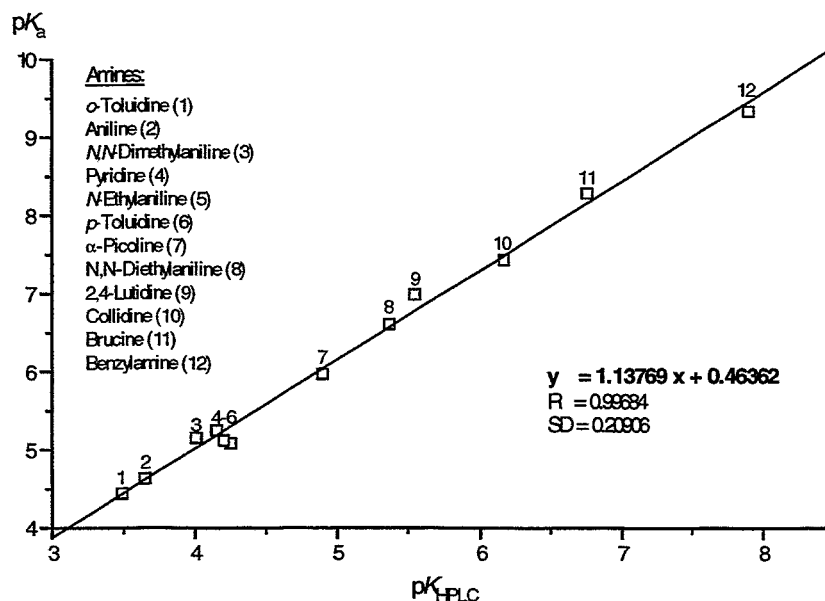


Fig. 2. Calibration curve for corrections of the pK_{HPLC} values of organic bases (acetonitrile/buffer = 2:1 (v/v))

Both calibration curves show a similar trend. In Fig.1 the curve presents an approximately parallel shift (by an amount of 1.5) to the function $pK_a = pK_{HPLC}$ (analogous to $y = x$). The curve in Fig. 2 is somewhat steeper. In both examples the curves represent rather good correlations.

In practice, the higher the proportion of acetonitrile in the eluant mixture, the shorter is the retention time of the solvent. A decrease in the proportion of the organic modifier prolongs the retention time. In the above chromatographic system a change in the acetonitrile/buffer volume ratio from 3:1 to 2:1 approximately doubles the retention time. A further change to 1:1 doubles it again. The continued reduction of the organic modifier in the elution mixture while maintaining the chromatographic system makes therefore no sense, economically or practically.

Organic acids:

The above studies were extended to organic acids. The pK_a and pK_{HPLC} values of some organic acids are listed and plotted in Table 3 and Fig. 3.

Table 3. pK_a values of some organic acids taken from the literature [6] and determined by HPLC, using a volume ratio of acetonitrile/buffer = 3:1

Organic acid	pK_a	pK_{HPLC}
<i>o</i> -Chlorobenzoic acid	2.92	4.56
Diphenylacetic acid	3.94	5.51
Benzoic acid	4.19	5.85
<i>trans</i> -Cinnamic acid	4.44	6.24
3-Phenylpropionic acid	4.37	6.40
4-Phenylbutyric acid	4.76	6.43
Thiophenol	6.52	8.44

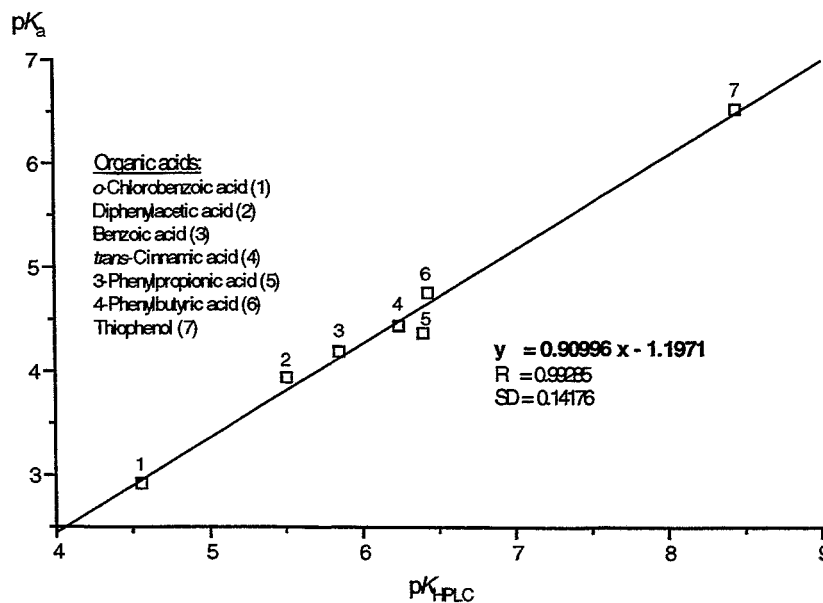


Fig. 3. Calibration curve for corrections of the pK_{HPLC} values of organic acids (acetonitrile/buffer = 3:1 (v/v))

Appropriate trend programs using the above calibration curves make it possible to calculate pK_{a(c)} from pK_{HPLC} values for organic bases and organic acids.

References

- [1] Berger R., Fietz T., Glaser M. and Spies H. (1995) Determination of partition coefficients for coordination compounds by using HPLC. *Annual Report 1995*, Institute of Bioinorganic and Radiopharmaceutical Chemistry, FZR-122, pp. 69-72.
- [2] Berger R., Scheunemann M., Pietzsch H.-J., Noll B., Noll St., Hoepping A., Glaser M., Fietz T., Spies H. and Johannsen B. (1995) pK_a value determinations by HPLC of some Tc and Re complexes containing an ionizable group. *Annual Report 1995*, Institute of Bioinorganic and Radiopharmaceutical Chemistry, FZR-122, pp. 73-79.
- [3] Hansch C., Sammes P. G. and Taylor J. B. eds. (1990) *Comprehensive Medicinal Chemistry, The Rational Design, Mechanistic Study & Therapeutic Application of Chemical Compounds, Vol. 6 (Cumulative Subject Index & Drug Compendium)*, Pergamon Press, Oxford, p. 330.
- [4] Leo A. J., Hansch C. and Elkins D. (1971) Partition coefficients and their uses. *Chem. Rev.* **71**, 525-616.
- [5] Pagliara A., Testa B., Carrupt P. A., Jolliet P., Morin C., Morin D., Urien S., Tillement J. P. and Rihoux J. P. (1998) Molecular properties and pharmacokinetic behavior of cetirizine, a zwitterionic H-1-receptor antagonist. *J. Med. Chem.* **41**, 853-863.
- [6] Lide D. R. ed. (1992-1993) *CRC Handbook of Chemistry and Physics*, CRC Press, Tokyo, pp. 8-37.
- [7] Berger R., Friebe M., Pietzsch H.-J., Scheunemann M., Noll B., Fietz T., Spies H. and Johannsen B. (1996) Lipophilicity and ionization properties of some amine-bearing technetium and rhenium "3+1" mixed-ligand chelates of the same ligand structure. *Annual Report 1996*, Institute of Bioinorganic and Radiopharmaceutical Chemistry, FZR-165, pp. 43-47.

54. Partition Coefficients for Steroidal Rhenium Coordination Compounds Determined by Using RP-HPLC

R. Berger, F. Wüst, M. Reisgys, H. Spies

Lipophilicity is an important parameter in the design of ^{99m}Tc steroid hormone receptor-binding ligands able to image hormone-dependent metabolic pathways of tumours [1, 2, 3]. This also applies to steroid hormone complexes with rhenium as an inactive surrogate of technetium.

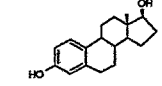
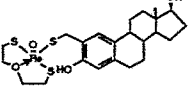
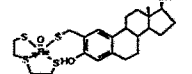
In order to determine the lipophilicity of steroid-derived Re complexes we used HPLC on a PRP-1 column eluted by an acetonitrile to buffer mixture in a volume ratio of 3 to 1 [4]. Following a preliminary report [5], we now publish all lipophilic data of steroid-derived Re complexes measured by us (Table 1). Column a) exhibits lipophilicity values based on known octanol/water partition coefficients ($\log P_{o/w}$) of aniline, benzene and bromobenzene as references [4, 6].

It is anticipated that structure-related steroids will be better reference molecules for the determination of $\log P_{o/w}$ of steroid complexes than the hitherto used aromatics aniline, benzene and bromobenzene. We therefore compare the above values with those obtained on the basis of some steroids for which $\log P_{o/w}$ values are known as references. In column b) P_{HPLC} data obtained by analogous calculations using the steroids 3,17 β -estradiol, testosterone and progesterone are shown. (Both series of values are based on the corresponding capacity factors which are listed in an additional column for comparison.)

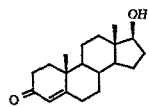
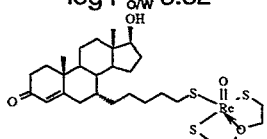
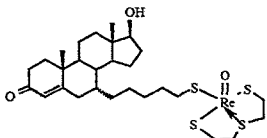
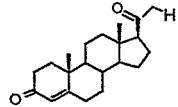
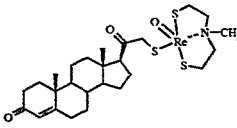
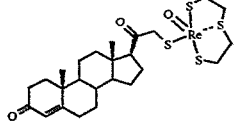
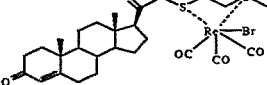
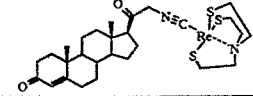
The P_{HPLC} values in column b) are generally larger by 1 - 2 orders of magnitude than those in column a). Because of the PRP-1 column matrix having aromatic properties, the results for steroids or steroidal ligands of chelates have to be interpreted with particular care. An interaction between the sterically marked steroidal structures and the column matrix obviously does not take place as could be expected. Presumably the functional groups of steroidal molecules are responsible for the relatively weak interaction with the column matrix, which is in a certain contrast to the behaviour concerning the partition between the phases of octanol and water. (In order to overcome this source of error as far as possible, the $\log P_{o/w}$ values of above-mentioned steroids available in [7] are used to calculate the P_{HPLC} values as was described earlier [4].)

A comparison of the lipophilic results obtained by using a) the aromatics and b) various steroids that are more structure-related to the chelates, revealed a certain correspondence. However, apart from the great difference between the values obtained by the two methods, the individual lipophilicity values are not sufficiently influenced by structural changes of functional groups of the steroidal Re complexes, i.e. an indirect determination of $P_{o/w}$ by using the above-mentioned chromatographic system is not advisable.

Table 1. P_{HPLC} and $\log P_{\text{HPLC}}$ values as well as the corresponding capacity factors (k') of several steroids and neutral rhenium complexes containing steroidal ligands [pH interval 5 - 9, $n = 3$],
a) reference substances: aniline, benzene, bromobenzene,
b) calculation by using 3,17 β -estradiol, testosterone and progesterone as references.

No.	Structure	P_{HPLC}		$\log P_{\text{HPLC}}$		k'	$\log k'$
		a)	b)	a)	b)		
1	 3,17 β -estradiol $\log P_{o/w}$ 4.01	9.3 ± 0.5	4944 ± 260	0.9685	3.6941	0.8995	-0.0460
2		51 ± 1.5	5441 ± 160	1.7076	3.7357	1.6894	0.2277
3		70 ± 2.5	5537 ± 200	1.8451	3.7433	1.8902	0.2765

4		96 ± 5	5660 ±300	1.9823	3.7528	2.1304	0.3285
5		111 ±6	5730 ±310	2.0453	3.7582	2.2113	0.3446
6		123 ±4	5798 ±190	2.0899	3.7633	2.2183	0.3460
7		154 ±5	5862 ±190	2.1875	3.7680	2.4008	0.3803
8		212 ±6	5970 ±170	2.3263	3.7760	2.7421	0.4381
9		251 ±8	6015 ±190	2.3997	3.7792	2.8948	0.4616
10		487 ±10	6224 ±130	2.6875	3.7941	3.7103	0.5694
11		390 ±25	6136 ±390	2.5911	3.7861	3.5312	0.5479
12		626 ±50	6303 ±500	2.7966	3.7968	4.2104	0.6243
13		771 ±50	6378 ±410	2.8871	3.8015	4.5488	0.6579
14		5760 ±200	7038 ±240	3.7604	3.8474	9.0460	0.9565
15		8780 ±200	7206 ±160	3.9435	3.8577	10.7325	1.0307
16		86 ±5	5629 ±330	1.9345	3.7504	2.0586	0.3136
17		219 ±15	5938 ±410	2.3404	3.7715	2.8488	0.4547
18		326 ±15	6068 ±280	2.5132	3.7830	3.3355	0.5232
19		1800 ±110	6692 ±410	3.2553	3.8233	6.2345	0.7948

20	 testosterone $\log P_{o/w}$ 3.32	19.5 ± 0.9	5175 ± 240	1.2900	3.7139	1.1993	0.0789
21		719 ± 30	6384 ± 270	2.8567	3.8051	4.7116	0.6732
22		900 ± 48	6408 ± 340	2.9542	3.8067	5.1206	0.7093
23	 progesterone $\log P_{o/w}$ 3.87	392 ± 10	6145 ± 160	2.5933	3.7885	3.5821	0.5541
24		2230 ± 90	6774 ± 270	3.3483	3.8287	6.7531	0.8295
25		4255 ± 100	7027 ± 160	3.6289	3.8432	8.5860	0.9338
26		1495 ± 90	6622 ± 400	3.1746	3.8189	5.8194	0.7649
27		16063 ± 600	7577 ± 280	4.2058	3.8765	14.0659	1.1482

As already deduced in our last report [5], the following general rules are valid:

- 1) Each formation of rhenium complexes with basic steroidal structures such as 3,17 β -estradiol, testosterone or progesterone has a growing lipophilicity as a consequence; however, the extent of the change in lipophilicity depends on the selection of references. Besides, the lipophilicity of these complexes is increased either by lengthening the carbon chain between the Re chelate moiety or removing a hydrophilic group as usual.
- 2) For a definite steroid moiety the lipophilicity is increased depending on the coordination mode in the following order: "4+1" (Nos. 18; 19, 27) > "3+1" (Nos. 4, 5; 12, 13; 24, 25) > "carbonyl-thioether" (Nos. 16; 17; 26).
- 3) In the "3+1" Re complexes, considering the tridentate ligand moiety, the lipophilicity grows in the following order: "SN(CH₃)S" (No. 11) < "SOS" (No. 12) < "SSS" (No. 13).

References

- [1] Wüst F., Spies H. and Johannsen B. (1996) Synthesis of "3+1" mixed-ligand oxorhenium(V) complexes containing modified 3,17 β -estradiol. *Bioorg. Med. Chem. Lett.* **6**, 2729-2734.
- [2] Wüst F., Spies H. and Johannsen B. (1997) Synthesis of 17 α -substituted mercaptoalkynyl derivatives of 3,17 β -estradiol. *Tetrahedron Lett.* **38**, 2931-2932.
- [3] Wüst F., Scheller D., Spies H. and Johannsen B. (1998) Synthesis of oxorhenium(V) complexes derived from 7 α -functionalized testosterone: First rhenium-containing testosterone derivatives. *Eur. J. Inorg. Chem.* **6**, 789-793.
- [4] Berger R., Fietz T., Glaser M. and Spies H. (1995) Determination of partition coefficients for coordination compounds by using HPLC. *Annual Report 1995*, Institute of Bioinorganic and Radiopharmaceutical Chemistry, FZR-122, pp. 69-72.
- [5] Berger R., Wüst F. and Spies H. (1997) Technetium and rhenium-labelled steroids
8. Lipophilicity of rhenium complexes with 1-mercapto-4-methylestra-1,3,5(10)-trien-17-one, 17 α -substituted estradiol as well as 7 α -substituted testosterone, determined by using RP-HPLC. *Annual Report 1997*, Institute of Bioinorganic and Radiopharmaceutical Chemistry, FZR-200, pp. 52-54.
- [6] Berger R., Friebe M. and Spies H. (1997) HPLC Troubleshooting: drifting retention times. *Annual Report 1997*, Institute of Bioinorganic and Radiopharmaceutical Chemistry FZR-200, pp. 132-134.
- [7] WWW (<http://esc.syrres.com/~esc1/kowexpdb.htm>)

55. Miscellaneous Results of Determining the Partition Coefficients and Ionization Constants for Rhenium and Technetium Coordination Compounds by Using HPLC

R. Berger, F. Wüst, A. Zablotskaya¹, M. Friebe, H.-J. Pietzsch, M. Scheunemann, M. Reigys, H. Spies, B. Johannsen

¹Latvian Institute of Organic Chemistry, Riga, Latvia

Introduction

In previous reports measurements of the lipophilicity and ionization behaviour of various substituted Tc/Re complexes with "3+1" mixed-ligand coordination priority were presented [1, 2]. This article is dedicated to analogous measurements of mixed-ligand complexes with a) variations in the tridentate ligands SXS (X=N-Me, S, O, N-Pyr) and monodentate ligands, to which b) a hydroxyl group or c) alkyl or aryl-silyl groups are substituted, d) which can be potentially bound to receptors as amines with a protonable nitrogen [3] and e) Re tricarbonyl dithioether complexes, which can be linked to bio-molecules [4].

The determination of lipophilicity resulting in apparent so-called log P_{HPLC} values was performed by applying an HPLC procedure involving a PRP-1 column eluted by an acetonitrile/buffer mixture in a volume ratio of 3 to 1 [1]. Ionization constants are measured as pK_{HPLC} and subsequently corrected to the form $pK_{\text{a(c)}}$ by using calibration curves both for organic bases and acids [2, 5, 6].

Results and Discussion

The lipophilicity values of some rhenium coordination compounds modified both in the tridentate and in the monodentate chelate unit substituted mostly by hydroxyl groups are listed in Table 1.

a) Influence of the exchange of the central atom in the tridentate ligands: The lipophilicity values show a structural dependence as expected, i.e. as already discussed, the replacement of the central heteroatom in the tridentate ligand increases P_{HPLC} in the rank order N-Me < O ≤ S [5, 7, 8] (Nos. 1-3). In the case of embedding the central nitrogen atom in a pyridine ring [S-N(pyr)-S] (No. 6), the P_{HPLC} value is higher than the one with the S-S-S unit (No. 5).

b) Effects of hydroxyl-group-containing substituents and the alkyl chain length in monodentate ligands: In general, ligands bearing hydroxyl substituents have the expected low P_{HPLC} values. For instance, P_{HPLC} values decrease when the monodentate benzene ring (No. 8) is substituted in the para position by oxygen-containing groups (Nos. 6, 7), among which the hydroxyl group has the greatest influence on diminishing P_{HPLC} (No. 6).

Lengthening the N-alkyl side chain in the monodentate ligand increases the P_{HPLC} value [5] (Nos. 3, 4).

c) Influence of the introduction of silyl groups into the monodentate ligands: Table 2 lists "3+1" rhenium complexes in which the proton of the hydroxyl group is substituted by a silyl group. A drastic increase in lipophilicity is observed. Regardless of the involvement of silicon in the chelate structure, the usual observations of lipophilic differences in the tridentate chelate units having various central atoms (Nos. 1, 2) and lengthening carbon chains (Nos. 2, 3) remain unchanged. The complex with three phenyl residues bound to silicon represents a certain exception. The relatively high P_{HPLC} value is a consequence of an intimate interaction with the aryllic column matrix (No. 4).

d) "3+1" Re/Tc complexes bearing protonable nitrogen: In continuation of previous studies, the supplementary lipophilicity and $pK_{\text{a(c)}}$ values relating to amine-group-bearing "3+1" rhenium and some technetium complexes are displayed in Table 3a and b. In particular, three novel monodentate ligands consisting of structural units such as 1,4-dioxo-8-azaspiro-N-2-mercaptoethylene-[4,5]-decane, 4-piperidinone or α -dimethylamino acetic acid methylester [cp. structure moieties of Nos. 1, 2, 5] are included in the determination.

Table 1. Lipophilicity values of some "3+1" rhenium complexes (N-pyridine in tridentate and hydroxyl substituents in monodentate ligands)

No.	Structure	P _{HPLC}	log P _{HPLC}
1		1.66 ±0.02	0.2201
2		2.06 ±0.12	0.3139
3		2.66 ±0.06	0.4249
4		2.73 ±0.04	0.4362
5		10.3 ±0.5	1.0128
6		21.3 ±1	1.3284
7		1128 ±50	3.0523
8		1586 ±70	3.2003

Table 2. "3+1" Rhenium complexes containing silyl groups in the monodentate structure unit

No.	Structure	P _{HPLC}	log P _{HPLC}
1		275 ±8	2.4393
2		577 ±14	2.7612
3		982 ±48	2.9921
4		237360 ±23000	5.3754

From these two compilations similar findings as earlier obtained [5] can be deduced, i.e. 1) looking at the tridentate moiety and keeping the monodentate unit constant, growing P_{HPLC} values can be observed in the following order [S-N(Me)-S] < [S-N(Et)-S] ~ [S-S-S] < [S-N(Pr)-S]; 2) for the compounds in Nos. 9, 10, greater lipophilicity values of the technetium species (maximum about double the amount) can be assumed;

3) directing attention to the D_{HPLC} values (obtained at pH 7.4), the relatively highest amount of the P_{HPLC} value can be observed in the case of the monodentate unit involving a ketone group;
 4) considering the pK_{a} values, an increase depending on monodentate structural groups can be deduced in the order of the typical groups: keto < ester < dioxa unit.
 Apart from that an evident difference between the $pK_{\text{a(c)}}$ values of technetium and rhenium complexes having the same structure cannot be recognized.

Table 3a. Lipophilicity values (P_{HPLC} , D_{HPLC}) and ionization constants ($pK_{\text{a(c)}}$) of "3+1" rhenium coordination compounds in continuation of previous results [5, 9]

No.	Structure	P_{HPLC}	$\log P_{\text{HPLC}}$	D_{HPLC}^*	$\log D_{\text{HPLC}}^*$	$pK_{\text{a(c)}}$
1		28	1.4471	3.5	0.5461	7.95
2		14	1.1461	11	1.0414	6.96
3		14	1.1461	1.9	0.2788	7.95
4		8	0.9031	5.6	0.7482	7.03
5		1.5	0.1761	0.7	-0.1549	7.46
6		28	1.4471	2.6	0.4150	8.09
7		15	1.1761	11	1.0414	7.05
8		2.5	0.3979	0.9	-0.0458	7.56

*) at pH 7.4; Me = methyl, Et = ethyl.

Table 3b. Lipophilicity values (P_{HPLC} , D_{HPLC}) and ionization constants ($pK_{\text{a(c)}}$) of "3+1" rhenium and technetium coordination compounds in continuation of previous results [5, 9]

No.	Structure	P_{HPLC}		$\log P_{\text{HPLC}}$		D_{HPLC}^*		$\log D_{\text{HPLC}}^*$		$pK_{\text{a(c)}}$	
		Tc	Re	Tc	Re	Tc	Re	Tc	Re	Tc	Re
9		104	49	2.0170	1.6902	16	3	1.2041	0.4771	8.04	8.42
10		46	29	1.6628	1.4624	35	21	1.5441	1.3222	7.07	7.06

M = Tc, Re; *) at pH 7.4; Pr = propyl.

Additional structures of "3+1" technetium and rhenium complexes modified at the monodentate ligand and the corresponding P_{HPLC} , D_{HPLC} at pH 7.4 as well as $pK_{\text{a(c)}}$ values are listed in Table 4 as a function of the growing P_{HPLC} values.

Table 4. P, D (at pH 7.4) and $pK_{\text{a(c)}}$ values of special "3+1" rhenium and technetium complexes modified at the monodentate ligand bearing protonable amine nitrogen

No.	Structure	P_{HPLC}	$\log P_{\text{HPLC}}$	D_{HPLC}	$\log D_{\text{HPLC}}$	$pK_{\text{a(c)}}$
1		350	2.5441	5	0.6990	9.46
2		410	2.6128	60	1.7782	7.97
3		665	2.8228	10	1.0000	9.12
4		1100	3.0414	5	0.6990	9.31
5		715	2.8543	10	1.0000	9.37
6		1300	3.1139	15	1.1761	9.13
7		1410	3.1492	20	1.3010	9.18
8		1750	3.2430	20	1.3010	9.47
9		2190	3.3404	370	2.5682	7.84
10		1540	3.1875	50	1.6990	8.41
11		2585	3.4125	100	2.0000	8.43
12		3096	3.4908	10	1.0000	9.85

13		3520	3.5465	45	1.6532	9.43
14		4410	3.6444	30	1.4771	9.60
15		6130	3.7875	175	2.2430	8.51
16		8890	3.9489	65	1.8129	9.65
17		9960	3.9983	180	2.2553	9.81
18		10375	4.0160	50	1.6990	10.04
19		18685	4.2715	160	2.2041	9.89
20		21230	4.3269	205	2.3118	9.90
21		27750	4.4433	60	1.7782	9.89

The following interdependences can be derived from Table 4:

- 1) In complexes of the same ligand structure those involving technetium have a higher lipophilicity than those containing rhenium (cp. pair Nos. 5, 6 and 10, 11).
- 2) The D_{HPLC} values increase with growing P_{HPLC} and diminishing $pK_{\text{a(c)}}$.
- 3) The smaller the $pK_{\text{a(c)}}$ values, the higher are the D_{HPLC} values.
- 4) Arrangement of oxygen in β -position (e.g. in the morpholine ring or within a chain) decreases the $pK_{\text{a(c)}}$ because of its electron-withdrawing effect on the amine nitrogen (No. 9). This effect is negligible over a distance of three carbon atoms (Nos. 8, 14, 18, 21).
- 5) Lengthening the N-alkyl side chain in the monodentate ligand from two to three carbon atoms increases the $pK_{\text{a(c)}}$ values by about 0.3 units (Nos. 13, 17 and 16, 20).

Some supplementary structures of "3+1" technetium and rhenium complexes modified chiefly at the tridentate ligand and the corresponding P_{HPLC} , D_{HPLC} at pH 7.4 as well as $pK_{\text{a(c)}}$ values are listed in Table 5.

Table 5. P_{HPLC} , D_{HPLC} (at pH 7.4) and $pK_{\text{a(c)}}$ values of special "3+1" rhenium and technetium complexes modified chiefly at the tridentate ligand

No.	Structur	P_{HPLC}	$\log P_{\text{HPLC}}$	D_{HPLC}	$\log D_{\text{HPLC}}$	$pK_{\text{a(c)}}$
1		850	2.9294	80	1.9031	8.19
2		3350	3.5250	260	2.4150	8.13
3		14340	4.15956	9500	3.9777	7.21
4		35500	4.5502	450	2.6532	8.92
5		15500	4.1903	380	2.5798	8.55
6		3500	3.5441	10	1.0000	9.05
7		11900	4.0755	100	2.0000	9.04
8		11735	4.06957	80	1.9031	9.34
9		22900	4.3598	210	2.3222	9.35
10		3325	3.5218	30	1.4771	9.20

In contrast to the discussion on oxygen in ether bridges (Table 4), an interesting example is listed in Table 5 under No. 3. An ether bridge in a chain containing another nitrogen atom bound through an ethylene bridge to the nitrogen of the tridentate ligand obviously results in a pronounced decrease in the $pK_{\text{a(c)}}$ value. The corresponding lipophilicity value at pH 7.4 grows reciprocally. As can be seen from Nos. 1 and 2, an ethylene bridge between two nitrogen atoms, one of which represents the central atom of the tridentate ligand, has a remarkable influence on diminishing basicity.

e) *Re tricarbonyl dithioether complexes*: The lipophilicity values as well as the ionization constants of several rhenium tricarbonyl dithioether complexes are listed in Table 6.

Table 6. The lipophilicity values (P_{HPLC} , $\log P_{\text{HPLC}}$) and ionization constants ($pK_{\text{a(c)}}$) of carbonyl-containing Re complexes

No.	Structure	P_{HPLC}	$\log P_{\text{HPLC}}$	pK_{HPLC}	$pK_{\text{a(c)}}$
1		93 ± 6	1.9685	-	-
2		3650	3.5623	7.47	8.88
3		1100	3.0414	7.11	8.52
4		0.43	-0.3665	5.18	3.5
5		1.79	0.2529	5.50	3.8
6		0.53 ± 0.03	-0.2757	-	-

The rhenium tricarbonyl dithioether complex (No.1) can be considered to be the parent compound from which the complexes (Nos. 2 - 6) with a relatively low lipophilicity derive. In complexes containing benzene rings the lipophilicity is enhanced to $\log P$ values greater than 3 (Nos. 2, 3), while the OH/COOH-group-containing compounds, as expected, show $\log P$ values at about 1. In accordance with their varying ionization properties Nos. 2, 3 behave as bases and the Nos. 4, 5 as acids. That can also be deduced by comparing the columns containing the pK_{HPLC} values, on the one hand, and the $pK_{\text{a(c)}}$ values, on the other. In cases of an acid or base the measured values have to be corrected by subtracting or adding a definite amount [cp. 10].

References

- [1] Berger R., Fietz T., Glaser M. and Spies H. (1995) Determination of partition coefficients for coordination compounds by using HPLC. *Annual Report 1995*, Institute of Bioinorganic and Radiopharmaceutical Chemistry, FZR-122, pp. 69-72.
- [2] Berger R., Scheunemann M., Pietzsch H.-J., Noll B., Noll St., Hoepping A., Glaser M., Fietz T., Spies H. and Johannsen B. (1995) pK_{a} value determinations by HPLC of some Tc and Re complexes containing an ionizable group. *Annual Report 1995*, Institute of Bioinorganic and Radiopharmaceutical Chemistry, FZR-122, pp. 73-79.
- [3] Johannsen B., Berger R., Brust P., Pietzsch H.-J., Scheunemann M., Seifert S., Spies H. and Syhre R. (1997) Structural modification of receptor-binding technetium-99m complexes in order to improve brain uptake. *Eur. J. Nucl. Med.* **24**, 316-319.
- [4] Alberto R., Schibli R., Angst D., Schubiger P. A., Abram U., Abram S. and Kaden T. A.. (1997) Application of technetium and rhenium carbonyl chemistry to nuclear medicine. Preparation of $[\text{NEt}_4]_2[\text{TcCl}_3(\text{CO})_3]$ from $[\text{NBu}_4][\text{TcO}_4]$ and structure of $[\text{NEt}_4][\text{Tc}_2(\mu\text{-Cl})_3(\text{CO})_6]$; structures of the model complexes $[\text{NEt}_4][\text{Re}_2(\mu\text{-OEt})_2(\mu\text{-OAc})(\text{CO})_6]$ and $[\text{ReBr}\{-\text{CH}_2\text{S}(\text{CH}_2)_2\text{Cl}\}_2(\text{CO})_3]$ *Transit. Metal. Chem.* **22** (6) pp. 597-601.

- [5] Berger R., Friebe M., Pietzsch H.-J., Scheunemann M., Noll B., Fietz T., Spies H. and Johannsen B. (1996) Lipophilicity and ionization properties of some amine-bearing technetium and rhenium "3+1" mixed-ligand chelates of the same ligand structure. *Annual Report 1996*, Institute of Bioinorganic and Radiopharmaceutical Chemistry FZR-165, pp. 43-47.
- [6] Berger R. and Spies H. (1999) Some additions to the determination of log P and pK_a values by using reversed phase HPLC. *This report*, pp. 192-195.
- [7] Berger R., Wüst F. and Spies H. (1997) Technetium and rhenium-labelled steroids.
8. Lipophilicity of rhenium complexes with 1-mercapto-4-methylestra-1,3,5(10)-trien-17-one, 17 α -substituted estradiol as well as 7 α -substituted testosterone, determined by using RP-HPLC. *Annual Report 1997*, Institute of Bioinorganic and Radiopharmaceutical Chemistry FZR-200, pp. 52-54.
- [8] Berger R., Wüst F., Reisgys M. and Spies H. (1999) Partition coefficients for steroidal rhenium coordination compounds determined by using RP-HPLC. *This report*, pp. 196-199.
- [9] Berger R., Friebe M., Spies H. and Johannsen B. (1997) Are there differences in lipophilicity between the transition metals technetium and rhenium? *Annual Report 1997*, Institute of Bioinorganic and Radiopharmaceutical Chemistry FZR-200, pp. 128-131.
- [10] Berger R. and Spies H. (1999) Some additions to the determination of log P and pK_a values by using reversed phase HPLC. *This report*, pp. 192-195.

56. Influence of Transport Conditions of the $[^{18}\text{F}]^-$ Water Target on the $[^{18}\text{F}]\text{FDG}$ Synthesis

St. Preusche, F. Füchtner, J. Steinbach

Introduction

The Rossendorf PET cyclotron 'CYCLONE 18/9' is equipped with a large-volume $[^{18}\text{F}]^-$ water target (irradiated volume ~ 1.5 ml). The $[^{18}\text{F}]\text{FDG}$ synthesis is based on a modified Nuclear Interface $[^{18}\text{F}]\text{FDG}$ module.

At the Rossendorf PET Center the PET cyclotron and the radiochemical laboratories are 500 meters apart. In case of the water target the distance is bridged by a pneumatic transport system. The principle of the transport of irradiated liquids is shown in Fig. 1. The irradiated liquid $[^{18}\text{O}]\text{H}_2\text{O}/[^{18}\text{F}]^-$ is transferred from the target to the loading unit of the pneumatic rabbit in a capillary tube 25 m in length, of 0.8 mm inner diameter (cyclotron site) and from the unloading unit to the $[^{18}\text{F}]\text{FDG}$ module in a 50 m long tube (radiochemistry site). The 500 m distance is bridged by the pneumatic rabbit. The whole unloading procedure (EOB to BOS) takes about 10 minutes.

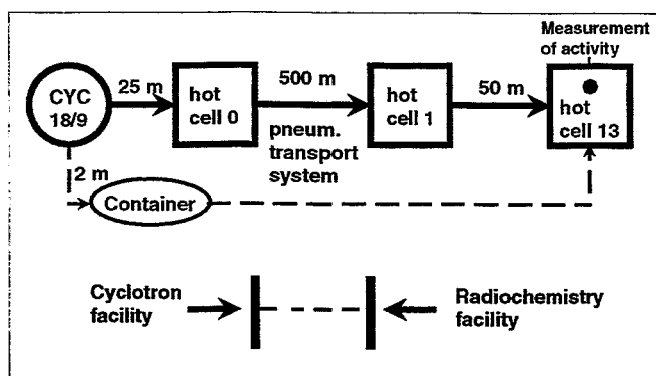


Fig. 1. Transport of irradiated liquids at the Rossendorf PET Center - principle -

When we started our routine $[^{18}\text{F}]^-$ production in 1997, we observed two phenomena:

- a relatively low saturation yield of the $[^{18}\text{F}]^-$ water target due to the reported data
 - a rapid decrease in the $[^{18}\text{F}]\text{FDG}$ yield when a high level of activity was produced the day before.
- Investigations were carried out to determine the activity losses during transport and the factors influencing the $[^{18}\text{F}]\text{FDG}$ yield.

Experimental

Activity losses during transport:

The activity is measured only at the radiochemistry site (see Fig. 1) just before starting the $[^{18}\text{F}]\text{FDG}$ synthesis. The decay-corrected target yield is the real target yield minus the activity losses of transport. To determine these losses we compared the activity of the unloading procedure described above (normal unloading) with that measured after an additional target and tube rinse and by direct unloading of the $[^{18}\text{F}]^-$ water target into a measuring vessel, using a container for transport (see Fig. 1, dotted line). The length of the capillary tube in case of container transport was only 2 m. The container was transported by handcart. The activity was always measured in hot cell 13.

$[^{18}\text{F}]\text{FDG}$ yield:

We observed that the $[^{18}\text{F}]\text{FDG}$ yield rapidly decreased when a high level of activity was produced the day before. Silver particles from the target were ruled out as the reason. This effect is mainly reported from CYCLONE 18/9 facilities with targets inside the yoke [1]. At our cyclotron the $[^{18}\text{O}]\text{H}_2\text{O}/[^{18}\text{F}]^-$ water target is placed outside the yoke and thus the beam spot is larger and the power density lower. When we opened the target for a preventive change of the target and vacuum windows, the inner

surface of the target was mostly clean. There were hardly any silver particles to be removed. Water drops remaining in the 75 m tube system (tubes and valves) after each unloading of the [¹⁸F]F⁻ water target could lead to the radiolysis effects in the tubes. This could be the reason for the low [¹⁸F]FDG yield on the next day. We performed a series of experiments with various tube materials to find the most suitable one in terms of a high [¹⁸F]FDG yield and minimum activity losses during transport. The following tube materials of 0.8 mm inner diameter were tested in one and a half years: silicone, teflon (PTFE), polyethylene (PE), PEEK and polypropylene (PP) [2].

Results

Activity losses during transport

The activity losses during transport can be described by the following equations:

$$L_{N,C} = (1 - A_N / A_C) \quad (1) \quad \text{and} \quad L_{N,R} = (1 - A_N / A_R) \quad (2)$$

(L = average activity losses, A = average activity of index N = normal unloading, C = container unloading, R = normal unloading with an additional target and tube rinse).

R1: $A_C \sim A_R$ (difference less than 3 %)

Nearly the same activity was achieved by container unloading and the normal unloading with an additional target and tube rinse. This is an indication that the target was always completely unloaded.

R2: $L_{N,C} \sim L_{N,R} = (14 \text{ to } 17) \%$

(14 to 17) % of the target yield are lost in the 75 m tube system. With our normal unloading procedure it is not possible to reduce the activity losses during transport. They depend on the length of the tube system and on the unloading principle.

R3: The results R1 and R2 are largely independent of the tube materials, the irradiation parameters and the particular charges of enriched water (level of enrichment = 96 %, 95 %, 94 %, recycled enriched water with lower level)

R4: The amount of activity that always remains in the vial of the pneumatic rabbit was estimated to be less than 3.5 % of the transported activity.

We also found that the vertical target position was not correct. To decrease the target pressure during the irradiation by increasing the gas expansion area above the water, the target was not completely filled. After correction of the vertical target position, the ion beam now touches the water completely and the target yield and also the saturation yield have thus been increased.

Properties of the tube materials in terms of transport of the water bolus and [¹⁸F]FDG synthesis:

Silicone:

- due to the surface, high resistance to transport of the water bolus
- transport time increased with the number of unloadings
- for 25 m (target to the hot cell 0 at the cyclotron site) transport time often much longer than 5 minutes
- water bolus was split into several parts

Silicon tubes are unsuitable for our purpose.

Polyethylene (PE):

- due to low mechanical stability unsuitable for long distances
- our experience in accordance with that of other research centers.

PE tubes are unsuitable for our purpose.

Teflon (PTFE):

- good properties for transporting the water bolus
- low resistance to radiation: tubes became brittle and often broke at the Rheodyne valve of the target system (entrance point of the activity into the tube) and in the FDG module, high risk of activated water squirting into the cyclotron vault and the module

PTFE tubes are unsuitable for our purpose.

PEEK:

- results of transport of the water bolus not reproducible
- sometimes good, sometimes bad transport of the water bolus, reasons for this behavior not clear
- no reliable transport of the water bolus

PEEK tubes are unsuitable for our purpose.

Polypropylene (PP):

- very good properties for transporting the water bolus
- high resistance to radiation
- FDG yield stable and sufficient

PP tubes are the most suitable ones for our purpose.

$[^{18}\text{F}]$ FDG yield

In addition to the use of the PP tubes, the activated water was removed from the 75 m tubes and the valves placed inside the tube system by rinsing them with deionized water after each unloading of the target.

The PP tubes have been used since July 14, 1998. The results are summarized in Fig. 2:

1. The absolute increase in the $[^{18}\text{F}]$ FDG yield is small but the standard deviation of the average $[^{18}\text{F}]$ FDG yield was reduced by a factor of two.
2. Every two to four months (see Fig. 2: 14 Jul. 98, 6 Nov. 98, 22 Jan. 99) the tube system is rinsed with the following procedure: rinse with 20 ml acetone, 20 ml heptane, 20 ml acetone, 100 ml deionized water, dry the tube system with nitrogen for half an hour. This leads to an improvement of the $[^{18}\text{F}]$ FDG yield.

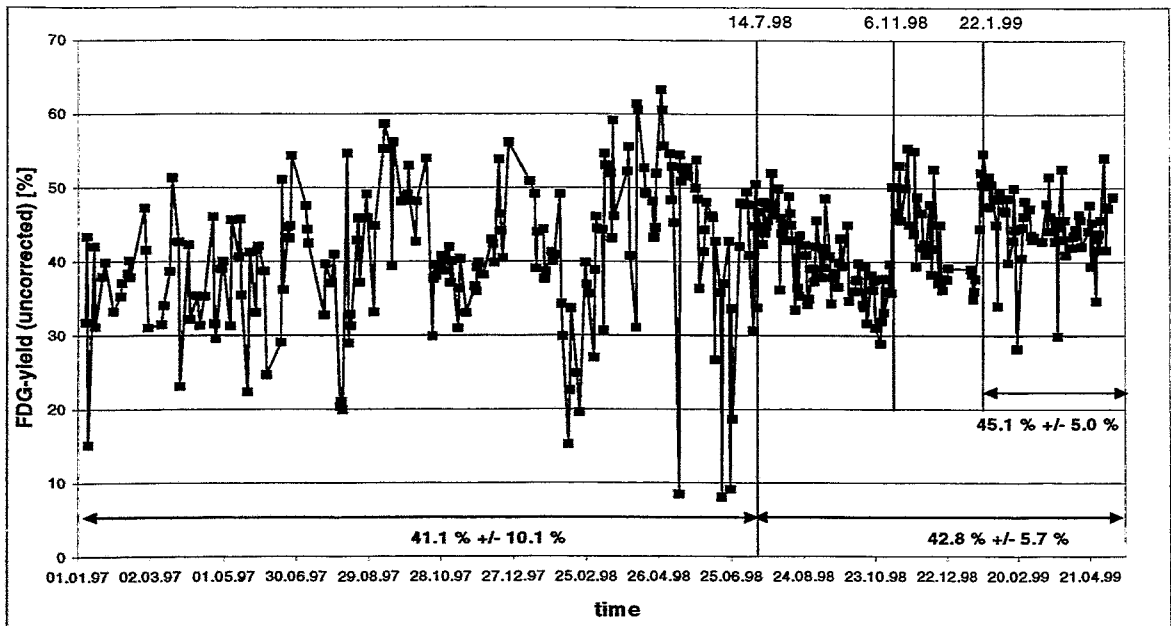


Fig. 2. $[^{18}\text{F}]$ FDG yield over two and a half years (not corrected for decay)

References

- [1] Eds. IBA and K.U. Leuven (1998) IBA PET CYCLONE USERS, second workshop, Leuven, Belgium, Dec 10 – 11.
- [2] Westera G. (1997), Universitätshospital Zürich, Nuklearmedizin, private communication.

57. Improvements at the Rossendorf PET Cyclotron "CYCLONE 18/9"

St. Preusche, H. Roß

Remote control for the azimuthal movement systems of the H⁺ and D⁻ ion sources

Introduction

The Rossendorf CYCLONE 18/9 is one of the first cyclotrons of the IBA CYCLONE 18/9 series. In our version the dees with their stems are fixed to the upper part of the yoke. Ion source adjustments have to be carried out after each opening and closing of the yoke, both for radial and azimuthal directions. This is a disadvantage for the effective running of the cyclotron and for radiation protection. To overcome it we equipped the azimuthal movement systems of both ion sources with remote-controlled electric drives. Now the azimuthal positions of the ion sources can be optimized under real ion beam conditions.

Technical solution and results

Two 24 V DC motors including gear units were added to the transmission spindles of the azimuthal movement systems of both ion sources (see Fig. 1). The 24 V power supply unit and the control buttons are placed close to the control terminal of the cyclotron in the control room.

The combination of radial and azimuthal movement of the ion sources causes their optimum positioning to the puller electrodes of the dees and thus maximizes the ion beam. After each opening and closing of the yoke the radial positions of the two ion sources are manually adjusted to the last operational positions with an accuracy of less than 0.3 mm. These radial positions are the result of our experience of operating of the CYCLONE 18/9.

We observed that during their lifetime the original sharp shapes of the slits of the ion sources and the puller electrodes are more and more burned out. These wear effects lead to losses in the ion beam. With our remote control for the azimuthal movement systems of both ion sources it is possible to adjust the azimuthal positions, if necessary, during particle acceleration to get maximum ion beam from the ion sources and at least on the targets.

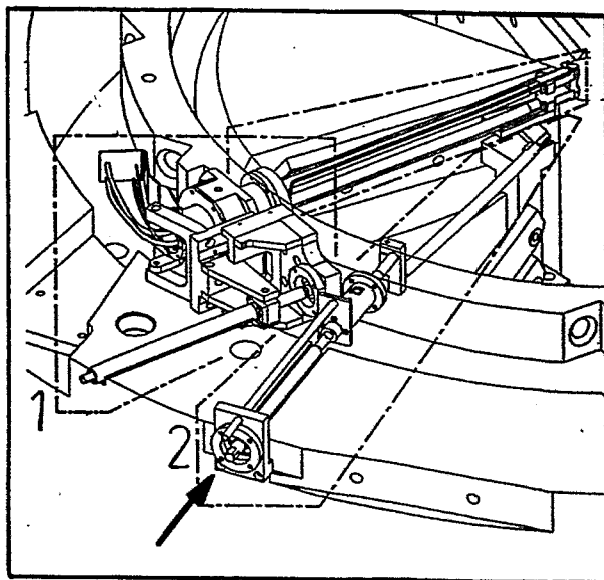


Fig 1. Radial (1) and azimuthal (2) movement systems of the H⁺ and D⁻ ion sources (part of IBA drawing 05.09.00.001) The arrow indicates the position of the motor.

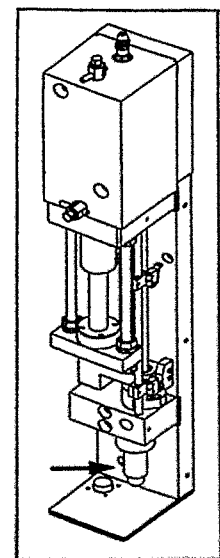


Fig 2. Hydraulic cylinder unit of the RF rough and fine tuning system (part of IBA drawing 05.09.26.000) The arrow indicates the position of the motor.

Remote control for the RF rough tuning system

Introduction

RF resonant tuning is by capacitive tuning. A pulse discriminator circuitry sends a signal which activates a DC motor on the cavity tuning drive mechanism. This mechanism consists of a tandem pair of small hydraulic cylinders, one for the rough and one for the fine tuning .

We observed that the fine tuning system always moves to the lower limit switch under the influence of temperature effects during long-time irradiation. To prevent RF instabilities when reaching the switch (reflected power increases and the RF system shuts down), we equipped the rough tuning system with remote control to correct its position in a small range as a compensation of the fine tuning movement during the irradiation process.

Technical solution and results

The small hydraulic cylinder of the rough tuning system was replaced by a 24 V DC motor including a gear unit and a transmission spindle (see Fig. 2). We used the same 24 V power supply as used for the azimuthal movement of the ion sources.

The tuning plate inside the cyclotron only moves in one direction under the influence of temperature effects. These observed effects are indicated by the movement of the fine tuning system to the lower limit switch. For optimum resonance conditions we positioned the rough tuning system so that the fine tuning system has nearly the full range of operation, starting from the cold cyclotron. When we reach the lower limit switch during long-time irradiation (the RF system is out of resonance and shuts down after a certain time) we can compensate the movement of the fine tuning system by remote-controlled moving of the rough tuning system in a small range. The RF system goes back to the resonant mode and the irradiation can go ahead.

Conclusion

Both the remote control for the azimuthal movement systems of the H⁺ and D⁺ ion sources and the RF rough tuning system have improved the handling and reliability of our CYCLONE 18/9. Ion source adjustments have been simplified and RF tuning has become more stable in long-time irradiation.

58. Operation of the Rossendorf PET Cyclotron "CYCLONE 18/9" in 1998/1999

St. Preusche, J. Steinbach

Introduction

A detailed description of the Rossendorf PET cyclotron "CYCLONE 18/9" facility and the 500 m long Radionuclide Transport System between the cyclotron and the radiochemical/radiopharmaceutical laboratories was given in [1] - [5]. Since we received the licence for routine operation in autumn 1996, the cyclotron has worked in its predicted way with high reliability.

Routine operation

Our standard radionuclides in routine operation are [^{18}F]F, [^{18}F]F₂ and ^{11}C , which makes a few radiotracers and radiopharmaceuticals available.

The Rossendorf PET Center uses the satellite concept and supplies clinics in Dresden, Gera, Jena, Suhl, Erfurt, Leipzig, Berlin and Bautzen (max. distance: 200 km) through Mallinckrodt Medical GmbH with the radiopharmaceutical [^{18}F]FDG. Do to this fact the need for [^{18}F]FDG has grown remarkably (s. Figs. 1 and 2).

The cyclotron runs 2 to 4 hours per day (Tuesdays to Fridays). Monday is the so-called service day both for the cyclotron and radiopharmacy. Table 1 gives an overview of the 1998/1999 radionuclide production (01 January 1998 to 30 June 1999) and typical irradiation conditions. The radionuclides ^{13}N and ^{15}O were produced to optimize the irradiation and extraction conditions and the 500 m on-line gas transport.

Table 1. Radionuclide production in 1998/1999 (01 January 1998 to 30 June 1999)

RN	Radionuclide production		Typical irradiation conditions			
	Number of irradiations	A _{EOB} GBq	Irrad. Time Min	I _T μA	Yield _{EOB} GBq	Sat. Yield GBq/μA
[^{18}F]F	338	20849	60	30	70	7.8
[^{18}F]F ₂	159 ⁾	555	120	18	10	1.1
^{11}C	155	825	4	5	4	6.2
^{15}O	89	440	30	10	7	0.7
^{13}N	10	84	15	10	8	1.2

⁾including pre-irradiations

Fig. 1 shows the number of irradiations and Fig. 2 the total amount of activity produced in 1998 in comparison with 1997.

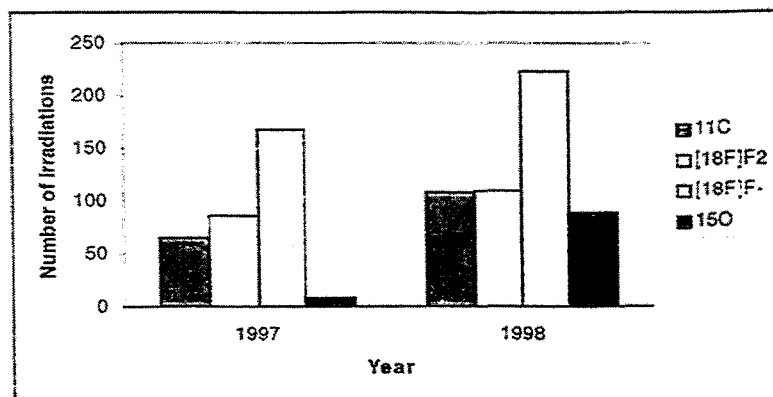


Fig. 1. Number of irradiations of radionuclides produced

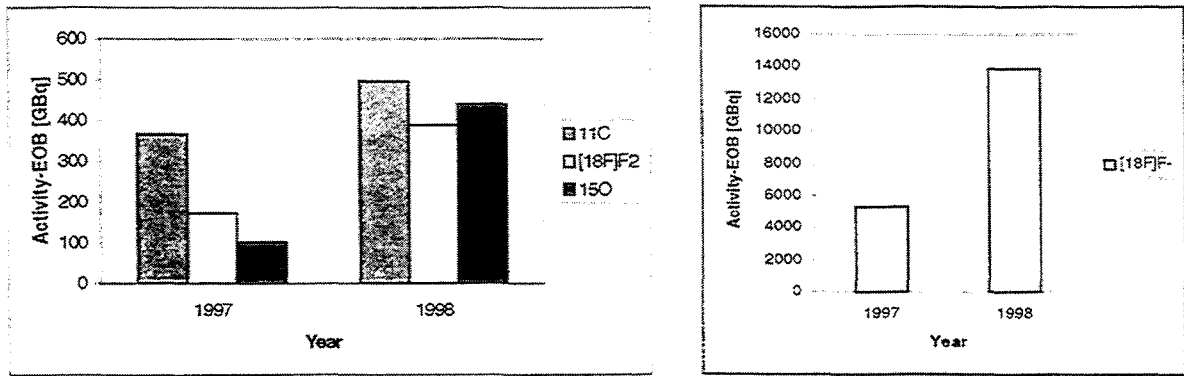


Fig. 2. Total amount of activity produced

Investigations and improvements at the cyclotron

- Remote control for the azimuthal movement systems of the H and D ion sources

The azimuthal movement systems of the H and D ion sources were equipped with remote-controlled electric drives to optimize their azimuthal positions under real ion beam conditions in terms of maximum ion beam on the targets [6, 8].

- Remote control for the RF rough tuning system

The RF rough tuning system was equipped with remote control to correct its position in a small range during long-time irradiation in terms of stabilization the RF tuning process [6, 8].

- Investigations of tube material for effective transport of irradiated liquids

Investigations were carried out to find the most suitable material for transport of the irradiated ^{18}F water target from the cyclotron to the pneumatic rabbit (cyclotron site, 25 m) and from the pneumatic rabbit to the ^{18}F FDG module (radiochemistry site, 50 m). Tubes of silicone, polyethylene, teflon, PEEK and polypropylene were tested in terms of minimum activity losses during transport and their influence on a stable ^{18}F FDG synthesis. Polypropylene tubes proved to be the most suitable ones [7, 8].

Maintenance and service

In view of our many years of experience in operation and maintenance of accelerators in Rossendorf, no maintenance contract was concluded with IBA. The CYCLONE 18/9 staff are responsible for all maintenance work and service of the cyclotron.

Maintenance at the open cyclotron and of the vacuum system is carried out annually in the first week of January and during two or three days in summer to:

- rebuild and clean the ion sources
- replace parts of the acceleration system
- check all parts inside the vacuum chamber
- check the forevacuum and the oil diffusion pumps

Several checks of the cyclotron subsystems are carried out on Mondays.

Destroyed stripper foils were the main reason for venting and opening the cyclotron until the middle of 1998. A new IBA stripper version with a higher area density and longer lifetime has been in use since then. Cyclotron openings as a result of destroyed strippers were reduced.

The strippers are mostly replaced in the late afternoon. Until the first irradiation in the following morning there is enough time for pumping the vacuum chamber down.

Unplanned turn-off periods:

1998: no turn-offs

1999: March: four days

- troubleshooting in the vacuum system to find a very small leak between the lower part of the vacuum chamber and the yoke
- compensated by additional irradiations on Mondays

June/July: thirteen days

- PLC communication processor destroyed by heavy storm
- intervention on site necessary by IBA and Siemens
- test and repair of the PLC system at IBA site

Once a year the CYCLONE 18/9 facility is checked by the TÜV Sachsen organization (TÜV = Association for Technical Inspection) for § 76 of the German Radiation Protection Order. Until now there have been no objections to further operation of the cyclotron.

Maintenance and service of the so-called peripheric facilities (ventilation, climatization facilities, etc.) is carried out by the ABB service firm.

Radiation protection

- Emission of radionuclides with the exhaust air

Exhaust air monitoring for radionuclides is carried out by a Berthold exhaust air emission measurement facility both for the CYCLONE 18/9 and the U-120 cyclotron, which is still used for various application purposes except PET. The annual limits for the emission of radionuclides have been confirmed by our authority. Investigations of the emission of radionuclides by both cyclotrons showed that the emission resulting from the CYCLONE 18/9 cyclotron is negligible. Table 2 gives an overview of the emission of radionuclides with the exhaust air and can be taken as an indication of the safe operation of the CYCLONE 18/9 cyclotron.

Table 2: Emission of radionuclides with the exhaust air resulting from operation of the CYCLONE 18/9 and U-120 cyclotrons

	01 January to 31 December 1998	01 January to 30 June 1999
⁴¹ Ar [Bq/a]	6.7E09	1.6E09
¹⁸ F [Bq/a]	4.8E09	1.1E09
¹³ N [Bq/a]	1.4E10	3.4E09
¹¹ C [Bq/a]	7.0E10	1.6E10
Percent of the annual limit	1.5	0.4

- Exposure to radiation of the cyclotron staff

The cyclotron staff belong to the category A of occupational exposed persons. The average exposure to radiation was 2.9 mSv in 1998, which is less than 6 % of the annual limit. In addition to the annual medical check-ups, there are quarterly measurements of incorporation with the whole body counter.

Miscellaneous

Since its foundation in 1996 on the initiative of our institut, the worldwide CYCLONE 18/9 & 10/5 USER COMMUNITY has worked as a forum of the CYCLONE 18/9 and CYCLONE 10/5 users, exchanging experience of operation and maintenance of these types of IBA cyclotrons and the corresponding chemistry modules [2]. It is also very helpful in case of problems and failures to discuss methods and ways of troubleshooting. The second workshop of our user community took place in Leuven, Belgium, in December 1998 [8].

References

- [1] Preusche St., Steinbach J., Füchtner F., Krug H., De Leenheer M. and Ghyoot M. (1996) The new cyclotron of the Rossendorf PET Center cyclotrons and their applications. World Scientific Publishing C. Pte. Ltd.
- [2] Johannsen B. and Preusche St. (1996) – Eds. CYCLONE 18/9 USER COMMUNITY, First Workshop, Rossendorf, Germany, Oct. 10-11, FZR-151.
- [3] Preusche St., Füchtner F., Steinbach F., Krug H. and Neumann W. (1996) The radionuclide transport system of the Rossendorf PET Center. XXX. European Cyclotron Progress Meeting, Catania, Italy, Sept. 04-07.
- [4] Preusche St., Füchtner F., Steinbach J., Krug H. and Neumann W. (1997) The Rossendorf radionuclide transport system for gases and liquids. 7th Int. Workshop on Targetry and Target Chemistry, Heidelberg, Germany, June 08-11.
- [5] Preusche St., Füchtner F., Steinbach F., Zessin J., Krug H. and Neumann W. (1999) Long-distance transport of radionuclides between PET cyclotron and PET radiochemistry. *Appl. Radiat. Isot.*, in press.
- [6] Preusche St. and Roß H. (1999) Improvements at the Rossendorf PET cyclotron "CYCLONE 18/9". *This report*, pp. 211-212.
- [7] Preusche St., Füchtner F. and Steinbach J. (1999) Influence of transport conditions of the [¹⁸F]F⁻ water target on the [¹⁸F]FDG synthesis. *This report*, pp. 208-210.
- [8] Editors: IBA and K.U. Leuven (1998) IBA PET CYCLONE USERS - second workshop. Leuven, Belgium, Dec. 10-11.

59. Sources of Radiation Exposure during FDG-PET Studies

H. Linemann¹, E. Will, B. Beuthien-Baumann¹, A. Wittmüß¹, H. Schröder¹, H. Kutzner¹,
A. Hauptmann²

¹TU Dresden, ²VKTA Rossendorf

The aim of this study was to identify the main sources of radiation doses to the medical personnel during PET studies so as to minimize the radiation exposure in routine scanning. The tasks to be undertaken under radiation exposure in preparing and performing a PET study are syringe preparation, injection, blood sampling (only for quantitative studies) and handling of the patient after injection of the radiopharmaceutical. The acquired radiation dose depends strongly on the work organization (distance and time) and on the shielding used.

The effects on the radiation dose were studied by the various working steps with the shielding used in the Rossendorf PET Center. We focused our work on 2-[¹⁸F]fluoro-2-deoxy-glucose ([¹⁸F]FDG) studies since this is the most frequently used PET radiopharmaceutical.

It is known, that radiation exposure during blood sampling is a major factor for the acquired dose per study [1]. We therefore designed a special movable radiation protection shield.

In the literature the radiation dose for the PET personnel is indicated either as annual value over all studies [2] or as values for a part of the tasks [1, 3]. Only limited information is available on hand dose values.

Experimental

The radiation exposure, personal dose and hand dose of the medical personnel were measured during the preparation and performance of [¹⁸F]FDG scans with the ECAT EXACT HR⁺ PET camera (Siemens - CTI).

The dosimeters used:

- dosimeter LB 133 (gamma probe) (Berthold) to measure the radiation emitted by the patient,
- personal digital dosimeter EDM 150A (Graetz) to obtain the body dose of the personnel.
- LiF-thermoluminescent dosimeters (Harshaw). We used finger rings to determine the radiation dose during injection and detectors of 8 mm diameter were taped to the fingertips of each hand to measure the radiation dose during syringe preparation.

The PET studies included dynamic brain scans with manual blood sampling (arterialized venous blood) as well as heart and whole body scans without blood sampling. The injected activities varied between 260 and 370 MBq.

The radiopharmaceutical for the day (max. 7 GBq) was transported and stored in a lead container of 3 cm wall thickness. The syringes containing the individual patient doses were prepared in a lead box with a window of 3 cm lead equivalent (Fig. 1). The syringes were handled with a special pair of tongs to minimize the radiation dose to the hands during preparation. During transport and injection the syringe was provided with a tungsten syringe shield of 8 mm wall thickness.

A movable radiation shield (2 cm lead) was designed

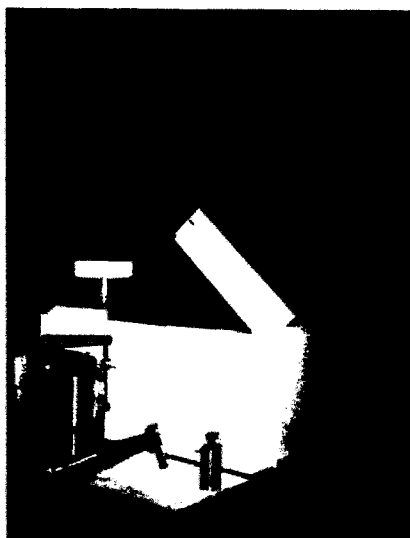


Fig. 1. Lead box with a lead glass window.
In front from left to right:
- container for radiopharmaceutical
- pair of tongs for syringe preparation
- syringe shield for injection.



Fig. 2. Radiation shield with hand heating box for blood sampling

(Fig. 2)¹⁾ to protect the technologist from radiation emitted by the patient during manual blood sampling. It can be placed between the patient and the technologist on both sides of the bed. Another advantage is the possibility of mounting on this device a hand heating box for pseudo arterial blood sampling.

Results and Discussion

Table 1 shows the results of the personal dose and hand dose measurements using protection devices.

Table 1. Results of the personal dose and hand dose measurements

Task	Number of studies	Dose per study [μ Sv]		
		Personal dose	Hand dose (rings)	Hand dose (finger tapes)
Syringe preparation (with tongs)	16	≤ 1		
	52			710 left, 710 right
Injection	45	3 (2 - 5)	27 left, 13 right	
Blood sampling	28	6 (3 - 11)		
Patient handling	28	7 (2 - 16)		

The detailed finger dose distribution values for the syringe preparation without and with using a pair of tongs are shown in Tables 2 and 3. The hand dose for the syringe preparation shown in Table 1 was derived from the mean of the highest finger dose values measured with the LiF dosimeters taped to the fingertips (Table 3).

Table 2. Highest finger doses for syringe preparation (manipulation without tongs, 1 technologist)

Measurement Nr.	Number of syringe preparations	Highest finger dose/syringe preparation] [mSv]	
		r	l
1	2	0.85	2.80
2	4	0.98	1.98
Σ : 6 mean (weighted)		0.94	2.25

The measurement of radiation exposure lateral to the unshielded patient thorax directly after injection of 340 MBq showed dose rates of 60 μ Sv/h and 20 μ Sv/h for distances of 30 cm and 80 cm.

With the movable radiation shield placed between the patient and the technologist, the radiation exposure of the technologist was reduced to 20% in comparison with the unshielded situation.

To estimate the radiation risk, we have to compare the measured dose for one year with the dose limits for exposed personnel (according to class A this means 50 mSv for the personal dose, 500 mSv for the hand dose). We assume a frequency of 13 PET studies/week and 52 working weeks/year.

Personal dose:

With the above-mentioned number of studies per year and the measured values from Table 1, a personal dose of about 10 mSv/a will be obtained for a technologist performing all tasks. This personal dose depends mainly on the time of close contact with the patients during blood sampling and patient handling.

Careful planning of the PET procedure is required to avoid unnecessary radiation exposure.

Hand dose:

The hand dose is mainly accumulated during syringe preparation. The use of a pair of tongs (left hand) reduced this dose to about 40% (Tables 2 and 3). For all these efforts the maximum permissible hand dose per year will be reached after preparation of 500 syringes. In PET facilities with a high patient throughput an automatic or remote-controlled filling device should therefore be used.

Table 3. Highest finger doses for syringe preparation (manipulation with tongs, 3 technologists)

Measurement Nr.	Number of syringe preparations	Highest finger dose/syringe preparation [mSv]	
		r	l
1	3	0.27	0.27
2	10	0.69	0.63
3	5	1.54	2.60
4	13	0.55	0.20
5	10	0.47	0.79
6	3	1.63	0.77
7	8	0.59	0.54
Σ : 52	mean (weighted):	0.71	0.71

¹⁾ The radiation shield was manufactured by Wälischmiller, Dresden.

References

- [1] McCormick V. and Miklos J. (1993) Radiation dose to positron emission tomography technologists during quantitative versus qualitative studies. *J. Nucl. Med.* **34**, 769-772.
- [2] Ostertag H. J., Krauss O., Kübler W. K., Kämmer M. and Strauss L. G. (1991) Measurement and calculation of local radiation doses in the vicinity of a positron emission tomograph (PET). *Radiation Protection Dosimetry* **36**, 37-41.
- [3] Chiesa C., DeSanctis V., Crippa F., Schiavini M., Fraigola C. E., Bogni A., Pascali C., Decise D., Marchesini R. and Bombardieri (1997) Radiation dose to technicians per nuclear procedure: comparison between technetium-99m, gallium-67, and iodine-131 radiotracers and fluorine-18 fluorodeoxyglucose. *Eur. J. Nucl. Med.* **24**, 1380-1389.

III. PUBLICATIONS, LECTURES, PATENTS, AWARDS AND THESES

PUBLICATIONS

- Alberto R., Schibli R., Schubiger A. P., Abram U., Pietzsch H.-J., Johannsen B. (1999)
First application of fac-[^{99m}Tc(OH₂)₃(CO)₃]⁺ in bioorganometallic chemistry: Design, structure and in vitro affinity of a 5-HT_{1A} receptor ligand labeled with ^{99m}Tc.
J. Am. Chem. Soc. **121**, 6076-6077.
- Bauer R., Bergmann R., Walter B., Brust P., Zwiener U., Johannsen B. (1999)
Regional distribution of cerebral blood volume and cerebral blood flow in newborn piglets – effect of hypoxia/hypercapnia.
Brain Res. Dev. Brain Res. **12**, 89-98.
- Bergmann R., Brust P., Johannsen B. (1998)
Differentiation between specific and non-specific effects related to P-glycoprotein inhibition in immortalised rat brain endothelial cells.
Int. J. Clin. Pharmacol. Ther. **36**, 46-49.
- Bouziotis P., Papadopoulos M., Pirmettis I., Pelecanou M., Raptopoulou C. P., Terzis A., Stassinopoulou Ch., Friebe M., Spies H., Johannsen B., Chiotellis E. (1999)
Synthesis and characterization of two P,S,N-coordinated cis-dioxorhenium(V) complexes.
In: *Technetium, Rhenium and Other Metals in Chemistry and Nuclear Medicine* (Edited by Nicolini M., Mazzi U.) SGEEditoriali Padova pp. 203-208.
- Brust P., Bauer R., Walter B., Bergmann R., Füchtner F., Vorwieger G., Steinbach J., Johannsen B., Zwiener U. (1998)
Simultaneous measurement of cerebral blood flow and [¹⁸F]FDOPA metabolism in newborn piglets.
Int. J. Dev. Neurosci. **16**, 353-364.
- Brust P., Scheffel U., Szabo Z. (1999)
Radioligands for the study of the 5-HT transporter in vivo.
IDrugs **2**, 129-145.
- Brust P., Bauer R., Vorwieger G., Walter B., Bergmann R., Füchtner F., Steinbach J., Zwiener U., Johannsen B. (1999)
Upregulation of the aromatic amino acid decarboxylase under neonatal asphyxia.
Neurobiol. Dis. **6**, 131-139.
- Friebe M., Jankowsky R., Spies H., Seichter W., Papadopoulos M., Chiotellis E., Johannsen B. (1998)
A mixed-ligand P,S,N,- cis-dioxorhenium(V) complex by ligand exchange reaction on trans-monooxo-trichlorobis(triphenylphosphine)rhenium(V): formation and structural studies.
Polyhedron **17**, 3711-3720.
- Friebe M., Spies H., Berger R., Syhre R., Papadopoulos M., Chiotellis E., Suda K., Wunderli-Allenspach H., Johannsen B. (1999)
Amine group bearing '3+1' oxotechnetium(V) and oxo-rhenium(V) complexes: synthesis, characterization of lipophilicity and permeation through the blood-brain barrier.
In: *Technetium, Rhenium and Other Metals in Chemistry and Nuclear Medicine* (Edited by Nicolini M., Mazzi U.) SGEEditoriali Padova, pp. 627-631.
- Füchtner F., Steinbach J., Vorwieger G., Bergmann R., Syhre R., Brust P., Beuthin-Baumann B., Burchert W., Zips D., Baumann M., Johannsen B. (1999)
3-O-methyl-6-[¹⁸F]fluoro-L-DOPA - a promising substance for tumour imaging.
J. Labelled Compd. Radiopharm. **42** (Suppl.1), S267-S269.
- Hilger C. S., Noll B., Blume F., Leibnitz P., Johannsen B. (1999)
Tc and Re complexes of N-(MAG₁)-histamine.
In: *Technetium, Rhenium and Other Metals in Chemistry and Nuclear Medicine* (Edited by Nicolini M., Mazzi U.) SGEEditoriali Padova, pp. 221-224.

- Hoepping A., Reisgys M., Brust P., Seifert S., Spies H., Alberto R., Johannsen B. (1998)
TROTEC-1, a new high-affinity ligand for labeling of the dopamine transporter.
J. Med. Chem. **41**, 4429-4432.
- Hoepping A., Brust P., Berger R., Spies H., Machill S., Scheller D., Johannsen B. (1998)
Novel rhenium complexes derived from α -tropanole as potential ligands for the dopamine transporter.
Bioorg. Med. Chem. **6**, 1663-1672.
- Jankowsky R., Kirsch S., Reich T., Spies H., Johannsen B. (1998)
Solution structures of rhenium(V) oxo peptide complexes of glycyglycylcysteine and cysteinylglycine as studied by capillary electrophoresis and X-ray absorption spectroscopy (EXAFS).
J. Inorg. Biochem. **70**, 99-106.
- Jankowsky R., Kirsch S., Spies H., Johannsen B. (1999)
Solution structures of technetium(V) and rhenium(V) peptide complexes as studies by EXAFS spectroscopy and capillary electrophoresis.
In: *Technetium, Rhenium and Other Metals in Chemistry and Nuclear Medicine* (Edited by Nicolini M., Mazzi U.) SGEEditoriali Padova, pp. 229-235.
- Jankowsky R., Friebe M., Noll B., Johannsen B. (1999)
Determination of dissociation constants of technetium-99m radiopharmaceuticals by capillary electrophoresis.
J. Chromatography A **833**, 83-96.
- Jankowsky R., Noll B., Johannsen B. (1999)
Capillary electrophoresis of technetium-99m radiopharmaceuticals.
J. Chromatography B **724**, 365-371.
- Jansen K., Steinbach J., Preusche St. (1998)
Fortluft-Emissionsüberwachung am PET-Zentrum im Forschungszentrum Rossendorf
Publikationsreihe Fortschritte im Strahlenschutz „Radioaktivität in Mensch und Umwelt“, Verlag TÜV Rheinland, pp.108-113.
- Johannsen B., Pietzsch H.-J., Reisgys M., Hoepping A., Scheunemann M., Spies H., Brust P., Schibli R., Schubiger P. A., Alberto R. (1999)
First application of the metallocarbonyl concept to design CNS receptor imaging agents based on technetium-99m.
J. Labelled Compd. Radiopharm. **42** (Suppl.1), S48-S50.
- Johannsen B., Pietzsch H.-J., Scheunemann M., Kretzschmar M., Seifert S., Brust P., Syhre R., Spies H. (1999)
Synthesis and autoradiographical evaluation of a novel high-affinity Tc-99m ligand for the serotonin-5-HT_{2A} receptor.
J. Labelled Compd. Radiopharm. **42** (Suppl.1), S345-S347.
- Kirsch S., Noll B., Spies H., Leibnitz P., Scheller D., Krueger T., Johannsen B. (1998)
Preparation and structural studies of neutral oxorhenium(V) complexes with D-penicillamine methyl ester.
J. Chem. Soc., Dalton Trans. 455-460.
- Kirsch S., Jankowsky R., Leibnitz P., Spies H., Johannsen B. (1999)
Crystal and solution structure of oxorhenium(V) complexes with cysteine and cysteine methyl ester.
J. Biol. Inorg. Chem. **4**, 48-55.
- Kirsch S., Jankowsky R., Leibnitz P., Spies H., Johannsen B. (1999)
Crystal and solution structure of oxorhenium(V) complexes with cysteine and cysteine methyl ester.
In: *Technetium, Rhenium and Other Metals in Chemistry and Nuclear Medicine* (Edited by Nicolini M., Mazzi U.) SGEEditoriali Padova, pp. 225-228.

- Knieß T., Spies H., Brandau W., Johannsen B. (1998)
Nicotinamide substituted rhenium and technetium mixed-ligand complexes as redox marker.
J. Labelled Compd. Radiopharm. **XLI**, 605-614.
- Knieß T., Noll St., Noll B., Spies H., Johannsen B. (1999)
Effective coupling of Re/Tc-MAG₃ complexes with amines and nucleobases in aprotic solvents.
J. Radioanal. Nucl. Chem. **240**, 657-660.
- Mäding P., Steinbach J. (1998)
N.c.a. ¹¹C-labelling of benzenoid compounds in ring positions: synthesis of 3-nitro-[3-¹¹C]toluene and 4-nitro-[4-¹¹C]toluene and their corresponding toluidines.
J. Labelled Compd. Radiopharm. **XLI**, 647-656.
- Meyer G.-J., Matzke K.H., Hamacher K., Füchtner F., Steinbach J., Notohamiprodjo G., Zijlstra S. (1999)
The stability of 2-[¹⁸F]fluoro-desoxy-D-glucose towards epimerisation under alkaline conditions.
Appl. Radiat. Isot. **51**, 37-41.
- Noll B., Noll St., Leibnitz P., Jankowsky R., Spies H., Johannsen B. (1999)
Technetium(V) and rhenium(V) complexes with mercaptoacetyl glycine (MAG₁).
In: *Technetium, Rhenium and Other Metals in Chemistry and Nuclear Medicine* (Edited by Nicolini M., Mazzi U.) SGEEditoriali Padova, pp. 241-244.
- Noll St., Noll B., Kniess T., Kampf G., Spies H., Johannsen B. (1999)
Rhenium and technetium complexes with nucleic acid components.
In: *Technetium, Rhenium and Other Metals in Chemistry and Nuclear Medicine* (Edited by Nicolini M., Mazzi U.) SGEEditoriali Padova, pp. 553-556.
- Papadopoulos M., Pirmettis I., Raptopoulou C., Chiotellis E., Friebe M., Berger R., Spies H., Johannsen B. (1998)
Synthesis, structure, lipophilicity and protonation behaviour of mixed-ligand rhenium chelates functionalised by amine groups.
Appl. Radiat. Isot. **49**, 961-966.
- Pietzsch H.-J., Reisgys M., Alberto R., Hoepfing A., Scheunemann M., Seifert S., Wüst F., Spies H., Schubiger P. A., Johannsen B. (1999)
Thioether ligands as anchor groups for coupling the "Tc(CO)₃" and "Re(CO)₃" moieties with biologically active molecules.
In: *Technetium, Rhenium and Other Metals in Chemistry and Nuclear Medicine* (Edited by Nicolini M., Mazzi U.) SGEEditoriali Padova pp. 313-316.
- Regina A., Koman A., Piciotti M., El Hafny B., Center M. S., Bergmann R., Couraud P. O., Roux F. (1998)
Mrp1 multidrug resistance-associated protein and P-glycoprotein expression in rat brain microvessel endothelial cells.
J. Neurochem. **71**, 705-715.
- Römer J., Füchtner F., Steinbach J., Johannsen B. (1999)
Automated production of 16α [¹⁸F]Fluoroestradiol for breast cancer imaging.
Nucl. Med. Biol. **26**, 473-479.
- Römer J., Füchtner F., Steinbach J., Johannsen B. (1999)
16α-[¹⁸F]Fluoroestradiol-3,17β-disulphamate for sulphatase imaging.
J. Labelled Compd. Radiopharm. **42** (Suppl.1), S715-S716
- Rother A., Knieß T., Pütz M., Jungclas H., Spies H., Johannsen B. (1999)
Nicotinamide-substituted complexes as redox markers.
2. Synthesis of a ⁹⁹Tc-dihydropyridine mixed-ligand complex and investigation of the stability in tissue homogenates
J. Labelled Compd. Radiopharm. **42**, 673-681.

- Scheunemann M., Mäding P., Steinbach J., Bergmann R., Iterbeke K., Tourwe D., Johannsen B. (1999)
Fluorine-18 labelling of neurotensin analogues for the development of tumour imaging agents.
J. Labelled Compd. Radiopharm. **42** (Suppl.1), S713-S714
- Schibli R., Alberto R., Schaffland A. O., Schubiger P. A., Abram U., Pietzsch H.-J., Johannsen B. (1999)
Derivatization strategies of small biomolecules for the labeling with the organometallic $^{99m}\text{Tc}(\text{CO})_3$ -core.
J. Labelled Compd. Radiopharm. **42** (Suppl.1), S147-S149
- Seifert S., Pietzsch H.-J., Scheunemann M., Spies H., Syhre R., Johannsen B. (1998)
No carrier added preparations of '3+1' mixed-ligand ^{99m}Tc complexes.
Appl. Radiat. Isot. **49**, 5-11.
- Seifert S., Syhre R., Gupta A., Spies H., Johannsen B. (1999)
Stability studies on "3+1" mixed-ligand technetium and rhenium complexes.
In: Technetium, Rhenium and Other Metals in Chemistry and Nuclear Medicine (Edited by Nicolini M., Mazzi U.) SGEEditoriali Padova pp. 687-690.
- Seifert S., Leibnitz P., Spies H. (1999)
Nitridorhenium(V)-Komplexe mit Dimercaptobernsteinsäuredimethylester. Präparation, Charakterisierung und Kristallstruktur von $[\text{Re}\{\text{NC}(\text{CH}_3)_2\text{PPhMe}_2\}(\text{DMSMe}_2)_2]$.
Z. anorg. allg. Chem. **625**, 1037-1040.
- Spies H., Pietzsch H.-J., Johannsen B. (1999)
The "n+1" mixed-ligand approach in the design of specific technetium radiopharmaceuticals: potentials and problems.
In: Technetium, Rhenium and Other Metals in Chemistry and Nuclear Medicine (Edited by Nicolini M., Mazzi U.) SGEEditoriali Padova, pp. 101-108.
- Spies H., Noll S., Noll B., Hilger C. S., Brust P., Syhre R., Johannsen B. (1999)
Derivatives of 6-methyl-8 α -amino-ergoline: synthesis and affinity to the dopamine D₂ receptor.
In: Technetium, Rhenium and Other Metals in Chemistry and Nuclear Medicine (Edited by Nicolini M., Mazzi U.) SGEEditoriali Padova, pp. 237-240.
- Spies H., Fietz T., Zablotskaya A., Beljakow S., Lukeviz E. (1999)
Siliinaja modifikacija biologitscheski aktivnich sojedenjenii. 6. Kremneorganitscheskije sojedenjenija kompleksow renija (V) co smeschannimi ligandami.
Chimija geterociklischeskaja sojedenjenija, (Chem.Heterocycl.Compds.) N1, 116-125.
- Syhre R., Seifert S., Spies H., Gupta A., Johannsen B. (1998)
Stability versus reactivity of "3+1" mixed-ligand technetium-99m complexes *in vitro* and *in vivo*.
Eur. J. Nucl. Med. **25**, 793-796.
- Vorwieger G., Brust P., Bergmann R., Bauer R., Walter B., Steinbach J., Füchtner F., Johannsen B. (1998)
HPLC-analysis of the metabolism of 6- ^{18}F -fluoro-L-DOPA (FDOPA) in the brain of neonatal pigs.
In: Quantitative Functional Brain Imaging with Positron Emission Tomography, (Carson, R. E., Daube-Witherspoon, M. E., Herscovitch, P., eds.) Academic Press, New York, pp. 285-292.
- Wüst F., Carlson K. E., Katzenellenbogen J. A., Spies H., Johannsen B. (1998)
Synthesis and binding affinities of new 17 α -substituted estradiol rhenium n+1 mixed-ligand and thioether-carbonyl complexes.
Steroids **63** (12), 665-671.
- Wüst F., Scheller D., Spies H., Johannsen B. (1998)
Synthesis of oxorhenium(V) complexes derived from 7 α -functionalized testosterone: first rhenium-containing testosterone derivatives.
Eur. J. Inorg. Chem., 789-793.

Wüst F., Skaddan M. B., Carlson K. E., Leibnitz P., Katzenellenbogen J. A., Spies H., Johannsen B. (1999)
Synthesis and receptor binding of novel progesterin-rhenium complexes.
In: Technetium, Rhenium and Other Metals in Chemistry and Nuclear Medicine (Edited by Nicolini M., Mazzi U.) SGEEditoriali Padova, pp. 491-495.

ABSTRACTS

Bauer R., Bergmann R., Walter B., Brust P., Zwiener U., Johannsen B. (1999)
Moderate asphyxia induces an increased perfusion velocity, but the concomitant cerebral blood volume (CBV) increase remains moderate in newborn piglets.
J. Cereb. Blood Flow Metab. **19**(Suppl. 1), S516.

Bergmann R., Brust P., Johannsen B. (1998)
Beeinflussung der ^{99m}Tc-MIBI- und [¹⁸F]FDG-Aufnahme durch Inhibitoren des P-Glycoproteins.
Nuklearmedizin **37**, A17.

Bergmann R., Brust P., Pietzsch H.-J., Johannsen B. (1998)
Evaluation of the in vitro and in vivo properties of a potential Tc-labelled inhibitor of the MDR gene product P-glycoprotein.
Eur. J. Nucl. Med. **25**, 865.

Beuthien-Baumann B., Handrick W., Schmidt T., Burchert W., Schackert G., Kropp J., Franke W. G. (1999)
¹⁸F-FDG-PET und ^{99m}Tc-ECD in der Hirn-Diagnostik bei Patienten mit apallischem Syndrom.
Nuklearmedizin **38**, A46.

Brust P., Vorwieger G., Bauer R., Bergmann R., Walter B., Füchtner F., Steinbach J., Johannsen B. (1998)
Upregulation of the aromatic amino acid decarboxylase under neonatal asphyxia.
Eur. J. Neuroscience **10** (Suppl. 10), 95.

Brust P., Friedrich A., Krizbai I. A., Bergmann R., Roux F., Johannsen B. (1999)
Functional expression of the serotonin transporter at the brain endothelium.
J. Cereb. Blood Flow Metab. **19**(Suppl. 1), S245.

Burchert W., Wolpers H. G., van den Hoff J., Hakimi M., Meyer G. J., Hausmann T., Pethig K., Knapp W. H. (1999)
¹³N-NH₃ PET zur Diagnostik der Transplantatvaskulopathie. Vergleich mit Koronarangiographie und intrakoronarem Ultraschall.
Nuklearmedizin **38**, A27.

Eisenhut M., Mohammed A., Mier W., Friebe M., Haberkorn U. (1999)
Melanoma affine Tc-99m complexes of N-(2-diethylaminoethyl)benzamides.
J. Nucl. Med. **40**, 120P-121P.

Franke W.-G., Beuthien-Baumann B., Kunath H. B., Reuner U., Füchtner F. (1998)
Zerebraler Glukosemetabolismus (MRGlu) und Hirmpfusion bei Patienten mit hereditärer myotoner Dystrophie (HMD).
Nuklearmedizin **37**, A28.

Friebe M., Spies H., Johannsen B., Mohammed A., Eisenhut M. (1998)
Präparation und in vivo-Testung von Melanom-affinen „3+1“ (^{99m}Tc)-Oxotechnetium(V)-Gemischt-Ligand-Komplexen.
Nuklearmedizin **37**, A49.

- Friedrich A., Brust P. (1998)
Evidence for a functionally active serotonin transporter at the blood-brain barrier.
Göttingen Neurobiology Report 1998 (Elsner N., Wehner R., eds.) Georg Thieme, Stuttgart, p. 580.
- Gerdson I., Pinkert J., Foetzsch R., Oehme L., Ripke B., Magyar-Lehmann S., Missimer J., Maguire R. P., Vollenweider F., Leenders K. L., Linemann H., Galley N., Hietschold V., Beuthien-Baumann B., Richter A., Müller A., Franke W.-G. (1999)
Spasmodicus torticollis shows impaired performance during numeric recognition and discrimination tasks – a study with ^{18}F -FDG-PET.
J. Cereb. Blood Flow Metab. **19**(Suppl.1), S128.
- Gupta A., Syhre R., Seifert S., Johannsen B. (1999)
Zur Stabilität von "3+1" Gemischtligandkomplexen des Technetiums: Umwandlung durch Glutathion.
Nuklearmedizin. **38**, A43.
- Hilger C.S., Noll B., Blume F., Leibnitz P., Johannsen B. (1998)
Tc(V) und Re(V) Komplexe von N-(MAG₁)-Histamin.
Nucl.-Med.**37**, A53.
- Jankowsky R., Kirsch S., Spies H., Johannsen B. (1999)
Strukturuntersuchungen an Peptidkomplexen von Technetium(V) und Rhenium(V).
Nuklearmedizin **38**, A43.
- Johannsen B., Pietzsch H.-J., Scheunemann M., Kretzschmar M., Brust P., Seifert S., Syhre R., Spies H. (1999)
Ein erster hochaffiner Technetium-99m-Ligand des Serotonin 5-HT_{2a} Rezeptors.
Nuklearmedizin **38**, A44.
- Kretzschmar M., Brust P., Syhre R., Scheunemann M., Gupta A., Seifert S., Pietzsch H.-J., Johannsen B. (1999)
Autoradiografische Darstellung der Rezeptorbindung eines 99m-Tc-Liganden des 5-HT_{2A}-Rezeptors in Hirnschnitten.
Nuklearmedizin **38**, A99.
- Kuwabara H., Brust P., Steinbach J., Johannsen B. (1999)
Blood-brain transport of large neutral amino acids (LNAAs) studied with O-methyl -[^{18}F]fluoro-L-DOPA ([^{18}F]OMFD).
J. Nucl. Med. **40** (5 Suppl.), 145P.
- Kuwabara H., Brust P., Steinbach J., Bergmann R. (1999)
Blood-brain transport and metabolic rate of glucose measured with [^{11}C]O-methyl-D-glucose (OMG).
J. Nucl. Med. **40** (5 Suppl.), 73P.
- Linemann H., Will E., Beuthien-Baumann B. (1998)
Zur Strahlenbelastung bei PET-Untersuchungen.
Nuklearmedizin **37**, A76.
- Matys S., Brust P., Scheunemann M., Pietzsch H.-J., Johannsen B. (1998)
Rezeptoraffine Oxorhenium (V)-Komplexe als Inhibitoren der Monoaminoxidase im Rattenhirn.
Nuklearmedizin **37**, A51.
- Römer J., Füchtner F., Steinbach J., Johannsen B. (1998)
 $^{16}\alpha$ -[^{18}F]Fluorestradiol für die Routine.
Nuklearmedizin **37**, A50.
- Stahl F., Lauer B., Junghans U., Beuthien-Baumann B., Schuler G. (1999)
Increased myocardial glucose-uptake after percutaneous myocardial laser revascularisation in patients with end-stage coronary artery disease.
JACC **33**, 335A.

Tiepolt C., Beuthien-Baumann B., Kühne A., Bredow J., Burchert W., Kropp J., Franke W.-G. (1999)
Diagnostische Treffsicherheit von ^{18}F -FDG bei differenziertem Schilddrüsenkarzinom: Vergleich von dediziertem PET und Koinzidenzkamera.
Nuklearmedizin **38**, A55.

Tsatalpas P., Spiegel, T., Manseck A., Beuthien-Baumann B., Kropp J., Franke W.-G. Wirth M. (1999)
 ^{18}F -FDG PET in the detection and treatment control of malignant germ cell tumours.
Eur. Urol. **35**, 122.

Van den Hoff J., Burchert W., Fricke H., Meyer G. J., Knapp W. H. (1999)
Eignung von $[1-^{11}\text{C}]$ -Acetat als quantitativer Perfusionstracer in der Myokard-PET.
Nuklearmedizin **38**, A27.

Vorwieger G., Brust P., Bauer R., Bergmann R., Walter B., Füchtner F., Steinbach J., Johannsen B. (1998)
The pharmacokinetics of FDOPA in newborn piglets.
Eur. J. Neuroscience **10** (Suppl. 10), 350.

Wittmüß A., Schröder H., Beuthien-Baumann B., Linemann H., Burchert W. (1999)
PET-Untersuchungen mit ^{18}F -FDG: Strahlenbelastung der MTAs beim Aufziehen der Spritzen.
Nuklearmedizin **38**, A107.

Wüst F., Berger R., Katzenellenbogen A.A., Alberto R., Schubiger P. A., Spies H., Johannsen B. (1998)
Rheniumkomplexe von steroidalen Estrogenen, Androgenen und Progestinen.
Nuklearmedizin **37**, A45.

Wüst F., Katzenellenbogen J. A., Spies H., Johannsen B. (1998)
Rhenium complexes of 17α -substituted estradiol capable of binding to the estrogen receptor.
Eur. J. Nucl. Med. **25**(8), 866.

Zessin J., Steinbach J., Johannsen B. (1998)
Triphenylarsonium- $[^{11}\text{C}]$ Methylid – Ein neuer ^{11}C -Präkursor zur Synthese von ^{11}C -Indolderivaten.
Nuklearmedizin **37**, A44.

LECTURES

Andreeff M., Hliscs R., Kropp J., Beuthien-Baumann B., Tiepolt C., Oehme L., Franke W.-G., Line-
mann H., Johannsen B.

Doppelkopf-Koinzidenz-Kamera im Vergleich zu einem PET-Ringtomographen – Erste physikalische
Untersuchungen und klinische Erfahrungen.

29. Wissenschaftlichen Tagung der Deutschen Gesellschaft für Medizinische Physik, Dresden,
14.-17.10.1998.

Bergmann R., Brust P., Johannsen B.

Beeinflussung der ^{99m}Tc -MIBI- und [^{18}F]-FDG-Aufnahme durch Inhibitoren des P-Glycoproteins.

36. Intern. Jahrestagung DGN, Leipzig, 01.-04.04.1998.

Bergmann R., Brust P., Pietzsch H.-J., Johannsen B.

Evaluation of the in vitro and in vivo properties of a potential Tc-labelled inhibitor of the MDR gene
product P-glycoprotein.

Joint Congress of European Association of Nuclear Medicine and the World Federation of Nuclear
Medicine and Biology, Berlin 30.08.-04.09.1998.

Beuthien-Baumann B.

Standortbestimmung der Positronen-Emissions-Tomographie in der Diagnostik von Herz, Mediasti-
num und Lunge.

8. Bastei-Symposium, Dresden, 17.-19.04.1998.

Beuthien-Baumann B.

Tutorial PET: Medizinische Diagnostik und Forschung mit Positronenstrahlen.

29. Wissenschaftlichen Tagung der Deutschen Gesellschaft für Medizinische Physik, Dresden,
14.-17.10.1998.

Beuthien-Baumann B., Franke W. G.

Refresherkurs: Aktuelle Informationen zu PET.

Tagung der Sächsischen Radiologischen Gesellschaft e.V. und der Thüringischen Gesellschaft für
Radiologie und Nuklearmedizin e.V., Radebeul/ Dresden, 09.-11.10.1998.

Beuthien-Baumann B., Handrick W., Schmidt T., Burchert W., Schackert G., Kropp J., Franke W.-G.

^{18}F -FDG-PET und ^{99m}Tc -ECD in der Hirn-Diagnostik bei Patienten mit apallischem Syndrom.

37. Intern. Jahrestagung DGN, Ulm, 14.-17.04.1999.

Bouziotis P., Papadopoulos M., Pirmettis I., Pelecanou M., Raptopoulou C. P., Terzis A., Stassinou-
poulou Ch., Friebe M., Spies H., Johannsen B., Chiotellis E.

Synthesis and characterization of two P,S,N-coordinated cis-dioxorhenium(V) complexes.

5th International Symposium on Technetium in Chemistry and Nuclear Medicine, Bressanone, Italy,
06.-09.09.1998.

Brust P.

Functional expression and regulation of the serotonin transporter at the blood-brain barrier.

Symp. on signal transduction pathways in the blood-brain barrier, Berlin, 01.07.1998.

Burchert W.

Beitrag der PET zur Diagnostik des Mammakarzinoms. In: Mammakarzinom. Empfehlungen zu Dia-
gnostik, Therapie und Nachsorge. Fortbildungsveranstaltung des Tumorzentrums Dresden.

Technische Universität Dresden, 09.12.1998.

Burchert W.

Alles über PET. In: 7. MTA Stammtisch der Gesellschaft für Nuklearmedizin Sachsens e.V.

Leipzig, 14.10.1998.

Burchert W.

Vergleich der Ergometerbelastung mit der Adenosin-Belastung bei der Myokardszintigraphie.

4. Dresdner Symposium „Invasive Kardiologie“, 09.-11.10.1998.

- Burchert W.
Stellenwert der Positronen-Emissions-Tomographie für die Kardiologie.
Nuklearkardiologisches Symposium der Firma Nycomed Amersham, Dresden, 10.10.1998.
- Burchert W.
PET – Revolution in Nuklearmedizin und Strahlentherapie.
75 Jahre Strahlentherapie in Dresden, Symposium, 27.11.1998.
- Burchert W., Wolpers H. G., van den Hoff J., Hakimi M., Meyer G. J., Hausmann T., Pethig K., Knapp W. H.
 $^{13}\text{N-NH}_3$ PET zur Diagnostik der Transplantatvaskulopathie. Vergleich mit Koronarangiographie und intrakoronarem Ultraschall.
37. Intern. Jahrestagung DGN, Ulm, 14.-17.04.1999.
- Franke W.-G., Beuthien-Baumann B., Kunath H. B., Reuner U., Füchtner F.
Zerebraler Glukosemetabolismus (MRGlu) und Hirnperfusion bei Patienten mit hereditärer myotoner Dystrophie (HMD).
36. Intern. Jahrestagung DGN, Leipzig, 01.-04.04.1998.
- Friebe M., Spies H., Johannsen B., Mohammed A., Eisenhut M.
Präparation und in vivo-Testung von Melanom-affinen „3+1“ ($^{99\text{m}}\text{Tc}$)-Oxotechnetium(V)-Gemischt-Ligand-Komplexen.
36. Intern. Jahrestagung DGN, Leipzig, 01.-04.04.1998.
- Friebe M., Spies H., Berger R., Syhre R., Papadopoulos M., Chiotellis E., Suda K., Wunderli-Allenspach H., Johannsen B.
Amine group bearing '3+1' oxotechnetium(V) and oxo-rhenium(V) complexes: synthesis, characterization of lipophilicity and permeation through the blood-brain barrier.
5th International Symposium on Technetium in Chemistry and Nuclear Medicine, Bressanone, Italy, 06.-09.09.1998.
- Füchtner F., Steinbach J., Brust P., Lücke R., Smuda C., Johannsen B.
Einfacher Zugang zu 3-O-Methyl-6- ^{18}F fluor-DOPA.
Vortragstagung GDCh-Fachgruppe Nuklearchemie, Dresden, 07.-09.09.1998.
- Füchtner F., Steinbach J., Zessin J., Brust P., Vorwieger G., Linemann H., Johannsen B.
Neues Herstellungsverfahren für 3-O-Methyl-6- ^{18}F fluor-DOPA und seine Anwendungen im PET-Experiment.
6. Arbeitstreffen AG Radiochemie/Radiopharmazie, Bad Nenndorf, 01.-03.10.1998.
- Füchtner F., Steinbach J., Bergmann R., Vorwieger G., Syhre R., Brust P., Beuthien-Baumann B., Burchert W., Zips D., Baumann M., Johannsen B.
3-O-methyl-6- ^{18}F fluoro-L-DOPA – a promising substance for tumour imaging.
13th Intern. Symp. on Radiopharm. Chem., St. Louis, USA, 27.06.-01.07.1999.
- Gupta A., Syhre R., Seifert S., Johannsen B.
Zur Stabilität von "3+1" Gemischtligandkomplexen des Technetiums: Umwandlung durch Glutathion.
37. Intern. Jahrestagung DGN, Ulm, 14.-17.04.1999.
- Heise K.-H., Nicolai R., Pompe S., Bubner M., Nitsche H.
Melanoidins as model humic acids in radioecological research.
13th Radiochemical Conference, Marienbad, 19.-24.04.1998.
- Hilger C. S., Noll B., Blume F., Leibnitz P., Johannsen B.
Tc and Re complexes of N-(MAG₁)-histamine.
5th International Symposium on Technetium in Chemistry and Nuclear Medicine, Bressanone, Italy, 06.-09.09.1998.

Hilger C. S., Noll B., Blume F., Leibnitz P., Johannsen B.
Tc(V) und Re(V) Komplexe von N-(MAG₁)-Histamin.
36. Intern. Jahrestagung DGN, Leipzig, 01.-04.04.1998.

Jankowsky R., Kirsch S., Spies H., Johannsen B.
Solution structures of technetium(V) and rhenium(V) peptide complexes as studies by EXAFS spectroscopy and capillary electrophoresis.
5th International Symposium on Technetium in Chemistry and Nuclear Medicine, Bressanone, Italy, 06.-09.09.1998.

Jankowsky R., Kirsch S., Spies H., Johannsen B.
Strukturuntersuchungen an Peptidkomplexen von Technetium(V) und Rhenium(V).
37. Intern. Jahrestagung DGN, Ulm, 14.-17.04.1999.

Jansen K., Steinbach J., Preusche St.
Fortluft-Emissionsüberwachung am PET-Zentrum im Forschungszentrum Rossendorf.
30. Jahrestagung Fachverband für Strahlenschutz „Radioaktivität in Mensch und Umwelt“, Lindau 28.9.-02.10.1998.

Johannsen B.
Auf dem Wege zu einer dritten Generation von Tc-99m-Radiopharmaka.
Minisymposium-Radiopharmazie. Biozentrum Johann Wolfgang Goethe-Universität Frankfurt am Main, 05.03.1998.

Johannsen B.
Towards a new generation of technetium-99m based radioactive probes for neuroreceptor imaging.
Bar-Ilan-University and Universities of Saxony. 2nd Scientific Conference, Bar-Ilan-Universität, Ramat Gan, Israel, 18.-19.03.1998.

Johannsen B.
Positronenemissionstomographie – ein modernes Verfahren der bildgebenden Diagnostik in der Medizin.
Technische Universität Chemnitz, Institut für Physik, 03.06.1998.

Johannsen B.
Recent advances in Tc-99m labelled compounds for CNS receptor imaging (Review).
2nd IAEA Research Co-ordination Meeting on "Development of agents for imaging CNS receptors based on Tc-99m", Athens, Greece, 21.-24. 09.1998.

Johannsen B.
Further attempts to design Tc-99m ligands for imaging CNS receptors.
2nd IAEA Research Co-ordination Meeting on "Development of agents for imaging CNS receptors based on Tc-99m", Athens, Greece, 21.-24.09.1998.

Johannsen B.
Radiopharmazeutische Sonden für die medizinische Diagnostik – möglichst auf der Basis des exotischen Elements Technetium.
Externe Pharmazeutische Seminarwoche der ETH Zürich, Lenzerheide, Schweiz, 10.-16.01.1999.

Johannsen B.
Radiopharmacy with ^{99m}Tc.
Miniworkshop on Medium-Mass Nuclei, FZR, Inst. für Kern- u. Hadronenphysik, 25.-26.02.1999.

Johannsen, B.
Radiopharmazeutische Sonden für die medizinische Diagnostik auf der Basis von Technetium-99m.
Kekulé-Institut für Organ. Chemie und Biochemie der Rheinischen Friedrich-Wilhelms-Universität Bonn, 30.03.1999.

Johannsen B., Pietzsch H.-J., Scheunemann M., Kretzschmar M., Brust P., Seifert S., Syhre R., Spies H.
Ein erster hochaffiner Technetium-99m-Ligand des Serotonin 5-HT_{2A}-Rezeptors.
37. Intern. Jahrestagung DGN, Ulm, 14.-17.04.1999.

Johannsen B., Friebe M., Pietzsch H.-J., Berger R., Syhre R., Papadopoulos M., Chiotellis E., Spies H.
Brain uptake of amine group bearing technetium complexes.
13th Intern.Symp. Radiopharmaceutical Chemistry, St.Louis, USA, 27.06.-01.07.1999.

Johannsen B., Pietzsch H.-J., Scheunemann M., Kretzschmar M., Seifert S., Brust P., Syhre R., Spies H.
Synthesis and autoradiographical evaluation of a novel high-affinity Tc-99m ligand for the serotonin-5-HT_{2A} receptor.
13th Intern.Symp. Radiopharmaceutical Chemistry, St.Louis, USA, 27.06.-01.07.1999.

Johannsen B., Pietzsch H.-J., Reigys M., Hoepfing A., Scheunemann M., Spies H., Brust P., Schibli R., Schubiger P. A., Alberto R.
First application of the metal tricarbonyl concept to design CNS receptor imaging agents based on technetium-99m.
13th Intern.Symp. Radiopharmaceutical Chemistry, St.Louis, USA, 27.06.-01.07.1999.

Kirsch S., Jankowsky R., Leibnitz P., Spies H., Johannsen B.
Crystal and solution structure of oxorhenium(V) complexes with cysteine and cysteine methyl ester.
5th International Symposium on Technetium in Chemistry and Nuclear Medicine, Bressanone, Italy, 06.-09.09.1998.

Kretzschmar M., Brust P., Syhre R., Scheunemann M., Gupta A., Seifert S., Pietzsch H.-J., Johannsen B.
Autoradiografische Darstellung der Rezeptorbindung eines ^{99m}Tc-Liganden des 5-HT_{2A}-Rezeptors in Hirnschnitten.
37. Intern. Jahrestagung DGN, Ulm, 14.-17.04.1999.

Linemann H., Will E., Beuthien-Baumann B.,
Zur Strahlenbelastung bei PET-Untersuchungen
36. Intern. Jahrestagung DGN, Leipzig, 01.-04.04.1998.

Linemann H.
Tutorial PET: Anforderungen an ein PET-Zentrum.
29. Wissenschaftliche Tagung der Deutschen Gesellschaft für Medizinische Physik, Dresden, 14.-17.10.1998.

Linemann H., Will E., Beuthien-Baumann B.
Strahlenbelastung des medizinischen Personals bei PET-Untersuchungen und Möglichkeiten der Reduzierung.
29. Wissenschaftliche Tagung der Deutschen Gesellschaft für Medizinische Physik, Dresden, 14.-17.10. 1998.

Linemann H., Will E., Beuthien-Baumann B., Wittmüß A., Schröder H., Kutzner H., Hauptmann A.
Sources of radiation dose to technologists by FDG-PET.
1999 ECAT USERS MEETING, Amsterdam, 21-24.04.1999.

Mädig P.
¹⁸F labelling strategy.
First Meeting of the EU project "Development of novel peptide-based radiopharmaceuticals"
Rossendorf, 19.06.1998.

Mädig P., Zessin J., Steinbach J., Chebani K., Johannsen B.
Einführung des kurzlebigen Radionuklids ¹¹C in aromatische Ringe.
Vortragstagung GDCh-Fachgruppe Nuklearchemie, Dresden, 07.-09.09.1998.

Mäding P.

Kernmarkierung von benzoiden und N-heterocyclischen Aromaten mit dem kurzlebigen Radionuklid ^{11}C .

BASF AG Ludwigshafen, 19.11.1998.

Mäding P., Scheunemann M., Steinbach J., Bergmann R., Iterbeke K., Tourwé D., Johannsen B.
Development of potential tumour imaging agents by 4- ^{18}F fluorobenzoylation of neurotensin analogues.

8th Conference of Central European Division of International Isotope Society, Bad Soden, 10.-11.06.1999.

Matys S., Brust P., Scheunemann M., Pietzsch H.-J., Johannsen B.

Rezeptoraffine Oxorhenium (V)-Komplexe als Inhibitoren der Monoaminoxidase im Rattenhirn.

36. Intern. Jahrestagung DGN, Leipzig, 01.-04.04.1998.

Noll B.

$^{186/188}\text{Re}$ -Markierung von Stents.

Workshop Schering AG, Fo Molekulare Diagnostik; 23.03.1999.

Noll B., Noll St., Leibnitz P., Jankowsky R., Spies H., Johannsen B.

Technetium(V) and rhenium(V) complexes with mercaptoacetyl glycine (MAG₁).

5th International Symposium on Technetium in Chemistry and Nuclear Medicine, Bressanone, Italy, 06.-09.09.1998.

Noll St., Noll B., Kniess T., Kampf G., Spies H., Johannsen B.

Rhenium and technetium complexes with nucleic acid components.

5th International Symposium on Technetium in Chemistry and Nuclear Medicine, Bressanone, Italy, 06.-09.09.1998.

Papadopoulos M., Pirmettis I., Tsoukalas C., Nock B., Maina T., Raptopoulou C. P., Terzis A., Friebe M., Spies H., Johannsen B., Chiotellis E.

Study of the formation of mixed-ligand oxorhenium and oxotechnetium complexes (SNS/S combination).

IAEA Intern. Symp. on modern trends in radiopharmaceuticals for diagnosis and therapy, Lissabon, 30.03.- 03.04.1998.

Pietzsch H.-J., Reisgys M., Alberto R., Hoepping A., Scheunemann M., Seifert S., Wüst F., Spies H., Schubiger P. A., Johannsen B.

Thioether ligands as anchor groups for coupling the " $\text{Tc}(\text{CO})_3$ " and " $\text{Re}(\text{CO})_3$ " moieties with biologically active molecules.

5th International Symposium on Technetium in Chemistry and Nuclear Medicine, Bressanone, Italy, 06.-09.09.1998.

Preusche St., Füchtner F., Steinbach J., Roß M.

Two years of experience in operation and maintenance of the Rossendorf PET cyclotron „CYCLONE 18/9“ facility“.

2. Workshop „CYCLONE 18/9 & 10/5 USER COMMUNITY“, Leuven/B, 10./11.12.1998.

Preusche St., Dupont C., Verbruggen R., Vamecq F., Bormans G.

CYCLONE 18/9 & 10/5 USER COMMUNITY: second workshop.

8th Intern. Workshop Targetry and Target Chemistry, St. Louis, 24.-27.06.1999.

Römer J., Füchtner F., Steinbach J., Johannsen B.

16α - ^{18}F Fluorestradiol für die Routine.

36. Intern. Jahrestagung DGN, Leipzig, 01.-04.04.1998.

Römer J.

Synthese von 16α - ^{18}F Fluoroestradiol-3,17 β -disulphamate.

8th Conference of Central European Division of International Isotope Society, Bad Soden, 10.-11.06.1999.

Römer J., Füchtner F., Steinbach J., Johannsen B.

16α -[^{18}F]Fluoroestradiol-3,17 β -disulphamate for sulphatase imaging.

13th Intern. Symp. Radiopharmaceutical Chemistry, St.Louis, USA, 27.06.-01.07.1999.

Scheunemann M., Elz S., Pietzsch H.-J., Brust P., Seifert S., Syhre R., Wober J., Kretzschmar M., Spies H., Johannsen B.

Konzeption und Synthese von Koordinationsverbindungen des Technetiums und des Rheniums mit Affinität zu neuronalen Serotoninrezeptoren.

Vortragstagung GDCh-Fachgruppe Nuklearchemie, Dresden, 07.-09.09.1998.

Scheunemann M.

^{18}F -labelling of NT(8-13) using activated 4-[^{18}F]fluorobenzoic acid.

2nd Meeting of the project partners of the Biomed 2 project "Novel peptide-based radiopharmaceuticals", Athens, 05.03.1999.

Scheunemann M., Mäding P., Steinbach J., Bergmann R., Iterbeke K., Tourwe D., Johannsen B.

Die Synthese von ^{18}F -markierten Derivaten des Neurotensins für die Entwicklung neuartiger Radiotracer zur Diagnose von Tumoren.

4. Deutsches Peptidsymposium 21.-24.03.1999.

Scheunemann M., Mäding P., Steinbach J., Bergmann R., Rodig H., Brust P., Johannsen B.

^{18}F labelling of neurotensins for the development of tumour imaging agents.

Portuguese-German Workshop, Rossendorf, 03.05.1999.

Scheunemann M., Mäding P., Steinbach J., Bergmann R., Iterbeke K., Tourwe D., Johannsen B.

Fluorine-18 labelling of neurotensin analogues for the development of tumour imaging agents.

13th Intern. Symp. Radiopharmaceutical Chemistry, St.Louis, USA, 27.06.-01.07.1999.

Schibli R., Alberto R., Schaffland A. O., Schubiger P. A., Abram U., Pietzsch H.-J., Johannsen B., Derivatization strategies of small biomolecules for the labeling with the organometallic $^{99\text{m}}\text{Tc}(\text{CO})_3$ -core.

13th Intern. Symp. Radiopharmaceutical Chemistry, St. Louis, USA, 27.06.-01.07.1999.

Seifert S., Syhre R., Gupta A., Spies H., Johannsen B.

Stability studies on "3+1" mixed-ligand technetium and rhenium complexes.

5th International Symposium on Technetium in Chemistry and Nuclear Medicine, Bressanone, Italy, 06.-09.09.1998.

Skaddan M. B., Wüst F., Welch M. J., Katzenellenbogen J. A.

Synthesis and biological evaluation of 7α Re/Tc "3+1" and cyclopentadienyltricarbonylmethyl (CpTM) estrogen mimics based on the conjugated design.

13th Intern. Symp. Radiopharmaceutical Chemistry, St. Louis, USA, 27.06.-01.07.1999.

Spies H., Pietzsch H.-J., Johannsen B.

The "n+1" mixed-ligand approach in the design of specific technetium radiopharmaceuticals: potentials and problems.

5th International Symposium on Technetium in Chemistry and Nuclear Medicine, Bressanone, Italy, 06.-09.09.1998.

Spies H., Noll S., Noll B., Hilger C. S., Brust P., Syhre R., Johannsen B.

Derivatives of 6-methyl-8 α -amino-ergoline: synthesis and affinity to the dopamine D_2 receptor.

5th International Symposium on Technetium in Chemistry and Nuclear Medicine, Bressanone, Italy, 06.-09.09.1998.

Spies H.

Technetiumtracer research at Rossendorf.

Instituto Tecnológico e Nuclear Lissabon/Savavem, Portugal, 25.-28.02.1999.

Spies H.
Technetium tracer research at Rossendorf.
Latvian Institute of Organic Synthesis, Riga, Latvia, 14.06.1999.

Steinbach J.
 ^{11}C -labelled aromatics and ^{18}F -electrophilic fluorinating agents as important prerequisites for the development of modern radiopharmaceuticals
Joint European International Isotope Society Conference (Central European Division and UK Chapter)
Bad Soden, 24.-26.06.1998.

Steinbach J.
Positronen-Emissions-Tomographie - ein modernes Diagnostik-Verfahren: Methodische Grundlagen und aktuelle radiochemische Ergebnisse.
Universität Marburg, 10.11.1998.

Steinbach J.
Positronen-Emissions-Tomographie - PET -ein bildgebendes Verfahren der Funktionsdiagnostik in der Medizin.
Tag der offenen Tür, 12.09.1998.

Steinbach J.
Physikochemische und technische Grundlagen der PET.
Symposium der Fa. Pfizer, 11.10.1998.

Steinbach J.
Radiopharmazie am PET-Zentrum Rossendorf.
Zentrumsseminar, 04.03.1999.

Stephan H.
Supramolekulare Rezeptoren zur Anionen- und Kationenerkennung.
Institutskolloquium, FZ Karlsruhe/Institut für Nukleare Entsorgungstechnik, 20.05.1999.

Stephan H.
Dendrimere: Anwendungsmöglichkeiten in der medizinischen Diagnostik und Therapie.
Institutskolloquium, Universität Bonn, Kekulé-Institut für Organische Chemie und Biochemie, 14.06.1999.

Stephan H., Berger R., Spies H., Johannsen B., Klein L., Vögtle F.
Dendrimere als selektive Carrier und medizinische Diagnostika.
DECHEMA-Statusseminar „Funktionale Supramolekulare Systeme“, Frankfurt am Main, 21.-22.06.1999.

Tiepolt C., Beuthien-Baumann B., Kühne A., Bredow J., Burchert W., Kropp J., Franke W.-G.
Diagnostische Treffsicherheit von ^{18}F -FDG bei differenziertem Schilddrüsenkarzinom: Vergleich von dediziertem PET und Koinzidenzkamera.
37. Intern. Jahrestagung DGN, Ulm, 14.-17.04.1999.

van den Hoff J., Burchert W., Fricke H., Meyer G. J., Knapp W. H.
Eignung von $[1-^{11}\text{C}]$ -Acetat als quantitativer Perfusionstracer in der Myokard-PET.
37. Int. Jahrestagung der DGN, Ulm, 14.-17.04.1999.

Witnüb A., Schröder H., Beuthien-Baumann B., Linemann H., Burchert W.
PET-Untersuchungen mit ^{18}F -FDG: Strahlenbelastung der MTAs beim Aufziehen der Spritzen.
37. Int. Jahrestagung der DGN, Ulm, 14.-17.04.1999.

Wüst F., Berger R., Katzenellenbogen A. A., Alberto R., Schubiger P. A., Spies H., Johannsen B.
Rheniumkomplexe von steroidalen Estrogenen, Androgenen und Progestinen
36. Intern. Jahrestagung DGN, Leipzig, 01.-04.04.1998.

Wüst F., Katzenellenbogen J. A., Spies H., Johannsen B.
Rhenium complexes of 17α -substituted estradiol capable of binding to the estrogen receptor.
Joint Congress of European Association of Nuclear Medicine and the World Federation of Nuclear
Medicine and Biology, Berlin, 30.08.-04.09.1998.

Wüst F., Skaddan M. B., Carlson K. E., Leibnitz P., Katzenellenbogen J. A., Spies H., Johannsen B.
Synthesis and receptor binding of novel progestin-rhenium complexes.
5th International Symposium on Technetium in Chemistry and Nuclear Medicine, Bressanone, Italy,
06.-09.09.1998.

Zessin J., Steinbach J., Johannsen B.
Triphenylarsonium- ^{11}C Methylid – Ein neuer ^{11}C -Präkursor zur Synthese von ^{11}C -Indolderivaten.
36. Intern. Jahrestagung DGN, Leipzig, 01.-04.04.1998.

PATENTS

Kasch H., Schumann W., Römer J., Steinbach J., DE 197 12 488 A 1
Steroid sulphamates, method for preparation and use thereof.

Füchtner F., Steinbach J., ha 1156, AZ 199 28 911.5
Verfahren zur Herstellung von 3-O-Methyl-6- ^{18}F Fluor-DOPA, (3-O-Methyl-6- ^{18}F Fluor-L-4-hydroxy-
phenylalanin, 3-(2- ^{18}F Fluor-4-hydroxy-5-methoxy-phenyl)-2-amino-propansäure).

Steinbach J., Füchtner F., Römer J., Johannsen B., ha 1164, AZ 199 28 910.7
Verfahren zur Herstellung von 16α - ^{18}F Fluorestradiol-3,17 β -disulfamat (FESDS).

Steinbach J., Füchtner F., Johannsen B., ha 1165, AZ 199 28 909.3
Aminosäurederivat und seine Verwendung.

Dinkelborg, Blume, Hilger, Heldmann, Platzeck, Niedballa, Miklautz, Speck, Duda, Tepe, Noll, Görner:
Oberflächlich radioaktiv beschichtete Stents, Verfahren zu ihrer Herstellung und ihre Verwendung zur
Restenoseprophylaxe (Verfahren zur Beschichtung von Stents).
submitted: 29.04.98

AWARDS

Mrs. M. Kretzschmar, Dr. P. Brust, Dr. R. Syhre, Dr. M. Scheunemann, Mrs. A. Gupta, Dr. S. Seifert,
Dr. H.-J. Pietzsch and Prof. B. Johannsen were awarded the 1999 Poster Prize of the Annual Meeting
of Deutsche Gesellschaft für Nuklearmedizin e.V for their development of a high affinity Tc-labelled
ligand for the 5-HT_{2A} -receptor.

Dr. H. Linemann, Dr. E. Will and Dr. B. Beuthien-Baumann were awarded the 1998 Varian Poster
Prize of the 29. Wissenschaftliche Tagung der Deutschen Gesellschaft für Medizinische Physik for
their contribution "Strahlenbelastung des medizinischen Personals bei PET-Untersuchungen und
Möglichkeiten der Reduzierung".

PhD THESES

Christian Fischer

Umpolung von nukleophilem no carrier added [^{18}F]Fluorid zu elektrophilem no carrier added [^{18}F]FCIO₃ mit hoher spezifischer Aktivität.

Dresden University of Technology, January 1998.

Sylvia Kirsch

Zur Koordination von Rhenium(V) und Technetium(V) mit SH-haltigen Aminosäuren und Peptiden.

Dresden University of Technology, May 1998.

Martina Reising

Rhenium- und Technetiumkomplexe mit Thioetherliganden.

Dresden University of Technology, October 1998.

Matthias Friebe

Amingruppentragende Technetium(V)- und Rhenium(V)-Verbindungen: Synthese und Untersuchungen von Zusammenhängen molekularer Eigenschaften und dem Transport über die Blut-Hirn-Schranke.

Dresden University of Technology, January 1999.

Rüdiger Jankowsky

Strukturuntersuchungen an Peptidkomplexen von Technetium und Rhenium.

Dresden University of Technology, January 1999.

Frank Wüst

Rhenium und technetium-containing steroids as ligands for the estrogen receptor, progesterone receptor and androgen receptor.

Dresden University of Technology, January 1999.

DIPLOMA THESES

Axel Rother

Synthese von Pyridinium-/Dihydropyridin-substituierten Oxotechnetium(V)-Gemischtligandkomplexen und Untersuchungen zu deren Redoxverhalten.

Philipps-Universität Marburg, Fachbereich Chemie (Prof. Jungclas), April 1998.

Mirko Kaffka

Softwarepaket zur 3D-Visualisierung von PET-Daten.

Hochschule für Technik und Wirtschaft Dresden (FH), Fachbereich Informatik/Mathematik, Oktober 1998.

Betreuer im FZR: Dr. E. Will.

Dr. Paul Bühler

Numerical methods for the analysis of blood sampler data.

Nachdiplomarbeit in Medizinphysik, Eidgenössische Technische Hochschule, Zürich, November 1998.

Betreuer im FZR: Dr. E. Will.

IV. SCIENTIFIC COOPERATION

COOPERATIVE RELATIONS AND JOINT PROJECTS

In multidisciplinary research such as carried out by this Institute, collaboration, the sharing of advanced equipment and, above all, exchanges of ideas and information play an important role. Effective collaboration has been established with colleagues at universities, in research centres and hospitals.

Dresden University of Technology has been a major partner in our cooperative relations. Cooperation with various groups in the Department of Chemistry and the Faculty of Medicine was again significantly extended last year. Common objects of radiopharmacological and medical research link the Institute with the Dresden University Hospital, above all with its Department of Nuclear Medicine (Prof. Franke). A joint team of staff members from both the Institute and the Clinic of Nuclear Medicine are currently working at the Rossendorf PET Centre.

The Institute cooperates with the Department of Surgical Research (Prof. Schackert) on a project concerning gene therapy monitoring. The Institute of Analytical Chemistry (Prof. Salzer) plays not only an important part in tracer research by performing analytical characterization (Dr. Scheller) but also cooperates in tumour research.

Very effective cooperation exists with the *Federal Material Research Institute in Berlin* (Dr. Reck, Mr. Leibnitz), whose staff members carried out X-ray crystal structure analysis of new technetium and rhenium complexes. The Institute of Organic Chemistry (Dr. Seichter) of the *Freiberg University of Mining & Technology* also contributes to analysing coordination compounds.

Our Institute is linked with the Institute of Pathology (Prof. Zwiener, Dr. Bauer) of *Jena's Friedrich-Schiller University* by long-standing fruitful cooperation on the pathophysiological aspects of brain functions.

In the field of PET tracers (steroid chemistry) the Institute works together with the *Hans-Knöll-Institute for Natural Products Research, Jena* (Prof. Hinnen, Dr. Kasch).

The fruitful collaboration with the *Paul Scherrer Institute* (Prof. Schubiger) of Villigen, Switzerland, which involves bioinorganic, radiochemical and biological topics, is much appreciated. PSI is also one of the main partners in the current BIOMED2 project on tumour-affine neuropeptides.

Our long-standing cooperation with the "*Demokritos*" *National Research Centre for Physical Sciences* in Athens (Dr. Chiotellis) has been continued. Various joint projects on technetium and rhenium chemistry were dealt with.

A field of cooperation with the Department of Pharmacy (Prof. Folkers, Prof. Wunderli-Allenspach) of the *Swiss Federal Institute of Technology Zurich (ETH Zürich)* was the chemical and biological characterization of technetium and rhenium complexes.

Based on PhD student and post doc visits, joint research into labelled steroids was carried out with the Department of Chemistry (Prof. Katzenellenbogen) of the *University of Illinois, Urbana, USA*, and the Division of Radiological Sciences (Prof. Welch) of the *Washington University School of Medicine, St. Louis, USA*.

Cooperation on a special subject concerning bioinorganic chemistry is in progress with *ASTA Medica Frankfurt* (Prof. Kutscher, Dr. Bernd).

In the field of supramolecular chemistry, successful cooperation was established with the Institute of Organic Chemistry and Biochemistry (Prof. Schmidtchen) of *Technische Universität München* and with the Kekulé Institute of Organic Chemistry and Biochemistry (Prof. Vögtle) of the *University of Bonn*.

The identification of common objects in PET radiopharmacy has led to collaborative research with the Department of Nuclear Medicine (Prof. Georgi) of the *University of Leipzig*.

Effective cooperation also exists with the *Riga Institute of Organic Chemistry* (Dr. Zablotskaya), Latvia. Cooperation in PET tracer chemistry has been established with the *Turku Medical PET Centre* (Dr. Solin).

The Institute works with the *Bar-Ilan University* in Ramat-Gan, Israel (Dr. G. Yadid), with the *West Virginia University Morgantown*, USA (Prof. H. Kuwabara), the *PET Centre Aarhus*, Denmark (Prof. A. Gjedde), the *Birla Institute of Technology and Science, Pilani*, India (Dr. P. Srinivas) on the biochemical aspects of radiotracer research.

During a PhD student's visit, joint research on the serotonin transporter was carried out in cooperation with the Department of Biochemistry and Molecular Biology (Prof. Ganapathy, Prof. Leibach) of the *Medical College of Georgia, Augusta*, USA.

LABORATORY VISITS

F. Wüst
University of Illinois, USA
Oct. 01, 1997-March 31, 1998

M. Friebe
Universität Heidelberg
February 10 – 13, 1998

M. Friebe
ETH Zurich, Switzerland
March 2 – April 1, 1998

B. Johannsen
Bar Ilan-University, Israel
March 17 – 22, 1998

R. Jankowsky
ETH Zurich, Switzerland
April 15 – June 15, 1998

R. Jankowsky
Hamburg, HASYLAB Synchrotron
August 2 – 9, 1998

M. Friebe
Hamburg, HASYLAB Synchrotron
August 2 – 10, 1998

M. Reigys
Hamburg, HASYLAB Synchrotron
August 2 – 10, 1998

P. Brust
Bar Ilan-University, Israel
September 6 – 18, 1998

R. Bergmann
PSI Villingen, Switzerland
September 22 – 25, 1998

S. Seifert
ESRF Grenoble, France
January 26 – February 3, 1999

J.-U. Künstler
ESRF Grenoble, France
January 26 – February 3, 1999

H. Spies
Instituto Tecnológico e Nuclear Lissabon/Savavem, Portugal
February 25 – 28, 1999

H.-J. Pietzsch
Karolinska Institute Stockholm, Sweden
May 29 – June 1, 1999

H. Spies
Latvian Institute of Organic Synthesis, Riga, Latvia
June 10 – 15, 1999

GUESTS

Dr. A. Zablotskaya
Latvian Institute of Organic Synthesis, Riga, Latvia
May 3 - 24, 1998

M. Netter
Universität Wien, Austria
July 1 – October 31, 1998

Prof. Dr. H. Kuwabara
West Virginia University, USA
July 2 – September 25, 1998

J. Zaers
Krebsforschungszentrum Heidelberg
August 14 – 17, 1998

O. Ublitz
Krebsforschungszentrum Heidelberg
August 14 – 17, 1998

Prof. Srivastava
University Brookhaven, USA
August 27 – 29, 1998

Dr. G. Byk
Bar Ilan-University, Israel
October 13 – 21, 1998

Prof. A. Nudelman
Bar Ilan-University, Israel
October 13 – 16, 1998

Dr. Knickmeier
Universität Münster
October 15 – 17, 1998

Dr. Bauer
Universität Jena
November 9 – 13, 1998

B. Walther
Universität Jena
November 9 – 13, 1998

El Sajed
Universität Jena
November 9 – 13, 1998

I. Benkovsky
Slovak Institute of Metrology Bratislava, Slovak Republic
January 14 – February 14, 1999

A. Alberti Ramirez
Centro de Isotopes, La Habana, Cuba
April 1 – May 31, 1999

Dr. A. Zablotskaya
Latvian Institute of Organic Synthesis, Riga, Latvia
April 6 – May 7, 1999

L. Patrico
Instituto Tecnologico e Nuclear Lissabon, Portugal
May 1 – 4, 1999

I. Santos
Instituto Tecnologico e Nuclear Lissabon, Portugal
May 1 – 4, 1999

Prof. M. Mintas
ETH Zurich
June 4 – 6, 1999

Prof. Dr. C. Streffer
Universität Essen
June 11 – 12, 1999

K. Chavatte
University Brussels, Belgium
June 20 – July 1, 1999

M. Vekeman
University Brussels, Belgium
June 20 – July 1, 1999

MEETINGS ORGANIZED

PET Centre Workshop „Die Anwendung der kinetischen Modellanalyse im klinischen PET (am Beispiel Hirn und Tumoren)“
Dresden, February 18, 1998.

First meeting of the partners of the EU project: “Development of novel peptide based radiopharmaceuticals for *in vivo* receptor associated tumour diagnosis and therapy“
Rossendorf, June 19, 1998

German-Portuguese Workshop on Aspects of Radiotracer Research
Rossendorf, May 3 – 4, 1999

OTHER ACTIVITIES

DGN Working Group on Radiochemistry and Radiopharmacy

Chairman: Johannsen, B.
(see also homepage <http://www.nuklearmedizin.de>)

Activities for the IAEA:

1. Agency Research Agreement No. 8959 (CNS receptor imaging agents)
Johannsen, B.
2. Two months fellowship training of Alberti Ramirez, A., Cuba
(supervisor: Spies, H.)
3. One-month fellowship training of Benkovsky, I, Slovak Republic
(supervisor: Steinbach, J.)
4. Consultation on setup of PET centres in Prague and Bratislava
5. Meeting with Dr. Vera Ruiz, Head of Industrial Applications and Chemistry Section, to discuss the implementation of PET reference centres.
6. Visits of scientists in the frame of network of IAEA from Pakistan Nuclear Research Centre and Peking Institute of Nuclear Research.

V. SEMINARS

TALKS OF VISITORS

Prof. Dr. W. Jaroß und Dr. S. Gehrisch, Institut für Klinische Chemie und Laboratoriumsmedizin,
Universitäts-Klinikum Carl Gustav Carus, Dresden
Genetische Grundlagen von Herz-Kreislauf-Erkrankungen und Methoden der DNA- und RNA-Analytik.
23. 01. 1998.

Prof. Dr. G. Folkers, Dept. Pharmazie, Eidgenössische Technische Hochschule Zürich
Integrierte Ansätze zur rationalen Entwicklung von Gentherapeutika auf der Basis Nukleosid-
prozessierender Proteine.
24. 04. 1998.

Dr. M. Glaser, Hammersmith Hospital London
Neue bifunktionelle Chelatbildner für Technetium und Rhenium.
28. 04. 1998.

Dr. O. Solin, National PET-Centre Turku, Finnland
Fluorine-18 radiochemistry at the Turku PET Centre.
30. 04. 1998.

Prof. T. Kuwert, Herz- und Diabeteszentrum Nordrhein-Westfalen, Bad Oeynhausen
Stoffwechseluntersuchungen an Hirntumoren.
12. 05. 1998.

Prof. H. Kuwabara, West Virginia University, USA
Clinical applications of F-DOPA-PET.
27. 07. 1998.

Prof. C. Srivastava, Brookhaven National Laboratory, USA
Research and production of medical radionuclides at Brookhaven National Laboratory.
28. 08. 1998.

Prof. Vögtle, Universität Bonn
Energie- und Elektronentransfer in Übergangsmetallen, Komplexchemie und Homocalixarenen und
dendritische Diagnostika.
18. 09. 1998.

Prof. O. Schober und Dr. M. Knickmeier, Westf. Wilhelms-Universität Münster
Sympathische Innervation des Herzmuskels
– Klinische Fragestellung und In-vivo-Darstellung
– Radiochemie der Transmitter und Rezeptoren.
16. 10. 1998.

Dr. G. Byk, Bar-Ilan-Universität Israel
Novel cationic lipids for gene delivery and gene therapy.
19. 10. 1998.

Herr Erler, Universitätsklinikum Dresden
Einführung in die Versuchstierzucht.
28. 10. 1998.

Prof. M. Schwaiger, Nuklearmedizinische Klinik der TU München
PET in der kardiologischen Forschung.
20. 11. 1998.

Prof. F. P. Schmidtchen, Technische Universität München
Die Guanidine: Vielseitige Bausteine für Katalysatoren und abiotische Wirte.
23. 11. 1998.

Prof. T. Jones, Hammersmith Hospital London
Einführung in PET – Prinzipien, Anwendungen, Probleme, Zukunft (Zentrumsseminar).
04. 02. 1999.

Prof. M. Schwaiger, Nuklearmedizinische Klinik der TU München
PET: Körperfunktionen auf dem Bildschirm (Zentrumsseminar).
18. 02. 1999.

Dr. J. Steinbach, FZR
Radiopharmazie am PET-Zentrum Rossendorf (Zentrumsseminar).
04. 03. 1999.

Prof. G. Vollmer, TU Dresden, Institut für Zoologie
Hormonabhängige Kanzerogenese des Endometriums – zur Bedeutung von Hormonen und
Komponenten der extrazellulären Matrix.
08. 04. 1999.

Dr. V. Otto, Universitätsspital Zürich
Das schwere Schädel-Hirn-Trauma in der Klinik und im Forschungslabor.
07. 05. 1999.

Prof. M. Mintas, Eidgenössische Hochschule Zürich
Novel pyrimidines and pyrimidine derivatives of L-ascorbic acid: synthesis and biological evaluation.
04. 06. 1999.

Prof. Dr. Dr. h.c. Streffer, Universitätsklinikum Essen
Hypoxie und Tumorstoffwechsel und ihr Einfluss auf die Strahlentherapie.
11. 06. 1999.

K. Chavatte und M. Vekeman, Freie Universität Brüssel
-The bioevaluation of radiolabelled neurotensin analogues
-Synthesis and the pre-clinical evaluation of 2-I-tyrosine.
21. 06. 1999.

INTERNAL SEMINARS 1998/99

U. Dintner (Hans-Knöll-Institut Jena)

Synthese von 16 α -Fluor-androst-5-en-3 β ,17 β -diol.
14.05.98.

H. Stephan

Supramolekulare Rezeptoren zur Anionenerkennung.
27.05.98.

M. Reisgys

Thioetherchelate, erfolgversprechende Kombination von Tc/Re und Biomolekül.
17.06.98.

B. Beuthien-Baumann

Stand der PET bei der Diagnostik von Mediastinal- und Lungen-Tumoren.
07.07.98.

M. Scheunemann

Neue Rheniumkomplexe mit Affinität zu Serotonin- HT_{1A}- und HT_{2A}-Rezeptoren.
19.08.98.

M. Kretzschmar

Die Autoradiographie – eine Methode zum Nachweis der Rezeptor- bzw. Transporter-Ligand-Bindung im Hirn und peripheren Gewebe verschiedener Tierspezies.
16.09.98.

J. Zessin

¹¹C-Kernmarkierung von aromatischen Heterocyclen.
28.10.98.

H. Spies, J. Kropp

Vorstellung des Gemeinschaftsprojekts Tc-Fettsäuren.
13.11.98.

R. Berger

Bestimmung von Lipophilie- und pK_a-Werten für Tc/Re-Komplexe mit RP-HPLC.
02.12.98.

R. Jankowsky

Strukturuntersuchungen an Peptid-Komplexen von Tc und Re.
09.12.98.

W. Seidel (Abt. FWKF)

Freie Elektronen-Laserstrahlung: Prinzip und mögliche Anwendungen.
17.03.99.

H. Linemann

Graphische Lösungen für das Kompartiment-Modell bei dynamischen PET-Untersuchungen.
7.04.99.

F. Füchtner

PET-Radiopharmaka-Herstellung.
12.05.99.

J. Römer

[¹⁸F]Fluorestradiolsulfamate.
26.05.99.

T. Knieß
Bifunktionelle Chelatagenzien im pre-Labeling von Biomolekülen mit ^{99m}Tc .
16.06.99.

VI. ACKNOWLEDGEMENTS

ACKNOWLEDGEMENTS FOR FINANCIAL AND MATERIAL SUPPORT

The Institute is part of the Research Center Rossendorf Inc., which is financed by the Federal Republic of Germany and the Free State of Saxony on a fifty-fifty basis.

Two projects were supported by Commission of the European Communities:

- Peptide radiopharmaceuticals in oncology
BIOMED II
in collaboration with Belgium, Greece and Switzerland
(PL 963198-SC), 04/1998 – 03/2001.
- Radiotracers for in vivo assessment of biological function
COST B12
in collaboration with Sweden, Italy and Switzerland
02/1999 – 02/2004.

Four research projects concerning technetium tracer design, biochemistry and PET radiochemistry were supported by the Deutsche Forschungsgemeinschaft (DFG):

- Development and characterization of mixed-ligand complexes of technetium and rhenium with multidentate chelating agents
Sp 401/2-4 (H. Spies), 01/1994 – 08/1998.
- Technetium complexes with thioether ligands
Pi 255/1-2 (H.-J. Pietzsch), 04/1992 – 12/1998.
- PET with steroids
Ste 601/3-3 (J. Steinbach), 01/1998 – 12/1999.
- Tc labelled fatty acids for myocardium diagnosis
Sp 401/6-1 (H. Spies), 06/1999 – 05/2001.
- Redox transport system for ^{99m}Tc radiopharmaceuticals
Sp 401/5-1 (H. Spies), 06/1999 – 06/2001.

The Sächsisches Staatsministerium für Wissenschaft und Kunst provided support for the following projects:

- Technetium(VII) complexes with supramolecular receptors
SMWK-No. 4-7533-70-844-98/4, 07/1998 – 12/2000.
- ¹⁸F labelled substrates of virus thymidine kinase for monitoring of gene therapy of cancer
SMWK-No. 4-7531.50-03-844-98/2, 07/1998 – 12/2000.
- Molecular modelling of solid tumours by molecule spectroscopy in combination with PET
SMWK-No. 4-7531.50-03-0370-98/3, 07/1998 – 12/2000.

The Free State of Saxony and the Free State of Thuringia support PET studies on DOPA metabolism in brain (P. Brust) – 04/1995 – 12/1998.

Supported by the "LIST" programme of the Free State of Saxonia studies on new ¹⁸F-labelled tracers were carried on in cooperation with TU Dresden and Hans-Knöll-Institut Jena. (Prof. W.-G. Franke) 03/1996 – 12/1998.

The International Atomic Energy Agency supported a co-ordinated research programme: "Development of agents for imaging central neural system receptors based on Tc-99m". Agreement No. 8959 – 12/1995 – 12/1998.

Two projects were supported by cooperation with the pharmaceutical industry:

- Receptor-binding technetium tracers
Mallinckrodt Medical B.V.
07/1993 – 06/1998.
- Cooperation in nuclear diagnostic
Schering AG Berlin
07/1996 – 06/2000.

Temporary work at cooperating institutions were supported by the following sponsors:

- EXAFS-Untersuchungen (Friebe M., Jankowsky R., Reisgys M.)
HASYLAB Synchrotron Hamburg
- Two months stay at ETH Zurich (Jankowsky R.)
ETH Zurich fund
- Five months stay at ETH Zurich (Friebe M.)
ETH Zurich fund
- Six months stay at University of Illinois, Urbana, USA (Wüst F.)
DAAD-Stipendium
- One year stay at the Medical College of Georgia, Augusta, USA (Friedrich A.)
fund of the host institution

VII. PERSONNEL

per 30 June 1999

Director

Prof. Dr. B. Johannsen

Administrative Staff

L. Kowe
G. Neubert
M. Kersten

Scientific Staff

Dr. Bergmann, R.
Dr. Brust, P.
Dr. Füchtner, F.
Dr. Heibold, I.*
Kretschmar, M.
Mädig, P.

Dr. Noll, B.
Dr. Noll, S.
Dr. Pietzsch, H.J
Preusche, S
Dr. Römer, J.*
Dr. Scheunemann, M.*

Dr. Steinbach, J.
Dr. Spies, H.
Dr. Seifert, S.
Dr. Syhre, R.
Dr. Will, E.

Technical Staff

Dohn, N.
Fischer, K.
Gläser, H.
Görner, H.
Große, B.
Herrlich, R.
Hüller, R.

Kasper, H.
Kolbe, U.
Krauß, E.*
Kreisl, B..
Kunadt, E
Lehnert, S.
Lösel, E

Lücke, R.
Nicolai,
Roß, H.
R Smuda, C.*
Sterzing, R.
Suhr, A.*

Post Docs

Dr. Knieß, T.
Dr. Krishnan, S.
Dr. Zessin, J.

PhD Students

Drews, A.
Grote, M.

Gupta, A.
Jordanova, A.

Künstler, J.-U.
Rodig, H.

* term contract

Former Personnel

(who left during the period covered by the report)

Scientific Staff:	DC Berger, R. Prof. Dr. Burchert, W.	Vorwieger, G.
Technical Staff:	Landrock, K.** Lenkeit, U.**	Schneider, F.
Post Docs:	Dr. Hoeping, A.	
PhD Students:	Dr. Friebe, M. Friedrich, A. Dr. Jankowsky, R.	Dr. Kirsch, S. Dr. Reisgys, M. Dr. Wüst, F.

** on maternity leave